

**Study of the cellular  
response, signaling, and  
repair pathways to confront  
DNA double-strand breaks  
in telophase**

**Jessel Ayra Plasencia  
2021**



Universidad  
de La Laguna

Este documento incorpora firma electrónica, y es copia auténtica de un documento electrónico archivado por la ULL según la Ley 39/2015.  
Su autenticidad puede ser contrastada en la siguiente dirección <https://sede.ull.es/validacion/>

Identificador del documento: 3075810 Código de verificación: smutbmB+

Firmado por: JESSEL AYRA PLASENCIA  
UNIVERSIDAD DE LA LAGUNA

Fecha: 30/11/2020 12:24:14

María de las Maravillas Aguiar Aguiar  
UNIVERSIDAD DE LA LAGUNA

08/02/2021 13:50:06



Este documento incorpora firma electrónica, y es copia auténtica de un documento electrónico archivado por la ULL según la Ley 39/2015.  
*Su autenticidad puede ser contrastada en la siguiente dirección <https://sede.ull.es/validacion/>*

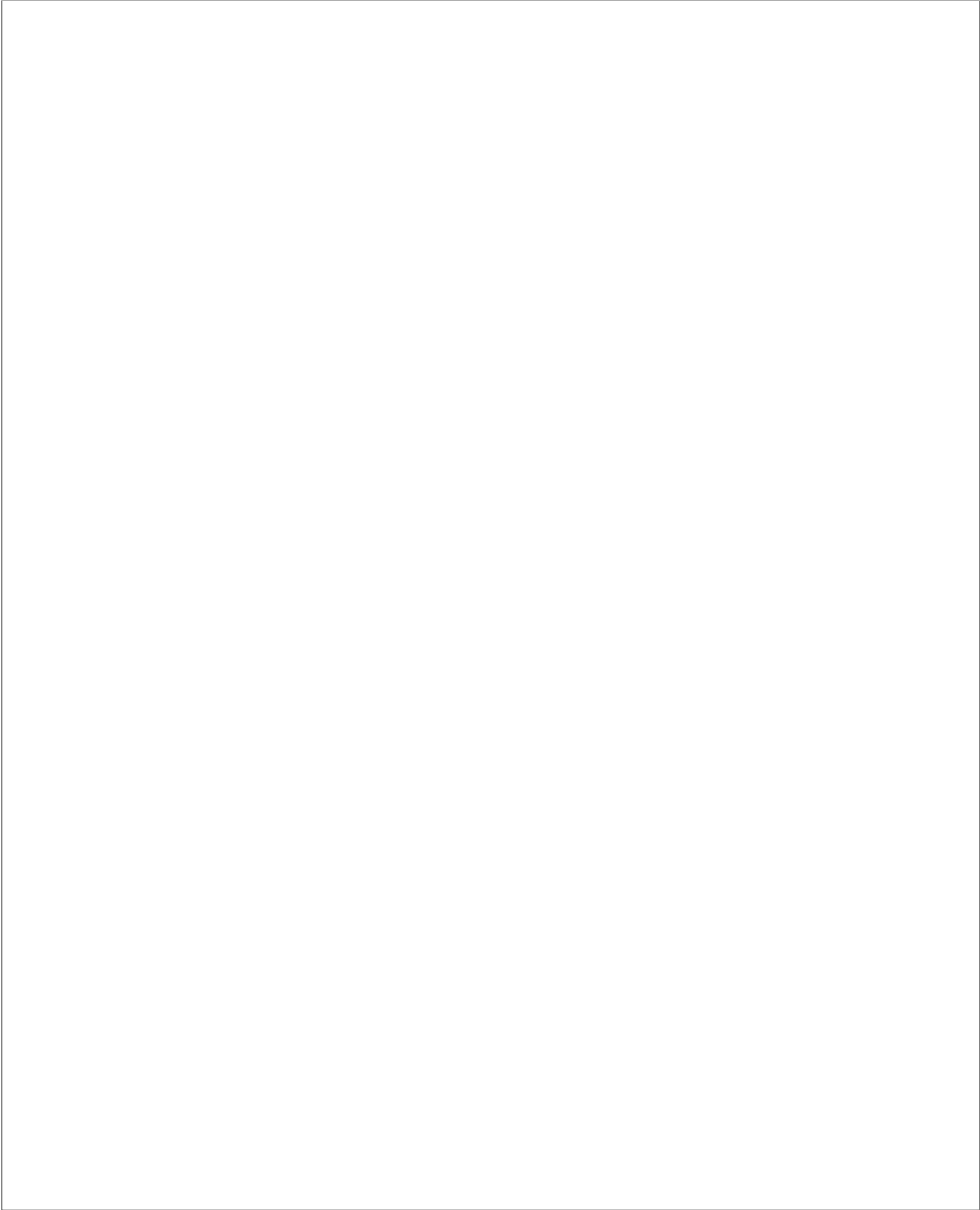
Identificador del documento: 3075810      Código de verificación: smutbmB+

Firmado por: JESSEL AYRA PLASENCIA  
UNIVERSIDAD DE LA LAGUNA

Fecha: 30/11/2020 12:24:14

María de las Maravillas Aguiar Aguiar  
UNIVERSIDAD DE LA LAGUNA

08/02/2021 13:50:06



Este documento incorpora firma electrónica, y es copia auténtica de un documento electrónico archivado por la ULL según la Ley 39/2015.  
*Su autenticidad puede ser contrastada en la siguiente dirección <https://sede.ull.es/validacion/>*

Identificador del documento: 3075810 Código de verificación: smutbmB+

Firmado por: JESSEL AYRA PLASENCIA  
UNIVERSIDAD DE LA LAGUNA

Fecha: 30/11/2020 12:24:14

María de las Maravillas Aguiar Aguiar  
UNIVERSIDAD DE LA LAGUNA

08/02/2021 13:50:06



Este documento incorpora firma electrónica, y es copia auténtica de un documento electrónico archivado por la ULL según la Ley 39/2015.  
*Su autenticidad puede ser contrastada en la siguiente dirección <https://sede.ull.es/validacion/>*

Identificador del documento: 3075810 Código de verificación: smutbmB+

Firmado por: JESSEL AYRA PLASENCIA  
UNIVERSIDAD DE LA LAGUNA

Fecha: 30/11/2020 12:24:14

María de las Maravillas Aguiar Aguiar  
UNIVERSIDAD DE LA LAGUNA

08/02/2021 13:50:06



Universidad  
de La Laguna

Study of the cellular response,  
signaling, and repair pathways to  
confront DNA double-strand breaks  
in telophase

Jessel Ayra Plasencia  
2021

Este documento incorpora firma electrónica, y es copia auténtica de un documento electrónico archivado por la ULL según la Ley 39/2015.  
Su autenticidad puede ser contrastada en la siguiente dirección <https://sede.ull.es/validacion/>

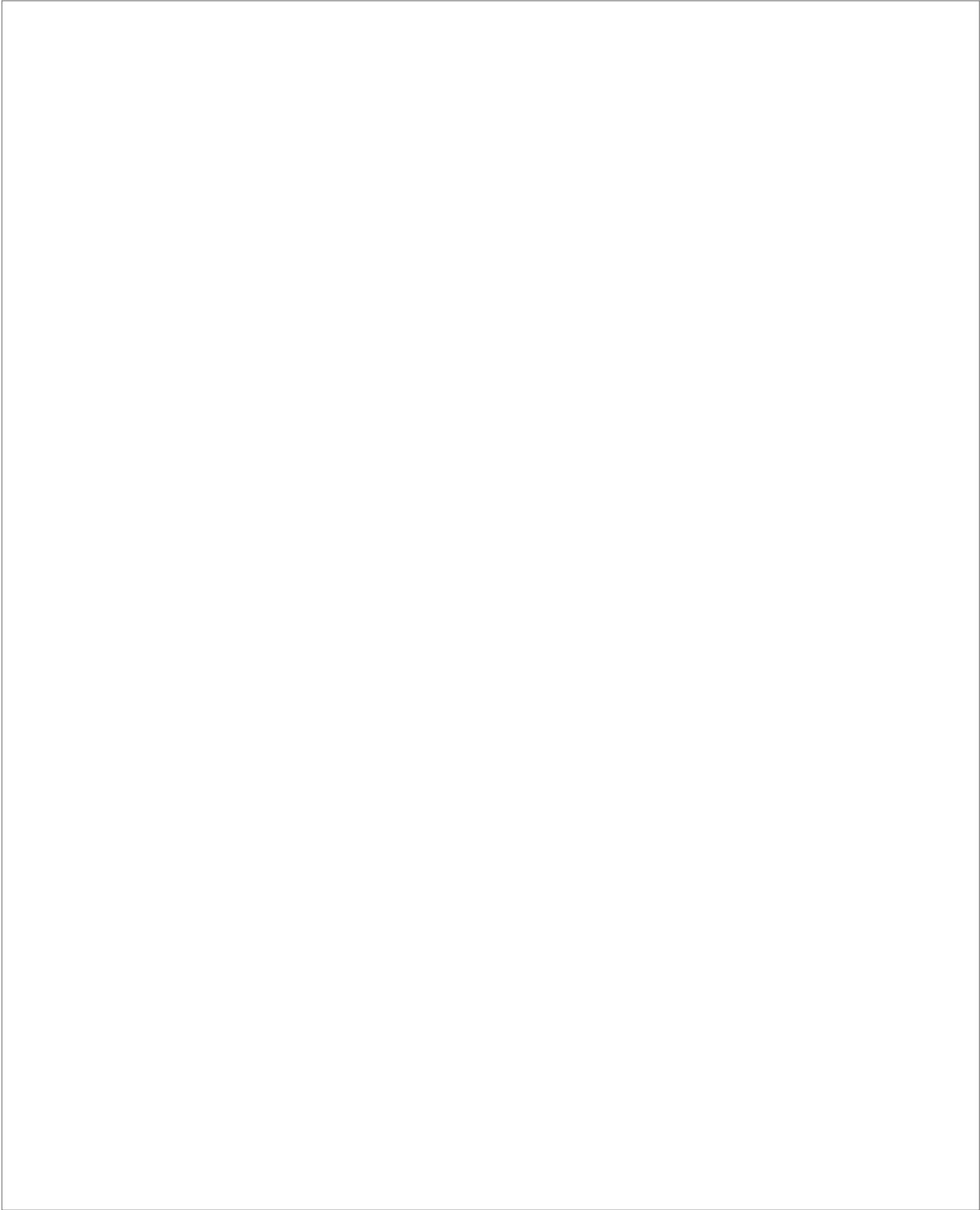
Identificador del documento: 3075810 Código de verificación: smutbmB+

Firmado por: JESSEL AYRA PLASENCIA  
UNIVERSIDAD DE LA LAGUNA

Fecha: 30/11/2020 12:24:14

María de las Maravillas Aguiar Aguiar  
UNIVERSIDAD DE LA LAGUNA

08/02/2021 13:50:06



Este documento incorpora firma electrónica, y es copia auténtica de un documento electrónico archivado por la ULL según la Ley 39/2015.  
*Su autenticidad puede ser contrastada en la siguiente dirección <https://sede.ull.es/validacion/>*

Identificador del documento: 3075810 Código de verificación: smutbmB+

Firmado por: JESSEL AYRA PLASENCIA  
UNIVERSIDAD DE LA LAGUNA

Fecha: 30/11/2020 12:24:14

María de las Maravillas Aguiar Aguiar  
UNIVERSIDAD DE LA LAGUNA

08/02/2021 13:50:06

## Autorización del director de tesis

Dr. Félix M. Machín Concepción, director de la tesis doctoral presentada por el Graduado en Biología Jessel Ayra Plasencia,

Certifica que:

La memoria presentada por el Graduado en Biología D. Jessel Ayra Plasencia titulada "Estudio de la respuesta celular, señalización, y mecanismos de reparación frente a la rotura de la doble cadena de ADN en telofase", ha sido realizada bajo mi dirección en la Unidad de Investigación del Hospital Universitario Nuestra Señora de Candelaria y, considerando que reúne las condiciones de calidad y rigor científico, autorizo para que pueda ser presentada y defendida ante la comisión nombrada al efecto para optar al grado de Doctor con Mención Internacional por la Universidad de La Laguna.

San Cristóbal de La Laguna, a 5 de noviembre de 2020

Fdo: **Dr. Félix M. Machín Concepción**

Este documento incorpora firma electrónica, y es copia auténtica de un documento electrónico archivado por la ULL según la Ley 39/2015.  
*Su autenticidad puede ser contrastada en la siguiente dirección <https://sede.ull.es/validacion/>*

Identificador del documento: 3075810 Código de verificación: smutbmB+

Firmado por: JESSEL AYRA PLASENCIA  
UNIVERSIDAD DE LA LAGUNA

Fecha: 30/11/2020 12:24:14

María de las Maravillas Aguiar Aguiar  
UNIVERSIDAD DE LA LAGUNA

08/02/2021 13:50:06



Este documento incorpora firma electrónica, y es copia auténtica de un documento electrónico archivado por la ULL según la Ley 39/2015.  
*Su autenticidad puede ser contrastada en la siguiente dirección <https://sede.ull.es/validacion/>*

Identificador del documento: 3075810      Código de verificación: smutbmB+

Firmado por: JESSEL AYRA PLASENCIA  
UNIVERSIDAD DE LA LAGUNA

Fecha: 30/11/2020 12:24:14

María de las Maravillas Aguiar Aguiar  
UNIVERSIDAD DE LA LAGUNA

08/02/2021 13:50:06



This work has been funded by:

- Ministerio de Ciencia, Innovación y Universidades (MICIU). Research grants to Félix Machín:
  - o BFU2015-63902-R.
  - o BFU2017-83954-R.
  
- Financial support was co-financed by the EU-ERDF program.



This work has been carried out under the supervision of Dr. Félix Manuel Machín Concepción at the Research Unit of Hospital Universitario Nuestra Señora de la Candelaria, Santa Cruz de Tenerife, Spain.

Jessel Ayra Plasencia performed this thesis while being affiliated with the Institute of Biomedical Technologies (ITB) of the University of La Laguna and the Canarian Health Research Institute Foundation (FCIISC), Santa Cruz de Tenerife, Spain.

The molecular monitoring study was partly carried out at Dr. Lorraine Symington's lab, at the Department of Microbiology and Immunology, Hammer Health Sciences Building, Columbia University, New York, USA. This research stay was funded by Cabildo de Tenerife and the Fostering Grads Mentoring program of the University of La Laguna, mainly directed by ECUSA (Españoles Científicos en USA).

Proteomics Mass Spectrometry was done by Dr. Lara Pérez Martínez at the Institute of Molecular Biology (IMB), Mainz, Germany.



Este documento incorpora firma electrónica, y es copia auténtica de un documento electrónico archivado por la ULL según la Ley 39/2015.  
Su autenticidad puede ser contrastada en la siguiente dirección <https://sede.ull.es/validacion/>

Identificador del documento: 3075810 Código de verificación: smutbmB+

Firmado por: JESSEL AYRA PLASENCIA  
UNIVERSIDAD DE LA LAGUNA

Fecha: 30/11/2020 12:24:14

María de las Maravillas Aguiar Aguiar  
UNIVERSIDAD DE LA LAGUNA

08/02/2021 13:50:06



Este documento incorpora firma electrónica, y es copia auténtica de un documento electrónico archivado por la ULL según la Ley 39/2015.  
*Su autenticidad puede ser contrastada en la siguiente dirección <https://sede.ull.es/validacion/>*

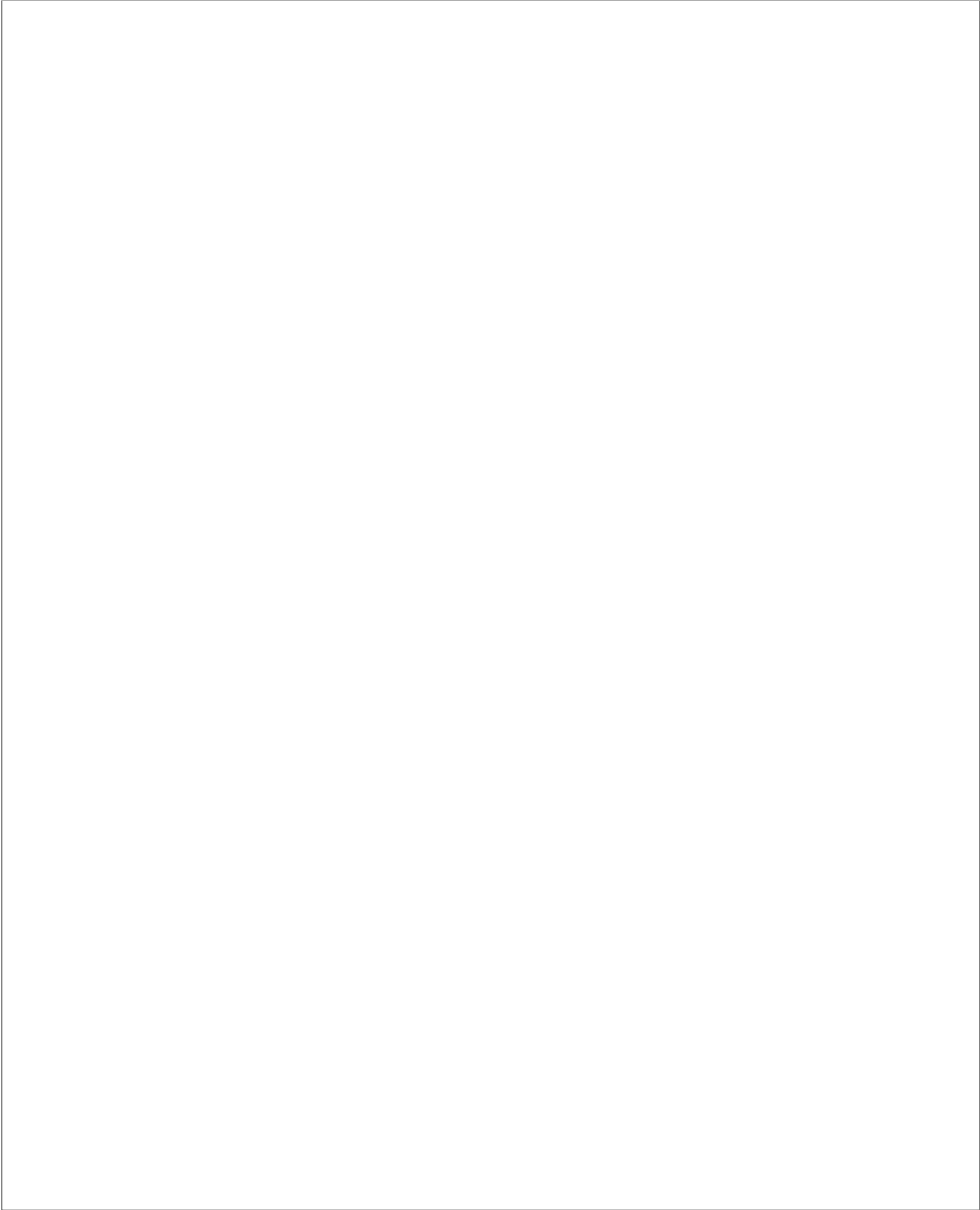
Identificador del documento: 3075810 Código de verificación: smutbmB+

Firmado por: JESSEL AYRA PLASENCIA  
UNIVERSIDAD DE LA LAGUNA

Fecha: 30/11/2020 12:24:14

María de las Maravillas Aguiar Aguiar  
UNIVERSIDAD DE LA LAGUNA

08/02/2021 13:50:06



Este documento incorpora firma electrónica, y es copia auténtica de un documento electrónico archivado por la ULL según la Ley 39/2015.  
*Su autenticidad puede ser contrastada en la siguiente dirección <https://sede.ull.es/validacion/>*

Identificador del documento: 3075810      Código de verificación: smutbmB+

Firmado por: JESSEL AYRA PLASENCIA  
UNIVERSIDAD DE LA LAGUNA

Fecha: 30/11/2020 12:24:14

María de las Maravillas Aguiar Aguiar  
UNIVERSIDAD DE LA LAGUNA

08/02/2021 13:50:06



Este documento incorpora firma electrónica, y es copia auténtica de un documento electrónico archivado por la ULL según la Ley 39/2015.  
*Su autenticidad puede ser contrastada en la siguiente dirección <https://sede.ull.es/validacion/>*

Identificador del documento: 3075810      Código de verificación: smutbmB+

Firmado por: JESSEL AYRA PLASENCIA  
UNIVERSIDAD DE LA LAGUNA

Fecha: 30/11/2020 12:24:14

María de las Maravillas Aguiar Aguiar  
UNIVERSIDAD DE LA LAGUNA

08/02/2021 13:50:06



# Abstract

Este documento incorpora firma electrónica, y es copia auténtica de un documento electrónico archivado por la ULL según la Ley 39/2015.  
Su autenticidad puede ser contrastada en la siguiente dirección <https://sede.ull.es/validacion/>

Identificador del documento: 3075810 Código de verificación: smutbmB+

Firmado por: JESSEL AYRA PLASENCIA  
UNIVERSIDAD DE LA LAGUNA

Fecha: 30/11/2020 12:24:14

María de las Maravillas Aguiar Aguiar  
UNIVERSIDAD DE LA LAGUNA

08/02/2021 13:50:06



Este documento incorpora firma electrónica, y es copia auténtica de un documento electrónico archivado por la ULL según la Ley 39/2015.  
*Su autenticidad puede ser contrastada en la siguiente dirección <https://sede.ull.es/validacion/>*

Identificador del documento: 3075810 Código de verificación: smutbmB+

Firmado por: JESSEL AYRA PLASENCIA  
UNIVERSIDAD DE LA LAGUNA

Fecha: 30/11/2020 12:24:14

María de las Maravillas Aguiar Aguiar  
UNIVERSIDAD DE LA LAGUNA

08/02/2021 13:50:06

Abstract

Cell survival depends on the genome integrity throughout the cell cycle and includes the faithful segregation of chromosomes in anaphase. DNA is continuously compromised by both exogenous and endogenous sources, such as ionizing radiation or reactive oxygen species (ROS) from the internal metabolism, respectively. In the last instance, insults to the integrity of the DNA can happen. DNA double-strand breaks (DSBs) are among the most harmful lesions that cells have to face. DNA breakage can result in severe mutations and promote genomic instability, leading to cancer, senescence, or cell death. However, cells have developed different repair pathways to confront DSBs.

DSB repair mechanisms can be classified into non-homologous end joining (NHEJ) and homologous recombination (HR). The NHEJ pathway is triggered during the G<sub>1</sub> phase, which is characterized by the absence of a sister chromatid to act as an intact DNA template for repair and the low CDK/cyclin activity. On the other hand, HR is used from the S phase onwards, when CDK/cyclin levels rise, and chromosomes comprise two sister chromatids. NHEJ entails an error-prone mechanism since broken DNA ends are barely processed and directly re-joined, causing short insertions and deletions at the flanking sites of the DSB. On the contrary, HR is an error-free repair pathway because the broken DNA is restored by copying the nucleotide information from the homolog intact template, usually the intact sister chromatid.

However, how cells deal with DSBs at late anaphase/telophase is still unknown. These latest stages of the cell cycle are paradoxical scenarios. First, CDK/cyclin levels are still high, and this would promote HR-mediated repair. Nonetheless, sister chromatids have been previously segregated in anaphase, supporting a more important role for NHEJ since the intact template is not close and well-aligned to be invaded.

In this work, the budding yeast *Saccharomyces cerevisiae* has been employed as a model to determine the cellular response and the repair pathways triggered to face DSBs in telophase. *Cdc15-2* conditional mutants have been used to generate stable telophase blocks where to generate single and multiple DSBs. Fluorescence microscopy analysis has uncovered: i) the approximation of the segregated DNA material, ii) the acceleration of chromosome movement, iii) the structural and dynamics changes produced in the microtubules apparatus, and iv) the generation of coalescence events between segregated sister chromatid loci. Also, cells delay the telophase-to-G<sub>1</sub> transition in a Rad9-dependent manner, and the partial dephosphorylation of the Cin8 kinesin motor protein is relevant to promote the reversion of segregation. The molecular monitorization of a single DSB repair also showed that cells favor HR over NHEJ in a Rad9-, Mre11-, and Yku70-independent but cohesin-dependent manner.

13

Este documento incorpora firma electrónica, y es copia auténtica de un documento electrónico archivado por la ULL según la Ley 39/2015.  
Su autenticidad puede ser contrastada en la siguiente dirección <https://sede.ull.es/validacion/>

Identificador del documento: 3075810 Código de verificación: smutbmB+

Firmado por: JESSEL AYRA PLASENCIA  
UNIVERSIDAD DE LA LAGUNA

Fecha: 30/11/2020 12:24:14

María de las Maravillas Aguiar Aguiar  
UNIVERSIDAD DE LA LAGUNA

08/02/2021 13:50:06

Abstract

---

Additionally, an experimental approximation on the HeLa cells response has also been performed. Cells delayed cytokinesis after being confronted with phleomycin-mediated DSBs at late anaphase/telophase stages. Contrary to what happened in yeast, HeLa cells did not modify the microtubular morphology. Instead, they responded to DSBs by phosphorylating the histone variant  $\gamma$ H2A.X. Strikingly, 53BP1, RIF1, and RPA2 foci appeared simultaneously. Although previous works have described that 53BP1 and RIF1 promote NHEJ and counteract resection, telophase-damaged cells showed a pattern where both NHEJ and HR pathways seem to cooperate.

Este documento incorpora firma electrónica, y es copia auténtica de un documento electrónico archivado por la ULL según la Ley 39/2015.  
*Su autenticidad puede ser contrastada en la siguiente dirección <https://sede.ull.es/validacion/>*

Identificador del documento: 3075810 Código de verificación: smutbmB+

Firmado por: JESSEL AYRA PLASENCIA  
UNIVERSIDAD DE LA LAGUNA

Fecha: 30/11/2020 12:24:14

María de las Maravillas Aguiar Aguiar  
UNIVERSIDAD DE LA LAGUNA

08/02/2021 13:50:06



## Table of contents

Abstract.....	11
Table of contents.....	15
List of figures.....	19
List of tables.....	21
List of abbreviations.....	23
1. Introduction.....	25
1.1. <i>Saccharomyces cerevisiae</i> as a model organism.....	27
1.2. Cell cycle regulation of <i>Saccharomyces cerevisiae</i> .....	28
1.2.1. Regulation from G <sub>1</sub> to Mitosis.....	28
1.2.2. Chromosome segregation.....	29
1.2.3. Exit from mitosis.....	31
1.3. The DNA Damage Response.....	33
1.4. DNA damage repair pathways.....	36
1.4.1. Single-stranded DNA damage repair.....	36
1.4.1.1. Direct Reversal.....	36
1.4.1.2. Base Excision Repair.....	36
1.4.1.3. Mismatch Repair.....	37
1.4.1.4. Nucleotide Excision Repair.....	37
1.4.2. Double-strand DNA damage repair.....	37
1.4.2.1. Non-homologous end joining.....	38
1.4.2.2. Homologous recombination.....	39
1.4.2.2.1. Break-induced replication (BIR).....	41
1.4.2.2.2. Synthesis-dependent strand annealing (SDSA).....	43
1.4.2.2.3. Double Holliday junction pathway (dHJs).....	43
1.5. Regulation of the DNA repair pathway choice.....	45
2. Aims.....	47
3. Materials and methods.....	51
3.1. Yeast cultures.....	53
3.1.1. Strains used in this work.....	53
3.1.2. Strain construction.....	55
3.1.2.1. Yeast transformation.....	55
3.1.2.1.1. Preparation of competent cells.....	55
3.1.2.1.2. Transformation procedure.....	56
3.1.2.2. Crossing method.....	56
3.1.2.2.1. Diploid generation.....	56
3.1.2.2.2. Sporulation.....	57
3.1.2.2.3. Tetrad dissection.....	57
3.1.2.2.4. Replica plating.....	57

15

Este documento incorpora firma electrónica, y es copia auténtica de un documento electrónico archivado por la ULL según la Ley 39/2015.  
 Su autenticidad puede ser contrastada en la siguiente dirección <https://sede.ull.es/validacion/>

Identificador del documento: 3075810 Código de verificación: smutbmB+

Firmado por: JESSEL AYRA PLASENCIA  
 UNIVERSIDAD DE LA LAGUNA

Fecha: 30/11/2020 12:24:14

María de las Maravillas Aguiar Aguiar  
 UNIVERSIDAD DE LA LAGUNA

08/02/2021 13:50:06

3.1.3. Culture conditions.....	58
3.1.3.1. Storage and maintenance.....	58
3.1.3.2. Experimental conditions.....	58
3.1.3.2.1. Asynchronous to G <sub>1</sub> arrest.....	60
3.1.2.2.2. Asynchronous to S arrest.....	60
3.1.2.2.3. Asynchronous to G <sub>2</sub> arrest.....	61
3.1.2.3.4. Asynchronous to telophase arrest.....	61
3.1.3.2.5. Auxin-mediated protein degradation.....	62
3.1.3.2.6. Clonogenic assays.....	62
3.1.3.3. Transformant cells.....	63
3.2. Cell cultures.....	63
3.2.1. Culture conditions.....	63
3.2.1.1. Cryopreservation and cell recovery.....	63
3.2.1.2. Experimental conditions.....	64
3.2.1.2.1. Asynchronous to S phase arrest.....	64
3.2.1.2.2. S phase arrest to prometaphase arrest.....	65
3.2.1.2.3. Prometaphase arrest to anaphase/telophase arrest.....	65
3.3. DNA techniques.....	66
3.3.1. DNA preparations.....	66
3.3.1.1. Genomic DNA extractions from <i>Saccharomyces cerevisiae</i> .....	66
3.3.1.1.1. Mechanical method.....	66
3.3.1.1.2. Lytic method.....	66
3.3.2. Polymerase chain reactions (PCRs).....	67
3.3.2.1. Primers.....	67
3.3.2.2. PCRs from linear DNA.....	69
3.3.2.3. PCRs from plasmids.....	70
3.3.2.4. Quantitative PCR (qPCR).....	71
3.3.3. DNA electrophoreses.....	72
3.3.3.1. Analytical electrophoresis.....	72
3.3.3.2. Experimental electrophoresis.....	73
3.3.4. Southern blot.....	73
3.3.4.1. Probe labeling.....	73
3.3.4.2. DNA transfer.....	73
3.3.4.3. Probe hybridization and detection.....	74
3.3.5. Flow cytometry.....	75
3.4. Protein techniques.....	75
3.4.1. Western blot.....	75
3.4.1.1. Protein extraction.....	75
3.4.1.2. SDS-PAGE.....	76
3.4.1.3. Protein transfer.....	76

Este documento incorpora firma electrónica, y es copia auténtica de un documento electrónico archivado por la ULL según la Ley 39/2015.  
 Su autenticidad puede ser contrastada en la siguiente dirección <https://sede.ull.es/validacion/>

Identificador del documento: 3075810 Código de verificación: smutbmB+

Firmado por: JESSEL AYRA PLASENCIA  
 UNIVERSIDAD DE LA LAGUNA

Fecha: 30/11/2020 12:24:14

María de las Maravillas Aguiar Aguiar  
 UNIVERSIDAD DE LA LAGUNA

08/02/2021 13:50:06

3.4.1.4. Antibodies hybridization and detection.....	77
3.4.2. Proteomics mass spectrometry.....	78
3.4.2.1. Whole-cell protein extraction.....	78
3.5. Fluorescence microscopy.....	78
3.5.1. Yeast microscopy.....	79
3.5.2. HeLa cells microscopy.....	80
3.5.2.1. Antibodies hybridization and detection.....	80
4. Results and discussion.....	83
4.1. Chapter 1: DNA double-strand breaks lead to coalescence between segregated sister chromatid loci.....	85
4.2. Chapter 2: Molecular monitorization of a single DSB repair in telophase.....	111
4.2.1. Yeast cells trigger homologous recombination when a single DSB arise in telophase.....	113
4.2.2. Processing of 3' ssDNA ends in telophase is as efficient as in G <sub>2</sub> .....	115
4.2.3. DDR, Mre11, and NHEJ do not directly interfere with HR-mediated MAT Switching in telophase.....	117
4.2.3.1. Rad9 depletion does not prevent from triggering MAT Switching.....	117
4.2.3.2. Mre11 is not essential to achieve GC in telophase.....	119
4.2.3.3. NHEJ does not play any residual role for MAT Switching repair in telophase, but Yku70 absence delays homologous recombination.....	120
4.2.4. Cohesin complex is activated after DSBs in telophase and plays a leading role in promoting coalescence events and HR.....	121
4.2.4.1. Yeast $\alpha$ -kleisin subunit Scc1 is translated <i>de novo</i> after DSB generation in telophase.....	122
4.2.4.2. Depletion of Smc3 prevents the generation of coalescence events.....	123
4.2.4.3. HR in telophase is significantly delayed in the absence of Smc3.....	125
4.2.5. Proteomics identify new factors specifically involved in DNA repair in telophase.....	128
4.3. Chapter 3: Are anaphase events really irreversible? The endmost stages of cell division and the paradox of the DNA double-strand break repair.....	133
4.4. Chapter 4: Experimental insights in higher eukaryotes response to DSBs.....	143
4.4.1. HeLa cells delay the anaphase/telophase transition when DSBs occur.....	145
4.4.2. HeLa cells react to DSBs in telophase by triggering different DNA repair pathways.....	147
5. Conclusions.....	151
6. Cited literature.....	155
Appendix I: Proteomics Mass Spectrometry.....	179
Appendix II: Media and solutions.....	187
Appendix III: Other scientific contributions during this thesis.....	195

Este documento incorpora firma electrónica, y es copia auténtica de un documento electrónico archivado por la ULL según la Ley 39/2015.  
 Su autenticidad puede ser contrastada en la siguiente dirección <https://sede.ull.es/validacion/>

Identificador del documento: 3075810      Código de verificación: smutbmB+

Firmado por: JESSEL AYRA PLASENCIA  
 UNIVERSIDAD DE LA LAGUNA

Fecha: 30/11/2020 12:24:14

María de las Maravillas Aguiar Aguiar  
 UNIVERSIDAD DE LA LAGUNA

08/02/2021 13:50:06



Este documento incorpora firma electrónica, y es copia auténtica de un documento electrónico archivado por la ULL según la Ley 39/2015.  
*Su autenticidad puede ser contrastada en la siguiente dirección <https://sede.ull.es/validacion/>*

Identificador del documento: 3075810      Código de verificación: smutbmB+

Firmado por: JESSEL AYRA PLASENCIA  
UNIVERSIDAD DE LA LAGUNA

Fecha: 30/11/2020 12:24:14

María de las Maravillas Aguiar Aguiar  
UNIVERSIDAD DE LA LAGUNA

08/02/2021 13:50:06

## List of figures

Figure 1.1. Life cycle of <i>S. cerevisiae</i> .....	27
Figure 1.2. Schematic view of the cell cycle of <i>S. cerevisiae</i> .....	28
Figure 1.3. Scheme depicting the signaling cascades that regulate FEAR and MEN networks....	32
Figure 1.4. Cell cycle phases depicting the main checkpoints of <i>S. cerevisiae</i> .....	34
Figure 1.5. General schematic of the NHEJ pathway.....	36
Figure 1.6. Schematic of the pre-synapsis step on homologous recombination pathways.....	40
Figure 1.7. Schematic of the synapsis step on homologous recombination pathways.....	41
Figure 1.8. Break-induced replication (BIR) model scheme.....	42
Figure 1.9. Synthesis-dependent strand annealing (SDSA) model scheme.....	43
Figure 1.10. Double Holliday junction pathway (dHJs) model scheme.....	44
Figure 3.1. Inserted cassette map and working mechanism for $\beta$ -estradiol-mediated HO expression.....	59
Figure 3.2. Schematic of the experiment of the G <sub>1</sub> block.....	60
Figure 3.3. Schematic of the experiment of the S block.....	61
Figure 3.4. Schematic of the experiment of the G <sub>2</sub> block.....	61
Figure 3.5. Schematic of the experiment of the telophase block.....	62
Figure 3.6. Schematic of the experiment of S phase arrest in HeLa cells.....	64
Figure 3.7. Schematic of the experiment of prometaphase arrest in HeLa cells.....	65
Figure 3.8. Schematic of the experiment of anaphase/telophase arrest in HeLa cells.....	65
Figure 3.9. Schematic overview of the PCR program used to amplify DNA from transformant colonies or to obtain transformant DNA from previously modified yeast strains.....	70
Figure 3.10. Schematic overview of the employed PCR program to amplify probes.....	70
Figure 3.11. Schematic overview of the employed PCR program to amplify transformant DNA from plasmids.....	70
Figure 3.12. Schematic overview of the applied qPCR program.....	71
Figure 3.13. Scheme of the setup for DNA transfer to membrane.....	74
Figure 4.1. Yeast cells use HR instead of NHEJ to repair a DSB in telophase.....	114
Figure 4.2. Resection in telophase is carried out at similar levels than G <sub>2</sub> .....	116
Figure 4.3. MAT Switching is carried out in the absence of DDR and Mre11, whereas Yku70 deletion does not improve recombination levels.....	118
Figure 4.4. Scc1 levels are restored after DNA damage in telophase.....	122
Figure 4.5. The absence of Smc3 inhibits telomere coalescence after DSBs in telophase.....	124
Figure 4.6. Smc3 degradation elicits a substantial delay in GC performance in telophase.....	126
Figure 4.7. Proteomics Mass Spectrometry results for DSBs in G <sub>2</sub> .....	129
Figure 4.8. Proteomics Mass Spectrometry results for DSBs in telophase.....	130
Figure 4.9. Subcellular location and post-translational modifications of Msc1 upon DSBs in telophase.....	131
Figure 4.10. Proportion of mitotic stages after 1 hour of DSBs in anaphase/telophase.....	146
Figure 4.11. Immunofluorescence of DNA damage factors to repair DSBs in telophase.....	148

Este documento incorpora firma electrónica, y es copia auténtica de un documento electrónico archivado por la ULL según la Ley 39/2015.  
 Su autenticidad puede ser contrastada en la siguiente dirección <https://sede.ull.es/validacion/>

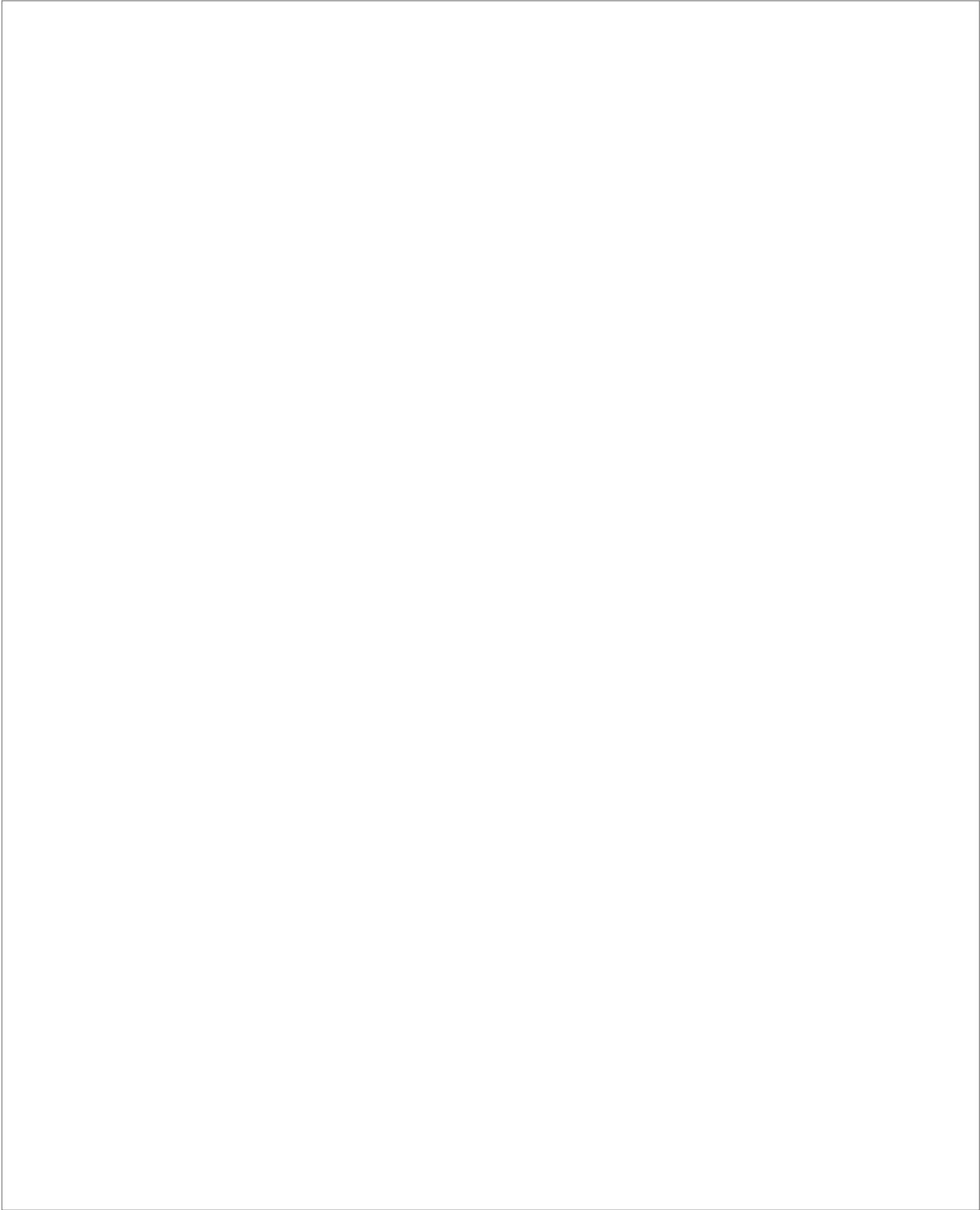
Identificador del documento: 3075810 Código de verificación: smutbmB+

Firmado por: JESSEL AYRA PLASENCIA  
 UNIVERSIDAD DE LA LAGUNA

Fecha: 30/11/2020 12:24:14

María de las Maravillas Aguiar Aguiar  
 UNIVERSIDAD DE LA LAGUNA

08/02/2021 13:50:06



Este documento incorpora firma electrónica, y es copia auténtica de un documento electrónico archivado por la ULL según la Ley 39/2015.  
*Su autenticidad puede ser contrastada en la siguiente dirección <https://sede.ull.es/validacion/>*

Identificador del documento: 3075810      Código de verificación: smutbmB+

Firmado por: JESSEL AYRA PLASENCIA  
UNIVERSIDAD DE LA LAGUNA

Fecha: 30/11/2020 12:24:14

María de las Maravillas Aguiar Aguiar  
UNIVERSIDAD DE LA LAGUNA

08/02/2021 13:50:06

## List of tables

Table 3.1. List of strains used in this work.....	53
Table 3.2. Stocks and final concentrations of used antibiotics for selection.....	63
Table 3.3. List of primers and their DNA sequences used in this thesis.....	67
Table 3.4. Primary and secondary antibodies used in this thesis.....	77
Table 3.5. List of filter cubes used in fluorescence microscopy.....	79
Table 3.6. List of parameters to visualize each protein.....	79
Table 3.7. List of used antibodies in HeLa cells IF.....	81

Este documento incorpora firma electrónica, y es copia auténtica de un documento electrónico archivado por la ULL según la Ley 39/2015.  
Su autenticidad puede ser contrastada en la siguiente dirección <https://sede.ull.es/validacion/>

Identificador del documento: 3075810 Código de verificación: smutbmB+

Firmado por: JESSEL AYRA PLASENCIA  
UNIVERSIDAD DE LA LAGUNA

Fecha: 30/11/2020 12:24:14

María de las Maravillas Aguiar Aguilár  
UNIVERSIDAD DE LA LAGUNA

08/02/2021 13:50:06



Este documento incorpora firma electrónica, y es copia auténtica de un documento electrónico archivado por la ULL según la Ley 39/2015.  
*Su autenticidad puede ser contrastada en la siguiente dirección <https://sede.ull.es/validacion/>*

Identificador del documento: 3075810 Código de verificación: smutbmB+

Firmado por: JESSEL AYRA PLASENCIA  
UNIVERSIDAD DE LA LAGUNA

Fecha: 30/11/2020 12:24:14

María de las Maravillas Aguiar Aguiar  
UNIVERSIDAD DE LA LAGUNA

08/02/2021 13:50:06



## List of abbreviations

- **AB buffer:** Antibody buffer
- **AID:** Auxin-inducible degron
- **aMTs:** Astral microtubules
- **APC:** Anaphase-promoting complex
- **AP site:** Apurinic/aprimidinic (abasic) site
- **β-E:** β-estradiol
- **BER:** Base Excision repair
- **BIR:** Break-induced replication
- **bp:** Base pairs
- **CDE:** Centromere DNA sequence elements
- **CDK:** Cyclin-dependent kinase
- **CI:** Confidence interval
- **COs:** Crossovers
- **DDC:** DNA damage checkpoint
- **DDR:** DNA damage response
- **DI-cohesion:** Damaged-induced cohesion
- **dHJs:** Double Holliday junctions
- **D-loop:** Displacement loop
- **DMEM:** Dulbecco's Modified Eagle Medium
- **DMSO:** Dimethyl sulfoxide
- **DNA:** Deoxyribonucleic acid
- **DSB:** DNA double-strand break
- **dsDNA:** Double-stranded DNA
- **ER:** Endoplasmic reticulum
- **FBS:** Fetal bovine serum
- **FEAR:** Cdc14-early anaphase release
- **GC:** Gene conversion
- **GCR:** Gross chromosome rearrangements
- **GGR:** Global genome repair
- **HOcs:** HO-mediated cut site
- **HR:** Homologous recombination
- **HU:** Hydroxyurea
- **IAA:** Indoleacetic acid
- **IF:** Immunofluorescence
- **iMTs:** Interpolar microtubules
- **kMTs:** Kinetochore microtubules
- **LFQ:** Label-free quantification
- **LOH:** Loss of heterozygosity
- **MAPs:** Microtubules-associated proteins
- **MEN:** Mitotic exit network
- **MMEJ:** Microhomology-mediated end joining
- **MMR:** Mismatch repair
- **MMS:** Methyl methanesulfonate
- **MPF:** Maturation promoting factor
- **MRX complex:** Mre11-Rad50-Xrs2 complex
- **NCOs:** Non crossovers
- **NER:** Nucleotide excision repair
- **NHEJ:** Non-homologous end joining
- **NM:** Nuclear membrane
- **OD<sub>600</sub>:** Optical density at 600 nm

23

Este documento incorpora firma electrónica, y es copia auténtica de un documento electrónico archivado por la ULL según la Ley 39/2015.  
Su autenticidad puede ser contrastada en la siguiente dirección <https://sede.ull.es/validacion/>

Identificador del documento: 3075810 Código de verificación: smutbmB+

Firmado por: JESSEL AYRA PLASENCIA  
UNIVERSIDAD DE LA LAGUNA

Fecha: 30/11/2020 12:24:14

María de las Maravillas Aguiar Aguiar  
UNIVERSIDAD DE LA LAGUNA

08/02/2021 13:50:06

- **PBS:** Phosphate buffer saline
- **PCNA:** Proliferating cell nuclear antigen
- **PCR:** Polymerase chain reaction
- **PEG:** Polyethylene glycol
- **pGal:** Gal promoter
- **Phle:** Phleomycin
- **qPCR:** Quantitative PCR.
- **rDNA:** Ribosomal DNA
- **REs:** Restriction enzymes
- **RFP:** Red fluorescent protein
- **RFs:** Replication forks
- **RPA:** Replication protein A complex
- **rpm:** revolutions per minute
- **ROS:** Reactive oxygen species
- **SAC:** Spindle assembly checkpoint
- **SBF:** Swi4/6 cell cycle box complex
- **SC:** Synthetic complete medium
- **SDSA:** Synthesis-dependent strand annealing
- **SDS-PAGE:** Sodium dodecyl sulfate polyacrylamide gel electrophoresis
- **SEM:** Standard error of the mean
- **SPB:** Spindle pole body
- **SPOC:** Spindle position checkpoint
- **SSA:** Single strand annealing
- **ssDNA:** Single-stranded DNA
- **SSEs:** Structure-specific endonucleases
- **STR complex:** Sgs1-Top3-Rmi1 complex
- **TBE buffer:** Tris base, Boric acid, and EDTA buffer
- **TCA:** Trichloroacetic acid
- **TCR:** Transcription-coupled repair
- **TE buffer:** Tris base and EDTA buffer
- **TetR:** Tetracycline repressor protein
- **TetO:** Tetracycline operator sequence
- **TIR1:** Auxin-binding receptor TIR1
- **TRITC:** Tetramethyl-rhodamine B isocyanate
- **UV:** Ultraviolet light
- **YPD:** Yeast extract, peptone, and dextrose growth medium
- **YFP:** Yellow fluorescent protein

24

Este documento incorpora firma electrónica, y es copia auténtica de un documento electrónico archivado por la ULL según la Ley 39/2015.  
Su autenticidad puede ser contrastada en la siguiente dirección <https://sede.ull.es/validacion/>

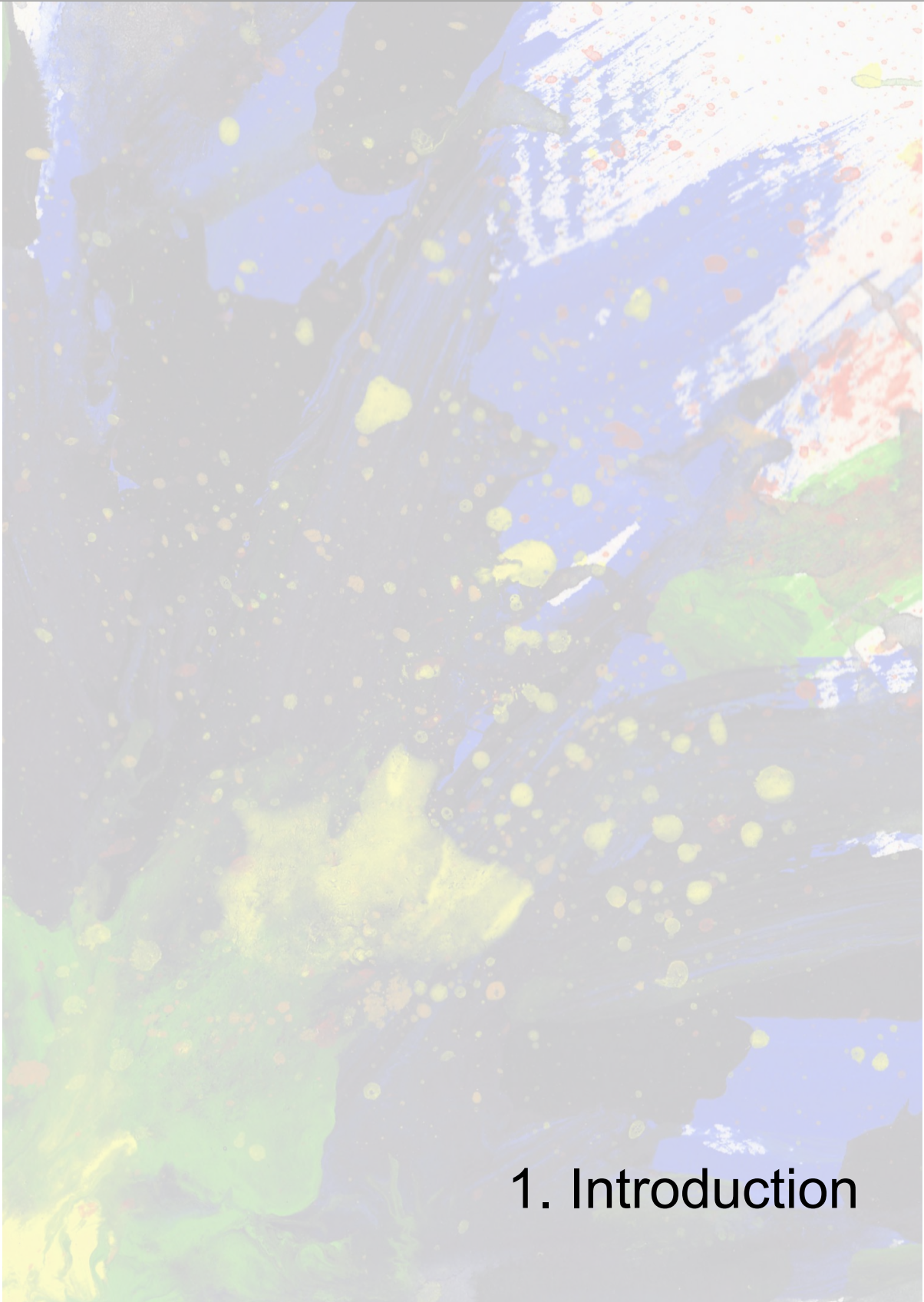
Identificador del documento: 3075810 Código de verificación: smutbmB+

Firmado por: JESSEL AYRA PLASENCIA  
UNIVERSIDAD DE LA LAGUNA

Fecha: 30/11/2020 12:24:14

María de las Maravillas Aguiar Aguiar  
UNIVERSIDAD DE LA LAGUNA

08/02/2021 13:50:06



# 1. Introduction

Este documento incorpora firma electrónica, y es copia auténtica de un documento electrónico archivado por la ULL según la Ley 39/2015.  
*Su autenticidad puede ser contrastada en la siguiente dirección <https://sede.ull.es/validacion/>*

Identificador del documento: 3075810 Código de verificación: smutbmB+

Firmado por: JESSEL AYRA PLASENCIA  
UNIVERSIDAD DE LA LAGUNA

Fecha: 30/11/2020 12:24:14

María de las Maravillas Aguiar Aguiar  
UNIVERSIDAD DE LA LAGUNA

08/02/2021 13:50:06



Este documento incorpora firma electrónica, y es copia auténtica de un documento electrónico archivado por la ULL según la Ley 39/2015.  
*Su autenticidad puede ser contrastada en la siguiente dirección <https://sede.ull.es/validacion/>*

Identificador del documento: 3075810 Código de verificación: smutbmB+

Firmado por: JESSEL AYRA PLASENCIA  
UNIVERSIDAD DE LA LAGUNA

Fecha: 30/11/2020 12:24:14

María de las Maravillas Aguiar Aguiar  
UNIVERSIDAD DE LA LAGUNA

08/02/2021 13:50:06

## 1.1. *Saccharomyces cerevisiae* as a model organism

The yeast *Saccharomyces cerevisiae*, also commonly known as baker's or budding yeast, is one of the most extensively used organisms for research. It is a model for a wide variety of eukaryotic cellular processes, such as cell cycle control and division, DNA replication and segregation, DNA repair, and aging, among many others. It supposes a handy tool because many essential proteins associated with fundamental cellular functions are highly conserved in mammals, including *Homo sapiens*.

It is a single-cell organism with a high cell division rate and a short cell cycle duration (~ 90 minutes). Indeed, it grows optimally in cheap and relatively straightforward conditions. Besides, it is very suitable for genetic engineering because of its remarkably effective homologous recombination. Thus, DNA can be easily modified to study the effect of gene deletions, N- or C-terminal protein tagging, or gene overexpression (Janke et al., 2004; Knop et al., 1999). Incidentally, it can stably propagate either as haploid or diploid through continuous mitotic divisions. Haploids are classified into two different sexual types, known as MAT<sub>a</sub> and MAT<sub>α</sub>. When both cell types fuse, they produce a diploid. If environmental conditions become stressful, such as during nutrient starvation, diploid cells undergo meiosis and generate four haploid spores, two for each sexual type (Fig. 1.1) (Schrick et al., 1997).

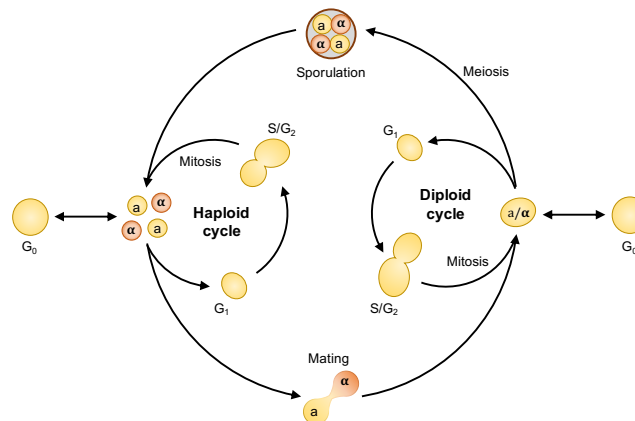


**Figure 1.1. Life cycle of *S. cerevisiae*.** Budding yeast grows mitotically as either haploid or diploid. The transition from haploid to diploid occurs by the fusion of two cells of different mating types, whereas sporulation happens through meiosis. Adapted from: <http://www.unifr.ch/biochem/index.php?id=11>.

The whole genomic nucleotide sequence is known since 1996, and it comprises 12.1 million base pairs (bp) distributed in 16 chromosomes and ~ 6,000 genes (~ 4,000 are not essential) (Goffeau et al., 1996).

Este documento incorpora firma electrónica, y es copia auténtica de un documento electrónico archivado por la ULL según la Ley 39/2015.  
 Su autenticidad puede ser contrastada en la siguiente dirección <https://sede.ull.es/validacion/>

Identificador del documento: 3075810 Código de verificación: smutbmB+

Firmado por: JESSEL AYRA PLASENCIA  
 UNIVERSIDAD DE LA LAGUNA

Fecha: 30/11/2020 12:24:14

María de las Maravillas Aguiar Aguiar  
 UNIVERSIDAD DE LA LAGUNA

08/02/2021 13:50:06

1. Introduction

## 1.2. Cell cycle regulation of *Saccharomyces cerevisiae*

As stated above, the cell cycle duration usually lasts ~ 90 – 120 minutes. The variation mainly depends on nutritional and environmental conditions, as *S. cerevisiae* divides in a wide variety of growing media at temperatures ranging from 23 to 37 °C.

The cell cycle is mainly differentiated into two phases: the S phase (when the DNA is replicated) and the M phase or mitosis (when the duplicated genome is segregated between two daughter cells). Two gaps temporally separate both steps: the G<sub>1</sub> (when cells grow in size and activate the metabolism) and the G<sub>2</sub> (which is almost inexistent in *S. cerevisiae*) (L. H. Hartwell, 1991) (Fig. 1.2).

Cdc28 protein is the only cyclin-dependent kinase (CDK) that drives every cell cycle event. Its action is regulated by 3 N-type cyclins specific for late G<sub>1</sub>, and 9 B-type cyclins expressed throughout S, G<sub>2</sub>, and M phases (D. J. Lew & Reed, 1993; Mendenhall & Hodge, 1998; Nasmyth, 1993).

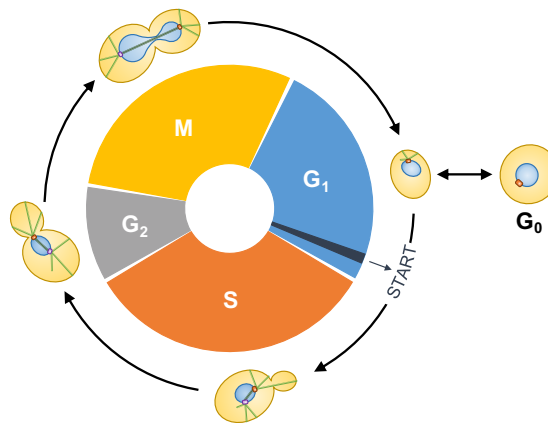


**Figure 1.2. Schematic view of the cell cycle of *S. cerevisiae*.** The draws depicted next to each phase represent the cell morphology (yellow), the nucleus shape (blue), and the spindle pole bodies (orange and violet) together with microtubules disposition (green) for each cell cycle stage.

### 1.2.1. Regulation from G<sub>1</sub> to Mitosis

Cells in G<sub>1</sub> increment their mass and size until reaching a point of no return (called START), from which they are committed to entering a new mitotic cycle (Dirick et al., 1995; L. H. Hartwell, 1974). After the START point, the Cln3-Cdc28 complex disassembles the transcription inhibitor Whi5. Cdc28 then activates the Swi4/6 cell cycle box complex (SBF) to enhance transcription at the G<sub>1</sub>-to-S transition (Costanzo et al., 2004; de Bruin et al., 2004, p.

Este documento incorpora firma electrónica, y es copia auténtica de un documento electrónico archivado por la ULL según la Ley 39/2015.  
 Su autenticidad puede ser contrastada en la siguiente dirección <https://sede.ull.es/validacion/>

Identificador del documento: 3075810 Código de verificación: smutbmB+

Firmado por: JESSEL AYRA PLASENCIA  
 UNIVERSIDAD DE LA LAGUNA

Fecha: 30/11/2020 12:24:14

María de las Maravillas Aguiar Aguiar  
 UNIVERSIDAD DE LA LAGUNA

08/02/2021 13:50:06

3). This way, *CLN1* and *CLN2* genes are transcribed. Cln1- and Cln2-Cdc28 complexes regulate the transcription of *CLB5-CLB6* and the degradation of the B-type mitotic cyclins inhibitor Sic1 (Levine et al., 1995; Nasmyth & Dirick, 1991; Ogas et al., 1991; Sidorova & Breeden, 1993). Through these changes in the Cdc28 partners, the spindle pole body (SPB) duplicates, and cells enter into the early S phase for replicating the DNA.

From the S phase onwards, every cellular process is governed by B-type cyclins. First, Clb5- and Clb6-Cdc28 inhibit the Cln cyclins and regulate the proper initiation of replication. Once Cln cyclins get degraded, Clb3 and Clb4 are translated to safeguard the SPB duplication and the reinitiation of already fired replication origins (Basco et al., 1995; Dahmann et al., 1995; Epstein & Cross, 1992, p. 5; Fitch et al., 1992; Schwob et al., 1994).

After replication and the entry in G<sub>2</sub>, the SBF-mediated transcription and the SPB duplication are inhibited by the Maturation Promoting Factor (MPF). MPF is under the control of Clb1 and Clb2 cyclins, and it regulates the phosphorylation and activation of the anaphase-promoting complex (APC) to perform the metaphase-to-anaphase transition (Booher et al., 1993; Ghiara et al., 1991; D. J. Lew & Reed, 1993; Surana et al., 1993).

### 1.2.2. Chromosome segregation

The DNA needs to be correctly replicated and faithfully transmitted to the progeny after each cell cycle. Cells ensure viability by triggering molecular mechanisms to control the sister chromatid cohesion, condensation into chromosomes with a critical length, the adequate formation and attachment of kinetochores at centromeres, and sister chromatid separation to the daughter cell.

From the S phase until the anaphase onset, the cohesin complex plays an essential role in the structural maintenance of sister chromatids. Cohesin is a multiprotein complex composed of Smc1, Smc3, Scc1 (also known as Mcd1), and Scc3 subunits (Hirano, 2000; Michaelis et al., 1997; Sjögren & Nasmyth, 2001). It forms a heterotrimeric ring that embraces and holds the replicated sister chromatids together and well-aligned until reaching late G<sub>2</sub> (Díaz-Martínez et al., 2008; Koshland & Guacci, 2000; Laloraya et al., 2000; Michaelis et al., 1997; Strunnikov et al., 1993, p. 1). Once the replication finishes, APC<sup>Cdc20</sup> (APC associated to its regulatory cofactor Cdc20) degrades the "securin" (Pds1), so that the "separase" (Esp1) becomes active. It then cleaves the Scc1 subunit by proteolysis, releasing sister chromatids from cohesion (Cohen-Fix et al., 1996; Michaelis et al., 1997; Uhlmann et al., 1999; Yamamoto et al., 1996b, 1996a).

Este documento incorpora firma electrónica, y es copia auténtica de un documento electrónico archivado por la ULL según la Ley 39/2015.  
Su autenticidad puede ser contrastada en la siguiente dirección <https://sede.ull.es/validacion/>

Identificador del documento: 3075810 Código de verificación: smutbmB+

Firmado por: JESSEL AYRA PLASENCIA  
UNIVERSIDAD DE LA LAGUNA

Fecha: 30/11/2020 12:24:14

María de las Maravillas Aguiar Aguiar  
UNIVERSIDAD DE LA LAGUNA

08/02/2021 13:50:06

## 1. Introduction

Apart from cohesin, the related condensin complex also plays a vital role. Yeast condensin is composed of Smc2, Smc4, Ycs4, Ycg1, and Brn1 subunits (Hudson et al., 2009; Ouspenski et al., 2000; Strunnikov et al., 1995; B.-D. Wang et al., 2006). DNA condensation is maintained from G<sub>2</sub> until telophase in an Aurora kinase (Ipl1)-dependent manner. The compaction is necessary to make the chromosome arms shorter than the spindle length and more manageable to segregate (Guacci et al., 1994; Machin et al., 2005; Vas et al., 2007).

Besides cohesin and condensin, sister chromatids are held together by topological linkages. Catenations are cohesin-independent subproducts of the replication and condensation processes. Before segregation, Topoisomerases II (Top2 in yeast) resolves catenations by creating a transient DNA double-strand break (DSB). Then, Top2 passes an intact portion of DNA through the cut and restore the gap, lowering the entanglement degree (Nitiss, 2009a, 2009b). Furthermore, physical DNA-DNA linkages may also maintain sister chromatids together, such as X-shaped DNA intermediates resulting from repair processes. Smc5-Smc6 complexes remove recombination intermediates and enhance the segregation of repetitive DNA sequences, such as the rDNA (Aragón, 2018; Bermúdez-López et al., 2010; Torres-Rosell, Machin, et al., 2005; Torres-Rosell, Machín, et al., 2005).

Cells regulate chromosome segregation not only by resolving intertwinings, recombination intermediates, and proteinaceous linkages between sister chromatids. They also modulate subcellular structures such as the SPBs, the microtubules apparatus, and the kinetochores. These structures are highly regulated and are necessary to pull apart the replicated chromosomes to the poles of the dividing nucleus. In yeast, the SPB is embedded in the nuclear membrane, which does not disappear during the so-called “closed” mitosis. This kind of mitotic division entails a fundamental difference between yeast and higher eukaryotes mitoses, as the nuclear membrane is disassembled in mammals when segregation is performed (Sazer et al., 2014).

SPBs (yeast microtubule-organizing center ortholog) is composed of three plaques, known as i) the inner plaque, where nucleation of interpolar (iMTs) and kinetochores microtubules (kMTs) occur, ii) the central plaque, which serves as a scaffold for the intra- and extra-nuclear SPBs domains and iii) the outer plaque, where cytoplasmic nucleation of astral microtubules (aMTs) is carried out. Also, SPBs contain a half-bridge whose function is associated with the duplication, formation, and nucleation of the new SPB (Fraschini, 2017; Sue L. Jaspersen & Winey, 2004; McIntosh & O’Toole, 1999; Rüttnick & Schiebel, 2016; Scarfone & Piatti, 2017).

The SPB cycle initiates when cells are in G<sub>1</sub>. The half-bridge elongates from the central plaque to produce the “satellite” structure. When the cells reach the START point, the duplication plaque is formed in a phosphorylated Spc42-dependent manner (Sue L. Jaspersen

30

Este documento incorpora firma electrónica, y es copia auténtica de un documento electrónico archivado por la ULL según la Ley 39/2015.  
Su autenticidad puede ser contrastada en la siguiente dirección <https://sede.ull.es/validacion/>

Identificador del documento: 3075810 Código de verificación: smutbmB+

Firmado por: JESSEL AYRA PLASENCIA  
UNIVERSIDAD DE LA LAGUNA

Fecha: 30/11/2020 12:24:14

María de las Maravillas Aguiar Aguiar  
UNIVERSIDAD DE LA LAGUNA

08/02/2021 13:50:06



## 1. Introduction

et al., 2004; Sue L. Jaspersen & Winey, 2004; Rüttnick & Schiebel, 2016, 2018). Thus, the duplication plaque starts maturing, and all components to form the new SPB are recruited. Both SPBs remain connected through a bridge until the end of the S-phase.

After replication, kinetochore proteins bind to centromeres. Kinetochores are multiprotein structures located at the plus ends of MTs. They attach to centromere-specific regions (known as CDE-I, -II, and -III) and serve as a scaffold to bind DNA and MTs, and thus separate chromosomes through the bipolar and elongated mitotic spindle (Keith & Fitzgerald-Hayes, 2000, p. 4; Murphy et al., 1991; Saunders et al., 1988; Tanaka, 2010). Kinetochores also enhance the nucleus polarization through the interaction and expansion of iMTs from both SPBs (Caydasi & Pereira, 2009; Hotz et al., 2012; Palmer et al., 1992; Pearson et al., 2001).

Segregation of kinetochores and centromeres along the iMTs is mediated by motor and microtubule-associated proteins (MAPs). Cin8 and Kip1 kinesins motors, Dyn1-3 dyneins, and Bim1-Kar9 MAPs (among others) lengthen and shorten iMTs and aMTs, respectively (Barnes et al., 1992; Tanaka, 2010; Tanaka et al., 2005; Winey & Bloom, 2012). Yeast kinesin-5 motor protein Cin8 is involved in anaphase progression. It contains three CDK sites in its motor domain (S277, T285, and S493), whose post-translational status modifies its location and activity along the spindle. In pre-anaphase spindles, Cin8 is dephosphorylated by PP2A<sup>Cdc55</sup> and accumulates near the SPBs. Then, at the anaphase onset, CDK partially phosphorylates Cin8 at S277 and S493 sites, promoting its relocation from the SPBs to the spindle midzone. FEAR-mediated Cdc14 release (see section 1.2.3) dephosphorylates the S493 residue and keeps the T285 site in a non-phosphorylated status. This way, Cin8 attaches stronger to the midzone and starts sliding away antiparallel MTs, leading to the elongation of iMTs and the separation of sister chromatids. In late anaphase, CDK phosphorylates all three sites, and Cin8 is inactivated and detached. Finally, iMTs are depolymerized, and cells perform the exit from mitosis (Avunie-Masala et al., 2011; D'Amours & Amon, 2004; Goldstein et al., 2017; Queralt et al., 2006; Shapira et al., 2017; Stegmeier et al., 2002).

### 1.2.3. Exit from mitosis

Whereas Cln- and Clb-Cdc28 complexes drive every cellular process from the S phase onwards, the exit from mitosis requires the adequate inhibition of the CDK activity. Yeast essential Cdc14 phosphatase, a tightly regulated protein, is directly involved in the CDK inactivation (Stegmeier & Amon, 2004). Cdc14 locates within the nucleolus and remains sequestered and inactive through the association to its specific inhibitor Net1 (Játiva et al., 2019; R. Visintin et al., 1999, p. 1). Yeast cells perform a double activation and subsequent Cdc14 release from the nucleolus for triggering mitotic exit. It occurs via two molecular

31

Este documento incorpora firma electrónica, y es copia auténtica de un documento electrónico archivado por la ULL según la Ley 39/2015.  
Su autenticidad puede ser contrastada en la siguiente dirección <https://sede.ull.es/validacion/>

Identificador del documento: 3075810 Código de verificación: smutbmB+

Firmado por: JESSEL AYRA PLASENCIA  
UNIVERSIDAD DE LA LAGUNA

Fecha: 30/11/2020 12:24:14

María de las Maravillas Aguiar Aguiar  
UNIVERSIDAD DE LA LAGUNA

08/02/2021 13:50:06

1. Introduction

signaling cascades known as the Cdc14-Early Anaphase Release (FEAR) and the Mitotic Exit Network (MEN) (Baro et al., 2017; Stegmeier & Amon, 2004; B.-D. Wang et al., 2004; Yoshida et al., 2002) (Fig. 1.3).

Cib1- and Cib2-Cdc28 phosphorylate the APC<sup>Cdc20</sup> in late G<sub>2</sub>. As stated above, APC leads to the ubiquitin-mediated degradation of the Pds1/securin inhibitor. Pds1 degradation promotes the activation of Esp1/separase, which cleaves the cohesin ring subunit Scc1 and liberates the sister chromatids to segregate (Cohen-Fix et al., 1996). Besides, Esp1 promotes the PP2A<sup>Cdc55</sup> inhibition (which precludes the inopportune Cdc14 release), and the Polo-like kinase Cdc5 activation (Buonomo et al., 2003; Rahal & Amon, 2008; Sullivan & Uhlmann, 2003; C. Visintin et al., 2008). Then, Cdc5 phosphorylates Net1 and promotes the first Cdc14 release.

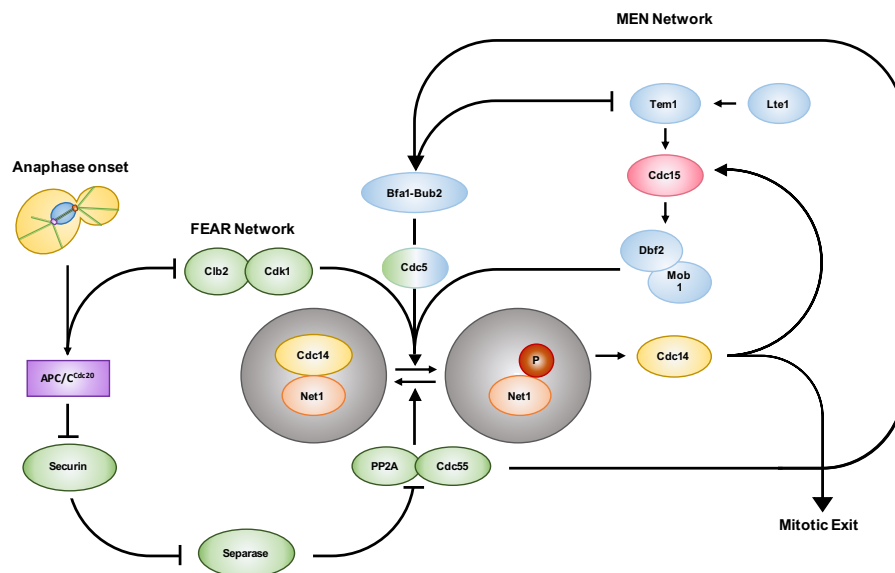


**Figure 1.3. Scheme depicting the signaling cascades that regulate FEAR and MEN networks.** Green ovals signal proteins involved in FEAR, whereas the blues points to those implied in MEN. APC: Anaphase Promoting Complex. P: Phosphorylated protein.

When FEAR is triggered, Cdc14 diffuses throughout the nucleus and dephosphorylates several targets. Cdc14 enhances the chromosome segregation (including the rDNA array) and controls the nuclear positioning and the spindle dynamics (Khmelninskii et al., 2009; Rocuzzo et al., 2015; Rozelle et al., 2011). Furthermore, it promotes the MEN regulatory network, which in turn leads to its second activation through a positive feedback.

Este documento incorpora firma electrónica, y es copia auténtica de un documento electrónico archivado por la ULL según la Ley 39/2015.  
 Su autenticidad puede ser contrastada en la siguiente dirección <https://sede.ull.es/validacion/>

Identificador del documento: 3075810 Código de verificación: smutbmB+

Firmado por: JESSEL AYRA PLASENCIA  
 UNIVERSIDAD DE LA LAGUNA

Fecha: 30/11/2020 12:24:14

María de las Maravillas Aguiar Aguiar  
 UNIVERSIDAD DE LA LAGUNA

08/02/2021 13:50:06

## 1. Introduction

The triggering of MEN depends on Tem1, a GTPase member of the Ras superfamily, which accumulates at SPBs and controls the actomyosin and septins dynamics during cytokinesis (Stegmeier et al., 2002; Stegmeier & Amon, 2004). Once the old SPB enters into the daughter cell, Lte1 counteracts the Bfa1-Bub2 complex (which blocks the cell cycle progression in response to spindle and kinetochore damage) and activates Tem1 (Segal, 2011; Varela et al., 2009; Yoshida et al., 2002, 2003). Tem1 interacts directly with Cdc15 kinase, which is then recruited to the SPBs and activated through Cdc14-mediated dephosphorylation (Cenamor et al., 1999; S. E. Lee et al., 2001; Rock & Amon, 2011, p. 15; Varela et al., 2009, p. 15). This way, Cdc15 acts over the Dbf2-Mob1 complex, which directly generates the second Cdc14 release responsible of cytokinesis (Mah et al., 2001, p. 2; Mohl et al., 2009, p. 2).

In the second release wave, Cdc14 dephosphorylates the transcription factor Swi5, which promotes the transcription of the B-type mitotic cyclins inhibitor Sic1. In turn, it also dephosphorylates translated Sic1 to prevent its degradation, and activates the APC/C<sup>Cdh1</sup> to degrade both Polo-like kinase Cdc5 and Clb1-Clb2 mitotic cyclins (S. L. Jaspersen et al., 1999; Prinz et al., 1998; C. Visintin et al., 2008; R. Visintin et al., 1998). Cdc5 degradation leads to the return of Cdc14 into the nucleolus (Schwab et al., 1997). Cdc14 release also activates the structure-specific endonuclease Yen1, which relocates into the nucleus to resolve remaining Holliday junctions (Eissler et al., 2014, p. 1; García-Luis et al., 2014).

Finally, MEN-released Cdc14 regulates the proper execution of cytokinesis. Once CDK/Cyclin and the Polo-like kinase levels decrease, the contractile actomyosin ring splits into two. It generates the mobilization of secretory vesicles containing the required factors to finish the actomyosin contraction and separation. Consequently, it causes a reorganization of the cytoskeleton and the formation of primary and secondary septums, resolving mother and daughter cells into two individual entities (Gladfelter et al., 2001; McMurray & Thorner, 2009; Meitinger et al., 2012; Palani et al., 2012; Rauter & Barral, 2006; Yoshida et al., 2006).

### 1.3. The DNA Damage Response

Cell survival mostly depends on DNA integrity. The genetic material, organized as chromosomes, must be appropriately duplicated and segregated during the cell cycle. The DNA molecule is highly stable and the sequence needs to be faithfully maintained. However, the double-helix is continuously subjected to a high metabolic activity, such as replication, transcription, recombination, or segregation, among others. DNA damage arises if the DNA molecule suffers alterations (either in the structure or nucleotide sequence). Most of the DNA damage can be classified as i) endogenous, caused as a consequence of metabolic activity

33

Este documento incorpora firma electrónica, y es copia auténtica de un documento electrónico archivado por la ULL según la Ley 39/2015.  
Su autenticidad puede ser contrastada en la siguiente dirección <https://sede.ull.es/validacion/>

Identificador del documento: 3075810 Código de verificación: smutbmB+

Firmado por: JESSEL AYRA PLASENCIA  
UNIVERSIDAD DE LA LAGUNA

Fecha: 30/11/2020 12:24:14

María de las Maravillas Aguiar Aguiar  
UNIVERSIDAD DE LA LAGUNA

08/02/2021 13:50:06

1. Introduction

(i.g., reactive oxygen species) and, ii) exogenous, promoted by physical or chemical agents (e.g., UV irradiation, genotoxins, etc.). Hence, cells face a constant challenge to maintain genome integrity.

Cells ensure the progression through the cell cycle by monitoring the appearance of DNA lesions. Each stage is protected from being prematurely triggered if the previous one has not adequately finished. Yeasts have developed several mechanisms that control DNA integrity. These pathways are known as checkpoints, and their performance depends on the type of DNA damage and the moment they appear (Fig. 1.4) (T. A. Weinert & Hartwell, 1990; T. Weinert & Hartwell, 1989, p. 2).

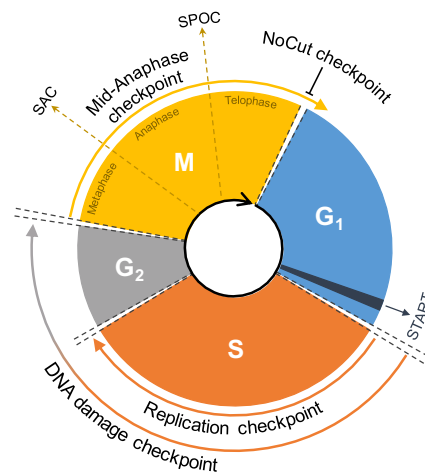


**Figure 1.4. Cell cycle phases scheme depicting the main checkpoints in *S. cerevisiae*.** SAC: Spindle Assembly Checkpoint. SPOC: Spindle Position Checkpoint.

Most of the checkpoints present in yeast are highly conserved through evolution. In all organisms, they are triggered to sense whether DNA is damaged through the cell cycle, even stopping the replication or segregation of chromosomes to repair (Foiani et al., 2000).

All molecular checkpoints pathways have a sensor, a transducer, and a final effector. Sensors are proteins involved in recognition of DNA damage. They monitor the situation and stimulate the transducer to increase the effector activation, which in turn promotes a signaling cascade that delays the cell cycle progression (Barnum & O'Connell, 2014; Clarke & Giménez-Abián, 2000; T. Weinert & Hartwell, 1989).

As DNA damage can arise during the S phase, cells have developed the Replication Checkpoint to cope with insults such as replication fork blocks or single-stranded DNA, among

Este documento incorpora firma electrónica, y es copia auténtica de un documento electrónico archivado por la ULL según la Ley 39/2015.  
 Su autenticidad puede ser contrastada en la siguiente dirección <https://sede.ull.es/validacion/>

Identificador del documento: 3075810 Código de verificación: smutbmB+

Firmado por: JESSEL AYRA PLASENCIA  
 UNIVERSIDAD DE LA LAGUNA

Fecha: 30/11/2020 12:24:14

María de las Maravillas Aguiar Aguiar  
 UNIVERSIDAD DE LA LAGUNA

08/02/2021 13:50:06

1. Introduction

others (Branzei & Foiani, 2010; L. Hartwell et al., 1994). When cells have replication stress, Mec1 kinase phosphorylates Mrc1, which in turn activates Rad53 and promotes the checkpoint response (Alcasabas et al., 2001; Osborn & Elledge, 2003, p. 1).

The DNA Damage Checkpoint (DDC) sensing relies on Mec1, Tel1, Rad53, and Chk1 kinases (ATM, ATR, CHK2, and CHK1 in humans, respectively) (Craven et al., 2002; de la Torre-Ruiz et al., 1998; O'Shaughnessy et al., 2006). Besides, Rad9 plays a central role in amplifying DNA damage signals since it binds to DNA double-strand breaks (Naiki et al., 2004). DDC can be performed from the S phase to late-G<sub>2</sub>, stopping the cell cycle by interfering with different cell cycle control factors.

Cells achieve mitosis by coordinating several elements involved in the segregation process. In yeast, the Spindle Assembly Checkpoint (SAC) assures that all centromeres and kinetochores have been attached to their corresponding MTs. It also preserves the correct orientation of sister chromatids to be separated along the mitotic spindle. If the tension between sister kinetochores is lost, the SAC delays the anaphase onset (Caydasi & Pereira, 2009, 2009; Lara-Gonzalez et al., 2012; Daniel J. Lew & Burke, 2003).

Interestingly, an extra delay has been described for anaphase bridges formed by dicentric chromosomes. Rad9 is closely implied in triggering the so-called Mid-Anaphase Checkpoint. It slows down (for almost 60 minutes) the mitotic spindle elongation when two centromeres within the same chromosome are pulled apart to the opposite nuclear poles (K. Bloom et al., 1989; Hill & Bloom, 1989; Yang et al., 1997).

Besides, spindle orientation is crucial for triggering MEN. SPBs must be adequately oriented, forming a bipolar spindle across the mother and daughter cellular bodies. If the mother-to-daughter polarity axis is not properly positioned, cells trigger the Spindle Position Checkpoint (SPOC), which delays the cell cycle until mitotic iMTs are correctly extended. The SPOC inhibits MEN through the Kin4 kinase. Kin4 counteracts Lte1 and prevents the inhibitory phosphorylation of Cdc5 that leads to Tem1 and Cdc15 activation, and so, the exit from mitosis (Caydasi & Pereira, 2009; Musacchio & Hardwick, 2002).

Finally, cells have developed another surveillance pathway before the completion of cytokinesis. The NoCut Checkpoint prevents the breakage of lagged chromosomes that remain across the bud neck (compulsory cytokinetic plane in yeast) when the nuclear membrane abscission is carried out. The Aurora kinase Ipl1 is activated by the chromatin arranged along the spindle midzone and translocates Boi1 and Boi2 from the nucleus to the cortex to abolish abscission (Kerry Bloom, 2006; Mendoza et al., 2009; Norden et al., 2006).

Este documento incorpora firma electrónica, y es copia auténtica de un documento electrónico archivado por la ULL según la Ley 39/2015.  
Su autenticidad puede ser contrastada en la siguiente dirección <https://sede.ull.es/validacion/>

Identificador del documento: 3075810 Código de verificación: smutbmB+

Firmado por: JESSEL AYRA PLASENCIA  
UNIVERSIDAD DE LA LAGUNA

Fecha: 30/11/2020 12:24:14

María de las Maravillas Aguiar Aguiar  
UNIVERSIDAD DE LA LAGUNA

08/02/2021 13:50:06

## 1.4. DNA damage repair pathways

Depending on the nature and the effect produced in the double-helix, DNA damage repair can be classified as single- and double-stranded. On the one hand, single-stranded DNA damage repair includes pathways such as direct reversal, base excision repair (BER), mismatch repair (MMR), and nucleotide excision repair (NER). By contrast, double-strand breaks (DSBs) are processed by non-homologous end joining (NHEJ) and homologous recombination (HR). HR, in turn, can be subdivided into synthesis-dependent strand annealing (SDSA), single-strand annealing (SSA), break-induced replication (BIR), and the pathway that leads to double Holliday junction (dHJs).

### 1.4.1. Single-stranded DNA damage repair

#### 1.4.1.1. Direct Reversal

Despite most of the repair pathways comprises complicated signaling cascades and numerous effectors, the Direct Reversal repair is based on removing the DNA damage by a simple chemical reaction. Depending on the nucleotide chemical modification, a specific enzyme is employed to restore the initial status. UV light or alkylating agents can generate pyrimidine dimers and methylation of DNA, respectively. Thus, cells use photolyases to split the covalent bonds between pyrimidine dimers, and the O<sub>6</sub>-methylguanine-DNA methyltransferase (MGMT) to remove methylated nucleotides (Eker et al., 2009; Memisoglu & Samson, 2001; Yi & He, 2013).

#### 1.4.1.2. Base Excision Repair

This pathway involves the repair of non-bulky DNA lesions through the activity of DNA glycosylases. These enzymes can recognize alkylated, oxidated, and deaminated DNA bases. Once activated, they release the nitrogen base by breaking the N-glycosylic bond, giving rise to a DNA abasic site. These apurinic/aprimidinic abasic sites (AP sites) can be restored through two distinct pathways. First, AP specific endonucleases can cut the AP site at the 5' end of the sugar-phosphate backbone to directly provide a primer for the DNA polymerase  $\beta$  and incorporate a new nucleotide. On the other hand, AP endonucleases can cleave at the 3' end, so that phosphodiesterases act to remove the fragmented sugar and allow the activity of DNA polymerase  $\beta$  as well. Finally, the DNA sequence is fully restored when DNA ligases seal the generated nicks (Boiteux & Guillet, 2004; Girard & Boiteux, 1997; Hegde et al., 2010; Krokan & Bjørås, 2013).

Este documento incorpora firma electrónica, y es copia auténtica de un documento electrónico archivado por la ULL según la Ley 39/2015.  
Su autenticidad puede ser contrastada en la siguiente dirección <https://sede.ull.es/validacion/>

Identificador del documento: 3075810 Código de verificación: smutbmB+

Firmado por: JESSEL AYRA PLASENCIA  
UNIVERSIDAD DE LA LAGUNA

Fecha: 30/11/2020 12:24:14

María de las Maravillas Aguiar Aguiar  
UNIVERSIDAD DE LA LAGUNA

08/02/2021 13:50:06

### 1.4.1.3. Mismatch Repair

This pathway is implied in restoring mismatches such as single-nucleotide loop insertions/deletions and mispairs from the endogenous replication process, that despite being highly accurate, it can introduce mistakes. Both MLH (Mlh1, -2, -3, and Pms1) and MSH (Msh2, -3, and -6) complexes work simultaneously to scan the DNA sequence. Once a mismatch is found, the newly synthesized single strand is nicked and degraded. This way, the ssDNA gap is re-synthesized and sealed by DNA ligases (Bowers et al., 2001; Habraken et al., 1998; Karahan et al., 2015).

### 1.4.1.4. Nucleotide Excision Repair

When UV light- and bulky lesions-mediated DNA modifications appear, cells can trigger the Nucleotide Excision Repair. This pathway can be subdivided into i) NER-mediated Global Genome Repair (GGR) and ii) NER-mediated Transcription-Coupled Repair (TCR). GGR is employed when DNA damage is restored all along the genome, whereas TCR is preferred when DNA lesions occur on transcribed DNA strands of active genes. In both subtypes, specific proteins unwind the DNA around the lesion. Then, they split off a 24-32 DNA sequence containing the damaged nucleotide through incisions at 3' and 5'. Finally, DNA synthesis and ligation are carried out (Apostolou et al., 2019; Kitsera et al., 2019; Marteiijn et al., 2014; Reardon & Sancar, 2005).

## 1.4.2. Double-strand DNA damage repair

Double-strand breaks are one of the most harmful types of DNA damage. They are generated when the phospho-sugars backbones of both complementary DNA strands are broken at the same (or nearly close) position, leading to the physical separation into two DNA molecules. In single-strand DNA breaks, the complementary strand is still available as an intact template. However, accurate repair of DSBs could cause loss of genetic information, chromosome fragmentation, rearrangements, and cell death. As stated before, several endogenous or exogenous sources can generate them, such as reactive oxygen species (ROS) from the metabolism or ionizing radiation, respectively. (Her & Bunting, 2018; Li & Xu, 2016; Shibata, 2017).

As also mentioned above, cells have developed distinct DSBs-associated repair pathways to restore the physical integrity and the genetic information. They can be classified into non-homologous end joining (NHEJ) and homologous recombination (HR) (Aparicio et al., 2014).

Este documento incorpora firma electrónica, y es copia auténtica de un documento electrónico archivado por la ULL según la Ley 39/2015.  
Su autenticidad puede ser contrastada en la siguiente dirección <https://sede.ull.es/validacion/>

Identificador del documento: 3075810 Código de verificación: smutbmB+

Firmado por: JESSEL AYRA PLASENCIA  
UNIVERSIDAD DE LA LAGUNA

Fecha: 30/11/2020 12:24:14

María de las Maravillas Aguiar Aguiar  
UNIVERSIDAD DE LA LAGUNA

08/02/2021 13:50:06

1. Introduction

**1.4.2.1. Non-homologous end joining**

This pathway works by directly fusing the two broken DNA ends after a minor processing. It is considered an error-prone mechanism since it can introduce short deletions or insertions at the break site (Fig. 1.5) (Chang et al., 2017; Chiruvella et al., 2013).

Once the DSB is generated and detected, the complex Yku70/80 (KU70/80 in humans) binds to broken DNA ends to prevent the exonucleases-mediated degradation. Then, the Mre11-Rad50-Xrs2 (MRX complex, MRE11-RAD50-NBS1 in humans) is subsequently recruited to the site of the break. Yku70/80 remains bound to limit the Rad50-mediated exonuclease activity. Still, MRX forms an end bridging factor that links broken DNA ends and creates a scaffold where the rest of NHEJ components are recruited and assembled.

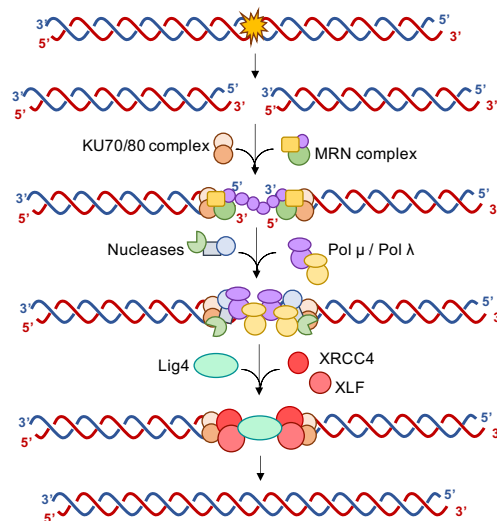


**Figure 1.5. General schematic of the NHEJ pathway.** DSBs are first recognized by KU70/80 complex, which also recruits the MRN complex to bind the two broken ends. Then, nucleases and polymerases are recruited to generate blunt ends. Finally, the Ligase IV complex is activated, and the DNA molecule is restored.

As NHEJ requires two blunt ends to repair, 3' non-cohesive DNA overhangs can be either filled by polymerases or trimmed by nucleases. It entails a significant cause of small deletions or insertions. Pol4 (Pol μ and Pol λ in humans) or Artemis nuclease (yeast ortholog Pso2, which is involved explicitly in interstrand cross-link repair) are recruited for processing the terminal ends. Then, Lig4, together with Lif1 and Nej1 (DNA ligase IV, XRCC4, and XLF in humans, respectively), are targeted to the DNA ends, and Yku70/80-mediated ligation is triggered (Chang et al., 2017; Daley et al., 2005; Galli et al., 2015; Lieber et al., 2003).

Este documento incorpora firma electrónica, y es copia auténtica de un documento electrónico archivado por la ULL según la Ley 39/2015.  
 Su autenticidad puede ser contrastada en la siguiente dirección <https://sede.ull.es/validacion/>

Identificador del documento: 3075810 Código de verificación: smutbmB+

Firmado por: JESSEL AYRA PLASENCIA  
 UNIVERSIDAD DE LA LAGUNA

Fecha: 30/11/2020 12:24:14

María de las Maravillas Aguiar Aguiar  
 UNIVERSIDAD DE LA LAGUNA

08/02/2021 13:50:06



## 1. Introduction

There exist another error-prone method based on microhomologous sequences on each side of the DSB. If KU proteins are absent or cells cannot trigger the canonical NHEJ, the resection machinery exposes extensive 3' ssDNA, promoting an alternative mechanism known as microhomology-mediated end joining (MMEJ). In this case, the MRX complex combined with phosphorylated Sae2 (MRN complex and CtIP in humans, respectively) initiate 5' to 3' end resection. Short resected ssDNA is sufficient to trigger MMEJ since exposed overhangs are annealed as intermediates with 3'-flap and gaps on both sides of the DSB. Then, the non-homologous 3' tails are removed by Rad1-Rad10 (XPF/ERCC1 in humans) endonucleases. Remaining ssDNA gaps are filled by a collection of polymerases such as Pol3 and Pol4 (Pol $\delta$  in humans). Finally, Cdc9-dependent activation of Lig4 promotes the nick ligation (LigIII in humans) (Galli et al., 2015; K. Lee et al., 2019; H. Wang & Xu, 2017).

### 1.4.2.2. Homologous recombination

HR-mediated DSBs repair includes various distinct pathways that rely on the error-free restoration of the broken DNA sequence. All of them share the availability of invading a homologous intact template from which the DNA sequence is faithfully copied. Despite specific differences, they present mechanisms based on three phases, known as:

- Pre-synapsis: It includes the recognition and processing of the DSB. Contrary to NHEJ, the MRX complex is first bound to the DNA ends. Phosphorylated Sae2 promotes a Rad50-mediated nucleolytic degradation of the 5' DNA ends, yielding ~ 100 nucleotides of 3' ssDNA overhangs. It then stimulates a more extensive 5' to 3' resection by Exo1 exonuclease, Sgs1 helicase, and Dna2 endonuclease (EXO1 and DNA2-BTR complex in humans, respectively) (Bonetti et al., 2015; Gravel et al., 2008; Mimitou & Symington, 2008; Symington, 2016; Zhu et al., 2008). Exo1 catalytically removes mononucleotides, whereas Sgs1-Top3-Rmi1 complex relaxes the negative supercoiling and Dna2 endonuclease degrades the unwound DNA (Huertas et al., 2008; Mimitou & Symington, 2008; Shim et al., 2010; Zhu et al., 2008). The generation of 3' ssDNA overhangs recruits the heterotrimeric replication protein A complex (RPA) to protect ssDNA from the nucleases-mediated degradation. Once RPA is loaded, Shu2-Csm2-Psy3 (SHU complex) and Rad51 mediators such as Rad52, -55, and -57 (BRCA2, PALB2, RAD51-paralogs and Shu Complex in humans), recruits Rad51 recombinase (RAD51 in humans) to replace RPA and create 3' protruding nucleofilaments (Anand et al., 2017, p. 52; Martino et al., 2019; Yan et al., 2019) (Fig. 1.6).

39

Este documento incorpora firma electrónica, y es copia auténtica de un documento electrónico archivado por la ULL según la Ley 39/2015.  
Su autenticidad puede ser contrastada en la siguiente dirección <https://sede.ull.es/validacion/>

Identificador del documento: 3075810 Código de verificación: smutbmB+

Firmado por: JESSEL AYRA PLASENCIA  
UNIVERSIDAD DE LA LAGUNA

Fecha: 30/11/2020 12:24:14

María de las Maravillas Aguiar Aguiar  
UNIVERSIDAD DE LA LAGUNA

08/02/2021 13:50:06

1. Introduction

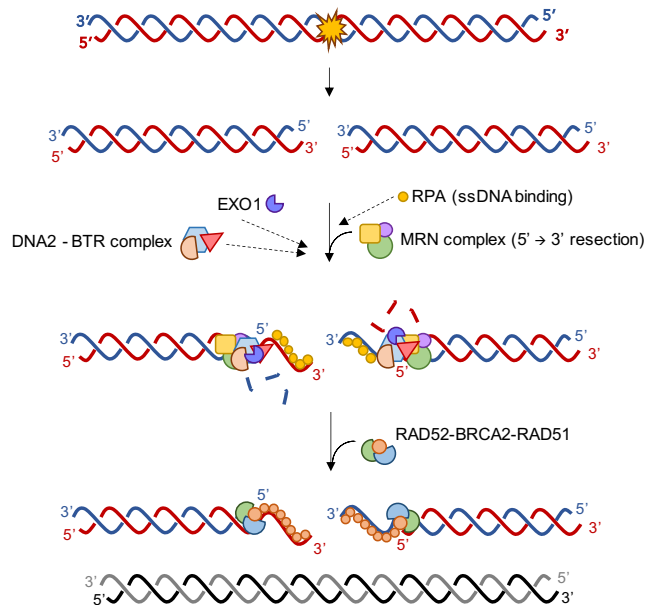


**Figure 1.6. Schematic of the pre-synapsis step on homologous recombination pathways.** MRN complex binds to broken DNA ends and promotes an extended resection through EXO1 and DNA2-BTR complex activities. Then, RPA is recruited to protect the 3' ssDNA from nucleases degradation. Then, RAD51 supersedes RPA and generates protruding nucleofilaments, which are ready to search for homology.

It should be noted that after this step, cells can trigger the single-strand annealing (SSA) pathway with no need to invade a donor sequence located in other chromosomes. It is highly restricted to DSBs flanked by repetitive regions, leading to rearrangements between the repeats. After 3' end resection, ssDNA repeats are exposed to recombine each other. SSA does not require to create a displacement loop (D-loop), but both Rad52 and Rad59 anneal homologous sequences and form a synapsed intermediate. Non-annealed flanking regions are cleaved by Rad1-Rad10 and Slx4, giving rise to polymerase-mediated filling of the resulting gaps (Bhargava et al., 2016; A. P. Davis & Symington, 2001; Evans et al., 2000; A. Malkova et al., 1996).

- **Synapsis:** This phase entails the Rad51-coated nucleofilament-mediated interrogation of the genome to look for an intact and homologous template to repair. Once found, the double-strand Rad54 motor protein (RAD54 in humans) simulates the nucleofilament invasion by opening the intact donor double-helix to form a D-loop (Heyer et al., 2006; Qi et al., 2015; Solinger et al., 2001; Sung et al., 2000, p. 199; Van Komen et al., 2000).

After D-loop formation, the 3' extension is carried out by polymerases in coordination with Dpb11 and the processivity clamp for DNA polymerases PCNA (pol $\delta$  and  $\epsilon$ , TOPBP1, and PCNA in humans) (Henninger & Pursell, 2014; Holmes & Haber, 1999; Symington, 2016; Symington et al., 2014; Wright et al., 2018). This way, error-free re-polymerization bypasses the broken DNA site by copying the intact template (Fig. 1.7).

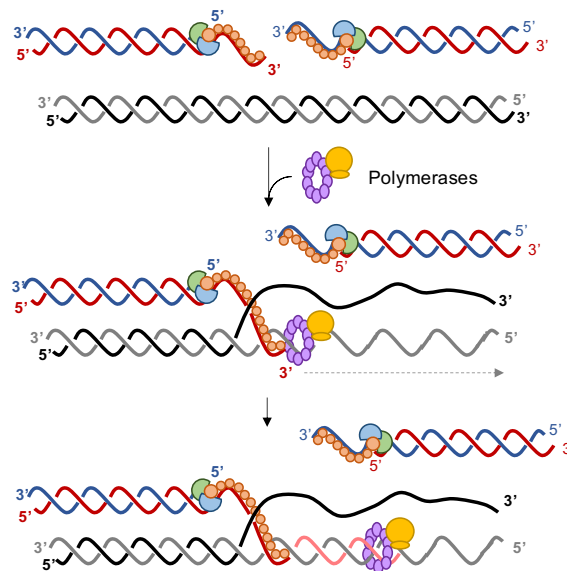


**Figure 1.7. Schematic of the synthesis step on homologous recombination pathways.** Rad51-coated nucleofilaments search for homology and invade the donor sequence by generating a D-loop. Then, polymerases, PCNA, and Dpb11 are recruited to perform the new DNA synthesis based on the template sequence.

- **Post-synapsis:** This last step comprises the resolution of the process, which depending on the number of invasions and the synthesis extension, can be performed through three distinct pathways, known as break-induced replication (BIR), synthesis-dependent strand annealing (SDSA), and the canonical DSBs repair (DSBR) pathway through double Holliday junctions (dHJs).

#### 1.4.2.2.1. Break-induced replication (BIR)

Cells mainly use this pathway to repair one-ended DSBs. Either the restart of collapsed replication forks (RFs) or the lengthening of eroded telomeres in telomerase-defective

1. Introduction

mutants, are performed through BIR. (Costantino et al., 2014; Kramara et al., 2018; Lydeard et al., 2007; A. Malkova et al., 1996; Mason-Osann et al., 2020; Teng et al., 2000).

Following DNA resection, the Rad51-coated 3' ssDNA invades the homologous DNA molecule and forms a D-loop. DNA synthesis is then initiated, and it persists as far as the donor sequence extends (Allison P. Davis & Symington, 2004; Elango et al., 2018; McEachern & Haber, 2006). Finally, the newly synthesized ssDNA is filled into dsDNA (Fig. 1.8).

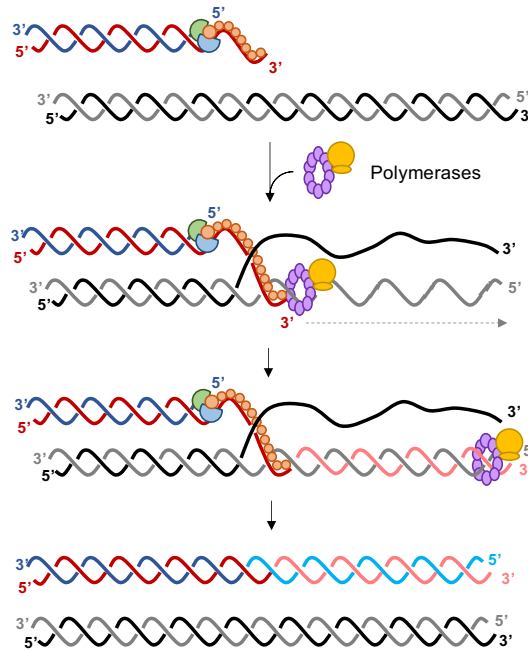


**Figure 1.8. Break-induced replication model scheme.** A Rad51-coated protruding nucleofilament from one-ended DSB invades a donor sequence. Primer extension leads to the synthesis of ssDNA until the full extension of the template. The newly synthesized ssDNA is finally re-filled to generate a double-strand product.

BIR can restore long tracks of DNA, which in case of repairing with the homolog chromosome, leads to extensive loss of heterozygosity (LOH). It can also occur at ectopic chromosome sites and promote gross chromosome rearrangements (GCRs) through sequential strand invasions, synthesis, and dissociation rounds (Bosco & Haber, 1998; Donnianni & Symington, 2013; Anna Malkova et al., 2005).

Este documento incorpora firma electrónica, y es copia auténtica de un documento electrónico archivado por la ULL según la Ley 39/2015.  
 Su autenticidad puede ser contrastada en la siguiente dirección <https://sede.ull.es/validacion/>

Identificador del documento: 3075810 Código de verificación: smutbmB+

Firmado por: JESSEL AYRA PLASENCIA  
 UNIVERSIDAD DE LA LAGUNA

Fecha: 30/11/2020 12:24:14

María de las Maravillas Aguiar Aguiar  
 UNIVERSIDAD DE LA LAGUNA

08/02/2021 13:50:06

#### 1.4.2.2.2. Synthesis-dependent strand annealing (SDSA)

In this pathway, the broken DNA sequence is usually replaced with a homologous DNA template copy while maintaining the original flanking regions. The strand invasion creates a D-loop, and DNA polymerases extend the 3' end of the invading nucleofilament. Contrary to what happens in BIR, polymerases do not synthesize through the full extension of the template. Instead, the newly ssDNA is quickly displaced from the donor template and paired again with the 3' end of the other DSB end. A second wave of DNA synthesis followed by a final ligation is then carried out to fill the broken strand gaps (Fig. 1.9) (Karlin & Fischhaber, 2013; Miura et al., 2012; Saponaro et al., 2010). SDSA is a conservative pathway since it exclusively produces non-crossover (NCO) recombination.

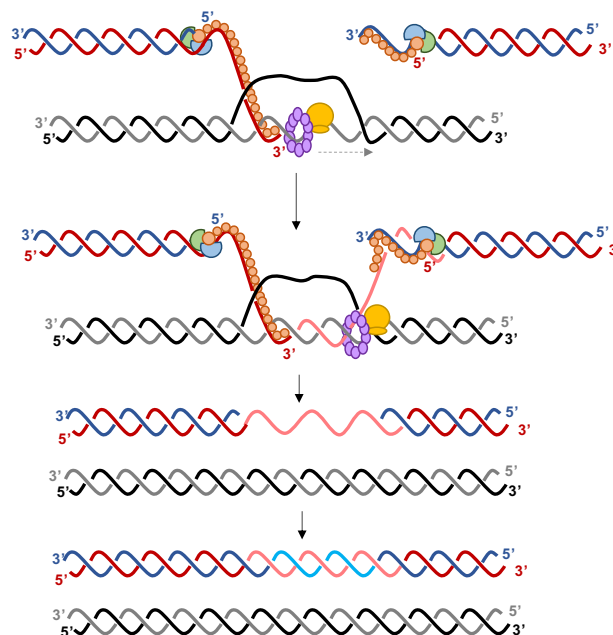


**Figure 1.9. Synthesis-dependent strand annealing model scheme.** A resected 3' end of a DSB invades its donor sequence and forms as D-loop. After a wave of DNA polymerization, the newly synthesized ssDNA is displaced from the D-loop and reannealed to the other resected 3' end of the DSB. Finally, the gaps are filled-in and ligated, restoring the original DNA sequence.

#### 1.4.2.2.3. Double Holliday junction pathway (dHJs)

This pathway is based on Holliday's early theoretical concepts, who proposed the correction of DNA base-pair mismatches through the generation of recombination intermediates and

Este documento incorpora firma electrónica, y es copia auténtica de un documento electrónico archivado por la ULL según la Ley 39/2015.  
 Su autenticidad puede ser contrastada en la siguiente dirección <https://sede.ull.es/validacion/>

Identificador del documento: 3075810 Código de verificación: smutbmB+

Firmado por: JESSEL AYRA PLASENCIA  
 UNIVERSIDAD DE LA LAGUNA

Fecha: 30/11/2020 12:24:14

María de las Maravillas Aguiar Aguiar  
 UNIVERSIDAD DE LA LAGUNA

08/02/2021 13:50:06

1. Introduction

provided the basis for gene conversion pathways (Esposito & Holliday, 1964; Holliday, 1964). The model has been redefined, and it currently comprises a D-loop structure formation followed by polymerases-mediated extension of the 3' protruding nucleofilament. Contrary to SDSA, the other 3' protruding nucleofilament anneals with the complementary displaced ssDNA from the template. The second-end capture promotes two physical linkages between homologous sequences known as Holliday junctions (HJs) (Mehta & Haber, 2014; Pâques & Haber, 1999).

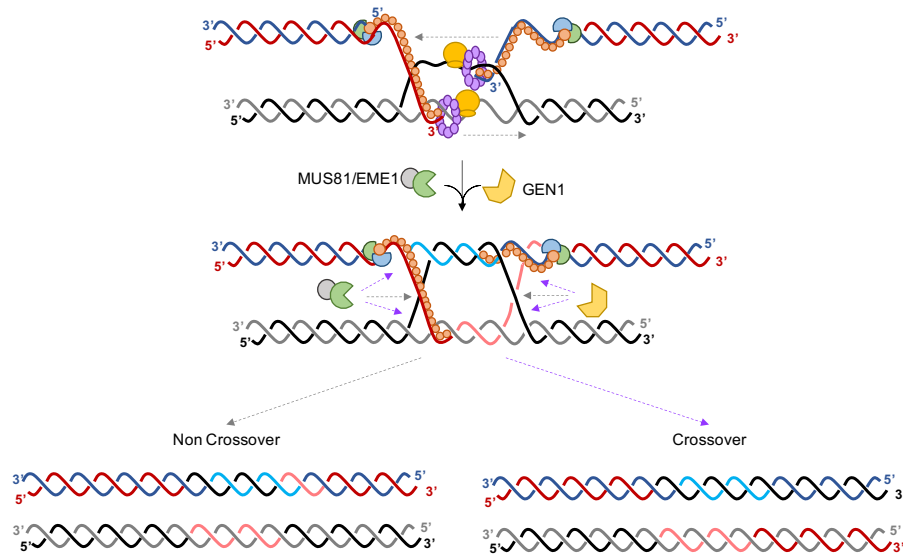


**Figure 1.10. Double Holliday Junctions model scheme.** A 3' protruding nucleofilament invades the homologous template through the formation of a D-loop. The other 3' resected DNA also anneals to the displaced ssDNA, creating two HJs as a consequence. Finally, dHJs dissolution by the STR complex or resolution by different SSEs gives rise to NCO or CO products, respectively.

Then, either Sgs1-Top3-Rmi1 (STR complex, BTR complex in humans) or different structure-specific endonucleases (SSEs) such as Mus81-Mms4, Yen1, and Slx1-Slx4 (MUS81-EME1, GEN1, and SLX1-SLX4 in humans), dissolve and resolve those DNA-DNA junctions, respectively (Fig. 1.10). The difference between STR-mediated dissolution and SSEs-dependent resolution relies on the DNA material exchange. STR-processed dHJs leads to NCO outcomes. On the other hand, SSEs promote crossovers (COs) events according to the pair of joint strands they cut (Eissler et al., 2014, p. 1; García-Luis & Machín, 2014, p. 81; Symington et al., 2014). COs can generate harmful effects since, in the case of homologous chromosomes, LOH can arise.

Este documento incorpora firma electrónica, y es copia auténtica de un documento electrónico archivado por la ULL según la Ley 39/2015.  
 Su autenticidad puede ser contrastada en la siguiente dirección <https://sede.ull.es/validacion/>

Identificador del documento: 3075810 Código de verificación: smutbmB+

Firmado por: JESSEL AYRA PLASENCIA  
 UNIVERSIDAD DE LA LAGUNA

Fecha: 30/11/2020 12:24:14

María de las Maravillas Aguiar Aguiar  
 UNIVERSIDAD DE LA LAGUNA

08/02/2021 13:50:06

## 1.5. Regulation of the DNA repair pathway choice

When DSBs occur, cells are committed to maintaining the genomic integrity through the DNA damage response. As DSBs can arise spontaneously, cells determine which mechanism is chosen based on the cell cycle stage, the biochemical environment, and the ploidy (Aylon et al., 2004; Aylon & Kupiec, 2004a, 2004b).

The CDK/cyclin levels regulate the choice between NHEJ- or HR-based repair. For this reason, the cell cycle results crucial to trigger the corresponding DNA repair pathway. After DSBs, both KU and MRX complexes are independently recruited to the broken ends. While Rad50 stimulates the resection of 3' ends and forces the cells to repair through HR, Yku70/80 inhibits the generation of protruding nucleofilaments (Mimitou & Symington, 2010). If DSBs arise in the G<sub>1</sub> phase, cells unbalance the preference to the KU complex activity. Yku70 is highly transcribed at the early stages of the cell cycle, whereas transcription levels are low at the S phase transition. However, transcription of ~ 20 HR-associated proteins is highly favored by Cdc28 activity, delimiting their presence after the S phase. Indeed, it has been shown that MRX-, Exo1-, STR- and Dna2-mediated resection, as well as Sae2 phosphorylation, is strictly dependent on the Cdc28 activity (Aylon et al., 2004).

Hence, it seems reasonable to use NHEJ in G<sub>1</sub> when sister chromatids are absent to be used as templates, and replication has not started. In contrast, HR is preferred from the S phase onwards, when CDK/cyclin levels are high, and strand invasion to copy the intact DNA sequence can be carried out (Mathiasen & Lisby, 2014).

Este documento incorpora firma electrónica, y es copia auténtica de un documento electrónico archivado por la ULL según la Ley 39/2015.  
Su autenticidad puede ser contrastada en la siguiente dirección <https://sede.ull.es/validacion/>

Identificador del documento: 3075810 Código de verificación: smutbmB+

Firmado por: JESSEL AYRA PLASENCIA  
UNIVERSIDAD DE LA LAGUNA

Fecha: 30/11/2020 12:24:14

María de las Maravillas Aguiar Aguiar  
UNIVERSIDAD DE LA LAGUNA

08/02/2021 13:50:06



Este documento incorpora firma electrónica, y es copia auténtica de un documento electrónico archivado por la ULL según la Ley 39/2015.  
*Su autenticidad puede ser contrastada en la siguiente dirección <https://sede.ull.es/validacion/>*

Identificador del documento: 3075810 Código de verificación: smutbmB+

Firmado por: JESSEL AYRA PLASENCIA  
UNIVERSIDAD DE LA LAGUNA

Fecha: 30/11/2020 12:24:14

María de las Maravillas Aguiar Aguilár  
UNIVERSIDAD DE LA LAGUNA

08/02/2021 13:50:06





## 2. Aims

Este documento incorpora firma electrónica, y es copia auténtica de un documento electrónico archivado por la ULL según la Ley 39/2015.  
Su autenticidad puede ser contrastada en la siguiente dirección <https://sede.ull.es/validacion/>

Identificador del documento: 3075810 Código de verificación: smutbmB+

Firmado por: JESSEL AYRA PLASENCIA  
UNIVERSIDAD DE LA LAGUNA

Fecha: 30/11/2020 12:24:14

María de las Maravillas Aguiar Aguiar  
UNIVERSIDAD DE LA LAGUNA

08/02/2021 13:50:06



Este documento incorpora firma electrónica, y es copia auténtica de un documento electrónico archivado por la ULL según la Ley 39/2015.  
*Su autenticidad puede ser contrastada en la siguiente dirección <https://sede.ull.es/validacion/>*

Identificador del documento: 3075810      Código de verificación: smutbmB+

Firmado por: JESSEL AYRA PLASENCIA  
UNIVERSIDAD DE LA LAGUNA

Fecha: 30/11/2020 12:24:14

María de las Maravillas Aguiar Aguiar  
UNIVERSIDAD DE LA LAGUNA

08/02/2021 13:50:06

2. Aims

Based on previous works in yeast, it is well established that cells mainly repair DSBs through non-homologous end joining (NHEJ) and homologous recombination (HR). Accordingly, cells have coupled the cyclin-dependent kinase (CDK) activity to the choice between them. HR is usually preferred in S-G<sub>2</sub> phases since intact sister chromatids are available (to be used as templates), and CDK/cyclin levels are high. In contrast, NHEJ is chosen in G<sub>1</sub> because neither donor templates nor CDK/cyclins activity are present. Interestingly, the telophase is a small window within the cell cycle that entails a paradoxical situation. On one side, the CDK/cyclin activity is still high compared to G<sub>1</sub>; however, sister chromatids are not physically available due to the previous segregation. Thus, cells could experience a crossroad if DSBs arise in late mitosis.

The aims of this work relate to addressing this paradoxical scenario:

1. To study the subcellular response to DSBs in telophase, determining whether changes in morphological structures and some specific effector proteins are directly involved in DNA repair.
2. To monitor a single DSB repair and discern whether the efficiency and kinetics are impaired in HR-, NHEJ-, and checkpoint-deficient cells.
3. To uncover essential protein factors specifically related to repair at late mitosis but dispensable for G<sub>2</sub>.
4. To approach whether the human cell responds to DSBs in late anaphase/telophase and distinguish whether it is comparable to the yeast response.

Este documento incorpora firma electrónica, y es copia auténtica de un documento electrónico archivado por la ULL según la Ley 39/2015.  
Su autenticidad puede ser contrastada en la siguiente dirección <https://sede.ull.es/validacion/>

Identificador del documento: 3075810 Código de verificación: smutbmB+

Firmado por: JESSEL AYRA PLASENCIA  
UNIVERSIDAD DE LA LAGUNA

Fecha: 30/11/2020 12:24:14

María de las Maravillas Aguiar Aguiar  
UNIVERSIDAD DE LA LAGUNA

08/02/2021 13:50:06



Este documento incorpora firma electrónica, y es copia auténtica de un documento electrónico archivado por la ULL según la Ley 39/2015.  
*Su autenticidad puede ser contrastada en la siguiente dirección <https://sede.ull.es/validacion/>*

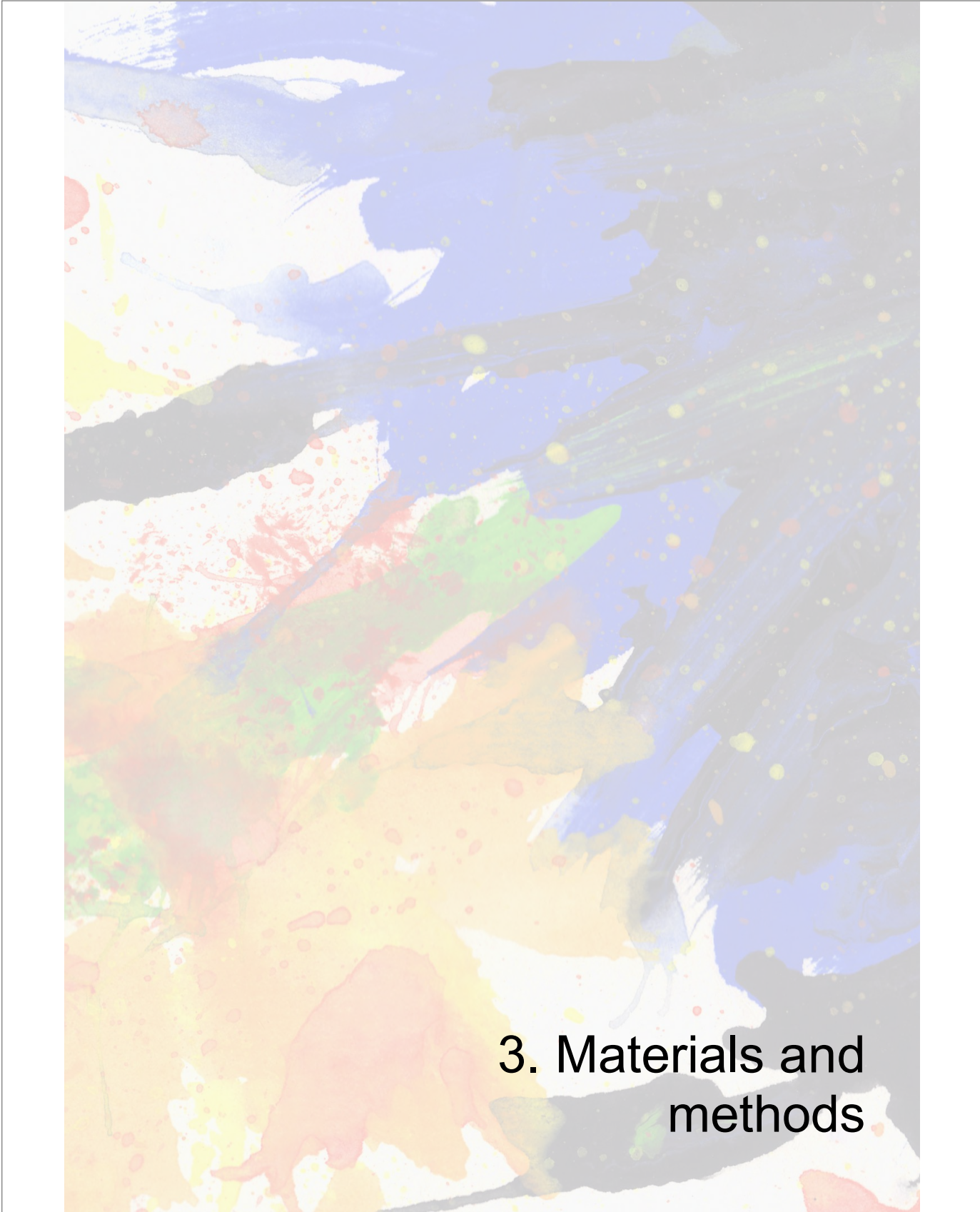
Identificador del documento: 3075810      Código de verificación: smutbmB+

Firmado por: JESSEL AYRA PLASENCIA  
UNIVERSIDAD DE LA LAGUNA

Fecha: 30/11/2020 12:24:14

María de las Maravillas Aguiar Aguiar  
UNIVERSIDAD DE LA LAGUNA

08/02/2021 13:50:06



### 3. Materials and methods

Este documento incorpora firma electrónica, y es copia auténtica de un documento electrónico archivado por la ULL según la Ley 39/2015.  
*Su autenticidad puede ser contrastada en la siguiente dirección <https://sede.ull.es/validacion/>*

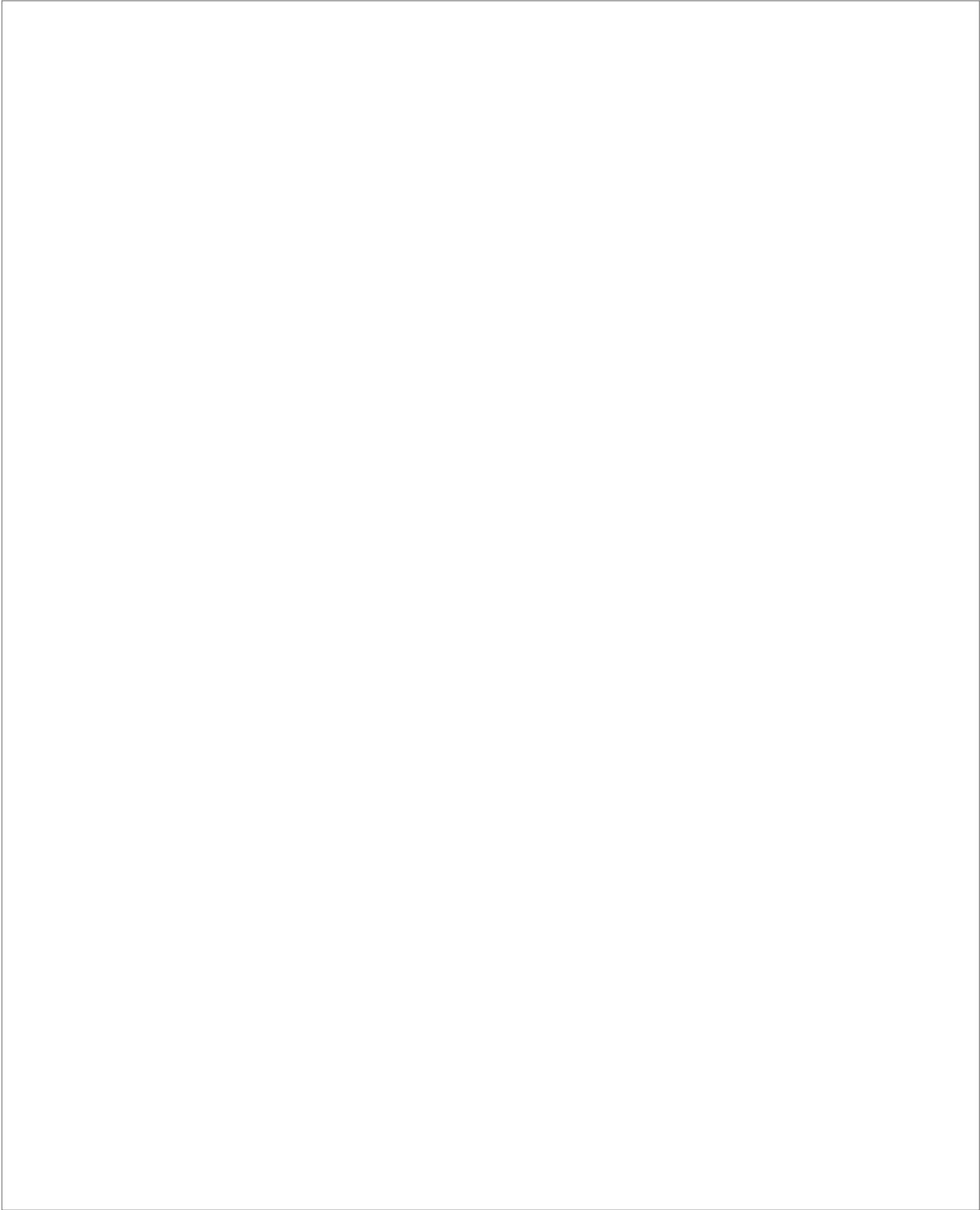
Identificador del documento: 3075810 Código de verificación: smutbmB+

Firmado por: JESSEL AYRA PLASENCIA  
UNIVERSIDAD DE LA LAGUNA

Fecha: 30/11/2020 12:24:14

María de las Maravillas Aguiar Aguiar  
UNIVERSIDAD DE LA LAGUNA

08/02/2021 13:50:06



Este documento incorpora firma electrónica, y es copia auténtica de un documento electrónico archivado por la ULL según la Ley 39/2015.  
*Su autenticidad puede ser contrastada en la siguiente dirección <https://sede.ull.es/validacion/>*

Identificador del documento: 3075810      Código de verificación: smutbmB+

Firmado por: JESSEL AYRA PLASENCIA  
UNIVERSIDAD DE LA LAGUNA

Fecha: 30/11/2020 12:24:14

María de las Maravillas Aguiar Aguiar  
UNIVERSIDAD DE LA LAGUNA

08/02/2021 13:50:06

### 3.1. Yeast cultures

#### 3.1.1. Strains used in this work

The following table contains the list of *Saccharomyces cerevisiae* strains used to develop this work. Genetic backgrounds are either W303 (Thomas & Rothstein, 1989) or derived from YPH499 (Sikorski & Hieter, 1989).

**Table 3.1. List of strains used in this work.**

<b>Strain</b>	<b>Relevant Genotype</b>	<b>Origin</b>
<b>AS499 (YPH499)</b>	<i>MATa ura3-52 lys2-801 ade2-101 trp1-Δ63 his3-Δ200 leu2-Δ1 bar1-Δ</i>	A. Strunnikov <sup>a</sup>
<b>FM593</b>	<i>AS499; ade2-101:TetR-YFP:ADE2; cXIIr (194 kb):tetOs:HIS3; cdc15-2:9myc:Hph</i>	F. Machín (Quevedo et al., 2012)
<b>FM588</b>	<i>AS499; ade2-101:TetR-YFP:ADE2; cXIIr (1061 kb):tetOs:HIS3; cdc15-2:9myc:Hph</i>	F. Machín (García-Luis & Machín, 2014)
<b>FM2329</b>	FM593; <i>RAD53:6HA:KanMX4</i>	This work
<b>FM2323</b>	FM593; <i>SIC1:6HA:KanMX4</i>	This work
<b>FM2354</b>	FM593; <i>HTA2:mCherry:KanMX6</i>	This work
<b>FM2301</b>	FM593; <i>NET1:eCFP:KanMX4</i>	This work
<b>FM2381</b>	<i>AS499; ura3-52:GFP:TUB1:URA3; cdc15-2:9myc:Hph</i>	This work
<b>FM2316</b>	FM593; <i>SPC42:mCherry:KanMX6</i>	This work
<b>FM2317</b>	FM593; <i>CIN8:mCherry:KanMX6</i>	This work
<b>FM2335</b>	FM593; <i>CIN8:9myc:natNT2</i>	This work
<b>FM916</b>	FM588; <i>Δrad9::natMX</i>	This work
<b>FM2477</b>	FM916; <i>SIC1:6HA:KanMX4</i>	This work
<b>FM567</b>	<i>MATa trp1-1 his3-11,15 leu2-3,112; Telomere cV-L:tetO:LEU2; ade2-1:URAp-TetR-YFP:ADE2; Telomere cV-R:lacO:TRP1; ura3-1:HISp-CFP-lacI:URA3; cdc15-2:9myc:Hph</i>	F. Machín (Quevedo et al., 2012), b
<b>FM2448 (W303)</b>	<i>MATa leu2-3,112 trp1-1 can1-100 ura3-1 ade2-1 his3-11,15 RAD5; cdc15-2</i>	This work
<b>LSY3902</b>	W303; <i>MATa lys2::GAL-I-Scel; Ura3:tetO; Leu2-LacO(YEL023C); HIS3-YFP-LacI; TetR-RFP; RAD52-CFP</i>	L.S. Symington (Oh et al., 2018)

Este documento incorpora firma electrónica, y es copia auténtica de un documento electrónico archivado por la ULL según la Ley 39/2015.  
 Su autenticidad puede ser contrastada en la siguiente dirección <https://sede.ull.es/validacion/>

Identificador del documento: 3075810 Código de verificación: smutbmB+

Firmado por: JESSEL AYRA PLASENCIA  
 UNIVERSIDAD DE LA LAGUNA

Fecha: 30/11/2020 12:24:14

María de las Maravillas Aguiar Aguilár  
 UNIVERSIDAD DE LA LAGUNA

08/02/2021 13:50:06

3. Materials and Methods

<b>FM2456*</b>	W303; <i>MATa lys2::GAL-I-SceI; Ura3-tetO; Leu2-LacO(YEL023C); HIS3-YFP-LacI; TetR-RFP; cdc15-2</i>	This work <sup>b</sup>
<b>FM889</b>	FM588; $\Delta rad52::KanMX$	F. Machín <sup>(García-Luis &amp; Machín, 2014)</sup>
<b>LG2055</b>	W303; <i>MATa <math>\Delta cin8::ura3MX; leu2-3,112::CIN8-3GFP-LEU2</math></i>	Gift from Larisa Gheber
<b>LG2058</b>	W303; <i>MATa <math>\Delta cin8::ura3MX; leu2-3,112::CIN8-3A-3GFP-LEU2</math></i>	Gift from Larisa Gheber
<b>LG2575</b>	W303; <i>MATa <math>\Delta cin8::ura3MX; leu2-3,112::CIN8-3D-3GFP-LEU2</math></i>	Gift from Larisa Gheber
<b>FM2505*</b>	W303; <i>MATa <math>\Delta cin8::ura3MX; leu2-3,112::CIN8-3GFP-LEU2; cdc15-2</math></i>	This work
<b>FM2506*</b>	W303; <i>MATa <math>\Delta cin8::ura3MX; leu2-3,112::CIN8-3A-3GFP-LEU2; cdc15-2</math></i>	This work
<b>FM2507*</b>	W303; <i>MATa <math>\Delta cin8::ura3MX; leu2-3,112::CIN8-3D-3GFP-LEU2; cdc15-2</math></i>	This work
<b>FM1293</b>	AS499; <i>cdc15-2:9myc:Hph</i>	This work
<b>FM2461</b>	FM1293; $\Delta cin8::HIS3MX4$	This work
<b>FM2465</b>	FM593; <i>CIN8:AID*:9myc:KanMX</i>	This work
<b>FM2466</b>	FM2465; <i>ura3-52::ADH1-OsTIR1-9myc:URA3</i>	This work
<b>FM2473</b>	FM2466; $\Delta kip1::HIS3MX4$	This work
<b>FM2302</b>	AS499; <i>CDC14:GFP:KanMX; cdc15-2:9myc:Hph</i>	This work
<b>FM518</b>	AS499; <i>ade2-101:TetR-YFP:ADE2; cXIIr(487kb):tetOs:HIS3; cdc14-1:9myc:TRP1</i>	F. Machín <sup>(Quevedo et al., 2012)</sup>
<b>FM2478</b>	FM518; <i>CIN8:9myc:KanMX4</i>	This work
<b>FM2449*</b>	W303; <i>MATa <math>\Delta hml HMR; pFM309^*; cdc15-2</math></i>	This work
<b>FM2450*</b>	W303; <i>MATa <math>\Delta hml \Delta hmr; pFM309^*; cdc15-2</math></i>	This work
<b>FM2520</b>	FM2450; <i>SCC1:3myc:HIS3MX</i>	This work
<b>FM2625</b>	FM588; <i>smc1::SMC1-AID*:9myc:KanMX</i>	This work
<b>FM2626</b>	FM588; <i>smc3::SMC3-AID*:9myc:KanMX</i>	This work
<b>FM2627</b>	FM2625; <i>ura3-52::ADH1-OsTIR1-9myc:URA3</i>	This work
<b>FM2628</b>	FM2626; <i>ura3-52::ADH1-OsTIR1-9myc:URA3</i>	This work

54

Este documento incorpora firma electrónica, y es copia auténtica de un documento electrónico archivado por la ULL según la Ley 39/2015.  
 Su autenticidad puede ser contrastada en la siguiente dirección <https://sede.ull.es/validacion/>

Identificador del documento: 3075810 Código de verificación: smutbmB+

Firmado por: JESSEL AYRA PLASENCIA  
 UNIVERSIDAD DE LA LAGUNA

Fecha: 30/11/2020 12:24:14

María de las Maravillas Aguiar Aguiar  
 UNIVERSIDAD DE LA LAGUNA

08/02/2021 13:50:06



3. Materials and Methods

<b>FM2633</b>	FM588; <i>scc1::SCC1-AID*-9myc:KanMX</i>	This work
<b>FM2634</b>	FM2633; <i>ura3-52::ADH1-OsTIR1-9myc:URA3</i>	This work
<b>FM2531</b>	FM1293; <i>pFM309*</i>	This work
<b>FM2662</b>	FM2531; <i>Δrad9::KanMX4</i>	This work
<b>FM2663</b>	FM2531; <i>Δyku70::KanMX4</i>	This work
<b>FM2672</b>	FM2531; <i>smc3::SMC3-AID*-9myc:KanMX</i>	This work
<b>FM2680</b>	FM2672; <i>ura3-52::ADH1-OsTIR1-9myc:URA3</i>	This work
<b>FM2684</b>	FM2531; <i>MSC1-eYFP:KanMX4</i>	This work
<b>FM2688</b>	FM2531; <i>Δmre11::kITRP1</i>	This work

<sup>a</sup> Parental strain; a *bar1Δ* derivative of YPH499, congenic to S288C.

<sup>b</sup> These strains carry *lacI*-YFP and *lacI*-CFP as fluorescent reporters along with TetR-RFP or TetR-YFP. *lacO*-based foci were unable to be detectable at 34 °C (used for the telophase arrest in *cdc15-2* strains).

\**pFM309* plasmid was inserted to express HO endonuclease under β-estradiol addition to the medium. See figure 3.1.a. for more details.

### 3.1.2. Strain construction

#### 3.1.2.1. Yeast transformation

The transformation protocol was slightly modified and adapted from (Janke et al., 2004; Knop et al., 1999). This version of the classical lithium acetate-based method implies working with pre-made frozen competent yeast stocks.

##### 3.1.2.1.1. Preparation of competent cells

For preparing competent cells, a single yeast colony was inoculated in 10 mL of YPD and grown overnight at 25 °C. The next day, 100 μL was transferred to a flask containing 40 mL of fresh YDP, letting the culture grow overnight until cells reached an OD<sub>600</sub> ~ 0.7 – 1.

Then, cells were harvested to discard the supernatant. The pellet was washed twice, once with 30 mL of sterile distilled water, and another with 10 mL of SORB solution. Finally, cells were resuspended in 350 μL of SORB solution and 50 μL of sonicated and denatured herring sperm DNA (serving as carrier DNA). Every competent yeast stock was stored at -80 °C until use.

55

Este documento incorpora firma electrónica, y es copia auténtica de un documento electrónico archivado por la ULL según la Ley 39/2015.  
 Su autenticidad puede ser contrastada en la siguiente dirección <https://sede.ull.es/validacion/>

Identificador del documento: 3075810 Código de verificación: smutbmB+

Firmado por: JESSEL AYRA PLASENCIA  
 UNIVERSIDAD DE LA LAGUNA

Fecha: 30/11/2020 12:24:14

María de las Maravillas Aguiar Aguiar  
 UNIVERSIDAD DE LA LAGUNA

08/02/2021 13:50:06

### 3. Materials and Methods

#### 3.1.2.1.2. Transformation procedure

Firstly, the competent stocks were thawed on ice. Then, 40 µL of cells and 10 µL of DNA (either directly obtained from a PCR or an enzymatic digestion) were mixed in a new Eppendorf tube. A six-fold volume of PEG solution was added before incubation at room temperature for 30 minutes.

After that, 1/9 volumes of DMSO were supplemented before incubation in a water bath at 42 °C for 15 minutes. Following this waiting time, cells were harvested by centrifugation before applying the appropriate resuspending and seeding method:

- **Auxotrophic markers:** The pellet was resuspended in 300 µL of distilled milli-Q water. Then, the cells were directly seeded on the corresponding minimum media.
- **Xenobiotic-resistance markers:** The pellet was resuspended in 300 µL of YPD and incubated at room temperature for at least 2 hours. This time is enough to express the resistance gene product before putting the cells in contact with the antibiotic (see section 3.1.3.3).

#### 3.1.2.2. Crossing method

In some cases, it was necessary to sporulate diploids and dissect tetrads for isolating new strains.

Most of the used lab yeast strains are homothallic, that is, mutants for HO endonuclease. This fact allows a stable propagation as haploids of a specific mating-type (a or alpha). When it is required, two different mating-type strains can fuse and form a heterozygous diploid. This new strain is susceptible to go through meiosis and generate four spores.

The procedure consists of four steps: i) to get a diploid from two haploid strains, ii) to force diploid cells to undergo meiosis, iii) to isolate independent spores, and iv) to select the corresponding haploid.

##### 3.1.2.2.1. Diploid generation

Two haploid strains (bearing the desired gene modifications and presenting different mating types) are required to create a diploid. Both target haploid strains were mixed as a patch on one edge of a YPDA plate. Then, an inoculating loop was used to streak three independent lines from this patch. This fact involves the progressive dilution of the initial inoculum, making easier the zygote isolation. Then, the plate was incubated at 25 °C for 2 hours. Next, 3 – 4 independent zygotes were separated by using a dissection microscope. Zygotes are easily

56

Este documento incorpora firma electrónica, y es copia auténtica de un documento electrónico archivado por la ULL según la Ley 39/2015.  
Su autenticidad puede ser contrastada en la siguiente dirección <https://sede.ull.es/validacion/>

Identificador del documento: 3075810 Código de verificación: smutbmB+

Firmado por: JESSEL AYRA PLASENCIA  
UNIVERSIDAD DE LA LAGUNA

Fecha: 30/11/2020 12:24:14

María de las Maravillas Aguiar Aguiar  
UNIVERSIDAD DE LA LAGUNA

08/02/2021 13:50:06

### 3. Materials and Methods

differentiable from cycling cells by their morphology. Once done, incubation at 25 °C was extended for two days.

#### 3.1.2.2.2. Sporulation

Diploid strains of *Saccharomyces cerevisiae* can go through meiosis. This process generates an ascus containing four genetically different and stress-resistant spores.

For promoting this event, diploids need to be under nitrogen starvation and poor carbon source conditions (Neiman, 2011). Thus, a sample of each pre-isolated diploid colony was seeded on a nutrient-deficient plate (composed of yeast extract 0.1 % w/v, potassium acetate 1 % w/v, bacto agar 1.5 % w/v, and glucose 0.05 % w/v), and incubated for two days at 25 °C.

#### 3.1.2.2.3. Tetrad dissection

The next step entails the ascus wall degradation. This step is necessary to ease the spore isolation. For doing that, a small portion of tetrads was scraped up and resuspended in 10 µL of digestion solution (1 mg·mL<sup>-1</sup> of Zymolyase in 1 M sorbitol). The mix was incubated at room temperature for 1 minute.

Next, 100 µL of sterile and double-distilled water was added to stop the reaction. A sample of 13 µL was then taken out and placed next to one edge of a YPDA plate. The dish was carefully inclined, letting the drop fall and creating a straight line through the medium.

Once the sample dried out, every spore was manually and accurately isolated with the dissection microscope. After incubation at 25 °C for three days, 96 genetically different haploid colonies were obtained on each plate.

#### 3.1.2.2.4. Replica plating

Every new independent haploid clone contains a different genotype. Replica plating helps transfer all colonies to other selective mediums in the same position as the master plate. Each new replicated plate provides a "growth/no growth" pattern dependent on the haploids genotype. This way, the selection of the desired strain becomes straightforward.

For doing this, a sterile velvet was attached to a cylindrical plastic block with a metal ring. After that, the master plate was placed on the top. Some pressure was made to transfer the colonies to the velvet. Then, the same was done with every selective plate required to determine the correct genotype. Finally, the haploid analysis and selection were performed after incubation at 25 °C for three days.

57

Este documento incorpora firma electrónica, y es copia auténtica de un documento electrónico archivado por la ULL según la Ley 39/2015.  
Su autenticidad puede ser contrastada en la siguiente dirección <https://sede.ull.es/validacion/>

Identificador del documento: 3075810 Código de verificación: smutbmB+

Firmado por: JESSEL AYRA PLASENCIA  
UNIVERSIDAD DE LA LAGUNA

Fecha: 30/11/2020 12:24:14

María de las Maravillas Aguiar Aguiar  
UNIVERSIDAD DE LA LAGUNA

08/02/2021 13:50:06

### 3. Materials and Methods

#### 3.1.3. Cultures conditions

##### 3.1.3.1. Storage and maintenance

All the strains were stored in YPD plus 20 % of glycerol at -80 °C in cryogenic tubes. Before every protocol, the cells were grown on YPDA plates for at least two days. The incubation was always performed at 25 °C since all employed strains were thermosensitive for Cdc15 kinase protein.

When required, the resulting colonies were used to prepare liquid cultures. For every experiment, the cells were cultured in YPD overnight with moderate shaking (180 rpm), unless stated otherwise. The next day, 100 µL of grown cells were diluted into a flask containing an appropriate YPD volume. Then, the incubation was prolonged overnight at 25 °C again.

Finally, the day after, exponentially growing cells were adjusted to  $OD_{600} = 0.5$  to start the experiment.

##### 3.1.3.2. Experimental conditions

Most of the experiments were made to compare how the cells react to DSBs in different cell cycle stages. For this reason, every procedure was followed by DSBs generation for 1 to 3 hours. Two methods were employed:

- **Phleomycin:** It is an intercalating agent of the bleomycin family. It binds to DNA and destroys its integrity, generating randomly distributed DSBs (Moore, 1989). When used,  $10 \mu\text{g}\cdot\text{mL}^{-1}$  was added to the culture for 1 to 3 hours.
- **Sequence-specific endonucleases:** It is a method that allows to create a single localized DSB. It is based on the specific recognition of DNA sequences by endonucleases, such as:
  - **HO endonuclease:** It is a site-specific endonuclease that creates a break at the MAT locus to switch the mating-type in heterothallic strains (Kostriken et al., 1983; Strathern et al., 1982). For this reason, many lab yeast strains are mutants for the *ho* gene. However, this protein has become a handy tool to study DSBs repair. Genetic engineering has generated replicative and integrative plasmids for transcribing and translating HO endonuclease conditionally. In this work, an integrative system based on a  $\beta$ -Estradiol-inducible promoter was employed (plasmid pFM309) (Fig. 3.1) (Ottoz et al., 2014). Then, HO was expressed through the addition of 2 µM of  $\beta$ -Estradiol for 1 to 3 hours.

58

Este documento incorpora firma electrónica, y es copia auténtica de un documento electrónico archivado por la ULL según la Ley 39/2015.  
Su autenticidad puede ser contrastada en la siguiente dirección <https://sede.ull.es/validacion/>

Identificador del documento: 3075810 Código de verificación: smutbmB+

Firmado por: JESSEL AYRA PLASENCIA  
UNIVERSIDAD DE LA LAGUNA

Fecha: 30/11/2020 12:24:14

María de las Maravillas Aguiar Aguiar  
UNIVERSIDAD DE LA LAGUNA

08/02/2021 13:50:06

3. Materials and Methods

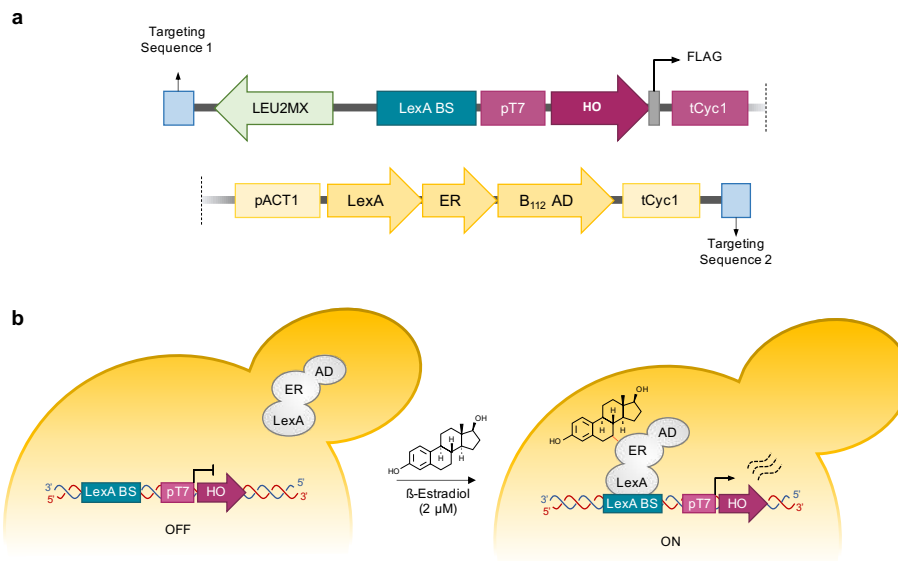


**Figure 3.1. Inserted cassette map and working mechanism for  $\beta$ -estradiol-mediated HO expression.** a) Scheme of the system to express HO. It is a linear fragment obtained from plasmid digestion with *AscI* restriction enzyme. Two homologous sequences for integration at the *leu2* locus flanks the cut DNA. *LEU2MX* cassette works as an auxotrophic marker. Flag-tagged HO endonuclease expression is silenced because of the presence of LexA binding sites sequences. Meanwhile, the constitutive *ACT1* promoter expresses a chimera formed by i) the LexA DNA binding protein, ii) the human estrogen receptor, and iii) the B<sub>112</sub> activation domain. b) Drawing of the mechanism of action. In standard growing conditions, HO endonuclease transcription is silenced. When  $\beta$ -Estradiol is added to the medium and joins the estrogen receptor, the chimera binds the LexA binding sites sequences and allows the HO translation. (Adapted from Ottoz et al., 2014). **LexA BS**: Lex A Binding Site. **pT7**: T7 promoter. **tCyc1**: *CYC1* terminator. **pACT1**: *ACT1* promoter. **ER**: Estrogen receptor. **B<sub>112</sub> AD**: B<sub>112</sub> Activation Domain.

- **I-SceI endonuclease**: It is a mitochondrial endonuclease whose primary function is the cleavage of intron-less genes at the site of intron insertion (Colleaux et al., 1986, 1986). It has also been widely used to study DNA DSBs repair mechanisms. For this work, a set of experiments was done with strains bearing an integrative construction of I-SceI under the Galactose promoter's control. When used, the cells were grown and duly arrested in YP medium + Raffinose (2 % w/v) as a carbon source. Then, I-SceI was induced by adding galactose (2 % w/v) for 1 to 3 hours. Finally, if required, expression was switched off through the glucose addition (2 % w/v).

Este documento incorpora firma electrónica, y es copia auténtica de un documento electrónico archivado por la ULL según la Ley 39/2015.  
 Su autenticidad puede ser contrastada en la siguiente dirección <https://sede.ull.es/validacion/>

Identificador del documento: 3075810 Código de verificación: smutbmB+

Firmado por: JESSEL AYRA PLASENCIA  
 UNIVERSIDAD DE LA LAGUNA

Fecha: 30/11/2020 12:24:14

María de las Maravillas Aguiar Aguiar  
 UNIVERSIDAD DE LA LAGUNA

08/02/2021 13:50:06

### 3. Materials and Methods

#### 3.1.3.2.1. Asynchronous to G<sub>1</sub> arrest

Asynchronous cultures were synchronized in G<sub>1</sub> by adding 50 ng·mL<sup>-1</sup> of  $\alpha$ -factor pheromone to the medium for 3 hours (Fig. 3.2).

All the strains used for these experiments were *bar1* $\Delta$ . Bar1 protease cleavages and inactivates the pheromone at the periplasmic space (Sprague et al., 1983). Its deletion allows long and efficient incubations by using a small  $\alpha$ -factor concentration.

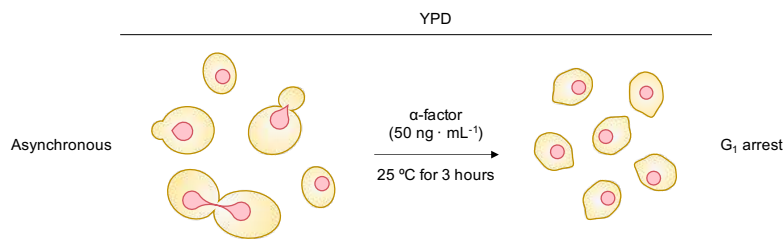


**Figure 3.2. Schematic of the experiment of the G<sub>1</sub> block.**  
Yellow color points to the cell cytoplasm. Pink shapes represent nuclei.

For specific experiments, it was necessary to release the cells from the G<sub>1</sub> block into a synchronous cell cycle. Thus, the previously arrested culture was centrifuged and washed twice with sterile water. Finally, the cells were resuspended in fresh YPD containing 0.1 mg·mL<sup>-1</sup> of Pronase E. The Pronase E addition (a protease mixture of endo- and exonucleases that hydrolyzes glycoprotein-peptide linkages) addresses the lack of Bar1 protein.

#### 3.1.3.2.2. Asynchronous to S arrest

The S phase is the period of the cell cycle when DNA is replicated. To produce a block in this stage, it becomes essential to interfere with this biological process.

There exist some chemicals reagents that inhibit replication by distinct pathways, such as hydroxyurea (HU) and methyl methanesulphonate (MMS).

HU inhibits DNA synthesis through the inactivation of the ribonucleotide reductase protein (Jw, 1992). On the other hand, MMS (which is an alkylating agent) leads to the formation of stalled replication forks that also inhibit the replication (Lundin et al., 2005).

For experiments in the S phase, cycling cells were incubated at 25 °C for 3 hours in the presence of either 0.2 M HU, either 0.01 % (v/v) MMS (Fig. 3.3).

3. Materials and Methods

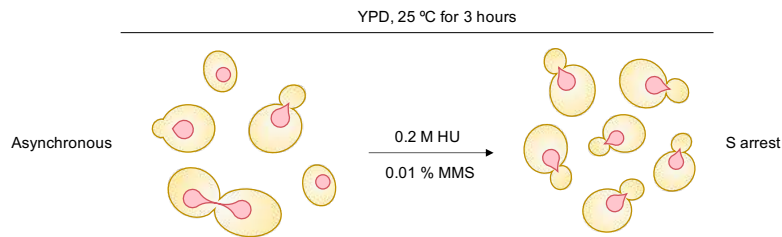


**Figure 3.3. Schematic of the experiment of the S block.**  
 Yellow color points to the cell cytoplasm. Pink shapes represent nuclei.

**3.1.3.2.3. Asynchronous to G<sub>2</sub> arrest**

There exist several methods to get a block in the G<sub>2</sub> phase. Some rely on inactivating clue proteins that promote the metaphase-to-anaphase transition, i.e., Cdc20 mutant alleles.

In this work, the G<sub>2</sub> block was performed by using nocodazole, which is a microtubule-depolymerizing drug. So, the cells finish the DNA replication but are unable to complete the segregation.

When required, asynchronous cells were arrested in the G<sub>2</sub> phase by adding 15 µg·mL<sup>-1</sup> of nocodazole and incubating for 3 hours. It is important to note that after 2 hours, additional nocodazole (7.5 µg·mL<sup>-1</sup>) was supplemented to reinforce the arrest (Fig. 3.4).

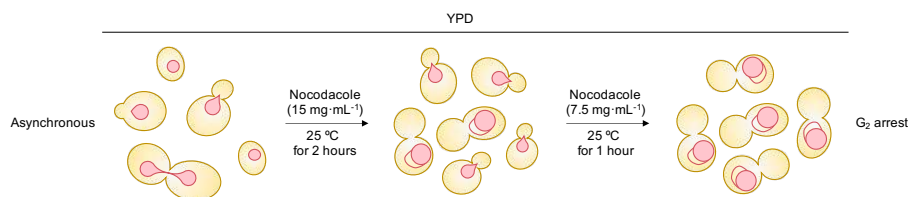


**Figure 3.4. Schematic of the experiment of the G<sub>2</sub> block.**  
 Yellow color points to the cell cytoplasm. Pink shapes represent nuclei.

**3.1.3.2.4. Asynchronous to telophase arrest**

The best technique to stably arrest yeast cells in telophase is through mutant proteins for the MEN, such as Cdc14 phosphatase or Cdc15 protein kinase.

Every strain in this thesis carried the *cdc15-2* thermosensitive allele. So, the cultures were blocked in telophase by only incubating the cells at 34 – 37 °C for 3 hours (Fig. 3.5).

Este documento incorpora firma electrónica, y es copia auténtica de un documento electrónico archivado por la ULL según la Ley 39/2015.  
 Su autenticidad puede ser contrastada en la siguiente dirección <https://sede.ull.es/validacion/>

Identificador del documento: 3075810 Código de verificación: smutbmB+

Firmado por: JESSEL AYRA PLASENCIA  
 UNIVERSIDAD DE LA LAGUNA

Fecha: 30/11/2020 12:24:14

María de las Maravillas Aguiar Aguiar  
 UNIVERSIDAD DE LA LAGUNA

08/02/2021 13:50:06

### 3. Materials and Methods

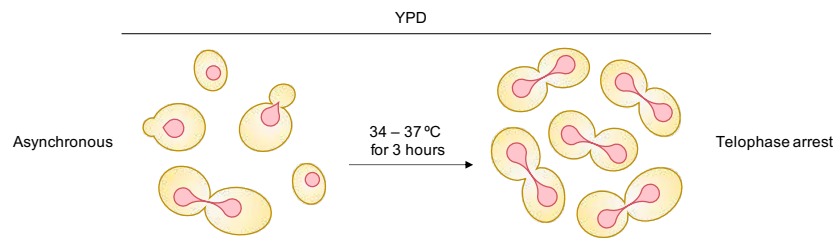


**Figure 3.5. Schematic of the experiment of the telophase block.**  
Yellow color points to the cell cytoplasm. Pink shapes represent nuclei.

Some specific experiments required a release into a new cell cycle. For achieving this goal, telophase-blocked cells were incubated again at 25 °C for 3 hours in fresh YPD. Thus, Cdc15-2 restored its activity and promoted the MEN.

Furthermore, when the accumulation of Sic1 (a specific inhibitor of mitotic cyclins) was the subject of study, 50 ng·mL<sup>-1</sup> of  $\alpha$ -factor pheromone was added to the medium at the time of shifting down the temperature to 25 °C.

#### 3.1.3.2.5. Auxin-mediated protein degradation

A set of experiments required the conditional depletion of proteins before DNA double-strand breaks generation.

The used method was the auxin-inducible degron (AID) (Morawska & Ulrich, 2013). This system works through the addition of the plant hormone auxin to the cell culture. This way, the auxin-binding receptor (TIR1), which is translated constitutively, targets the AID-tagged proteins for degradation by the proteasome.

When necessary, cells were treated with 5 – 8 mM of indoleacetic acid (IAA) for 1 hour at 34 – 37 °C. This time was enough to degrade >80 % of the protein of interest. Then, DSBs were created.

#### 3.1.3.2.6. Clonogenic assays

The clonogenic assay is used to determine the survival rate of a cell population. It works by plating a known number of cells after a specific treatment. Then, the number of grown colonies is compared to that obtained in the control plate.

For this work, cells from specific experiments were subjected to 1:10,000 dilutions. Finally, 100  $\mu$ L was spread onto YPDA plates and incubated at 25 °C for three days.



### 3.1.3.3. Transformant cells

After the transformation procedure (section 3.1.2.1.), transformant cells were plated on a solid selective medium according to the marker used for selection.

For auxotrophic genes, the cells were seeded on Synthetic Complete (SC) medium lacking particular amino acids or nucleotides. This media was prepared by mixing Yeast Nitrogen Base (YNB) and a dropout of amino acids and nucleotides. Glucose (2 % w/v) was chosen as the carbon source. In the case of xenobiotic-resistance markers, cells were plated on YPDA supplemented with the right antibiotic. The working concentration for each one is listed in the following table.

**Table 3.2. Stock and final concentrations of used antibiotics for selection.**

<i>Antibiotic</i>	<i>Stock concentration</i>	<i>Final concentration</i>
<b>Hygromycin (Hph)</b>	50 mg·mL <sup>-1</sup>	300 µg·mL <sup>-1</sup>
<b>Nourseothricin (Nat)</b>	200 mg·mL <sup>-1</sup>	100 µg·mL <sup>-1</sup>
<b>Ampicillin</b>	50 mg·mL <sup>-1</sup>	50 µg·mL <sup>-1</sup>
<b>Geneticin (G-418)</b>	50 mg·mL <sup>-1</sup>	200 µg·mL <sup>-1</sup>

## 3.2. Cell cultures

The last part of this thesis assessed whether yeast phenotypes were reproducible in human cells.

For this reason, Henrietta Lacks' cervix epithelial cancer cells (HeLa cell line) were employed as a eukaryotic model, taking into account the differences between the model organism and the higher eukaryotes.

### 3.2.1. Culture conditions

#### 3.2.1.1. Cryopreservation and cell recovery

The cell line was stored in Fetal Bovine Serum (FBS) + 10 % of DMSO at -80 °C in cryovial tubes. Before the experiments, HeLa cells were defrosted from liquid nitrogen in a water bath at 37 °C. Then, 150 µL were diluted into a flask containing 5 mL of growing medium. The cell culture media was composed of Dulbecco's Modified Eagle Medium (DMEM) containing high glucose and L-glutamine, 10 % FBS, and 1 % penicillin-streptomycin mix solution. Once done, the flask was maintained at 37 °C in a humidified 5 % CO<sub>2</sub> incubator for two days.

### 3. Materials and Methods

Since HeLa cells are subconfluent, it was necessary to perform cell passaging every three days. For doing that, the old medium was discarded, and the cells were washed twice with a pre-warm PBS 1x solution. Then, 2 mL of "detaching solution" (0.5 % Trypsin in 1 X EDTA) were added following incubation at room temperature for 3 minutes. After checking the cell detachment under the microscope, the reaction was stopped by dissolving the cells in 2 mL of full growth media. After centrifugation at 1,500 rpm for 5 minutes, the liquid phase was replaced by 3 mL of fresh medium. The cell pellet was gently resuspended by pipetting up and down several times. Finally, 150  $\mu$ L was diluted in a new flask containing 5 mL of cell culture media.

#### 3.2.1.2. Experimental conditions

Experiments in human cells were developed to create DSBs in telophase exclusively. It was unable to employ  $\gamma$ -irradiation, so phleomycin ( $50 \mu\text{g}\cdot\text{mL}^{-1}$ ) was used instead.

Blocking human cells in anaphase/telophase is more challenging than yeast. Due to these stages' short duration, the index of cells transiting late mitosis can be increased by first synchronizing the culture in previous phases, such as in S and prometaphase. The employed method is a modified protocol from (Matsui et al., 2012; Wee & Wang, 2017).

##### 3.2.1.2.1. Asynchronous to S phase arrest

The method consists of interfering with the DNA replication process through the addition of thymidine. This pyrimidine deoxynucleoside interrupts the nucleotide metabolism pathway at high concentrations through competitive inhibition, leading to an early S phase arrest.

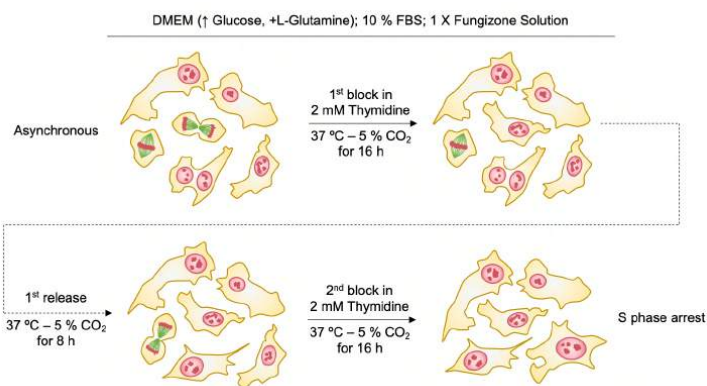


**Figure 3.6. Schematic of the experiment of S phase arrest in HeLa cells.**  
 Yellow points to the cytoplasm. Red shapes represent chromosomes. Green shows microtubules.

3. Materials and Methods

Healthy grown HeLa cells were incubated in culture media supplemented with 2 mM of thymidine for 16 hours. After washing twice with 1x PBS and replacing the medium, the cells were released for 8 hours. Finally, a second treatment of 2 mM of thymidine for 16 hours was performed again to induce a more uniform arrest (Fig. 3.6).

**3.2.1.2.2. S phase arrest to prometaphase arrest**

After the second block in the early S phase, the thymidine-containing medium was washed away. Then, the cells were released for 9 hours to replicate the DNA. After this time, 20 ng·mL<sup>-1</sup> of nocodazole was supplemented for 5 hours to promote a synchronous arrest in prometaphase (Fig. 3.7).

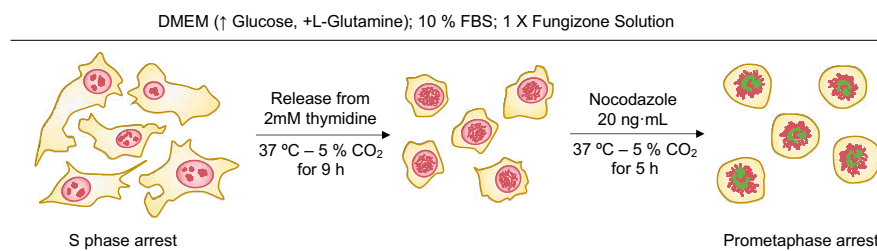


**Figure 3.7. Schematic of the experiment of prometaphase arrest in HeLa cells.**  
 Yellow points to the cytoplasm. Red shapes represent chromosomes. Green shows microtubules.

**3.2.1.2.3. Prometaphase arrest to anaphase/telophase arrest**

Finally, prometaphase arrested cells were released from nocodazole for 1 hour. After 20 minutes from the release, the specific myosin inhibitor (S)-(-)-Blebbistatin (50 μM) (Toronto Research Chemicals) was added to the medium. This drug delays the cytokinesis and increases the proportion of cells transiting anaphase/telophase (Fig. 3.8).

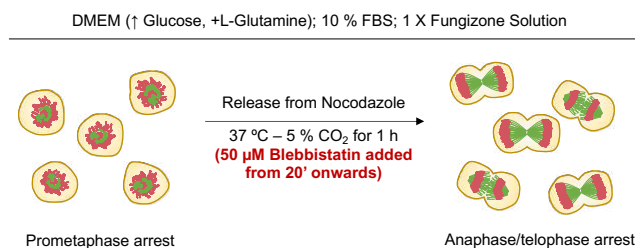


**Figure 3.8. Schematic of the experiment of anaphase/telophase arrest in HeLa cells**  
 Yellow points to the cytoplasm. Red shapes represent chromosomes. Green shows microtubules.

Este documento incorpora firma electrónica, y es copia auténtica de un documento electrónico archivado por la ULL según la Ley 39/2015.  
 Su autenticidad puede ser contrastada en la siguiente dirección <https://sede.ull.es/validacion/>

Identificador del documento: 3075810 Código de verificación: smutbmB+

Firmado por: JESSEL AYRA PLASENCIA  
 UNIVERSIDAD DE LA LAGUNA

Fecha: 30/11/2020 12:24:14

María de las Maravillas Aguiar Aguiar  
 UNIVERSIDAD DE LA LAGUNA

08/02/2021 13:50:06

### 3. Materials and Methods

## 3.3. DNA techniques

### 3.3.1. DNA preparations

Most of the employed methods for this thesis relied on different DNA preparations. Some of them were used for obtaining DNA to transform with, and many others were performed to study cellular processes *in vitro*.

#### 3.3.1.1. Genomic DNA extractions from *Saccharomyces cerevisiae*

##### 3.3.1.1.1. Mechanical method

The genomic DNA was obtained from liquid cultures and colonies. In liquid cultures, 5 mL of growing cells were centrifuged at maximum speed for 1 minute. Then, the supernatant was discarded. After that, the pellet or the colonies directly taken from plates were resuspended in 200  $\mu$ L of breaking buffer in a 1.5 mL tube.

Next, 200  $\mu$ L of ice-cold phenol:chloroform:isoamyl alcohol (25:24:1) and ~ 200 mg of glass beads were added, proceeding to vortex for 4 minutes. For separating the organic and aqueous layers, 200  $\mu$ L of 1x TE buffer was added, and the sample was centrifuged at 13,000 rpm at room temperature for 5 minutes.

The top aqueous layer was transferred to a new 1.5 mL tube and mixed with 1 mL of ice-cold ethanol 100 %. The DNA was precipitated by incubation in a nutator for 10 minutes at room temperature. Next, the sample was centrifuged for 2 minutes and the supernatant was carefully aspirated. The DNA pellet was desiccated (in an Eppendorf Vacufuge Concentrator) and resuspended in 50  $\mu$ L of 1x TE buffer. Finally, the sample was stored at 4 °C until use.

##### 3.3.1.1.2. Lytic method

This method was performed to maintain the DNA integrity and avoid the glass beads-mediated chromosomes breakage. For proceeding, a sample of 10 mL of growing yeast cells was centrifuged at 2,500 rpm for 3 minutes. The cell lysis was then performed by incubating the pellet in 500  $\mu$ L of digestion buffer for 5 minutes (40 units of Zymolyase 100T (Zymoresearch) in 1 % SDS, 100 mM NaCl, 50 mM Tris-HCl, and 10 mM EDTA).

Once the digestion was confirmed under the microscope, DNA was isolated by phenol:chloroform:isoamyl alcohol (25:24:1) as in the mechanical method (see section 3.3.1.1.1). After desiccation, the DNA pellet was resuspended in 10  $\mu$ L of 5 M of ammonium acetate and 340  $\mu$ L of 1x TE containing 10  $\mu$ g·mL<sup>-1</sup> RNase A. The sample was incubated at room temperature for 15 minutes, and a second ice-cold ethanol 100 % precipitation was

66

Este documento incorpora firma electrónica, y es copia auténtica de un documento electrónico archivado por la ULL según la Ley 39/2015.  
Su autenticidad puede ser contrastada en la siguiente dirección <https://sede.ull.es/validacion/>

Identificador del documento: 3075810 Código de verificación: smutbmB+

Firmado por: JESSEL AYRA PLASENCIA  
UNIVERSIDAD DE LA LAGUNA

Fecha: 30/11/2020 12:24:14

María de las Maravillas Aguiar Aguiar  
UNIVERSIDAD DE LA LAGUNA

08/02/2021 13:50:06

3. Materials and Methods

performed. Finally, the purified DNA was resuspended in 70 µL of 1x TE and stored at 4 °C until use.

### 3.3.2. Polymerase chain reactions (PCRs)

#### 3.3.2.1. Primers

The following table shows the full list of primers used in this work. Most PCRs were done using the GoTaq 2<sup>®</sup> G2 Flexi DNA polymerase from Promega. For amplifications longer than 4 kb, PCR BIO High Fidelity polymerase from Biosigma was used instead. In all cases, the applied components and conditions were the ones recommended by the provider.

Table 3.3. List of primers and their DNA sequences used in this thesis.

<b>Primers for tagging genes in C-terminal</b>	
<b>Primer name*</b>	<b>Sequence (5' → 3')</b>
<b>CIN8-S2</b>	TAGTTTGAATATATATTCGACTGAAAGGCAATATCAACTAATCGATGAATTCGAGCTCG
<b>CIN8-S3</b>	TGTGGACAATGAGGGCTCGAGAAAAATGTTAAAGATTGAACGTACGCTGCAGGTCGAC
<b>HTA2-S2</b>	ACAAGAATGTTTGATTTGCTTTGTTTCTTTCAACTCAGTTCTTAATCGATGAATTCGAGCTCG
<b>HTA2-S3</b>	TTGCCAAAGAAGTCTGCCAAGACTGCCAAAGCTTCTCAAGAAGTCCGTACGCTGCAGGTCGAC
<b>MSC1-S2</b>	TTGGGGAGAAAAGTACATTACGTTGACACCCCAATCATTAAATCGATGAATTCGAGCTCG
<b>MSC1-S3</b>	TAACGTAAAAACTGGTGGAAAAGCATATTAGGGTTCAACCGTACGCTGCAGGTCGAC
<b>NET1-S2</b>	ACTAGCTTTCTGTGACGTGATTCTACTGAGACTTTCTGGTATCAATCGATGAATTCGAGCTCG
<b>NET1-S3</b>	CCAAGTGGTGGATTTGCATCATTAAAAAGATTTCAAGAAAAACGTACGCTGCAGGTCGAC
<b>NET1-S2</b>	ACTAGCTTTCTGTGACGTGATTCTACTGAGACTTTCTGGTATCAATCGATGAATTCGAGCTCG
<b>NET1-S3</b>	CCAAGTGGTGGATTTGCATCATTAAAAAGATTTCAAGAAAAACGTACGCTGCAGGTCGAC
<b>RAD53-S2</b>	AAAAGGGGCAGCATTTTCTATGGGTATTTGTCCTTGGTTAATCGATGAATTCGAGCTCG
<b>RAD53-S3</b>	GGACCAAACCTCAAAGGCCCGAGAATTTGCAATTTTCGCGTACGCTGCAGGTCGAC
<b>SCC1-S2</b>	ATCAGCTTATTGGGTCCACCAAGAAATCCCCTCGGCGTAACTAGGTTTTAATCGATGAATTCGA GCTCG
<b>SCC1-S3</b>	ATATTAATAATAGACGCCAAACCTGCACTATTTGAAAGGTTTATCAATGCTCGTACGCTGCAGGTC GAC
<b>SIC1-S2</b>	AAGTAAATAAAATATAATCGTTCAGAAACTTTTTTTTTTCATTTCTTCAATCGATGAATTCGAGCT CG
<b>SIC1-S3</b>	AAGTAAATAAAATATAATCGTTCAGAAACTTTTTTTTTTCATTTCTTCAATCGATGAATTCGAGCT CG
<b>SMC1-S2</b>	GTCGAAGATCATAACTTTGACTTGAGCAATTACGCAGAAGTACGCTGCAGGTCGAC
<b>SMC1-S3</b>	TTATTTGACGGTTATAGCAGAGTTGGTTTCATAGATTAATCGATGAATTCGAGCTCG
<b>SMC3-S2</b>	ACTGATATTTTATATACAAATCGTTTCAAATATCTTAATCGATGAATTCGAGCTCG
<b>SMC3-S3</b>	AATCGGATTCATTAGAGGTAGCAATAAATTCGCTGAAGTCCGTACGCTGCAGGTCGAC
<b>SPC42-S2</b>	AGAACGCTTTAAGAATGCGCCATACTCCTTAACGCTTTTTAAATCATCAATCGATGAATTCGAG CTCG
<b>SPC42-S3</b>	CTGAAAAATAATATGTCAGAAACATTGCAACTCCCACTCCCAATAATCGACGTACGCTGCAGGT CGAC

Este documento incorpora firma electrónica, y es copia auténtica de un documento electrónico archivado por la ULL según la Ley 39/2015.  
 Su autenticidad puede ser contrastada en la siguiente dirección <https://sede.ull.es/validacion/>

Identificador del documento: 3075810 Código de verificación: smutbmB+

Firmado por: JESSEL AYRA PLASENCIA  
 UNIVERSIDAD DE LA LAGUNA

Fecha: 30/11/2020 12:24:14

María de las Maravillas Aguiar Aguiar  
 UNIVERSIDAD DE LA LAGUNA

08/02/2021 13:50:06

3. Materials and Methods

**Primers to amplify WT genes and ORFs deletions cassettes**

<b>CIN8-F(-396)</b>	TCCCATTATTTTCAATCTG
<b>CIN8-R(+3444)</b>	GTAATATGCCGAAACTCAGC
<b>CDC14-F(-600)</b>	TTTACCACTACGAAATCTTGAGATCGG
<b>CDC14-R(+1900)</b>	TACGGTGAAGTTATTCCTAGGTACCAG
<b>CDC15-F(-132)</b>	TCTTCCGCTTTTCTTGCTG
<b>CDC15-R(+3023)</b>	TGCGTTTTTCAGTATTGGAAGG
<b>HML-F(-234)</b>	GGTTCTCATTGCGACTATTGG
<b>HML-R(+3836)</b>	CAATATACTTACAGAGACCT
<b>HTA2-F(-382)</b>	GAGAACACCGCTTTATTAGG
<b>HTA2-R (+732)</b>	CATGAAAAGGATGAAAATGG
<b>KIP1-F(-473)</b>	TGGGTGACCTTTTGTATATTG
<b>KIP1-R(+3674)</b>	TGGTATTAACCGGTTCTG
<b>RAD9-F(-326)</b>	GCAGCTCCCCATCAAAATAA
<b>RAD9-R(+4158)</b>	TCATTACAAGATGCAAGCCTAAA
<b>RAD52-F(-150)</b>	TAAGAAAAGACGAAAAATATAG
<b>RAD52-R(+150)</b>	AAGTAAATATTAATACGACAC
<b>SCC1-F(+1000)</b>	CGAATAATTTATTGACTCCACAGCCCAATTTTAC
<b>SCC1-R(+450)</b>	GCATAATGTTTCTCTGGCTGCTAATGTACCAAAGC
<b>SMC1-F(+2700)</b>	GAAACAACGATAGATGATTTACCAATATCTTCC
<b>SMC1 3'-R(+500)</b>	GGCATATAGCCTAGACTTTTACGTTTTATCTCG
<b>SMC3-F(-474)</b>	GTATTTTGGCAAGGATTCAG
<b>SMC3-R(+4169)</b>	CTGATGACTCAGGGGATTC
<b>SPC42-F(+770)</b>	AGCTGAAGCGTGTGAAGAA
<b>SPC42-R(+1402)</b>	TGACACTAACCATCCACCATT
<b>S3-untailed-RC</b>	GTCGACCTGCAGCGTACG
<b>YKU70-F(-361)</b>	TCCGTTTTGACAACAGGTCACCTTCT
<b>YKU-R(+300)</b>	CCACAAAGTAATTGTCAGGAAGTGGAACCCCTTG

**Primers to delete genes from marker cassettes**

<b>CIN8-S1</b>	GTATATAAAAGCGCAAAAAATACAACAAGAAAGATTTGTTTGTATGCGTACGCTGCAGGTCGAC
<b>KIP1-S1</b>	CTTCCCTCACTAAATATGGCGAGATAGTTAAACAATCATGCGTACGCTGCAGGTCGAC
<b>KIP1-S2</b>	TATAGTGATACAAATATTTACAATGGCTATATCCCTTAATCGATGAATTCGAGCTCG
<b>HML-S1</b>	CATTTTATTTTTTCGCCTTTTATACAGACTTCAACACAATCAGAACGTACGCTGCAGGTCGAC
<b>HML-S2</b>	GCTCCCGCTTAATTATATATATGCGACTGTTACGGAGATGCAAAGCTTACATCGATGAATTCGAGCTCG
<b>MRE11-S1</b>	GCAAGTTGTACCTGCTCAGATCCGATAAACTCGACTATGCGTACGCTGCAGGTCGAC
<b>MRE11-S2</b>	TTATAAATAGGATATAATATAATATAGGGATCAAGTACAACCTAATCGATGAATTCGAGCTCG

**Primers for getting DNA probes**

<b>ACT1-F</b>	CGAACAAGAAATGCAAACCGC
<b>ACT1-R</b>	CTTGTGGTGAACGATAGATGG

68

Este documento incorpora firma electrónica, y es copia auténtica de un documento electrónico archivado por la ULL según la Ley 39/2015.  
 Su autenticidad puede ser contrastada en la siguiente dirección <https://sede.ull.es/validacion/>

Identificador del documento: 3075810 Código de verificación: smutbmB+

Firmado por: JESSEL AYRA PLASENCIA UNIVERSIDAD DE LA LAGUNA Fecha: 30/11/2020 12:24:14

María de las Maravillas Aguiar Aguilera UNIVERSIDAD DE LA LAGUNA 08/02/2021 13:50:06

3. Materials and Methods

<b>HIS3-F</b>	GAGCAGAAAGCCCTAGTAAAG
<b>HIS3-R</b>	TAAGAACACCTTTGGTGGAGG
<b>MAT-F</b>	CTTAGCATCATTCTTTGTTCTATC
<b>MAT-R</b>	CCAAGGGAGAGAAGACTTG
<b>MAT distal-F</b>	CATGCGTTTCACATGACTTTTGAC
<b>MAT distal-R</b>	AGGATGCCCTTGTTTGTACTG

**Primers for qPCR**

<b>726 bp dsHOcs_F</b>	TCATCTTCGCCACAAGTCTTCTCTC
<b>726 bp dsHOcs_R</b>	CCTGTTCTTAGCTTGTACCAGAGGA
<b>5.7 kb dsHOcs_F</b>	CCACCTTCATCGGTAACGTAC
<b>5.7 kb dsHOcs_R</b>	TAAGAACACCTTTGGTGGAGG
<b>ADH1 to qPCR_F</b>	GTAAAGGGCTGGAAGATCGG
<b>ADH1 to qPCR_R</b>	TTGTTGGAAAGAACCCTCGT
<b>MATa HOcs_F to qPCR</b>	TCAATGATTAATAAGCATAGTCGGGT
<b>MATa HOcs_R to qPCR</b>	CGTCAACCACTCTACAAAACCA

\*The number in brackets points the 5' nucleotide position relative to the ATG start codon of the gene. Negative values for upstream nucleotides and positive for downstream. F: Forward. R: Reverse. S2: Reverse in Janke's tagging and deletion system. S3: Forward in Janke's tagging system. S1: Forward in Janke's deletion system (Janke et al., 2004).

**3.3.2.2. PCRs from linear DNA**

Linear DNA fragments amplifications were performed for: i) checking yeast transformant colonies, ii) amplifying transformant products previously inserted in other yeast strains, and iii) labeling DNA probes with Fluorescein-12-dUTP.

A T100™ Thermal Cycle (Bio-Rad) was used in every case. For checking new transformants and amplifying PCR products from other yeast strains, genomic DNA was extracted by mechanical method (see section 3.3.1.1.1). Then, desired fragments were amplified with the PCR BIO High Fidelity polymerase (Biosigma) and corresponding primers (0.2 μM each one) according to the supplier's recommended program (Fig. 3.9).

On the other hand, Fluorescein-labeled probes were amplified using the Expand High Fidelity polymerase (Roche) and a dNTPs mix composed of 0.2 μM of dATP – dGTP – dCTP; 0.13 μM of dTTP, and 0.07 μM of Fluorescein-12-dUTP. The rest of the supplemented PCR components and the amplification program were performed following the supplier's instructions (Fig. 3.10).

Este documento incorpora firma electrónica, y es copia auténtica de un documento electrónico archivado por la ULL según la Ley 39/2015.  
 Su autenticidad puede ser contrastada en la siguiente dirección <https://sede.ull.es/validacion/>

Identificador del documento: 3075810 Código de verificación: smutbmB+

Firmado por: JESSEL AYRA PLASENCIA  
 UNIVERSIDAD DE LA LAGUNA

Fecha: 30/11/2020 12:24:14

María de las Maravillas Aguiar Aguiar  
 UNIVERSIDAD DE LA LAGUNA

08/02/2021 13:50:06

3. Materials and Methods

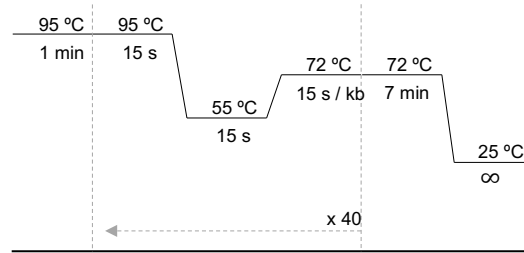


**Figure 3.9. Schematic overview of the PCR program used to amplify DNA from transformant colonies or to obtain transformant DNA from previously modified yeast strains.**

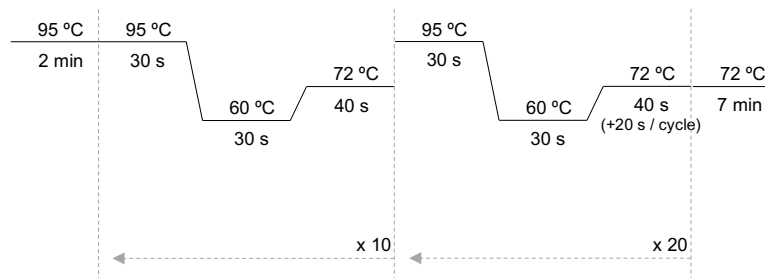


**Figure 3.10. Schematic overview of the employed PCR program to amplify probes.**

**3.3.2.3. PCRs from plasmids**

In most cases, transformation products were amplified from a set of plasmids with marker cassettes to tag proteins in the C- or N-terminal (Janke et al., 2004). For this purpose, PCRs were done with the GoTaq 2<sup>®</sup> G2 Flexi Polymerase (Promega). The PCR master mix was composed of 2.5 mM of Mg<sup>2+</sup>, 0.5 mM of each dNTP, 0.2 μM of each primer, and 0.07 U·μL<sup>-1</sup> of the enzyme with the provided buffer. The amplification program is shown below (Fig. 3.11):

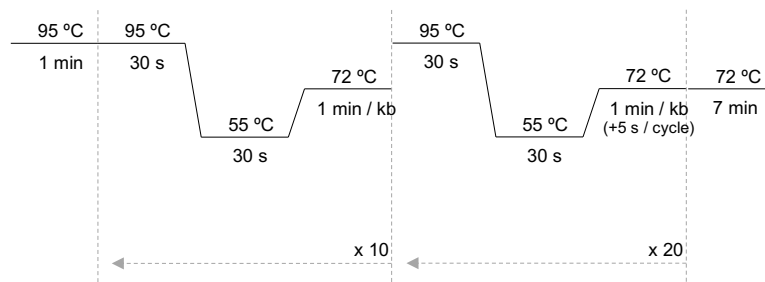


**Figure 3.11. Schematic overview of the employed PCR program to amplify transformant DNA from plasmids.**



### 3.3.2.4. Quantitative PCR (qPCR)

This technique was used to measure the resection rate of broken DNA ends after the generation of an HO-mediated DSB (Zierhut & Diffley, 2008).

The strategy is based on designing primers to amplify sequences located downstream of the break and study how far resection extends. The amplicons must contain target sites for restriction endonuclease enzymes (REs). Thus, amplification in digested samples is only possible when resection has overpassed the target site and renders it at single-stranded DNA, avoiding REs activity.

For this purpose, the DNA samples were obtained through the lytic method (see section 3.3.1.1.2). Once extracted, every sample was measured and normalized with a Nanodrop Lite Spectrophotometer (ThermoFisher Scientific). For every time point, a mock digestion was also required as control. Then, mock digestions and digestion reactions (4.4 µL per well of the qPCR plate containing 2.5 µg·µL<sup>-1</sup> of genomic DNA) were digested with 5 U of the corresponding restriction enzyme per µg of DNA for 2 hours at 37 °C. After that, a mix of 0.3 µL of each primer and 5 µL of PowerUp™ SYBR™ Green Master Mix (Applied Biosystems) was added to each well, getting 10 µL as final volume.

The qPCR plates were subjected to the following program (Fig. 3.12) in a QuantStudio 5 Real-Time PCR System (ThermoFisher Scientific), taking into account the technical triplicates per sample for three independent experiments:

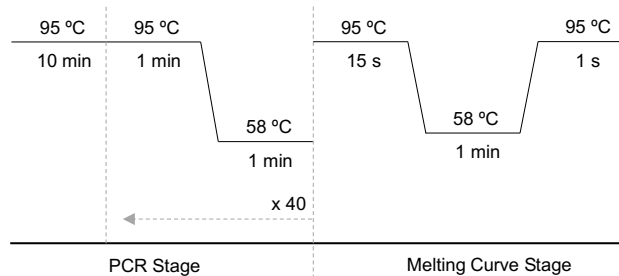


**Figure 3.12. Schematic overview of the applied qPCR program.**

Once obtained the data, the next formula was employed to quantify resection rates:

$$x = \frac{2}{\left( \frac{(E_{RS})^{\Delta C_q(\text{digest-mock})}}{(E_{ADH})^{\Delta C_q(\text{digest-mock})}} + 1 \right)} \cdot f$$

### 3. Materials and Methods

Where  $E_{RS}$  and  $E_{ADH1}$  are the primer efficiencies for the restriction site (RS) and the *ADH1* gene (used as a control to correct differences in template concentrations).  $\Delta C_q(\text{digest} - \text{mock})$  is the difference between the quantification cycles ( $C_q$ ) for the digested and the mock-digested sample.  $f$  is the fraction of the genome where the HO-mediated DSB was generated.  $f$  is calculated as follows:

$$f = 1 - \frac{(E_{HOcs})^{\Delta C_q(t_0-t)}}{(E_{ADH1})^{\Delta C_q(t_0-t)}}$$

where  $E_{HOcs}$  and  $E_{ADH1}$  are the primer efficiencies for the HO-cut site and *ADH1* amplicons, and  $\Delta C_q(t_0 - t)$  is the difference between the quantification cycles before HO induction and the evaluated time point.

The primer efficiencies are determined through the analysis of 1:10 serial dilutions of undigested genomic DNA in a qPCR assay. Then, a plot of  $C_q$  values vs. log (DNA concentration) should show a linear distribution. Finally, efficiencies ( $E$ ) can be calculated by applying the following formula:

$$E = 10^{-\left(\frac{1}{b}\right)}$$

where  $b$  is the slope of the linear regression.

### 3.3.3. DNA electrophoresis

#### 3.3.3.1. Analytical electrophoresis

This kind of electrophoresis was routinely performed to i) check transformant DNA, ii) check transformant colonies, and iii) measure the efficiency of restriction digestion reactions.

DNA fragments were separated in 1 % w/v of Agarose E gels (Pronadisa) dissolved in 1x TBE buffer. 0.5x TBE was the used concentration of the running buffer. Before loading the samples, 5  $\mu\text{L}$  of each was mixed with 1  $\mu\text{L}$  of 6x of EZ-Vision<sup>®</sup> One DNA dye (Amresco). The GeneRuler 1 kb DNA Ladder (ThermoFisher Scientific) was employed as a molecular weight marker.

Running conditions were always 90 V for 1 hour at room temperature. Finally, DNA bands were visualized under the UV light of the Gel-Doc System (Bio-Rad).

Este documento incorpora firma electrónica, y es copia auténtica de un documento electrónico archivado por la ULL según la Ley 39/2015.  
Su autenticidad puede ser contrastada en la siguiente dirección <https://sede.ull.es/validacion/>

Identificador del documento: 3075810 Código de verificación: smutbmB+

Firmado por: JESSEL AYRA PLASENCIA  
UNIVERSIDAD DE LA LAGUNA

Fecha: 30/11/2020 12:24:14

María de las Maravillas Aguiar Aguiar  
UNIVERSIDAD DE LA LAGUNA

08/02/2021 13:50:06

### 3.3.3.2. Experimental electrophoresis

The molecular study of DSBs repair was performed through the MAT switching assay (Haber, 2012; Kaplun et al., 2006; Kostriken et al., 1983; Strathern et al., 1982).

This method is used as a DNA repair model. It determines if cells can repair an HO-mediated DSB and whether they trigger homologous recombination or non-homologous end joining. Digestion of samples with a restriction enzyme gives rise to DNA fragments whose sizes depend on whether they are intact, cut, or repaired.

Digested DNA fragments were separated in 1.2 % w/v Agarose Low EEO LS (Panreac) dissolved in 1x TBE. 0.5x TBE was again employed as the running buffer, whereas the wells were loaded with the samples mixed with Loading Dye Purple (6x) (New England Biolabs). Finally, running conditions were performed at 90 V for 2 hours at room temperature.

### 3.3.4. Southern blot

Gels from experimental electrophoreses were always subjected to the Southern blot technique. Previously separated DNA fragments are first transferred to positive-charged nylon membranes. Then, DNA bands of interest are detected through specific binding of Fluorescein-12-dUTP-labeled DNA probes.

#### 3.3.4.1. Probe labeling

Specific probes were created in three steps. Firstly, linear DNA fragments of interest were amplified by PCR from genomic DNA. After checking in a conventional electrophoresis, PCR products were purified using a Wizard® SV Gel and PCR Clean-Up System (Promega). Finally, purified DNA was used as a template to create Fluorescein-12-dUTP-labeled probes by PCR (see section 3.3.2.2).

#### 3.3.4.2. DNA transfer

After experimental electrophoreses, separated DNA samples were stained in a 0.5 µg·mL<sup>-1</sup> ethidium bromide solution for 10 minutes and visualized under UV light. Then, a three-steps treatment was performed to ease the transfer to membranes.

First, gels were soaked in Milli-Q water for 10 minutes at room temperature. Next, they were submerged in a depurination solution (0.4 % HCl) for 10 minutes. Second, Milli-Q water was added for 5 minutes to clean up the tray, and gels were soaked in a denaturing solution for 30

Este documento incorpora firma electrónica, y es copia auténtica de un documento electrónico archivado por la ULL según la Ley 39/2015.  
Su autenticidad puede ser contrastada en la siguiente dirección <https://sede.ull.es/validacion/>

Identificador del documento: 3075810 Código de verificación: smutbmB+

Firmado por: JESSEL AYRA PLASENCIA  
UNIVERSIDAD DE LA LAGUNA

Fecha: 30/11/2020 12:24:14

María de las Maravillas Aguiar Aguilár  
UNIVERSIDAD DE LA LAGUNA

08/02/2021 13:50:06

### 3. Materials and Methods

minutes. Finally, a brief step of Milli-Q water was applied for 3 minutes before equilibrating gels in a neutralization solution for additional 30 minutes.

Once finished, downward capillary transfer onto Hybond-N<sup>+</sup> Nylon membranes positively charged (Amersham) was performed overnight (Fig. 3.13). 10x SSC solution was used as the transfer buffer.

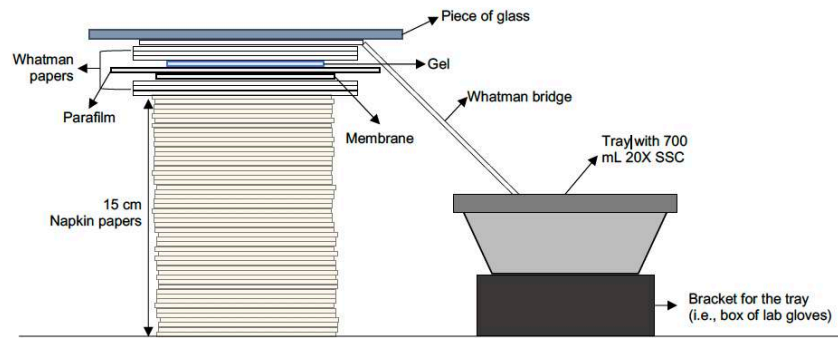


Figure 3.13. Scheme of the setup for DNA transfer to membranes.

#### 3.3.4.3. Probe hybridization and detection

Transferred DNA was crosslinked by exposing membranes to 1,200 J·cm<sup>-2</sup> in a Stratalinker UV crosslinker (Hoefer). Then, they were washed in a 5x SSC solution for 30 minutes at room temperature.

Next, membranes were introduced in a glass tube containing 50 mL of blocking solution and incubated at 68 °C for 1 hour in a hybridization oven (Stuart Scientific). Once passed this time, denatured Fluorescein-12-dUTP-labeled probes were added to the blocking solution, and hybridization continued at 68 °C overnight.

The day after, hybridized membranes were washed at 68 °C in a primary washing buffer (two times for 10 minutes), and then in a secondary washing buffer (two times for 5 minutes). Next, they were rinsed in AB buffer for 5 minutes and blocked in AB buffer + 1 % skimmed milk (w/v) for 1 hour at room temperature. After that, the solution was replaced by AB buffer + 0.5 % skimmed milk (w/v) containing a 1:100,000 dilution of anti-Fluorescein antibody conjugated to alkaline phosphatase (Merck) for 1 hour. Lastly, AB buffer + 0.1 % Tween 20 (Promega) was used to make three washes for 30 minutes.

### 3. Materials and Methods

The detection was performed by adding CDP-Star Detection Reagent (Amersham) over the membranes. Then, they were placed between two transparent plastic sheets avoiding bubbles. The chemiluminescent signal was developed in a Fusion Solo S Documentation Chamber (Vilber Lourmat). Quantifications were measured with the Bio1-D Software.

#### 3.3.5. Flow Cytometry

This technique was performed to measure the DNA content of cell populations and study the cell cycle transition.

Samples of 1 mL were taken and centrifuged at top speed for 1 minute. The pellet was then fixed by resuspension in 1 mL of 100 % ethanol and centrifuged again at maximum speed for 1 minute to discard the supernatant. The cells were resuspended and incubated in 250  $\mu$ L of 1x SSC solution containing 10 mg·mL<sup>-1</sup> of RNase A at 37 °C overnight. The next day, 50  $\mu$ L of 1x SSC solution containing 1 mg·mL<sup>-1</sup> of Proteinase K was added, and the incubation was prolonged for 1 hour at 50 °C. Finally, 500  $\mu$ L of 1x SSC solution containing 3  $\mu$ g·mL<sup>-1</sup> of propidium iodide was supplemented, and incubation was extended again for 1 hour at room temperature. Processed samples were stored at 4 °C until use.

The analysis was carried out using a BD FACSCalibur equipment and the CellQuest Pro Software (BD Biosciences). An exponentially growing culture was used for each experiment to calibrate the 1C and 2C peaks relative to the DNA content before reading the samples.

### 3.4. Protein techniques

#### 3.4.1. Western blot

A significant part of this thesis consisted of studying proteins. Western blots of proteins of interest were performed to evaluate their presence/absence, post-translational modifications, and in some cases, their auxin-mediated degradation.

##### 3.4.1.1. Protein extraction

Whole-cell proteins were precipitated by using the Trichloroacetic Acid (TCA) method. TCA helps to conserve post-translational modifications, avoiding enzymatic reactions such as dephosphorylations.

75

Este documento incorpora firma electrónica, y es copia auténtica de un documento electrónico archivado por la ULL según la Ley 39/2015.  
Su autenticidad puede ser contrastada en la siguiente dirección <https://sede.ull.es/validacion/>

Identificador del documento: 3075810 Código de verificación: smutbmB+

Firmado por: JESSEL AYRA PLASENCIA  
UNIVERSIDAD DE LA LAGUNA

Fecha: 30/11/2020 12:24:14

María de las Maravillas Aguiar Aguiar  
UNIVERSIDAD DE LA LAGUNA

08/02/2021 13:50:06

### 3. Materials and Methods

5 mL of liquid cultures were taken per sample. After centrifugation for 1 minute at 4,000 rpm, pellets were resuspended in 1 mL of TCA 20 % and stored at -20 °C until use. Once collected all samples to analyze, they were thawed and centrifuged at top speed for 1 minute. Supernatants were discarded, and pellets were resuspended again in 100 µL cold 20 % TCA. Breakage of cell walls was done by adding ~ 200 mg of glass beads and vortexing for 4 minutes. Then, TCA-containing cell debris was diluted to 10 % by adding 200 µL of 5 % TCA. The liquid phase was transferred to new 1.5 mL tubes, and cell debris/proteins were collected by centrifugation at top speed for 1 minute. Finally, pellets were resuspended in 150 µL of Laemmli Sample Buffer (Bio-Rad) + β-mercaptoethanol and boiled at 95 °C for 10 minutes. Quantification and normalization of total proteins was performed by using a Qubit 4 Fluorometer (ThermoFisher Scientific).

#### 3.4.1.2. SDS-PAGE

Quantified samples were fractionated by one-dimension polyacrylamide gel electrophoresis under denaturing conditions (SDS-PAGE). Acrylamide/bisacrylamide 37.5:1 proportion (Bio-Rad) was used to polymerize 7.5 % and 10 % continuous separating gels. 4 % was the percentage used for the stacking gels in all cases.

Electrophoreses were performed in a Mini-PROTEAN® Tetra Cell (Bio-Rad). Before loading the samples, gels were subjected to a pulse of 160 V for 12 minutes. Then, 10 µL per sample containing 30 µg of proteins were loaded on the wells. Precision Plus Protein™ Dual Color Standard was used as the molecular weight marker. Running conditions consisted of 20 minutes at 90 V, followed by 30 minutes at 120 V, and 150 V until the end of the electrophoresis.

When phosphorylation was not seen in conventional SDS-PAGE gels, 5 µmol·mL<sup>-1</sup> Phos-tag™ Acrylamide (Fujifilm Wako Chemicals) and 10 µmol·mL<sup>-1</sup> of Manganese Chloride (Sigma-Aldrich) were added to resolving gels. Phos-tag™ is a molecule that binds to phosphorylated residues. Thus, phosphorylated proteins migrate slower, and the detection of phosphorylated forms becomes clearer. When used, samples were loaded in the absence of the molecular weight marker, as it interferes with the proteins' regular migration.

#### 3.4.1.3. Protein transfer

The resolving part of SDS-PAGE gels were equilibrated in 50 mL of transfer buffer for 30 minutes at room temperature. Meanwhile, Immobilon-FL PVDF membranes (Merck Millipore) were soaked in 100 % methanol for 20 seconds. They were then rinsed in milli-Q water and transferred to 50 mL of transfer buffer for 30 minutes.

76

Este documento incorpora firma electrónica, y es copia auténtica de un documento electrónico archivado por la ULL según la Ley 39/2015.  
Su autenticidad puede ser contrastada en la siguiente dirección <https://sede.ull.es/validacion/>

Identificador del documento: 3075810 Código de verificación: smutbmB+

Firmado por: JESSEL AYRA PLASENCIA  
UNIVERSIDAD DE LA LAGUNA

Fecha: 30/11/2020 12:24:14

María de las Maravillas Aguiar Aguiar  
UNIVERSIDAD DE LA LAGUNA

08/02/2021 13:50:06

3. Materials and Methods

In the case of Phos-tag™ gels, they were briefly incubated in 10 mmol·L<sup>-1</sup> EDTA to remove divalent MnCl<sub>2</sub>. Transfer was done on a Mini Trans-Blot® Cell (Bio-Rad) in the presence of 20 % methanol. Transfer conditions were 90 V for 1 hour at 4 °C. When Phos-tag™ gels were transferred, 0.1 % SDS (w/v) was added to the buffer.

**3.4.1.4. Antibodies hybridization and detection**

When finished, membranes were briefly activated in 100 % methanol for 20 seconds, rinsed in milli-Q water, and submerged in Ponceau S Solution BC (Panreac) for 5 minutes at room temperature. Ponceau S staining served to check the protein transfer and to cut the membranes for hybridization with different antibodies.

After three washes for 5 minutes in milli-Q water, Ponceau S was destained by re-activating membranes in 100 % methanol for 20 seconds and incubating in TBS buffer + 0.1 % Tween 20 (TBST) for 10 minutes at room temperature.

When membranes whitened, they were blocked in TBST + 5 % skimmed milk (in the presence of 0.1 % sodium azide) for 1 hour at 4 °C. The blocking solution was then replaced by TBST + 5 % skimmed milk (in 0.1 % sodium azide) containing primary antibodies, and incubations were prolonged overnight at 4 °C.

The day after, membranes were washed six times in TBST for 5 minutes each at room temperature. Secondary antibodies were added in TBST + 5 % skimmed milk for 1 hour at room temperature. After washing six times in TBST, the ECL Prime Western Blotting Detection Reagent (Amersham) was added over the membranes. Finally, they were revealed as in the Southern blot technique (see section 3.3.4.3). The following table shows the origin, the hosts, and the working dilution for each antibody used in this thesis:

**Table 3.4. Primary and secondary antibodies used in this thesis.**

<i>Antibody</i>	<i>Working dilution</i>	<i>Host</i>	<i>Origin</i>
α-c-Myc (clone 9E10)	1:5,000	Mouse	Sigma-Aldrich (M4439)
α-HA (clone HA-7)	1:5,000	Mouse	Sigma-Aldrich (H9658)
α-Rad53 (clone EL7.E1)	1:5,000	Mouse	Abcam (ab166859)
α-PGK1 (clone 22C5D8)	1:10,000	Mouse	ThermoFisher™ (459250)
α-Flag® (clone M2)	1:5,000	Mouse	Sigma-Aldrich (F3165)

77

Este documento incorpora firma electrónica, y es copia auténtica de un documento electrónico archivado por la ULL según la Ley 39/2015.  
 Su autenticidad puede ser contrastada en la siguiente dirección <https://sede.ull.es/validacion/>

Identificador del documento: 3075810 Código de verificación: smutbmB+

Firmado por: JESSEL AYRA PLASENCIA  
 UNIVERSIDAD DE LA LAGUNA

Fecha: 30/11/2020 12:24:14

María de las Maravillas Aguiar Aguiar  
 UNIVERSIDAD DE LA LAGUNA

08/02/2021 13:50:06

### 3. Materials and Methods

$\alpha$ -mini-AID-tag (clone 1E4)	1:5,000	Mouse	MBL Life Sciences (M214-3)
$\alpha$ -GFP	1:10,000	Rabbit	Abcam (ab6556)
$\alpha$ -acSmc3	1:5,000	Mouse	Dr. Katsu Shirahig gift
$\alpha$ -Mouse IgG (H+L) (HRP conjugated)	1:10,000	Goat	Promega (W4021)
$\alpha$ -Rabbit IgG (H+L) (HRP conjugated)	1:20,000	Goat	Abcam (ab97051)

#### 3.4.2. Proteomics mass spectrometry

This technique was assessed to determine differences in the proteome when DSBs arise in G<sub>2</sub> and telophase. For this purpose, only the extraction of whole-cell proteins was performed. The analysis through mass spectrometry was carried out at the Institute of Molecular Biology gGmbH of Mainz, Germany.

##### 3.4.2.1. Whole-cell protein extraction

1 OD<sub>600</sub> of cells blocked in different cell cycle stages (with and without one or multiple DSBs) was centrifuged in a 1.5 mL tube. The pellet was then resuspended in 25  $\mu$ L of 1x NuPAGE™ LDS Sample Buffer (ThermoFisher Scientific) + 10 mM DTT (Promega). Collected samples were placed in a 96-well plate and boiled for 10 minutes at 95 °C. Storage was done at 4 °C until shipment to Germany. It should be noted that four independent replicates per sample were needed.

### 3.5. Fluorescence microscopy

Much of the current work is versed in studying the subcellular location and changes in different proteins upon DSBs. For this purpose, wide-field fluorescence microscopy has supposed a fundamental pillar, both in yeast and HeLa cells.

The Leica DMI6000B epifluorescence microscope (Leica) has been used, employing a 63x/1.30 immersion objective and an ultrasensitive DFC350 digital camera. Immersion oil (UV-transparent, fluorescence-free) with a refractive index of 1.515 – 1-517 (Fluka) has also been employed. The following table shows the properties of filter cubes for each fluorescent protein.



3. Materials and Methods

**Table 3.5. List of filter cubes used in fluorescence microscopy.**

<i>Filter cube</i>	<i>Fluorochrome</i>	<i>Excitation range</i>	<i>Excitation filter</i>	<i>Dichromatic mirror</i>	<i>Suppression filter</i>
A	Hoechst/DAPI	UV	BP 360/40	400	BP 470/40
CFP	eCFP	Violet-blue	BP 436/20	455	BP 480/40
RFP	RFP, mCherry	Red	BP 546/12	560	BP 605/75
YFP	YFP, GFP	Green	BP 500/20	515	BP 535/30

### 3.5.1. Yeast microscopy

Fluorescence microscopy of yeast was always performed in live cells. For each time point, an aliquot of 100  $\mu$ L of cells was transferred to a 1.5 mL tube. After a brief pulse of centrifugation, part of the pellet was taken out and spread over a microscope slide. A coverslip was then placed on the sample with slight pressure, and a little drop of immersion oil was disposed over. The cells were directly subjected to visualization.

Only when the plasma membrane and DNA was subject to study, 0.5  $\mu$ L of 1 mg·mL<sup>-1</sup> Hoechst 33258 (Promega) was mixed with live cells before placing the coverslip. The following table shows the list of microscope settings employed for each tagged protein.

**Table 3.6. List of parameters to visualize each protein.**

<i>Protein/compound</i>	<i>Exposure (seconds)</i>	<i>Gain</i>	<i>Intensity</i>
Hoechst	0.02	2	2
TetR-YFP	2	5	5
TetR-RFP	2	6	5
Hta2-mCherry	2	6	4
Net1-eCFP	2	6	5
GFP-Tub1	2	6	4
Spc42-mCherry	2	6	5
Cin8-mCherry	4	6	5
Cin8-3GFP*	3	6	5
Cdc14-GFP	2	6	4
Msc1-eYFP	4	6	5

\* Cin8-3GFP and its phosphor-mutant versions (Cin8-3A-3GFP and Cni8-3D-3GFP) were visualized under the same settings.

Este documento incorpora firma electrónica, y es copia auténtica de un documento electrónico archivado por la ULL según la Ley 39/2015.  
 Su autenticidad puede ser contrastada en la siguiente dirección <https://sede.ull.es/validacion/>

Identificador del documento: 3075810 Código de verificación: smutbmB+

Firmado por: JESSEL AYRA PLASENCIA  
 UNIVERSIDAD DE LA LAGUNA

Fecha: 30/11/2020 12:24:14

María de las Maravillas Aguiar Aguilár  
 UNIVERSIDAD DE LA LAGUNA

08/02/2021 13:50:06

### 3. Materials and Methods

---

Single captures and series of 20 z-focal plane images (0.3  $\mu\text{m}$  depth between each consecutive photo) were taken for each protein.

For analyzing the dynamics of some structures, such as chromatin (Hta2-mCherry) and chromosome loci (TetR-YFP/TetR-RFP) movement, or the microtubule apparatus (GFP-Tub1), short time-lapse movies were recorded. In this case, 60 consecutive pictures were captured per field using z-focal settings stuck in a single focal plane.

Specific measurements, such as interloci distances, were performed with the Leica AF6000 software (Leica). Quantifications for categories charts were done with FIJI software (Schindelin et al., 2012).

#### 3.5.2. HeLa cells microscopy

Contrary to yeast, HeLa cells are visualized by immunofluorescence (IF). The IF technique requires to fix the cells before hybridization with specific antibodies.

For this, cells were grown, incubated, and blocked in anaphase/telophase (see section 3.2.1.2.) directly over circular microscope cover glasses 13 mm  $\varnothing$ , thickness N° 1 (VWR) previously coated with 0.1 mg·mL<sup>-1</sup> poly-L-Lysine (Sigma-Aldrich).

Once the samples were ready, DMEM was discarded, and cells were washed twice in 1x PBS. They were treated with a pre-extraction buffer (which eases the visualization of proteins tightly associated with the chromatin) for 7 minutes at room temperature. Next, cells were washed twice with 1x PBS and fixed in 1x PBS containing 4% paraformaldehyde (Sigma-Aldrich) for 15 minutes at room temperature. After two washes in 1x PBS, cells were permeabilized in a solution containing 0.2 % Triton X-100 (Promega) in 1x PBS for 10 minutes at room temperature. Finally, coverslips were again washed twice in 1x PBS before starting the IF.

##### 3.5.2.1. Antibodies hybridization and detection

First, cells were blocked in 1x PBS containing 1 % FBS for 1 hour at room temperature. Then, the blocking solution was replaced by fresh 1x PBS + 1% FBS in the primary antibody's presence overnight at 4 °C. The next day, three consecutive washes in 1x PBS were performed, and cells were incubated in 1x PBS + 1 % FBS containing the secondary antibody for 1 hour at room temperature. These incubations can be achieved with two different primary and secondary antibodies simultaneously, provided that they have been raised in distinct species.

80

Este documento incorpora firma electrónica, y es copia auténtica de un documento electrónico archivado por la ULL según la Ley 39/2015.  
Su autenticidad puede ser contrastada en la siguiente dirección <https://sede.ull.es/validacion/>

Identificador del documento: 3075810 Código de verificación: smutbmB+

Firmado por: JESSEL AYRA PLASENCIA  
UNIVERSIDAD DE LA LAGUNA

Fecha: 30/11/2020 12:24:14

María de las Maravillas Aguiar Aguilár  
UNIVERSIDAD DE LA LAGUNA

08/02/2021 13:50:06

### 3. Materials and Methods

For actin cytoskeleton staining, phalloidin conjugated with tetramethyl-rhodamine B isothiocyanate (TRITC) (Sigma-Aldrich) was employed. Phalloidin-TRITC staining was always post-antibodies hybridizations. Thus, an additional incubation in 1x PBS containing 1% DMSO + 50  $\mu\text{g}\cdot\text{mL}^{-1}$  phalloidin-TRITC was done for 40 minutes at room temperature in darkness. Finally, several washes in 1x PBS were needed to clean up the unbound phalloidin-TRITC.

The following table shows the antibodies, as well as their host and working concentrations:

**Table 3.7. List of used antibodies in HeLa cells IF.**

<b>Antibody</b>	<b>Working dilution</b>	<b>Host</b>	<b>Origin</b>
$\alpha$ -53BP1	1:600	Rabbit	Abcam (ab172580)
$\alpha$ -RPA2 (JE45-59)	1:600	Rabbit	ThermoFisher™ (MA5-34843)
$\alpha$ -Phospho-Histone H2A.X Ser139 ( $\gamma$ -H2A.X)	1:600	Mouse	Merck-Millipore (JBW301)
$\alpha$ -RIF1 (D2F2M)	1:600	Rabbit	Cell Signalling Technology (95558)
$\alpha$ -Tubulin alpha (clone YOL1/34)	1:500	Rat	Bio-Rad (MCA78G)
$\alpha$ -Rat IgG (H+L) (Alexa Fluor® 488)	1:600	Goat	Abcam (ab150157)
$\alpha$ -Rabbit IgG (H+L) (Alexa Fluor® 488)	1:600	Goat	Abcam (A150007)
$\alpha$ -Mouse IgG (H+L) (Alexa Fluor® 594)	1:600	Goat	Abcam (ab150116)

Finally, when all incubations were ready, microscopy slides were assembled by adding a drop of Fluoroshield™ with DAPI mounting medium (Sigma-Aldrich) over the samples. Then, coverslips were sealed to the slides with nail polish, and cells were subjected to visualization.

Every statistical calculation and graphical representation were performed through the use of Prism 8 software (GraphPad).

Este documento incorpora firma electrónica, y es copia auténtica de un documento electrónico archivado por la ULL según la Ley 39/2015.  
 Su autenticidad puede ser contrastada en la siguiente dirección <https://sede.ull.es/validacion/>

Identificador del documento: 3075810 Código de verificación: smutbmB+

Firmado por: JESSEL AYRA PLASENCIA  
 UNIVERSIDAD DE LA LAGUNA

Fecha: 30/11/2020 12:24:14

María de las Maravillas Aguiar Aguiar  
 UNIVERSIDAD DE LA LAGUNA

08/02/2021 13:50:06



Este documento incorpora firma electrónica, y es copia auténtica de un documento electrónico archivado por la ULL según la Ley 39/2015.  
*Su autenticidad puede ser contrastada en la siguiente dirección <https://sede.ull.es/validacion/>*

Identificador del documento: 3075810 Código de verificación: smutbmB+

Firmado por: JESSEL AYRA PLASENCIA  
UNIVERSIDAD DE LA LAGUNA

Fecha: 30/11/2020 12:24:14

María de las Maravillas Aguiar Aguiar  
UNIVERSIDAD DE LA LAGUNA

08/02/2021 13:50:06



## 4. Results and discussion

Este documento incorpora firma electrónica, y es copia auténtica de un documento electrónico archivado por la ULL según la Ley 39/2015.  
Su autenticidad puede ser contrastada en la siguiente dirección <https://sede.ull.es/validacion/>

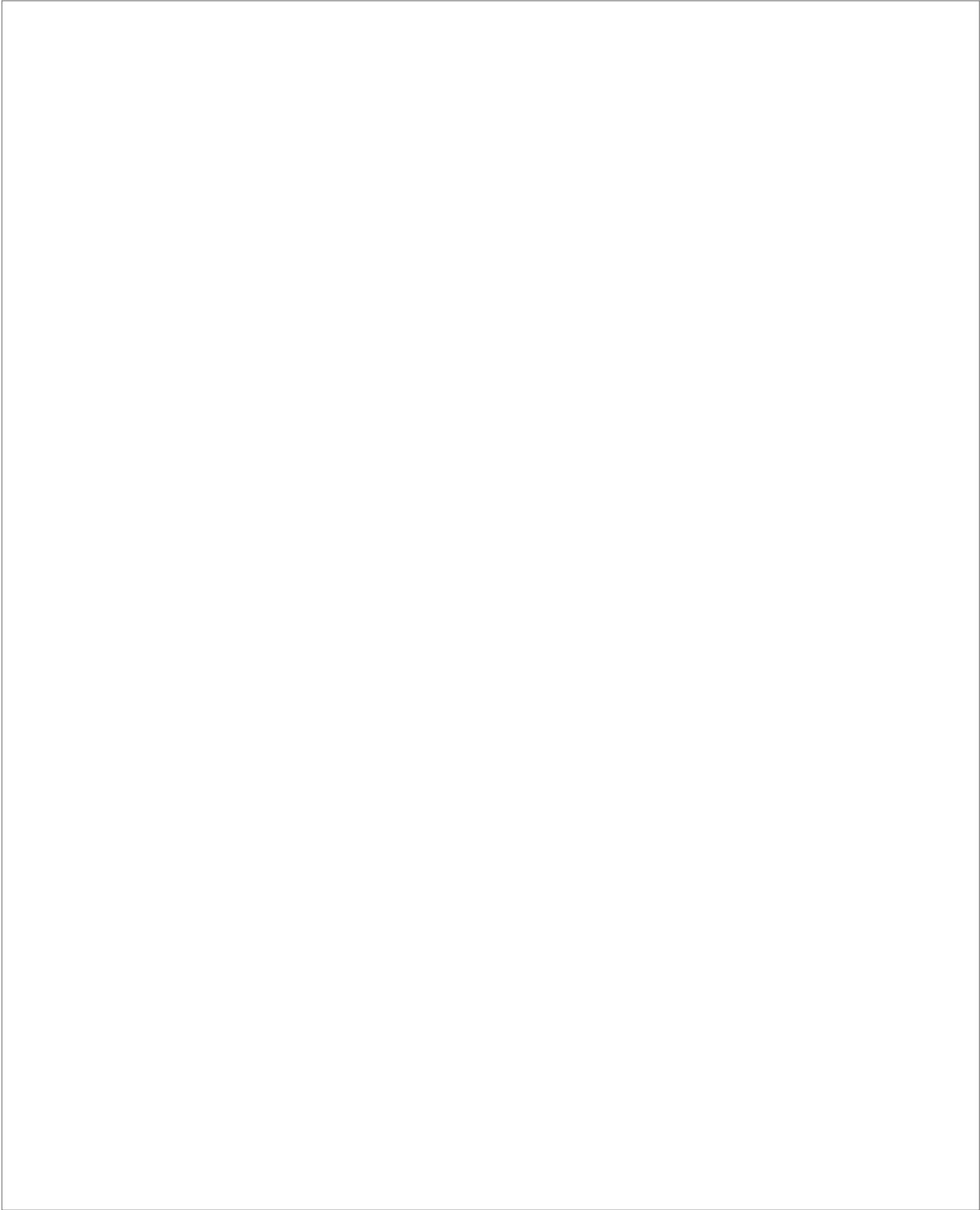
Identificador del documento: 3075810 Código de verificación: smutbmB+

Firmado por: JESSEL AYRA PLASENCIA  
UNIVERSIDAD DE LA LAGUNA

Fecha: 30/11/2020 12:24:14

María de las Maravillas Aguiar Aguiar  
UNIVERSIDAD DE LA LAGUNA

08/02/2021 13:50:06



Este documento incorpora firma electrónica, y es copia auténtica de un documento electrónico archivado por la ULL según la Ley 39/2015.  
*Su autenticidad puede ser contrastada en la siguiente dirección <https://sede.ull.es/validacion/>*

Identificador del documento: 3075810      Código de verificación: smutbmB+

Firmado por: JESSEL AYRA PLASENCIA  
UNIVERSIDAD DE LA LAGUNA

Fecha: 30/11/2020 12:24:14

María de las Maravillas Aguiar Aguiar  
UNIVERSIDAD DE LA LAGUNA

08/02/2021 13:50:06

## 4.1. Chapter 1

### DNA double-strand breaks lead to coalescence between segregated sister chromatid loci

The first chapter is dedicated to the study of the subcellular response to DSBs in telophase. This mitotic stage was synchronously established by using mutant strains for the Cdc15 kinase. Once blocked, cells were submitted to DSBs by incubation in the presence of phleomycin ( $10 \mu\text{g}\cdot\text{mL}^{-1}$ ).

DSBs lead the cells to delay the telophase-to- $G_1$  transition through Rad53 hyperphosphorylation and the Rad9-dependent DNA damage checkpoint (DDC). Furthermore, chromosomes accelerate their interloci movement, and the microtubule apparatus (MTs) changes its morphology and dynamics. This phenomenon causes a partial regression of chromosome segregation to generate events of coalescence between sister loci. This fact is likely due to DSB repair through homologous recombination with the sister, as deficient cells for this pathway ( $\Delta rad52$ ) do not survive after DSBs in telophase. Moreover, cells partially dephosphorylate the Cin8 kinesin motor protein. This post-translational modification promotes its relocation from inter-polar microtubules (iMTs) to spindle pole bodies (SPBs), and this is required for the approximation of segregated DNA material and cell survival.

This set of results has been published as a peer-reviewed article. For this reason, it is presented as a copy of the original paper.

- **Scientific journal:** Nature communications.
- **Area:** Multidisciplinary sciences.
- **Quartile:** Q1.
- **Impact factor (2019):** 12.121.
- **Authors:** Jessel Ayra Plasencia and Félix Manuel Machín Concepción
- **DOI:** <https://doi.org/10.1038/s41467-019-10742-8>.



QR code for supplementary multimedia material

Este documento incorpora firma electrónica, y es copia auténtica de un documento electrónico archivado por la ULL según la Ley 39/2015.  
Su autenticidad puede ser contrastada en la siguiente dirección <https://sede.ull.es/validacion/>

Identificador del documento: 3075810 Código de verificación: smutbmB+

Firmado por: JESSEL AYRA PLASENCIA  
UNIVERSIDAD DE LA LAGUNA

Fecha: 30/11/2020 12:24:14

María de las Maravillas Aguiar Aguiar  
UNIVERSIDAD DE LA LAGUNA

08/02/2021 13:50:06



Este documento incorpora firma electrónica, y es copia auténtica de un documento electrónico archivado por la ULL según la Ley 39/2015.  
*Su autenticidad puede ser contrastada en la siguiente dirección <https://sede.ull.es/validacion/>*

Identificador del documento: 3075810      Código de verificación: smutbmB+

Firmado por: JESSEL AYRA PLASENCIA  
UNIVERSIDAD DE LA LAGUNA

Fecha: 30/11/2020 12:24:14

María de las Maravillas Aguiar Aguiar  
UNIVERSIDAD DE LA LAGUNA

08/02/2021 13:50:06





Corrected: Publisher correction

ARTICLE

<https://doi.org/10.1038/s41467-019-10742-8>

OPEN

# DNA double-strand breaks in telophase lead to coalescence between segregated sister chromatid loci

Jessel Ayra-Plasencia <sup>1,2</sup> & Félix Machín <sup>1,3</sup>

DNA double strand breaks (DSBs) pose a high risk for genome integrity. Cells repair DSBs through homologous recombination (HR) when a sister chromatid is available. HR is upregulated by the cyclin dependent kinase (CDK) despite the paradox of telophase, where CDK is high but a sister chromatid is not nearby. Here we study in the budding yeast the response to DSBs in telophase, and find they activate the DNA damage checkpoint (DDC), leading to a telophase-to-G<sub>1</sub> delay. Outstandingly, we observe a partial reversion of sister chromatid segregation, which includes approximation of segregated material, de novo formation of anaphase bridges, and coalescence between sister loci. We finally show that DSBs promote a massive change in the dynamics of telophase microtubules (MTs), together with dephosphorylation and relocalization of kinesin-5 Cin8. We propose that chromosome segregation is not irreversible and that DSB repair using the sister chromatid is possible in telophase.

<sup>1</sup>Unidad de Investigación, Hospital Universitario Nuestra Señora de Candelaria, Santa Cruz de Tenerife, Spain. <sup>2</sup>Escuela de Doctorado y Estudios de Posgrado, Universidad de La Laguna, Santa Cruz de Tenerife, Spain. <sup>3</sup>Instituto de Tecnologías Biomédicas, Universidad de La Laguna, Santa Cruz de Tenerife, Spain. Correspondence and requests for materials should be addressed to F.M. (email: [fmachin@funcanis.es](mailto:fmachin@funcanis.es))

Este documento incorpora firma electrónica, y es copia auténtica de un documento electrónico archivado por la ULL según la Ley 39/2015.  
Su autenticidad puede ser contrastada en la siguiente dirección <https://sede.ull.es/validacion/>

Identificador del documento: 3075810 Código de verificación: smutbmB+

Firmado por: JESSEL AYRA PLASENCIA  
UNIVERSIDAD DE LA LAGUNA

Fecha: 30/11/2020 12:24:14

María de las Maravillas Aguiar Aguiar  
UNIVERSIDAD DE LA LAGUNA

08/02/2021 13:50:06

#### 4. Results and Discussion

### ARTICLE

NATURE COMMUNICATIONS | <https://doi.org/10.1038/s41467-019-10742-8>

**D**NA double-strand breaks (DSBs) represent one of the most toxic forms of DNA damage, which, if left unrepaired, leads to cell death. Cells repair DSBs through two major mechanisms: non-homologous end joining (NHEJ) and homologous recombination (HR). Whereas DSB repair prevents cells from dying, inaccurate repair might be a major source of mutagenesis and genomic instability. The budding yeast *Saccharomyces cerevisiae* has served for several decades as one of the most useful model organisms to study both repair mechanisms, including their influence in the stability of the genome. Thus, NHEJ is generally considered error-prone as it often creates short deletions or insertions at the site of the DNA junction<sup>1,2</sup>. In addition, NHEJ can lead to chromosome translocations when two or more DSBs coincide in space and time. By contrast, HR is generally considered an error-free repair mechanism when the intact sister chromatid serves as a template. Nevertheless, the risk of choosing alternative partially homologous sequences during HR repair may actually feed chromosome rearrangements. For instance, the use in diploid cells of the homologous chromosome, instead of the sister chromatid, may result in loss of heterozygosity. Hence, it is not surprising that yeast, and many other organisms, prefers HR only when a sister chromatid is available in close proximity. Cells lack sister chromatids in G<sub>1</sub>, the resting period of the cell cycle between the segregation of the sister chromatids to the daughter cells and the next replication of the chromosomal DNA. Because G<sub>1</sub> is the only cell cycle stage where the activity of the cyclin dependent kinase (CDK) is low, it appears logical that cells have coupled the CDK activity to the selection between NHEJ and HR<sup>3–8</sup>. Accordingly, low CDK activity inhibits HR in favour of NHEJ, whereas high CDK promotes HR. However, there is a small window in the cell cycle, where CDK is high, despite a sister chromatid is not physically available for HR: late anaphase/telophase.

Herein, we address this paradox by studying the cell response to DSBs in telophase. We find that such response resembles in many ways what is seen in S/G<sub>2</sub>, including the activation of the DNA damage checkpoint (DDC), which leads to a delay in the telophase-G<sub>1</sub> transition in this case. Surprisingly, we observe that the segregation of sister chromatids is partly reverted and that sister loci can coalesce after generation of DSBs. We further show that this regression phenotype mechanistically depends on the DDC, as well as the kinesin-5 microtubule motor protein Cin8. We conclude that chromosome segregation can be a reversible process.

### Results

**DSBs in telophase activate the DDC to block the entry in G<sub>1</sub>.** We took advantage that *S. cerevisiae* cells can be easily and stably arrested in telophase to check the DSB response at this cell cycle stage. We arrested cells in telophase through the broadly used thermosensitive allele *cdc15-2*. Cdc15 is a key kinase in the Mitotic Exit Network (MEN) that allows cytokinesis and reduction of CDK activity, a hallmark of G<sub>1</sub><sup>9</sup>. We created randomly distributed DSBs using phleomycin, a radiomimetic drug<sup>10</sup>. Treatment with phleomycin (10 µg mL<sup>-1</sup>, 1 h) caused hyperphosphorylation of Rad53 (Fig. 1a), a classical marker for the activation of the DDC<sup>11</sup>. The degree of hyperphosphorylation was equivalent to those seen in G<sub>1</sub>- and G<sub>2</sub>/M-blocked cells, where Rad53 amplifies the corresponding checkpoint responses that delay G<sub>1</sub>-to-S transition and anaphase onset, respectively<sup>12</sup>. We thus checked whether a telophase-to-G<sub>1</sub> delay was also observed after phleomycin treatment. Indeed, concomitant removal of phleomycin and re-activation of Cdc15-2 (shift the temperature from 37 to 25 °C) showed a delay in both cytokinesis and G<sub>1</sub> entry relative to cells which were not treated with phleomycin (mock treatment). For instance, plasma membrane

ingression and resolution at the bud neck (abscission) was clear for ~70% of cells just 1 h after Cdc15 re-activation (Fig. 1b); note that most mother–daughter doublets remain together during a *cdc15-2* release, at least for the upcoming cell cycle<sup>13,14</sup>. When telophase cells were treated with phleomycin, abscission was severely delayed; <50% by 3 h (Fig. 1b). The telophase-to-G<sub>1</sub> delay was also evident through three additional markers. Firstly, only G<sub>1</sub> cells respond to the alpha-factor pheromone (αF) acquiring a shmoo-like morphology. We thus added αF after reactivating Cdc15 and found that <50% of phleomycin-treated cells had responded by 3 h, versus ~75% of mock-treated cells (Supplementary Fig. 1). Secondly, the CDK-inhibitor Sic1 is only present in G<sub>1</sub> cells<sup>15</sup>. We checked Sic1 levels after Cdc15 re-activation and found a clear delay in its production after phleomycin treatment (Fig. 1c). Thirdly, flow cytometry (FACS) showed that the 2C content, expected in cells arrested in telophase, was long-lasting after phleomycin. By contrast, a mock-treated culture shortly turned this 2C peak into either 1C content (a subset of mother–daughter doublets are separated during the harsh treatment for FACS, provided that cytokinesis is completed) or 4C (DNA replication of the immediate progeny without mother–daughter separation) (Fig. 1d). Finally, we confirmed genetically that the DDC was responsible for this telophase-G<sub>1</sub> delay. This checkpoint relies on a biochemical cascade that goes from signalling kinases, such as Mec1 and Tel1, to effector kinases such as Rad53 and Chk1<sup>8,16</sup>. In between, the adaptor kinase Rad9 transduces the checkpoint signal from the signalling to the effector kinases; with *rad9Δ* mutants being incapable of blocking the G<sub>1</sub>-to-S and G<sub>2</sub>/M-to-anaphase transitions after DSBs<sup>17–19</sup>. In our scenario, *cdc15-2 rad9Δ* mutants failed to block the telophase-G<sub>1</sub> transition after phleomycin treatment (Fig. 1e, f), strongly pointing towards an active role of the DDC in this delay.

**Segregated sister loci can coalesce after DSBs in telophase.** We next focussed on the behaviour of chromosome loci during and after phleomycin treatment in the telophase arrest. We first took advantage of the fact that our *cdc15-2* strains also carried YFP-labelled loci along the chromosome XII right arm (cXIIr; *tetO/TetR*-YFP system)<sup>13</sup>. We started with cXII centromere (cXII-Cen), as a representative of the centromere cluster according to the Rabl configuration<sup>20</sup>. We noted that, whereas mock-treated telophase cells maintained a constant distance of ~8 µm between segregated sister centromeres, phleomycin caused a shortening of this distance to <6 µm (Fig. 2a and Supplementary Fig. 2a). This approximation between sister centromeres occurred around 1 h after phleomycin addition and was maintained for at least another hour upon phleomycin removal. Furthermore, we noted that the approximation was asymmetric (Fig. 2b and Supplementary Fig. 2b), and up to 25% of phleomycin-treated telophase cells had one sister centromere at the bud neck (versus <5% in mock-treated cells; *p* < 0.001, Fisher's exact test). Sister centromere approximation appeared specific to phleomycin (i.e. DSBs) since other DNA damaging agents expected not to generate DSBs in telophase did not bring about this phenotype. Neither methyl methanesulfonate (MMS) nor hydroxyurea (HU) led to cXII-Cen approximation (Fig. 2c). Note that these two agents should generate DSBs only during ongoing DNA replication (S phase), and just after prolonged incubation or in checkpoint-deficient mutants<sup>21</sup>. Accordingly, both agents minimally increased Rad53 phosphorylation in telophase-blocked cells (Supplementary Fig. 3). Furthermore, sister loci approximation was not restricted to centromeres or the extra-long chromosome XII. When we looked at sister loci located in the middle of the longest arm of chromosome V, a representative medium size chromosome, we also observed approximation (Fig. 2d).

2

NATURE COMMUNICATIONS | (2019) 10:2862 | <https://doi.org/10.1038/s41467-019-10742-8> | www.nature.com/naturecommunications

88

Este documento incorpora firma electrónica, y es copia auténtica de un documento electrónico archivado por la ULL según la Ley 39/2015.

Su autenticidad puede ser contrastada en la siguiente dirección <https://sede.ull.es/validacion/>

Identificador del documento: 3075810

Código de verificación: smutbmB+

Firmado por: JESSEL AYRA PLASENCIA  
UNIVERSIDAD DE LA LAGUNA

Fecha: 30/11/2020 12:24:14

María de las Maravillas Aguiar Aguilár  
UNIVERSIDAD DE LA LAGUNA

08/02/2021 13:50:06

4. Results and Discussion

NATURE COMMUNICATIONS | <https://doi.org/10.1038/s41467-019-10742-8>

ARTICLE

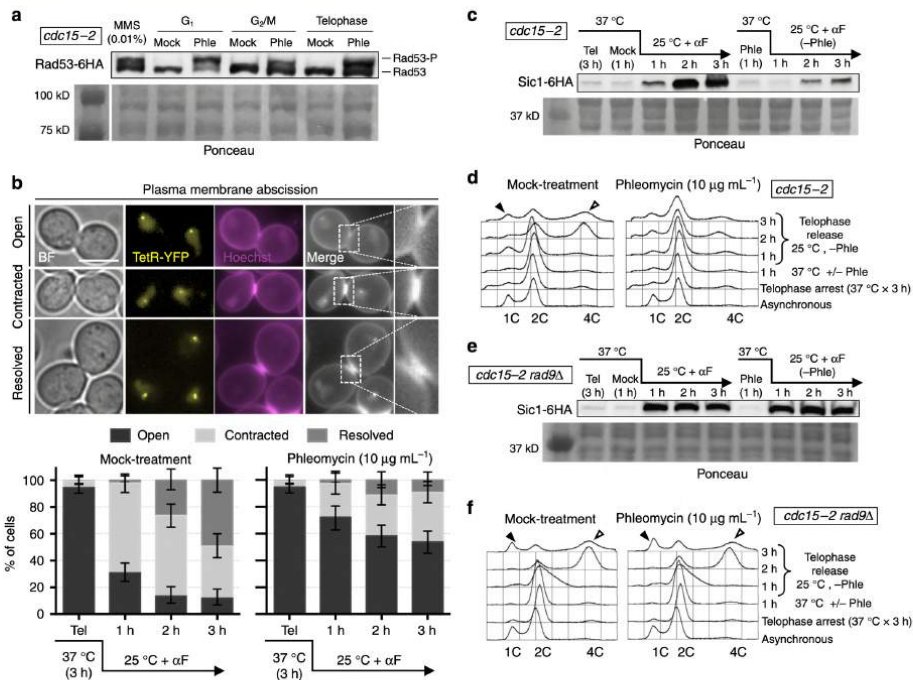


**Fig. 1** Phleomycin triggers the DNA damage checkpoint to delay telophase-G<sub>1</sub> transition. **a** Rad53 gets hyperphosphorylated in telophase after phleomycin treatment. Strain FM2329 was arrested at the indicated cell cycle stages. Phleomycin (10 μg mL<sup>-1</sup>) was then added and cells were harvested after 1 h for western blot analysis. MMS (0.01%), added to an asynchronous culture, was used as Rad53 hyperphosphorylation control. The leftmost lane in the Ponceau staining corresponds to the protein weight markers. **b** Cytokinesis is delayed after phleomycin treatment in telophase. Strain FM593 was arrested in telophase, the culture split into two and one subculture treated with phleomycin. After 1 h, phleomycin was washed away and both subcultures were released from the telophase block, taking samples every hour for plasma membrane abscission analysis using Hoechst staining. The G<sub>1</sub>-blocking pheromone alpha-factor (αF) was added at the time of the telophase release to simplify cell outcomes. On the top, representative micrographs of telophase cells with different degrees of cytokinesis completion. Scale bar corresponds to 5 μm; BF, bright field. At the bottom, charts showing the march of cytokinesis during the telophase release (one representative experiment ± CI95). **c** Sic1 synthesis (G<sub>1</sub> marker) is delayed after DSBs in telophase. FM2323 was treated as described in panel (b), taking samples for western blot analysis. **d** Cell separation and entry in a new S phase is blocked after DSBs in telophase. FM593 was treated as described in panel (b). In this case, though, αF addition was omitted. Samples were taken for FACS analysis. DNA content (1C, 2C or 4C) is indicated under each FACS profile. Filled arrowheads point to the 1C peak; hollow arrowhead points to the 4C peak. **e** Sic1 synthesis is not delayed in strains impaired for the DNA damage checkpoint. FM2477 was treated and samples processed as described in panel (c). **f** Cell separation and entry in a new S phase is not blocked after DSBs in telophase in strains impaired for the DNA damage checkpoint. FM916 was treated and samples processed as described in panel (d). Source data are provided as a Source Data file

Similar shortening for the distance between sister loci was seen for telomeres (Fig. 3a and Supplementary Fig. 4). Strikingly, we also observed coalescence between sister telomeres (Fig. 3a; ~7% in phleomycin vs ~2% in mock treatment for cXIIr-Tel;  $p < 0.001$ , Fisher's exact test), which was further confirmed through short-term videomicroscopy (Fig. 3b; Supplementary Movies 1–3). Filming individual cells also showed acceleration of interloci movement and how coalescence lasted longer than expected from simple Brownian motion (Fig. 3b, c). Approximation and eventual coalescence of a fraction of sister loci appeared to be a general phenomenon after DNA damage caused by phleomycin. Firstly, using the histone variant H2A-mCherry, which labels all nuclear DNA,

we confirmed that phleomycin treatment shortens the distance of the bulk of the segregated nuclear masses (Supplementary Fig. 5a). In addition, we observed confined trafficking of segregated DNA across the bud neck (Supplementary Fig. 5b and Supplementary Movies 4–6). This trafficking involved chromatin that appears partly depleted of histones (at least H2A) or is less condensed than the average segregated masses. Strikingly, phleomycin caused the formation of de novo histone-labelled anaphase bridges (Fig. 3d). These bridges included chromatin confined in bulgy nuclear domains (Fig. 3e, Supplementary Fig. 5a and Supplementary Movie 7). We had described before these bulgy bridges in *top2* mutants arrested in telophase and in the *cdc14-1* late anaphase block, but

NATURE COMMUNICATIONS | (2019) 10:2862 | <https://doi.org/10.1038/s41467-019-10742-8> | www.nature.com/naturecommunications

3

89

Este documento incorpora firma electrónica, y es copia auténtica de un documento electrónico archivado por la ULL según la Ley 39/2015.  
 Su autenticidad puede ser contrastada en la siguiente dirección <https://sede.ull.es/validacion/>

Identificador del documento: 3075810 Código de verificación: smutbmB+

Firmado por: JESSEL AYRA PLASENCIA  
 UNIVERSIDAD DE LA LAGUNA

Fecha: 30/11/2020 12:24:14

María de las Maravillas Aguiar Aguilár  
 UNIVERSIDAD DE LA LAGUNA

08/02/2021 13:50:06

4. Results and Discussion

ARTICLE

NATURE COMMUNICATIONS | <https://doi.org/10.1038/s41467-019-10742-8>

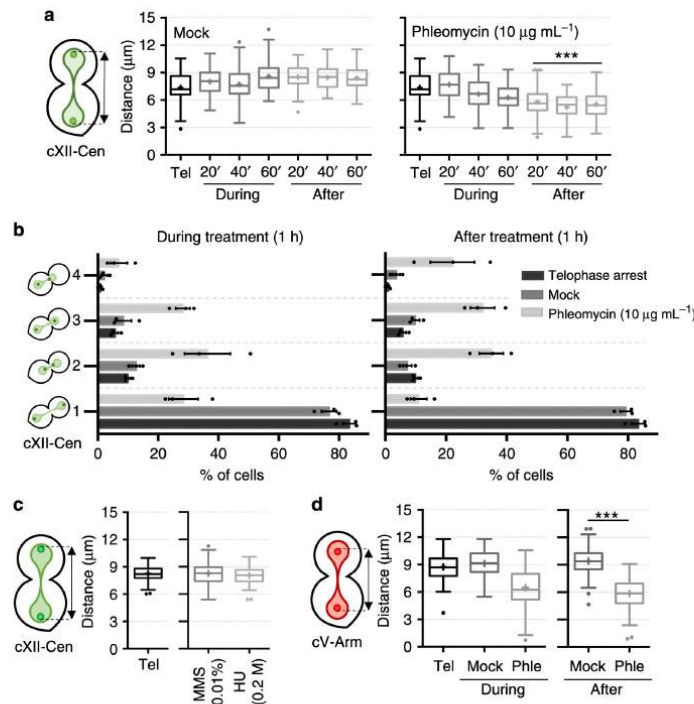


**Fig. 2** DNA double-strand breaks in telophase lead to sister loci approximation. **a** Sister centromeres approach each other during and after generating DSBs in telophase. FM593 was treated as in Fig. 1d, except for the fact that the telophase block was maintained (37 °C) even after phleomycin was washed away. Samples were taken every 20' during and after phleomycin (or mock) treatment and visualised under the microscope. Distance between sister cXII centromeres was measured and box-plotted for each time point ( $N = 70$  cells per box; \*\*\* indicates  $p < 0.0001$  in mock/phleomycin comparisons at each time point, Mann-Whitney  $U$  Test). **b** Relative position of cXII sister centromeres from the former experiment was categorised as depicted on the left (mean  $\pm$  s.e.m.,  $n = 3$  independent experiments); category 1, both centromeres at near polar locations; category 2, closer centromeres with symmetrical distances to the bud neck; category 3, closer centromeres with asymmetrical distances to the bud neck; category 4, one sister centromere at the bud neck. **c** DNA damage caused by MMS (0.01% v/v) or HU (0.2 M) do not trigger approximation of sister cXII centromeres in telophase. FM593 was treated as in (a) except for the drug, and the distance between sister cXII centromeres was box-plotted. Only the telophase block and 1 h following drug addition (during treatment) are represented. **d** Sister loci in the middle of chromosome V also get closer during and after phleomycin treatment. FM2456 was treated like in (a) and the distance between sister cXII centromeres was box-plotted (\*\* indicates  $p < 0.0001$ ; Mann-Whitney  $U$  Test). Source data are provided as a Source Data file

always arising from metaphase-anaphase transitions<sup>13,22</sup>. Secondly, approximation and coalescence were also observed for the repetitive ribosomal DNA array (rDNA), coated with the rDNA binding protein Net1-eCFP (Fig. 3f and Supplementary Fig. 6).

Having shown that DSBs generated by phleomycin in telophase partially turned back sister chromatid segregation, we next wondered about the specificity of this behaviour. Firstly, we addressed if the sustained telophase block contributed to these outstanding cytological phenotypes. Thus, we added phleomycin to cells normally transiting through telophase. There are at least two critical caveats in this experiment; (i) the fact that phleomycin elicits a  $G_2/M$  block in asynchronous cells and (ii) the relatively short duration of telophase. Hence, we performed the experiment in a synchronous  $G_1$  release and closely monitored the peak of cells transiting through anaphase; i.e.,

maximizing budded cells with segregating cXII-Cen and a nucleoplasmic bridge, as reported by the soluble pool of TetR-YFP (Supplementary Fig. 7; 120' from the  $G_1$  release). Phleomycin addition at that peak led to a higher proportion of cells with closer cXII-Cen and shorter nucleoplasmic bridges across the bud neck (Supplementary Fig. 7; ~20% vs <5% in the mock treatment;  $p < 0.001$ , Fisher's exact test). In addition, this experiment also points out that phleomycin blocks the cell cycle in telophase since: (i) fewer cells reached a second cell cycle, as indicated by binucleated dumbbells without a nucleoplasmic bridge (Supplementary Fig. 7a, b)<sup>13</sup> and (ii) almost all Rad53 appeared hyperphosphorylated despite <5% of cells stayed in  $G_2/M$  (mononucleated dumbbells) 1 h after adding phleomycin (Supplementary Fig. 7c). Secondly, we wondered if approximation and coalescence were specific for DSBs generated via phleomycin. For this purpose, we endonucleolytically cleaved a

4

NATURE COMMUNICATIONS | (2019) 10:2862 | <https://doi.org/10.1038/s41467-019-10742-8> | www.nature.com/naturecommunications

90

Este documento incorpora firma electrónica, y es copia auténtica de un documento electrónico archivado por la ULL según la Ley 39/2015.  
 Su autenticidad puede ser contrastada en la siguiente dirección <https://sede.ull.es/validacion/>

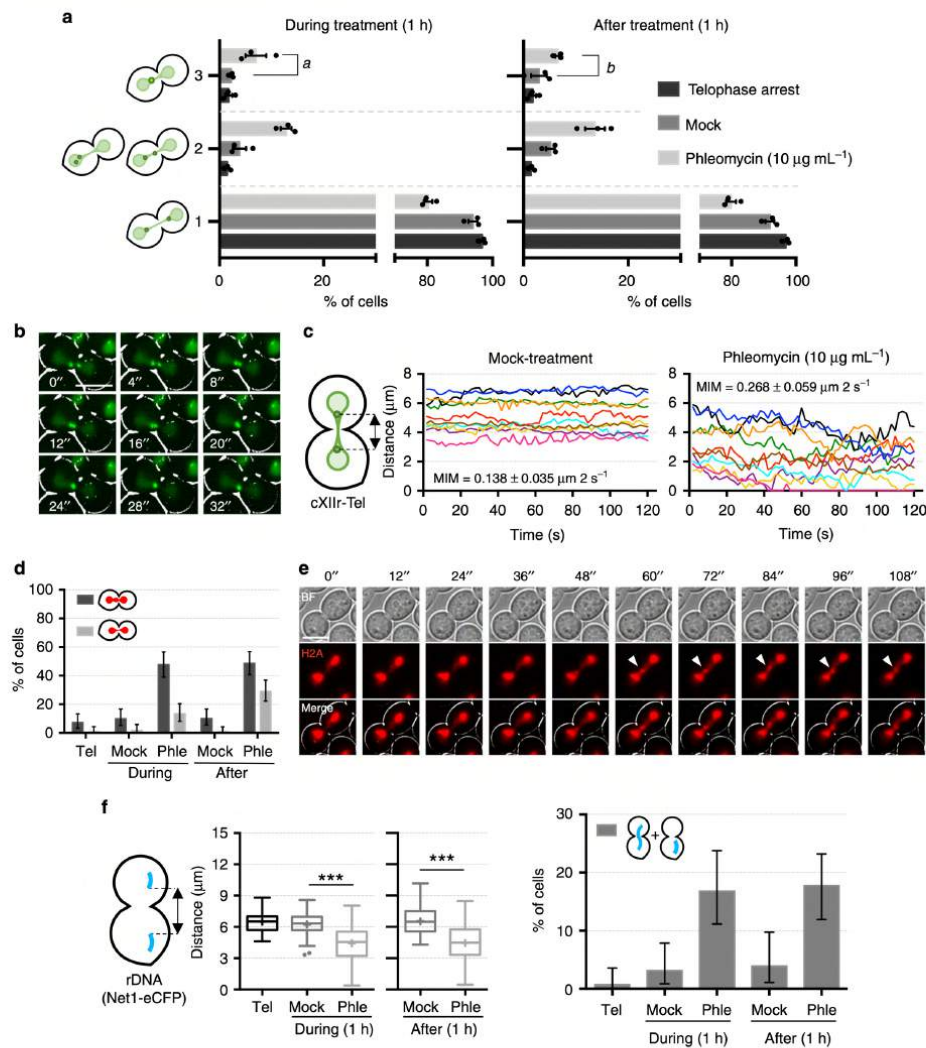
Identificador del documento: 3075810 Código de verificación: smutbmB+

Firmado por: JESSEL AYRA PLASENCIA  
 UNIVERSIDAD DE LA LAGUNA

Fecha: 30/11/2020 12:24:14

María de las Maravillas Aguiar Aguiar  
 UNIVERSIDAD DE LA LAGUNA

08/02/2021 13:50:06



single locus by expressing the I-SceI endonuclease in a strain that carried the I-SceI recognition sequence adjacent to the YEL023C gene, ~44 kbs from chromosome V centromere<sup>23</sup>. This locus has a *tetOs* array on one of its flanks (*URA3* locus), which allowed us to monitor sister loci position before and after I-SceI cleavage. We observed both approximation and coalescence of segregated YEL023C loci after inducing I-SceI for 1 h (Supplementary Fig. 8 and Supplementary Movies 8–10), strongly pointing to coalescence of sister loci as a result of nearby DSBs. Incidentally, we also observed that when one of the loci moved through the bud neck to seek its sister, it stretched to a point where the *tetOs* array

appeared as a line rather than a focus. This striking finding supports the aforementioned statement about local decondensation of chromatin when passing through the bud neck.

Taken together, we conclude in this chapter that all segregated nuclear and nucleolar material gets closer after the generation of DSBs in telophase; and that, under these circumstances, events of sister loci coalescence occur.

**Regression of segregation depends on DDC but not on HR.** Having shown that DSBs in telophase rendered a cell cycle block

#### 4. Results and Discussion

### ARTICLE

NATURE COMMUNICATIONS | <https://doi.org/10.1038/s41467-019-10742-8>

**Fig. 3** DSBs in telophase cause sister loci acceleration, coalescence and de novo anaphase bridges. **a** Sister telomeres move to the same cell body and coalesce after phleomycin treatment. FM588 was treated like in Fig. 2a. Relative position of cXIIr sister telomeres was categorised as depicted on the left (mean  $\pm$  s.e.m.,  $n = 3$ ); category 1, sister telomeres in different cell bodies; category 2, telomeres localise in the same cell body or at the bud neck; category 3, sister telomeres coalesce ( $a [p < 0.001]$  and  $b [p = 0.04]$  denote the corresponding mock/phleomycin comparisons; Fisher's exact tests from the pooled experiments). **b** Sister telomeres dynamically coalesce during DSBs in telophase. FM588 was treated like in (a) and cells were filmed for 2 min after 1 h of phleomycin (or mock) addition. A representative example of coalescence is shown. **c** Inter sister telomere movement accelerates after DSBs. Kinetograms of 10 randomly selected cells. The mean interloci movement (MIM) is displayed within the charts (mean  $\pm$  s.d.,  $n = 10$  cells;  $p < 0.0001$  in mock/phleomycin comparison, Student's  $t$  test). **d** DSBs in telophase generate de novo chromatin bridges. FM2354 was treated like in (a) and the histone-labelled nuclear masses categorised in three: binuclear (not shown), with a gross/bulgy bridge (dark grey) and with a thinner/fainter histone-poor bridge (light grey). A representative experiment is shown ( $\pm$ CI95). **e** The de novo chromatin bridges are dynamic. FM2354 was filmed as in (c). A representative cell in which a bulgy bridge is dynamically formed from a histone-poor bridge. Filled arrowheads point to the bulge along the chromatin bridge. **f** Approximation and coalescence also occur for the rDNA/nucleolus. Strain FM2301 was treated like in (a). On the left, box-plots of minimum distances between sister rDNA signals under the indicated treatments ( $N = 70$  cells per box; \*\*\* indicates  $p < 0.0001$ ; Mann-Whitney  $U$  Test). Single nucleolar signals were ignored for this calculation. On the right, bar chart for proportion of cells with a single nucleolus either in one cell body or stretched across the bud neck ( $\pm$ CI95). Scale: white bars correspond to 5  $\mu$ m; BF, bright field. Source data are provided as a Source Data file

at that stage and that segregation is partially regressed to allow sister loci coalescence, we next wondered about the significance of these phenotypes. We began asking whether regression and coalescence were also under control of the DDC. Thus, we checked sister loci approximation, coalescence and acceleration in *rad9 $\Delta$*  mutants. We found that sister cXIIr-Tel loci did not move to the same cell body and coalesce in this mutant upon phleomycin addition (Fig. 4a). Moreover, interloci acceleration was rather modest in phleomycin (Fig. 4b); whereas in DDC-proficient cells the acceleration was twofold (from 0.14 to 0.27  $\mu$ m per frame), in *rad9 $\Delta$*  was only 33% faster (from 0.16 to 0.20  $\mu$ m per frame). These results demonstrate that the observed cytological responses to DSBs in telophase are regulated by the DDC. Therefore, they are part of the cell reprogramming aimed to cope with DSBs in telophase.

We noticed that dynamic coalescent events between sister loci could represent a chance for HR to repair DSBs with the intact sister chromatid. Therefore, we next drove our attention to HR itself. In yeast, HR is thoroughly impaired by deleting the *RAD52* gene<sup>24</sup>. Thus, we also checked sister loci approximation, coalescence and acceleration in *rad52 $\Delta$*  mutants. Surprisingly, we found that none of these DSB-induced phenotypes was abolished in *rad52 $\Delta$* ; rather, cXIIr-Tel coalescence was more frequent than that in the wild type (~20% vs ~7%) (Fig. 4c). Strikingly, not only interloci movement was the highest in *rad52 $\Delta$*  with phleomycin (0.37  $\mu$ m per frame) but it was also high even without DNA damage (0.31  $\mu$ m per frame) (Fig. 4d). The latter suggests that Rad52 plays an unexpected role in restraining loci movement in cells not challenged with exogenously generated DSBs. Lastly, we addressed whether Rad52 may influence the formation of de novo chromatin bridges, finding no differences between the wild type (Fig. 3d) and *rad52 $\Delta$*  strain (Fig. 4e). Altogether, we concluded that HR itself (Rad52) is not responsible for the aforementioned phenotypes in response to DSBs in telophase. This situates the DDC (Rad9) upstream the observed phenotypes after DSBs, while placing any putative role of HR downstream.

**HR repairs DSBs in telophase.** In order to assess whether HR repairs DSBs in telophase, we performed a series of clonogenic survival experiments. We reasoned that, if DSBs were repaired in telophase using the sister chromatid, sensitivity to phleomycin would be more similar to that of a  $G_2/M$  arrest. Conversely, if DSBs are either left unrepaired for the next cell cycle or repaired via NHEJ, the sensitivity would resemble that observed during a  $G_1$  block. Importantly, because HR is chosen for DSBs repair when a sister chromatid is available (i.e. in  $G_2/M$  but not in  $G_1$ ), comparison of survival rates between the wild type and *rad52 $\Delta$*

would further inform whether HR is used in telophase for DSB repair. Thus, we arrested both strains in  $G_1$  ( $\alpha$ DF),  $G_2/M$  (Noc) and telophase (*cdc15-2*), and surveyed survival after 1 h of phleomycin treatment (Fig. 4f). We found that (i) survival to DSBs in telophase was similar to  $G_2/M$  in the wild type, not  $G_1$ ; and (ii) Rad52 was directly responsible for such survival since there was a threefold drop of survivors in *rad52 $\Delta$*  for DSBs generated in both  $G_2/M$  and telophase. Taken together, we conclude that DSBs in telophase are repaired by HR during the ensuing arrest and before cells transit into  $G_1$ .

**Cin8 drives reversion of chromosome segregation.** Having observed the approximation of segregated sister loci, we next wondered about the cell forces underlying this behaviour. We consequently drove our attention to the spindle apparatus and engineered *cdc15-2* strains where we labelled the microtubules (MTs) (GFP-Tub1) and the spindle pole bodies (SPBs) (Spc42-mCherry), budding yeast equivalent to centrosomes. Phleomycin turned the elongated spindle, characteristic of telophase, into a rather dynamic star-like distribution (Fig. 5a and Supplementary Movies 11–14). This new morphology points to a redistribution of Tubulin towards astral MTs, while nuclear MTs appear misaligned and with a weakened interpolar MT interaction. The change in the spindle morphology shortened the spindle length, which was confirmed by the approximation of the segregated SPBs from ~9 to ~6  $\mu$ m (Fig. 5b). The separation of SPBs in anaphase pulls attached centromeres apart, favouring the centromere-to-telomere segregation of sister chromatids<sup>25</sup>. Co-visualization of SPBs and cXII sister centromeres showed that SPBs often headed centromeres in the approximation (Fig. 5c), suggesting that either the strengthened astral microtubules or the weakened spindle indirectly drive sister loci approximation by pushing SPBs to each other.

These results led us to check the behaviour of Cin8 upon DSBs in telophase. Cin8 is a bidirectional mitotic kinesin-5 motor protein that makes antiparallel interpolar microtubules slide apart, thus favouring spindle elongation in anaphase<sup>26,27</sup>. Upon phleomycin treatment, Cin8 relocated from the spindle to two discrete foci in telophase-blocked cells (Fig. 6a). These foci likely correspond to SPBs and/or kinetochore clusters<sup>28–30</sup>. Cin8 localization throughout the cell cycle depends on its phosphorylation status, with dephosphorylated Cin8 mostly located at the mitotic spindle<sup>31</sup>. We checked phosphorylation levels of Cin8 after DSBs in telophase and found they are intermediate between  $S/G_2$  (fully dephosphorylated) and an unperturbed telophase (Fig. 6b). Consequently, a partial dephosphorylation of Cin8 occurs upon DSBs in telophase. We also checked if Cdc14, the master phosphatase in anaphase/telophase, played an active role

6

NATURE COMMUNICATIONS | (2019) 10:2862 | <https://doi.org/10.1038/s41467-019-10742-8> | www.nature.com/naturecommunications

92

Este documento incorpora firma electrónica, y es copia auténtica de un documento electrónico archivado por la ULL según la Ley 39/2015.

Su autenticidad puede ser contrastada en la siguiente dirección <https://sede.ull.es/validacion/>

Identificador del documento: 3075810

Código de verificación: smutbmB+

Firmado por: JESSEL AYRA PLASENCIA  
UNIVERSIDAD DE LA LAGUNA

Fecha: 30/11/2020 12:24:14

María de las Maravillas Aguiar Aguilár  
UNIVERSIDAD DE LA LAGUNA

08/02/2021 13:50:06

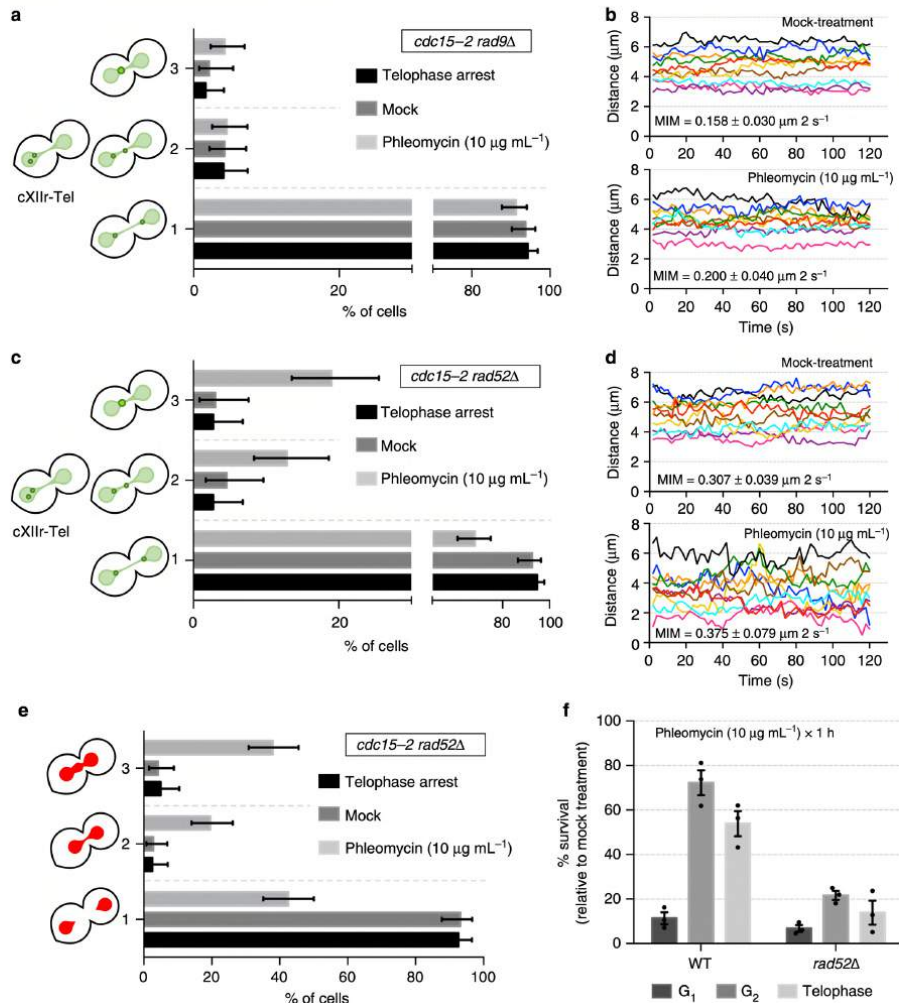


**Fig. 4** Sister loci acceleration and coalescence in telophase depends on Rad9 but is independent of Rad52. **a** Sister telomeres need the DNA damage checkpoint (Rad9 branch) to move to the same cell body and coalesce after DSBs in telophase. FM916 (*rad9Δ*) was treated like in Fig. 2a. Relative position of cXIIr sister telomeres was categorised as depicted on the left (one representative experiment  $\pm$  CI95); categories 1, 2 and 3 as defined in Fig. 3a. **b** The increase in inter sister telomere movement also depends on Rad9. Kinetograms of 2-min movies from 10 randomly selected cells in the previous experiment. The MIM is also displayed within the charts (mean  $\pm$  s.d.,  $n = 10$  cells). Note that the acceleration in interloci movement after phleomycin addition is only one-third of that observed in DDC-proficient cells (compare with Fig. 3c). **c** Sister telomeres coalescence is independent of a functional HR. FM889 (*rad52Δ*) was treated like in Fig. 2a. Relative position of cXIIr sister telomeres was categorised as depicted on the left (one representative experiment  $\pm$  CI95); categories 1, 2 and 3 as defined in Fig. 3a. **d** Rad52 restrains inter sister telomere movement in telophase. Kinetograms of 2-min movies from 10 randomly selected cells in the previous experiment. The MIM is also displayed within the charts (mean  $\pm$  s.d.,  $n = 10$  cells). Note how MIM is already doubled in the mock treatment when compared with the wild type (Fig. 3c). **e** Formation of de novo chromatin bridges is independent of Rad52. Samples from the previous experiments were taken and the nuclear mass stained with Hoechst. Nuclear morphology was categorised as followed: 1, binuclear; 2, thin bridge; 3, gross/bulgy bridge ( $\pm$ CI95). **f** HR repairs DSBs in telophase. Clonogenic survival of strains FM588 (WT) and FM889 (*rad52Δ*) arrested in G<sub>1</sub>, G<sub>2</sub> or telophase before treated with phleomycin (mean  $\pm$  s.e.m.,  $n = 3$  independent experiments). Survival is normalised to a parallel mock-treated culture (reference for 100% survival). Source data are provided as a Source Data file

Este documento incorpora firma electrónica, y es copia auténtica de un documento electrónico archivado por la ULL según la Ley 39/2015.  
 Su autenticidad puede ser contrastada en la siguiente dirección <https://sede.ull.es/validacion/>

Identificador del documento: 3075810

Código de verificación: smutbmB+

Firmado por: JESSEL AYRA PLASENCIA  
 UNIVERSIDAD DE LA LAGUNA

Fecha: 30/11/2020 12:24:14

María de las Maravillas Aguiar Aguiar  
 UNIVERSIDAD DE LA LAGUNA

08/02/2021 13:50:06

4. Results and Discussion

ARTICLE

NATURE COMMUNICATIONS | <https://doi.org/10.1038/s41467-019-10742-8>

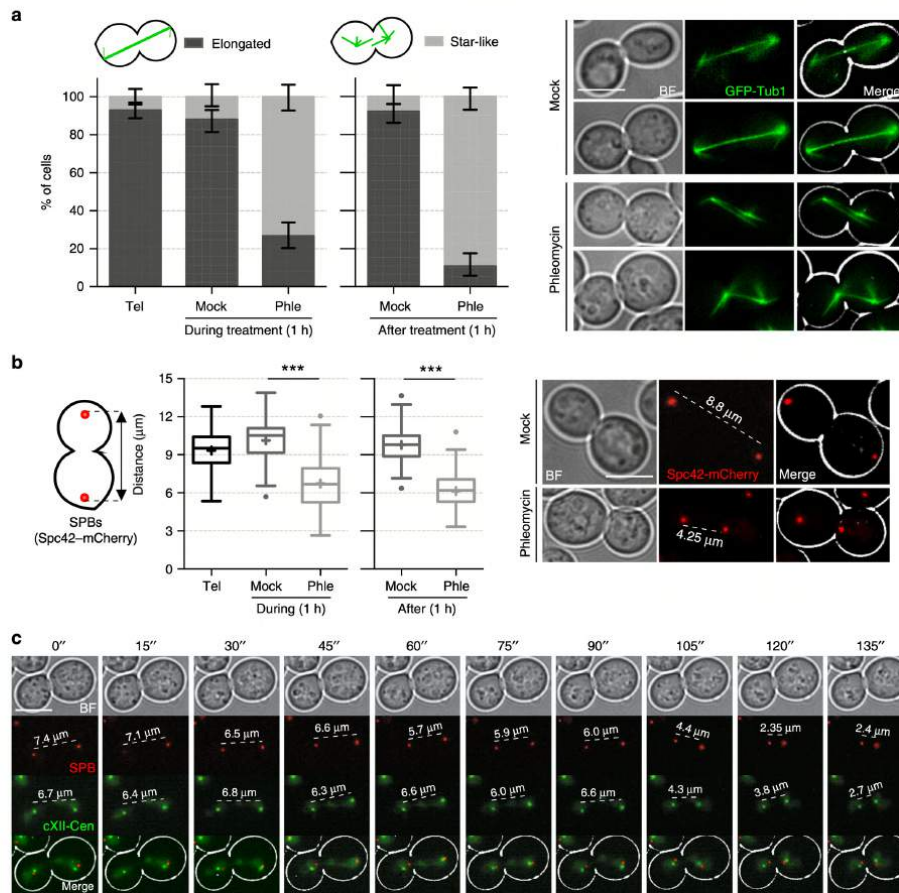


**Fig. 5** Dynamics of microtubules after DNA double-strand breaks in telophase. **a** Microtubules are repositioned after DSBs in telophase. Strain FM2381 was treated as in Fig. 2a. At the indicated conditions, samples were taken and microtubules visualised under the microscope. Two categories were considered for quantification of the spindle: elongated and star-like, the latter being formed by multiple and shorter microtubule fibres arising from each SPB (% cells  $\pm$  CI95, one representative experiment). **b** SPBs approach each other after DSBs. Strain FM2316 was treated like in Fig. 2a. On the left, box-plots of distances between SPBs under the indicated treatments (\*\*\*) indicates  $p < 0.0001$ ; Mann-Whitney *U* Test). On the right, representative cells for the major phenotypes observed during each treatment. **c** SPBs often move ahead centromeres during the approximation that follows DSB generation in telophase. Strain FM2316 was treated and filmed like in Fig. 3b. Scale: white bars correspond to 5  $\mu$ m; BF, bright field. Source data are provided as a Source Data file

in dephosphorylating Cin8. Two sequential waves of Cdc14 activation coordinate anaphase events and the telophase- $G_1$  transition<sup>32</sup>. Cdc14 is activated through its release out of the nucleolus, where it is sequestered for most of the cell cycle. At the *cdc15-2* block, Cdc14 is back in the nucleolus after completion of the first activation wave in early anaphase. It is conceivable, though, that a new partial release upon phleomycin addition could drive Cin8 dephosphorylation. In fact, two previous reports encourage this possibility: Cin8 is a target of Cdc14 in early anaphase<sup>33</sup>, and phleomycin promotes Cdc14 release in metaphase-blocked cells<sup>34</sup>. However, we could not observe

Cdc14 release upon phleomycin in *cdc15*-arrested cells (Supplementary Fig. 9a). Furthermore, Cin8 still became dephosphorylated upon phleomycin in the *cdc14-1* mutant (Supplementary Fig. 9b).

We hypothesised that the Cin8 relocation was a consequence of its novel minus-end-directed motility<sup>27</sup>, which might reset the spindle to revert its elongation in cells already in late anaphase. To gain insight on this, we looked at how a set of Cin8 phosphomutants in the motor domain responded to phleomycin during the telophase block. In the Cin8-3A mutant, which mimics a constitutive non-phosphorylated Cin8 in the motor domain (i.e.,

8

NATURE COMMUNICATIONS | (2019) 10:2862 | <https://doi.org/10.1038/s41467-019-10742-8> | www.nature.com/naturecommunications

94

Este documento incorpora firma electrónica, y es copia auténtica de un documento electrónico archivado por la ULL según la Ley 39/2015.  
 Su autenticidad puede ser contrastada en la siguiente dirección <https://sede.ull.es/validacion/>

Identificador del documento: 3075810 Código de verificación: smutbmB+

Firmado por: JESSEL AYRA PLASENCIA  
 UNIVERSIDAD DE LA LAGUNA

Fecha: 30/11/2020 12:24:14

María de las Maravillas Aguiar Aguiar  
 UNIVERSIDAD DE LA LAGUNA

08/02/2021 13:50:06



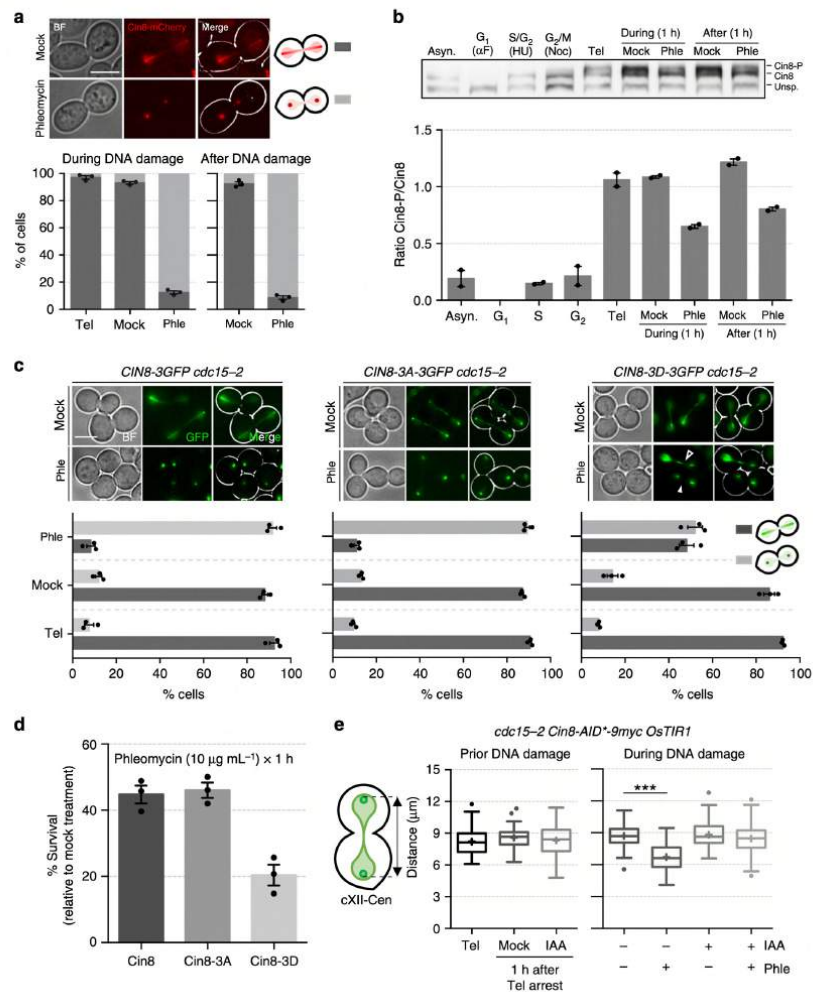


**Fig. 6** Kinesin-5 Cin8 drives sister loci approximation in telophase. **a** Cin8 relocates from the spindle into SPBs/kinetochores after DSBs. Strain FM2317 was treated like in Fig. 2a and checked under the microscope at indicated times. Location of Cin8 was categorised into two: all along the spindle (dark grey bars) and concentrated in two foci (light grey bars) (mean  $\pm$  s.e.m.,  $n = 3$  experiments). **b** A pool of Cin8 becomes dephosphorylated in telophase after DSBs. Strain FM2335 was treated like in Fig. 2a and, in addition, blocked at the indicated cell cycle stages. The upper picture shows western blot of Cin8-9myc, where myc signal appears as a triplet as reported before<sup>53</sup>. The lowest band is unspecific and serves as a loading control. The highest (slowest in PAGE migration) corresponds to the Cin8 phosphorylated forms (Cin8-P). Cin8 is absent in G<sub>1</sub><sup>53</sup>. The lower chart depicts quantification of the Cin8-P/Cin8 ratios (mean  $\pm$  s.e.m.,  $n = 2$  independent experiments). **c** The relocation of Cin8 upon DSBs is partly dependent on its motor domain. Relocalization of WT Cin8 (FM2505) was compared with Cin8 phosphomutants for its motor domain (Cin8-3A, FM2506; Cin8-3D, FM2507). All strains were treated as in Fig. 2a. Upper images show representative micrographs during treatment (1 h). Lower charts depict quantifications (mean  $\pm$  s.e.m.,  $n = 3$  independent experiments). **d** Relocalization of Cin8 contributes to cell tolerance to DSBs in telophase. Clonogenic survival of strains in (c). Cells were arrested in telophase before being treated with phleomycin (mean  $\pm$  s.e.m.,  $n = 3$  independent experiments). Survival is normalised to a parallel mock-treated culture (reference for 100% survival). **e** Cin8 is needed to bring closer sister loci upon double-strand breakage in telophase. FM2466 (bearing a conditional degen Cin8-aid variant) was treated as in Fig. 2a, except for the fact that Cin8-aid degradation was induced 1 h before mock/phleomycin treatments. Scale: white bars correspond to 5  $\mu$ m; BF, bright field. Source data are provided as a Source Data file

Este documento incorpora firma electrónica, y es copia auténtica de un documento electrónico archivado por la ULL según la Ley 39/2015.  
 Su autenticidad puede ser contrastada en la siguiente dirección <https://sede.ull.es/validacion/>

Identificador del documento: 3075810 Código de verificación: smutbmB+

Firmado por: JESSEL AYRA PLASENCIA  
 UNIVERSIDAD DE LA LAGUNA

Fecha: 30/11/2020 12:24:14

María de las Maravillas Aguiar Aguiar  
 UNIVERSIDAD DE LA LAGUNA

08/02/2021 13:50:06

#### 4. Results and Discussion

### ARTICLE

NATURE COMMUNICATIONS | <https://doi.org/10.1038/s41467-019-10742-8>

active motility along MTs), phleomycin still led to Cin8 relocalization (Fig. 6c). Nonetheless, only partial relocalization was obtained with the Cin8-3D mutant, which mimics a constitutive phosphorylated Cin8 (i.e., reduced binding to and motility along MTs). The most obvious conclusion from this experiment is that phleomycin polarises Cin8 movement towards the SPBs through its minus-end motility, using MTs as motorways, while it also drives Cin8 dephosphorylation to recruit soluble Cin8 to MTs. This two-step mechanism, recruitment to MTs and walking towards the SPBs, suggests that Cin8 relocalization could play an active role at the poles. In agreement with this, we found that clonogenic survival after phleomycin treatment in telophase was dependent on the Cin8 ability to get dephosphorylated, with Cin8-3D having worse survival than wild-type Cin8 and Cin8-3A (Fig. 6d). In order to confirm the active role hypothesis, we employed a conditional degen version of Cin8 (Cin8-aid) and exposed cells to phleomycin. Indeed, without Cin8, telophase cells were unable to bring closer the segregated genetic material (Fig. 6e).

Finally, we addressed whether the shift in MT distribution resulted in an active mechanism for the approximation of the segregated material. We reasoned that Cin8 relocalization weakens interpolar MTs, and perhaps also enforces astral MTs, which, in turn, would favour new pulling forces to bring closer SPB/kinetochores/centromeres. With this aim, we studied the consequences of eliminating MTs in telophase-blocked cells, with or without concomitant DSBs. Nocodazole, a microtubule depolymerizing drug, mimicked most of the phenotypes just described for phleomycin; i.e., shortening of sister loci distances and acceleration of interloci movement (Fig. 7a–c). In general, nocodazole masked the effect of phleomycin. For instance, nocodazole led to a more symmetric approximation of sister loci (compare categories 2 and 3 between Figs. 2b and 7b), with double phleomycin–nocodazole treatment resembling the phenotype of just nocodazole. A similar relationship was seen for those cells where sister centromeres ended up within the same cell body (category 5 in Fig. 7b). This was a very rare event in cells just treated with phleomycin, likely because astral MTs prevented SPBs from passing through the bud neck (Supplementary Movies 13 and 14). Importantly, nocodazole and phleomycin had an additive effect on loci movement for a subset of cells (Fig. 7d), demonstrating that other cell components aside from MTs participate in loci acceleration after the generation of DSBs in telophase. Altogether, these results position weakening of interpolar MTs on top of reinforcing astral MTs as the main cell force that partially regress sister chromatid segregation. Noteworthy, phleomycin did not depolymerise microtubules. Firstly, the effect of nocodazole and phleomycin in telophase MTs was clearly different; nocodazole caused GFP-Tub1 to appear homogeneously distributed throughout the cell, with signs of neither nuclear nor astral microtubules (Supplementary Fig. 10a). Secondly, when added to an asynchronous culture, phleomycin arrested cells in G<sub>2</sub>/M with the characteristic metaphase spindle (Supplementary Fig. 10b).

### Discussion

In this study, we demonstrate that DSBs can partially regress chromosome segregation in late anaphase. The results shown above question the irreversible nature of chromosome segregation, at least in budding yeast. Importantly, we also provide mechanistic bases for this regression (Fig. 8): (i) weakening of the elongated spindle, likely through dephosphorylation-dependent relocalization of the bipolar kinesin-5 Cin8, which allows sister loci to get closer; (ii) local decondensation of chromatin, which favours passage through the bud neck (i.e., cytokinetic plane); and

(iii) acceleration of loci movement, which increases the probability of closer sister loci to coalesce. Furthermore, we provide evidence that these processes depend on the activation of the DDC to DSBs. We hypothesise that sister loci coalescence in telophase provides a chance to repair DSBs through the efficient and error-free HR pathway; a hypothesis supported by the marked drop of survivors in HR-deficient strains (Fig. 4f). A time window for such repair exists as we also demonstrate that DSBs delay cytokinesis and telophase–G<sub>1</sub> transition for more than 2 h (Fig. 1). This telophase checkpoint also depends on Rad9. Even though we have not mechanistically addressed in detail this checkpoint, it is likely that the axis that connects Rad9/Rad53 with MEN inhibition is responsible for the cell cycle arrest<sup>35,36</sup>.

DSBs generated in anaphase/telophase have been barely studied despite they pose an even higher risk for genome integrity than those generated in G<sub>1</sub>, S phase, G<sub>2</sub> and prophase/metaphase (M-phase). The reasons for this lay in both, the absence of a nearby sister chromatid and the increased risk of having DSB ends in different compartments (daughters nuclei). In our study, we have generated DSBs once the cells were already in telophase (*cdc15-2* block). This scenario physically resembles G<sub>1</sub> (no sister chromatid nearby but the two DSB ends locate in the same compartment), yet it shares with S/G<sub>2</sub>/M the high CDK activity that favours HR for repair. We generated DSBs through two different approaches. On the one hand, the radiomimetic drug phleomycin, whose major advantage resides in that DSBs are random. This is critical because the probability of having two DSBs in the same pair of sister loci is virtually zero. In this way, we assure that the intact sister chromatid may serve as a genuine template for HR. On the other hand, we also used DSBs generated by the controlled expression of the I-SceI endonuclease. Whereas this approach has the advantage of restricting the DSB to a defined region, which can then be followed by fluorescent tags, it often generates DSBs in both sister loci. Either way, we observed coalescence of selected sister loci (Fig. 3 and Supplementary Fig. 8). In both cases, coalescence was relatively low in end-point experiments (~10% of telophase cells), yet significantly higher than the background levels seen without DSBs (2–3%). This is somehow expected for randomly generated DSBs (phleomycin) since only a minor proportion of cells would have a DSB near the sister loci being monitored by tags. In the case of endonucleolytic cleavage, even though coalescence might appear lower than expected, we must bear in mind that most cells would carry two equivalent DSBs, one per sister chromatid; and this could hinder the capture of an intact sister for HR repair. Because we also filmed individual cells during short periods of sustained DNA damage, we actually suggest that coalescence occurs more often than what we observed in fixed end-point experiments. We reach this conclusion since we could capture dynamic coalescent events in 2-min movies, long (1 h) after the initial DSBs were generated. It is likely that successive DSBs are continuously generated and repaired in telophase under ongoing DNA damage, and transient coalescence reflects cycles of repair attempts of a nearby DSB.

Despite sister loci coalescence was seen at any given time point in ~10% of cells, the approximation of sister loci was almost a general phenomenon after double-strand breakage in telophase (>75% of cells approximate centromeres and SPBs; Figs. 2 and 5). In addition, ~20% of segregated sister loci end up in the same cell body after DSBs, irrespective of whether they then coalesce or not. This implies that one of the labelled sister loci travels back through the narrow bud neck. Accordingly, we observed the appearance of de novo anaphase bridges where before there were binucleated cells (in up to 50% of telophase cells; Figs. 3, 4 and Supplementary Fig. 5). Merging of the segregated nucleoli into a single entity in up to 20% of telophase cells was another indicator of regression in sister chromatid segregation. Altogether, we

10

NATURE COMMUNICATIONS | (2019) 10:2862 | <https://doi.org/10.1038/s41467-019-10742-8> | www.nature.com/naturecommunications

96

Este documento incorpora firma electrónica, y es copia auténtica de un documento electrónico archivado por la ULL según la Ley 39/2015.

Su autenticidad puede ser contrastada en la siguiente dirección <https://sede.ull.es/validacion/>

Identificador del documento: 3075810

Código de verificación: smutbmB+

Firmado por: JESSEL AYRA PLASENCIA  
UNIVERSIDAD DE LA LAGUNA

Fecha: 30/11/2020 12:24:14

María de las Maravillas Aguiar Aguilár  
UNIVERSIDAD DE LA LAGUNA

08/02/2021 13:50:06

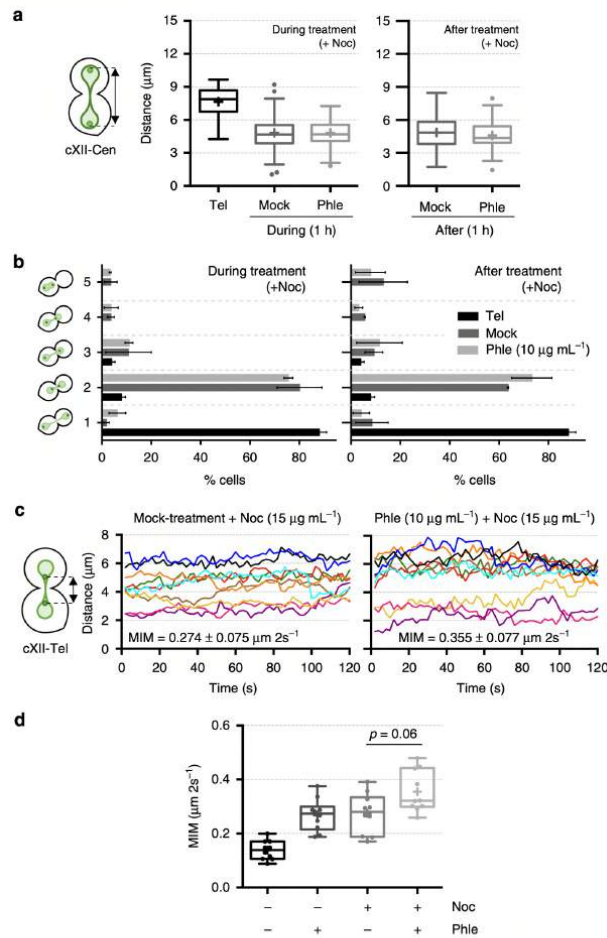


**Fig. 7** Microtubule depolymerization masks the effects of DSBs on sister loci approximation. **a** Sister centromeres also approach each other after depolymerizing telophase microtubules, masking the effect of phleomycin. Strain FM593 was treated as in Fig. 2a, except for the fact that nocodazole (Noc,  $15 \mu\text{g mL}^{-1}$ ) was added at the time of mock/phleomycin treatments and maintained after that. Distance between sister cXII centromeres was measured and box-plotted as in previous experiments. **b** Relative position of cXII sister centromeres from experiments like in panel (a) was categorised as indicated on the left (mean  $\pm$  s.e.m.,  $n = 3$  independent experiments). Categories 1-4 are described in Fig. 2b. Category 5, two centromeres laying within the same cell body (very rare in Noc-free experiments). **c** Inter sister telomere movement accelerates upon microtubule depolymerization. Kinetograms of 10 randomly selected FM588 cells previously treated for 1 h with either nocodazole (Noc) alone or Noc plus phleomycin. The MIM during the 2-min movies is also displayed within the charts (mean  $\pm$  s.d.,  $n = 10$  cells). **d** Box-plots of MIMs ( $N = 10$  cells per box) at the indicated treatment combinations (1 h after addition of the drugs). Note how nocodazole and phleomycin give an additive effect on interloci acceleration for a subset of cells. Source data are provided as a Source Data file

conclude that chromosome segregation in *S. cerevisiae* is more fluid than previously anticipated. This situates cytokinesis, rather than chromosome segregation, as the putative point of no return for using the sister chromatid as template for DSB repair. Whether or not this is extensible to other organisms remains to be determined. Technical caveats greatly difficult such studies since

telophase synchronization is not easily achievable. In metazoans, unlike yeast, there is a clear distinction between  $G_2$  and the M-phase. DSBs in  $G_2$  lead to immediate cell cycle arrest, whereas DSBs in M-phase lead to distinct responses depending on the type of damage and the model cell line (reviewed in ref. 37). In all these studies, mitotic DSBs were generated in

Este documento incorpora firma electrónica, y es copia auténtica de un documento electrónico archivado por la ULL según la Ley 39/2015.  
 Su autenticidad puede ser contrastada en la siguiente dirección <https://sede.ull.es/validacion/>

Identificador del documento: 3075810 Código de verificación: smutbmB+

Firmado por: JESSEL AYRA PLASENCIA  
 UNIVERSIDAD DE LA LAGUNA

Fecha: 30/11/2020 12:24:14

María de las Maravillas Aguiar Aguiar  
 UNIVERSIDAD DE LA LAGUNA

08/02/2021 13:50:06

4. Results and Discussion

ARTICLE

NATURE COMMUNICATIONS | <https://doi.org/10.1038/s41467-019-10742-8>

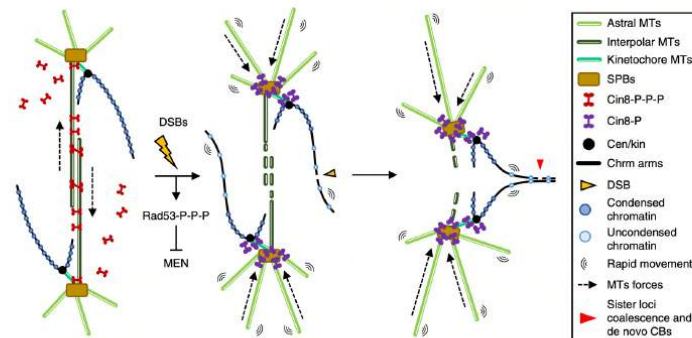


**Fig. 8** Model for the effect of DSBs on segregated sister chromatids. Segregated sister chromatids are maintained away from each other in telophase. Two complementary mechanisms aid to this aim. Firstly, an elongated spindle is maintained by the action of kinesin-5 Cin8 on interpolar microtubules (iMTs). Secondly, segregated sister chromatids are in a hypercondensed state<sup>54</sup>. DSBs locally mobilise the affected chromatid through decondensation, so the histone-poor signal in de novo chromatin bridges, and globally accelerate loci movement. In addition, Cin8 is displaced out of iMTs by partial dephosphorylation, abrogating the spindle forces that keep SPBs far from each other. It is likely that enforced astral MTs also participate in bringing closer the SPBs. All these circumstances make possible for sister loci at chromosome arms to coalesce and repair DSBs through HR with the sister chromatid, even when cells are in telophase

prophase/metaphase. Interestingly, these DSBs in cells committed to mitosis but that have not reached anaphase causes defects in the ensuing chromosome segregation. So far, there has been only one attempt to comprehend how DSBs affect cells transiting through anaphase<sup>38</sup>. In this study, authors used a model marsupial cell line suitable for laser-mediated DNA damage. However, they focused on the consequences for cytokinesis, rather than the behaviour of segregating sister chromatids.

We here also provide mechanistic insights into the regression process. We have found that the spindle undergoes a dramatic change after phleomycin addition (Figs. 5 and 6): (i) the intranuclear spindle collapses and astral MTs appeared reinforced; (ii) the SPBs approximate to each other while keeping themselves in different compartments; and (iii) Kinesin-5 Cin8, a master motor protein for spindle assembly and elongation, fully relocates to SPBs (and/or kinetochores). We also provide several evidences that all these changes actively contribute to the observed regression and are not simply circumstantial. For instance, sister chromatid approximation requires an active Cin8 localised at the SPBs/kinetochores (Fig. 6). These same players, MTs and Cin8 kinesin-5 orthologs, could be tested in higher eukaryotes if regression were observed after DSBs in anaphase/telophase. Lastly, we demonstrate that Cin8 dephosphorylation in the motor domain is required, yet not sufficient, for full relocation. It is required because a Cin8 phospho-mimetic version of this kinesin-5 (Cin8-3D) was partially impaired in relocating. However, it is not sufficient because a Cin8 phospho-mutant (Cin8-3A) behaved like wild-type Cin8; i.e., (i) it was not enriched at poles in telophase without damage, and (ii) it was fully relocated to the poles after phleomycin addition. We envision a two-step model to explain these results (Fig. 8). Firstly, Cin8 dephosphorylation recruits soluble Cin8 pools to nuclear MTs, and then, MT-bound Cin8 concentrates at the poles upon further post-translational modifications. These modifications must correspond to residues other than the two serines (S277 and S493) and one threonine (T285) mutated in the Cin8-3D and Cin8-3A variants<sup>31</sup>. Whether the partial dephosphorylation we observed by western blots (Fig. 6) corresponds to dephosphorylation of these three residues or any other(s) that drive Cin8 concentration at the SPBs/kinetochores is presently unknown. Interestingly, the anaphase master

phosphatase Cdc14 does not dephosphorylate Cin8 in telophase after DSBs (Supplementary Fig. 9). Cdc14 does dephosphorylate CDK residues in Cin8 at anaphase onset<sup>33</sup>; and S277, T285 and S493 are all CDK residues<sup>31</sup>. Thus, we propose that a phosphatase other than Cdc14 dephosphorylates non-CDK Cin8 residues upon DSBs. A clue for such phosphatase could be found in a recent report whereby a physical interaction between protein phosphatase 1 (PP1) and Cin8 has been described at kinetochores<sup>30</sup>.

While Cin8 appears to entirely control sister chromatid approximation, it is likely that coalescence needs more players. We found higher movement of sister loci after DSBs. This kind of movement is oscillatory when comparing the interloci distances, as if pulling and pushing forces were operating successively (Figs. 3, 4 and 7). This increase in oscillatory movement depends on the DDC (Fig. 4). A higher motility of chromatin after DNA damage has been reported before<sup>39,40</sup>. Several nuclear and chromatin rearrangements favour chromatin movement in the confined space of the nucleus, including nucleosomal repositioning, untethering of telomeres from the nuclear envelope and relaxation of the kinetochore-MT interaction<sup>41-44</sup>. It is likely that these processes also contribute to coalescence. Regardless, rapid oscillatory movements and coalescence were highly dependent on Rad9 (i.e., DDC) but not Rad52 (i.e., synopsis between DSB ends and the intact sister chromatid). This raises the possibility that coalescence occurs through a Rad52-independent mechanism, which, nonetheless, is a prerequisite for later execution of HR (Fig. 4f). At present, we can only speculate about the nature of this coalescence facilitator. For instance, very recent findings report that sister chromatid replication is not completed until late anaphase<sup>45</sup>. The maintenance of physical linkages between segregated sister chromatids may catalyse coalescence by zipping sisters from these linkages (e.g., persistent replication forks).

**Methods**

**Yeast strains and experimental procedures.** All yeast strains used in this work are listed in Supplementary Table 1. Strain construction was undertaken through standard transformation and crossing methods<sup>46</sup>. C-terminal tags and gene deletions were engineered using PCR methods<sup>46,47</sup>. Strains were grown overnight in air orbital incubators at 25 °C in YEPD media (10 g L<sup>-1</sup> yeast extract, 20 g L<sup>-1</sup> peptone and 20 g L<sup>-1</sup> glucose). To arrest cells in telophase, log-phase asynchronous cultures

Este documento incorpora firma electrónica, y es copia auténtica de un documento electrónico archivado por la ULL según la Ley 39/2015.  
 Su autenticidad puede ser contrastada en la siguiente dirección <https://sede.ull.es/validacion/>

Identificador del documento: 3075810 Código de verificación: smutbmB+

Firmado por: JESSEL AYRA PLASENCIA  
 UNIVERSIDAD DE LA LAGUNA

Fecha: 30/11/2020 12:24:14

María de las Maravillas Aguiar Aguiar  
 UNIVERSIDAD DE LA LAGUNA

08/02/2021 13:50:06

were adjusted to  $OD_{600} = 0.3\text{--}0.4$  and the temperature shifted to  $37^\circ\text{C}$  for 3 h. In most experiments, the arrested culture was split into two and one of them was treated with phleomycin ( $10\ \mu\text{g mL}^{-1}$ ) while the second was just treated with the vehicle (mock treatment). After 1 h incubation, both cultures were washed twice with fresh YEPD and further incubated for 1–3 h to recover from DNA damage. In experiments aimed to check the telophase- $G_1$  transition, temperature was shifted back to  $25^\circ\text{C}$  to allow Cdc15-2 re-activation. To simplify morphological outcomes during the *cdc15-2* release, the alpha-factor pheromone (aF) was added after the washing steps unless stated otherwise ( $50\ \text{ng mL}^{-1}$ ; all strains are *bar1*, so hyper-sensitive to aF). For experiments other than telophase- $G_1$  time courses, telophase arrest was maintained after phleomycin/mock treatments by keeping the temperature at  $37^\circ\text{C}$ . Particular experiments such as plasma membrane ingress and responsiveness to aF have been described before<sup>13,22</sup>. Hoechst 33258, utilised to stain both nuclear DNA and plasma membrane, was used at  $5\ \mu\text{g mL}^{-1}$ . To arrest cells in  $G_1$ ,  $50\ \text{ng mL}^{-1}$  aF were directly added to an asynchronous culture growing at  $25^\circ\text{C}$  and incubated at that temperature for 3 h. To arrest cells in  $G_2/M$ ,  $15\ \mu\text{g mL}^{-1}$  Nocodazole (Noc) was added instead of aF. To arrest cells in  $S/G_2$ , either  $0.01\%$  v/v methyl methanesulfonate (MMS) or  $0.2\ \text{M}$  hydroxyurea (HU) were added instead. The same concentrations of aF, Noc, HU and MMS were used in experiments where cells were already in telophase before the drug treatment. In experiments with conditional Cin8 degen variants for the auxin system (*aid tags*)<sup>48</sup>, the protein was targeted for degradation by adding  $5\ \text{mM}$  3-indol-acetic acid (IAA) 1 h prior to adding phleomycin. Because Cin8 is not essential, we tested the effective degradation range by combining Cin8-aid with *kipp1Δ* (Supplementary Fig. 11); *cin8Δ* is synthetic lethal with *kipp1Δ*<sup>49,50</sup>. For clonogenic survival assays, log-phase asynchronous cultures were adjusted to  $OD_{600} = 0.4$  before the corresponding arrest and ensuing treatment. After that,  $100\ \mu\text{L}$  of  $1:10,000$  dilutions were spread onto YPD plates. The mock treatments yielded 300–500 CFU/plate in these experiments. Spot sensitivity assays were performed as described before<sup>51</sup>. Briefly, cultures were grown exponentially and adjusted to an  $OD_{600} = 0.5$  and then 10-fold serially diluted in YEPD. A 48-pin replica plater (Sigma-Aldrich, R2383) was used to spot  $\sim 5\ \mu\text{L}$  onto the corresponding plates, which were incubated at  $25^\circ\text{C}$  for 3–4 days before taking the photo.

**Microscopy.** A fully motorised Leica DMI6000B wide-field fluorescence microscope was used in all experiments. In time courses, a stack of 20 z-focal plane images ( $0.3\ \mu\text{m}$  depth) were collected using a  $63\times/1.30$  immersion objective and an ultrasensitive DFC 350 digital camera. Micrographs were taken from freshly collected cells without further processing; 200–300 cells were quantified per experimental data point. Videomicroscopy was also performed in freshly collected cells in a single focal plane (no more than 2 min, time frames of 2 s). The AF6000 (Leica) and Fiji (NIH) softwares were used for image processing and quantifications. The distances between sister loci and SPBs, as well as minimum distances between segregated rDNA and histone-labelled nuclear masses, were measured manually with the AF6000 software. Mean interloci movement (MIM) was calculated from the cumulative absolute variation of distances during videomicroscopy recording divided by the number of frames:  $(\sum |d_i - d_{i-1}|)/n$ ; where  $d$  is distance,  $f$  is the frame number,  $n$  is total number of frames, and the summation goes from  $f = 2$  to  $f = n$ . Coalescent events were not considered for calculations.

**Western blots.** For western blotting,  $10\ \text{mL}$  of the yeast liquid culture were collected to extract total protein using the trichloroacetic acid (TCA) method. Briefly, cell pellets were fixed in  $2\ \text{mL}$  of  $20\%$  TCA. After centrifugation ( $2500 \times g$  for 3 min), cells were resuspended in fresh  $100\ \mu\text{L}$   $20\%$  TCA and  $\sim 200\ \text{mg}$  of glass beads were added. After 3 min of breakage by vortex, extra  $200\ \mu\text{L}$   $5\%$  TCA were added to the tubes and  $\sim 300\ \mu\text{L}$  of the mix were collected in new  $1.5\ \text{mL}$  tubes. Samples were then centrifuged ( $2500 \times g$  for 5 min) and pellets were resuspended in  $100\ \mu\text{L}$  of PAGE Laemmli Sample Buffer (Bio-Rad, 1610747) mixed with  $50\ \mu\text{L}$  TE 1X pH 8.0. Finally, tubes were boiled for 3 min at  $95^\circ\text{C}$  and pelleted again. Total proteins were quantified with a Qubit 4 Fluorometer (Thermo Fisher Scientific, Q33227). Proteins were resolved in  $10\%$  (7.5% for Rad53 hyperphosphorylation assay) SDS-PAGE gels and transferred to PVDF membranes (Pall Corporation, PYM020C-099). The HA epitope was recognised with a primary mouse monoclonal anti-HA antibody (Sigma-Aldrich, H9658;  $1:5,000$ ); and the myc epitope was recognised with a primary mouse monoclonal anti-myc antibody (Sigma-Aldrich, M4439;  $1:5,000$ ). A polyclonal goat anti-mouse conjugated to horseradish peroxidase (Promega, W4021;  $1:10,000$ ) was used as secondary antibody. Chemiluminescence method was selected for detection, using the ECL reagent (GE Healthcare, RPN2232) and a Vilber-Lourmat Fusion Solo S documentation chamber. The membrane was finally stained with Ponceau S-solution (PanReac AppliChem, A2935) for a loading reference.

**Flow cytometry.** Flow cytometry was performed to determine DNA content<sup>52</sup>. In brief,  $1\ \text{mL}$  samples were fixed in  $75\%$  ethanol. Cells were resuspended in  $250\ \mu\text{L}$   $1\times$  SSC buffer containing  $0.1\ \text{mg mL}^{-1}$  of RNaseA and incubated overnight at  $37^\circ\text{C}$ . Then,  $50\ \mu\text{L}$  of  $1\times$  SSC containing  $1\ \text{mg mL}^{-1}$  of proteinase K was added and incubated at  $50^\circ\text{C}$  for 1 h. Finally,  $500\ \mu\text{L}$  of  $1\times$  SSC with  $3\ \mu\text{g mL}^{-1}$  propidium iodide was added and incubated at room temperature for 1 h. BD FACScalibur machine was used to analyse the samples.

**Data representation and statistics.** Bar charts represent proportions of cells which have been categorised (e.g., relative position of sister loci, plasma membrane ingress, etc.). Error bars in these charts generally depict the standard error of the mean (s.e.m.), with the aim of quickly showing the interexperimental variability. At least three experiments, performed in different days, were considered for each figure panel. In case only one representative experiment is shown, error bars represent exact 95% confidence interval (CI95) of the proportion. Continuous data (e.g., interloci distance in  $\mu\text{m}$ ) were represented in box-plots ( $N = 100$  cells per box, unless stated otherwise); the centre line depicts the medians, the cross depicts the mean, box limits indicate the 25th and 75th percentile, whiskers extend to the 5th and 95th, and dots represent outliers. R software (<https://www.r-project.org/>) was used for statistical tests. Differences between experimental data points with continuous data were estimated through a Mann-Whitney  $U$  Test. Differences between experimental data points with categorical data were estimated through a Fisher's exact test. In this case, cells counted in all three independent experiments were pooled ( $>500$  cells per data point) to make the contingency tables. All reported  $p$  values are two-tailed.

**Reporting summary.** Further information on research design is available in the Nature Research Reporting Summary linked to this article.

#### Data availability

The authors declare that all data supporting the findings of this study are available within the paper, its supplementary information, or from the corresponding author upon request. The source data underlying Figs. 1a–c, e, 2a–d, 3a, c, d, f, 4a–f, 5a, b, 6a–e and 7a–c and Supplementary Figs. 1, 3, 4, 5a, 7a, 7c, 8a, 8b and 9b are provided as a Source Data file.

Received: 16 October 2018 Accepted: 30 May 2019

Published online: 28 June 2019

#### References

- Kramer, K. M., Brock, J. A., Bloom, K., Moore, J. K. & Haber, J. E. Two different types of double-strand breaks in *Saccharomyces cerevisiae* are repaired by similar RAD52-independent, nonhomologous recombination events. *Mol. Cell. Biol.* **14**, 1293–1301 (1994).
- Emerson, C. H. & Bertuch, A. A. Consider the workhorse: nonhomologous end-joining in budding yeast. *Biochem. Cell Biol.* **94**, 396–406 (2016).
- Symington, L. S., Rothstein, R. & Lisby, M. Mechanisms and regulation of mitotic recombination in *Saccharomyces cerevisiae*. *Genetics* **198**, 795–835 (2014).
- Aylon, Y., Liefshitz, B. & Kupiec, M. The CDK regulates repair of double-strand breaks by homologous recombination during the cell cycle. *EMBO J.* **23**, 4868–4875 (2004).
- Ira, G. et al. DNA end resection, homologous recombination and DNA damage checkpoint activation require CDK1. *Nature* **431**, 1011–1017 (2004).
- Chiruvella, K. K., Liang, Z. & Wilson, T. E. Repair of double-strand breaks by end joining. *Cold Spring Harb. Perspect. Biol.* **5**, a012757 (2013).
- Mathiasen, D. P. & Lisby, M. Cell cycle regulation of homologous recombination in *Saccharomyces cerevisiae*. *FEMS Microbiol. Rev.* **38**, 172–184 (2014).
- Zhao, X. et al. Cell cycle-dependent control of homologous recombination. *Acta Biochim. Biophys. Sin.* **49**, 655–668 (2017).
- D'Amours, D. & Amon, A. At the interface between signaling and executing anaphase-Cdc14 and the FEAR network. *Genes Dev.* **18**, 2581–2595 (2004).
- Moore, C. W. Cleavage of cellular and extracellular *Saccharomyces cerevisiae* DNA by bleomycin and phleomycin. *Cancer Res.* **49**, 6935–6940 (1989).
- Finn, K., Lowndes, N. F. & Grenon, M. Eukaryotic DNA damage checkpoint activation in response to double-strand breaks. *Cell. Mol. Life Sci.* **69**, 1447–1473 (2012).
- Allen, J. B., Zhou, Z., Siede, W., Friedberg, E. C. & Elledge, S. J. The SAD1/RAD53 protein kinase controls multiple checkpoints and DNA damage-induced transcription in yeast. *Genes Dev.* **8**, 2401–2415 (1994).
- Quevedo, O., García-Luis, J., Matos-Perdomo, E., Aragón, L. & Machin, F. Nondisjunction of a single chromosome leads to breakage and activation of DNA damage checkpoint in *g2*. *PLoS Genet.* **8**, e1002509 (2012).
- Spellman, P. T. et al. Comprehensive identification of cell cycle-regulated genes of the yeast *Saccharomyces cerevisiae* by microarray hybridization. *Mol. Biol. Cell* **9**, 3273–3297 (1998).
- Schwob, E., Böhm, T., Mendenhall, M. D. & Nasmyth, K. The B-type cyclin kinase inhibitor p40SIC1 controls the G1 to S transition in *S. cerevisiae*. *Cell* **79**, 233–244 (1994).
- Gobbinì, E., Cesena, D., Galbiati, A., Lockhart, A. & Longhese, M. P. Interplays between ATM/Tel1 and ATR/Mec1 in sensing and signaling DNA double-strand breaks. *DNA Repair (Amst.)* **12**, 791–799 (2013).

Este documento incorpora firma electrónica, y es copia auténtica de un documento electrónico archivado por la ULL según la Ley 39/2015.

Su autenticidad puede ser contrastada en la siguiente dirección <https://sede.ull.es/validacion/>

Identificador del documento: 3075810

Código de verificación: smutbmB+

Firmado por: JESSEL AYRA PLASENCIA  
 UNIVERSIDAD DE LA LAGUNA

Fecha: 30/11/2020 12:24:14

María de las Maravillas Aguiar Aguiar  
 UNIVERSIDAD DE LA LAGUNA

08/02/2021 13:50:06

#### 4. Results and Discussion

### ARTICLE

NATURE COMMUNICATIONS | <https://doi.org/10.1038/s41467-019-10742-8>

17. Weinert, T. A. & Hartwell, L. H. The RAD9 gene controls the cell cycle response to DNA damage in *Saccharomyces cerevisiae*. *Science* **241**, 317–322 (1988).
18. Gerald, J. N. F., Benjamin, J. M. & Kron, S. J. Robust G1 checkpoint arrest in budding yeast: dependence on DNA damage signaling and repair. *J. Cell Sci.* **115**, 1749–1757 (2002).
19. Hunt, D. F. et al. *Saccharomyces cerevisiae* Rad9 acts as a Mec1 adaptor to allow Rad53 activation. *Curr. Biol.* **15**, 1364–1375 (2005).
20. Zimmer, C. & Fabre, E. Principles of chromosomal organization: lessons from yeast. *J. Cell Biol.* **192**, 723–733 (2011).
21. Branzei, D. & Foiani, M. Interplay of replication checkpoints and repair proteins at stalled replication forks. *DNA Repair* **6**, 994–1003 (2007).
22. Ramos-Pérez, C. et al. Genome-scale genetic interactions and cell imaging confirm cytokinesis as deleterious to transient topoisomerase II deficiency in *Saccharomyces cerevisiae*. *G3 (Bethesda)* **7**, 3379–3391 (2017).
23. Oh, J., Lee, S. J., Rothstein, R. & Symington, L. S. Xrs2 and Tel1 independently contribute to MR-mediated DNA tethering and replisome stability. *Cell Rep.* **25**, 1681–1692.e4 (2018).
24. Symington, L. S. Role of RAD52 epistasis group genes in homologous recombination and double-strand break repair. *Microbiol. Mol. Biol. Rev.* **66**, 630–670 (2002).
25. Machin, F., Torres-Rosell, J., Jarmuz, A. & Aragón, L. Spindle-independent condensation-mediated segregation of yeast ribosomal DNA in late anaphase. *J. Cell Biol.* **168**, 209–219 (2005).
26. Khmelinskii, A., Roostalu, J., Roque, H., Antony, C. & Schiebel, E. Phosphorylation-dependent protein interactions at the spindle midzone mediate cell cycle regulation of spindle elongation. *Dev. Cell* **17**, 244–256 (2009).
27. Singh, S. K., Pandey, H., Al-Bassam, J. & Gheber, L. Bidirectional motility of kinesin-5 motor proteins: structural determinants, cumulative functions and physiological roles. *Cell. Mol. Life Sci.* **75**, 1–15 (2018).
28. De Wulf, P., McAinsh, A. D. & Sorger, P. K. Hierarchical assembly of the budding yeast kinetochore from multiple subcomplexes. *Genes Dev.* **17**, 2902–2921 (2003).
29. Shapira, O., Goldstein, A., Al-Bassam, J. & Gheber, L. A potential physiological role for bi-directional motility and motor clustering of mitotic kinesin-5 Cin8 in yeast mitosis. *J. Cell Sci.* **130**, 725–734 (2017).
30. Suzuki, A. et al. A Kinesin-5, Cin8, recruits protein phosphatase 1 to kinetochores and regulates chromosome segregation. *Curr. Biol.* **28**, 2697–2704.e3 (2018).
31. Goldstein, A. et al. Three Cdk1 sites in the kinesin-5 Cin8 catalytic domain coordinate motor localization and activity during anaphase. *Cell. Mol. Life Sci.* **74**, 3395–3412 (2017).
32. Stegmeier, F. & Amon, A. Closing mitosis: the functions of the Cdc14 phosphatase and its regulation. *Annu. Rev. Genet.* **38**, 203–232 (2004).
33. Rocuzzo, M., Visintin, C., Tili, F. & Visintin, R. FEAR-mediated activation of Cdc14 is the limiting step for spindle elongation and anaphase progression. *Nat. Cell Biol.* **17**, 251–261 (2015).
34. Villoria, M. T. et al. Stabilization of the metaphase spindle by Cdc14 is required for recombinational DNA repair. *EMBO J.* **36**, 79–101 (2017).
35. Hu, F. et al. Regulation of the Bub2/Bfa1 GAP complex by Cdc5 and cell cycle checkpoints. *Cell* **107**, 655–665 (2001).
36. Valerio-Santiago, M., de los Santos-Velázquez, A. I. & Monje-Casas, F. Inhibition of the mitotic exit network in response to damaged telomeres. *PLoS Genet.* **9**, 1–15 (2013).
37. Bakhroum, S. F., Kabeche, L., Compton, D. A., Powell, S. N. & Bastians, H. Mitotic DNA damage response: at the crossroads of structural and numerical cancer chromosome instabilities. *Trends cancer* **3**, 225–234 (2017).
38. Baker, N. M., Zeitlin, S. G., Shi, L. Z., Shah, J. & Berns, M. W. Chromosome tips damaged in anaphase inhibit cytokinesis. *PLoS ONE* **5**, e12398 (2010).
39. Miné-Hattab, J. & Rothstein, R. Increased chromosome mobility facilitates homology search during recombination. *Nat. Cell Biol.* **14**, 510–517 (2012).
40. Dion, V., Kalkk, V., Horigome, C., Towbin, B. D. & Gasser, S. M. Increased mobility of double-strand breaks requires Mec1, Rad9 and the homologous recombination machinery. *Nat. Cell Biol.* **14**, 502–509 (2012).
41. Strecker, J. et al. DNA damage signalling targets the kinetochore to promote chromatin mobility. *Nat. Cell Biol.* **18**, 281–290 (2016).
42. Lawrimore, J. et al. Microtubule dynamics drive enhanced chromatin motion and mobilize telomeres in response to DNA damage. *Mol. Biol. Cell* **28**, 1701–1711 (2017).
43. Horigome, C. et al. SWR1 and INO80 chromatin remodelers contribute to DNA double-strand break perinuclear anchorage site choice. *Mol. Cell* **55**, 626–639 (2014).
44. Chung, D. K. C. et al. Perinuclear tethers license telomeric DSBs for a broad kinesin- and NPC-dependent DNA repair process. *Nat. Commun.* **6**, 7742 (2015).
45. Ivanova, T. et al. Budding yeast complete DNA replication after chromosome segregation begins. Preprint at <https://www.biorxiv.org/content/10.1101/407957v1> (2018).
46. Smith, J. S. & Burke, D. J. *Yeast Genetics: Methods and Protocols*. 1205 (Springer New York, 2014).
47. Malcova, I., Farkasovsky, M., Senohrabkova, L., Vasicova, P. & Hasek, J. New integrative modules for multicolor-protein labeling and live-cell imaging in *Saccharomyces cerevisiae*. *FEMS Yeast Res.* **16**, fow027 (2016).
48. Morawska, M. & Ulrich, H. D. An expanded tool kit for the auxin-inducible degron system in budding yeast. *Yeast* **30**, 341–351 (2013).
49. Hoyt, M. A., He, L., Loo, K. K. & Saunders, W. S. Kinesin-related gene products. *J. Biol. Chem.* **118**, 109–120 (1992).
50. Roof, D. M., Meluh, P. B. & Rose, M. D. Kinesin-related proteins required for assembly of the mitotic spindle. *J. Cell Biol.* **118**, 95–108 (1992).
51. Matos-Perdomo, E. & Machin, F. The ribosomal DNA metaphase loop of *Saccharomyces cerevisiae* gets condensed upon heat stress in a Cdc14-independent TORC1-dependent manner. *Cell Cycle* **17**, 200–215 (2018).
52. García-Luis, J. & Machin, F. Mus81-Mms4 and Yen1 resolve a novel anaphase bridge formed by noncanonical Holliday junctions. *Nat. Commun.* **5**, 5652 (2014).
53. Avunie-Masala, R. et al. Phospho-regulation of kinesin-5 during anaphase spindle elongation. *J. Cell Sci.* **124**, 873–878 (2011).
54. Machin, F., Quevedo, O., Ramos-Pérez, C. & García-Luis, J. Cdc14 phosphatase: warning, no delay allowed for chromosome segregation! *Curr. Genet.* **62**, 7–13 (2016).

#### Acknowledgements

We thank Larisa Gheber and Lorraine Symington for yeast strains, and Ivana Malcova for tagging plasmids. We also thank Emiliano Matos-Perdomo and Jonay García-Luis for technical help. This work was supported by Spanish Ministry of Economy, Industry and Competitiveness (research grants BFU2015-63902-R and BFU2017-83954-R to F.M.). Both grants were co-financed with the European Commission's ERDF structural funds.

#### Author contributions

F.M. conceived the original project. J.A.-P. performed all the experimental work and prepared the figures. F.M. and J.A.-P. planned and analysed the experiments. F.M. wrote the paper.

#### Additional information


**Supplementary Information** accompanies this paper at <https://doi.org/10.1038/s41467-019-10742-8>.

**Competing interests:** The authors declare no competing interests.

**Reprints and permission** information is available online at <http://npg.nature.com/reprintsandpermissions/>

**Peer review information:** *Nature Communications* thanks the anonymous reviewer(s) for their contribution to the peer review of this work. Peer reviewer reports are available.

**Publisher's note:** Springer Nature remains neutral with regard to jurisdictional claims in published maps and institutional affiliations.

 **Open Access** This article is licensed under a Creative Commons Attribution 4.0 International License, which permits use, sharing, adaptation, distribution and reproduction in any medium or format, as long as you give appropriate credit to the original author(s) and the source, provide a link to the Creative Commons license, and indicate if changes were made. The images or other third party material in this article are included in the article's Creative Commons license, unless indicated otherwise in a credit line to the material. If material is not included in the article's Creative Commons license and your intended use is not permitted by statutory regulation or exceeds the permitted use, you will need to obtain permission directly from the copyright holder. To view a copy of this license, visit <http://creativecommons.org/licenses/by/4.0/>.

© The Author(s) 2019

14 NATURE COMMUNICATIONS | (2019) 10:2862 | <https://doi.org/10.1038/s41467-019-10742-8> | www.nature.com/naturecommunications

100

Este documento incorpora firma electrónica, y es copia auténtica de un documento electrónico archivado por la ULL según la Ley 39/2015.  
Su autenticidad puede ser contrastada en la siguiente dirección <https://sede.ull.es/validacion/>

Identificador del documento: 3075810 Código de verificación: smutbm+

Firmado por: JESSEL AYRA PLASENCIA  
UNIVERSIDAD DE LA LAGUNA

Fecha: 30/11/2020 12:24:14

María de las Maravillas Aguiar Aguiar  
UNIVERSIDAD DE LA LAGUNA

08/02/2021 13:50:06

**SUPPLEMENTARY INFORMATION**

**DNA double-strand breaks in telophase lead to coalescence between segregated sister chromatid loci.**

Jessel Ayra-Plasencia<sup>1,2</sup>, Félix Machín<sup>1,3\*</sup>.

<sup>1</sup> Unidad de Investigación, Hospital Universitario Nuestra Señora de Candelaria, Santa Cruz de Tenerife, Spain.

<sup>2</sup> Escuela de Doctorado y Estudios de Posgrado. Universidad de La Laguna, Santa Cruz de Tenerife, Spain

<sup>3</sup> Instituto de Tecnologías Biomédicas. Universidad de La Laguna, Santa Cruz de Tenerife, Spain.

\* Contact: [fmachin@funcanis.es](mailto:fmachin@funcanis.es)

Unidad de Investigación, Hospital Universitario Nuestra Señora de Candelaria.  
Carretera del Rosario, 145. 38010. Santa Cruz de Tenerife, Spain.

Este documento incorpora firma electrónica, y es copia auténtica de un documento electrónico archivado por la ULL según la Ley 39/2015.  
Su autenticidad puede ser contrastada en la siguiente dirección <https://sede.ull.es/validacion/>

Identificador del documento: 3075810 Código de verificación: smutbmB+

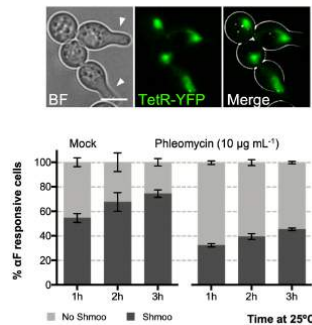
Firmado por: JESSEL AYRA PLASENCIA  
UNIVERSIDAD DE LA LAGUNA

Fecha: 30/11/2020 12:24:14

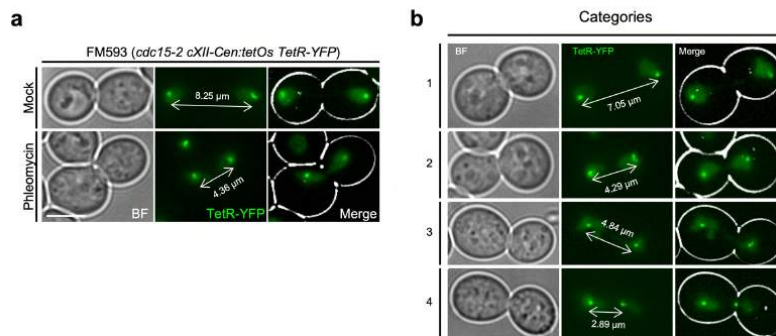
María de las Maravillas Aguiar Aguiar  
UNIVERSIDAD DE LA LAGUNA

08/02/2021 13:50:06

4. Results and Discussion



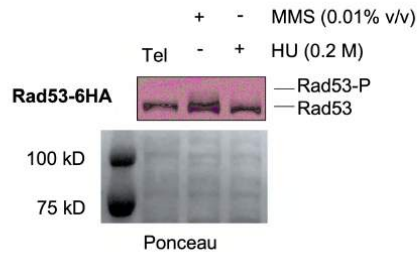
**Supplementary Figure 1. Responsiveness to  $\alpha F$  (as a marker of  $G_1$ ) is delayed after DNA damage in telophase.** FM593 was treated as described in Figure 1b. On the top, a representative micrograph showing two telophase-like cells (binucleated dumbbells) in which one daughter cell responds to  $\alpha F$  by acquiring the shmoo morphology (filled arrowheads). Scale white bar corresponds to 5  $\mu m$ ; BF, bright field. At the bottom, chart depicting the evolution of the  $\alpha F$ -responsive cells after the telophase release (mean  $\pm$  s.e.m., n=3 independent experiments). Source data are provided as a Source Data file.



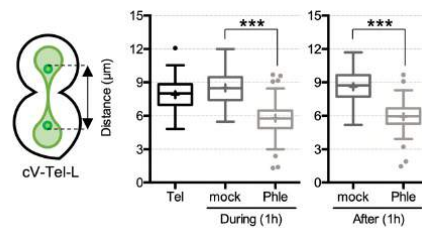
**Supplementary Figure 2. (a)** Representative cells from Figure 2a (1h after initiation of treatment). Note how sister centromeres are kept close to opposite poles throughout the telophase block. DNA damage after phleomycin addition breaks this disposition so the inter sister centromere distance is reduced. **(b)** Examples of cell categories included in the Figure 2b. Note how in category 4 one of the sister centromeres is at the bud neck. Scale bar corresponds to 5  $\mu m$ ; BF, bright field.



4. Results and Discussion



**Supplementary Figure 3. DNA damages other than DSBs do not trigger a strong DNA Damage Response in telophase.** Related to Figure 2c. Rad53 is weakly phosphorylated in telophase after treatments with the DNA alkylating agent MMS or the ribonucleotide reductase inhibitor hydroxyurea (HU). Strain FM2329 was arrested for 3h at telophase before splitting the culture in two. MMS and HU were added to the indicated subcultures and cells were harvested after 1h for Western blot analysis. Tel, sample at the telophase arrest, before splitting the culture in two. The leftmost lane in the Ponceau staining corresponds to the protein weight markers (shared with the Western blot shown in Supplementary Figure 7c). Source data are provided as a Source Data file.



**Supplementary Figure 4. Telomeres other than cXIIr-Tel get closer after DSBs in telophase.** Related to Figures 2 and 3. Strain FM567 was treated as in Figure 2a and samples taken at the indicated experimental time points for fluorescence microscopy. The distance between sister chromosome V left telomeres was measured and box-plotted (\*\*\*) indicates  $p < 0.0001$  in mock/phleomycin comparisons at each time point; Mann-Whitney U Test). Source data are provided as a Source Data file.

Este documento incorpora firma electrónica, y es copia auténtica de un documento electrónico archivado por la ULL según la Ley 39/2015.  
 Su autenticidad puede ser contrastada en la siguiente dirección <https://sede.ull.es/validacion/>

Identificador del documento: 3075810 Código de verificación: smutbmB+

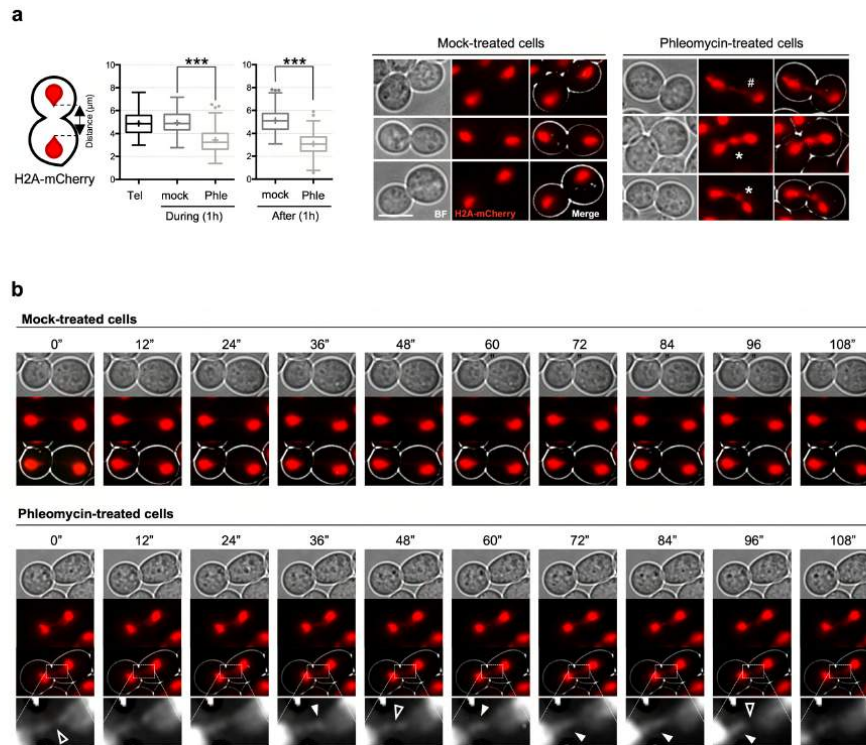
Firmado por: JESSEL AYRA PLASENCIA  
 UNIVERSIDAD DE LA LAGUNA

Fecha: 30/11/2020 12:24:14

María de las Maravillas Aguiar Aguiar  
 UNIVERSIDAD DE LA LAGUNA

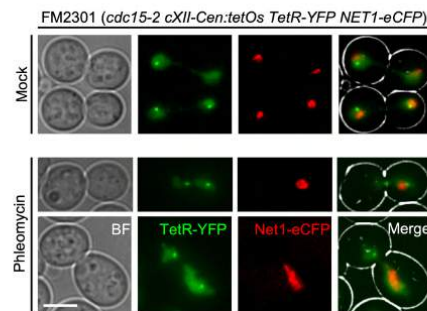
08/02/2021 13:50:06

4. Results and Discussion

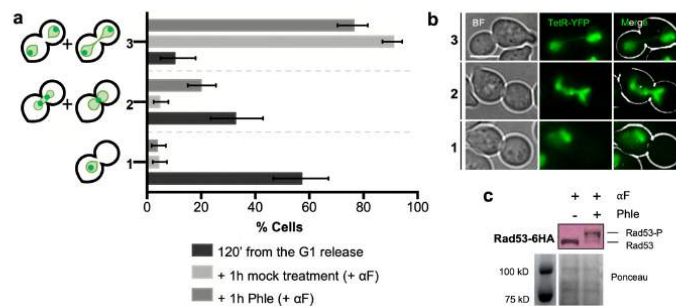


**Supplementary Figure 5. The bulk of segregated nuclear masses moves closer and forms *de novo* chromatin bridges after DNA damage in telophase.** FM2354 was treated like in Figure 2a. **(a)** Boxplots of minimum distances between bright (condensed) histone-labelled segregated nuclear masses (\*\*\*) indicates  $p < 0.0001$ ; Mann-Whitney U Test). On the right, representative cells observed during treatments. Note the presence of distinct chromatin bridges in phleomycin formed by either thin histone-poor inter nuclear connections (#) or bulgy string-like bridges (\*). For the plot, it was considered for calculation of the minimum distances neither the bulgy minor chromatin fraction in the bridge nor the histone-poor signal along the bridge. **(b)** Time frames of representative cell examples during mock (above) and phleomycin (below) treatments. Phleomycin led to the two above-mentioned outcomes. Here it is represented the dynamics of a *de novo* bridge comprised of apparently decondensed and histone-poor DNA (zoomed in at the bottom). Filled arrowheads point to histone-poor DNA moving along the bridge, whereas hollow arrowheads show empty spaces. For the second outcome (bulgy string-like bridge) refer to Figure 3e. BF, bright field; scale white bar represents 5 µm. Source data are provided as a Source Data file.

4. Results and Discussion



**Supplementary Figure 6.** Representative cells from **Figure 2f** (1h after initiation of treatment). Note how sister rDNAs (coated with Net1-eCFP) merged into a single nucleolus upon phleomycin treatment. BF, bright field; scale white bar represents 5  $\mu$ m.



**Supplementary Figure 7. Sister loci stay close more often when DSBs are generated in cells normally transiting through anaphase.** Strain FM593 was released from a G<sub>1</sub> arrest at 25 °C and monitor each 10' seeking the beginning of chromosome segregation. When cells were entering anaphase (120' from G<sub>1</sub> release in this particular experiment), the culture was split in two and phleomycin was added to one subculture. To simplify subsequent cell figures,  $\alpha$ F was also added to both subcultures. (a) Categorization of cell and nuclear morphologies (soluble tetR-YFP pool) at the indicated experimental points ( $\pm$  CI95). (b) Representative cells for each category in the subculture treated with phleomycin. (c) Western blot for Rad53 showing that phleomycin elicited a strong DNA damage response. Note that when phleomycin was added cells underwent progression into anaphase (i.e., category 1 of mononucleated dumbbells accounts for only 5% of cells at the end point); however, up to 20% of cells have an elongated nucleus with two very close centromeres. Rad53 was highly hyperphosphorylated, pointing out that a strong DNA damage response also occurs if DSBs are generated in anaphase. The leftmost lane in the Ponceau staining corresponds to the protein weight markers (shared with the Western blot shown in Supplementary Figure 3). Source data are provided as a Source Data file.

Este documento incorpora firma electrónica, y es copia auténtica de un documento electrónico archivado por la ULL según la Ley 39/2015.  
 Su autenticidad puede ser contrastada en la siguiente dirección <https://sede.ull.es/validacion/>

Identificador del documento: 3075810 Código de verificación: smutbmB+

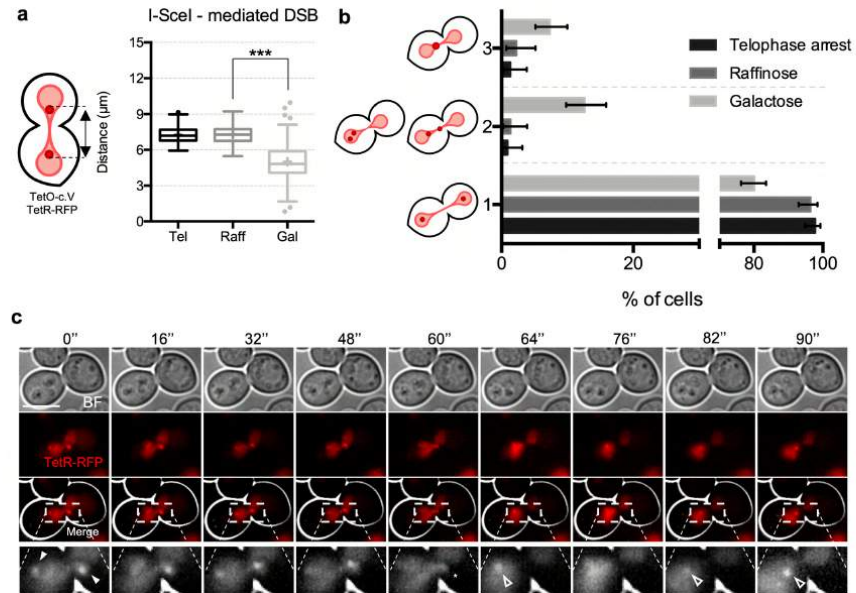
Firmado por: JESSEL AYRA PLASENCIA  
 UNIVERSIDAD DE LA LAGUNA

Fecha: 30/11/2020 12:24:14

María de las Maravillas Aguiar Aguiar  
 UNIVERSIDAD DE LA LAGUNA

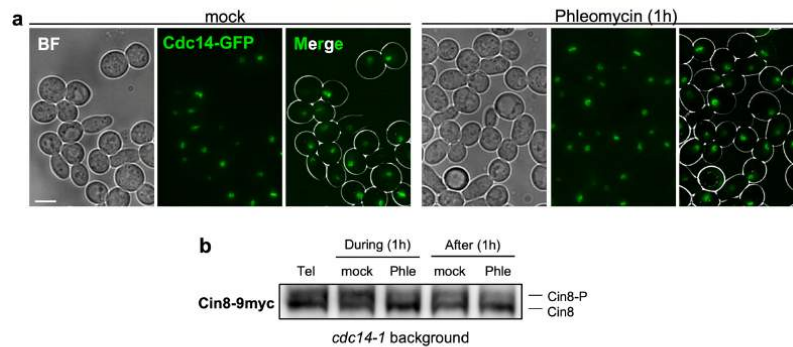
08/02/2021 13:50:06

4. Results and Discussion

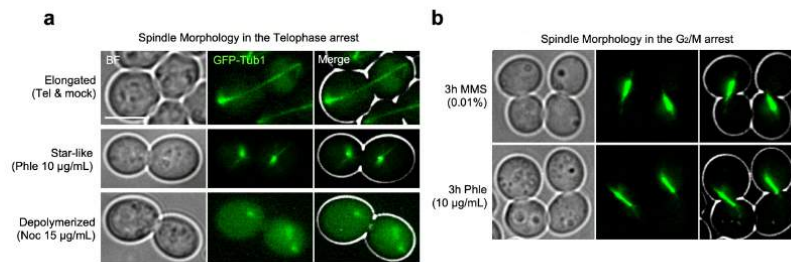


**Supplementary Figure 8. DSBs generated by endonucleases also lead to approximation and coalescence of adjacent sister loci.** The strain FM2456 was grown at 25 °C in raffinose (2% w/v) and arrested in telophase (3h at 37 °C) before splitting the culture in two (Tel). One subculture was left in raffinose for another hour (Raff), while galactose (2% w/v) was added to the second one to induce the I-SceI endonuclease (Gal). Samples were taken at the indicated experimental points for analysis under the fluorescence microscope. **(a)** the distance between the sister loci adjacent to the I-SceI recognition site was measured and box-plotted (\*\*\*) indicates  $p < 0.0001$ ; Mann-Whitney U Test). Note that cells with only one focus (coalescent sister loci) were omitted in the box plots. **(b)** Categorization of sister loci as in Figure 3a ( $\pm$  CI95). **(c)** A sample of "Gal" was filmed for 2 minutes. A representative cell with dynamic coalescence near the bud neck is shown. Source data are provided as a Source Data file.

4. Results and Discussion



**Supplementary Figure 9. Cdc14 does not dephosphorylate Cin8 upon DSB generation in telophase. (a)** Cdc14 remains in the nucleolus upon phleomycin treatment in telophase. The strain FM2302 was treated as in Figure 2a. One hour within phleomycin (or mock) incubation, samples were photographed under the microscope. Note that Cdc14-GFP appears as concentrated clusters, lines or small loops; all characteristics of rDNA in telophase. **(b)** The strain FM2478 was treated and samples processed as in Figure 6b. BF, bright field. Source data are provided as a Source Data file.



**Supplementary Figure 10. Phleomycin does not depolymerize microtubules. (a)** Representative Tub1 figures after telophase cells are (i) left untreated, (ii) treated with phleomycin or (iii) treated with nocodazole. The elongated spindle was the major phenotype at the telophase block (3h) or after 1h of mock treatment. Phleomycin yielded the star-like morphology with or without evident interpolar microtubules (iMTs). Here a representative cell without iMTs is shown in order to compare with the extreme Noc phenotype. For cells with iMTs see Figure 5a. For iMTs changing dynamics see Supplementary Movies 11-14. Unlike phleomycin, Nocodazole caused Tub1 to appear soluble throughout the cell, with no signs of organized MTs and only a Tub1 fraction concentrated as one focus per cell body (probably at the SPBs). **(b)** DNA damage exerted with Phleomycin over an asynchronous culture induced a G<sub>2</sub>/M block (mononucleated dumbbell cell) with a characteristic short and thick spindle, similar to the G<sub>2</sub>/M blocks caused by other DNA damaging agents (MMS in included for comparison). BF, bright field; scale white bar represents 5 µm.

Este documento incorpora firma electrónica, y es copia auténtica de un documento electrónico archivado por la ULL según la Ley 39/2015.  
 Su autenticidad puede ser contrastada en la siguiente dirección <https://sede.ull.es/validacion/>

Identificador del documento: 3075810 Código de verificación: smutbmB+

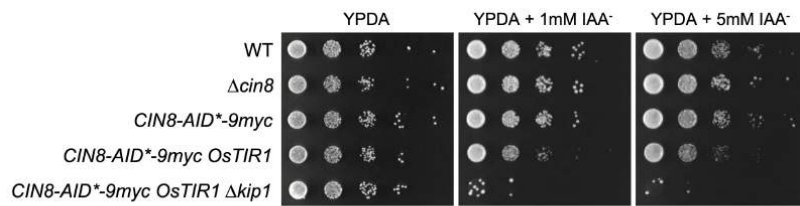
Firmado por: JESSEL AYRA PLASENCIA  
 UNIVERSIDAD DE LA LAGUNA

Fecha: 30/11/2020 12:24:14

María de las Maravillas Aguiar Aguiar  
 UNIVERSIDAD DE LA LAGUNA

08/02/2021 13:50:06

4. Results and Discussion



**Supplementary Figure 11. Cin8-aid levels drop beyond functionality after auxin addition.** Strains FM518, FM2461, FM2465, FM2466 and FM2473 were grown in YPD, normalized to 0.5 OD<sub>600</sub>, 1:10 serially diluted and spotted onto the indicated plates. Note that loss of Cin8 is not deleterious unless it is combined with a *kip1Δ* mutant. We made use of this synthetic lethality to confirm auxin-mediated degradation of Cin8-aid.

Este documento incorpora firma electrónica, y es copia auténtica de un documento electrónico archivado por la ULL según la Ley 39/2015.  
 Su autenticidad puede ser contrastada en la siguiente dirección <https://sede.ull.es/validacion/>

Identificador del documento: 3075810 Código de verificación: smutbmB+

Firmado por: JESSEL AYRA PLASENCIA  
 UNIVERSIDAD DE LA LAGUNA

Fecha: 30/11/2020 12:24:14

María de las Maravillas Aguiar Aguiar  
 UNIVERSIDAD DE LA LAGUNA

08/02/2021 13:50:06

4. Results and Discussion

**Supplementary Table 1. Strains used in this work.**

Strain	Genotype	Origin
AS499 (YPH499)	<i>MATa ura3-52 lys2-801 ade2-101 trp1-Δ63 his3-Δ200 leu2-Δ1 bar1-Δ</i>	A. Strunnikov <sup>a</sup>
FM593	AS499; <i>ade2-101::TetR-YFP::ADE2</i> ; <i>cXIIr(194Kb)::tetOs::HIS3</i> ; <i>cdc15-2::9myc::Hph</i>	F. Machin <sup>b</sup>
FM588	AS499; <i>ade2-101::TetR-YFP::ADE2</i> ; <i>cXIIr(1061Kb)::tetOs::HIS3</i> ; <i>cdc15-2::9myc::Hph</i>	F. Machin <sup>b</sup>
FM2329	FM593; <i>RAD53::6HA::KanMX4</i>	This Study
FM2323	FM593; <i>SIC1::6HA::KanMX4</i>	This Study
FM2329	FM593; <i>HTA2::mCherry::KanMX4</i>	This Study
FM2301	FM593; <i>NET1::eCFP::KanMX4</i>	This Study
FM2381	AS499; <i>ura3-52::GFP::TUB1::URA3</i> ; <i>cdc15-2::9myc::Hph</i>	This Study
FM2316	FM593; <i>SPC42::mCherry::KanMX6</i>	This Study
FM2317	FM593; <i>CIN8::mCherry::KanMX6</i>	This Study
FM2335	FM593; <i>CIN8::9myc::natNT2</i>	This Study
FM916	FM588; <i>Δrad9::natMX</i>	This Study
FM2477	FM916; <i>SIC1::6HA::KanMX4</i>	This Study
FM567	<i>MATa trp1-1 his3-11,15 leu2-3,112</i> ; <i>Telomere cV-L::tetO::LEU2</i> ; <i>ade2-1::URAp-TetR-YFP::ADE2</i> ; <i>Telomere cV-R::lacO::TRP1</i> ; <i>ura3-1::HISp-CFP-lacI::URA3</i> ; <i>cdc15-2::9myc::Hph</i>	F. Machin <sup>b,c</sup>
FM2448 (W303)	<i>MATa leu2-3,112 trp1-1 can1-100 ura3-1 ade2-1 his3-11,15 RAD5</i> ; <i>cdc15-2</i>	This study
LSY3902	W303; <i>MATa lys2::GAL-I-SceI Ura3::tetO Leu2-LacO(YEL023C)</i> <i>HIS3-YFP-LacI TetR-RFP RAD52-CFP</i>	L.S. Symington <sup>d</sup>
FM2456*	W303; <i>MATa lys2::GAL-I-SceI Ura3::tetO Leu2-LacO(YEL023C)</i> <i>HIS3-YFP-LacI TetR-RFP</i> ; <i>cdc15-2</i>	This study <sup>c</sup>
FM889	FM588; <i>Δrad52::KanMX</i>	F. Machin <sup>e</sup>
LGY2055	W303; <i>MATa Δcin8::ura3MX</i> ; <i>leu2-3,112::CIN8-3GFP-LEU2</i>	Gift from Larisa Gheber
LGY2058	W303; <i>MATa Δcin8::ura3MX</i> ; <i>leu2-3,112::CIN8-3A-3GFP-LEU2</i>	Gift from Larisa Gheber

Este documento incorpora firma electrónica, y es copia auténtica de un documento electrónico archivado por la ULL según la Ley 39/2015.  
 Su autenticidad puede ser contrastada en la siguiente dirección <https://sede.ull.es/validacion/>

Identificador del documento: 3075810 Código de verificación: smutbmB+

Firmado por: JESSEL AYRA PLASENCIA  
 UNIVERSIDAD DE LA LAGUNA

Fecha: 30/11/2020 12:24:14

María de las Maravillas Aguiar Aguilera  
 UNIVERSIDAD DE LA LAGUNA

08/02/2021 13:50:06

4. Results and Discussion

LGY2575	W303; <i>MATa Δcin8::ura3MX; leu2-3,112::CIN8-3D-3GFP-LEU2</i>	Gift from Larisa Gheber
FM2505*	W303; <i>MATa Δcin8::ura3MX; leu2-3,112::CIN8-3GFP-LEU2; cdc15-2</i>	This Study
FM2506*	W303; <i>MATa Δcin8::ura3MX; leu2-3,112::CIN8-3A-3GFP-LEU2; cdc15-2</i>	This Study
FM2507*	W303; <i>MATa Δcin8::ura3MX; leu2-3,112::CIN8-3D-3GFP-LEU2; cdc15-2</i>	This Study
FM1293	AS499; <i>cdc15-2:9myc:Hph</i>	This Study
FM2461	FM1293; <i>Δcin8::HIS3MX4</i>	This Study
FM2465	FM593; <i>CIN8:AID*:9myc:KanMX</i>	This Study
FM2466	FM2465; <i>ura3-52::ADHI-OsTIR1-9myc-URA3</i>	This Study
FM2473	FM2466; <i>Δkip1::HIS3MX4</i>	This Study
FM2302	AS499; <i>CDC14:GFP:KanMX; cdc15-2:9myc:Hph</i>	This Study
FM518	AS499; <i>ade2-101:TetR-YFP:ADE2; cXIIr(487Kb):tetOs:HIS3; cdc14-1:9myc:TRP1</i>	F. Machín <sup>b</sup>
FM2478	FM518; <i>CIN8:9myc:KanMX4</i>	This Study

<sup>a</sup> Parental strain; a *bar1-Δ* a derivative of YPH499, congenic to S288C.

<sup>b</sup> Quevedo, O., García-Luis, J., Matos-Perdomo, E., Aragón, L., and Machín, F. (2012). Nondisjunction of a single chromosome leads to breakage and activation of DNA damage checkpoint in *g2*. *PLoS Genet.* 8, e1002509.

<sup>c</sup> These strains carry either *lacI-YFP* or *lacI-CFP* as fluorescent reporters, along with *TetR-RFP* or *TetR-YFP*. We were unable to detect *lacO*-based foci at 34-37 °C (used for the telophase arrest in *cdc15-2* strains).

<sup>d</sup> Oh, J., Lee, S.J., Rothstein, R., and Symington, L.S. (2018). Xrs2 and Tel1 Independently Contribute to MR-Mediated DNA Tethering and Replisome Stability. *Cell Reports.* 25(7):1681-1692.e4.

<sup>e</sup> García-Luis, J., and Machín, F. (2014). Mus81-Mms4 and Yen1 resolve a novel anaphase bridge formed by noncanonical Holliday junctions. *Nature communications.* 5:5652.

\* Strains created by crosses with FM2448, followed by spore selection for the annotated genotypes.

Este documento incorpora firma electrónica, y es copia auténtica de un documento electrónico archivado por la ULL según la Ley 39/2015.  
 Su autenticidad puede ser contrastada en la siguiente dirección <https://sede.ull.es/validacion/>

Identificador del documento: 3075810 Código de verificación: smutbmB+

Firmado por: JESSEL AYRA PLASENCIA  
 UNIVERSIDAD DE LA LAGUNA

Fecha: 30/11/2020 12:24:14

María de las Maravillas Aguiar Aguilár  
 UNIVERSIDAD DE LA LAGUNA

08/02/2021 13:50:06



## 4.2. Chapter 2

### Molecular monitorization of a single DSB repair in telophase

The second chapter is focused on the study of the molecular processing, kinetics, and pathways to repair DSB in late mitosis. *Cdc15-2* blocked cells were submitted to 2  $\mu$ M  $\beta$ -estradiol to express the HO endonuclease and follow the cut at the MAT locus. Thus, the MAT Switching process was monitored as a model of DSB repair

Similar to what happened with phleomycin, cells also respond to a single DSB through the hyperphosphorylation Rad53. Besides, cells prefer using HR instead of NHEJ, although HR is Rad9- and Mre11-independent. Processing single-stranded 3' DNA occurs as efficiently as in G<sub>2</sub>, and cohesin complex plays an essential role in directing the interloci coalescence and promoting HR. Finally, proteomics mass spectrometry uncovers new factors specifically involved in DNA repair in telophase, compared to those essential for the DNA damage response in G<sub>2</sub>.

Este documento incorpora firma electrónica, y es copia auténtica de un documento electrónico archivado por la ULL según la Ley 39/2015.  
Su autenticidad puede ser contrastada en la siguiente dirección <https://sede.ull.es/validacion/>

Identificador del documento: 3075810 Código de verificación: smutbmB+

Firmado por: JESSEL AYRA PLASENCIA  
UNIVERSIDAD DE LA LAGUNA

Fecha: 30/11/2020 12:24:14

María de las Maravillas Aguiar Aguiar  
UNIVERSIDAD DE LA LAGUNA

08/02/2021 13:50:06



Este documento incorpora firma electrónica, y es copia auténtica de un documento electrónico archivado por la ULL según la Ley 39/2015.  
*Su autenticidad puede ser contrastada en la siguiente dirección <https://sede.ull.es/validacion/>*

Identificador del documento: 3075810      Código de verificación: smutbmB+

Firmado por: JESSEL AYRA PLASENCIA  
UNIVERSIDAD DE LA LAGUNA

Fecha: 30/11/2020 12:24:14

María de las Maravillas Aguiar Aguiar  
UNIVERSIDAD DE LA LAGUNA

08/02/2021 13:50:06

#### 4.2.1. Yeast cells trigger homologous recombination when a single DSB arise in telophase

Based on the premise that establishes the choice of the repair pathway (this is, the levels of Cdk/cyclins and the availability of having an intact DNA template to repair with), the MAT Switching assay was performed to define the cells preference to restore the broken DNA (Haber, 2012).

This process comprises the specific cut of the MAT locus through the conditional expression of the HO endonuclease. Once the DSB is created, HO is quickly repressed and degraded, enabling cells to repair. If HR is triggered, MAT a cells recombine with the HML locus and change the DNA sequence to MAT $\alpha$  through the Gene Conversion (GC) pathway (Yamaguchi & Haber, 2021). Thus, it is possible to analyze by Southern blot the appearance of bands with different sizes resulting from enzymatic digestions. The restriction enzyme must contain a target site within the sequence of either MAT $\alpha$  or MATa. This way, HR is employed if the initial band changes its size when repaired, whereas NHEJ occurs if the DSB switches back to its original size (Fig. 4.1.a).

*Cdc15-2* cells were blocked in telophase for 3 hours at 34 °C. Then, 2  $\mu$ M of  $\beta$ -estradiol was added for one extra hour. The culture medium was washed away and replaced by fresh YPD. Samples were taken at indicated time points to be processed for Southern and western blotting.

Southern blot analysis showed that cells trigger HR instead of NHEJ (Fig. 4.1.b). The initial band corresponds to the intact *StyI*-digested MATa fragment. After 1 hour of HO expression (1h + $\beta$ -E lane), ~ 70 % of cells had created the DSB (Fig. 4.1.b – d). It is a high percentage according to the  $\beta$ -estradiol system, which does not overexpress HO as it occurs with the widely used galactose promoter (pGal) (Gnügge et al., 2018; Klein et al., 2019; Yamaguchi & Haber, 2021). Considering that the HO cut band signal was 100 %, cells efficiently repaired ~ 75 % of MAT $\alpha$  sequence (~ 50 % relative to the MATa telophase band) after 3 hours of recovery (Fig. 1.b – d).

Such repair was accompanied by the hyperphosphorylation of Rad53 (Fig. 4.1.c). After the HO cut, the DNA damage was recognized, but Rad53 was completely hyperphosphorylated from 30 minutes onwards. Taking the advantage that HO endonuclease was tagged with the Flag epitope, its translation was also analyzed by western blot (Fig. 4.1.c). HO, as expected, only appeared after  $\beta$ -estradiol addition and coinciding with the DSB detection. After that, it was quickly degraded, as previously reported (Kaplun et al., 2006).

Este documento incorpora firma electrónica, y es copia auténtica de un documento electrónico archivado por la ULL según la Ley 39/2015.  
Su autenticidad puede ser contrastada en la siguiente dirección <https://sede.ull.es/validacion/>

Identificador del documento: 3075810 Código de verificación: smutbmB+

Firmado por: JESSEL AYRA PLASENCIA  
UNIVERSIDAD DE LA LAGUNA

Fecha: 30/11/2020 12:24:14

María de las Maravillas Aguiar Aguiar  
UNIVERSIDAD DE LA LAGUNA

08/02/2021 13:50:06

#### 4. Results and Discussion

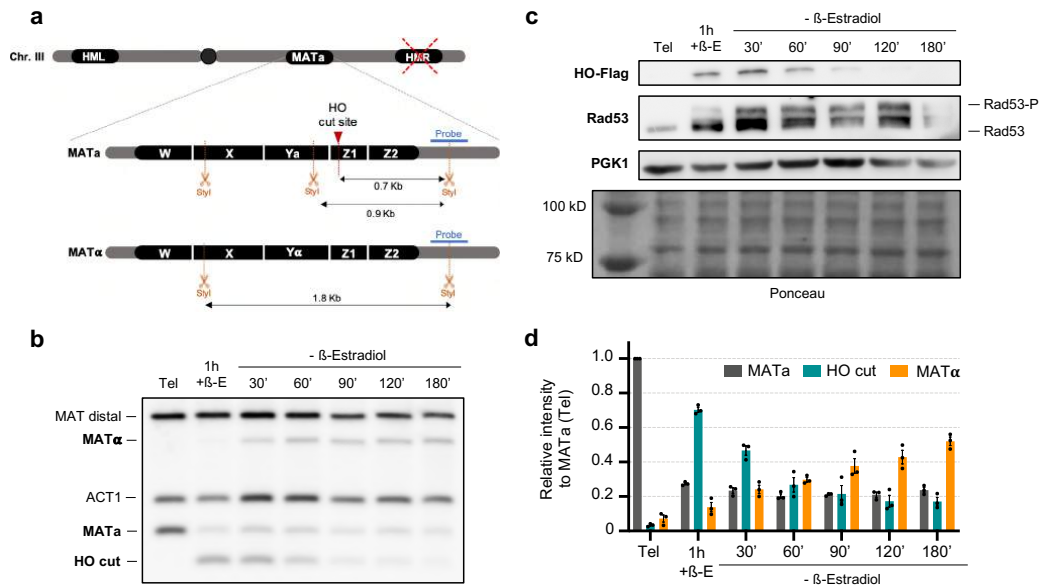


**Figure 4.1. Yeast cells use HR instead of NHEJ to repair a DSB in telophase.** **a)** Schematic of the fragments obtained after a *StyI* digestion and detected with a specific DNA probe for both MATa and MATα sequences. When the MATa locus is intact, the digestion gives rise to a fragment of 0.9 kb. The HOcs is targeted within the *StyI*-digested MATa fragment. Then, when cells create the DSB, the band decreases to 0.7 kb. HR leads the change of sequence to MATα, losing a *StyI* restriction site. Thus, the detected band migrates slower and is seen as a fragment of 1.8 kb. **b)** Representative Southern blot for MAT Switching assay in the wild-type strain. FM2531 was first blocked in telophase at 34 °C for 3 hours. Then, DSB was generated by adding β-estradiol. After 1 hour, the medium was washed away, and samples were taken to monitor the repair for 3 hours. The DNA was extracted, digested with *StyI*, separated in 1 % Agarose Low EEO LS gel, and submitted to Southern blot. The probes hybridized with the MAT locus and the ACT1 gene as a loading control (1.1 kb). The MAT probe was designed to hybridize in a *StyI* cut site sequence, leading to MAT distal bands (2.2 kb) that served as a second loading control. **c)** Representative western blot analyses for HO translation (tagged with Flag epitope) and the DSB detection through Rad53 hyperphosphorylation. PGK1 western blot served as housekeeping and Ponceau S staining of the membrane as the loading control for all lanes. The leftmost lane corresponds to the protein weight marker. **d)** Quantification of relative band intensities for MAT Switching Southern blots. Individual values were normalized to the ACT1 signals. Then, every lane was normalized to MATa (Tel). Error bars represent standard errors of the mean (SEMs) of three independent experiments. Tel: Telophase. +β-E: β-Estradiol addition.

At this point, it is not unreasonable to think that cells execute HR in telophase for the MAT Switching process. Contrary to what is seen when multiple DSBs emerge, *HML* and *HMR* cryptic copies are also located in chromosome III, just like the MAT locus. It may ease the GC pathway with no need to produce a sister loci coalescence event, making HR more efficient than expected.

#### 4. Results and Discussion

Based on the initial paradox to repair in late mitosis, it would perhaps be simpler going through cytokinesis and repair in  $G_1$  by NHEJ (Gao et al., 2016). Noteworthy, cells appear to give more importance to the Cdk1/cyclin levels than the chromosome segregation status. It results quite impressive since every biological process is developed to be as straightforward as possible, and reverting the segregation seems troubling. Likely, cells trigger HR in telophase and favor safeguarding the DNA integrity before entering a new cell cycle. What would happen if a DSB were generated within an essential gene? NHEJ would cause gain or loss of nucleotides at the junction, altering the DNA sequence and sentencing the cells to a certain death. Hence, HR positions itself as the best way to preserve life in telophase.

Another remaining question is, how would diploid cells respond to DSBs in telophase? It should be kept in mind that yeast strains used in this thesis are haploids, and they must recombine with the previously segregated sister chromatid. However, diploids could either promote sister loci coalescence events or recombine with the homolog chromosome located in the same nucleus. Would it be preferable to lose heterogeneity at the expense of avoiding the reversion of segregation? Further work is required to answer this question.

#### 4.2.2. Processing of 3' ssDNA ends in telophase is as efficient as in $G_2$

A clue signal of HR is the resection of the broken DNA ends to generate 3' ssDNA tails. This process is necessary to form protruding 3' nucleofilaments and invade the donor sequence to restore the break (Ferrari et al., 2020, p. 9; Peng et al., 2021; Yun & Kim, 2019).

Once resection begins, cells are committed to recombine because long ssDNA fragments do not work as efficient substrates for NHEJ. Cdk1 activates resection, and as shown above, Cdk/cyclin levels seem to predominate over the presence of a close and well-aligned sister chromatid to choose the repair pathway (Ewald, 2018; Kelliher et al., 2018; Lew & Reed, 1993; Litsios et al., 2019).

For this reason, the qPCR technique was employed as previously done (Gnügge et al., 2018; Zierhut & Diffley, 2008) to determine if resection occurs and how long it extends compared to  $G_2$ . A strain carrying deletions for both *HML* and *HMR* (unable to repair) was employed. Mutants for the cryptic copies leads to a static scenario for studying the processing of the broken end. So, cells were blocked in  $G_2$  and telophase. Then,  $\beta$ -estradiol was added and maintained until the end of the experiment, taking samples each hour. The technique is based on the amplification of different regions located downstream of the HOcs. These sequences contain a target site for *StyI* restriction enzyme, so that amplification can only occur if resection overpasses it (Fig. 4.2.a – b).

115

Este documento incorpora firma electrónica, y es copia auténtica de un documento electrónico archivado por la ULL según la Ley 39/2015.  
Su autenticidad puede ser contrastada en la siguiente dirección <https://sede.ull.es/validacion/>

Identificador del documento: 3075810 Código de verificación: smutbmB+

Firmado por: JESSEL AYRA PLASENCIA  
UNIVERSIDAD DE LA LAGUNA

Fecha: 30/11/2020 12:24:14

María de las Maravillas Aguiar Aguiar  
UNIVERSIDAD DE LA LAGUNA

08/02/2021 13:50:06

4. Results and Discussion

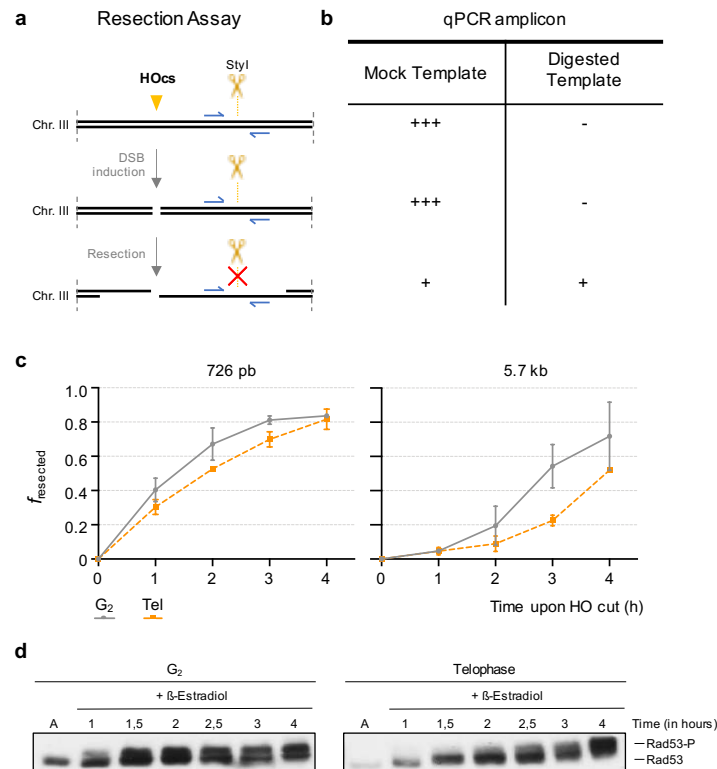


**Figure 4.2. Resection in telophase is carried out at similar levels than G<sub>2</sub>.** **a)** Schematic representation of the working system. Primers (blue arrows) are designed to amplify a sequence that contains a *StyI* target site. When this restriction enzyme is used on the sample, amplification is inhibited. If resection extends beyond the target site, *StyI* does not cut, and the primers can amplify. **b)** Summary table of the amplification yield obtained for each situation (drawn in **a**) after the restriction digestion and the mock control for each case. **c)** Charts depicting the resection kinetics for two different amplicons located at 726 bp and 5.7 kb downstream the break. Error bars represent SEMs of three independent experiments. *f* means the percentage of resected DNA. **d)** Representatives western blots against Rad53 to follow the DNA damage detection while 3' ssDNA ends are being processed. A: Arrest (G<sub>2</sub> → 15 µg·mL<sup>-1</sup> nocodazole for 3 hours. Telophase → incubation at 34 °C for 3 hours).

Two different DNA sequences located at 726 bp and 5.7 kb were analyzed. These locations were chosen to discern the efficiency of initial resection and the kinetics far away from the HOcs. Although Cdk/cyclin levels differ between G<sub>2</sub> and telophase, being lower in the latter stage, the resection rate does not present differences at 726 bp (Fig. 4.2.c). The HR machinery seems to be fully active, but, as previously discussed (see Chapter 1), there is no evidence whether it only happens for MAT Switching or every kind of DSB. MAT Switching suppose a pre-set mechanism genetically programmed, and many of the findings described here may be

#### 4. Results and Discussion

due to this condition. It would be interesting to generate a DSB in only one of the segregated sister chromatids, forcing the cells to revert segregation to trigger HR. The intact sister template would be located in the opposite nucleus, and cells would not have another way to restore the DNA sequence but regressing segregation, unless they activate NHEJ.

The outcomes for this experiment remain on the unavailability of creating just one DSB. First, sequence-specific endonucleases are the only way to make and monitor them locally. Still, both segregated sister chromatids contain the target sites, promoting the cut of both chromosomes. On the other hand, chemical compounds like phleomycin create randomly distributed DSBs but lead to differences in their location and number between each cell of a yeast culture. This fact would impede to follow the repair at a molecular level.

There exists a slight difference when resection takes place far away from the break. Even though yeast cells also resect ~ 50 % at 5.7 kb in telophase, it is not as efficient as the ~ 75 % shown in G<sub>2</sub> (Fig. 4.2.c). This finding could support the idea that the HR machinery is fully active in telophase, but its regulation is contingent upon the cell cycle phase. Thus, HR machinery would be functional at the initial stages to inhibit NHEJ. Then, the resection rate would slow down, stabilizing 3' ssDNA protruding nucleofilaments and preparing them to revert segregation for finding the intact donor. Long ssDNA tracks could hamper the regression.

As sister chromatids are still held together by proteinaceous linkages in G<sub>2</sub> (Shibata, 2017), cells might continue resecting 3' ends until finding a point when invasion could occur, although this experiment has been done in strains that cannot repair. In favor of that, Rad53 phosphorylation in G<sub>2</sub> is lightly faster than in telophase. It could mean that cells in G<sub>2</sub> (since homolog templates are already close) are at a more advanced level of repair. In contrast, telophase cells could promote a thorough adjustment between the initial processing, the homology search, and the final recombination (Fig. 4.2.d).

#### 4.2.3. DDR, Mre11, and NHEJ do not directly interfere with HR-mediated MAT Switching in telophase

##### 4.2.3.1. Rad9 depletion does not prevent from triggering MAT Switching

Since cells trigger MAT Switching in telophase, the study of HR factors was carried out. Results shown in the previous chapter described that the telophase-to-G<sub>1</sub> transition, acceleration of interloci movement, and coalescence events were directly dependent on the DDR. For this reason, a mutant strain for this checkpoint ( $\Delta rad9$ ) was tested in a MAT Switching assay (Fig. 4.3.a – c).

117

Este documento incorpora firma electrónica, y es copia auténtica de un documento electrónico archivado por la ULL según la Ley 39/2015.  
Su autenticidad puede ser contrastada en la siguiente dirección <https://sede.ull.es/validacion/>

Identificador del documento: 3075810 Código de verificación: smutbmB+

Firmado por: JESSEL AYRA PLASENCIA  
UNIVERSIDAD DE LA LAGUNA

Fecha: 30/11/2020 12:24:14

María de las Maravillas Aguiar Aguiar  
UNIVERSIDAD DE LA LAGUNA

08/02/2021 13:50:06

#### 4. Results and Discussion

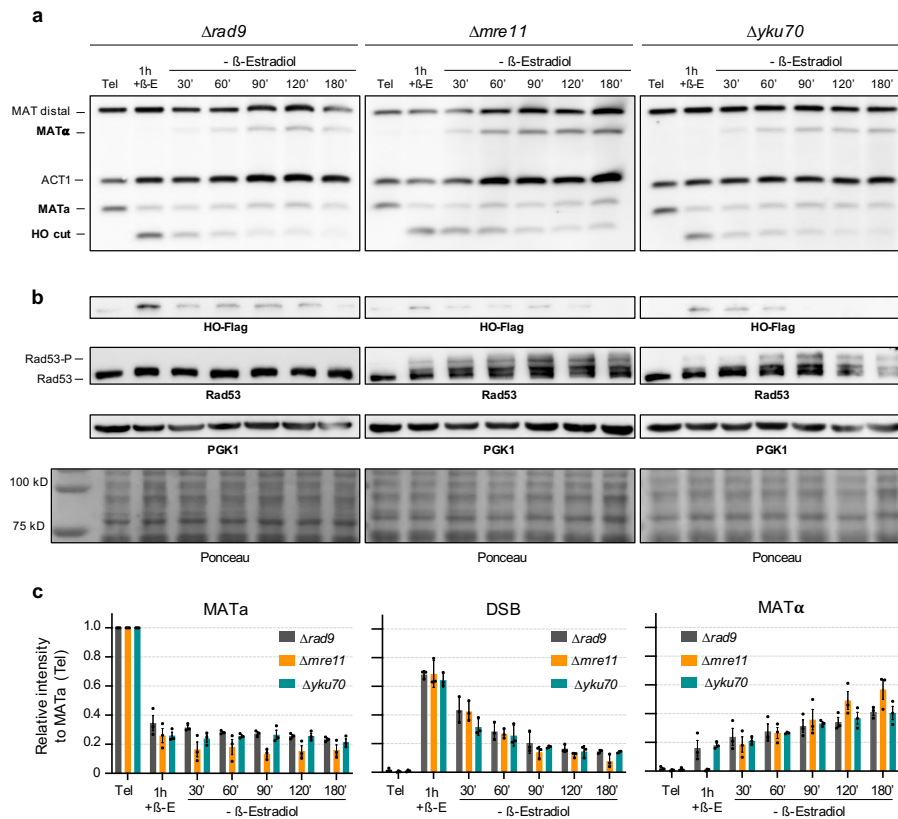


**Figure 4.3. MAT Switching is carried out in the absence of DDR and Mre11, whereas Yku70 deletion does not improve recombination levels.** **a)** Representative Southern blots to monitor MAT Switching in mutant strains for Rad9, Mre11, and Yku70. Strains were blocked in telophase at 34 °C for 3 hours. Then, experimental samples were taken and treated as explained in Fig. 4.1.b. **b)** Representative Western blots against the levels of translated HO (α-Flag), the levels of DNA damage detection (α-Rad53), the housekeeping protein (α-PGK1), and the loading sample control (Ponceau S staining) for each set of experiments. **c)** Charts of the relative signal for each band relative to the MATa control (Tel lane). Bars show the average of three independent experiments. Error bars are the SEMs.

Rad9 is known to be an adaptor of the DNA damage signaling, whose function is required for cell cycle arrest after DNA damage (Weinert & Hartwell, 1988, 1990). It is recruited to chromatin by the methylation of the histone H3-K79 and phosphorylation of H2A and Dpb11. Then, it enhances the Tel1- and Mec1-mediated activation of Rad53 (Finn et al., 2012).

Depletion of Rad9 did not cause any recombination deficiency (Fig. 4.3.a, leftmost Southern blot). Even though DNA damage is not detected by Rad53 phosphorylation (Fig. 4.3.b), in some way, cells recombine to similar levels (~ 60 % considering HOcs signal as 100 %) than



#### 4. Results and Discussion

the wild-type. Recent findings have reported that excessive Rad9 accumulation at DSBs inhibits the DNA end processing by Dna2-Sgs1 and Exo1 nucleases (Yu et al., 2018). It might be a reason by which cells can repair in its absence.

Rad9-independent repair in telophase likely relies on the Mre11-Rad50-Xrs2 (MRX) complex. Mre11 could initiate the 3' to 5' end resection stimulated by Cdk1-phosphorylated Sae2 (which antagonizes Rad9 accumulation and inhibits Rad53 activation). Besides, the Sgs1-Dna2 would be recruited to the DSB in a non-catalytic way, leading to a more extensive resection. It would then entail the RPA coating of resected 3' ssDNA and the recruitment of Mec1-Dna2, which would promote the genome integrity checkpoint in the absence of Rad9. Thus, the generation of protruding nucleofilaments would finally recruit Rad51 to replace RPA, enabling the GC at MAT locus (Bonetti et al., 2015; Clerici et al., 2006; Gobbin et al., 2013).

Western blot control against HO translation levels shows that it degrades slower than wild-type (Fig. 4.3.b). According to (Kaplan et al., 2003, 2006), the endonuclease has a half-life of only 10 minutes and is phosphorylated by Chk1 to be rapidly degraded. Accordingly, dead mutations for DDR as  $\Delta chk1$  or  $\Delta rad9$  stabilize HO, which does not seem to cause any residual effect in the course of the MAT Switching experiment.

#### 4.2.3.2. Mre11 is not essential to achieve GC in telophase.

Whether the MRX complex had an essential role for MAT Switching in telophase was tested next. As explained above, the MRX complex competes with the KU complex (Ku70/Ku80) for binding to broken DNA ends and then promoting HR or NHEJ, respectively.

In this case, Mre11 depletion did not cause any inhibition or retardation for GC in telophase (Fig. 4.3.a, central Southern blot). It seems that the DDR was activated through Tel1- and Rad9-mediated Rad53 phosphorylation, which was even more pronounced than in the wild-type (Fig. 4.3.b).

In line with previous studies (Nicolette et al., 2010, p. 11; Shibata et al., 2014; Shim et al., 2010), Exo1 and Sgs1, in concert with Dna2, are recruited to DSBs by MRX and Sae2. However,  $\Delta mre11$  *per se* does not delay the Exo1 resection. It has been shown that nuclease-deficient MRX complexes bound to DSBs, also exhibits ~ 80 % Exo1 activity compared to wild-type. In contrast, mutations in Rad50 decrease resection to ~ 25 – 30 %. Thus, Mre11 might be required for slight processing at DSB ends when some proteins (such as Spo11 or non-degradable nucleases) remain bound to the DNA and impede Rad50 activity. In those cases, Mre11 endonuclease may initiate the 3' to 5' resection, which is continued by Rad50 and then replaced by Exo1 or Sgs1-Dna2.

119

Este documento incorpora firma electrónica, y es copia auténtica de un documento electrónico archivado por la ULL según la Ley 39/2015.  
Su autenticidad puede ser contrastada en la siguiente dirección <https://sede.ull.es/validacion/>

Identificador del documento: 3075810 Código de verificación: smutbmB+

Firmado por: JESSEL AYRA PLASENCIA  
UNIVERSIDAD DE LA LAGUNA

Fecha: 30/11/2020 12:24:14

María de las Maravillas Aguiar Aguiar  
UNIVERSIDAD DE LA LAGUNA

08/02/2021 13:50:06

#### 4. Results and Discussion

HO endonuclease degradation is not affected when MRX cannot work (Fig. 4.3.b). Besides, the Mre11 function is dispensable for MAT Switching, but whether it becomes essential in DDC-deficient cells remains unknown. Curiously, cells repaired more efficiently than the  $\Delta rad9$  strain since the MAT $\alpha$  band was restored in ~ 90 % from the HOcs signal (vs. ~ 60 % in  $\Delta rad9$ ). Nonetheless, whether Mre11 becomes essential in the absence of Rad9 remains unknown.

##### **4.2.3.3. NHEJ does not play any residual role for MAT Switching repair in telophase, but Yku70 absence delays homologous recombination**

The next point addressed relied on whether NHEJ was hampering MAT Switching or remained inactive. Competition between MRX and KU complexes could be delaying the kinetics of GC in telophase compared to G<sub>2</sub> since HOcs was not entirely repaired after 3 hours (see Fig. 4.1.b).

Experiments performed in a mutant strain for NHEJ ( $\Delta yku70$ ) gave similar Southern and Western blots profiles than those previously seen (Fig. 4.3.b). If it were functional, a proportion of the MAT $\alpha$  signal should be restored after the DSB in the wild-type. However, once MAT $\alpha$  falls to ~ 20 %, it remains unchanged for the rest of the experiment (see Fig. 4.1.b). On the other hand, the  $\Delta yku70$  mutant should increase the percentage of MAT $\alpha$  signal, but it was formed even lower than expected (~ 70 % vs. ~ 80 % in the wild-type).

This result positions NHEJ as inactive in telophase. It should be considered that it might be the only way to repair when HR is abolished. Although the  $\Delta mre11$  strain did not serve as a mutant for HR,  $\Delta rad51$  and  $\Delta rad52$  strains could be employed instead in future approaches.

It has not escaped the idea that Yku70 is also involved in telomere length maintenance, structure, and epigenetic silencing (Bertuch & Lundblad, 2003a, 2003b; Gravel et al., 1998; Laroche et al., 1998; Taddei et al., 2004). The explanation for the delay seen in the MAT locus repair efficiency could lie in the chromosomal location of *HML*. It is located at the subtelomeric region of the left arm of chromosome III (from 11146 – 14849 bp). These regions should be correctly silenced, and the KU complex, in coordination with proteins like Esc1 or Sir2-Sir4, plays an essential role. In a  $\Delta yku70$  mutant, cells might experience some challenges to move and make the silent chromatin more accessible to the recombination machinery. This could explain why the MAT Switching process is slightly delayed relative to wild-type.

These results also suggest that those protein complexes located at the nuclear membrane and periphery, which are involved in the threedimensional distribution and structural maintenance of chromosomes, could have important roles at the time of moving back the damaged chromatin across the bud neck.

120

Este documento incorpora firma electrónica, y es copia auténtica de un documento electrónico archivado por la ULL según la Ley 39/2015.  
Su autenticidad puede ser contrastada en la siguiente dirección <https://sede.ull.es/validacion/>

Identificador del documento: 3075810 Código de verificación: smutbmB+

Firmado por: JESSEL AYRA PLASENCIA  
UNIVERSIDAD DE LA LAGUNA

Fecha: 30/11/2020 12:24:14

María de las Maravillas Aguiar Aguiar  
UNIVERSIDAD DE LA LAGUNA

08/02/2021 13:50:06

#### 4.2.4. Cohesin complex is activated after DSBs in telophase and plays a leading role in promoting coalescence events and HR

Considering the possible roles for proteins involved in chromatin silencing and structural maintenance, the cohesin complex was run as an exciting candidate. The cohesin is a chromosome-associated multisubunit complex highly conserved from yeast to humans. Its primary function is to mediate the physical cohesion between replicated sister chromatids for ensuring a normal segregation. However, it has also been enrolled in the efficient repair of DNA, as well as regulating gene expression (Peters et al., 2008).

The cohesin complex forms a ring-shaped structure that traps replicated sister chromatids before segregation. Once the cells enter anaphase, the securin Pds1 is degraded, and the separase Esp1 is released. Then, Esp1 cleaves the  $\alpha$ -kleisin subunit Scc1 (also known as Mcd1), and sister chromatids are pulled apart through MTs-mediated mechanical forces to the opposite nucleus (Uhlmann et al., 2000).

In terms of DNA repair, it has been shown that cohesin plays an essential role. In addition to the sister chromatid cohesion generated from S to G<sub>2</sub> phases, DSBs produce the damage-induced cohesion (DI-cohesion) (Kim et al., 2010). Following DNA damage, cohesin is recruited and accumulated along 50 – 100 kb surrounding the DSB site, and surprisingly, also genome-wide (Ström et al., 2004; Unal et al., 2004). In some way, the cohesin recruitment creates a firm anchoring of two well-aligned sister chromatids, easing recombination. Although it has been shown that cohesion depends on the acetyltransferase Eco1 (Ström et al., 2007; Unal et al., 2007), it has also been demonstrated that Mec1 and Chk1 phosphorylate Scc1 to initiate the cohesion establishment in post-replicative cells (Heidinger-Pauli et al., 2008).

This way, the cohesin complex regulation situates the telophase as a particular scenario compared to G<sub>2</sub>. Whereas it is active at the end of replication, only Smc1 and Smc3 subunits remain attached to chromatin after segregation to be recycled in the next cell cycle. In contrast, Scc1 needs to be translated *de novo* since cleaved fragments are unstable and degraded by the proteasome (Cheng et al., 2020; Rao et al., 2001). Thus, since coalescence events shown in Chapter 1 imply the joining of two segregated loci for relatively long periods, it would not be unreasonable to think of an active role for the cohesin complex, maybe holding close and well-aligned the sister chromatids.

For these reasons, different experiments were performed to discern whether cohesin was acting as an HR enhancer or was dispensable.

Este documento incorpora firma electrónica, y es copia auténtica de un documento electrónico archivado por la ULL según la Ley 39/2015.  
Su autenticidad puede ser contrastada en la siguiente dirección <https://sede.ull.es/validacion/>

Identificador del documento: 3075810 Código de verificación: smutbmB+

Firmado por: JESSEL AYRA PLASENCIA  
UNIVERSIDAD DE LA LAGUNA

Fecha: 30/11/2020 12:24:14

María de las Maravillas Aguiar Aguiar  
UNIVERSIDAD DE LA LAGUNA

08/02/2021 13:50:06

#### 4. Results and Discussion

##### 4.2.4.1. Yeast $\alpha$ -kleisin subunit Scc1 is translated *de novo* after DSB generation in telophase

It is known that the Scc1 subunit is necessary to generate cohesion. Indeed, the main difference between G<sub>2</sub> and telophase is its presence or absence, respectively.

For testing how this subunit was regulated, a strain unable to repair the HO-mediated DSB at the MAT locus ( $\Delta hml \Delta hmr$  double mutant) but bearing Scc1 tagged with three tandem copies of the Myc epitope was first blocked in telophase at 34 °C for 3 hours. Then, the culture was divided into three. The first one served as a mock control, whereas the others were used to generate a single (2  $\mu$ M  $\beta$ -estradiol) and multiple (10  $\mu$ g·mL<sup>-1</sup> phleomycin) DSBs. Incubation of subcultures was prolonged at 34 °C for 2 extra hours. Samples were processed and subjected to the Western blot technique.

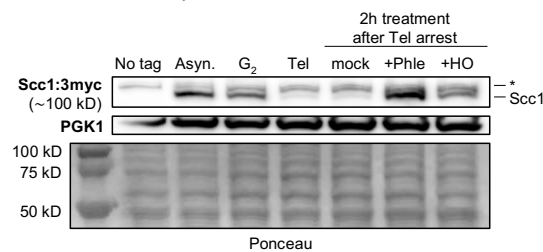


**Figure 4.4. Scc1 levels are restored after DNA damage in telophase.** Western blot against Scc1-3myc ( $\alpha$ -myc antibody) comparing its levels between asynchronous, G<sub>2</sub>- and telophase-blocked cultures. Cells arrested in telophase were subdivided into three conditions for two hours (mock, phleomycin, and HO endonuclease). The leftmost lane is a control for Scc1 without the 3myc epitope tag. PGK1 protein levels served as the housekeeping. Ponceau S staining is also shown as a loading control. Asyn.: Asynchronous. Tel: Telophase. +Phle: 10 mg·mL<sup>-1</sup> Phleomycin. +HO: 2  $\mu$ M  $\beta$ -estradiol addition. \*: Unspecific band detected by the  $\alpha$ -myc antibody just over Scc1 signal.

As expected, Scc1 band was detected for both cycling cells and those blocked in G<sub>2</sub>. The Scc1 signal disappeared almost entirely when cells were arrested in telophase and remained low in the mock control two hours later. Surprisingly, full-length Scc1 was restored after single and multiple DSBs generation (Fig. 4.4).

This finding points towards the hypothesis that positions the cohesin complex as an essential factor during the reversion of segregation. Cells might require synthesizing Scc1 *de novo*. Thus, the ring-shaped cohesin structure could be newly formed and loaded onto the breaks, promoting the DI-cohesion and easing the recombinational coalescent events. Nevertheless, the Scc1 recruitment by Smc1-Smc3 and the re-formation of the cohesin complex remains to be studied.

#### 4. Results and Discussion

Whether Scc1 is protected from Esp1-mediated degradation is still unknown; however, its regulation could be performed through three distinct pathways. The first one would involve the physical inactivation of Esp1 through the *de novo* synthesis of the inhibitor Pds1. The second one would rely on the transient suppression of Esp1 enzymatic activity by a PP2A<sup>cdc55</sup>-mediated dephosphorylation (Liang et al., 2018). Finally, the third one could entail a Mec1- and Chk1-mediated Scc1 phosphorylation, thus inducing cohesion (Heidinger-Pauli et al., 2008). It is not even improbable that some of the pathways may be triggered simultaneously.

##### 4.2.4.2. Depletion of Smc3 prevents the generation of coalescence events

Smc1-Smc3 cohesin subunits are loaded onto chromosomes at the telophase-to-G<sub>1</sub> transition. When cells enter S phase, the acetyl-transferase Eco1 acetylates Smc3, thus preventing the ATPase activity of Smc1-Smc3 heads and inhibiting the opening of the Smc3-Scc1 interface (Çamdere et al., 2015; Chan et al., 2012; Huber et al., 2016; Murayama & Uhlmann, 2015). Thus, sister chromatids are stably held together until the onset of anaphase through the Scc1 cleavage (Nasmyth & Haering, 2009).

Whether Smc1-Smc3 dimers are loaded onto chromosomes in telophase and lead the coalescence upon DSBs was next tested. The same strain for the coalescence study under the fluorescence microscope (see Chapter 1) was transformed to degrade Smc3 conditionally. The strain carries several *TetO* sequences at the telomeric region of the right arm of chromosome XII and the *TetR-YFP* as the fluorescent reporter. Smc3 was modified to be degraded conditionally. For doing that, a cassette containing the auxin-inducible degen (AID) sequence and nine tandem repeats of the Myc epitope was fused at C-termini. Also, a cassette for translating the auxin preceptive F-box protein TIR1 (OsTIR1), which forms a functional ubiquitin-ligase, was inserted at the *URA3* locus.

For checking the system was working correctly, a serial dilution spot assay was carried out (Fig. 4.5.a). The strain described above and its counterpart with no presence of OsTIR1 were plated in YPDA and YPDA + 8 mM indole-acetic acid (IAA). When IAA enters inside the cells, it binds to the AID epitope. Then, OsTIR targets it for degradation by the proteasome, leading to a conditional depletion of every AID-tagged protein (Morawska & Ulrich, 2013). If the tagged protein is essential, the spot assay gives rise to a no-growth pattern.

Este documento incorpora firma electrónica, y es copia auténtica de un documento electrónico archivado por la ULL según la Ley 39/2015.  
Su autenticidad puede ser contrastada en la siguiente dirección <https://sede.ull.es/validacion/>

Identificador del documento: 3075810 Código de verificación: smutbmB+

Firmado por: JESSEL AYRA PLASENCIA  
UNIVERSIDAD DE LA LAGUNA

Fecha: 30/11/2020 12:24:14

María de las Maravillas Aguiar Aguiar  
UNIVERSIDAD DE LA LAGUNA

08/02/2021 13:50:06

#### 4. Results and Discussion

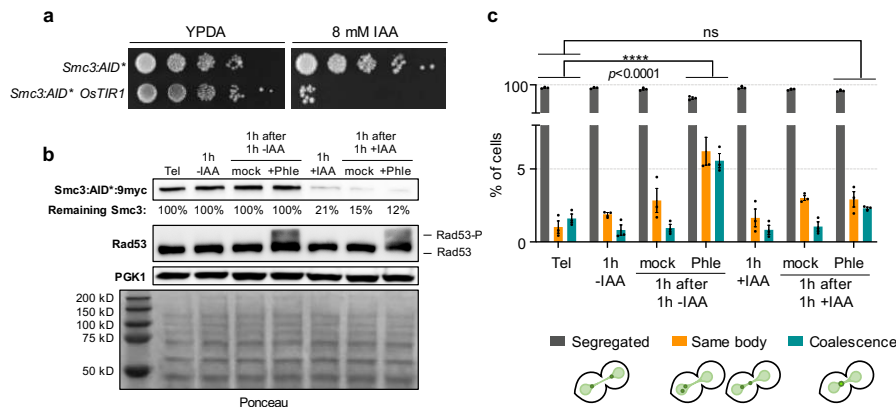


**Figure 4.5. The absence of Smc3 inhibits telomere coalescence after DSBs in telophase. a)** Serial dilution spot assay depicting the no-growth pattern of the Smc3:AID tagged strain in the presence of 8 mM IAA. The same strain without the ubiquitin-ligase was also used as control. **b)** Representative Western blot from experimental samples. Telophase blocked cells were divided into two. One subculture was treated with 8 mM IAA for 1 hour. Then, each subculture was, in turn, divided into two, one serving as mock control and the other to be treated with 10  $\mu\text{g}\cdot\text{mL}^{-1}$  phleomycin. As cells carried Smc3, *cdc15-2*, and the OsTIR1 tagged with the Myc epitope, the degradation of Smc3 was monitored by using an  $\alpha$ -mini-AID-tag monoclonal antibody (MBL Life Sciences, see table 3.4 in Materials and Methods section). Besides, the  $\alpha$ -myc antibody even recognizes an unspecific band ( $\sim 100$  kb), which could hamper the identification of Smc3, giving a multiband pattern. Rad53 was also monitored as a control for DNA damage detection. PGK1 was revealed as the housekeeping to quantify the remaining Smc3 signal. Ponceau S staining is showed as a loading control for each lane. **c)** Chart representing quantifications from fluorescence microscopy. Cells were classified into three categories depending on sister cXII right arm telomeres (*TetR-YFP*) location within the nucleus: i) Segregated, showing two foci well separated; ii) Same body, presenting the telomeres retained in one of the cells; and iii) Coalescence, only one TetR-YFP focus. Error bars represent the SEM of three independent experiments. Statistical significance was calculated through 2-way ANOVA and multiple comparisons analysis. IAA: Indole-acetic acid. Tel: Telophase. ns: non-significant statistical difference.

Telophase cells were submitted to Smc3 degradation and subsequent generation of DSBs. Western blot analyses showed that cells degraded  $\sim 80$  % of Smc3 after 1 hour (Fig. 4.5.b). Besides, cells could trigger Smc3-independent Rad53 phosphorylation at similar levels than the mock control, positioning any cohesin role downstream of the DDC.

Quantification of fluorescence microscopy gave rise to important information about the relevance of the cohesin role in coalescence. Cells that were not treated with IAA but suffered DSBs reverted segregation of *TetR-YFP* in  $\sim 13$  % of the telophase-blocked cells [ $p < 0.0001$  relative to categories quantified in Tel time-point] (Fig. 4.5.c). As it occurred in Chapter 1,  $\sim 7$  % of cells showed two foci in the same cellular body, whereas  $\sim 6$  % had coalescence events. The reversion of segregation represents a low percentage, but it could be due to the nature of

#### 4. Results and Discussion

phleomycin-generated DSBs and the method employed to quantify. After all, and despite the whole nuclear material suffers gross changes when DSBs arise in telophase, only the telomere of chromosome XII is being monitored. The cells may choose the sister loci-to-revert depending on the DSB location. As phleomycin creates randomly-distributed DSBs, it would be possible to think that the low percentage of partial reversion represents only the fraction of chromosome XII where DSBs occurred.

Nonetheless, the quantification of cells deficient for Smc3 did not show a significant statistical difference from the control situation (Fig. 4.5.c). This result could support that the cohesin complex is essential to hold coalescence and promote the passing of broken chromosomes across the bud neck. Besides replication and segregation, the cohesin complex is also involved in the structural maintenance of chromosome distribution within the nucleus. It might be a starting point to decipher how cohesin absence precludes coalescence. Indeed, the Smc3 subunit has been shown to interact physically with several nuclear envelope (NE) factors closely involved in nuclear organization such as Mps3 (Ghosh et al., 2012). Thus, it would be interesting to study further whether chromatin-associated cohesins anchor to NE complexes and promote the chromosomes reversion. In conclusion, chromosome reversion and sister loci coalescence could work through a dual mechanism based on i) the Cin8 kinesin motor protein, and ii) the displacement of broken chromatin by the interaction with nuclear membrane complexes and chromatin-associated cohesins.

#### 4.2.4.3. HR in telophase is significantly delayed in the absence of Smc3 subunit

Having seen the cohesin role for repairing random DSBs in telophase, its absence was also studied in the MAT Switching assay.

It has previously been reported that cohesin is vital for efficient post-replicative repair, but not for regulating intrachromosomal GC nor forming ssDNA at the DSBs ends (Unal et al., 2004). However, those experiments were performed using thermosensitive mutants for cohesin (*mcd1-1*) in cells blocked in G<sub>2</sub>. Although the *mcd1-1* allele has broadly been employed, it might not be the most appropriate for this kind of experiments. It is known that thermosensitive mutations are typically missense, retaining a specific essential gene function only at permissive temperatures. When it is raised at non-permissive conditions, the gene product loses its activity, leading to an unfunctional protein. Nevertheless, the lack of functions may not necessarily promote a rapid degradation. In G<sub>2</sub>, the ring-shaped cohesin structure is completely formed and loaded onto sister chromatids. It means that replicated sisters are held nearby and well-aligned each other. This way, to what extent could the misfolding of *mcd1-1* affect the process of recombination?

125

Este documento incorpora firma electrónica, y es copia auténtica de un documento electrónico archivado por la ULL según la Ley 39/2015.  
Su autenticidad puede ser contrastada en la siguiente dirección <https://sede.ull.es/validacion/>

Identificador del documento: 3075810 Código de verificación: smutbmB+

Firmado por: JESSEL AYRA PLASENCIA  
UNIVERSIDAD DE LA LAGUNA

Fecha: 30/11/2020 12:24:14

María de las Maravillas Aguiar Aguiar  
UNIVERSIDAD DE LA LAGUNA

08/02/2021 13:50:06

#### 4. Results and Discussion

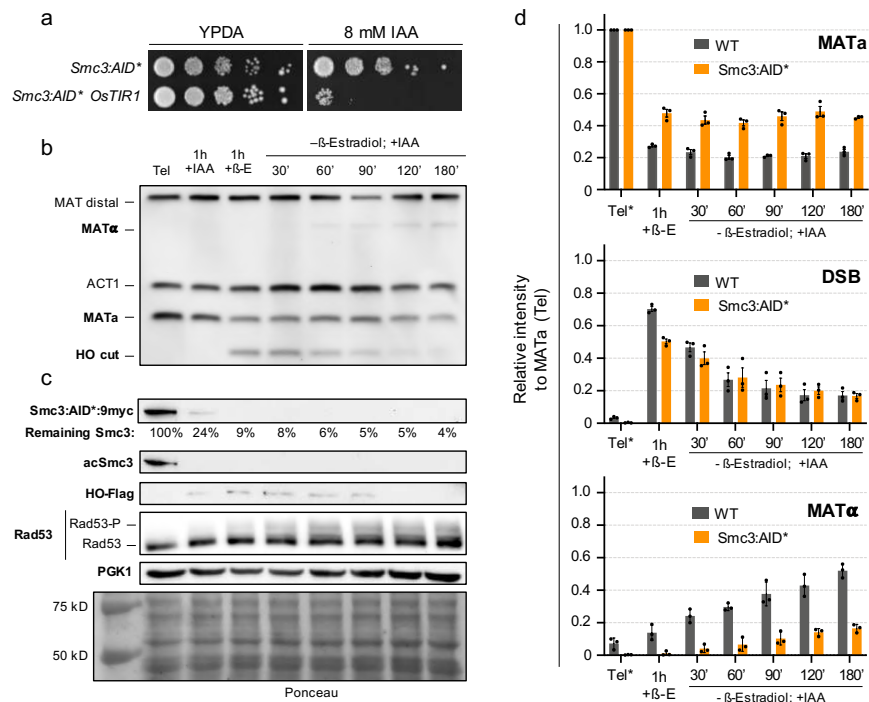


**Figure 4.6. Smc3 degradation elicits a substantial delay in GC performance in telophase.** **a)** Serial dilution spot assay as it was performed in Fig. 4.5.a. In this case, the strain constructed for MAT Switching was transformed to degrade Smc3 conditionally. **b)** Representative Southern blot to monitor MAT Switching in the absence of Smc3. Telophase cells were first submitted to Smc3 depletion through the addition of 8 mM IAA for 1 hour. Then, the culture was subjected to 2  $\mu$ M  $\beta$ -estradiol to create the HO cut for another extra hour. Finally, the medium was replaced by fresh YPD containing 8 mM IAA (maintaining Smc3 degradation), and repair was monitored for 3 hours. **c)** Representative Western blots from samples taken in **b**. As in Fig. 4.5.b, Remaining Smc3 levels were followed using the  $\alpha$ -mini-AID-tag monoclonal antibody. A monoclonal  $\alpha$ -acetylated-Smc3 antibody was also employed to determine the fraction of Smc3 bound to chromatin. The HO translation, as well as the DNA damage detection marker, are also shown. PGK1 served as the housekeeping to relativize the remaining Smc3, and Ponceau S staining was performed as a loading control for each lane. **d)** Quantification of relative band intensities for MAT Switching Southern blots. Individual values were normalized to the ACT1 signals and then normalized to MATa (Tel lane). Error bars represent SEMs of three independent experiments. Tel: Telophase. + $\beta$ -E:  $\beta$ -Estradiol addition. +IAA: Indole-acetic acid.

In the end, the role of cohesin in DNA double-strand repair is to facilitate and favor the use of the sister chromatid during recombination, thus reducing the loss of heterozygosity or gross chromosomal rearrangements (Litwin et al., 2018).

Therefore, once the cohesion is established in  $G_2$ : i) How long should *mcd1-1* be degraded to generate interference on DNA repair? ii) Is the misfolding of *mcd1-1* sufficient for precluding



#### 4. Results and Discussion

HR despite sister chromatids are already together? iii) Are Smc1-Smc3 also targeted for degradation? Moreover, if it occurs, how is the Smc1-Smc3-Scc1 interaction disrupted without disturbing the trapped DNA? iv) Despite cohesion between sister chromatids is lost through *mcd1-1* inactivation, do they separate enough to avoid MAT Switching? All these questions still remain unknown.

Whether the cohesin complex is involved in promoting gene conversion in telophase was next tested. A strain ready for studying MAT Switching was also transformed to degrade Smc3 conditionally (Fig. 4.6.a). The advantage of telophase is that the Smc1-Smc3 remaining pool cannot trap the DNA. Assuming that Scc1 *de novo* translation after DSBs (see Fig. 4.4) serves to generate the ring-structure, telophase cohesion can be abolished by degrading Smc1 or Smc3 before the DNA damage. For doing that, cells were arrested in telophase at 34 °C for 3 hours. Then, 8 mM IAA was added to the medium to deplete Smc3 for one hour. After this time, 2 µM β-estradiol was supplemented to generate the HO-mediated DSB for another hour. The medium was then replaced by YPD plus 8 mM IAA to continue monitoring the repair in the absence of cohesin. The samples were taken at indicated time-points for Southern and Western blotting.

Contrary to what is seen in the wild-type, the Smc3 absence delayed GC drastically (Fig. 4.6.b). The HO cut seems to be adequately processed as the band started fading after 30 minutes from the break. Even though the cut efficiency is lower than in wild-type (~ 50 % vs. ~ 70 %, respectively), its fading implies that cells trigger resection. However, the quantification of band intensities showed that the MATα repair is severely impaired. Whereas wild-type cells perform GC with ~ 80 % efficiency, Smc3-depleted cells only repaired ~ 35 % (considering the HO cut band as 100 %). Also, the detection of DNA damage through Rad53 phosphorylation seems fainter and slightly delayed (Fig. 4.6.c).

Not less important, Western blot against the acetylation of lysine residues (K112 and K113) of Smc3 showed that a large pool is indeed acetylated in telophase (Fig. 4.6.c). It is known that the Eco1-acetylation of Smc3 during the S phase stabilizes its association with chromosomes. Then, Hos1-mediated deacetylation in anaphase eases the sister chromatids release and allows its re-use in the next cell cycle (Chan et al., 2012; Huber et al., 2016; Murayama & Uhlmann, 2015). Strikingly, this result reveals a chromatin-bound Smc3 pool in telophase. It might be a consequence of blocking cells before cytokinesis. Telophase-blocked cells may stay one step ahead and start bounding the Smc1-Smc3 to chromatin for two reasons. The first one would consist of the entrance in G<sub>1</sub> with an Smc1-Smc3 pool already bound to chromosomes. In some way, it would compensate for cytokinesis delay by advancing for the next S phase events, resulting in a more efficient replication. The second one would

127

Este documento incorpora firma electrónica, y es copia auténtica de un documento electrónico archivado por la ULL según la Ley 39/2015.  
Su autenticidad puede ser contrastada en la siguiente dirección <https://sede.ull.es/validacion/>

Identificador del documento: 3075810 Código de verificación: smutbmB+

Firmado por: JESSEL AYRA PLASENCIA  
UNIVERSIDAD DE LA LAGUNA

Fecha: 30/11/2020 12:24:14

María de las Maravillas Aguiar Aguiar  
UNIVERSIDAD DE LA LAGUNA

08/02/2021 13:50:06

#### 4. Results and Discussion

---

involve the prevention of DSBs generation and their consequences in telophase. In the case they appeared, cells should respond as fast as possible. Hence, counting with a chromatin-bound Smc1-Smc3 pool would be advantageous. It would speed the formation of the ring-shaped structure after Scc1 *de novo* translation, leading to a more effective reversion of segregation and repair.

This set of experiments give insights into the potential molecular regulation of a DSB in telophase. However, further work needs to be carried out to solve numerous issues. For now, it can be claimed that cells respond to DSBs through the DDC. Thus, they trigger resection of 3' DNA ends and promote a Yku70-, Rad9- and Mre-11 independent, but Smc3-dependent homologous recombination repair.

#### 4.2.5. Proteomics identifies new factors specifically involved in DNA repair in telophase.

As a final experimental approximation to frame the context of DNA repair in telophase, proteomics through mass spectrometry was performed. This technique allows the high-throughput characterization and quantification of the proteome levels.

Proteomics mass spectrometry helps to identify both downregulated and upregulated proteins relative to control situations. It eases the finding of factors involved in cellular processes, such as DNA repair, by comparing the proteome resulting from different experimental conditions.

For this reason, four independent experiments were carried out to compare G<sub>2</sub> and telophase scenarios, both in the presence and absence of one single (HO-mediated) or multiple (phleomycin) DSBs. Experiments, sample extractions, and protein preparations were performed as explained in the Materials and Methods section. The mass spectrometry experimental procedure was performed by Dr. Lara Pérez Martínez, at the Institute of Molecular Biology (IMB), Mainz, Germany, as explained in (L et al., 2020).

This technique was performed to find new factors that may specifically involve DSBs repair in telophase compared to G<sub>2</sub>. The results are shown in Figs. 4.7 – 4.8 as volcano plots, and can also be found in the Appendix I section. It summarizes up- and downregulated proteins for DSBs repair in G<sub>2</sub> and telophase DNA, as well as their biological function.

Many of the hit proteins were involved in processes such as metabolism regulation. However, it was also possible to identify some telophase-specific factors related to DNA repair.

128

Este documento incorpora firma electrónica, y es copia auténtica de un documento electrónico archivado por la ULL según la Ley 39/2015.  
Su autenticidad puede ser contrastada en la siguiente dirección <https://sede.ull.es/validacion/>

Identificador del documento: 3075810 Código de verificación: smutbmB+

Firmado por: JESSEL AYRA PLASENCIA  
UNIVERSIDAD DE LA LAGUNA

Fecha: 30/11/2020 12:24:14

María de las Maravillas Aguiar Aguiar  
UNIVERSIDAD DE LA LAGUNA

08/02/2021 13:50:06

4. Results and Discussion

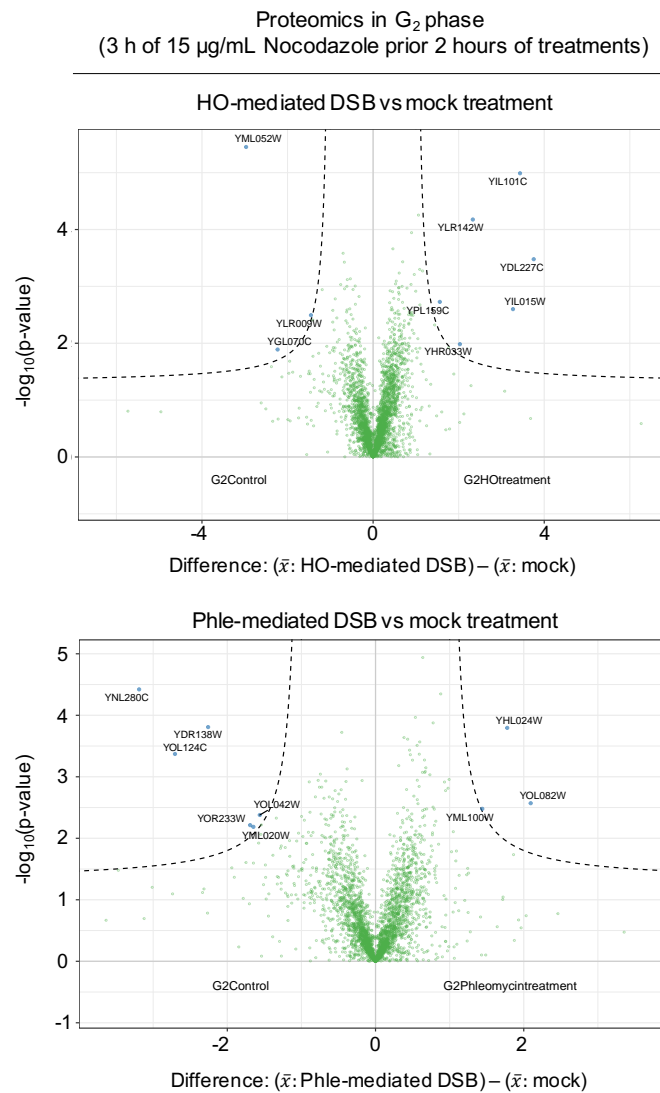


**Figure 4.7. Proteomics Mass Spectrometry results for DSBs in G<sub>2</sub>.** Volcano plots representing the quantified proteins. Cells were first arrested in G<sub>2</sub> by adding 15 µg·mL<sup>-1</sup> Nocodazole and incubating at 25 °C for 3 hours. Then, the culture was divided into three. One served as mock control, whereas the others were treated with 2 µM β-estradiol and 10 µg·mL<sup>-1</sup> phleomycin to generate DSBs. Samples were processed as required to perform the technique. Up- and downregulated proteins were represented by plotting  $-\log_{10}(p\text{-value})$  for each found peptide vs. the Log<sub>2</sub> fold change. In turn, Log<sub>2</sub> change was determined as the difference between the mean of label-free quantification (LFQ) intensity of the four damaged replicates with DSBs or the control samples. *P*-values were calculated with a Welch *t*-test, and proteins above the threshold (dashed line defined empirically as  $p = 0.05$ ) are considered enriched.

Este documento incorpora firma electrónica, y es copia auténtica de un documento electrónico archivado por la ULL según la Ley 39/2015.  
 Su autenticidad puede ser contrastada en la siguiente dirección <https://sede.ull.es/validacion/>

Identificador del documento: 3075810 Código de verificación: smutbmB+

Firmado por: JESSEL AYRA PLASENCIA  
 UNIVERSIDAD DE LA LAGUNA

Fecha: 30/11/2020 12:24:14

María de las Maravillas Aguiar Aguiar  
 UNIVERSIDAD DE LA LAGUNA

08/02/2021 13:50:06

4. Results and Discussion

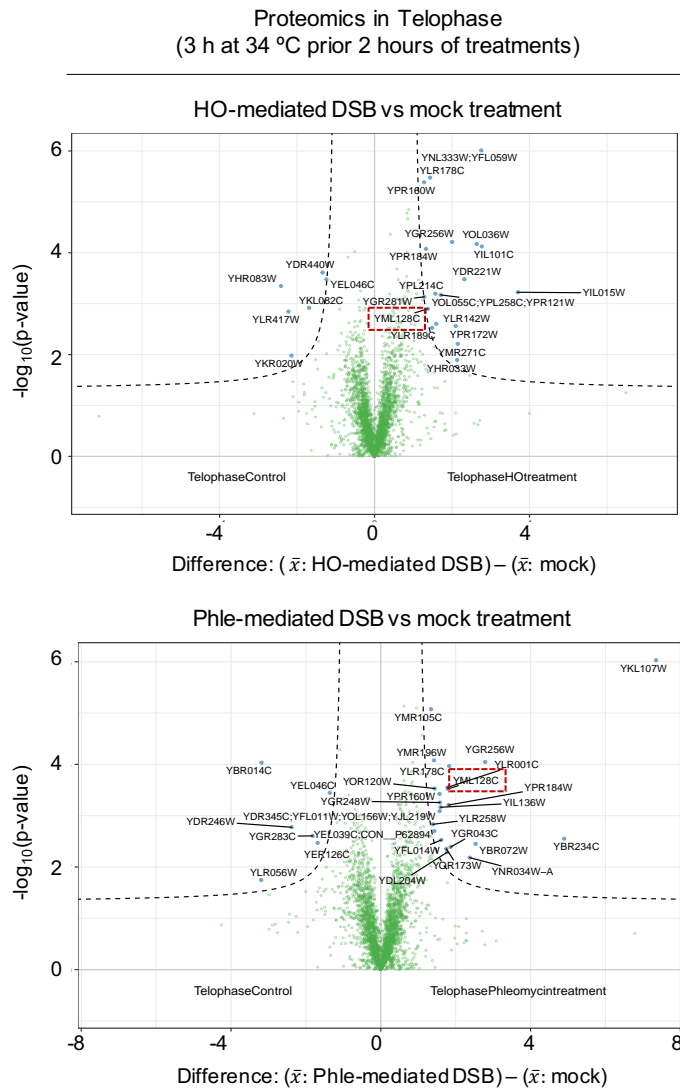


**Figure 4.8. Proteomics Mass Spectrometry results for DSBs in telophase.** Volcano plots representing the quantified proteins. Cells were first arrested in telophase by incubating at 34 °C for 3 hours. Then, the culture was divided into three. Samples were treated, taken, and processed, as explained in Fig. 4.7. Up- and downregulated proteins were also represented by plotting  $-\log_{10}(\text{p-value})$  for each found peptide vs. the  $\text{Log}_2$  fold change.

There was an interesting protein among the factors shown in volcano plots. It was upregulated upon DSBs in telophase, but not in  $G_2$ . The protein is encoded by the YML128C gene (depicted inside a red dashed-line rectangle in Fig. 4.8), and it is also known as Msc1. It

130

Este documento incorpora firma electrónica, y es copia auténtica de un documento electrónico archivado por la ULL según la Ley 39/2015.  
 Su autenticidad puede ser contrastada en la siguiente dirección <https://sede.ull.es/validacion/>

Identificador del documento: 3075810 Código de verificación: smutbmB+

Firmado por: JESSEL AYRA PLASENCIA  
 UNIVERSIDAD DE LA LAGUNA

Fecha: 30/11/2020 12:24:14

María de las Maravillas Aguiar Aguiar  
 UNIVERSIDAD DE LA LAGUNA

08/02/2021 13:50:06

4. Results and Discussion

is a protein of unknown function, but null mutants ( $\Delta msc1$ ) seem to be defective in directing meiotic recombination events to homologous chromatids (Huh et al., 2003; Reinders et al., 2007; Thompson & Stahl, 1999).

Thus, a subcellular and biochemical analysis was performed to discern whether it could be directly implied in DSBs repair in telophase. For doing that, the strain ready for studying MAT Switching was transformed to analyze the Msc1 subcellular location under the fluorescence microscope and its post-translational modification upon DSBs in telophase (Fig. 4.9).

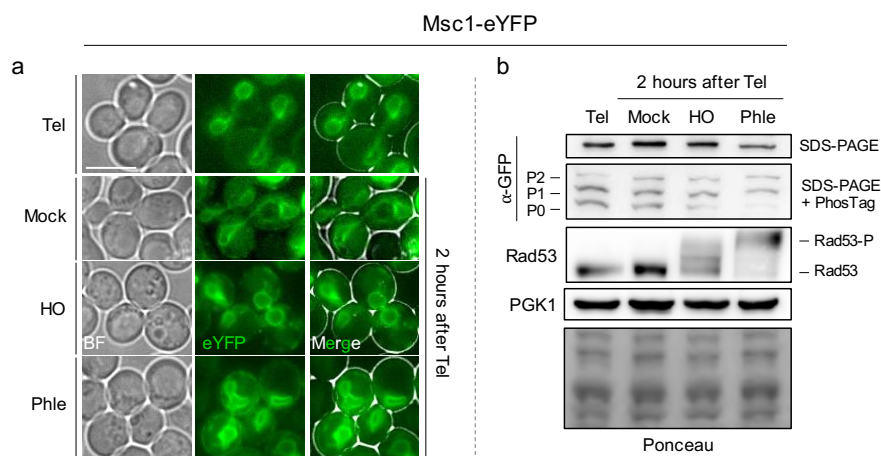


**Figure 4.9. Subcellular location and post-translational modifications of Msc1 upon DSBs in telophase.** **a)** Fluorescence microscopy pictures of the Msc1-eYFP subcellular distribution. Cells were blocked in telophase at 34 °C for 3 hours. Then, the culture was split into three. One served as mock control, whereas the others were subsequently treated with 2  $\mu\text{M}$   $\beta$ -estradiol and 10  $\mu\text{g}\cdot\text{mL}^{-1}$  for 2 extra hours. Then, live-cell imaging was performed. **b)** Representative Western blots for samples from **a**. Rad53 was analyzed as the marker of DNA damage detection, and PGK1 was used as housekeeping. Ponceau S staining was done as loading control for each lane. Taking advantage that cells were already transformed with Msc1-eYFP fusion, an  $\alpha$ -GFP antibody was employed to study the Msc1 post-translational states. The upper panel shows the Msc1 levels in an SDS-PAGE gel. Below, a PhosTag-containing SDS-PAGE gel exhibits the different Msc1-phosphorylated isoforms. Tel: Telophase. Phle: 10  $\mu\text{g}\cdot\text{mL}^{-1}$  phleomycin. SDS-PAGE: Sodium dodecyl-sulfate polyacrylamide gel electrophoresis). eYFP: enhanced Yellow Fluorescent Protein.

Visualization of Msc1-eYFP under the microscope suggested an expected distribution for proteins located at the endoplasmic reticulum (ER) and the nuclear membrane (NM) (Fig. 4.9.a). In telophase, it was defined as two separated rounded entities connected by a thin bridge. These elongated nuclei structures were maintained for 2 hours in the case of mock control. Contrary to what happened with Cin8 kinesin protein (see Chapter 1), Msc1-eYFP did not relocate at all after DSBs. Instead, it remained attached to the ER-NM interface, where it

#### 4. Results and Discussion

---

served as a reporter to confirm that not only the DNA or MTs but also the NM suffered structural changes when DSBs occurred.

SDS-PAGEs was not enough to differentiate phosphorylated isoforms. For this reason, the same samples were loaded and separated into an SDS-PAGE containing PhosTag™. The PVDF membrane exposure revealed that Msc1, at least in telophase, had 3 phosphorylation levels (Fig. 4.9.b). The same pattern was seen 2 hours later in the mock control, even though the P2 level appeared slightly enriched. However, after DSBs generation, the P0 level faded almost to be undetectable, whereas P1 and P2 remained unchangeable.

According to recent works, it is well known that DSBs promote the movement of chromatin to be repaired at the nuclear periphery (Lemaître et al., 2014; Seeber & Gasser, 2017). Msc1 seems to be phosphorylated, but whether the fading of the P0 level supposes an enzymatic activation or protein relocalization remains unclear. Msc1 could be relocated from the ER-NM interface to the inner nuclear periphery to repair DNA. However, limitations of epifluorescence microscopy do not allow to discern whether Msc1 changes its location. It might be more appropriate to use super-resolution confocal or even transmission electron microscopy instead. Besides, it would be interesting to test whether  $\Delta msc1$  cells revert segregation, perform MAT Switching, or survive to DSBs in telophase at similar levels than the wild-type. This set of experiments could provide a novel role for a protein of unknown function specific for telophase repair.

Este documento incorpora firma electrónica, y es copia auténtica de un documento electrónico archivado por la ULL según la Ley 39/2015.  
Su autenticidad puede ser contrastada en la siguiente dirección <https://sede.ull.es/validacion/>

Identificador del documento: 3075810 Código de verificación: smutbmB+

Firmado por: JESSEL AYRA PLASENCIA  
UNIVERSIDAD DE LA LAGUNA

Fecha: 30/11/2020 12:24:14

María de las Maravillas Aguiar Aguiar  
UNIVERSIDAD DE LA LAGUNA

08/02/2021 13:50:06

### 4.3. Chapter 3

#### **Are anaphase events really irreversible? The endmost stages of cell division and the paradox of the DNA double-strand break repair**

The third chapter is dedicated to the theoretical contemplation and future perspectives of the facts discovered in yeast. It is essential to understand the DSBs repair at the latest mitotic stages. The partial reversion of segregation (if it happened in higher eukaryotes) could open a new research field, even for anticancer therapies.

Whether the coalescence of segregated sister loci is a telophase-specific response or a result of the pre-existing DNA damage response in G<sub>2</sub> remains unclear. Regardless, kinesin proteins, microtubules, and HR machinery are conserved in mammal cells. It should be considered, though, that there are numerous differences between yeast and mammals (such as the yeast close mitosis with no disruption of the nuclear membrane or its ability to live as haploid), which may impede mammals repairing with the sister when cells divide.

This set of ideas and speculations have also been published as an original peer-reviewed paper. For this reason, these insights are presented as a copy of the original manuscript.

- **Scientific journal:** BioEssays.
- **Area:** Biochemistry, cell biology, and molecular biology.
- **Quartile:** Q1.
- **Impact factor (2019):** 4.627.
- **Authors:** Félix Manuel Machín Concepción and Jessel Ayra Plasencia
- **DOI:** <https://doi.org/10.1002/bies.202000085>.

Este documento incorpora firma electrónica, y es copia auténtica de un documento electrónico archivado por la ULL según la Ley 39/2015.  
Su autenticidad puede ser contrastada en la siguiente dirección <https://sede.ull.es/validacion/>

Identificador del documento: 3075810 Código de verificación: smutbmB+

Firmado por: JESSEL AYRA PLASENCIA  
UNIVERSIDAD DE LA LAGUNA

Fecha: 30/11/2020 12:24:14

María de las Maravillas Aguiar Aguilera  
UNIVERSIDAD DE LA LAGUNA

08/02/2021 13:50:06



Este documento incorpora firma electrónica, y es copia auténtica de un documento electrónico archivado por la ULL según la Ley 39/2015.  
*Su autenticidad puede ser contrastada en la siguiente dirección <https://sede.ull.es/validacion/>*

Identificador del documento: 3075810      Código de verificación: smutbmB+

Firmado por: JESSEL AYRA PLASENCIA  
UNIVERSIDAD DE LA LAGUNA

Fecha: 30/11/2020 12:24:14

María de las Maravillas Aguiar Aguiar  
UNIVERSIDAD DE LA LAGUNA

08/02/2021 13:50:06



## Are Anaphase Events Really Irreversible? The Endmost Stages of Cell Division and the Paradox of the DNA Double-Strand Break Repair

Félix Machín\* and Jessel Ayra-Plasencia

It has been recently demonstrated that yeast cells are able to partially regress chromosome segregation in telophase as a response to DNA double-strand breaks (DSBs), likely to find a donor sequence for homology-directed repair (HDR). This regression challenges the traditional concept that establishes anaphase events as irreversible, hence opening a new field of research in cell biology. Here, the nature of this new behavior in yeast is summarized and the underlying mechanisms are speculated about. It is also discussed whether it can be reproduced in other eukaryotes. Overall, this work brings forwards the need of understanding how cells attempt to repair DSBs when transiting the latest stages of mitosis, i.e., anaphase and telophase.

repair, HR is by far the most common form of HDR; being also the most reliable and error-free.

The selection of the repair mechanism is related to the expected rate of success. As HR needs the presence of a well-aligned and physically close sister chromatid for an error-free repair, it is preferred in the S and G<sub>2</sub> phases of the cell cycle. On the other hand, NHEJ is preferred in G<sub>1</sub> phase, when chromosomes have not been yet replicated and HR would thus use the incorrect template (e.g., the homologous chromosome, ectopic homologous sequences, etc.) The

question of how cells coordinate the choice between NHEJ and HR with the absence and presence of a sister chromatid, respectively, seems to have a simple answer at first glance: make the choice based on the cyclin dependent kinase (CDK) activity. The CDK activity is only low in G<sub>1</sub>, exactly when HR is riskiest. Accordingly, CDK upregulates HR when its activity begins to rise in the G<sub>1</sub>/S transition.<sup>17,81</sup> CDK activity is maximum in G<sub>2</sub>; correspondingly, cells rely almost entirely on HR to repair DSBs. This coordination between CDK activity and HR appears universal in eukaryotes, despite the rise in complexity of the CDK networks when going from simple to complex organisms (i.e., from yeast to humans). However, once cells enter M-phase, the relationship between CDK and HR becomes more diverse.<sup>91</sup> Likewise, the role that HR plays in DSB repair is controversial.<sup>10,111</sup>

Two poorly explored DSB scenarios are those where sister chromatids have been resolved through condensation and segregated by the spindle. We can group these scenarios in a window that goes from prophase to early telophase in most eukaryotes; that is, from condensation of chromosome arms to the reassembly of the nuclear envelope around the daughter nuclei. In yeast, this window stretches from the anaphase onset to cytokinesis completion in late telophase. The reasons for this difference are that i) yeast undergoes chromosome segregation without dismantling the nuclear envelope (close mitosis); and ii) sister chromosome arms are not resolved and condensed before anaphase onset.<sup>12,13</sup> In late mitosis, CDK is relatively high, though not as high as in the previous cell cycle stages. The questions we can ask are: Do cells still try to repair DSBs here or, alternatively, they postpone the repair to the next cell cycle? Do cells use a HR pathway despite a sister chromatid is not nearby? What is the outcome of such repair attempt? One limitation to address these questions in eukaryotes is the technical caveats to stably synchronize cells in the endmost stages of the cell

### 1. Introduction

DNA double-strand breaks (DSBs) entail a dangerous threat for the genome stability, introducing mutations that promote carcinogenesis.<sup>11-41</sup> Due to their toxicity for cancer cells, DSBs also represent the basis of the therapeutical effectiveness of radiotherapy and most antitumor chemotherapy.<sup>12,51</sup>

Cells have developed two major DNA repair mechanisms to deal with DSBs: i) Non-homologous end joining (NHEJ), comprising the error-prone mechanisms that fuse two broken DNA ends; and ii) homology-directed repair (HDR), comprising the mechanisms that use intact homologous sequences to restore the broken DNA sequence.<sup>1,31</sup> HDR can be separated in three major subpathways: single strand annealing, break-induced replication, and homologous recombination (HR).<sup>1,3,61</sup> In the context of DSB

Dr. F. Machín, J. Ayra-Plasencia  
Unidad de Investigación  
Hospital Universitario Nuestra Señora de Candelaria  
Santa Cruz de Tenerife 38010, Spain  
E-mail: fmachin@funcanis.es

Dr. F. Machín, J. Ayra-Plasencia  
Instituto de Tecnologías Biomédicas  
Universidad de La Laguna  
Santa Cruz de Tenerife 38200, Spain

Dr. F. Machín  
Universidad Fernando Pessoa Canarias  
Las Palmas de Gran Canaria 35450, Spain

The ORCID identification number(s) for the author(s) of this article can be found under <https://doi.org/10.1002/bies.202000021>

This article is commented on in the Idea to Watch paper by Matthew K. Summers, <https://doi.org/10.1002/bies.202000085>.

DOI: 10.1002/bies.202000021

Este documento incorpora firma electrónica, y es copia auténtica de un documento electrónico archivado por la ULL según la Ley 39/2015.

Su autenticidad puede ser contrastada en la siguiente dirección <https://sede.ull.es/validacion/>

Identificador del documento: 3075810

Código de verificación: smutbmB+

Firmado por: JESSEL AYRA PLASENCIA  
UNIVERSIDAD DE LA LAGUNA

Fecha: 30/11/2020 12:24:14

María de las Maravillas Aguiar Aguiar  
UNIVERSIDAD DE LA LAGUNA

08/02/2021 13:50:06

#### 4. Results and Discussion

cycle. However, this inconvenience can be overcome in the yeast *Saccharomyces cerevisiae*, in which cells can be stably arrested in late M-phase. We have recently used this model to explore the cell response to DSBs in telophase. Surprisingly, we observed a partial reversion of sister chromatid segregation, including retrograde formation of anaphase bridges and coalescence of previously segregated sister loci.<sup>[14]</sup> These findings defy the irreversible nature of chromosome segregation and open new avenues of research in cell biology, with possible implications in cancer biology as well.

In this essay, we outline our recent findings in yeast, putting them in the context of the canonical DSBs response, and speculate whether partial regression of sister chromatid segregation is feasible in other eukaryotes. Generally, we intend to highlight the importance of understanding better how cells deal with DSBs that arise in the endmost stages of the cell cycle in order to complete the picture of DNA repair mechanisms in the maintenance of genome stability.

### 2. Double Strand Break Repair in Late Mitosis: Does it Make Sense Having High CDK Favoring HR?

CDKs and their cyclins govern orderly progression through the cell cycle. In multicellular eukaryotes, the plethora of different CDKs (up to five with cell cycle functions; CDK1–4 and 6) and cyclins to partner with (also five types with cell cycle functions; A to E, each with several members) allow an exquisite control and fine-tuning of the cell cycle events.<sup>[15,16]</sup> In the unicellular yeast *S. cerevisiae*, there is only one essential CDK (CDK1/Cdc28) and only three cyclin types: G<sub>1</sub> cyclins (Cln1–3), S-specific A-type cyclins (Clb5 and Clb6), and mitotic B-type cyclins (Clb1–4). Thus, only one CDK controls all the cell cycle, including the critical G<sub>1</sub>-S and metaphase-anaphase transitions. Despite this simplification, Cyclin-CDK control of yeast cell cycle is rather complex, and a detailed description is beyond the scope of this essay. It is worth mentioning, though, that CDK activity and specificity is not only controlled by cyclins but also through post-translational modification of Cdc28 by other kinases such as Cak1 and Wee1, as well as CDK inhibitors such as the Clb-CDK inhibitor Sic1.<sup>[17–20]</sup>

In two seminal papers published in 2004, Foiani's and Kupiec's labs showed that high CDK activity was essential for establishing and maintaining HR as the preferred repair pathway against DSBs.<sup>[21,22]</sup> When Cdc28 was inhibited in S/G<sub>2</sub> through conditional mutants, HR was abolished completely and DSB repair occurred by NHEJ. However, other layers of control by CDK, both transcriptionally and post-translationally, enhance HR and inhibit NHEJ as well (for reviews see refs. [7,23]). In addition, the DNA damage checkpoint (DDC), which gets activated over the new local environment created around the broken ends (i.e., the 3'-single stranded DNA overhangs generated after DSB end resection), positively feedbacks HR (reviewed in refs. [3,24]). It is not clear whether specific cyclin partners drive CDK to promote HR. HR becomes predominant once cells enter S-phase: therefore, Cln1/2/3-Cdc28—which permit G<sub>1</sub>-S transition—and Clb5/6-Cdc28—which controls DNA replication—are likely to trigger HR initially. However, it appears that late mitotic CDK, such as the important Clb2-Cdc28 complex, can take this respon-

sibility later. Indeed, Cln2-Cdc28, Clb5-Cdc28, and Clb2-Cdc28 are all recruited to DSBs after resection, where they could activate important DDC and HR factors.<sup>[25]</sup>

The CDK activity is maintained high from the beginning of S-phase until the end of mitosis. At G<sub>2</sub> and metaphase, CDK activity is highest because all Clb-Cdc28 complexes are present. When cells fulfil the requirements to correctly segregate their sister chromatids, a burst of biochemical changes takes place that partly drops CDK activity. In particular, the anaphase-promoting complex/cyclosome (APC/C) gets activated after coupling with one of its co-activators, Cdc20. APC/C-Cdc20 degrades most Clbs but fails to drop Clb2 entirely.<sup>[26,27]</sup> Hence, full inactivation of CDK cannot be accomplished by APC/C-Cdc20 alone. This is done in telophase through the mitotic exit network (MEN), whereby the master cell cycle phosphatase Cdc14 drives both the degradation of Clb2 by APC/C-Cdh1 (Cdh1 is another APC/C co-activator, activated by Cdc14) and the transcription/stabilization of Sic1.<sup>[26,28,29]</sup> In addition, Cdc14 dephosphorylates other CDK targets that avert mitotic exit. The corollary of this multistep regulation is that, even in a normal cell cycle, there is a delay between the physical separation of the sister chromatids and the full inhibition of CDK (Figure 1A). This creates scenarios whereby HR could be attempted to repair DSBs in late mitosis, despite the absence of the sister chromatid. This is what we stress as a paradox in the current models of regulation of HR by CDK, and this was the initial purpose of our study.<sup>[14]</sup>

### 3. The Partial Regression of Sister Chromatid Segregation as a Solution for the CDK/HR Paradox?

In our recent study, we used a yeast system that stably synchronizes cells in telophase through a thermosensitive allele for the MEN kinase Cdc15 (*cdc15-2*) (Figure 1A, Box 1). The alternative approach of using mutants for Cdc14 adds other layers of complexity because Cdc14 plays critical functions in early anaphase to lengthen the mitotic spindle and resolve transient anaphase bridges.<sup>[30–32]</sup> DSBs in the context of anaphase bridges are indeed interesting, but they are one-ended in nature as stretching tension on the bridge would pull each DSB end apart (see ref. [12] for our own review on this matter). By contrast, at the restrictive condition, *cdc15-2* arrests cells in telophase with sister chromatids segregated.<sup>[33,34]</sup> Thus, a DSB in a *cdc15-2* block mimics a G<sub>1</sub> nucleus with just two important differences; namely, the presence of Clb2-CDK activity and the presence of an opposite sister nuclear mass. In this circumstance, we were shocked to observe that random DSBs originated with phleomycin (a bleomycin-zeocin-like radiomimetic compound) brought closer the two segregated masses, up to a point where retrograde anaphase bridges are formed and sister loci of distal subtelomeric regions coalesce.<sup>[14]</sup> The physical nature of such coalescence (e.g., not governed by Brownian rules), as well as its dependency on the DDC and its extended persistence in HR mutants point out that coalescence of previously segregated sister loci might allow HDR of DSBs with the intact sister. With randomly-generated DSBs, this conclusion cannot be fully demonstrated at present; however, G<sub>1</sub>:G<sub>2</sub>:Telophase comparative survival points towards this direction (Box 1).

Este documento incorpora firma electrónica, y es copia auténtica de un documento electrónico archivado por la ULL según la Ley 39/2015.  
Su autenticidad puede ser contrastada en la siguiente dirección <https://sede.ull.es/validacion/>

Identificador del documento: 3075810 Código de verificación: smutbm+

Firmado por: JESSEL AYRA PLASENCIA  
UNIVERSIDAD DE LA LAGUNA

Fecha: 30/11/2020 12:24:14

María de las Maravillas Aguiar Aguiar  
UNIVERSIDAD DE LA LAGUNA

08/02/2021 13:50:06

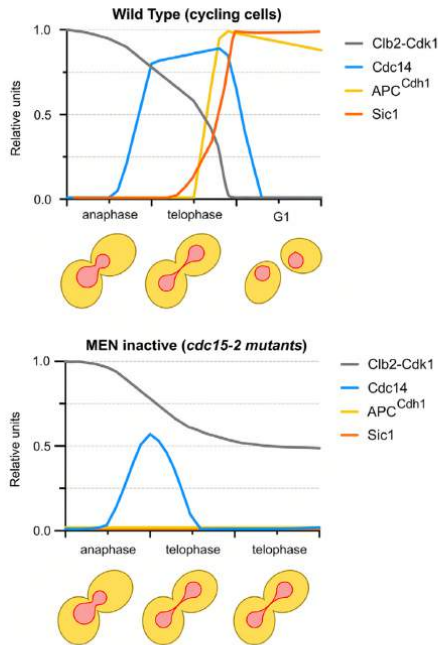


**Figure 1.** The course of CDK activity in M-phase of *S. cerevisiae*. From previous experimental and quantitative studies,<sup>[33,34]</sup> it appears that a minor reduction of CDK activity is enough for early anaphase events, whereas later events require full CDK inactivation. A. In a wild type strain, anaphase onset (0 in the x-axis) occurs once APC/C-Cdc20 (not depicted) becomes active. Among other targets, APC/C-Cdc20 starts Clb2 degradation and indirectly activates the CDK-counteracting phosphatase Cdc14 through the FEAR network. A positive feedback loop driven by the mitotic exit network (MEN) sustains and spreads Cdc14 activity, which, in parallel, activates the late APC/C-Cdh1 complex and leads to the accumulation of the Clb-CDK inhibitor Sic1. APC/C-Cdh1 boosts Clb2 degradation. The concerted actions of APC/C-Cdh1 and Sic1 switch off CDK activity. Zero levels of CDK and full Cdc14 activity reset CDK targets to a dephosphorylated state. In the case of HR-promoting factors, dephosphorylation leads to their inactivation such that NHEJ takes over for the upcoming G<sub>1</sub>, B. In MEN mutants (or when MEN is blocked by the DDC in a wild type early anaphase), Cdc14 activity cannot be maintained and extinguishes in mid-anaphase. This leaves high CDK activity after sister chromatid separation; a paradox considering that high CDK upregulates HR. The role of the CDK-counteracting phosphatase Cdc14 on HR in early anaphase remains to be determined in order to refine the paradox, although it is likely that any dephosphorylation on HR players is transient.

Even though we performed much of our study in cells artificially blocked in telophase,<sup>[14]</sup> we obtained data that support that our findings are present in cycling cells and that partial regression represents a real chance for a late mitotic cell to repair DSBs before reaching the following cell cycle. The most impor-

tant piece of data we obtained is that telophase-G<sub>1</sub> transition is blocked by the DDC, even after we reactivated Cdc15.

We noticed that regression of sister chromatid segregation is a straightforward solution for the CDK-HR paradox. Nevertheless, this solution comes at the expense of a shocking observation that challenges the notion that anaphase events are irreversible. Whether or not this partial regression is an efficient mechanism for HDR, the simple fact that DSBs in telophase bring about such regression is a remarkable and unexpected phenotype that deserves a deeper evaluation in the future.

#### 4. Mechanisms Underlying the Partial Regression

Even though the daughter nuclear masses do get closer after DSBs in telophase, it is important to make clear that the observed regression of sister chromatid segregation is far from being complete. In fact, only a minor portion of the segregated masses contact each other again (Figure 2). It appears there are other barriers to pass in order to coalesce. For instance, we observed local changes in the chromatin morphology that we interpret as decondensation. From our cytological data, decondensation appears necessary to pass through the bud neck (yeast predefined cytokinetic plane). In addition, we observed a DDC-dependent acceleration of loci movement within the telophase nucleus, acquiring an oscillatory nature between sister loci (Box 1). This acceleration may well account for increasing the chance to pass the cytokinetic plane and find the sister.

In our study,<sup>[14]</sup> we provided data on what allows segregated masses to get closer after DSBs (Box 1). The elongated anaphase B spindle is characterized by antiparallel interpolar microtubules (MTs) being slid away by the kinesin-5 Cin8 from the spindle to the spindle pole bodies (SPBs), the centrosome equivalents in yeast. This relocalization abrogates the outwards pushing forces that interpolar MTs exert over the SPBs, hence they can get closer. However, Cin8 also seems to play an active role at the SPBs because nuclear masses do not get that close if we experimentally degrade Cin8 prior to generating DSBs. This raises the possibility of other inward forces acting on the SPBs. Indeed, we observed reinforced astral MTs after DSB generation. In upcoming studies, it would be logical to look into cytoplasmic dyneins and the actin cytoskeleton on the sister nuclei approximation.

#### 5. Is the Regression a Deliberate Solution or an Accidental Consequence of a Pre-Existing Response to DSBs in G<sub>2</sub>/M?

An interesting issue raised by our finding is whether what we described is a novel mechanism evolutionarily selected for the repair of late mitotic DSBs or just the consequence of a pre-existing response to deal with DSBs in S/G<sub>2</sub>. In favor of the latter, we must admit that the DDC not only blocks metaphase-anaphase transition but also backs up any leakage into the next cell cycle by blocking MEN.<sup>[36]</sup> We must also consider that the retrograde formation of anaphase bridges may activate the NoCut/Abscission checkpoint, which would further stop cytokinesis and transition into G<sub>1</sub>.<sup>[37,38]</sup> This checkpoint is present to prevent severing of

Este documento incorpora firma electrónica, y es copia auténtica de un documento electrónico archivado por la ULL según la Ley 39/2015.  
 Su autenticidad puede ser contrastada en la siguiente dirección <https://sede.ull.es/validacion/>

Identificador del documento: 3075810 Código de verificación: smutbmB+

Firmado por: JESSEL AYRA PLASENCIA  
 UNIVERSIDAD DE LA LAGUNA

Fecha: 30/11/2020 12:24:14

María de las Maravillas Aguiar Aguiar  
 UNIVERSIDAD DE LA LAGUNA

08/02/2021 13:50:06

#### 4. Results and Discussion

##### Box 1 Outline of the Key Experiments

How did we generate DSBs in telophase cells? We first blocked the cells at telophase with the *cdc15-2* thermosensitive allele. Then, we either added the radiomimetic drug phleomycin or induced the endonuclease I-SceI. Phleomycin generates multiple DSBs at random locations, thus an intact homologous sequence is expected in the segregated sister chromatid. I-SceI endonuclease gives rise to two DSBs at a unique chromosomal I-SceI site; one DSB per sister chromatid.

How did we detect sister nuclei approximation, sister loci coalescence and retrograde formation of anaphase bridges? All using fluorescence microscopy and videomicroscopy. For the bulk of the DNA masses we labelled the histone H2A with mCherry. For chromosomal loci we employed locus-specific insertions of bacterial *tetO* arrays detected as fluorescent dots through its binding with tetR-YFP. For the spindle pole bodies (yeast centrioles) we used Spc42-mCherry. For the ribosomal DNA array, we used Net1-eCFP. For the microtubules we followed GFP-Tub1.

What do we mean by acceleration of sister loci movement? While performing short-term videomicroscopy of sister loci we noticed a faster and broader oscillatory movement between segregated loci after DSBs. An increased movement of chro-

mosomes within a G<sub>2</sub> nucleus has been reported before. It is likely our observation relates to the latter; however, we must point out that we did not measure if a larger nuclear area is visited by each locus in telophase.

Why did we conclude that HR plays a role in repairing DSBs after chromosome segregation? A critical experiment was comparative clonogenic survival between cells blocked at different cell cycle stages. Only 10% of the G<sub>1</sub>-blocked cells survived after 1 h treatment with 10 µg mL<sup>-1</sup> phleomycin. G<sub>2</sub>-blocked cells increased survival to 75%. Telophase-blocked cells raised 55% survivability, 5-fold over G<sub>1</sub>-blocked cells and only slightly lower than G<sub>2</sub>-blocked cells. Importantly, when HR was impaired (*rad52* mutant), clonogenic survival dropped in G<sub>2</sub>- and telophase-blocked cells, but not in G<sub>1</sub>.

How did we find out that changes in the spindle dynamics drive sister nuclei approximation? We observed a dramatic change in the spindle morphology after DSBs. We hypothesized that the kinesin-5 Cin8, a major player in spindle elongation in anaphase, may be regulated by DSBs. We then observed DSB-dependent dephosphorylation and relocation of Cin8 out of the spindle. We finally confirmed this Cin8 role by using engineered alleles that either control Cin8 levels or change its phosphorylation status.

canonical anaphase bridges, whose origin can be traced back to chromosomal stresses that occurred before anaphase onset, including DNA damage.<sup>[39]</sup> In addition, loci acceleration within the nucleus is also observed in G<sub>2</sub>.<sup>[40,41]</sup> Blocking spindle elongation also appears logical to prevent cells from segregating the sister chromatids before they repair any S/G<sub>2</sub> DSB. Local decondensation around a DSB also appears as a logical step to accomplish HR in G<sub>2</sub>.

On the contrary, in favor of a genuine mechanism to deal with DSBs in late mitosis, we argue that the previous connection between the DCC and MEN should be reinterpreted in the new context of DSBs in anaphase and telophase. Thus, the purpose of the DCC would be that G<sub>2</sub> DSBs block anaphase onset and M-phase DSBs block mitotic exit. If MEN inactivation has been observed after G<sub>2</sub> DSBs is because MEN targets for the DCC are available for most of the cell cycle. Likewise, it seems counterintuitive to accelerate chromosome movement to find a partner to recombine with in G<sub>2</sub>, when sister chromatids are aligned and firmly held together by cohesin; the ring-shaped complex that embraces the two sisters.<sup>[42]</sup> Acceleration would be more needed when homologous sequences in the sisters are not close to each other and they have to be brought together again; that is, when cohesion has been removed.

Our work was undertaken in haploid cells. However, it would be interesting to investigate the DSB response in diploids. Because diploids are expected to be highly homozygous in wild type heterothallic yeast strains, it ought to be error-free to recombine with the homolog chromosome in late mitosis. Therefore,

the telophase-G<sub>1</sub> block, loci acceleration and the perseverance of HDR in anaphase/telophase could be just predesigned for this diploid wild-type context. In haploids, when the homolog cannot be found, telophase cells might engage in lengthy “searching” of their chromosomes until they find the right homolog sequence in the opposite nucleus—which, incidentally, would have become closer because of the DSB-mediated Cin8 relocation described before.

#### 6. Could Other Eukaryotes Bring Back Together Segregated Sister Chromatids?

A quick look at the mechanisms that favor sister loci approximation and coalescence in yeast shows that they are conserved in most eukaryotes. For instance, kinesin-5 also plays a central role in the anaphase spindle.<sup>[35]</sup> Likewise, DSBs decondense chromosomes in prophase as well as generally increasing chromatin motion.<sup>[9,43]</sup> In addition, there exists a window of opportunity since there is a delay between chromosome segregation and full CDK inactivation.<sup>[44]</sup>

There are, however, key differences in M-phase between the budding yeast and other eukaryotic cell types, including human cells. In particular, resolution of sister chromatids starts before anaphase in humans, when cohesin is removed from chromosome arms in prophase and these become highly condensed.<sup>[45,46]</sup> Even earlier, in G<sub>2</sub>, when chromosomes are still decondensed and DSB repair is highly efficient, numerous sister

Este documento incorpora firma electrónica, y es copia auténtica de un documento electrónico archivado por la ULL según la Ley 39/2015.

Su autenticidad puede ser contrastada en la siguiente dirección <https://sede.ull.es/validacion/>

Identificador del documento: 3075810

Código de verificación: smutbmB+

Firmado por: JESSEL AYRA PLASENCIA  
UNIVERSIDAD DE LA LAGUNA

Fecha: 30/11/2020 12:24:14

María de las Maravillas Aguiar Aguiar  
UNIVERSIDAD DE LA LAGUNA

08/02/2021 13:50:06

*Saccharomyces cerevisiae*

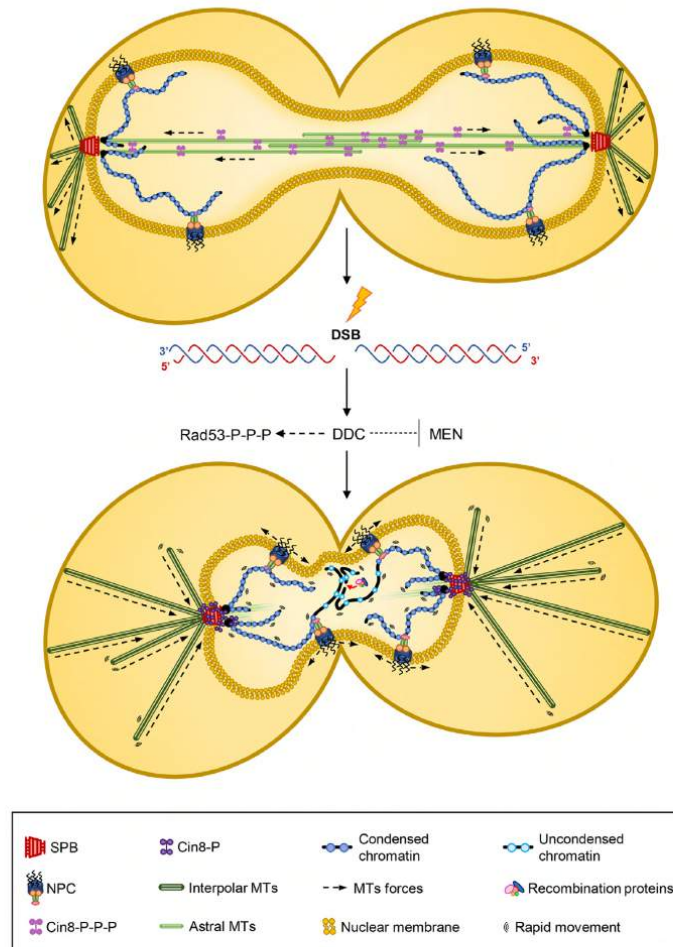


**Figure 2.** Summary of the events underlying partial regression of sister chromatid segregation in the budding yeast *S. cerevisiae*. The weakening of the elongated inter-polar MTs by Cin8 relocalization, the acceleration of sister loci movement, and the local decondensation were reported in our original work (see also ref. [55] for further comments).<sup>[14]</sup> Reinforced astral MTs that may exert inwards forces over the SPBs are likely as well. Because *S. cerevisiae* undertakes a close mitosis, it is also likely that the physics of the nuclear envelope after weakening the spindle contribute to the approximation of the sister chromatids. Likewise, the fact that part of the chromatin is attached to the nuclear envelope (e.g., telomeres and ribosomal DNA) may facilitate the search for homologous sequences. Rad53-P-P-P, hyperphosphorylated and active Rad53 (central effector kinase of the DDC); NPC, nuclear pore complex; Cin8-P; low phosphorylated Cin8; Cin8-P-P-P, hyperphosphorylated Cin8. Refer to the main text for other abbreviations.

Este documento incorpora firma electrónica, y es copia auténtica de un documento electrónico archivado por la ULL según la Ley 39/2015.  
 Su autenticidad puede ser contrastada en la siguiente dirección <https://sede.ull.es/validacion/>

Identificador del documento: 3075810 Código de verificación: smutbmB+

Firmado por: JESSEL AYRA PLASENCIA  
 UNIVERSIDAD DE LA LAGUNA

Fecha: 30/11/2020 12:24:14

María de las Maravillas Aguiar Aguiar  
 UNIVERSIDAD DE LA LAGUNA

08/02/2021 13:50:06

4. Results and Discussion

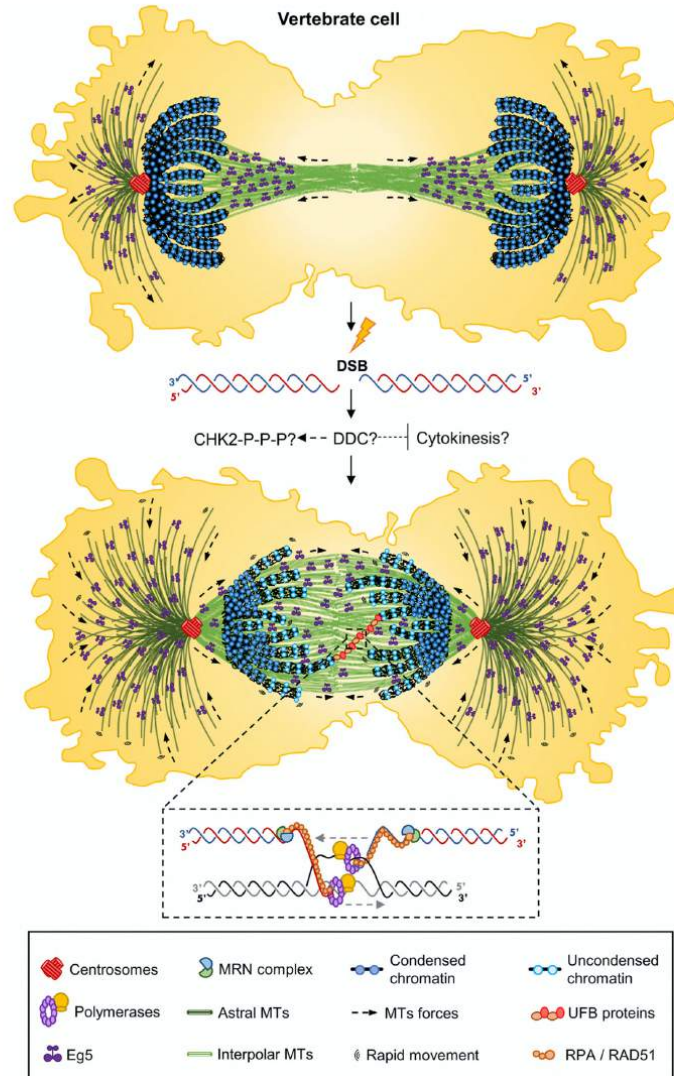


**Figure 3.** Putative scenarios of partial regression of sister chromatid segregation in other eukaryotes (vertebrate cells). Unlike budding yeast cells, vertebrate cells undertake an open mitosis; hence, weakening the spindle may not be enough to bring the segregated sister chromatids closer. We speculate that the contribution of reinforced astral microtubules ought to be more important in these cells. Note that the Cin8 homologue Eg5 can reach astral MTs here. A representation of the DSB repair through HR with the sister is also depicted (within an UFB in the example); MRN, MRE11-RAD50-NBS1; RPA/RAD51, replication protein A and/or recombinase RAD51; CHK2-P-P-P, hyperphosphorylated and active CHK2 (Rad53-like effector kinase of the vertebrate DDC).

Este documento incorpora firma electrónica, y es copia auténtica de un documento electrónico archivado por la ULL según la Ley 39/2015.  
 Su autenticidad puede ser contrastada en la siguiente dirección <https://sede.ull.es/validacion/>

Identificador del documento: 3075810 Código de verificación: smutbmB+

Firmado por: JESSEL AYRA PLASENCIA  
 UNIVERSIDAD DE LA LAGUNA

Fecha: 30/11/2020 12:24:14

María de las Maravillas Aguiar Aguiar  
 UNIVERSIDAD DE LA LAGUNA

08/02/2021 13:50:06

loci appear physically separated.<sup>[47,48]</sup> Condensation itself is another major difference between yeast and other eukaryotes. In fact, the high degree of compaction observed in the latter might hamper DSB repair. Eukaryotes are however rather diverse, not only different cell architectures among species but also different cell types within the same species, for instance, between differentiated and stem cells. Another layer of complexity includes disposition of nucleosomes in the chromatin, especially between euchromatin and heterochromatin, which may respond in different ways to mitotic DSBs. Thus, a more accurate question to ask is whether there exist eukaryotic cell types in which sister chromatids can be brought together again after mitotic DSBs.

For a cell in prophase-metaphase, with sister chromatids resolved at the arms but not the centromeres, to bring back the sister arms together does not seem an extraordinary achievement in principle. Even a less complicated situation can be envisioned for sister loci that are resolved in G<sub>2</sub>,<sup>[47,48]</sup> as cohesin is still loaded on the arms and may serve to nucleate loci coalescence. On the contrary, for cells already in anaphase and telophase, the regression would mean a scenario as impressive as, or even more than, the one we observed in yeast. After all, yeast cells perform a closed mitosis, in which the sister nuclear masses are separated without dismantling the nuclear envelope.<sup>[13]</sup> It is likely that after abrogating the interpolar forces that push the SPBs apart, the elasticity of the nuclear envelope facilitates that the SPBs come closer again as the nucleus tends to readopt a rounded shape (Figure 2). This feature is absent in complex eukaryotes that carry out an open mitosis (Figure 3). In this case, active centripetal forces on the centrosomes are needed if they are to come close enough to allow sister loci coalescence in late mitosis, before the reassembling of the nuclear envelope and before kinetochores and centrosomes get detached. These forces could be exerted by either inverting the sliding of interpolar MTs or directing the astral MTs to push inwards, perhaps with the aid of the actin cytoskeleton and dyneins.<sup>[49]</sup> Of note, we observed reinforced astral MTs in yeast alongside a weakened mitotic spindle.<sup>[14]</sup>

Regression of sister chromatid segregation in human cells ought to be relatively simple to observe. It is thus surprising it has not been reported as far as we know. Perhaps, as pointed out for yeast, human diploid cells may already find a template within each telophase nucleus. Another interesting scenario is that the approximation of the segregated DNA masses might not be a prerequisite for partial regression. Hence, this approximation could be occurring without being noticed by standard cell biology techniques; for instance, through the retrograde formation of ultrafine anaphase bridges (UFB). This kind of connections between segregated sister chromatids can only be visualized through specific DNA-binding proteins.<sup>[50]</sup>

In addition to the physical challenges of executing regression, there are several hints that point out that what we observed in the budding yeast is unlikely in multicellular eukaryotes. First, the aforementioned barrier that condensation imposes over DSB repair. Second, most studies pinpoint a general downregulation of DSB repair in M-phase.<sup>[10,11,51]</sup> Therefore, mitotic DSB could be left unrepaired until the next G<sub>1</sub>. Thirdly, NHEJ is more commonly used in these cell types. In fact, HR preference is often restricted to cells in S-phase;<sup>[52]</sup> thereby, there is no need to seek a sister chromatid in M-phase. Finally, and related to the latter,

the CDK paradox might not be present in these cells because HR is actually downregulated by CDKs in M-phase.<sup>[3,9]</sup>

## 7. Conclusions and Perspectives

The observation that sister chromatid segregation can be partly reversed in the yeast telophase after DNA damage challenges firmly established principles in cell biology. Whether this phenomenon is a mechanism conceived for DNA repair through HR after the sister chromatids are not held together by proteinaceous and/or topological linkages has yet to be determined. Another key question is whether the regression behavior can be observed in eukaryotes other than *S. cerevisiae*, more specifically eukaryotic cells that undertake an open mitosis. Other avenues of future research should deal with refining the mechanisms responsible for both the partial regression and the maintenance of the telophase block. Altogether, our findings point towards a more dynamic and fluid vision of chromosome segregation in anaphase.

## Acknowledgements

The authors apologize to authors whose relevant contributions were not cited due to space restrictions. This work was supported by Spanish Ministry of Science and Innovation through the research grant BFU2017-83954-R (to F.M.), co-financed with the European Commission's ERDF structural funds.

## Conflict of Interest

The authors declare no conflict of interest.

## Keywords

anaphase, chromosome segregation, DNA double-strand breaks, homologous recombination, telophase

Received: February 6, 2020  
Revised: March 16, 2020  
Published online: May 4, 2020

- [1] E. Mladenov, S. Magin, A. Soni, G. Iliakis, *Semin. Cancer Biol.* **2016**, 37–38, 51.
- [2] L. Krenning, J. van den Berg, R. H. Medema, *Mol. Cell* **2019**, 76, 346.
- [3] J. Her, S. F. Bunting, *J. Biol. Chem.* **2018**, 293, 10502.
- [4] T. Aparicio, R. Baer, J. Gautier, *DNA Repair* **2014**, 19, 169.
- [5] E. Berthel, M. L. Ferlazzo, C. Devic, M. Bourguignon, N. Foray, *Int. J. Mol. Sci.* **2019**, 20, 5339.
- [6] J. E. Haber, *BioEssays* **2018**, 40, 1700229.
- [7] X. Zhao, C. Wei, J. Li, P. Xing, J. Li, S. Zheng, X. Chen, *Acta Biochim. Biophys. Sin.* **2017**, 49, 655.
- [8] N. Hustedt, D. Durocher, *Nat. Cell Biol.* **2017**, 19, 1.
- [9] R. Thompson, R. Gatenby, S. Sidi, *Cells* **2019**, 8, 1049.
- [10] S. Giunta, R. Belotserkovskaya, S. P. Jackson, *J. Cell Biol.* **2010**, 190, 197.
- [11] A. Orthwein, A. Fradet-Turcotte, S. M. Noordermeer, M. D. Canny, C. M. Brun, J. Strecker, C. Escribano-Diaz, D. Durocher, *Science* **2014**, 344, 189.

Este documento incorpora firma electrónica, y es copia auténtica de un documento electrónico archivado por la ULL según la Ley 39/2015.

Su autenticidad puede ser contrastada en la siguiente dirección <https://sede.ull.es/validacion/>

Identificador del documento: 3075810

Código de verificación: smutbmB+

Firmado por: JESSEL AYRA PLASENCIA  
UNIVERSIDAD DE LA LAGUNA

Fecha: 30/11/2020 12:24:14

María de las Maravillas Aguiar Aguiar  
UNIVERSIDAD DE LA LAGUNA

08/02/2021 13:50:06

4. Results and Discussion

**ADVANCED  
SCIENCE NEWS**

www.advancedsciencenews.com

**BioEssays**

www.bioessays-journal.com

- [12] F. Machín, O. Quevedo, C. Ramos-Pérez, J. García-Luis, *Curr. Genet.* **2016**, *62*, 7.
- [13] B. Boettcher, Y. Barral, *Nucleus* **2013**, *4*, 160.
- [14] J. Ayra-Plasencia, F. Machín, *Nat. Commun.* **2019**, *10*, 2862.
- [15] J. Bloom, F. R. Cross, *Nat. Rev. Mol. Cell Biol.* **2007**, *8*, 149.
- [16] M. Malumbres, *Genome Biol.* **2014**, *15*, 122.
- [17] R. N. Booher, R. J. Deshaies, M. W. Kirschner, *EMBO J.* **1993**, *12*, 3417.
- [18] P. Kaldis, A. Sutton, M. J. Solomon, *Cell* **1996**, *86*, 553.
- [19] M. D. Mendenhall, *Science* **1993**, *259*, 216.
- [20] E. Schwob, T. Böhm, M. D. Mendenhall, K. Nasmyth, *Cell* **1994**, *79*, 233.
- [21] G. Ira, A. Pellicoli, A. Balija, X. Wang, S. Fiorani, W. Carotenuto, G. Liberi, D. Bressan, L. Wan, N. M. Hollingsworth, J. E. Haber, M. Foiani, *Nature* **2004**, *431*, 1011.
- [22] Y. Aylon, B. Liefshitz, M. Kupiec, *EMBO J.* **2004**, *23*, 4868.
- [23] L. S. Symington, R. Rothstein, M. Lisby, *Genetics* **2014**, *198*, 795.
- [24] J. C. Harrison, J. E. Haber, *Annu. Rev. Genet.* **2006**, *40*, 209.
- [25] X. Chen, H. Niu, Y. Yu, J. Wang, S. Zhu, J. Zhou, A. Papusha, D. Cui, X. Pan, Y. Kwon, P. Sung, G. Ira, *Nucleic Acids Res.* **2016**, *44*, 2742.
- [26] F. M. Yeong, H. H. Lim, C. G. Padmashree, U. Surana, *Mol. Cell* **2000**, *5*, 501.
- [27] M. Shirayama, A. Tóth, M. Gálóvá, K. Nasmyth, *Nature* **1999**, *402*, 203.
- [28] R. Visintin, K. Craig, E. S. Hwang, S. Prinz, M. Tyers, A. Amon, *Mol. Cell* **1998**, *2*, 709.
- [29] S. L. Jaspersen, J. F. Charles, D. O. Morgan, *Curr. Biol.* **1999**, *9*, 227.
- [30] M. Rocuzzo, C. Visintin, F. Tili, R. Visintin, *Nat. Cell Biol.* **2015**, *17*, 251.
- [31] F. Machín, J. Torres-Rosell, A. Jarmuz, L. Aragón, *J. Cell Biol.* **2005**, *168*, 209.
- [32] D. D'Amours, F. Stegmeier, A. Amon, *Cell* **2004**, *117*, 455.
- [33] O. Quevedo, J. García-Luis, E. Matos-Perdomo, L. Aragón, F. Machín, *PLoS Genet.* **2012**, *8*, e1002509.
- [34] J. García-Luis, F. Machín, *Nat. Commun.* **2014**, *5*, 5652.
- [35] S. K. Singh, H. Pandey, J. Al-Bassam, L. Gheber, *Cell. Mol. Life Sci.* **2018**, *75*, 1757.
- [36] F. Hu, Y. Wang, D. Liu, Y. Li, J. Qin, S. J. Elledge, *Cell* **2001**, *107*, 655.
- [37] V. Nähse, L. Christ, H. Stenmark, C. Campsteijn, *Trends Cell Biol.* **2017**, *27*, 1.
- [38] T. Karg, B. Warecki, W. Sullivan, *Mol. Biol. Cell* **2015**, *26*, 2227.
- [39] N. Amaral, A. Vendrell, C. Funaya, F.-Z. Idrissi, M. Maier, A. Kumar, G. Neurohr, N. Colomina, J. Torres-Rosell, M.-I. Geli, M. Mendoza, *Nat. Cell Biol.* **2016**, *18*, 516.
- [40] J. Miné-Hattab, R. Rothstein, *Nat. Cell Biol.* **2012**, *14*, 510.
- [41] V. Dion, V. Kalck, C. Horigome, B. D. Towbin, S. M. Gasser, *Nat. Cell Biol.* **2012**, *14*, 502.
- [42] C. H. Haering, A.-M. Farcas, P. Arumugam, J. Metson, K. Nasmyth, *Nature* **2008**, *454*, 297.
- [43] R. Oshidari, K. Mekhail, A. Seeber, *Trends Cell Biol.* **2019**, *30*, 144.
- [44] M. J. Cundell, R. N. Bastos, T. Zhang, J. Holder, U. Gruneberg, B. Novak, F. A. Barr, *Mol. Cell* **2013**, *52*, 393.
- [45] C. Morales, A. Losada, *Curr. Opin. Cell Biol.* **2018**, *52*, 51.
- [46] P. Batty, D. W. Gerlich, *Trends Cell Biol.* **2019**, *29*, 717.
- [47] J. K. Eykelenboom, M. Gierlinski, Z. Yue, N. Hegarat, H. Pollard, T. Fukagawa, H. Hochegger, T. U. Tanaka, *J. Cell Biol.* **2019**, *218*, 1531.
- [48] R. Stanyte, J. Nuebler, C. Blaukopf, R. Hoeffler, R. Stocsits, J. M. Peters, D. W. Gerlich, *J. Cell Biol.* **2018**, *217*, 1985.
- [49] F. Pietro, A. Echard, X. Morin, *EMBO Rep.* **2016**, *17*, 1106.
- [50] A. H. Bizard, I. D. Hickson, *Curr. Opin. Cell Biol.* **2018**, *52*, 112.
- [51] M. A. T. M. Van Vugt, A. K. Gardino, R. Linding, G. J. Ostheimer, H. C. Reinhardt, S. E. Ong, C. S. Tan, H. Miao, S. M. Keezer, J. Li, T. Pawson, T. A. Lewis, S. A. Carr, S. J. Smerdon, T. R. Brummelkamp, M. B. Yaffe, M. Lichten, *PLoS Biol.* **2010**, *8*, e1000287.
- [52] K. Karanam, R. Kafri, A. Loewer, G. Lahav, *Mol. Cell* **2012**, *47*, 320.
- [53] E. Queralt, C. Lehane, B. Novak, F. Uhlmann, *Cell* **2006**, *125*, 719.
- [54] I. W. Campbell, X. Zhou, A. Amon, *eLife* **2019**, *8*, e41139.
- [55] J. Ayra-Plasencia, F. Machín, *Mol. Cell. Oncol.* **2019**, *6*, e1648027.

Este documento incorpora firma electrónica, y es copia auténtica de un documento electrónico archivado por la ULL según la Ley 39/2015.  
Su autenticidad puede ser contrastada en la siguiente dirección <https://sede.ull.es/validacion/>

Identificador del documento: 3075810 Código de verificación: smutbmB+

Firmado por: JESSEL AYRA PLASENCIA  
UNIVERSIDAD DE LA LAGUNA

Fecha: 30/11/2020 12:24:14

María de las Maravillas Aguiar Aguiar  
UNIVERSIDAD DE LA LAGUNA

08/02/2021 13:50:06



## 4.4. Chapter 4

### Experimental insights in higher eukaryotes response to DSBs in telophase

The fourth chapter is dedicated to studying the first early signs of eukaryotic reaction to DSBs in telophase. HeLa cells were synchronized in anaphase/telophase in a stepwise manner. Phleomycin ( $100 \mu\text{g}\cdot\text{mL}^{-1}$ ) was employed as the DSBs source.

HeLa cells responded by delaying the late telophase-to- $G_1$  transition when DSBs occurred. Fluorescence microscopy of MTs served to detect cells transiting a longer anaphase B. Besides, immunofluorescence of DNA damaging reporter proteins such as  $\gamma\text{H2A.X}$ , 53BP1, RIF1, and RPA2 showed that human cells appear to trigger different repair pathways. These results reveal the mammal ability to cope with DNA damage in this paradoxical scenario and the similarities and differences with yeast.

Este documento incorpora firma electrónica, y es copia auténtica de un documento electrónico archivado por la ULL según la Ley 39/2015.  
Su autenticidad puede ser contrastada en la siguiente dirección <https://sede.ull.es/validacion/>

Identificador del documento: 3075810 Código de verificación: smutbmB+

Firmado por: JESSEL AYRA PLASENCIA  
UNIVERSIDAD DE LA LAGUNA

Fecha: 30/11/2020 12:24:14

María de las Maravillas Aguiar Aguiar  
UNIVERSIDAD DE LA LAGUNA

08/02/2021 13:50:06



Este documento incorpora firma electrónica, y es copia auténtica de un documento electrónico archivado por la ULL según la Ley 39/2015.  
*Su autenticidad puede ser contrastada en la siguiente dirección <https://sede.ull.es/validacion/>*

Identificador del documento: 3075810      Código de verificación: smutbmB+

Firmado por: JESSEL AYRA PLASENCIA  
UNIVERSIDAD DE LA LAGUNA

Fecha: 30/11/2020 12:24:14

María de las Maravillas Aguiar Aguiar  
UNIVERSIDAD DE LA LAGUNA

08/02/2021 13:50:06

#### 4.4.1. HeLa cells delay the anaphase/telophase transition when DSBs occur

There exist numerous similarities and differences between yeast and mammals. The DNA damage response in telophase could be conserved, but whether it occurs equally may depend on shared key factors as well as remarkable cytological differences between yeast and mammals

Yeast can live as haploids, whereas mammalian cells are diploids (except gametes). This difference could be crucial for the reversion of segregation. As haploids do not have a close and well-aligned sister chromatid, they appear to be forced to find an intact donor in the opposite nucleus. In contrast, diploid organisms may prefer recombining with the homolog chromosome (despite causing LOH) than reverting segregation.

Another difference relies on the presence of the nuclear envelope at the moment of mitosis. Whereas yeast divides and segregates by enlarging the nuclear membrane (NM), mammals break it down temporally to synthesize a new one after telophase (Sazer et al., 2014). Closed mitoses keep nuclear membrane protein complexes bound to heterochromatin domains. They may act in hand with the MTs apparatus as an extra force to induce the reversion of segregation. However, mammalian cells suffer a temporal dissipation of protein embedded in the nuclear envelope, and thus, the transient degradation of those NM multiprotein complexes.

Another factor to take into consideration is the duration of the cell cycle stages in both cell types. Yeast exhibits an average length of metaphase plus anaphase of ~ 48 minutes (both in synchronous and asynchronous cultures) (Leitao & Kellogg, 2017), and this represents ~ 50 % of the cell cycle. On the other hand, whereas the mammalian cell cycle (HeLa cell line specifically) lasts ~ 20 hours, the entire mitosis covers only ~ 1 hour, representing ~ 5 % (Puck & Steffen, 1963). The fact that the mammalian mitosis lasts ten-fold less than yeast might suppose a reason for not reverting segregation. Yeast could have time enough to repair through HR. In contrast, mammals usually prefer triggering NHEJ and not compromise the entire cell cycle in 1 hour, besides considering the absence of protein complexes of the nuclear membrane that could enable DNA repair by promoting coalescence events.

Amongst the similarities that could accomplish the reversion, both organisms show a fully functional and extended MTs apparatus and active kinesin motor proteins. As MTs changed their morphology and dynamics and Cin8 protein was partially dephosphorylated for DNA repair in yeast telophase, mammalian cells could also use their elongated MTs and kinesins (such as Eg5/KIF11) to produce the same behavior, i.e., they could also change the segregation directionality to repair.

Este documento incorpora firma electrónica, y es copia auténtica de un documento electrónico archivado por la ULL según la Ley 39/2015.  
Su autenticidad puede ser contrastada en la siguiente dirección <https://sede.ull.es/validacion/>

Identificador del documento: 3075810 Código de verificación: smutbmB+

Firmado por: JESSEL AYRA PLASENCIA  
UNIVERSIDAD DE LA LAGUNA

Fecha: 30/11/2020 12:24:14

María de las Maravillas Aguiar Aguiar  
UNIVERSIDAD DE LA LAGUNA

08/02/2021 13:50:06

4. Results and Discussion

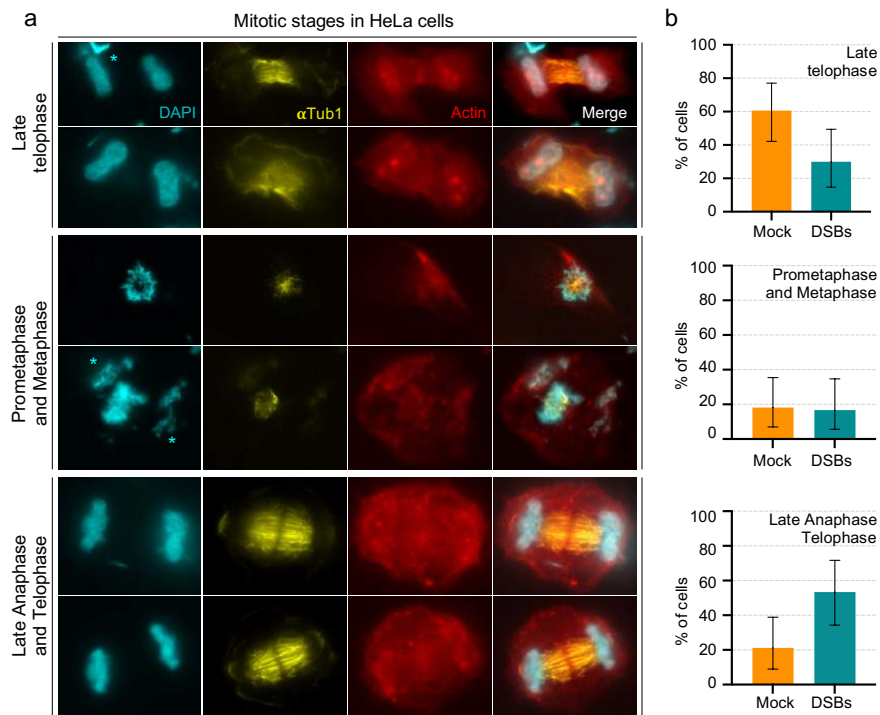


**Figure 4.10. Proportion of mitotic stages after 1 hour of DSBs in anaphase/telophase.** Healthy HeLa cells were grown over poly-L-Lysine coated coverslips and blocked twice in the G<sub>1</sub> phase with double sequential incubations in the presence of 2 mM thymidine for 16 hours. Then, they were released for 9 hours to allow DNA replication. After that, the growth medium was replaced by DMEM containing 20 ng·mL<sup>-1</sup> Nocodazole and incubation was prolonged for 5 hours. Once the cells were in prometaphase, they were released for 20 minutes to let the MTs polymerizate. After this time, 50 μM blebbistatin and 100 μg·mL<sup>-1</sup> phleomycin were added (only blebbistatin for the mock control), extending the incubation for 40 - 45 minutes extra to reach late telophase. Samples were pre-extracted, fixed, and permeabilized before using the corresponding antibodies to perform immunofluorescence. **a)** Microscopy pictures showing examples of different mitotic stages (late telophase, pro- and metaphase, and late anaphase/telophase). Nuclear DNA was stained with DAPI, the actin cytoskeleton with TRITC-phalloidin, and the MTs apparatus was detected through α-Tub1alpha antibody immunostaining. **b)** Quantification of mitotic stages for mock and DSBs treatments in a representative experiment (error bars depict ± CI 95 %, n = 45 cells per treatment). Asterisks point to insoluble blebbistatin crystals that also fluoresce under UV light exposure.

As MTs morphology showed the most prominent phenotypic change in yeast, HeLa cells were subjected to MTs immunofluorescence to study whether they presented a similar behavior. For visualization, HeLa cells were first grown over coverslips previously coated with poly-L-Lysine to improve cell adhesion. They were then adequately synchronized in anaphase/telophase (see section Materials and Methods), and 100 mg·mL<sup>-1</sup> phleomycin was

#### 4. Results and Discussion

used to create DSBs. Once the incubation period finished, cytoplasmic particles and small organelles were pre-extracted for 10 minutes. For that, the cells were fixed in 4 % paraformaldehyde and permeabilized. Finally, coverslips were blocked and hybridized with the required antibodies to perform immunofluorescence.

Microscope visualization allowed to differentiate three different mitotic stages: i) late telophase (two separated DAPI nuclei within an elongated cytoplasmic space and extended non-uniform MTs); ii) prometaphase and metaphase (very condensed chromosomes in the middle of a rounded-cytoplasm with almost-inexistent MTs) and; iii) late anaphase/early telophase (two separated DNA masses inside a rounded-cytoplasm and joint by very uniform, gross and extended MTs) (Fig. 4.10a). Whereas the “late telophase” category was the most abundant in the mock control, phleomycin-treated cells tended to accumulate earlier cell cycle stages before entering a new cell cycle (Fig. 4.10b). The fact that ~ 50 % of phleomycin-treated cells were found as late anaphase/early telophase versus ~ 20 % in the mock control suggests that mammals could trigger a late mitotic checkpoint. This is the most likely scenario. Alternatively, the reversion of segregation could be taking place. Further works based on live-cell movies of fluorescent-tagged MTs and chromatin are required to compare the phenotypes seen in yeasts.

Nonetheless, telophase-stuck cells did not present any modification in MTs morphology. It does not necessarily reflect that human cells avoid the reversion of segregation. Indeed, keeping it extended and uniform could serve as a scaffold to regress only the broken chromosomes through kinesins activation. Besides, immunofluorescence has some experimental caveats. Images have been taken in fixed cells after 40 minutes of DSBs generation. Continuous exposure to DSBs could be the reason to observe a static MTs disposition. Further experiments might be required to visualize the outcome after washing away the phleomycin, letting the cells time enough to react and repair.

#### 4.4.2. HeLa cells react to DSBs in telophase by triggering different DNA repair pathways

Immunofluorescence of essential DNA repair factors was also performed. Having seen that damaged cells accumulate in late anaphase/early telophase, whether HeLa detect DSBs, process DNA 3' ssDNA ends, and activate DNA repair pathways, was next addressed.

Among numerous activated factors after DSBs, phosphorylation of H2AX ( $\gamma$ H2A.X) variant plays a key role at sites containing damaged chromatin. Once phosphorylated, it promotes the assembly and recruitment of protein factors required for DNA repair, such as 53BP1, RIF1,

147

Este documento incorpora firma electrónica, y es copia auténtica de un documento electrónico archivado por la ULL según la Ley 39/2015.  
Su autenticidad puede ser contrastada en la siguiente dirección <https://sede.ull.es/validacion/>

Identificador del documento: 3075810 Código de verificación: smutbmB+

Firmado por: JESSEL AYRA PLASENCIA  
UNIVERSIDAD DE LA LAGUNA

Fecha: 30/11/2020 12:24:14

María de las Maravillas Aguiar Aguiar  
UNIVERSIDAD DE LA LAGUNA

08/02/2021 13:50:06

4. Results and Discussion

RPA2 (Podhorecka et al., 2010). Thus, double immunostaining was carried out to determine if cells not only detected DSBs through  $\gamma$ H2A.X but also triggered either HR or NHEJ.

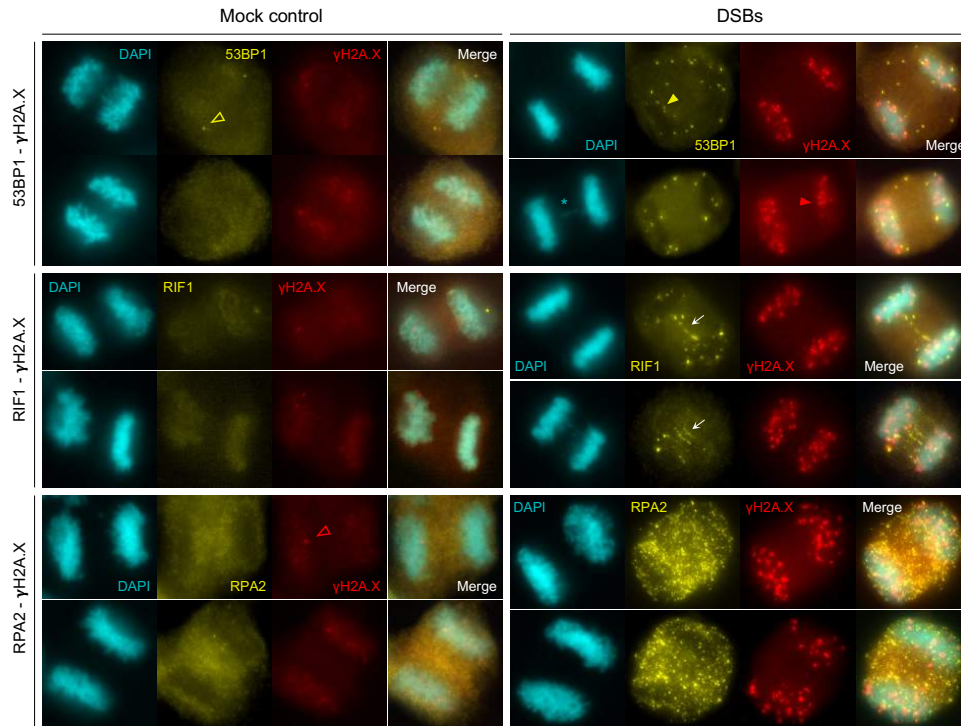


**Figure 4.11. Immunofluorescence of DNA damage factors to repair DSBs in telophase.** Fixed telophase cells were treated as in Fig. 4.10a and immunostained with  $\alpha$ - $\gamma$ H2A.X,  $\alpha$ -53BP1,  $\alpha$ -RIF1, and  $\alpha$ -RPA2 antibodies to determine the DNA damage response to DSBs. DNA was stained with DAPI. Yellow and red hollow arrowheads signal 53BP1 and  $\gamma$ H2A.X spontaneous foci, whereas yellow- and red-filled arrowheads show protein aggregates formed after DSBs. The blue asterisk depicts a DNA bridge joining two DNA masses. White arrows signal RIF1 proteins forming bridges likely coating ultrafine anaphase bridges.

53BP1 is a key regulator of DSB repair pathway choice. It promotes NHEJ by antagonizing DNA end-resection, which is essential for HR-mediated DSB repair (Bártová et al., 2019; Ferrari et al., 2020; Panier & Boulton, 2014). Surprisingly, recent studies have demonstrated that BP531 also has several implications in promoting GC in the late S phase and G<sub>2</sub> (Malewicz, 2016; Ochs et al., 2016, p. 1). For these reasons, it was analyzed as a regulator of DNA repair after H2A.X phosphorylation.

Although the yeast Rif1 protein is associated with telomeres length maintenance, human

Este documento incorpora firma electrónica, y es copia auténtica de un documento electrónico archivado por la ULL según la Ley 39/2015.  
 Su autenticidad puede ser contrastada en la siguiente dirección <https://sede.ull.es/validacion/>

Identificador del documento: 3075810 Código de verificación: smutbmB+

Firmado por: JESSEL AYRA PLASENCIA  
 UNIVERSIDAD DE LA LAGUNA

Fecha: 30/11/2020 12:24:14

María de las Maravillas Aguiar Aguiar  
 UNIVERSIDAD DE LA LAGUNA

08/02/2021 13:50:06

#### 4. Results and Discussion

RIF1 is translocated to DSBs in a 53BP1-dependent manner. Its accumulation at broken DNA ends antagonizes DNA end resection (Chapman et al., 2013, p. 1; Feng et al., 2013, p. 1; Silverman et al., 2004, p. 1). Hence, RIF1 was also analyzed to check whether the repair pathway choice was unbalanced in favor of NHEJ.

RPA2 is a subunit of the RPA complex. In addition to the initiation and elongation of DNA replication, this human protein is involved in the resection of 3' ssDNA to promote HR events (Anantha et al., 2008; Ghospurkar et al., 2015; Stephan et al., 2009). Thus, it was examined as a marker of the processing of broken DNA ends, which is a sign that precedes HR.

Microscopy analysis (fig. 4.11) showed that mock-treated cells only had spontaneous foci of  $\gamma$ H2A.X and 53BP1, which can occur even in the absence of exogenous DNA damage (Grudzenski et al., 2010; Pustovalova et al., 2016). In contrast, when DSBs occurred, a remarkable increase in  $\gamma$ H2A.X foci abundance throughout all chromosomes was visualized. This result pinpoints that human cells, as yeast, detect DSBs when transiting late anaphase/telophase. Consequently, 53BP1 also formed foci disposed along the whole cytoplasm. It could mean that cells were inhibiting BRCA1, and therefore HR, so promoting NHEJ. However, as CDK/cyclin levels are still high in telophase (as it occurs in the late S phase and G<sub>2</sub>), it cannot be ruled out that 53BP1 forms foci to foster GC-mediated HR (Malewicz, 2016; Ochs et al., 2016, p. 1).

Similar to  $\gamma$ H2A.X and 53BP1, both RIF1 and RPA2 generated foci upon DSBs. While it is true that RPA2 was visualized in more abundance, RIF1 can also be seen as filaments disposed between segregated chromosomes. They might be coating ultrafine anaphase bridges formed by single-stranded DNA or protecting chromosome telomeres from telomere fusion as HR is active to repair DSBs (Fig. 4.11, white arrows). It is not unreasonable to think that both were acting simultaneously. Indeed, phleomycin does not produce a single type of DSB but promotes the generation of "dirty" DNA ends that might influence the repair pathway to choose. Thus, DSBs in telophase promote  $\gamma$ H2A.X foci generation and the 53BP1 recruitment to the broken DNA, which depending on the DSB type, might enhance the induction of NHEJ or HR through RIF1 and RPA2, respectively

Further experiments are required to study how the mammalian cells respond to DNA damage in late mitosis, such as visualization of BRCA1 and MRE11 proteins or the molecular monitorization of a single DSB repair. Nevertheless, this approximation has demonstrated that telophase is not only a short and eventual cell cycle stage where cells are committed to divide. Telophase is a paradoxical scenario in which mammals (at least HeLa cells) also react to DSBs by i) promoting a cell cycle delay and ii) triggering both NHEJ and HR before cytokinesis.

149

Este documento incorpora firma electrónica, y es copia auténtica de un documento electrónico archivado por la ULL según la Ley 39/2015.  
Su autenticidad puede ser contrastada en la siguiente dirección <https://sede.ull.es/validacion/>

Identificador del documento: 3075810 Código de verificación: smutbmB+

Firmado por: JESSEL AYRA PLASENCIA  
UNIVERSIDAD DE LA LAGUNA

Fecha: 30/11/2020 12:24:14

María de las Maravillas Aguiar Aguiar  
UNIVERSIDAD DE LA LAGUNA

08/02/2021 13:50:06



Este documento incorpora firma electrónica, y es copia auténtica de un documento electrónico archivado por la ULL según la Ley 39/2015.  
*Su autenticidad puede ser contrastada en la siguiente dirección <https://sede.ull.es/validacion/>*

Identificador del documento: 3075810 Código de verificación: smutbmB+

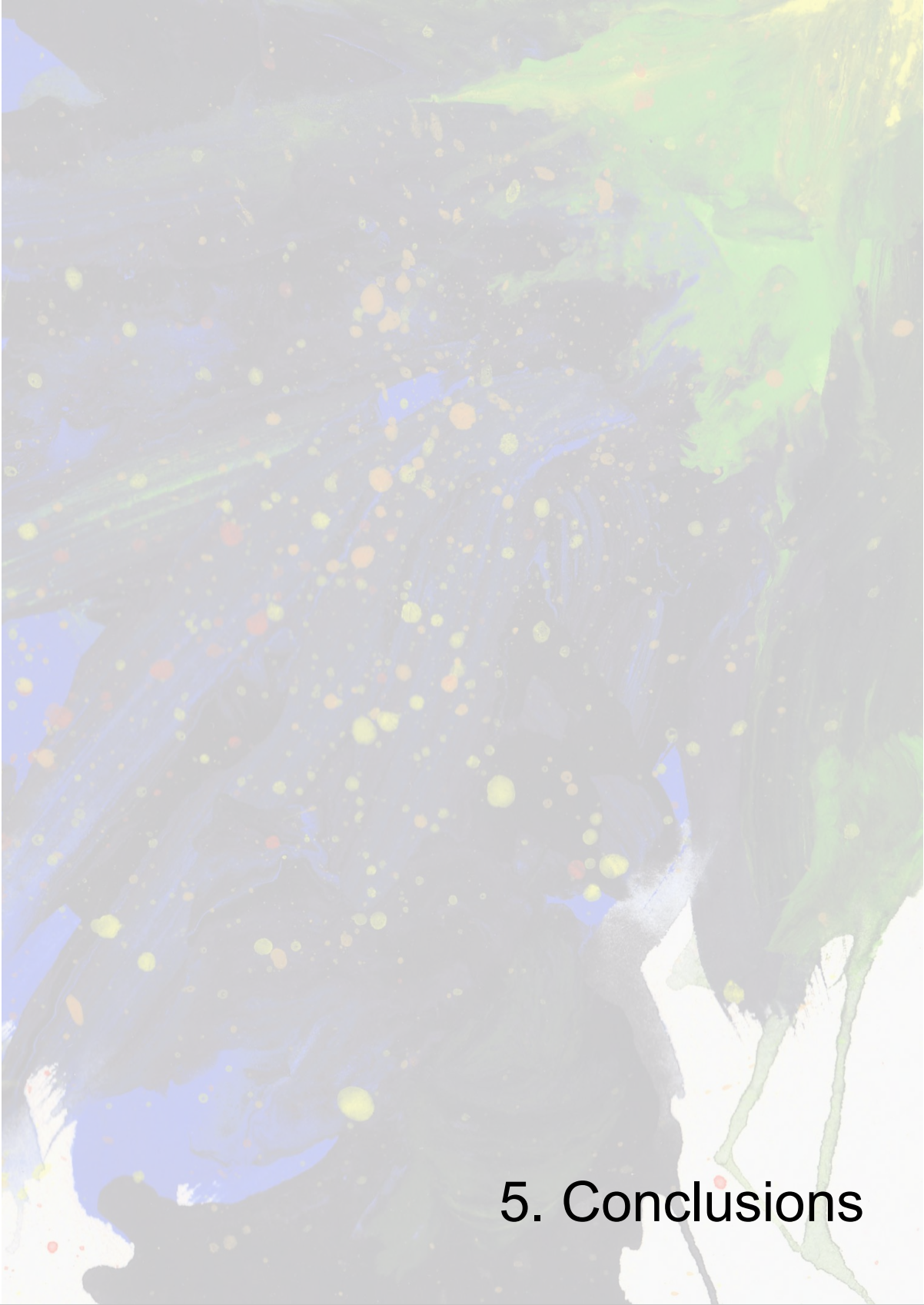
Firmado por: JESSEL AYRA PLASENCIA  
UNIVERSIDAD DE LA LAGUNA

Fecha: 30/11/2020 12:24:14

María de las Maravillas Aguiar Aguiar  
UNIVERSIDAD DE LA LAGUNA

08/02/2021 13:50:06





## 5. Conclusions

Este documento incorpora firma electrónica, y es copia auténtica de un documento electrónico archivado por la ULL según la Ley 39/2015.  
*Su autenticidad puede ser contrastada en la siguiente dirección <https://sede.ull.es/validacion/>*

Identificador del documento: 3075810 Código de verificación: smutbmB+

Firmado por: JESSEL AYRA PLASENCIA  
UNIVERSIDAD DE LA LAGUNA

Fecha: 30/11/2020 12:24:14

María de las Maravillas Aguiar Aguiar  
UNIVERSIDAD DE LA LAGUNA

08/02/2021 13:50:06



Este documento incorpora firma electrónica, y es copia auténtica de un documento electrónico archivado por la ULL según la Ley 39/2015.  
*Su autenticidad puede ser contrastada en la siguiente dirección <https://sede.ull.es/validacion/>*

Identificador del documento: 3075810      Código de verificación: smutbmB+

Firmado por: JESSEL AYRA PLASENCIA  
UNIVERSIDAD DE LA LAGUNA

Fecha: 30/11/2020 12:24:14

María de las Maravillas Aguiar Aguiar  
UNIVERSIDAD DE LA LAGUNA

08/02/2021 13:50:06

## 5. Conclusions

Conclusions from this work are listed below and shed light on how the cells attempt to repair DSBs in telophase.

1. Yeast cells recognize DSBs in telophase through the hyperphosphorylation of Rad53. Besides, they also stop the cell cycle and delay the telophase-to-G<sub>1</sub> transition through the DDR.
2. DSBs in telophase promote a substantial change in microtubules morphology and dynamics, generating active cellular pulling forces that approximate previously segregated chromosomes.
3. DSBs also stimulate the acceleration of chromatin movement in telophase and, ultimately, produce coalescence events between segregated sister chromatid loci.
4. Coalescence is dependent on the DDR, whereas survival seems to be related to HR. Rad9 mutants cannot re-join segregated loci, and Rad52-deficient cells do not survive as the wild-type.
5. Cin8 kinesin motor protein is partially dephosphorylated in a Cdc14-independent manner. This fact promotes its relocation from interpolar microtubules to the spindle pole bodies. Such post-translational modification results essential for reverting chromosome segregation and for survival.
6. DSBs in telophase are efficiently repaired, at least with a proximal donor sequence. Similar to G<sub>2</sub>, 3' ssDNA ends are resected, and the chosen HR repair model is Rad9- and Mre11 independent.
7. The cohesin complex seems to be heavily involved in enhancing DNA repair in telophase. Scc1 subunit is stabilized after the generation of DSBs, whereas Smc3 conditional depletion precludes and slows down the invasion and completion of the HR.
8. Proteomics mass spectrometry reports Msc1 as an upregulated protein specific for DSBs in telophase. Msc1 locates at the nuclear envelope and does not change its location upon DNA damage. However, biochemical analyses showed a post-translational modification, suggesting a possible important role.
9. HeLa cells seem to slow down cytokinesis when DSBs arise in telophase. Besides, they phosphorylate  $\gamma$ H2A.X and form 53BP1, RIF1, and RPA2 foci, likely upregulating HR and NHEJ repair pathways in this cell cycle stage.

153

Este documento incorpora firma electrónica, y es copia auténtica de un documento electrónico archivado por la ULL según la Ley 39/2015.  
Su autenticidad puede ser contrastada en la siguiente dirección <https://sede.ull.es/validacion/>

Identificador del documento: 3075810 Código de verificación: smutbmB+

Firmado por: JESSEL AYRA PLASENCIA  
UNIVERSIDAD DE LA LAGUNA

Fecha: 30/11/2020 12:24:14

María de las Maravillas Aguiar Aguiar  
UNIVERSIDAD DE LA LAGUNA

08/02/2021 13:50:06



Este documento incorpora firma electrónica, y es copia auténtica de un documento electrónico archivado por la ULL según la Ley 39/2015.  
*Su autenticidad puede ser contrastada en la siguiente dirección <https://sede.ull.es/validacion/>*

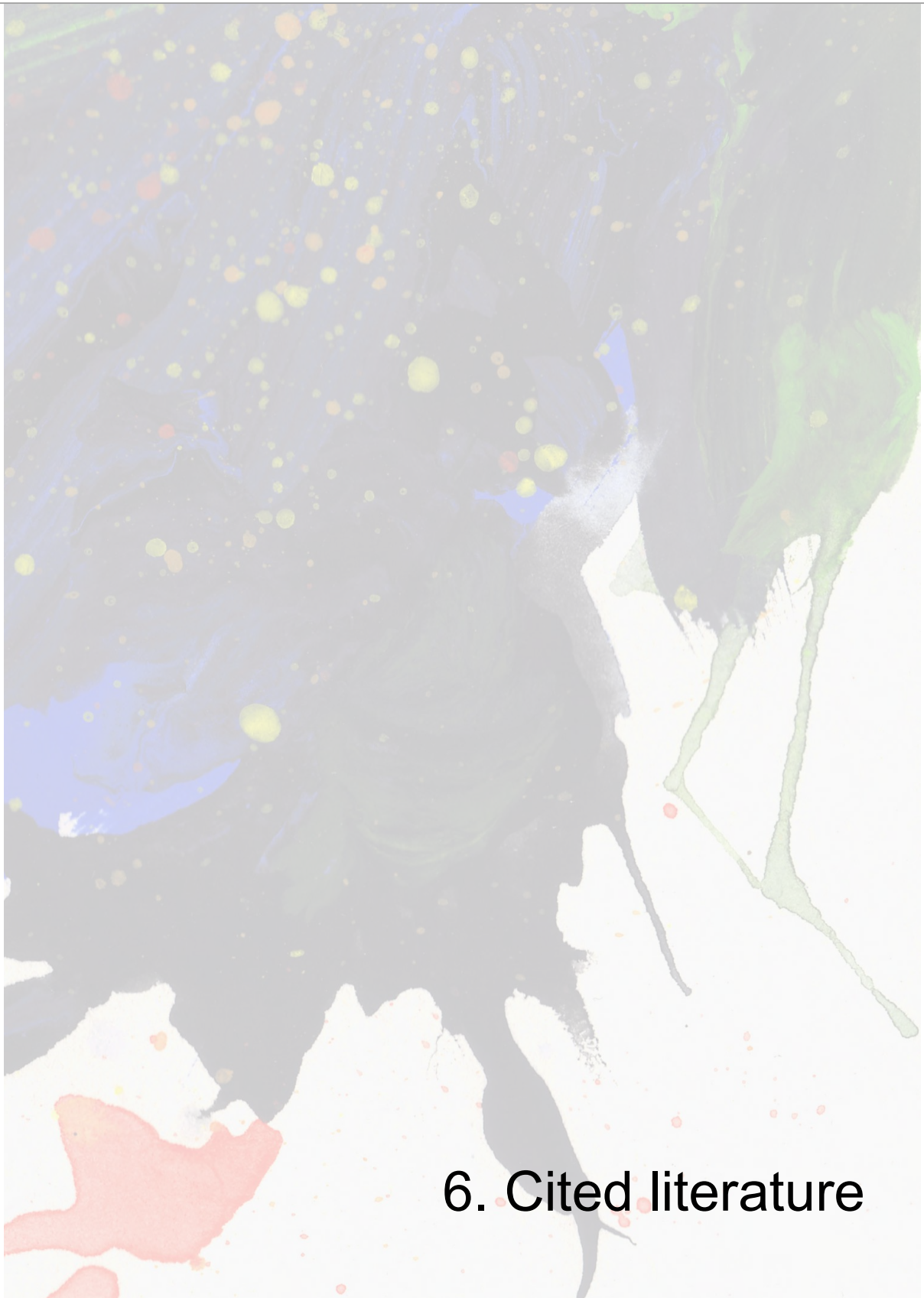
Identificador del documento: 3075810      Código de verificación: smutbmB+

Firmado por: JESSEL AYRA PLASENCIA  
UNIVERSIDAD DE LA LAGUNA

Fecha: 30/11/2020 12:24:14

María de las Maravillas Aguiar Aguiar  
UNIVERSIDAD DE LA LAGUNA

08/02/2021 13:50:06



## 6. Cited literature

Este documento incorpora firma electrónica, y es copia auténtica de un documento electrónico archivado por la ULL según la Ley 39/2015.  
*Su autenticidad puede ser contrastada en la siguiente dirección <https://sede.ull.es/validacion/>*

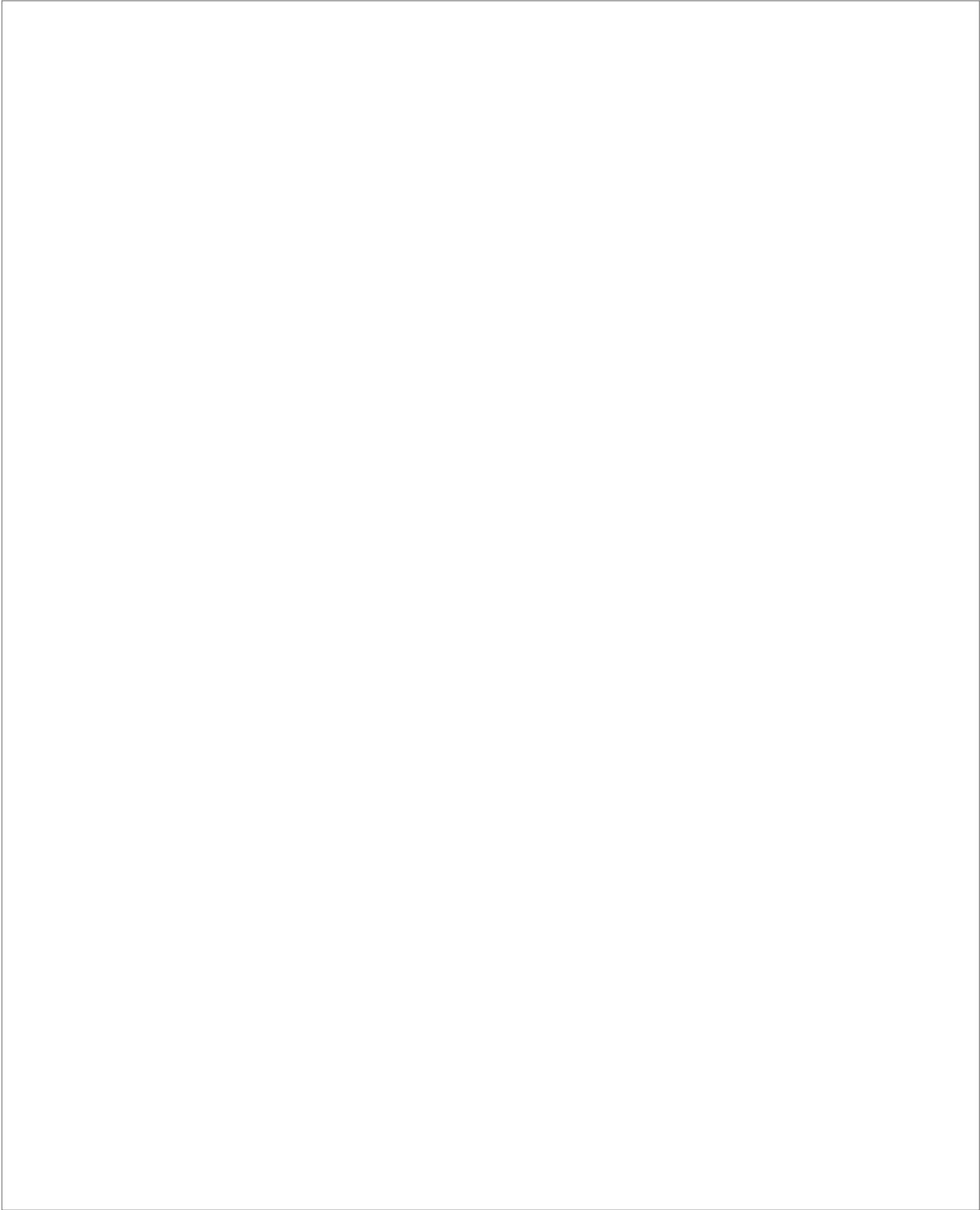
Identificador del documento: 3075810 Código de verificación: smutbmB+

Firmado por: JESSEL AYRA PLASENCIA  
UNIVERSIDAD DE LA LAGUNA

Fecha: 30/11/2020 12:24:14

María de las Maravillas Aguiar Aguiar  
UNIVERSIDAD DE LA LAGUNA

08/02/2021 13:50:06



Este documento incorpora firma electrónica, y es copia auténtica de un documento electrónico archivado por la ULL según la Ley 39/2015.  
*Su autenticidad puede ser contrastada en la siguiente dirección <https://sede.ull.es/validacion/>*

Identificador del documento: 3075810      Código de verificación: smutbmB+

Firmado por: JESSEL AYRA PLASENCIA  
UNIVERSIDAD DE LA LAGUNA

Fecha: 30/11/2020 12:24:14

María de las Maravillas Aguiar Aguiar  
UNIVERSIDAD DE LA LAGUNA

08/02/2021 13:50:06

6. Cited literature

- Alcasabas, A. A., Osborn, A. J., Bachant, J., Hu, F., Werler, P. J., Bousset, K., Furuya, K., Diffley, J. F., Carr, A. M., & Elledge, S. J. (2001). Mrc1 transduces signals of DNA replication stress to activate Rad53. *Nature Cell Biology*, 3(11), 958–965. <https://doi.org/10.1038/ncb1101-958>
- Anand, R., Beach, A., Li, K., & Haber, J. (2017). Rad51-mediated double-strand break repair and mismatch correction of divergent substrates. *Nature*, 544(7650), 377–380. <https://doi.org/10.1038/nature22046>
- Anantha, R. W., Sokolova, E., & Borowiec, J. A. (2008). RPA phosphorylation facilitates mitotic exit in response to mitotic DNA damage. *Proceedings of the National Academy of Sciences of the United States of America*, 105(35), 12903–12908. <https://doi.org/10.1073/pnas.0803001105>
- Aparicio, T., Baer, R., & Gautier, J. (2014). DNA double-strand break repair pathway choice and cancer. *DNA Repair*, 19, 169–175. <https://doi.org/10.1016/j.dnarep.2014.03.014>
- Apostolou, Z., Chatzinikolaou, G., Stratigi, K., & Garinis, G. A. (2019). Nucleotide Excision Repair and Transcription-Associated Genome Instability. *BioEssays: News and Reviews in Molecular, Cellular and Developmental Biology*, 41(4), e1800201. <https://doi.org/10.1002/bies.201800201>
- Aragón, L. (2018). The Smc5/6 Complex: New and Old Functions of the Enigmatic Long-Distance Relative. *Annual Review of Genetics*, 52(1), 89–107. <https://doi.org/10.1146/annurev-genet-120417-031353>
- Avunie-Masala, R., Movshovich, N., Nissenkorn, Y., Gerson-Gurwitz, A., Fridman, V., Köivomägi, M., Loog, M., Hoyt, M. A., Zaritsky, A., & Gheber, L. (2011). Phospho-regulation of kinesin-5 during anaphase spindle elongation. *Journal of Cell Science*, 124(6), 873–878. <https://doi.org/10.1242/jcs.077396>
- Aylon, Y., & Kupiec, M. (2004a). New insights into the mechanism of homologous recombination in yeast. *Mutation Research*, 566(3), 231–248. <https://doi.org/10.1016/j.mrrev.2003.10.001>
- Aylon, Y., & Kupiec, M. (2004b). DSB repair: The yeast paradigm. *DNA Repair*, 3(8–9), 797–815. <https://doi.org/10.1016/j.dnarep.2004.04.013>
- Aylon, Y., Liefshitz, B., & Kupiec, M. (2004). The CDK regulates repair of double-strand breaks by homologous recombination during the cell cycle. *The EMBO Journal*, 23(24), 4868–4875. <https://doi.org/10.1038/sj.emboj.7600469>
- Barnes, G., Louie, K. A., & Botstein, D. (1992). Yeast proteins associated with microtubules in vitro and in vivo. *Molecular Biology of the Cell*, 3(1), 29–47. <https://doi.org/10.1091/mbc.3.1.29>
- Barnum, K. J., & O'Connell, M. J. (2014). Cell cycle regulation by checkpoints. *Methods in Molecular Biology (Clifton, N.J.)*, 1170, 29–40. [https://doi.org/10.1007/978-1-4939-0888-2\\_2](https://doi.org/10.1007/978-1-4939-0888-2_2)
- Baro, B., Queralt, E., & Monje-Casas, F. (2017). Regulation of Mitotic Exit in *Saccharomyces cerevisiae*. *Methods in Molecular Biology (Clifton, N.J.)*, 1505, 3–17. [https://doi.org/10.1007/978-1-4939-6502-1\\_1](https://doi.org/10.1007/978-1-4939-6502-1_1)
- Bártová, E., Legartová, S., Dundr, M., & Suchánková, J. (2019). A role of the 53BP1 protein in genome protection: Structural and functional characteristics of 53BP1-dependent DNA repair. *Aging (Albany NY)*, 11(8), 2488–2511. <https://doi.org/10.18632/aging.101917>
- Basco, R. D., Segal, M. D., & Reed, S. I. (1995). Negative regulation of G1 and G2 by S-phase cyclins of *Saccharomyces cerevisiae*. *Molecular and Cellular Biology*, 15(9), 5030–5042. <https://doi.org/10.1128/mcb.15.9.5030>

157

Este documento incorpora firma electrónica, y es copia auténtica de un documento electrónico archivado por la ULL según la Ley 39/2015.  
Su autenticidad puede ser contrastada en la siguiente dirección <https://sede.ull.es/validacion/>

Identificador del documento: 3075810 Código de verificación: smutbmB+

Firmado por: JESSEL AYRA PLASENCIA  
UNIVERSIDAD DE LA LAGUNA

Fecha: 30/11/2020 12:24:14

María de las Maravillas Aguiar Aguiar  
UNIVERSIDAD DE LA LAGUNA

08/02/2021 13:50:06

6. Cited literature

- Bermúdez-López, M., Ceschia, A., de Piccoli, G., Colomina, N., Pasero, P., Aragón, L., & Torres-Rosell, J. (2010). The Smc5/6 complex is required for dissolution of DNA-mediated sister chromatid linkages. *Nucleic Acids Research*, 38(19), 6502–6512. <https://doi.org/10.1093/nar/gkq546>
- Bertuch, A. A., & Lundblad, V. (2003a). Which end: Dissecting Ku's function at telomeres and double-strand breaks. *Genes & Development*, 17(19), 2347–2350. <https://doi.org/10.1101/gad.1146603>
- Bertuch, A. A., & Lundblad, V. (2003b). The Ku heterodimer performs separable activities at double-strand breaks and chromosome termini. *Molecular and Cellular Biology*, 23(22), 8202–8215. <https://doi.org/10.1128/mcb.23.22.8202-8215.2003>
- Bhargava, R., Onyango, D. O., & Stark, J. M. (2016). Regulation of Single-Strand Annealing and its Role in Genome Maintenance. *Trends in Genetics: TIG*, 32(9), 566–575. <https://doi.org/10.1016/j.tig.2016.06.007>
- Bloom, K., Hill, A., & Jones, E. (1989). Conditional dicentric chromosomes in yeast. *Progress in Clinical and Biological Research*, 318, 149–158.
- Bloom, Kerry. (2006). NoCut: Cytokinesis in check. *Cell*, 125(1), 17–18. <https://doi.org/10.1016/j.cell.2006.03.016>
- Boiteux, S., & Guillet, M. (2004). Abasic sites in DNA: Repair and biological consequences in *Saccharomyces cerevisiae*. *DNA Repair*, 3(1), 1–12. <https://doi.org/10.1016/j.dnarep.2003.10.002>
- Bonetti, D., Villa, M., Gobbin, E., Cassani, C., Tedeschi, G., & Longhese, M. P. (2015). Escape of Sgs1 from Rad9 inhibition reduces the requirement for Sae2 and functional MRX in DNA end resection. *EMBO Reports*, 16(3), 351–361. <https://doi.org/10.15252/embr.201439764>
- Booher, R. N., Deshaies, R. J., & Kirschner, M. W. (1993). Properties of *Saccharomyces cerevisiae* wee1 and its differential regulation of p34CDC28 in response to G1 and G2 cyclins. *The EMBO Journal*, 12(9), 3417–3426.
- Bosco, G., & Haber, J. E. (1998). Chromosome break-induced DNA replication leads to nonreciprocal translocations and telomere capture. *Genetics*, 150(3), 1037–1047.
- Bowers, J., Tran, P. T., Joshi, A., Liskay, R. M., & Alani, E. (2001). MSH-MLH complexes formed at a DNA mismatch are disrupted by the PCNA sliding clamp. *Journal of Molecular Biology*, 306(5), 957–968. <https://doi.org/10.1006/jmbi.2001.4467>
- Branzei, D., & Foiani, M. (2010). Leaping forks at inverted repeats. *Genes & Development*, 24(1), 5–9. <https://doi.org/10.1101/gad.1884810>
- Buonomo, S. B. C., Rabitsch, K. P., Fuchs, J., Gruber, S., Sullivan, M., Uhlmann, F., Petronczki, M., Tóth, A., & Nasmyth, K. (2003). Division of the nucleolus and its release of CDC14 during anaphase of meiosis I depends on separase, SPO12, and SLK19. *Developmental Cell*, 4(5), 727–739. [https://doi.org/10.1016/s1534-5807\(03\)00129-1](https://doi.org/10.1016/s1534-5807(03)00129-1)
- Çamdere, G., Guacci, V., Stricklin, J., & Koshland, D. (2015). The ATPases of cohesin interface with regulators to modulate cohesin-mediated DNA tethering. *ELife*, 4. <https://doi.org/10.7554/eLife.11315>
- Caydasi, A. K., & Pereira, G. (2009). Spindle alignment regulates the dynamic association of checkpoint proteins with yeast spindle pole bodies. *Developmental Cell*, 16(1), 146–156. <https://doi.org/10.1016/j.devcel.2008.10.013>

158

Este documento incorpora firma electrónica, y es copia auténtica de un documento electrónico archivado por la ULL según la Ley 39/2015.  
Su autenticidad puede ser contrastada en la siguiente dirección <https://sede.ull.es/validacion/>

Identificador del documento: 3075810 Código de verificación: smutbmB+

Firmado por: JESSEL AYRA PLASENCIA  
UNIVERSIDAD DE LA LAGUNA

Fecha: 30/11/2020 12:24:14

María de las Maravillas Aguiar Aguiar  
UNIVERSIDAD DE LA LAGUNA

08/02/2021 13:50:06



6. Cited literature

- Cenamor, R., Jiménez, J., Cid, V. J., Nombela, C., & Sánchez, M. (1999). The budding yeast Cdc15 localizes to the spindle pole body in a cell-cycle-dependent manner. *Molecular Cell Biology Research Communications: MCBRC*, 2(3), 178–184. <https://doi.org/10.1006/mcbr.1999.0173>
- Chan, K.-L., Roig, M. B., Hu, B., Beckouët, F., Metson, J., & Nasmyth, K. (2012). Cohesin's DNA Exit Gate Is Distinct from Its Entrance Gate and Is Regulated by Acetylation. *Cell*, 150(5), 961–974. <https://doi.org/10.1016/j.cell.2012.07.028>
- Chang, H. H. Y., Pannunzio, N. R., Adachi, N., & Lieber, M. R. (2017). Non-homologous DNA end joining and alternative pathways to double-strand break repair. *Nature Reviews. Molecular Cell Biology*, 18(8), 495–506. <https://doi.org/10.1038/nrm.2017.48>
- Chapman, J. R., Barral, P., Vannier, J.-B., Borel, V., Steger, M., Tomas-Loba, A., Sartori, A. A., Adams, I. R., Batista, F. D., & Boulton, S. J. (2013). RIF1 Is Essential for 53BP1-Dependent Nonhomologous End Joining and Suppression of DNA Double-Strand Break Resection. *Molecular Cell*, 49(5), 858–871. <https://doi.org/10.1016/j.molcel.2013.01.002>
- Cheng, H., Zhang, N., & Pati, D. (2020). Cohesin subunit RAD21: From biology to disease. *Gene*, 758, 144966. <https://doi.org/10.1016/j.gene.2020.144966>
- Chiruvella, K. K., Liang, Z., & Wilson, T. E. (2013). Repair of double-strand breaks by end joining. *Cold Spring Harbor Perspectives in Biology*, 5(5), a012757. <https://doi.org/10.1101/cshperspect.a012757>
- Clarke, D. J., & Giménez-Abián, J. F. (2000). Checkpoints controlling mitosis. *BioEssays: News and Reviews in Molecular, Cellular and Developmental Biology*, 22(4), 351–363. [https://doi.org/10.1002/\(SICI\)1521-1878\(200004\)22:4<351::AID-BIES5>3.0.CO;2-W](https://doi.org/10.1002/(SICI)1521-1878(200004)22:4<351::AID-BIES5>3.0.CO;2-W)
- Clerici, M., Mantiero, D., Lucchini, G., & Longhese, M. P. (2006). The *Saccharomyces cerevisiae* Sae2 protein negatively regulates DNA damage checkpoint signalling. *EMBO Reports*, 7(2), 212–218. <https://doi.org/10.1038/sj.embor.7400593>
- Cohen-Fix, O., Peters, J. M., Kirschner, M. W., & Koshland, D. (1996). Anaphase initiation in *Saccharomyces cerevisiae* is controlled by the APC-dependent degradation of the anaphase inhibitor Pds1p. *Genes & Development*, 10(24), 3081–3093. <https://doi.org/10.1101/gad.10.24.3081>
- Colleaux, L., d'Auriol, L., Betermier, M., Cottarel, G., Jacquier, A., Galibert, F., & Dujon, B. (1986). Universal code equivalent of a yeast mitochondrial intron reading frame is expressed into *E. coli* as a specific double strand endonuclease. *Cell*, 44(4), 521–533. [https://doi.org/10.1016/0092-8674\(86\)90262-X](https://doi.org/10.1016/0092-8674(86)90262-X)
- Costantino, L., Sotiriou, S. K., Rantala, J. K., Magin, S., Mladenov, E., Helleday, T., Haber, J. E., Iliakis, G., Kallioniemi, O. P., & Halazonetis, T. D. (2014). Break-induced replication repair of damaged forks induces genomic duplications in human cells. *Science (New York, N.Y.)*, 343(6166), 88–91. <https://doi.org/10.1126/science.1243211>
- Costanzo, M., Nishikawa, J. L., Tang, X., Millman, J. S., Schub, O., Breitzkreuz, K., Dewar, D., Rupes, I., Andrews, B., & Tyers, M. (2004). CDK activity antagonizes Whi5, an inhibitor of G1/S transcription in yeast. *Cell*, 117(7), 899–913. <https://doi.org/10.1016/j.cell.2004.05.024>
- Craven, R. J., Greenwell, P. W., Dominska, M., & Petes, T. D. (2002). Regulation of genome stability by TEL1 and MEC1, yeast homologs of the mammalian ATM and ATR genes. *Genetics*, 161(2), 493–507.

159

Este documento incorpora firma electrónica, y es copia auténtica de un documento electrónico archivado por la ULL según la Ley 39/2015.  
Su autenticidad puede ser contrastada en la siguiente dirección <https://sede.ull.es/validacion/>

Identificador del documento: 3075810 Código de verificación: smutbmB+

Firmado por: JESSEL AYRA PLASENCIA  
UNIVERSIDAD DE LA LAGUNA

Fecha: 30/11/2020 12:24:14

María de las Maravillas Aguiar Aguiar  
UNIVERSIDAD DE LA LAGUNA

08/02/2021 13:50:06

6. Cited literature

- Dahmann, C., Diffley, J. F., & Nasmyth, K. A. (1995). S-phase-promoting cyclin-dependent kinases prevent re-replication by inhibiting the transition of replication origins to a pre-replicative state. *Current Biology: CB*, 5(11), 1257–1269. [https://doi.org/10.1016/s0960-9822\(95\)00252-1](https://doi.org/10.1016/s0960-9822(95)00252-1)
- Daley, J. M., Palmbo, P. L., Wu, D., & Wilson, T. E. (2005). Nonhomologous end joining in yeast. *Annual Review of Genetics*, 39, 431–451. <https://doi.org/10.1146/annurev.genet.39.073003.113340>
- D'Amours, D., & Amon, A. (2004). At the interface between signaling and executing anaphase—Cdc14 and the FEAR network. *Genes & Development*, 18(21), 2581–2595. <https://doi.org/10.1101/gad.1247304>
- Davis, A. P., & Symington, L. S. (2001). The yeast recombinational repair protein Rad59 interacts with Rad52 and stimulates single-strand annealing. *Genetics*, 159(2), 515–525.
- Davis, Allison P., & Symington, L. S. (2004). RAD51-dependent break-induced replication in yeast. *Molecular and Cellular Biology*, 24(6), 2344–2351. <https://doi.org/10.1128/mcb.24.6.2344-2351.2004>
- de Bruin, R. A. M., McDonald, W. H., Kalashnikova, T. I., Yates, J., & Wittenberg, C. (2004). Cln3 activates G1-specific transcription via phosphorylation of the SBF bound repressor Whi5. *Cell*, 117(7), 887–898. <https://doi.org/10.1016/j.cell.2004.05.025>
- de la Torre-Ruiz, M. A., Green, C. M., & Lowndes, N. F. (1998). RAD9 and RAD24 define two additive, interacting branches of the DNA damage checkpoint pathway in budding yeast normally required for Rad53 modification and activation. *The EMBO Journal*, 17(9), 2687–2698. <https://doi.org/10.1093/emboj/17.9.2687>
- Díaz-Martínez, L. A., Giménez-Abián, J. F., & Clarke, D. J. (2008). Chromosome cohesion—Rings, knots, orcs and fellowship. *Journal of Cell Science*, 121(Pt 13), 2107–2114. <https://doi.org/10.1242/jcs.029132>
- Dirick, L., Böhm, T., & Nasmyth, K. (1995). Roles and regulation of Cln-Cdc28 kinases at the start of the cell cycle of *Saccharomyces cerevisiae*. *The EMBO Journal*, 14(19), 4803–4813.
- Donnianni, R. A., & Symington, L. S. (2013). Break-induced replication occurs by conservative DNA synthesis. *Proceedings of the National Academy of Sciences of the United States of America*, 110(33), 13475–13480. <https://doi.org/10.1073/pnas.1309800110>
- Eissler, C. L., Mazón, G., Powers, B. L., Savinov, S. N., Symington, L. S., & Hall, M. C. (2014). The Cdk/cDc14 module controls activation of the Yen1 holliday junction resolvase to promote genome stability. *Molecular Cell*, 54(1), 80–93. <https://doi.org/10.1016/j.molcel.2014.02.012>
- Eker, A. P. M., Quayle, C., Chaves, I., & van der Horst, G. T. J. (2009). DNA repair in mammalian cells: Direct DNA damage reversal: elegant solutions for nasty problems. *Cellular and Molecular Life Sciences: CMLS*, 66(6), 968–980. <https://doi.org/10.1007/s00018-009-8735-0>
- Elango, R., Kockler, Z., Liu, L., & Malkova, A. (2018). Investigation of Break-Induced Replication in Yeast. *Methods in Enzymology*, 601, 161–203. <https://doi.org/10.1016/bs.mie.2017.12.010>
- Epstein, C. B., & Cross, F. R. (1992). CLB5: A novel B cyclin from budding yeast with a role in S phase. *Genes & Development*, 6(9), 1695–1706. <https://doi.org/10.1101/gad.6.9.1695>
- Esposito, R. E., & Holliday, R. (1964). THE EFFECT OF 5-FLUORODEOXYURIDINE ON GENETIC REPLICATION AND MITOTIC CROSSING OVER IN SYNCHRONIZED CULTURES OF *USTILAGO MAYDIS*. *Genetics*, 50, 1009–1017.

160

Este documento incorpora firma electrónica, y es copia auténtica de un documento electrónico archivado por la ULL según la Ley 39/2015.  
Su autenticidad puede ser contrastada en la siguiente dirección <https://sede.ull.es/validacion/>

Identificador del documento: 3075810 Código de verificación: smutbmB+

Firmado por: JESSEL AYRA PLASENCIA  
UNIVERSIDAD DE LA LAGUNA

Fecha: 30/11/2020 12:24:14

María de las Maravillas Aguiar Aguilár  
UNIVERSIDAD DE LA LAGUNA

08/02/2021 13:50:06

6. Cited literature

- Evans, E., Sugawara, N., Haber, J. E., & Alani, E. (2000). The *Saccharomyces cerevisiae* Msh2 mismatch repair protein localizes to recombination intermediates in vivo. *Molecular Cell*, 5(5), 789–799. [https://doi.org/10.1016/s1097-2765\(00\)80319-6](https://doi.org/10.1016/s1097-2765(00)80319-6)
- Ewald, J. C. (2018). How yeast coordinates metabolism, growth and division. *Current Opinion in Microbiology*, 45, 1–7. <https://doi.org/10.1016/j.mib.2017.12.012>
- Feng, L., Fong, K.-W., Wang, J., Wang, W., & Chen, J. (2013). RIF1 Counteracts BRCA1-mediated End Resection during DNA Repair. *The Journal of Biological Chemistry*, 288(16), 11135–11143. <https://doi.org/10.1074/jbc.M113.457440>
- Ferrari, M., Rawal, C. C., Lodovichi, S., Vietri, M. Y., & Pellicoli, A. (2020). Rad9/53BP1 promotes DNA repair via crossover recombination by limiting the Sgs1 and Mph1 helicases. *Nature Communications*, 11(1), 3181. <https://doi.org/10.1038/s41467-020-16997-w>
- Finn, K., Lowndes, N. F., & Grenon, M. (2012). Eukaryotic DNA damage checkpoint activation in response to double-strand breaks. *Cellular and Molecular Life Sciences*, 69(9), 1447–1473. <https://doi.org/10.1007/s00018-011-0875-3>
- Fitch, I., Dahmann, C., Surana, U., Amon, A., Nasmyth, K., Goetsch, L., Byers, B., & Futcher, B. (1992). Characterization of four B-type cyclin genes of the budding yeast *Saccharomyces cerevisiae*. *Molecular Biology of the Cell*, 3(7), 805–818. <https://doi.org/10.1091/mbc.3.7.805>
- Foiani, M., Pellicoli, A., Lopes, M., Lucca, C., Ferrari, M., Liberi, G., Muzi Falconi, M., & Plevani, P. (2000). DNA damage checkpoints and DNA replication controls in *Saccharomyces cerevisiae*. *Mutation Research*, 451(1–2), 187–196. [https://doi.org/10.1016/s0027-5107\(00\)00049-x](https://doi.org/10.1016/s0027-5107(00)00049-x)
- Fraschini, R. (2017). Factors that Control Mitotic Spindle Dynamics. *Advances in Experimental Medicine and Biology*, 925, 89–101. [https://doi.org/10.1007/5584\\_2016\\_74](https://doi.org/10.1007/5584_2016_74)
- Galli, A., Chan, C. Y., Parfenova, L., Cervelli, T., & Schiestl, R. H. (2015). Requirement of POL3 and POL4 on non-homologous and microhomology-mediated end joining in *rad50/xrs2* mutants of *Saccharomyces cerevisiae*. *Mutagenesis*, 30(6), 841–849. <https://doi.org/10.1093/mutage/gev046>
- Gao, S., Honey, S., Futcher, B., & Grollman, A. P. (2016). The non-homologous end-joining pathway of *S. cerevisiae* works effectively in G1-phase cells, and religates cognate ends correctly and non-randomly. *DNA Repair*, 42, 1. <https://doi.org/10.1016/j.dnarep.2016.03.013>
- García-Luis, J., Clemente-Blanco, A., Aragón, L., & Machín, F. (2014). Cdc14 targets the Holliday junction resolvase Yen1 to the nucleus in early anaphase. *Cell Cycle (Georgetown, Tex.)*, 13(9), 1392–1399. <https://doi.org/10.4161/cc.28370>
- García-Luis, J., & Machín, F. (2014). Mus81-Mms4 and Yen1 resolve a novel anaphase bridge formed by noncanonical Holliday junctions. *Nature Communications*, 5(1), 5652. <https://doi.org/10.1038/ncomms6652>
- Ghiara, J. B., Richardson, H. E., Sugimoto, K., Henze, M., Lew, D. J., Wittenberg, C., & Reed, S. I. (1991). A cyclin B homolog in *S. cerevisiae*: Chronic activation of the Cdc28 protein kinase by cyclin prevents exit from mitosis. *Cell*, 65(1), 163–174. [https://doi.org/10.1016/0092-8674\(91\)90417-w](https://doi.org/10.1016/0092-8674(91)90417-w)
- Ghosh, S., Gardner, J. M., Smoyer, C. J., Friederichs, J. M., Unruh, J. R., Slaughter, B. D., Alexander, R., Chisholm, R. D., Lee, K. K., Workman, J. L., & Jaspersen, S. L. (2012). Acetylation of the SUN protein Mps3 by Eco1 regulates its function in nuclear organization. *Molecular Biology of the Cell*, 23(13), 2546–2559. <https://doi.org/10.1091/mbc.E11-07-0600>

161

Este documento incorpora firma electrónica, y es copia auténtica de un documento electrónico archivado por la ULL según la Ley 39/2015.  
Su autenticidad puede ser contrastada en la siguiente dirección <https://sede.ull.es/validacion/>

Identificador del documento: 3075810 Código de verificación: smutbmB+

Firmado por: JESSEL AYRA PLASENCIA  
UNIVERSIDAD DE LA LAGUNA

Fecha: 30/11/2020 12:24:14

María de las Maravillas Aguiar Aguiar  
UNIVERSIDAD DE LA LAGUNA

08/02/2021 13:50:06

6. Cited literature

- Ghospurkar, P. L., Wilson, T. M., Liu, S., Herauf, A., Steffes, J., Mueller, E. N., Oakley, G. G., & Haring, S. J. (2015). Phosphorylation and cellular function of the human Rpa2 N-terminus in the budding yeast *Saccharomyces cerevisiae*. *Experimental Cell Research*, 331(1), 183–199. <https://doi.org/10.1016/j.yexcr.2014.12.002>
- Girard, P. M., & Boiteux, S. (1997). Repair of oxidized DNA bases in the yeast *Saccharomyces cerevisiae*. *Biochimie*, 79(9–10), 559–566. [https://doi.org/10.1016/s0300-9084\(97\)82004-4](https://doi.org/10.1016/s0300-9084(97)82004-4)
- Gladfelter, A. S., Pringle, J. R., & Lew, D. J. (2001). The septin cortex at the yeast mother-bud neck. *Current Opinion in Microbiology*, 4(6), 681–689. [https://doi.org/10.1016/s1369-5274\(01\)00269-7](https://doi.org/10.1016/s1369-5274(01)00269-7)
- Grünigge, R., Oh, J., & Symington, L. S. (2018). Chapter One—Processing of DNA Double-Strand Breaks in Yeast. In M. Spies & A. Malkova (Eds.), *Methods in Enzymology* (Vol. 600, pp. 1–24). Academic Press. <https://doi.org/10.1016/bs.mie.2017.11.007>
- Gobbini, E., Cesena, D., Galbiati, A., Lockhart, A., & Longhese, M. P. (2013). Interplays between ATM/Tel1 and ATR/Mec1 in sensing and signaling DNA double-strand breaks. *DNA Repair*, 12(10), 791–799. <https://doi.org/10.1016/j.dnarep.2013.07.009>
- Goffeau, A., Barrell, B. G., Bussey, H., Davis, R. W., Dujon, B., Feldmann, H., Galibert, F., Hoheisel, J. D., Jacq, C., Johnston, M., Louis, E. J., Mewes, H. W., Murakami, Y., Philippsen, P., Tettelin, H., & Oliver, S. G. (1996). Life with 6000 genes. *Science (New York, N.Y.)*, 274(5287), 546, 563–567. <https://doi.org/10.1126/science.274.5287.546>
- Goldstein, A., Siegler, N., Goldman, D., Judah, H., Valk, E., Kõivomägi, M., Loog, M., & Gheber, L. (2017). Three Cdk1 sites in the kinesin-5 Cin8 catalytic domain coordinate motor localization and activity during anaphase. *Cellular and Molecular Life Sciences: CMLS*, 74(18), 3395–3412. <https://doi.org/10.1007/s00018-017-2523-z>
- Gravel, S., Larrivée, M., Labrecque, P., & Wellinger, R. J. (1998). Yeast Ku as a regulator of chromosomal DNA end structure. *Science (New York, N.Y.)*, 280(5364), 741–744. <https://doi.org/10.1126/science.280.5364.741>
- Gravel, Serge, Chapman, J. R., Magill, C., & Jackson, S. P. (2008). DNA helicases Sgs1 and BLM promote DNA double-strand break resection. *Genes & Development*, 22(20), 2767–2772. <https://doi.org/10.1101/gad.503108>
- Grudzinski, S., Raths, A., Conrad, S., Rube, C. E., & Löbrich, M. (2010). Inducible response required for repair of low-dose radiation damage in human fibroblasts. *Proceedings of the National Academy of Sciences*, 107(32), 14205–14210. <https://doi.org/10.1073/pnas.1002213107>
- Guacci, V., Hogan, E., & Koshland, D. (1994). Chromosome condensation and sister chromatid pairing in budding yeast. *The Journal of Cell Biology*, 125(3), 517–530. <https://doi.org/10.1083/jcb.125.3.517>
- Haber, J. E. (2012). Mating-Type Genes and MAT Switching in *Saccharomyces cerevisiae*. *Genetics*, 191(1), 33–64. <https://doi.org/10.1534/genetics.111.134577>
- Habraken, Y., Sung, P., Prakash, L., & Prakash, S. (1998). ATP-dependent assembly of a ternary complex consisting of a DNA mismatch and the yeast MSH2-MSH6 and MLH1-PMS1 protein complexes. *The Journal of Biological Chemistry*, 273(16), 9837–9841. <https://doi.org/10.1074/jbc.273.16.9837>
- Hartwell, L. H. (1974). *Saccharomyces cerevisiae* cell cycle. *Bacteriological Reviews*, 38(2), 164–198.
- Hartwell, L. H. (1991). Twenty-five years of cell cycle genetics. *Genetics*, 129(4), 975–980.

162

Este documento incorpora firma electrónica, y es copia auténtica de un documento electrónico archivado por la ULL según la Ley 39/2015.  
Su autenticidad puede ser contrastada en la siguiente dirección <https://sede.ull.es/validacion/>

Identificador del documento: 3075810 Código de verificación: smutbmB+

Firmado por: JESSEL AYRA PLASENCIA  
UNIVERSIDAD DE LA LAGUNA

Fecha: 30/11/2020 12:24:14

María de las Maravillas Aguiar Aguiar  
UNIVERSIDAD DE LA LAGUNA

08/02/2021 13:50:06

6. Cited literature

- Hartwell, L., Weinert, T., Kadyk, L., & Garvik, B. (1994). Cell cycle checkpoints, genomic integrity, and cancer. *Cold Spring Harbor Symposia on Quantitative Biology*, 59, 259–263. <https://doi.org/10.1101/sqb.1994.059.01.030>
- Hegde, M. L., Hazra, T. K., & Mitra, S. (2010). Functions of disordered regions in mammalian early base excision repair proteins. *Cellular and Molecular Life Sciences: CMLS*, 67(21), 3573–3587. <https://doi.org/10.1007/s00018-010-0485-5>
- Heidinger-Pauli, J. M., Unal, E., Guacci, V., & Koshland, D. (2008). The kleisin subunit of cohesin dictates damage-induced cohesion. *Molecular Cell*, 31(1), 47–56. <https://doi.org/10.1016/j.molcel.2008.06.005>
- Henninger, E. E., & Pursell, Z. F. (2014). DNA polymerase  $\epsilon$  and its roles in genome stability. *IUBMB Life*, 66(5), 339–351. <https://doi.org/10.1002/iub.1276>
- Her, J., & Bunting, S. F. (2018). How cells ensure correct repair of DNA double-strand breaks. *The Journal of Biological Chemistry*, 293(27), 10502–10511. <https://doi.org/10.1074/jbc.TM118.000371>
- Heyer, W.-D., Li, X., Rolfsmeier, M., & Zhang, X.-P. (2006). Rad54: The Swiss Army knife of homologous recombination? *Nucleic Acids Research*, 34(15), 4115–4125. <https://doi.org/10.1093/nar/gkl481>
- Hill, A., & Bloom, K. (1989). Acquisition and processing of a conditional dicentric chromosome in *Saccharomyces cerevisiae*. *Molecular and Cellular Biology*, 9(3), 1368–1370. <https://doi.org/10.1128/mcb.9.3.1368>
- Hirano, T. (2000). Chromosome cohesion, condensation, and separation. *Annual Review of Biochemistry*, 69, 115–144. <https://doi.org/10.1146/annurev.biochem.69.1.115>
- Holliday, R. (1964). THE INDUCTION OF MITOTIC RECOMBINATION BY MITOMYCIN C IN *USTILAGO* AND *SACCHAROMYCES*. *Genetics*, 50, 323–335.
- Holmes, A. M., & Haber, J. E. (1999). Double-strand break repair in yeast requires both leading and lagging strand DNA polymerases. *Cell*, 96(3), 415–424. [https://doi.org/10.1016/s0092-8674\(00\)80554-1](https://doi.org/10.1016/s0092-8674(00)80554-1)
- Hotz, M., Leisner, C., Chen, D., Manatschal, C., Wegleiter, T., Ouellet, J., Lindstrom, D., Gottschling, D. E., Vogel, J., & Barral, Y. (2012). Spindle pole bodies exploit the mitotic exit network in metaphase to drive their age-dependent segregation. *Cell*, 148(5), 958–972. <https://doi.org/10.1016/j.cell.2012.01.041>
- Huber, R. G., Kulemzina, I., Ang, K., Chavda, A. P., Suranthran, S., Teh, J.-T., Kenanov, D., Liu, G., Rancati, G., Szmyd, R., Kaldis, P., Bond, P. J., & Ivanov, D. (2016). Impairing Cohesin Smc1/3 Head Engagement Compensates for the Lack of Eco1 Function. *Structure*, 24(11), 1991–1999. <https://doi.org/10.1016/j.str.2016.09.001>
- Hudson, D. F., Marshall, K. M., & Earnshaw, W. C. (2009). Condensin: Architect of mitotic chromosomes. *Chromosome Research: An International Journal on the Molecular, Supramolecular and Evolutionary Aspects of Chromosome Biology*, 17(2), 131–144. <https://doi.org/10.1007/s10577-008-9009-7>
- Huertas, P., Cortés-Ledesma, F., Sartori, A. A., Aguilera, A., & Jackson, S. P. (2008). CDK targets Sae2 to control DNA-end resection and homologous recombination. *Nature*, 455(7213), 689–692. <https://doi.org/10.1038/nature07215>

163

Este documento incorpora firma electrónica, y es copia auténtica de un documento electrónico archivado por la ULL según la Ley 39/2015.  
Su autenticidad puede ser contrastada en la siguiente dirección <https://sede.ull.es/validacion/>

Identificador del documento: 3075810 Código de verificación: smutbmB+

Firmado por: JESSEL AYRA PLASENCIA  
UNIVERSIDAD DE LA LAGUNA

Fecha: 30/11/2020 12:24:14

María de las Maravillas Aguiar Aguilera  
UNIVERSIDAD DE LA LAGUNA

08/02/2021 13:50:06

6. Cited literature

- Huh, W.-K., Falvo, J. V., Gerke, L. C., Carroll, A. S., Howson, R. W., Weissman, J. S., & O'Shea, E. K. (2003). Global analysis of protein localization in budding yeast. *Nature*, 425(6959), 686–691. <https://doi.org/10.1038/nature02026>
- Janke, C., Magiera, M. M., Rathfelder, N., Taxis, C., Reber, S., Maekawa, H., Moreno-Borchart, A., Doenges, G., Schwob, E., Schiebel, E., & Knop, M. (2004). A versatile toolbox for PCR-based tagging of yeast genes: New fluorescent proteins, more markers and promoter substitution cassettes. *Yeast*, 21(11), 947–962. <https://doi.org/10.1002/yea.1142>
- Jaspersen, S. L., Charles, J. F., & Morgan, D. O. (1999). Inhibitory phosphorylation of the APC regulator Hct1 is controlled by the kinase Cdc28 and the phosphatase Cdc14. *Current Biology: CB*, 9(5), 227–236. [https://doi.org/10.1016/s0960-9822\(99\)80111-0](https://doi.org/10.1016/s0960-9822(99)80111-0)
- Jaspersen, Sue L., Huneycutt, B. J., Giddings, T. H., Resing, K. A., Ahn, N. G., & Winey, M. (2004). Cdc28/Cdk1 regulates spindle pole body duplication through phosphorylation of Spc42 and Mps1. *Developmental Cell*, 7(2), 263–274. <https://doi.org/10.1016/j.devcel.2004.07.006>
- Jaspersen, Sue L., & Winey, M. (2004). The budding yeast spindle pole body: Structure, duplication, and function. *Annual Review of Cell and Developmental Biology*, 20, 1–28. <https://doi.org/10.1146/annurev.cellbio.20.022003.114106>
- Játiva, S., Calabria, I., Moyano-Rodríguez, Y., García, P., & Queralt, E. (2019). Cdc14 activation requires coordinated Cdk1-dependent phosphorylation of Net1 and PP2A-Cdc55 at anaphase onset. *Cellular and Molecular Life Sciences: CMLS*, 76(18), 3601–3620. <https://doi.org/10.1007/s00018-019-03086-5>
- Jw, Y. (1992). Mechanism of action of hydroxyurea. *Seminars in Oncology*, 19(3 Suppl 9), 1–10.
- Kaplun, L., Ivantsiv, Y., Bakhrat, A., & Raveh, D. (2003). DNA damage response-mediated degradation of Ho endonuclease via the ubiquitin system involves its nuclear export. *The Journal of Biological Chemistry*, 278(49), 48727–48734. <https://doi.org/10.1074/jbc.M308671200>
- Kaplun, L., Ivantsiv, Y., Bakhrat, A., Tzirkin, R., Baranes, K., Shabek, N., & Raveh, D. (2006). The F-box protein, Ufo1, maintains genome stability by recruiting the yeast mating switch endonuclease, Ho, for rapid proteasome degradation. *The Israel Medical Association Journal: IMAJ*, 8(4), 246–248.
- Karahan, B., Argon, A., Yildirim, M., & Vardar, E. (2015). Relationship between MLH-1, MSH-2, PMS-2, MSH-6 expression and clinicopathological features in colorectal cancer. *International Journal of Clinical and Experimental Pathology*, 8(4), 4044–4053.
- Karlin, J., & Fischhaber, P. L. (2013). Rad51 ATP binding but not hydrolysis is required to recruit Rad10 in synthesis-dependent strand annealing sites in *S. cerevisiae*. *Advances in Biological Chemistry*, 3(3), 295–303. <https://doi.org/10.4236/abc.2013.33033>
- Keith, K. C., & Fitzgerald-Hayes, M. (2000). CSE4 genetically interacts with the *Saccharomyces cerevisiae* centromere DNA elements CDE I and CDE II but not CDE III. Implications for the path of the centromere dna around a cse4p variant nucleosome. *Genetics*, 156(3), 973–981.
- Kelliher, C. M., Foster, M. W., Motta, F. C., Deckard, A., Soderblom, E. J., Moseley, M. A., & Haase, S. B. (2018). Layers of regulation of cell-cycle gene expression in the budding yeast *Saccharomyces cerevisiae*. *Molecular Biology of the Cell*, 29(22), 2644–2655. <https://doi.org/10.1091/mbc.E18-04-0255>
- Khmelinskii, A., Roostalu, J., Roque, H., Antony, C., & Schiebel, E. (2009). Phosphorylation-dependent protein interactions at the spindle midzone mediate cell cycle regulation of spindle elongation. *Developmental Cell*, 17(2), 244–256. <https://doi.org/10.1016/j.devcel.2009.06.011>

164

Este documento incorpora firma electrónica, y es copia auténtica de un documento electrónico archivado por la ULL según la Ley 39/2015.  
Su autenticidad puede ser contrastada en la siguiente dirección <https://sede.ull.es/validacion/>

Identificador del documento: 3075810 Código de verificación: smutbmB+

Firmado por: JESSEL AYRA PLASENCIA  
UNIVERSIDAD DE LA LAGUNA

Fecha: 30/11/2020 12:24:14

María de las Maravillas Aguiar Aguiar  
UNIVERSIDAD DE LA LAGUNA

08/02/2021 13:50:06

6. Cited literature

- Kim, B.-J., Li, Y., Zhang, J., Xi, Y., Li, Y., Yang, T., Jung, S. Y., Pan, X., Chen, R., Li, W., Wang, Y., & Qin, J. (2010). Genome-wide Reinforcement of Cohesin Binding at Pre-existing Cohesin Sites in Response to Ionizing Radiation in Human Cells. *The Journal of Biological Chemistry*, 285(30), 22784–22792. <https://doi.org/10.1074/jbc.M110.134577>
- Kitsera, N., Rodríguez-Alvarez, M., Emmert, S., Carell, T., & Khobta, A. (2019). Nucleotide excision repair of abasic DNA lesions. *Nucleic Acids Research*, 47(16), 8537–8547. <https://doi.org/10.1093/nar/gkz558>
- Klein, H. L., Bačinskaja, G., Che, J., Cheblal, A., Elango, R., Epshtein, A., Fitzgerald, D. M., Gómez-González, B., Khan, S. R., Kumar, S., Leland, B. A., Marie, L., Mei, Q., Miné-Hattab, J., Piotrowska, A., Polleys, E. J., Putnam, C. D., Radchenko, E. A., Saada, A. A., ... Malkova, A. (2019). Guidelines for DNA recombination and repair studies: Cellular assays of DNA repair pathways. *Microbial Cell (Graz, Austria)*, 6(1), 1–64. <https://doi.org/10.15698/mic2019.01.664>
- Knop, M., Siegers, K., Pereira, G., Zachariae, W., Winsor, B., Nasmyth, K., & Schiebel, E. (1999). Epitope tagging of yeast genes using a PCR-based strategy: More tags and improved practical routines. *Yeast*, 15(10B), 963–972. [https://doi.org/10.1002/\(SICI\)1097-0061\(199907\)15:10B<963::AID-YEA399>3.0.CO;2-W](https://doi.org/10.1002/(SICI)1097-0061(199907)15:10B<963::AID-YEA399>3.0.CO;2-W)
- Koshland, D. E., & Guacci, V. (2000). Sister chromatid cohesion: The beginning of a long and beautiful relationship. *Current Opinion in Cell Biology*, 12(3), 297–301. [https://doi.org/10.1016/s0955-0674\(00\)00092-2](https://doi.org/10.1016/s0955-0674(00)00092-2)
- Kostriken, R., Strathern, J. N., Klar, A. J. S., Hicks, J. B., & Heffron, F. (1983). A site-specific endonuclease essential for mating-type switching in *Saccharomyces cerevisiae*. *Cell*, 35(1), 167–174. [https://doi.org/10.1016/0092-8674\(83\)90219-2](https://doi.org/10.1016/0092-8674(83)90219-2)
- Kramara, J., Osia, B., & Malkova, A. (2018). Break-Induced Replication: The Where, The Why, and The How. *Trends in Genetics: TIG*, 34(7), 518–531. <https://doi.org/10.1016/j.tig.2018.04.002>
- Krokan, H. E., & Bjørås, M. (2013). Base excision repair. *Cold Spring Harbor Perspectives in Biology*, 5(4), a012583. <https://doi.org/10.1101/cshperspect.a012583>
- L, P.-M., M, Ö, F, B., & B, L. (2020, April 3). *Npl3 stabilizes R-loops at telomeres to prevent accelerated replicative senescence*. EMBO Reports; EMBO Rep. <https://doi.org/10.15252/embr.201949087>
- Laloraya, S., Guacci, V., & Koshland, D. (2000). Chromosomal addresses of the cohesin component Mcd1p. *The Journal of Cell Biology*, 151(5), 1047–1056. <https://doi.org/10.1083/jcb.151.5.1047>
- Lara-Gonzalez, P., Westhorpe, F. G., & Taylor, S. S. (2012). The spindle assembly checkpoint. *Current Biology: CB*, 22(22), R966-980. <https://doi.org/10.1016/j.cub.2012.10.006>
- Laroche, T., Martin, S. G., Gotta, M., Gorham, H. C., Pryde, F. E., Louis, E. J., & Gasser, S. M. (1998). Mutation of yeast Ku genes disrupts the subnuclear organization of telomeres. *Current Biology: CB*, 8(11), 653–656. [https://doi.org/10.1016/s0960-9822\(98\)70252-0](https://doi.org/10.1016/s0960-9822(98)70252-0)
- Lee, K., Ji, J.-H., Yoon, K., Che, J., Seol, J.-H., Lee, S. E., & Shim, E. Y. (2019). Microhomology Selection for Microhomology Mediated End Joining in *Saccharomyces cerevisiae*. *Genes*, 10(4). <https://doi.org/10.3390/genes10040284>
- Lee, S. E., Frenz, L. M., Wells, N. J., Johnson, A. L., & Johnston, L. H. (2001). Order of function of the budding-yeast mitotic exit-network proteins Tem1, Cdc15, Mob1, Dbf2, and Cdc5. *Current Biology: CB*, 11(10), 784–788. [https://doi.org/10.1016/s0960-9822\(01\)00228-7](https://doi.org/10.1016/s0960-9822(01)00228-7)

165

Este documento incorpora firma electrónica, y es copia auténtica de un documento electrónico archivado por la ULL según la Ley 39/2015.  
Su autenticidad puede ser contrastada en la siguiente dirección <https://sede.ull.es/validacion/>

Identificador del documento: 3075810 Código de verificación: smutbmB+

Firmado por: JESSEL AYRA PLASENCIA  
UNIVERSIDAD DE LA LAGUNA

Fecha: 30/11/2020 12:24:14

María de las Maravillas Aguiar Aguiar  
UNIVERSIDAD DE LA LAGUNA

08/02/2021 13:50:06

6. Cited literature

- Leitao, R. M., & Kellogg, D. R. (2017). The duration of mitosis and daughter cell size are modulated by nutrients in budding yeast. *Journal of Cell Biology*, 216(11), 3463–3470. <https://doi.org/10.1083/jcb.201609114>
- Lemaître, C., Grabarz, A., Tsouroula, K., Andronov, L., Furst, A., Pankotai, T., Heyer, V., Rogier, M., Attwood, K. M., Kessler, P., Dellaire, G., Klaholz, B., Reina-San-Martin, B., & Soutoglou, E. (2014). Nuclear position dictates DNA repair pathway choice. *Genes & Development*, 28(22), 2450–2463. <https://doi.org/10.1101/gad.248369.114>
- Levine, K., Tinkelenberg, A. H., & Cross, F. (1995). The CLN gene family: Central regulators of cell cycle Start in budding yeast. *Progress in Cell Cycle Research*, 1, 101–114. [https://doi.org/10.1007/978-1-4615-1809-9\\_8](https://doi.org/10.1007/978-1-4615-1809-9_8)
- Lew, D. J., & Reed, S. I. (1993). Morphogenesis in the yeast cell cycle: Regulation by Cdc28 and cyclins. *The Journal of Cell Biology*, 120(6), 1305–1320. <https://doi.org/10.1083/jcb.120.6.1305>
- Lew, Daniel J., & Burke, D. J. (2003). The spindle assembly and spindle position checkpoints. *Annual Review of Genetics*, 37, 251–282. <https://doi.org/10.1146/annurev.genet.37.042203.120656>
- Li, J., & Xu, X. (2016). DNA double-strand break repair: A tale of pathway choices. *Acta Biochimica Et Biophysica Sinica*, 48(7), 641–646. <https://doi.org/10.1093/abbs/gmw045>
- Liang, N., Doré, C., Kennedy, E. K., Yeh, E., Williams, E. C., Fortinez, C. M., Wang, A., Bloom, K. S., & Rudner, A. D. (2018). Cdk1 phosphorylation of Esp1/Separase functions with PP2A and SIK19 to regulate pericentric Cohesin and anaphase onset. *PLoS Genetics*, 14(3), e1007029. <https://doi.org/10.1371/journal.pgen.1007029>
- Lieber, M. R., Ma, Y., Pannicke, U., & Schwarz, K. (2003). Mechanism and regulation of human non-homologous DNA end-joining. *Nature Reviews Molecular Cell Biology*, 4(9), 712–720. <https://doi.org/10.1038/nrm1202>
- Litsios, A., Huberts, D. H. E. W., Terpstra, H. M., Guerra, P., Schmidt, A., Buczak, K., Papagiannakis, A., Rovetta, M., Hekelaar, J., Hubmann, G., Exterkate, M., Miliadis-Argeitis, A., & Heinemann, M. (2019). Differential scaling between G1 protein production and cell size dynamics promotes commitment to the cell division cycle in budding yeast. *Nature Cell Biology*, 21(11), 1382–1392. <https://doi.org/10.1038/s41556-019-0413-3>
- Litwin, I., Pilarczyk, E., & Wysocki, R. (2018). The Emerging Role of Cohesin in the DNA Damage Response. *Genes*, 9(12). <https://doi.org/10.3390/genes9120581>
- Lundin, C., North, M., Erixon, K., Walters, K., Jenssen, D., Goldman, A. S. H., & Helleday, T. (2005). Methyl methanesulfonate (MMS) produces heat-labile DNA damage but no detectable in vivo DNA double-strand breaks. *Nucleic Acids Research*, 33(12), 3799–3811. <https://doi.org/10.1093/nar/gki681>
- Lydeard, J. R., Jain, S., Yamaguchi, M., & Haber, J. E. (2007). Break-induced replication and telomerase-independent telomere maintenance require Pol32. *Nature*, 448(7155), 820–823. <https://doi.org/10.1038/nature06047>
- Machín, F., Torres-Rosell, J., Jarmuz, A., & Aragón, L. (2005). Spindle-independent condensation-mediated segregation of yeast ribosomal DNA in late anaphase. *The Journal of Cell Biology*, 168(2), 209–219. <https://doi.org/10.1083/jcb.200408087>
- Mah, A. S., Jang, J., & Deshaies, R. J. (2001). Protein kinase Cdc15 activates the Dbf2-Mob1 kinase complex. *Proceedings of the National Academy of Sciences of the United States of America*, 98(13), 7325–7330. <https://doi.org/10.1073/pnas.141098998>

166

Este documento incorpora firma electrónica, y es copia auténtica de un documento electrónico archivado por la ULL según la Ley 39/2015.  
Su autenticidad puede ser contrastada en la siguiente dirección <https://sede.ull.es/validacion/>

Identificador del documento: 3075810 Código de verificación: smutbmB+

Firmado por: JESSEL AYRA PLASENCIA  
UNIVERSIDAD DE LA LAGUNA

Fecha: 30/11/2020 12:24:14

María de las Maravillas Aguiar Aguilár  
UNIVERSIDAD DE LA LAGUNA

08/02/2021 13:50:06



6. Cited literature

- Malewicz, M. (2016). The role of 53BP1 protein in homology-directed DNA repair: Things get a bit complicated. *Cell Death & Differentiation*, 23(12), 1902–1903. <https://doi.org/10.1038/cdd.2016.88>
- Malkova, A., Ivanov, E. L., & Haber, J. E. (1996). Double-strand break repair in the absence of RAD51 in yeast: A possible role for break-induced DNA replication. *Proceedings of the National Academy of Sciences of the United States of America*, 93(14), 7131–7136. <https://doi.org/10.1073/pnas.93.14.7131>
- Malkova, Anna, Naylor, M. L., Yamaguchi, M., Ira, G., & Haber, J. E. (2005). RAD51-dependent break-induced replication differs in kinetics and checkpoint responses from RAD51-mediated gene conversion. *Molecular and Cellular Biology*, 25(3), 933–944. <https://doi.org/10.1128/MCB.25.3.933-944.2005>
- Marteijn, J. A., Lans, H., Vermeulen, W., & Hoeijmakers, J. H. J. (2014). Understanding nucleotide excision repair and its roles in cancer and ageing. *Nature Reviews. Molecular Cell Biology*, 15(7), 465–481. <https://doi.org/10.1038/nrm3822>
- Martino, J., Brunette, G. J., Barroso-González, J., Moiseeva, T. N., Smith, C. M., Bakkenist, C. J., O'Sullivan, R. J., & Bernstein, K. A. (2019). The human Shu complex functions with PDS5B and SPIDR to promote homologous recombination. *Nucleic Acids Research*, 47(19), 10151–10165. <https://doi.org/10.1093/nar/gkz738>
- Mason-Osann, E., Terranova, K., Lupo, N., Lock, Y. J., Carson, L. M., & Flynn, R. L. (2020). RAD54 promotes alternative lengthening of telomeres by mediating branch migration. *EMBO Reports*, 21(6), e49495. <https://doi.org/10.15252/embr.201949495>
- Mathiasen, D. P., & Lisby, M. (2014). Cell cycle regulation of homologous recombination in *Saccharomyces cerevisiae*. *FEMS Microbiology Reviews*, 38(2), 172–184. <https://doi.org/10.1111/1574-6976.12066>
- Matsui, Y., Nakayama, Y., Okamoto, M., Fukumoto, Y., & Yamaguchi, N. (2012). Enrichment of cell populations in metaphase, anaphase, and telophase by synchronization using nocodazole and blebbistatin: A novel method suitable for examining dynamic changes in proteins during mitotic progression. *European Journal of Cell Biology*, 91(5), 413–419. <https://doi.org/10.1016/j.ejcb.2011.12.008>
- McEachern, M. J., & Haber, J. E. (2006). Break-induced replication and recombinational telomere elongation in yeast. *Annual Review of Biochemistry*, 75, 111–135. <https://doi.org/10.1146/annurev.biochem.74.082803.133234>
- McIntosh, J. R., & O'Toole, E. T. (1999). Life cycles of yeast spindle pole bodies: Getting microtubules into a closed nucleus. *Biology of the Cell*, 91(4–5), 305–312.
- McMurray, M. A., & Thorner, J. (2009). Septins: Molecular partitioning and the generation of cellular asymmetry. *Cell Division*, 4, 18. <https://doi.org/10.1186/1747-1028-4-18>
- Mehta, A., & Haber, J. E. (2014). Sources of DNA double-strand breaks and models of recombinational DNA repair. *Cold Spring Harbor Perspectives in Biology*, 6(9), a016428. <https://doi.org/10.1101/cshperspect.a016428>
- Meitinger, F., Palani, S., & Pereira, G. (2012). The power of MEN in cytokinesis. *Cell Cycle (Georgetown, Tex.)*, 11(2), 219–228. <https://doi.org/10.4161/cc.11.2.18857>
- Memisoglu, A., & Samson, L. D. (2001). DNA Repair by Reversal of Damage. In *ELS*. American Cancer Society. <https://doi.org/10.1038/npg.els.0000579>

167

Este documento incorpora firma electrónica, y es copia auténtica de un documento electrónico archivado por la ULL según la Ley 39/2015.  
Su autenticidad puede ser contrastada en la siguiente dirección <https://sede.ull.es/validacion/>

Identificador del documento: 3075810 Código de verificación: smutbmB+

Firmado por: JESSEL AYRA PLASENCIA  
UNIVERSIDAD DE LA LAGUNA

Fecha: 30/11/2020 12:24:14

María de las Maravillas Aguiar Aguiar  
UNIVERSIDAD DE LA LAGUNA

08/02/2021 13:50:06

6. Cited literature

- Mendenhall, M. D., & Hodge, A. E. (1998). Regulation of Cdc28 cyclin-dependent protein kinase activity during the cell cycle of the yeast *Saccharomyces cerevisiae*. *Microbiology and Molecular Biology Reviews: MMBR*, 62(4), 1191–1243.
- Mendoza, M., Norden, C., Durrer, K., Rauter, H., Uhlmann, F., & Barral, Y. (2009). A mechanism for chromosome segregation sensing by the NoCut checkpoint. *Nature Cell Biology*, 11(4), 477–483. <https://doi.org/10.1038/ncb1855>
- Michaelis, C., Ciosk, R., & Nasmyth, K. (1997). Cohesins: Chromosomal proteins that prevent premature separation of sister chromatids. *Cell*, 91(1), 35–45. [https://doi.org/10.1016/s0092-8674\(01\)80007-6](https://doi.org/10.1016/s0092-8674(01)80007-6)
- Mimitou, E. P., & Symington, L. S. (2008). Sae2, Exo1 and Sgs1 collaborate in DNA double-strand break processing. *Nature*, 455(7214), 770–774. <https://doi.org/10.1038/nature07312>
- Mimitou, E. P., & Symington, L. S. (2010). Ku prevents Exo1 and Sgs1-dependent resection of DNA ends in the absence of a functional MRX complex or Sae2. *The EMBO Journal*, 29(19), 3358–3369. <https://doi.org/10.1038/emboj.2010.193>
- Miura, T., Yamana, Y., Usui, T., Ogawa, H. I., Yamamoto, M.-T., & Kusano, K. (2012). Homologous Recombination via Synthesis-Dependent Strand Annealing in Yeast Requires the Irc20 and Srs2 DNA Helicases. *Genetics*, 191(1), 65–78. <https://doi.org/10.1534/genetics.112.139105>
- Mohl, D. A., Huddleston, M. J., Collingwood, T. S., Annan, R. S., & Deshaies, R. J. (2009). Dbf2-Mob1 drives relocalization of protein phosphatase Cdc14 to the cytoplasm during exit from mitosis. *The Journal of Cell Biology*, 184(4), 527–539. <https://doi.org/10.1083/jcb.200812022>
- Moore, C. W. (1989). Cleavage of cellular and extracellular *Saccharomyces cerevisiae* DNA by bleomycin and phleomycin. *Cancer Research*, 49(24 Pt 1), 6935–6940.
- Morawska, M., & Ulrich, H. D. (2013). An expanded tool kit for the auxin-inducible degron system in budding yeast. *Yeast (Chichester, England)*, 30(9), 341–351. <https://doi.org/10.1002/yea.2967>
- Murayama, Y., & Uhlmann, F. (2015). DNA Entry into and Exit out of the Cohesin Ring by an Interlocking Gate Mechanism. *Cell*, 163(7), 1628–1640. <https://doi.org/10.1016/j.cell.2015.11.030>
- Murphy, M. R., Fowlkes, D. M., & Fitzgerald-Hayes, M. (1991). Analysis of centromere function in *Saccharomyces cerevisiae* using synthetic centromere mutants. *Chromosoma*, 101(3), 189–197. <https://doi.org/10.1007/BF00355368>
- Musacchio, A., & Hardwick, K. G. (2002). The spindle checkpoint: Structural insights into dynamic signalling. *Nature Reviews. Molecular Cell Biology*, 3(10), 731–741. <https://doi.org/10.1038/nrm929>
- Naiki, T., Wakayama, T., Nakada, D., Matsumoto, K., & Sugimoto, K. (2004). Association of Rad9 with double-strand breaks through a Mec1-dependent mechanism. *Molecular and Cellular Biology*, 24(8), 3277–3285. <https://doi.org/10.1128/mcb.24.8.3277-3285.2004>
- Nasmyth, K. (1993). Control of the yeast cell cycle by the Cdc28 protein kinase. *Current Opinion in Cell Biology*, 5(2), 166–179. [https://doi.org/10.1016/0955-0674\(93\)90099-c](https://doi.org/10.1016/0955-0674(93)90099-c)
- Nasmyth, K., & Dirick, L. (1991). The role of SWI4 and SWI6 in the activity of G1 cyclins in yeast. *Cell*, 66(5), 995–1013. [https://doi.org/10.1016/0092-8674\(91\)90444-4](https://doi.org/10.1016/0092-8674(91)90444-4)
- Nasmyth, Kim, & Haering, C. H. (2009). Cohesin: Its Roles and Mechanisms. *Annual Review of Genetics*, 43(1), 525–558. <https://doi.org/10.1146/annurev-genet-102108-134233>

168

Este documento incorpora firma electrónica, y es copia auténtica de un documento electrónico archivado por la ULL según la Ley 39/2015.  
Su autenticidad puede ser contrastada en la siguiente dirección <https://sede.ull.es/validacion/>

Identificador del documento: 3075810 Código de verificación: smutbmB+

Firmado por: JESSEL AYRA PLASENCIA  
UNIVERSIDAD DE LA LAGUNA

Fecha: 30/11/2020 12:24:14

María de las Maravillas Aguiar Aguiar  
UNIVERSIDAD DE LA LAGUNA

08/02/2021 13:50:06

6. Cited literature

- Neiman, A. M. (2011). Sporulation in the budding yeast *Saccharomyces cerevisiae*. *Genetics*, 189(3), 737–765. <https://doi.org/10.1534/genetics.111.127126>
- Nicolette, M. L., Lee, K., Guo, Z., Rani, M., Chow, J. M., Lee, S. E., & Paull, T. T. (2010). Mre11–Rad50–Xrs2 and Sae2 promote 5' strand resection of DNA double-strand breaks. *Nature Structural & Molecular Biology*, 17(12), 1478–1485. <https://doi.org/10.1038/nsmb.1957>
- Nitiss, J. L. (2009a). DNA topoisomerase II and its growing repertoire of biological functions. *Nature Reviews. Cancer*, 9(5), 327–337. <https://doi.org/10.1038/nrc2608>
- Nitiss, J. L. (2009b). Targeting DNA topoisomerase II in cancer chemotherapy. *Nature Reviews. Cancer*, 9(5), 338–350. <https://doi.org/10.1038/nrc2607>
- Norden, C., Mendoza, M., Dobbelaere, J., Kotwaliwale, C. V., Biggins, S., & Barral, Y. (2006). The NoCut pathway links completion of cytokinesis to spindle midzone function to prevent chromosome breakage. *Cell*, 125(1), 85–98. <https://doi.org/10.1016/j.cell.2006.01.045>
- Ochs, F., Somyajit, K., Altmeyer, M., Rask, M.-B., Lukas, J., & Lukas, C. (2016). 53BP1 fosters fidelity of homology-directed DNA repair. *Nature Structural & Molecular Biology*, 23(8), 714–721. <https://doi.org/10.1038/nsmb.3251>
- Ogas, J., Andrews, B. J., & Herskowitz, I. (1991). Transcriptional activation of CLN1, CLN2, and a putative new G1 cyclin (HCS26) by SWI4, a positive regulator of G1-specific transcription. *Cell*, 66(5), 1015–1026. [https://doi.org/10.1016/0092-8674\(91\)90445-5](https://doi.org/10.1016/0092-8674(91)90445-5)
- Oh, J., Lee, S. J., Rothstein, R., & Symington, L. S. (2018). Xrs2 and Tel1 Independently Contribute to MR-Mediated DNA Tethering and Replisome Stability. *Cell Reports*, 25(7), 1681–1692.e4. <https://doi.org/10.1016/j.celrep.2018.10.030>
- Osborn, A. J., & Elledge, S. J. (2003). Mrc1 is a replication fork component whose phosphorylation in response to DNA replication stress activates Rad53. *Genes & Development*, 17(14), 1755–1767. <https://doi.org/10.1101/gad.1098303>
- O'Shaughnessy, A. M., Grenon, M., Gilbert, C., Toh, G. W.-L., Green, C. M., & Lowndes, N. F. (2006). Multiple approaches to study *S. cerevisiae* Rad9, a prototypical checkpoint protein. *Methods in Enzymology*, 409, 131–150. [https://doi.org/10.1016/S0076-6879\(05\)09008-7](https://doi.org/10.1016/S0076-6879(05)09008-7)
- Ottoz, D. S. M., Rudolf, F., & Stelling, J. (2014). Inducible, tightly regulated and growth condition-independent transcription factor in *Saccharomyces cerevisiae*. *Nucleic Acids Research*, 42(17), e130. <https://doi.org/10.1093/nar/gku616>
- Ouspenski, I. I., Cabello, O. A., & Brinkley, B. R. (2000). Chromosome condensation factor Brn1p is required for chromatid separation in mitosis. *Molecular Biology of the Cell*, 11(4), 1305–1313. <https://doi.org/10.1091/mbc.11.4.1305>
- Palani, S., Meitinger, F., Boehm, M. E., Lehmann, W. D., & Pereira, G. (2012). Cdc14-dependent dephosphorylation of Inn1 contributes to Inn1–Cyk3 complex formation. *Journal of Cell Science*, 125(Pt 13), 3091–3096. <https://doi.org/10.1242/jcs.106021>
- Palmer, R. E., Sullivan, D. S., Huffaker, T., & Koshland, D. (1992). Role of astral microtubules and actin in spindle orientation and migration in the budding yeast, *Saccharomyces cerevisiae*. *The Journal of Cell Biology*, 119(3), 583–593. <https://doi.org/10.1083/jcb.119.3.583>
- Panier, S., & Boulton, S. J. (2014). Double-strand break repair: 53BP1 comes into focus. *Nature Reviews Molecular Cell Biology*, 15(1), 7–18. <https://doi.org/10.1038/nrm3719>

169

Este documento incorpora firma electrónica, y es copia auténtica de un documento electrónico archivado por la ULL según la Ley 39/2015.  
Su autenticidad puede ser contrastada en la siguiente dirección <https://sede.ull.es/validacion/>

Identificador del documento: 3075810 Código de verificación: smutbmB+

Firmado por: JESSEL AYRA PLASENCIA  
UNIVERSIDAD DE LA LAGUNA

Fecha: 30/11/2020 12:24:14

María de las Maravillas Aguiar Aguiar  
UNIVERSIDAD DE LA LAGUNA

08/02/2021 13:50:06

6. Cited literature

- Pâques, F., & Haber, J. E. (1999). Multiple pathways of recombination induced by double-strand breaks in *Saccharomyces cerevisiae*. *Microbiology and Molecular Biology Reviews: MMBR*, 63(2), 349–404.
- Pearson, C. G., Maddox, P. S., Salmon, E. D., & Bloom, K. (2001). Budding yeast chromosome structure and dynamics during mitosis. *The Journal of Cell Biology*, 152(6), 1255–1266. <https://doi.org/10.1083/jcb.152.6.1255>
- Peng, H., Zhang, S., & Chen, X. (2021). Monitoring 5'-End Resection at Site-Specific Double-Strand Breaks by Southern Blot Analysis. *Methods in Molecular Biology (Clifton, N.J.)*, 2196, 245–255. [https://doi.org/10.1007/978-1-0716-0868-5\\_20](https://doi.org/10.1007/978-1-0716-0868-5_20)
- Peters, J.-M., Tedeschi, A., & Schmitz, J. (2008). The cohesin complex and its roles in chromosome biology. *Genes & Development*, 22(22), 3089–3114. <https://doi.org/10.1101/gad.1724308>
- Podhorecka, M., Skladanowski, A., & Bozko, P. (2010). H2AX Phosphorylation: Its Role in DNA Damage Response and Cancer Therapy. *Journal of Nucleic Acids*, 2010. <https://doi.org/10.4061/2010/920161>
- Prinz, S., Hwang, E. S., Visintin, R., & Amon, A. (1998). The regulation of Cdc20 proteolysis reveals a role for APC components Cdc23 and Cdc27 during S phase and early mitosis. *Current Biology: CB*, 8(13), 750–760. [https://doi.org/10.1016/s0960-9822\(98\)70298-2](https://doi.org/10.1016/s0960-9822(98)70298-2)
- Puck, T. T., & Steffen, J. (1963). LIFE CYCLE ANALYSIS OF MAMMALIAN CELLS. I. A METHOD FOR LOCALIZING METABOLIC EVENTS WITHIN THE LIFE CYCLE, AND ITS APPLICATION TO THE ACTION OF COLCEMIDE AND SUBLETHAL DOSES OF X-IRRADIATION. *Biophysical Journal*, 3, 379–397. [https://doi.org/10.1016/s0006-3495\(63\)86828-9](https://doi.org/10.1016/s0006-3495(63)86828-9)
- Pustovalova, M., Grekhova, A., Astrelina, T., Nikitina, V., Dobrovolskaya, E., Suchkova, Y., Kobzeva, I., Usupzhanova, D., Vorobyeva, N., Samoylov, A., Bushmanov, A., Ozerov, I. V., Zhavoronkov, A., Leonov, S., Klokov, D., & Osipov, A. N. (2016). Accumulation of spontaneous  $\gamma$ H2AX foci in long-term cultured mesenchymal stromal cells. *Aging (Albany NY)*, 8(12), 3498–3506. <https://doi.org/10.18632/aging.101142>
- Qi, Z., Redding, S., Lee, J. Y., Gibb, B., Kwon, Y., Niu, H., Gaines, W. A., Sung, P., & Greene, E. C. (2015). DNA sequence alignment by microhomology sampling during homologous recombination. *Cell*, 160(5), 856–869. <https://doi.org/10.1016/j.cell.2015.01.029>
- Queralt, E., Lehane, C., Novak, B., & Uhlmann, F. (2006). Downregulation of PP2A(Cdc55) phosphatase by separase initiates mitotic exit in budding yeast. *Cell*, 125(4), 719–732. <https://doi.org/10.1016/j.cell.2006.03.038>
- Quevedo, O., García-Luis, J., Matos-Perdomo, E., Aragón, L., & Machín, F. (2012). Nondisjunction of a Single Chromosome Leads to Breakage and Activation of DNA Damage Checkpoint in G2. *PLoS Genetics*, 8(2), e1002509. <https://doi.org/10.1371/journal.pgen.1002509>
- Rahal, R., & Amon, A. (2008). The Polo-like kinase Cdc5 interacts with FEAR network components and Cdc14. *Cell Cycle (Georgetown, Tex.)*, 7(20), 3262–3272. <https://doi.org/10.4161/cc.7.20.6852>
- Rao, H., Uhlmann, F., Nasmyth, K., & Varshavsky, A. (2001). Degradation of a cohesin subunit by the N-end rule pathway is essential for chromosome stability. *Nature*, 410(6831), 955–959. <https://doi.org/10.1038/35073627>
- Rauter, H., & Barral, Y. (2006). Cytokinesis goes polo. *Developmental Cell*, 11(2), 136–137. <https://doi.org/10.1016/j.devcel.2006.07.010>

170

Este documento incorpora firma electrónica, y es copia auténtica de un documento electrónico archivado por la ULL según la Ley 39/2015.  
Su autenticidad puede ser contrastada en la siguiente dirección <https://sede.ull.es/validacion/>

Identificador del documento: 3075810 Código de verificación: smutbmB+

Firmado por: JESSEL AYRA PLASENCIA  
UNIVERSIDAD DE LA LAGUNA

Fecha: 30/11/2020 12:24:14

María de las Maravillas Aguiar Aguiar  
UNIVERSIDAD DE LA LAGUNA

08/02/2021 13:50:06

6. Cited literature

- Reardon, J. T., & Sancar, A. (2005). Nucleotide excision repair. *Progress in Nucleic Acid Research and Molecular Biology*, 79, 183–235. [https://doi.org/10.1016/S0079-6603\(04\)79004-2](https://doi.org/10.1016/S0079-6603(04)79004-2)
- Reinders, J., Wagner, K., Zahedi, R. P., Stojanovski, D., Eylich, B., van der Laan, M., Rehling, P., Sickmann, A., Pfanner, N., & Meisinger, C. (2007). Profiling phosphoproteins of yeast mitochondria reveals a role of phosphorylation in assembly of the ATP synthase. *Molecular & Cellular Proteomics: MCP*, 6(11), 1896–1906. <https://doi.org/10.1074/mcp.M700098-MCP200>
- Rocuzzo, M., Visintin, C., Tili, F., & Visintin, R. (2015). FEAR-mediated activation of Cdc14 is the limiting step for spindle elongation and anaphase progression. *Nature Cell Biology*, 17(3), 251–261. <https://doi.org/10.1038/ncb3105>
- Rock, J. M., & Amon, A. (2011). Cdc15 integrates Tem1 GTPase-mediated spatial signals with Polo kinase-mediated temporal cues to activate mitotic exit. *Genes & Development*, 25(18), 1943–1954. <https://doi.org/10.1101/gad.17257711>
- Rozelle, D. K., Hansen, S. D., & Kaplan, K. B. (2011). Chromosome passenger complexes control anaphase duration and spindle elongation via a kinesin-5 brake. *The Journal of Cell Biology*, 193(2), 285–294. <https://doi.org/10.1083/jcb.201011002>
- Rüthnick, D., & Schiebel, E. (2016). Duplication of the Yeast Spindle Pole Body Once per Cell Cycle. *Molecular and Cellular Biology*, 36(9), 1324–1331. <https://doi.org/10.1128/MCB.00048-16>
- Rüthnick, D., & Schiebel, E. (2018). Duplication and Nuclear Envelope Insertion of the Yeast Microtubule Organizing Centre, the Spindle Pole Body. *Cells*, 7(5). <https://doi.org/10.3390/cells7050042>
- Saponaro, M., Callahan, D., Zheng, X., Krejci, L., Haber, J. E., Klein, H. L., & Liberi, G. (2010). Cdk1 targets Srs2 to complete synthesis-dependent strand annealing and to promote recombinational repair. *PLoS Genetics*, 6(2), e1000858. <https://doi.org/10.1371/journal.pgen.1000858>
- Saunders, M., Fitzgerald-Hayes, M., & Bloom, K. (1988). Chromatin structure of altered yeast centromeres. *Proceedings of the National Academy of Sciences of the United States of America*, 85(1), 175–179. <https://doi.org/10.1073/pnas.85.1.175>
- Sazer, S., Lynch, M., & Needleman, D. (2014). Deciphering the Evolutionary History of Open and Closed Mitosis. *Current Biology*, 24(22), R1099–R1103. <https://doi.org/10.1016/j.cub.2014.10.011>
- Scarfone, I., & Piatti, S. (2017). Asymmetric Localization of Components and Regulators of the Mitotic Exit Network at Spindle Pole Bodies. *Methods in Molecular Biology (Clifton, N.J.)*, 1505, 183–193. [https://doi.org/10.1007/978-1-4939-6502-1\\_14](https://doi.org/10.1007/978-1-4939-6502-1_14)
- Schindelin, J., Arganda-Carreras, I., Frise, E., Kaynig, V., Longair, M., Pietzsch, T., Preibisch, S., Rueden, C., Saalfeld, S., Schmid, B., Tinevez, J.-Y., White, D. J., Hartenstein, V., Eliceiri, K., Tomancak, P., & Cardona, A. (2012). Fiji: An open-source platform for biological-image analysis. *Nature Methods*, 9(7), 676–682. <https://doi.org/10.1038/nmeth.2019>
- Schrick, K., Garvik, B., & Hartwell, L. H. (1997). Mating in *Saccharomyces cerevisiae*: The role of the pheromone signal transduction pathway in the chemotropic response to pheromone. *Genetics*, 147(1), 19–32.
- Schwab, M., Lutum, A. S., & Seufert, W. (1997). Yeast Hct1 is a regulator of Clb2 cyclin proteolysis. *Cell*, 90(4), 683–693. [https://doi.org/10.1016/s0092-8674\(00\)80529-2](https://doi.org/10.1016/s0092-8674(00)80529-2)
- Schwob, E., Böhm, T., Mendenhall, M. D., & Nasmyth, K. (1994). The B-type cyclin kinase inhibitor p40SIC1 controls the G1 to S transition in *S. cerevisiae*. *Cell*, 79(2), 233–244. [https://doi.org/10.1016/0092-8674\(94\)90193-7](https://doi.org/10.1016/0092-8674(94)90193-7)

171

Este documento incorpora firma electrónica, y es copia auténtica de un documento electrónico archivado por la ULL según la Ley 39/2015.  
Su autenticidad puede ser contrastada en la siguiente dirección <https://sede.ull.es/validacion/>

Identificador del documento: 3075810 Código de verificación: smutbmB+

Firmado por: JESSEL AYRA PLASENCIA  
UNIVERSIDAD DE LA LAGUNA

Fecha: 30/11/2020 12:24:14

María de las Maravillas Aguiar Aguiar  
UNIVERSIDAD DE LA LAGUNA

08/02/2021 13:50:06

6. Cited literature

- Seeber, A., & Gasser, S. M. (2017). Chromatin organization and dynamics in double-strand break repair. *Current Opinion in Genetics & Development*, 43, 9–16. <https://doi.org/10.1016/j.gde.2016.10.005>
- Segal, M. (2011). Mitotic exit control: A space and time odyssey. *Current Biology: CB*, 21(20), R857–R859. <https://doi.org/10.1016/j.cub.2011.09.023>
- Shapira, O., Goldstein, A., Al-Bassam, J., & Gheber, L. (2017). A potential physiological role for bi-directional motility and motor clustering of mitotic kinesin-5 Cin8 in yeast mitosis. *Journal of Cell Science*, 130(4), 725–734. <https://doi.org/10.1242/jcs.195040>
- Shibata, A. (2017). Regulation of repair pathway choice at two-ended DNA double-strand breaks. *Mutation Research*, 803–805, 51–55. <https://doi.org/10.1016/j.mrfmmm.2017.07.011>
- Shibata, A., Moiani, D., Arvai, A. S., Perry, J., Harding, S. M., Genois, M.-M., Maity, R., van Rossum-Fikkert, S., Kertokallio, A., Romoli, F., Ismail, A., Ismalaj, E., Petricci, E., Neale, M. J., Bristow, R. G., Masson, J.-Y., Wyman, C., Jeggo, P. A., & Tainer, J. A. (2014). DNA double-strand break repair pathway choice is directed by distinct MRE11 nuclease activities. *Molecular Cell*, 53(1), 7–18. <https://doi.org/10.1016/j.molcel.2013.11.003>
- Shim, E. Y., Chung, W.-H., Nicolette, M. L., Zhang, Y., Davis, M., Zhu, Z., Paull, T. T., Ira, G., & Lee, S. E. (2010). Saccharomyces cerevisiae Mre11/Rad50/Xrs2 and Ku proteins regulate association of Exo1 and Dna2 with DNA breaks. *The EMBO Journal*, 29(19), 3370–3380. <https://doi.org/10.1038/emboj.2010.219>
- Sidorova, J., & Breeden, L. (1993). Analysis of the SWI4/SWI6 protein complex, which directs G1/S-specific transcription in Saccharomyces cerevisiae. *Molecular and Cellular Biology*, 13(2), 1069–1077. <https://doi.org/10.1128/mcb.13.2.1069>
- Sikorski, R. S., & Hieter, P. (1989). A system of shuttle vectors and yeast host strains designed for efficient manipulation of DNA in Saccharomyces cerevisiae. *Genetics*, 122(1), 19–27.
- Silverman, J., Takai, H., Buonomo, S. B. C., Eisenhaber, F., & de Lange, T. (2004). Human Rif1, ortholog of a yeast telomeric protein, is regulated by ATM and 53BP1 and functions in the S-phase checkpoint. *Genes & Development*, 18(17), 2108–2119. <https://doi.org/10.1101/gad.1216004>
- Sjögren, C., & Nasmyth, K. (2001). Sister chromatid cohesion is required for postreplicative double-strand break repair in Saccharomyces cerevisiae. *Current Biology: CB*, 11(12), 991–995. [https://doi.org/10.1016/s0960-9822\(01\)00271-8](https://doi.org/10.1016/s0960-9822(01)00271-8)
- Solinger, J. A., Lutz, G., Sugiyama, T., Kowalczykowski, S. C., & Heyer, W. D. (2001). Rad54 protein stimulates heteroduplex DNA formation in the synaptic phase of DNA strand exchange via specific interactions with the presynaptic Rad51 nucleoprotein filament. *Journal of Molecular Biology*, 307(5), 1207–1221. <https://doi.org/10.1006/jmbi.2001.4555>
- Sprague, G. F., Jensen, R., & Herskowitz, I. (1983). Control of yeast cell type by the mating type locus: Positive regulation of the  $\alpha$ -specific STE3 gene by the MAT $\alpha$  1 product. *Cell*, 32(2), 409–415. [https://doi.org/10.1016/0092-8674\(83\)90460-9](https://doi.org/10.1016/0092-8674(83)90460-9)
- Stegmeier, F., & Amon, A. (2004). Closing Mitosis: The Functions of the Cdc14 Phosphatase and Its Regulation. *Annual Review of Genetics*, 38(1), 203–232. <https://doi.org/10.1146/annurev.genet.38.072902.093051>
- Stegmeier, F., Visintin, R., & Amon, A. (2002). Separase, polo kinase, the kinetochore protein Slk19, and Spo12 function in a network that controls Cdc14 localization during early anaphase. *Cell*, 108(2), 207–220. [https://doi.org/10.1016/s0092-8674\(02\)00618-9](https://doi.org/10.1016/s0092-8674(02)00618-9)

172

Este documento incorpora firma electrónica, y es copia auténtica de un documento electrónico archivado por la ULL según la Ley 39/2015.  
Su autenticidad puede ser contrastada en la siguiente dirección <https://sede.ull.es/validacion/>

Identificador del documento: 3075810 Código de verificación: smutbmB+

Firmado por: JESSEL AYRA PLASENCIA  
UNIVERSIDAD DE LA LAGUNA

Fecha: 30/11/2020 12:24:14

María de las Maravillas Aguiar Aguiar  
UNIVERSIDAD DE LA LAGUNA

08/02/2021 13:50:06

6. Cited literature

- Stephan, H., Concannon, C., Kremmer, E., Carty, M. P., & Nasheuer, H.-P. (2009). Ionizing radiation-dependent and independent phosphorylation of the 32-kDa subunit of replication protein A during mitosis. *Nucleic Acids Research*, 37(18), 6028–6041. <https://doi.org/10.1093/nar/gkp605>
- Strathern, J. N., Klar, A. J. S., Hicks, J. B., Abraham, J. A., Ivy, J. M., Nasmyth, K. A., & McGill, C. (1982). Homothallic switching of yeast mating type cassettes is initiated by a double-stranded cut in the MAT locus. *Cell*, 31(1), 183–192. [https://doi.org/10.1016/0092-8674\(82\)90418-4](https://doi.org/10.1016/0092-8674(82)90418-4)
- Ström, L., Karlsson, C., Lindroos, H. B., Wedahl, S., Katou, Y., Shirahige, K., & Sjögren, C. (2007). Postreplicative formation of cohesion is required for repair and induced by a single DNA break. *Science (New York, N.Y.)*, 317(5835), 242–245. <https://doi.org/10.1126/science.1140649>
- Ström, L., Lindroos, H. B., Shirahige, K., & Sjögren, C. (2004). Postreplicative recruitment of cohesin to double-strand breaks is required for DNA repair. *Molecular Cell*, 16(6), 1003–1015. <https://doi.org/10.1016/j.molcel.2004.11.026>
- Strunnikov, A. V., Hogan, E., & Koshland, D. (1995). SMC2, a *Saccharomyces cerevisiae* gene essential for chromosome segregation and condensation, defines a subgroup within the SMC family. *Genes & Development*, 9(5), 587–599. <https://doi.org/10.1101/gad.9.5.587>
- Strunnikov, A. V., Larionov, V. L., & Koshland, D. (1993). SMC1: An essential yeast gene encoding a putative head-rod-tail protein is required for nuclear division and defines a new ubiquitous protein family. *The Journal of Cell Biology*, 123(6 Pt 2), 1635–1648. <https://doi.org/10.1083/jcb.123.6.1635>
- Sullivan, M., & Uhlmann, F. (2003). A non-proteolytic function of separase links the onset of anaphase to mitotic exit. *Nature Cell Biology*, 5(3), 249–254. <https://doi.org/10.1038/ncb940>
- Sung, P., Trujillo, K. M., & Van Komen, S. (2000). Recombination factors of *Saccharomyces cerevisiae*. *Mutation Research*, 451(1–2), 257–275. [https://doi.org/10.1016/s0027-5107\(00\)00054-3](https://doi.org/10.1016/s0027-5107(00)00054-3)
- Surana, U., Amon, A., Dowzer, C., McGrew, J., Byers, B., & Nasmyth, K. (1993). Destruction of the CDC28/CLB mitotic kinase is not required for the metaphase to anaphase transition in budding yeast. *The EMBO Journal*, 12(5), 1969–1978.
- Symington, L. S. (2016). Mechanism and regulation of DNA end resection in eukaryotes. *Critical Reviews in Biochemistry and Molecular Biology*, 51(3), 195–212. <https://doi.org/10.3109/10409238.2016.1172552>
- Symington, L. S., Rothstein, R., & Lisby, M. (2014). Mechanisms and regulation of mitotic recombination in *Saccharomyces cerevisiae*. *Genetics*, 198(3), 795–835. <https://doi.org/10.1534/genetics.114.166140>
- Taddei, A., Hediger, F., Neumann, F. R., Bauer, C., & Gasser, S. M. (2004). Separation of silencing from perinuclear anchoring functions in yeast Ku80, Sir4 and Esc1 proteins. *The EMBO Journal*, 23(6), 1301–1312. <https://doi.org/10.1038/sj.emboj.7600144>
- Tanaka, T. U. (2010). Kinetochore-microtubule interactions: Steps towards bi-orientation. *The EMBO Journal*, 29(24), 4070–4082. <https://doi.org/10.1038/emboj.2010.294>
- Tanaka, T. U., Stark, M. J. R., & Tanaka, K. (2005). Kinetochore capture and bi-orientation on the mitotic spindle. *Nature Reviews. Molecular Cell Biology*, 6(12), 929–942. <https://doi.org/10.1038/nrm1764>
- Teng, S. C., Chang, J., McCowan, B., & Zakian, V. A. (2000). Telomerase-independent lengthening of yeast telomeres occurs by an abrupt Rad50p-dependent, Rif-inhibited recombinational process. *Molecular Cell*, 6(4), 947–952. [https://doi.org/10.1016/s1097-2765\(05\)00094-8](https://doi.org/10.1016/s1097-2765(05)00094-8)

173

Este documento incorpora firma electrónica, y es copia auténtica de un documento electrónico archivado por la ULL según la Ley 39/2015.  
Su autenticidad puede ser contrastada en la siguiente dirección <https://sede.ull.es/validacion/>

Identificador del documento: 3075810 Código de verificación: smutbmB+

Firmado por: JESSEL AYRA PLASENCIA  
UNIVERSIDAD DE LA LAGUNA

Fecha: 30/11/2020 12:24:14

María de las Maravillas Aguiar Aguiar  
UNIVERSIDAD DE LA LAGUNA

08/02/2021 13:50:06

6. Cited literature

- Thomas, B. J., & Rothstein, R. (1989). The genetic control of direct-repeat recombination in *Saccharomyces*: The effect of *rad52* and *rad1* on mitotic recombination at *GAL10*, a transcriptionally regulated gene. *Genetics*, 123(4), 725–738.
- Thompson, D. A., & Stahl, F. W. (1999). Genetic control of recombination partner preference in yeast meiosis. Isolation and characterization of mutants elevated for meiotic unequal sister-chromatid recombination. *Genetics*, 153(2), 621–641.
- Torres-Rosell, J., Machin, F., & Aragón, L. (2005). Smc5-Smc6 complex preserves nucleolar integrity in *S. cerevisiae*. *Cell Cycle (Georgetown, Tex.)*, 4(7), 868–872. <https://doi.org/10.4161/cc.4.7.1825>
- Torres-Rosell, J., Machín, F., Farmer, S., Jarmuz, A., Eydmann, T., Dalgaard, J. Z., & Aragón, L. (2005). SMC5 and SMC6 genes are required for the segregation of repetitive chromosome regions. *Nature Cell Biology*, 7(4), 412–419. <https://doi.org/10.1038/ncb1239>
- Uhlmann, F., Lottspeich, F., & Nasmyth, K. (1999). Sister-chromatid separation at anaphase onset is promoted by cleavage of the cohesin subunit *Scc1*. *Nature*, 400(6739), 37–42. <https://doi.org/10.1038/21831>
- Uhlmann, Frank, Wernic, D., Poupard, M.-A., Koonin, E. V., & Nasmyth, K. (2000). Cleavage of Cohesin by the CD Clan Protease Separin Triggers Anaphase in Yeast. *Cell*, 103(3), 375–386. [https://doi.org/10.1016/S0092-8674\(00\)00130-6](https://doi.org/10.1016/S0092-8674(00)00130-6)
- Unal, E., Arbel-Eden, A., Sattler, U., Shroff, R., Lichten, M., Haber, J. E., & Koshland, D. (2004). DNA damage response pathway uses histone modification to assemble a double-strand break-specific cohesin domain. *Molecular Cell*, 16(6), 991–1002. <https://doi.org/10.1016/j.molcel.2004.11.027>
- Unal, E., Heidinger-Pauli, J. M., & Koshland, D. (2007). DNA double-strand breaks trigger genome-wide sister-chromatid cohesion through *Eco1* (*Ctf7*). *Science (New York, N. Y.)*, 317(5835), 245–248. <https://doi.org/10.1126/science.1140637>
- Van Komen, S., Petukhova, G., Sigurdsson, S., Stratton, S., & Sung, P. (2000). Superhelicity-driven homologous DNA pairing by yeast recombination factors *Rad51* and *Rad54*. *Molecular Cell*, 6(3), 563–572. [https://doi.org/10.1016/s1097-2765\(00\)00055-1](https://doi.org/10.1016/s1097-2765(00)00055-1)
- Varela, E., Shimada, K., Laroche, T., Leroy, D., & Gasser, S. M. (2009). *Lte1*, *Cdc14* and MEN-controlled Cdk inactivation in yeast coordinate rDNA decompaction with late telophase progression. *The EMBO Journal*, 28(11), 1562–1575. <https://doi.org/10.1038/emboj.2009.111>
- Vas, A. C. J., Andrews, C. A., Kirkland Matesky, K., & Clarke, D. J. (2007). In vivo analysis of chromosome condensation in *Saccharomyces cerevisiae*. *Molecular Biology of the Cell*, 18(2), 557–568. <https://doi.org/10.1091/mbc.e06-05-0454>
- Visintin, C., Tomson, B. N., Rahal, R., Paulson, J., Cohen, M., Taunton, J., Amon, A., & Visintin, R. (2008). APC/C-Cdh1-mediated degradation of the Polo kinase *Cdc5* promotes the return of *Cdc14* into the nucleolus. *Genes & Development*, 22(1), 79–90. <https://doi.org/10.1101/gad.1601308>
- Visintin, R., Craig, K., Hwang, E. S., Prinz, S., Tyers, M., & Amon, A. (1998). The phosphatase *Cdc14* triggers mitotic exit by reversal of Cdk-dependent phosphorylation. *Molecular Cell*, 2(6), 709–718. [https://doi.org/10.1016/s1097-2765\(00\)80286-5](https://doi.org/10.1016/s1097-2765(00)80286-5)
- Visintin, R., Hwang, E. S., & Amon, A. (1999). *Cfi1* prevents premature exit from mitosis by anchoring *Cdc14* phosphatase in the nucleolus. *Nature*, 398(6730), 818–823. <https://doi.org/10.1038/19775>

174

Este documento incorpora firma electrónica, y es copia auténtica de un documento electrónico archivado por la ULL según la Ley 39/2015.  
Su autenticidad puede ser contrastada en la siguiente dirección <https://sede.ull.es/validacion/>

Identificador del documento: 3075810 Código de verificación: smutbmB+

Firmado por: JESSEL AYRA PLASENCIA  
UNIVERSIDAD DE LA LAGUNA

Fecha: 30/11/2020 12:24:14

María de las Maravillas Aguiar Aguiar  
UNIVERSIDAD DE LA LAGUNA

08/02/2021 13:50:06



6. Cited literature

- Wang, B.-D., Butylin, P., & Strunnikov, A. (2006). Condensin function in mitotic nucleolar segregation is regulated by rDNA transcription. *Cell Cycle (Georgetown, Tex.)*, 5(19), 2260–2267. <https://doi.org/10.4161/cc.5.19.3292>
- Wang, B.-D., Yong-Gonzalez, V., & Strunnikov, A. V. (2004). Cdc14p/FEAR pathway controls segregation of nucleolus in *S. cerevisiae* by facilitating condensin targeting to rDNA chromatin in anaphase. *Cell Cycle (Georgetown, Tex.)*, 3(7), 960–967. <https://doi.org/10.4161/cc.3.7.1003>
- Wang, H., & Xu, X. (2017). Microhomology-mediated end joining: New players join the team. *Cell & Bioscience*, 7(1), 6. <https://doi.org/10.1186/s13578-017-0136-8>
- Wee, P., & Wang, Z. (2017). Cell Cycle Synchronization of HeLa Cells to Assay EGFR Pathway Activation. In Z. Wang (Ed.), *ErbB Receptor Signaling: Methods and Protocols* (pp. 167–181). Springer. [https://doi.org/10.1007/978-1-4939-7219-7\\_13](https://doi.org/10.1007/978-1-4939-7219-7_13)
- Weinert, T. A., & Hartwell, L. H. (1988). The RAD9 gene controls the cell cycle response to DNA damage in *Saccharomyces cerevisiae*. *Science (New York, N.Y.)*, 241(4863), 317–322. <https://doi.org/10.1126/science.3291120>
- Weinert, T. A., & Hartwell, L. H. (1990). Characterization of RAD9 of *Saccharomyces cerevisiae* and evidence that its function acts posttranslationally in cell cycle arrest after DNA damage. *Molecular and Cellular Biology*, 10(12), 6554–6564. <https://doi.org/10.1128/mcb.10.12.6554>
- Weinert, T., & Hartwell, L. (1989). Control of G2 delay by the rad9 gene of *Saccharomyces cerevisiae*. *Journal of Cell Science. Supplement*, 12, 145–148. [https://doi.org/10.1242/jcs.1989.supplement\\_12.12](https://doi.org/10.1242/jcs.1989.supplement_12.12)
- Winey, M., & Bloom, K. (2012). Mitotic spindle form and function. *Genetics*, 190(4), 1197–1224. <https://doi.org/10.1534/genetics.111.128710>
- Wright, W. D., Shah, S. S., & Heyer, W.-D. (2018). Homologous recombination and the repair of DNA double-strand breaks. *The Journal of Biological Chemistry*, 293(27), 10524–10535. <https://doi.org/10.1074/jbc.TM118.000372>
- Yamaguchi, M., & Haber, J. E. (2021). Monitoring Gene Conversion in Budding Yeast by Southern Blot Analysis. *Methods in Molecular Biology (Clifton, N.J.)*, 2153, 221–238. [https://doi.org/10.1007/978-1-0716-0644-5\\_16](https://doi.org/10.1007/978-1-0716-0644-5_16)
- Yamamoto, A., Guacci, V., & Koshland, D. (1996a). Pds1p, an inhibitor of anaphase in budding yeast, plays a critical role in the APC and checkpoint pathway(s). *The Journal of Cell Biology*, 133(1), 99–110. <https://doi.org/10.1083/jcb.133.1.99>
- Yamamoto, A., Guacci, V., & Koshland, D. (1996b). Pds1p is required for faithful execution of anaphase in the yeast, *Saccharomyces cerevisiae*. *The Journal of Cell Biology*, 133(1), 85–97. <https://doi.org/10.1083/jcb.133.1.85>
- Yan, Z., Xue, C., Kumar, S., Crickard, J. B., Yu, Y., Wang, W., Pham, N., Li, Y., Niu, H., Sung, P., Greene, E. C., & Ira, G. (2019). Rad52 Restrains Resection at DNA Double-Strand Break Ends in Yeast. *Molecular Cell*, 76(5), 699–711.e6. <https://doi.org/10.1016/j.molcel.2019.08.017>
- Yang, S. S., Yeh, E., Salmon, E. D., & Bloom, K. (1997). Identification of a mid-anaphase checkpoint in budding yeast. *The Journal of Cell Biology*, 136(2), 345–354. <https://doi.org/10.1083/jcb.136.2.345>
- Yi, C., & He, C. (2013). DNA repair by reversal of DNA damage. *Cold Spring Harbor Perspectives in Biology*, 5(1), a012575. <https://doi.org/10.1101/cshperspect.a012575>

175

Este documento incorpora firma electrónica, y es copia auténtica de un documento electrónico archivado por la ULL según la Ley 39/2015.  
Su autenticidad puede ser contrastada en la siguiente dirección <https://sede.ull.es/validacion/>

Identificador del documento: 3075810 Código de verificación: smutbmB+

Firmado por: JESSEL AYRA PLASENCIA  
UNIVERSIDAD DE LA LAGUNA

Fecha: 30/11/2020 12:24:14

María de las Maravillas Aguiar Aguiar  
UNIVERSIDAD DE LA LAGUNA

08/02/2021 13:50:06

6. Cited literature

---

- Yoshida, S., Asakawa, K., & Toh-e, A. (2002). Mitotic exit network controls the localization of Cdc14 to the spindle pole body in *Saccharomyces cerevisiae*. *Current Biology: CB*, 12(11), 944–950. [https://doi.org/10.1016/s0960-9822\(02\)00870-9](https://doi.org/10.1016/s0960-9822(02)00870-9)
- Yoshida, S., Ichihashi, R., & Toh-e, A. (2003). Ras recruits mitotic exit regulator Lte1 to the bud cortex in budding yeast. *The Journal of Cell Biology*, 161(5), 889–897. <https://doi.org/10.1083/jcb.200301128>
- Yoshida, S., Kono, K., Lowery, D. M., Bartolini, S., Yaffe, M. B., Ohya, Y., & Pellman, D. (2006). Polo-like kinase Cdc5 controls the local activation of Rho1 to promote cytokinesis. *Science (New York, N.Y.)*, 313(5783), 108–111. <https://doi.org/10.1126/science.1126747>
- Yu, T.-Y., Kimble, M. T., & Symington, L. S. (2018). Sae2 antagonizes Rad9 accumulation at DNA double-strand breaks to attenuate checkpoint signaling and facilitate end resection. *Proceedings of the National Academy of Sciences*, 115(51), E11961–E11969. <https://doi.org/10.1073/pnas.1816539115>
- Yun, H., & Kim, K. (2019). Ku complex suppresses recombination in the absence of MRX activity during budding yeast meiosis. *BMB Reports*, 52(10), 607–612.
- Zhu, Z., Chung, W.-H., Shim, E. Y., Lee, S. E., & Ira, G. (2008). Sgs1 helicase and two nucleases Dna2 and Exo1 resect DNA double-strand break ends. *Cell*, 134(6), 981–994. <https://doi.org/10.1016/j.cell.2008.08.037>
- Zierhut, C., & Diffley, J. F. X. (2008). Break dosage, cell cycle stage and DNA replication influence DNA double strand break response. *The EMBO Journal*, 27(13), 1875–1885. <https://doi.org/10.1038/emboj.2008.111>

Este documento incorpora firma electrónica, y es copia auténtica de un documento electrónico archivado por la ULL según la Ley 39/2015.  
Su autenticidad puede ser contrastada en la siguiente dirección <https://sede.ull.es/validacion/>

Identificador del documento: 3075810 Código de verificación: smutbmB+

Firmado por: JESSEL AYRA PLASENCIA  
UNIVERSIDAD DE LA LAGUNA

Fecha: 30/11/2020 12:24:14

María de las Maravillas Aguiar Aguiar  
UNIVERSIDAD DE LA LAGUNA

08/02/2021 13:50:06



# Appendix I. Proteomics Mass Spectrometry

Este documento incorpora firma electrónica, y es copia auténtica de un documento electrónico archivado por la ULL según la Ley 39/2015.  
Su autenticidad puede ser contrastada en la siguiente dirección <https://sede.ull.es/validacion/>

Identificador del documento: 3075810 Código de verificación: smutbmB+

Firmado por: JESSEL AYRA PLASENCIA  
UNIVERSIDAD DE LA LAGUNA

Fecha: 30/11/2020 12:24:14

María de las Maravillas Aguiar Aguiar  
UNIVERSIDAD DE LA LAGUNA

08/02/2021 13:50:06



Este documento incorpora firma electrónica, y es copia auténtica de un documento electrónico archivado por la ULL según la Ley 39/2015.  
*Su autenticidad puede ser contrastada en la siguiente dirección <https://sede.ull.es/validacion/>*

Identificador del documento: 3075810      Código de verificación: smutbmB+

Firmado por: JESSEL AYRA PLASENCIA  
UNIVERSIDAD DE LA LAGUNA

Fecha: 30/11/2020 12:24:14

María de las Maravillas Aguiar Aguiar  
UNIVERSIDAD DE LA LAGUNA

08/02/2021 13:50:06

## Proteomics Mass Spectrometry Results

- **G<sub>2</sub>-Control (Downregulated proteins with HO-mediated DSB):**
  - **Sur7:** Plasma membrane protein, component of eisosomes; long-lived protein that remains stable in eisosomes of mother cells while other eisosome proteins, Pil1p and Lsp1p, turn over; may function to anchor the eisosome in place; sporulation and plasma membrane sphingolipid content are altered in mutants; localizes to furrow-like invaginations (MCC patches).
  - **Rlp24:** Essential protein required for ribosomal large subunit biogenesis; associated with pre-60S ribosomal subunits; stimulates the ATPase activity of Afg2p, which is required for release of Rlp24p from the pre-60S particle; has similarity to Rpl24Ap and Rpl24Bp.
  - **Rpb9:** RNA polymerase II subunit B12.6; contacts DNA; mutations affect transcription start site selection and fidelity of transcription.
- **G<sub>2</sub>-HO (Upregulated proteins with HO-mediated DSB):**
  - **Xbp1:** Transcriptional repressor; binds promoter sequences of cyclin genes, CYS3, and SMF2; not expressed during log phase of growth, but induced by stress or starvation during mitosis, and late in meiosis; represses 15% of all yeast genes as cells transition to quiescence; important for maintaining G1 arrest and for longevity of quiescent cells; member of Swi4p/Mbp1p family; phosphorylated by Cdc28p; relative distribution to nucleus increases upon DNA replication stress.
  - **Put1:** Proline oxidase; nuclear-encoded mitochondrial protein involved in utilization of proline as sole nitrogen source; PUT1 transcription is induced by Put3p in the presence of proline and the absence of a preferred nitrogen source.
  - **HO:** Site-specific endonuclease; required for gene conversion at the MAT locus (homothallic switching) through the generation of a dsDNA break; expression restricted to mother cells in late G1 as controlled by Swi4p-Swi6p, Swi5p, and Ash1p.
  - **Bar1:** Aspartyl protease; secreted into the periplasmic space of mating type a cell; helps cells find mating partners; cleaves and inactivates alpha factor allowing cells to recover from alpha-factor-induced cell cycle arrest.
  - **Pet20:** Mitochondrial protein; required for respiratory growth under some conditions and for stability of the mitochondrial genome.
  - **YHR033W:** Putative protein of unknown function; epitope-tagged protein localizes to the cytoplasm; YHR033W has a paralog, PRO1, that arose from the whole genome duplication.
- **G<sub>2</sub>-Control (Downregulated proteins with Phleomycin-mediated DSB):**
  - **Erg24:** C-14 sterol reductase; acts in ergosterol biosynthesis; mutants accumulate the abnormal sterol ignosterol (ergosta-8,14 dienol), and are viable under anaerobic growth conditions but inviable on rich medium under aerobic conditions.

Este documento incorpora firma electrónica, y es copia auténtica de un documento electrónico archivado por la ULL según la Ley 39/2015.  
Su autenticidad puede ser contrastada en la siguiente dirección <https://sede.ull.es/validacion/>

Identificador del documento: 3075810 Código de verificación: smutbmB+

Firmado por: JESSEL AYRA PLASENCIA  
UNIVERSIDAD DE LA LAGUNA

Fecha: 30/11/2020 12:24:14

María de las Maravillas Aguiar Aguiar  
UNIVERSIDAD DE LA LAGUNA

08/02/2021 13:50:06

Appendix I

- **Hpr1**: Subunit of THO/TREX complexes; this complex couple transcription elongation with mitotic recombination and with mRNA metabolism and export, subunit of an RNA Pol II complex; regulates lifespan; involved in telomere maintenance; similar to Top1p.
- **Trm11**: Catalytic subunit of adoMet-dependent tRNA methyltransferase complex; required for the methylation of the guanosine nucleotide at position 10 (m2G10) in tRNAs; contains a THUMP domain and a methyltransferase domain; another complex member is Trm112p.
- **Kin4**: Serine/threonine protein kinase; inhibits the mitotic exit network (MEN) when the spindle position checkpoint is activated; localized asymmetrically to mother cell cortex, spindle pole body and bud neck; KIN4 has a paralog, FRK1, that arose from the whole genome duplication.
- **Ng1**: Putative endonuclease; has a domain similar to a magnesiumdependent endonuclease motif in mRNA deadenylase Ccr4p; the authentic, non-tagged protein is detected in highly purified mitochondria in high-throughput studies.
- **YML020W**: Putative protein of unknown function.
- **G2-Phleomycin (Upregulated proteins with Phleomycin-mediated DSB):**
  - **Rim4**: Putative RNA-binding protein; required for the expression of early and middle sporulation genes.
  - **Atg19**: Receptor protein for the cytoplasm-to-vacuole targeting (Cvt) pathway; delivers cargo proteins aminopeptidase I (Ape1p) and alphanmannosidase (Ams1p) to the phagophore assembly site for packaging into Cvt vesicles; interaction with Atg19p during the Cvt pathway requires phosphorylation by Hrr25p.
  - **Tsl1**: Large subunit of trehalose 6-phosphate synthase/phosphatase complex; Tps1p-Tps2p complex converts uridine-5'-diphosphoglucose and glucose 6-phosphate to trehalose; contributes to survival to acute lethal heat stress; mutant has aneuploidy tolerance; protein abundance increases in response to DNA replication stress; TSL1 has a paralog, TPS3, that arose from the whole genome duplication.
- **Tel-Control (Downregulated proteins with HO-mediated DSB):**
  - **Sam35**: Component of the sorting and assembly machinery (SAM) complex; the SAM (or TOB) complex is located in the mitochondrial outer membrane; the complex binds precursors of beta-barrel proteins and facilitates their insertion into the outer membrane.
  - **Dot1**: Nucleosomal histone H3-Lys79 methylase; methylation is required for telomeric silencing, meiotic checkpoint control, and DNA damage response.
  - **Gly1**: Threonine aldolase; catalyzes the cleavage of L-allo-threonine and L-threonine to glycine; involved in glycine biosynthesis.
  - **Rrp14**: Essential protein, constituent of 66S pre-ribosomal particles; interacts with proteins involved in ribosomal biogenesis and cell polarity; member of the SURF-6 family.

180

Este documento incorpora firma electrónica, y es copia auténtica de un documento electrónico archivado por la ULL según la Ley 39/2015.  
Su autenticidad puede ser contrastada en la siguiente dirección <https://sede.ull.es/validacion/>

Identificador del documento: 3075810 Código de verificación: smutbmB+

Firmado por: JESSEL AYRA PLASENCIA  
UNIVERSIDAD DE LA LAGUNA

Fecha: 30/11/2020 12:24:14

María de las Maravillas Aguiar Aguiar  
UNIVERSIDAD DE LA LAGUNA

08/02/2021 13:50:06

- **Vps36**: Component of the ESCRT-II complex; contains the GLUE (GRAM Like Ubiquitin binding in EAP45) domain which is involved in interactions with ESCRT-I and ubiquitin-dependent sorting of proteins into the endosome; plays a role in the formation of mutant huntingtin (Htt) aggregates in yeast.
- **Vps51**: Component of the GARP (Golgi-associated retrograde protein) complex; GARP is required for the recycling of proteins from endosomes to the late Golgi, and for mitosis after DNA damage induced checkpoint arrest; links the (VFT/GARP) complex to the SNARE Tlg1p; members of the GARP complex are Vps51p-Vps52p-Vps53p-Vps54p.
- **Tel-HO (Upregulated proteins with HO-mediated DSB):**
  - **Snz2**: Protein involved in thiamine and pyridoxine biosynthesis; member of a stationary phase-induced gene family where transcriptional induction precedes the diauxic shift; induced in the absence of thiamine in a Thi2/3pdependent manner and repressed in its presence; forms a co-regulated gene pair with SNO2; interacts with Thi11p; paralog of SNZ1 and SNZ3.
  - **Snz3**: Pyridoxal-5'-phosphate synthase; involved in thiamine and pyridoxine biosynthesis; member of a stationary phase-induced gene family where transcriptional induction precedes the diauxic shift; induced in the absence of thiamine in a Thi2/3p-dependent manner and repressed in its presence; forms a co-regulated gene pair with SNO3; paralog of SNZ1 and SNZ2.
  - **Tfs1**: Inhibitor of carboxypeptidase Y (Prc1p), and Ras GAP (Ira2p); phosphatidylethanolamine-binding protein (PEBP) family member and ortholog of hPEBP1/RKIP, a natural metastasis suppressor; targets to vacuolar membranes during stationary phase; acetylated by NatB N-terminal acetyltransferase; protein abundance increases in response to DNA replication stress.
  - **Gph1**: Glycogen phosphorylase required for the mobilization of glycogen; non-essential; regulated by cyclic AMP-mediated phosphorylation; phosphorylation by Cdc28p may coordinately regulate carbohydrate metabolism and the cell cycle; expression is regulated by stress-response elements and by the HOG MAP kinase pathway.
  - **Gnd2**: 6-phosphogluconate dehydrogenase (decarboxylating); catalyzes an NADPH regenerating reaction in the pentose phosphate pathway; required for growth on D-glucono-delta-lactone; GND2 has a paralog, GND1, that arose from the whole genome duplication.
  - **YOL036W**: Protein of unknown function; potential Cdc28p substrate; YOL036W has a paralog, YIR016W, that arose from the whole genome duplication. (YIR016W: Putative protein of unknown function; expression directly regulated by the metabolic and meiotic transcriptional regulator of Ume6p; overexpression causes a cell cycle delay or arrest; non-essential gene; YIR016W has a paralog, YOL036W, that arose from the whole genome duplication).
  - **Gdb21**: Glycogen debranching enzyme; contains glucanotranferase and alpha-1,6-amyloglucosidase activities; required for glycogen degradation; phosphorylated in

Este documento incorpora firma electrónica, y es copia auténtica de un documento electrónico archivado por la ULL según la Ley 39/2015.  
Su autenticidad puede ser contrastada en la siguiente dirección <https://sede.ull.es/validacion/>

Identificador del documento: 3075810 Código de verificación: smutbmB+

Firmado por: JESSEL AYRA PLASENCIA  
UNIVERSIDAD DE LA LAGUNA

Fecha: 30/11/2020 12:24:14

María de las Maravillas Aguiar Aguiar  
UNIVERSIDAD DE LA LAGUNA

08/02/2021 13:50:06

Appendix I

mitochondria; activity is inhibited by Igd1p; protein abundance increases in response to DNA replication stress.

- **Xbp1**: Transcriptional repressor; binds promoter sequences of cyclin genes, CYS3, and SMF2; not expressed during log phase of growth, but induced by stress or starvation during mitosis, and late in meiosis; represses 15% of all yeast genes as cells transition to quiescence; important for maintaining G1 arrest and for longevity of quiescent cells; member of Swi4p/Mbp1p family; phosphorylated by Cdc28p; relative distribution to nucleus increases upon DNA replication stress.
- **Gtb1**: Glucosidase II beta subunit, forms a complex with alpha subunit Rot2p; involved in removal of two glucose residues from N-linked glycans during glycoprotein biogenesis in the ER; relocalizes from ER to cytoplasm upon DNA replication stress.
- **Thi6**: Thiamine-phosphate diphosphorylase and hydroxyethylthiazole kinase; required for thiamine biosynthesis; GFP-fusion protein localizes to the cytoplasm in a punctate pattern.
- **Bar1**: Aspartyl protease; secreted into the periplasmic space of mating type a cell; helps cells find mating partners; cleaves and inactivates alpha factor allowing cells to recover from alpha-factor-induced cell cycle arrest.
- **Yor1**: Plasma membrane ATP-binding cassette (ABC) transporter; multidrug transporter mediates export of many different organic anions including oligomycin; homolog of human cystic fibrosis transmembrane receptor (CFTR).
- **Thi20**: Trifunctional enzyme of thiamine biosynthesis, degradation and salvage; has hydroxymethylpyrimidine (HMP) kinase, HMP-phosphate (HMP-P) kinase and thiaminase activities; member of a gene family with THI21 and THI22; HMP and HMP-P kinase activity redundant with Thi21p.
- **Thi21**: Hydroxymethylpyrimidine (HMP) and HMP-phosphate kinase; involved in thiamine biosynthesis; member of a gene family with THI20 and THI22; functionally redundant with Thi20p.
- **Thi22**: Protein with similarity to hydroxymethylpyrimidine phosphate kinases; member of a gene family with THI20 and THI21; not required for thiamine biosynthesis; SWAT-GFP and mCherry fusion proteins localize to the endoplasmic reticulum and vacuole respectively.
- **Msc1**: Protein of unknown function; mutant is defective in directing meiotic recombination events to homologous chromatids; the authentic, nontagged protein is detected in highly purified mitochondria and is phosphorylated.
- **Put1**: Proline oxidase; nuclear-encoded mitochondrial protein involved in utilization of proline as sole nitrogen source; PUT1 transcription is induced by Put3p in the presence of proline and the absence of a preferred nitrogen source.
- **Atg26**: UDP-glucose:sterol glucosyltransferase; conserved enzyme involved in synthesis of sterol glucoside membrane lipids; in contrast to ATG26 from *P. pastoris*, *S. cerevisiae* ATG26 is not involved in autophagy.
- **YPR172W**: Protein of unknown function; predicted to encode a pyridoxal 5'-phosphate synthase based on sequence similarity but purified protein does not possess this activity, nor does it bind flavin mononucleotide (FMN); transcriptionally activated by

182

Este documento incorpora firma electrónica, y es copia auténtica de un documento electrónico archivado por la ULL según la Ley 39/2015.  
 Su autenticidad puede ser contrastada en la siguiente dirección <https://sede.ull.es/validacion/>

Identificador del documento: 3075810 Código de verificación: smutbmB+

Firmado por: JESSEL AYRA PLASENCIA  
 UNIVERSIDAD DE LA LAGUNA

Fecha: 30/11/2020 12:24:14

María de las Maravillas Aguiar Aguiar  
 UNIVERSIDAD DE LA LAGUNA

08/02/2021 13:50:06



Yrm1p along with genes involved in multidrug resistance; YPR172W has a paralog, YLR456W, that arose from the whole genome duplication.

- **Ura10**: Minor orotate phosphoribosyltransferase (OPRTase) isozyme; catalyzes the fifth enzymatic step in the de novo biosynthesis of pyrimidines, converting orotate into orotidine-5'-phosphate; URA10 has a paralog, URA5, that arose from the whole genome duplication.
- **YHR033W**: Putative protein of unknown function; epitope-tagged protein localizes to the cytoplasm; YHR033W has a paralog, PRO1, that arose from the whole genome duplication. (PRO1: Gamma-glutamyl kinase; catalyzes the first step in proline biosynthesis; required for nitrogen starvation-induced ribophagy but not for nonselective autophagy; PRO1 has a paralog, YHR033W, that arose from the whole genome duplication).
- **Tel-Control (Downregulated proteins with Phleomycin-mediated DSB):**
  - **Grx7**: Cis-golgi localized monothiol glutaredoxin; more similar in activity to dithiol than other monothiol glutaredoxins; involved in the oxidative stress response; does not bind metal ions; GRX7 has a paralog, GRX6, that arose from the whole genome duplication.
  - **Gly1**: Threonine aldolase; catalyzes the cleavage of L-allo-threonine and L-threonine to glycine; involved in glycine biosynthesis.
  - **Trs23**: Core component of transport protein particle (TRAPP) complexes I-III; TRAPP complexes are related multimeric guanine nucleotideexchange factor for the GTPase Ypt1p, regulating ER-Golgi traffic (TRAPPI), intra-Golgi traffic (TRAPP II), endosome-Golgi traffic (TRAPP II and III) and autophagy (TRAPP III); human homolog is TRAPPC4.
  - **YGR283C**: Putative methyltransferase; may interact with ribosomes, based on co-purification experiments; predicted to be involved in ribosome biogenesis; null mutant is resistant to fluconazole; GFP-fusion protein localizes to the nucleolus; YGR283C has a paralog, YMR310C, that arose from the whole genome duplication. (YGR283C: Putative methyltransferase; predicted to be involved in ribosome biogenesis; green fluorescent protein (GFP)-fusion protein localizes to the nucleus; not an essential gene; YMR310C has a paralog, YGR283C, that arose from the whole genome duplication).
  - **Nsa2**: Protein constituent of 66S pre-ribosomal particles; contributes to processing of the 27S pre-rRNA; recruited by ribosomal proteins L17, L35, and L37 to assembling ribosomes after 27SB pre-rRNA is generated, immediately preceding removal of ITS2.
  - **Erg3**: C-5 sterol desaturase; glycoprotein that catalyzes the introduction of a C-5(6) double bond into episterol, a precursor in ergosterol biosynthesis; transcriptionally down-regulated when ergosterol is in excess; mutants are viable, but cannot grow on non-fermentable carbon sources; substrate of HRD ubiquitin ligase; mutation is functionally complemented by human SC5D.
- **Tel-Phleomycin (Upregulated proteins with Phleomycin-mediated DSB):**
  - **YKL107W**: Aldehyde reductase; involved in detoxification of acetaldehyde, glycolaldehyde, and furfural; localized in ER.

Este documento incorpora firma electrónica, y es copia auténtica de un documento electrónico archivado por la ULL según la Ley 39/2015.  
Su autenticidad puede ser contrastada en la siguiente dirección <https://sede.ull.es/validacion/>

Identificador del documento: 3075810 Código de verificación: smutbmB+

Firmado por: JESSEL AYRA PLASENCIA  
UNIVERSIDAD DE LA LAGUNA

Fecha: 30/11/2020 12:24:14

María de las Maravillas Aguiar Aguilár  
UNIVERSIDAD DE LA LAGUNA

08/02/2021 13:50:06

Appendix I

- **Pgm2**: Phosphoglucomutase; catalyzes the conversion from glucose-1-phosphate to glucose-6-phosphate, which is a key step in hexose metabolism; functions as the acceptor for a Glc-phosphotransferase; protein abundance increases in response to DNA replication stress; PGM2 has a paralog, PGM1, that arose from the whole genome duplication.
- **YMR196W**: Putative protein of unknown function; green fluorescent protein (GFP)-fusion protein localizes to the cytoplasm; YMR196W is not an essential gene.
- **Gnd2**: 6-phosphogluconate dehydrogenase (decarboxylating); catalyzes an NADPH regenerating reaction in the pentose phosphate pathway; required for growth on D-glucono-delta-lactone; GND2 has a paralog, GND1, that arose from the whole genome duplication.
- **Tfs1**: Inhibitor of carboxypeptidase Y (Prc1p), and Ras GAP (Ira2p); phosphatidylethanolamine-binding protein (PEBP) family member and ortholog of hPEBP1/RKIP, a natural metastasis suppressor; targets to vacuolar membranes during stationary phase; acetylated by NatB N-terminal acetyltransferase; protein abundance increases in response to DNA replication stress.
- **YLR001C**: Putative protein of unknown function; the authentic, nontagged protein detected in highly purified mitochondria in highthroughput studies; predicted to be palmitoylated.
- **Gcy1**: Glycerol dehydrogenase; involved in an alternative pathway for glycerol catabolism used under microaerobic conditions; also has mRNA binding activity; member of the aldo-keto reductase (AKR) family; human homolog AKR1B1 can complement yeast null mutant; protein abundance increases in response to DNA replication stress; GCY1 has a paralog, YPR1, that arose from the whole genome duplication.
- **Msc1**: Protein of unknown function; mutant is defective in directing meiotic recombination events to homologous chromatids; the authentic, nontagged protein is detected in highly purified mitochondria and is phosphorylated.
- **Sol4**: 6-phosphogluconolactonase; protein abundance increases in response to DNA replication stress; SOL4 has a paralog, SOL3, that arose from the whole genome duplication.
- **Gph1**: Glycogen phosphorylase required for the mobilization of glycogen; non-essential; regulated by cyclic AMP-mediated phosphorylation; phosphorylation by Cdc28p may coordinately regulate carbohydrate metabolism and the cell cycle; expression is regulated by stress-response elements and by the HOG MAP kinase pathway.
- **Gdb1**: Glycogen debranching enzyme; contains glucanotransferase and alpha-1,6-amyloglucosidase activities; required for glycogen degradation; phosphorylated in mitochondria; activity is inhibited by Igd1p; protein abundance increases in response to DNA replication stress.
- **Hxt3**: Low affinity glucose transporter of the major facilitator superfamily; expression is induced in low or high glucose conditions; HXT3 has a paralog, HXT5, that arose from the whole genome duplication.

184

Este documento incorpora firma electrónica, y es copia auténtica de un documento electrónico archivado por la ULL según la Ley 39/2015.  
 Su autenticidad puede ser contrastada en la siguiente dirección <https://sede.ull.es/validacion/>

Identificador del documento: 3075810 Código de verificación: smutbmB+

Firmado por: JESSEL AYRA PLASENCIA  
 UNIVERSIDAD DE LA LAGUNA

Fecha: 30/11/2020 12:24:14

María de las Maravillas Aguiar Aguiar  
 UNIVERSIDAD DE LA LAGUNA

08/02/2021 13:50:06

- **Htx10**: Putative hexose transporter; expressed at low levels and expression is repressed by glucose.
- **Htx11**: Hexose transporter; capable of transporting a broad range of substrates including: glucose, fructose, mannose and galactose; polyol transporter that supports the growth on and uptake of xylitol with low affinity when overexpressed in a strain deleted for hexose family members; nearly identical in sequence to Hxt9p; has similarity to major facilitator superfamily (MFS) transporters; involved in pleiotropic drug resistance.
- **Hxt9**: Putative hexose transporter that is nearly identical to Hxt11p; has similarity to major facilitator superfamily (MFS) transporters, expression of HXT9 is regulated by transcription factors Pdr1p and Pdr3p.
- **Cst6**: Basic leucine zipper (bZIP) transcription factor from ATF/CREB family involved in stress-responsive regulatory network; mediates transcriptional activation of NCE103 in response to low CO<sub>2</sub> levels; proposed to be a regulator of oleate responsive genes; involved in utilization of non-optimal carbon sources and chromosome stability; relocalizes to the cytosol in response to hypoxia; CST6 has a paralogue, ACA1, that arose from the whole genome duplication. (ACA1: ATF/CREB family basic leucine zipper (bZIP) transcription factor; binds as a homodimer to the ATF/CREB consensus sequence TGACGTCA; important for carbon source utilization; target genes include GRE2 and COS8; ACA1 has a paralogue, CST6, that arose from the whole genome duplication).
- **Gsy2**: Glycogen synthase; expression induced by glucose limitation, nitrogen starvation, heat shock, and stationary phase; activity regulated by cAMP-dependent, Snf1p and Pho85p kinases as well as by the Gac1p-Glc7p phosphatase; GSY2 has a paralogue, GSY1, that arose from the whole genome duplication; relocalizes from cytoplasm to plasma membrane upon DNA replication stress.
- **Cyc7**: Cytochrome c isoform 2, expressed under hypoxic conditions; also known as iso-2-cytochrome c; electron carrier of the mitochondrial intermembrane space that transfers electrons from ubiquinone cytochrome c oxidoreductase to cytochrome c oxidase during cellular respiration; protein abundance increases in response to DNA replication stress; CYC7 has a paralogue, CYC1, that arose from the whole genome duplication. (CYC1: Cytochrome c, isoform 1; also known as iso-1-cytochrome c; electron carrier of mitochondrial intermembrane space that transfers electrons from ubiquinone-cytochrome c oxidoreductase to cytochrome c oxidase during cellular respiration; CYC1 has a paralogue, CYC7, that arose from the whole genome duplication; human homolog CYC1 can complement yeast null mutant; mutations in human CYC1 cause insulin-responsive hyperglycemia).
- **Hsp12**: Plasma membrane protein involved in maintaining membrane organization; involved in maintaining organization during stress conditions; induced by heat shock, oxidative stress, osmotic stress, stationary phase, glucose depletion, oleate and alcohol; protein abundance increased in response to DNA replication stress and dietary restriction; regulated by the HOG and Ras-Pka pathways; required for dietary restriction-induced lifespan extension.
- **Nqm1**: Transaldolase of unknown function; transcription is repressed by Mot1p and induced by alpha-factor and during diauxic shift; NQM1 has a paralogue, TAL1, that arose from the whole genome duplication. (TAL1: Transaldolase, enzyme in the non-oxidative pentose phosphate pathway; converts sedoheptulose 7-phosphate and

Este documento incorpora firma electrónica, y es copia auténtica de un documento electrónico archivado por la ULL según la Ley 39/2015.  
Su autenticidad puede ser contrastada en la siguiente dirección <https://sede.ull.es/validacion/>

Identificador del documento: 3075810 Código de verificación: smutbmB+

Firmado por: JESSEL AYRA PLASENCIA  
UNIVERSIDAD DE LA LAGUNA

Fecha: 30/11/2020 12:24:14

María de las Maravillas Aguiar Aguilár  
UNIVERSIDAD DE LA LAGUNA

08/02/2021 13:50:06

Appendix I

glyceraldehyde 3-phosphate to erythrose 4-phosphate and fructose 6-phosphate; TAL1 has a paralog, NQM1, that arose from the whole genome duplication).

- **Hsp26**: Small heat shock protein (sHSP) with chaperone activity; forms hollow, sphere-shaped oligomers that suppress unfolded proteins aggregation; long-lived protein that is preferentially retained in mother cells and forms cytoplasmic foci; oligomer activation requires heat-induced conformational change; also has mRNA binding activity.
- **Arc40**: Subunit of the ARP2/3 complex; ARP2/3 is required for the motility and integrity of cortical actin patches.
- **Rtn2**: Reticulon protein; involved in nuclear pore assembly and maintenance of tubular ER morphology; promotes membrane curvature; regulates the ER asymmetry-induced inheritance block during ER stress; role in ER-derived peroxisomal biogenesis; interacts with Sec6p, Yip3p, and Sbh1p; less abundant than RTN1; member of RTNLA (reticulon-like A) subfamily; protein increases in abundance and relocalizes to plasma membrane upon DNA replication stress. (RTN1: Reticulon protein; involved in nuclear pore assembly and maintenance of tubular ER morphology; promotes membrane curvature; regulates the ER asymmetry-induced inheritance block during ER stress; role in ER-derived peroxisomal biogenesis; increases tubular ER when overexpressed; mutants have reduced phosphatidylserine transfer between the ER and mitochondria; interacts with exocyst subunit Sec6p, Yip3p, and Sbh1p; member of the RTNLA subfamily).
- **Dcs2**: m(7)GpppX pyrophosphatase regulator; non-essential, stress induced regulatory protein; modulates m7G-oligoribonucleotide metabolism; inhibits Dcs1p; regulated by Msn2p, Msn4p, and the RascAMP- cAPK signaling pathway; mutant has increased aneuploidy tolerance; DCS2 has a paralog, DCS1, that arose from the whole genome duplication. (DCS1: Non-essential hydrolase involved in mRNA decapping; activates Xrn1p; may function in a feedback mechanism to regulate deadenylation, contains pyrophosphatase activity and a HIT (histidine triad) motif; acts as inhibitor of neutral trehalase Nth1p; required for growth on glycerol medium; protein abundance increases in response to DNA replication stress; DCS1 has a paralog, DCS2, that arose from the whole genome duplication).
- **Ego4**: Protein of unknown function; expression is regulated by Msn2p/Msn4p; YNR034W-A has a paralog, YCR075W-A, that arose from the whole genome duplication. (EGO2: Subunit of the EGO/GSE complex; the vacuolar/endosomal membrane associated EGO/GSE complex regulates exit from rapamycin-induced growth arrest, stimulating microautophagy and sorting of Gap1p from the endosome to the plasma membrane; identified by homology to Ashbya gossypii; EGO2 has a paralog, EGO4, that arose from the whole genome duplication).

Este documento incorpora firma electrónica, y es copia auténtica de un documento electrónico archivado por la ULL según la Ley 39/2015.  
 Su autenticidad puede ser contrastada en la siguiente dirección <https://sede.ull.es/validacion/>

Identificador del documento: 3075810 Código de verificación: smutbmB+

Firmado por: JESSEL AYRA PLASENCIA  
 UNIVERSIDAD DE LA LAGUNA

Fecha: 30/11/2020 12:24:14

María de las Maravillas Aguiar Aguiar  
 UNIVERSIDAD DE LA LAGUNA

08/02/2021 13:50:06



## Appendix II. Media and solutions

Este documento incorpora firma electrónica, y es copia auténtica de un documento electrónico archivado por la ULL según la Ley 39/2015.  
Su autenticidad puede ser contrastada en la siguiente dirección <https://sede.ull.es/validacion/>

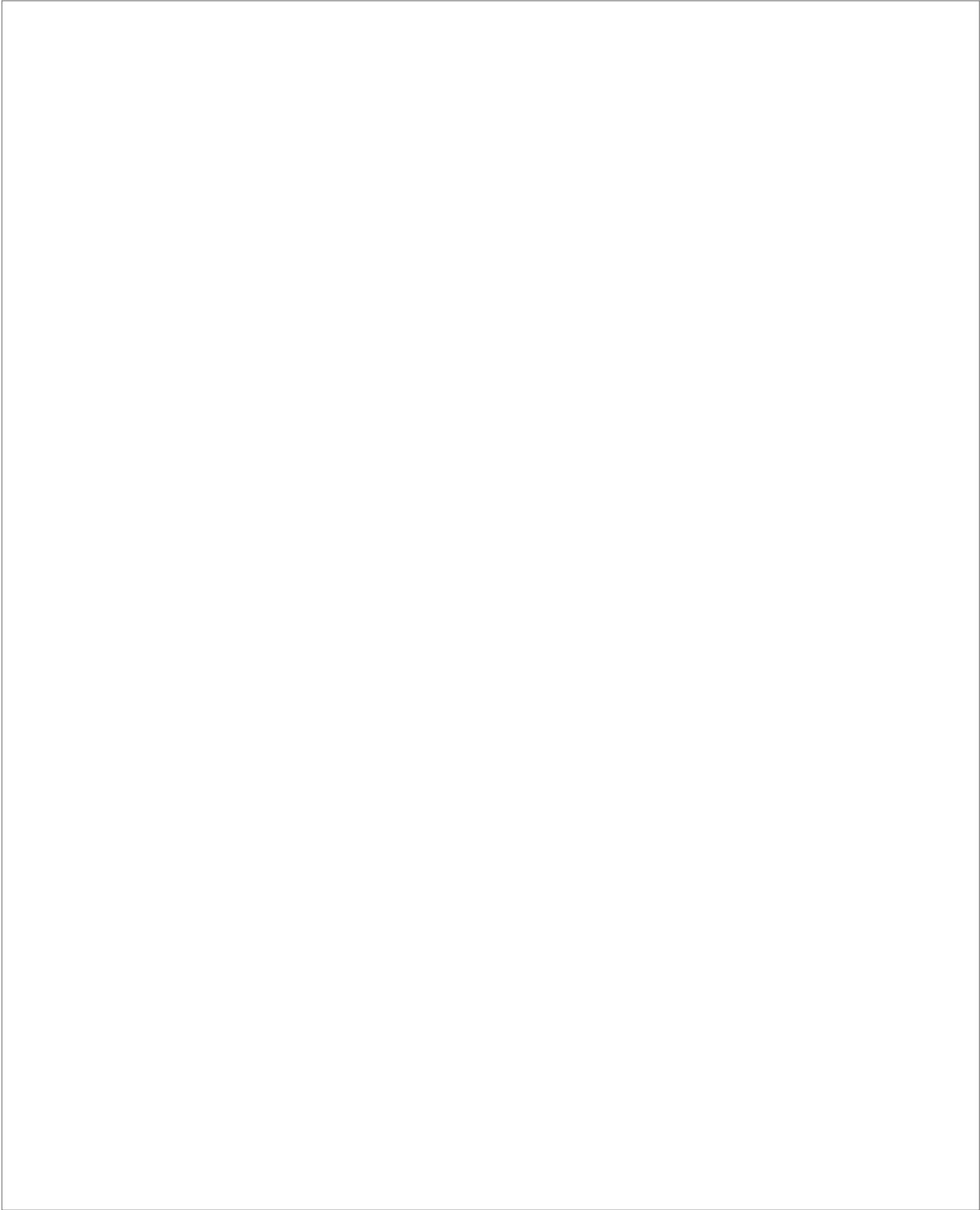
Identificador del documento: 3075810 Código de verificación: smutbmB+

Firmado por: JESSEL AYRA PLASENCIA  
UNIVERSIDAD DE LA LAGUNA

Fecha: 30/11/2020 12:24:14

María de las Maravillas Aguiar Aguiar  
UNIVERSIDAD DE LA LAGUNA

08/02/2021 13:50:06



Este documento incorpora firma electrónica, y es copia auténtica de un documento electrónico archivado por la ULL según la Ley 39/2015.  
*Su autenticidad puede ser contrastada en la siguiente dirección <https://sede.ull.es/validacion/>*

Identificador del documento: 3075810      Código de verificación: smutbmB+

Firmado por: JESSEL AYRA PLASENCIA  
UNIVERSIDAD DE LA LAGUNA

Fecha: 30/11/2020 12:24:14

María de las Maravillas Aguiar Aguiar  
UNIVERSIDAD DE LA LAGUNA

08/02/2021 13:50:06

## Media and Solutions

### Media for *Saccharomyces cerevisiae* culture

• **Liquid YPD medium (w/v)**

- 1 % Yeast extract
- 2 % Peptone
- 2% Glucose

• **Solid YPD medium (w/v)**

- 1 % Yeast extract
- 2 % Peptone
- 2 % Glucose
- 2% Agar

• **Sporulation medium (w/v)**

- 1% potassium acetate
- 0.1% yeast extract
- 0.05% glucose
- 0.01% amino acid mix (1:1:1:5 Ura:His:Lys:Leu)
- 2% agar

• **Synthetic Complete medium (SC)**

- 0.17 % Yeast Nitrogen Base without ammonium sulphate and amino acids
- 0.1 % Monosodium glutamic acid
- 0.2 % Amino acid mix without uracil and tryptophan (see table I)
- 2 % Glucose
- 2 % Agar (only in solid medium)

**Table I. Amino acids mix for drop out media.**

<i>Nutrient</i>	<i>Amount (mg·L<sup>-1</sup>)</i>	<i>Nutrient</i>	<i>Amount (mg·L<sup>-1</sup>)</i>
Adenine	40	Lysine	50
Arginine	50	Methionine	20
Aspartate	80	Phenylalanine	50
Histidine	20	Threonine	100
Isoleucine	50	Tyrosine	50
Leucine	100	Valine	140

Este documento incorpora firma electrónica, y es copia auténtica de un documento electrónico archivado por la ULL según la Ley 39/2015.  
 Su autenticidad puede ser contrastada en la siguiente dirección <https://sede.ull.es/validacion/>

Identificador del documento: 3075810 Código de verificación: smutbmB+

Firmado por: JESSEL AYRA PLASENCIA  
 UNIVERSIDAD DE LA LAGUNA

Fecha: 30/11/2020 12:24:14

María de las Maravillas Aguiar Aguiar  
 UNIVERSIDAD DE LA LAGUNA

08/02/2021 13:50:06

Appendix I

---

**Media for HeLa cells**

• **Growth media (w/v)**

- 1X DMEM with high glucose and L-glutamine
- 10 % Fetal Bovine Serum
- 1 % Antibiotic/Antimycotic solution

• **PBS**

- 2 mM KH<sub>2</sub>PO<sub>4</sub>
- 10 mM NaHPO<sub>4</sub>
- 2.7 mM KCl
- 137 mM NaCl
- o pH 7.4

**Solutions**

**Preparation of competent cells and transformation of *Saccharomyces cerevisiae***

• **SORB Solution**

- 100 mM Lithium acetate
- 10 mM Tris-HCl pH, 8.0
- 1 mM EDTA
- 1 M Sorbitol pH, 8.0 (adjusted using 1M Acetic acid)

• **PEG Solution**

- 100 mM Lithium acetate
- 10 mM Tris-HCl pH 8.0
- 1 mM EDTA
- 40 % Polyethylene glycol 3350 (w/v)

**Genomic DNA extraction of *Saccharomyces cerevisiae***

• **Breaking Buffer**

- 2 % Triton X-100 (v/v)
- 1 % SDS (w/v)
- 100 mM NaCl
- 10 mM Tris-HCl, pH 8.0
- 1 mM EDTA, pH 8.0

• **TE buffer**

- 10 mM Tris-HCl
- 1 mM EDTA, pH 8.0

190

Este documento incorpora firma electrónica, y es copia auténtica de un documento electrónico archivado por la ULL según la Ley 39/2015.  
Su autenticidad puede ser contrastada en la siguiente dirección <https://sede.ull.es/validacion/>

Identificador del documento: 3075810 Código de verificación: smutbmB+

Firmado por: JESSEL AYRA PLASENCIA  
UNIVERSIDAD DE LA LAGUNA

Fecha: 30/11/2020 12:24:14

María de las Maravillas Aguiar Aguiar  
UNIVERSIDAD DE LA LAGUNA

08/02/2021 13:50:06



• **Digestion Buffer**

- 1 % SDS (w/v)
- 100 mM NaCl
- 50 mM Tris-HCl, pH 8.0
- 10 mM EDTA, pH 8.0
- 40 units of Zymolyase 100-T

**Agarose Gel Electrophoresis**

• **TBE**

- 89 mM Tris base % Triton X-100 (v/v)
- 89 mM Boric acid
- 2 mM EDTA, pH 8.0

**Southern blot**

• **Depurination solution**

- 0.125 M HCl

• **Denaturing solution**

- 0.4 M NaOH
- 1M NaCl

• **Neutralization solution**

- 1.5 M NaCl
- 0.5 M Tris base
- o pH adjusted to 7.5 with HCl

• **20 X SSC buffer**

- 3 M NaCl
- 0.3 M Sodium citrate
- o pH adjusted to 7 with HCl

• **Blocking membrane solution**

- 5x SSC buffer (final concentration)
- 0.1 % SDS (v/v)
- 5 % Dextran sulphate (w/v)
- 5 % Blocking liquid (v/v) (Rapid-hyb Buffer – GE Healthcare)

• **Primary washing solution**

- 1x SSC buffer (final concentration)
- 0.1 % SDS (v/v)

Este documento incorpora firma electrónica, y es copia auténtica de un documento electrónico archivado por la ULL según la Ley 39/2015.  
Su autenticidad puede ser contrastada en la siguiente dirección <https://sede.ull.es/validacion/>

Identificador del documento: 3075810 Código de verificación: smutbmB+

Firmado por: JESSEL AYRA PLASENCIA  
UNIVERSIDAD DE LA LAGUNA

Fecha: 30/11/2020 12:24:14

María de las Maravillas Aguiar Aguiar  
UNIVERSIDAD DE LA LAGUNA

08/02/2021 13:50:06

Appendix I

---

• **Secondary washing solution**

- 0.5x SSC buffer (final concentration)
- 0.1 % SDS (v/v)

• **Antibody buffer (AB)**

- 0.1 M Tris-HCl
- 0.15 M NaCl

Adjust pH to 7.5 with NaOH

• **Blocking solution for antibody**

- AB buffer
- 1 % milk powder (w/v)

• **Hybridization solution for antibody**

- AB buffer
- 0.5 % milk powder (w/v)
- 1:100,000 Anti-Fluorescein-AP Fab fragments (Roche)

• **Washing solution for antibody**

- AB buffer
- 0.2 % Tween (v/v)

**Western blot**

• **Laemmli buffer (2X)**

- 120 mM Tris/HCl pH 6.8
- 20 % glycerol
- 4% SDS
- 4%  $\beta$ -mercaptoethanol
- 0.02 % bromophenol blue

• **Running buffer**

- 3 g/l Tris base
- 14,4 g/l glycine
- 0.6 g/l SDS

• **Transfer buffer**

- 25 mM Tris/HCl pH 8.3
- 192 mM glycine
- 20% methanol
- 0.1% SDS

192

Este documento incorpora firma electrónica, y es copia auténtica de un documento electrónico archivado por la ULL según la Ley 39/2015.  
Su autenticidad puede ser contrastada en la siguiente dirección <https://sede.ull.es/validacion/>

Identificador del documento: 3075810 Código de verificación: smutbmB+

Firmado por: JESSEL AYRA PLASENCIA  
UNIVERSIDAD DE LA LAGUNA

Fecha: 30/11/2020 12:24:14

María de las Maravillas Aguiar Aguiar  
UNIVERSIDAD DE LA LAGUNA

08/02/2021 13:50:06

• **TBST solution**

- 100 mM Tris-HCl, pH 7.5
- 150 mM NaCl
- 0.1 % Tween 20

**Hela cells immunofluorescence**

• **Pre-extraction buffer**

- 20 mM Hepes, pH 8.0
- 20 mM NaCl
- 5 mM MgCl<sub>2</sub>
- 0.5 % Nonidet® P-40

• **Fixation buffer**

- 4 % Paraformaldehyde
- 1X PBS

• **Permeabilization buffer**

- 0.2 % Triton® X-100
- 1X PBS

• **Blocking and hybridization solution for antibodies**

- 1 % FBS
- 1X PBS
- o When used, 1:600 antibody dilution was employed.

• **Phalloidin-TRITC**

- 1 mg·mL<sup>-1</sup> Phalloidin-TRITC
- 1X PBS
- 1 % DMSO

Este documento incorpora firma electrónica, y es copia auténtica de un documento electrónico archivado por la ULL según la Ley 39/2015.  
Su autenticidad puede ser contrastada en la siguiente dirección <https://sede.ull.es/validacion/>

Identificador del documento: 3075810 Código de verificación: smutbmB+

Firmado por: JESSEL AYRA PLASENCIA  
UNIVERSIDAD DE LA LAGUNA

Fecha: 30/11/2020 12:24:14

María de las Maravillas Aguiar Aguiar  
UNIVERSIDAD DE LA LAGUNA

08/02/2021 13:50:06



Este documento incorpora firma electrónica, y es copia auténtica de un documento electrónico archivado por la ULL según la Ley 39/2015.  
*Su autenticidad puede ser contrastada en la siguiente dirección <https://sede.ull.es/validacion/>*

Identificador del documento: 3075810 Código de verificación: smutbmB+

Firmado por: JESSEL AYRA PLASENCIA  
UNIVERSIDAD DE LA LAGUNA

Fecha: 30/11/2020 12:24:14

María de las Maravillas Aguiar Aguiar  
UNIVERSIDAD DE LA LAGUNA

08/02/2021 13:50:06



## Appendix III. Other scientific contributions during this thesis

Este documento incorpora firma electrónica, y es copia auténtica de un documento electrónico archivado por la ULL según la Ley 39/2015.  
Su autenticidad puede ser contrastada en la siguiente dirección <https://sede.ull.es/validacion/>

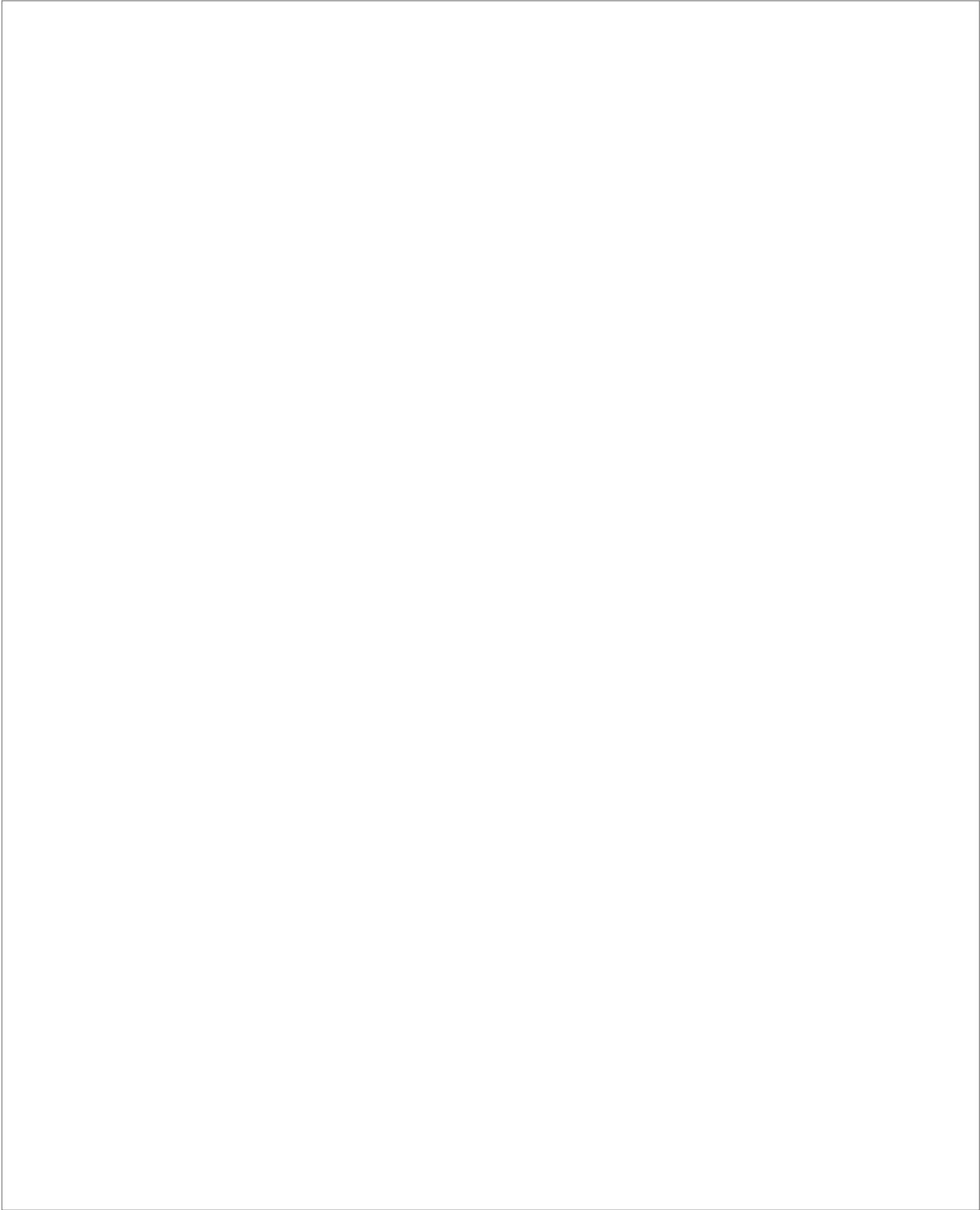
Identificador del documento: 3075810 Código de verificación: smutbmB+

Firmado por: JESSEL AYRA PLASENCIA  
UNIVERSIDAD DE LA LAGUNA

Fecha: 30/11/2020 12:24:14

María de las Maravillas Aguiar Aguiar  
UNIVERSIDAD DE LA LAGUNA

08/02/2021 13:50:06



Este documento incorpora firma electrónica, y es copia auténtica de un documento electrónico archivado por la ULL según la Ley 39/2015.  
*Su autenticidad puede ser contrastada en la siguiente dirección <https://sede.ull.es/validacion/>*

Identificador del documento: 3075810      Código de verificación: smutbmB+

Firmado por: JESSEL AYRA PLASENCIA  
UNIVERSIDAD DE LA LAGUNA

Fecha: 30/11/2020 12:24:14

María de las Maravillas Aguiar Aguiar  
UNIVERSIDAD DE LA LAGUNA

08/02/2021 13:50:06



## Molecular & Cellular Oncology



ISSN: (Print) 2372-3556 (Online) Journal homepage: <https://www.tandfonline.com/loi/kmco20>

### Yeast cells can partially revert chromosome segregation to repair late DNA double-strand breaks through homologous recombination

Jessel Ayra-Plasencia & Félix Machín

To cite this article: Jessel Ayra-Plasencia & Félix Machín (2019) Yeast cells can partially revert chromosome segregation to repair late DNA double-strand breaks through homologous recombination, *Molecular & Cellular Oncology*, 6:5, e1648027, DOI: [10.1080/23723556.2019.1648027](https://doi.org/10.1080/23723556.2019.1648027)

To link to this article: <https://doi.org/10.1080/23723556.2019.1648027>



© 2019 The Author(s). Published with license by Taylor & Francis Group, LLC.



Published online: 06 Aug 2019.



[Submit your article to this journal](#)



Article views: 348



[View related articles](#)



[View Crossmark data](#)



[Citing articles: 2 View citing articles](#)

Full Terms & Conditions of access and use can be found at  
<https://www.tandfonline.com/action/journalInformation?journalCode=kmco20>

Este documento incorpora firma electrónica, y es copia auténtica de un documento electrónico archivado por la ULL según la Ley 39/2015.  
Su autenticidad puede ser contrastada en la siguiente dirección <https://sede.ull.es/validacion/>

Identificador del documento: 3075810 Código de verificación: smutbmB+

Firmado por: JESSEL AYRA PLASENCIA  
UNIVERSIDAD DE LA LAGUNA

Fecha: 30/11/2020 12:24:14

María de las Maravillas Aguiar Aguiar  
UNIVERSIDAD DE LA LAGUNA

08/02/2021 13:50:06

## Yeast cells can partially revert chromosome segregation to repair late DNA double-strand breaks through homologous recombination

Jessel Ayra-Plasencia <sup>a,b</sup> and Félix Machín <sup>a,c,d</sup>

<sup>a</sup>Unidad de Investigación, Hospital Universitario Nuestra Señora de Candelaria, Santa Cruz de Tenerife, Spain; <sup>b</sup>Escuela de Doctorado y Estudios de Posgrado, Universidad de La Laguna, Santa Cruz de Tenerife, Spain; <sup>c</sup>Instituto de Tecnologías Biomédicas, Universidad de La Laguna, Santa Cruz de Tenerife, Spain; <sup>d</sup>Facultad de Ciencias de la Salud, Universidad Fernando Pessoa Canarias, Las Palmas de Gran Canaria, Spain

### ABSTRACT

DNA repair in late mitosis sets paradoxical scenarios. Cyclin-dependent kinase (CDK) activity is high, which favors homologous recombination (HR), despite a sister chromatid is not physically close to recombine with. We have found that DNA double-strand breaks partially revert chromosome segregation to find an intact template and repair through HR.

### ARTICLE HISTORY

Received 17 July 2019  
Revised 19 July 2019  
Accepted 23 July 2019

### KEYWORDS

DNA double-strand breaks;  
homologous recombination;  
chromosome segregation;  
kinesin; telophase

### Main body

DNA double-strand breaks (DSBs) are one of the most toxic forms of DNA damage. DSBs are carcinogenic, but also the key triggering event that kills cancer cells upon radiotherapy and most chemotherapy treatments. Cells have developed several pathways to repair DSBs. They can generally be classified in (i) non-homologous end joining (NHEJ) and, (ii) homologous recombination (HR). The first one works by fusing two DNA ends lightly processed. It is an error-prone mechanism since short deletions, insertions or even chromosome translocations can be generated. On the other hand, HR is considered as error-free. To heal the DSB and restore the original sequence, HR needs the presence of a well aligned sister chromatid to be invaded with a highly processed broken end.<sup>1</sup>

Cells have coupled the choice between different DNA repair pathways to the cyclin-dependent kinase (CDK) activity. Thus, NHEJ is used during G<sub>1</sub> phase, when CDK/cyclins levels are low and no sister DNA is present. On the contrary, HR is preferred in S and G<sub>2</sub> phases, when DNA replication has started (or has been completed) and sister chromatids are available as templates.<sup>2–4</sup>

Late anaphase and telophase constitute short stages within the cell cycle where it is not clear which pathway should be chosen. On the one hand, the biochemical environment of the cell would facilitate HR, as CDK/cyclins levels are still high. Conversely, these stages are similar to G<sub>1</sub> as there not exist a close sister chromatid to recombine with because they have just been segregated. This paradoxical scenario, which can be found in a proportion of tumoral cells treated with chemo- and radiotherapy, has been barely studied. All efforts in understanding what happens when a DSB is generated during mitosis have mainly been focused on cells transiting prophase/metaphase. This

issue is probably due to the technical caveats of specifically generating DSBs in late anaphase/telophase. Mammal and human cell cultures can be easily arrested in early mitosis (prophase/metaphase), but not in the latest stages.<sup>5,6</sup> This fact has hindered the study and comprehension of this unique situation.

In a recent publication,<sup>7</sup> we studied DSB repair in *Saccharomyces cerevisiae* cells that can be easily and stably arrested in late anaphase/telophase. Treatment of telophase-blocked cultures with the radiomimetic drug phleomycin led us to see that cells detect DSBs through the hyperphosphorylation of Rad53 kinase (CHK2 in humans). This posttranslational modification is closely linked to the activation of a specific DNA damage checkpoint (DDC). Accordingly, we observed a delay at the telophase-to-G<sub>1</sub> transition by analyzing the kinetics of plasma membrane abscission and the accumulation of the specific G<sub>1</sub> protein Sic1. Furthermore, we demonstrated that the observed delay depends on the DDC. Indeed, cells impaired for this checkpoint (*rad9Δ*; yeast Rad9 is the functional analog to human 53BP1 and BRCA1) were unable to block the G<sub>1</sub> entry.

Fluorescence microscopy monitorization of different chromosome loci revealed a new striking phenomenon. After DSBs, the distance between previously segregated centromere clusters was greatly reduced. Surprisingly, filming *in vivo* short movies unrevealed events of coalescence between sister chromatid loci, such as telomeres and the ribosomal DNA array (rDNA). We also observed *de novo* formation of two types of anaphase bridges (ABs): (i) thick ABs formed by bulgy nuclear masses and (ii) thin ABs with confined trafficking of less condensed DNA across the bud neck (i.e., cytokinetic plane in yeast). Coalescence was also observed when

**CONTACT** Félix Machín  [fmachin@funcanis.es](mailto:fmachin@funcanis.es)  Unidad de Investigación, Hospital Universitario Nuestra Señora de Candelaria, Carretera del Rosario 145, Santa Cruz de Tenerife 38010, Spain

© 2019 The Author(s). Published with license by Taylor & Francis Group, LLC.  
This is an Open Access article distributed under the terms of the Creative Commons Attribution-NonCommercial-NoDerivatives License (<http://creativecommons.org/licenses/by-nc-nd/4.0/>), which permits non-commercial re-use, distribution, and reproduction in any medium, provided the original work is properly cited, and is not altered, transformed, or built upon in any way.

Este documento incorpora firma electrónica, y es copia auténtica de un documento electrónico archivado por la ULL según la Ley 39/2015.  
Su autenticidad puede ser contrastada en la siguiente dirección <https://sede.ull.es/validacion/>

Identificador del documento: 3075810 Código de verificación: smutbmB+

Firmado por: JESSEL AYRA PLASENCIA  
UNIVERSIDAD DE LA LAGUNA

Fecha: 30/11/2020 12:24:14

María de las Maravillas Aguiar Aguiar  
UNIVERSIDAD DE LA LAGUNA

08/02/2021 13:50:06



e1648027-2 J. AYRA-PLASENCIA AND F. MACHÍN

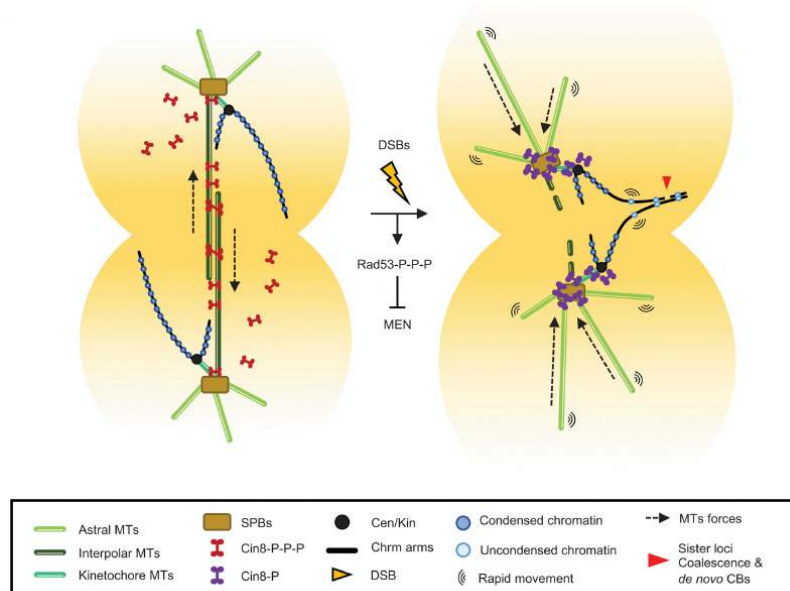


**Figure 1.** Events underlying sister chromatid approximation and coalescence after DNA double-strand breaks (DSBs) in late anaphase/telophase. DSBs elicit Rad53 hyperphosphorylation (Rad53-P-P-P) in telophase, inhibiting the mitotic exit network (MEN). Alongside, a partial dephosphorylation of Cin8 (from Cin8-P-P-P to Cin8-P), and its relocation from the interpoles microtubules (MTs) to the spindle pole bodies (SPBs), drive a massive change in MT dynamics. This brings closer the segregated chromosomes (chr), including centromeres/kinetochores (Cen/Kin) and telomeres, leading to the formation of *de novo* chromatin bridges (CBs) and coalescence between sister loci.

a single DSB was generated through the inducible expression of the sequence-specific endonuclease I-SceI.

It is known that cells mobilize damaged chromatin to the nuclear periphery, where HR is frequently used to repair.<sup>8-10</sup> In telophase, we also visualized a remarkable increase mobility of damaged loci. The DDC is directly responsible of this behavior, since the *rad9Δ* strain did not accelerate interloco movement. In contrast, cells deficient for HR (*rad52Δ*; analog to human BRCA2) were unable to diminish coalescence events and the interloco movement, despite we found a clear contribution in the survival to DSBs in telophase. Comparative survival between G<sub>1</sub>, G<sub>2</sub>/M and telophase revealed that cells use HR instead of NHEJ.

Finally, we also characterized a massive change in the morphology and dynamics of microtubules (MTs) after DSBs. The elongated mitotic spindle typical from telophase turns into a dynamic and star-shaped structure, in which interpoles MTs are no longer present. Short videomicroscopy movies showed that distances between segregated spindle pole bodies (SPBs, equivalent to human centrosomes) are also reduced, yet constrained, by the enforced astral MTs, which work as the new pushing and pulling forces inside the cell. In addition, we identified that Cin8 (kinesin-5 motor protein) is partially dephosphorylated and relocated from the mitotic spindle to SPBs/kinetochores to drive the approximation of

segregated nuclear masses. A conditional Cin8-aid degenon did not bring closer the DNA material, and a phosphomimic version of Cin8 for its motor domain (partially impaired to relocate after DSBs) gave rise to reduced survival rates.

Altogether, our exciting results demonstrate that DSBs in telophase lead to a partial reversion of chromosome segregation (Figure 1; adapted from<sup>7</sup>). Cells recognise the damage and trigger the DDC. This promotes a partial dephosphorylation and relocation of Cin8 to drive a massive change in MT dynamics. In addition, chromatin is partly decondensed and increases its mobility, while nuclear masses begin to approximate each other. Finally, coalescence events between segregated sister chromatid loci are produced, so HR can be used to repair the damage and survive.

#### Disclosure of potential conflicts of interest

No potential conflicts of interest were disclosed.

#### Funding

This work was supported by the Spanish Ministry of Science, Innovation and Universities (research grant BFU2017-83954-R to Félix Machín), co-financed with the European Commission's ERDF structural funds.

Este documento incorpora firma electrónica, y es copia auténtica de un documento electrónico archivado por la ULL según la Ley 39/2015.  
 Su autenticidad puede ser contrastada en la siguiente dirección <https://sede.ull.es/validacion/>

Identificador del documento: 3075810

Código de verificación: smutbmB+


Firmado por: JESSEL AYRA PLASENCIA  
 UNIVERSIDAD DE LA LAGUNA

Fecha: 30/11/2020 12:24:14

María de las Maravillas Aguiar Aguiar  
 UNIVERSIDAD DE LA LAGUNA

08/02/2021 13:50:06

Appendix III

MOLECULAR & CELLULAR ONCOLOGY  e1648027-3

**ORCID**

Jessel Ayra-Plasencia  <http://orcid.org/0000-0003-1052-4214>  
Félix Machín  <http://orcid.org/0000-0003-4559-7798>

**References**

1. Symington LS, Rothstein R, Lisby M. Mechanisms and regulation of mitotic recombination in *Saccharomyces cerevisiae*. *Genetics*. 2014;198:795–835. doi:10.1534/genetics.114.166140.
2. Emerson CH, Bertuch AA. Consider the workhorse: nonhomologous end-joining in budding yeast. *Biochem Cell Biol*. 2016;94:396–406. doi:10.1139/bcb-2016-0001.
3. Aylon Y, Liefshitz B, Kupiec M. The CDK regulates repair of double-strand breaks by homologous recombination during the cell cycle. *Embo J*. 2004;23:4868–4875. doi:10.1038/sj.emboj.7600469.
4. Ira G, Pellicoli A, Balijja A, Wang X, Fiorani S, Carotenuto W, Liberi G, Bressan D, Wan L, Hollingsworth NM, et al. DNA end resection, homologous recombination and DNA damage checkpoint activation require CDK1. *Nature*. 2004;431:1011–1017. doi:10.1038/nature02964.
5. Baker NM, Zeitlin SG, Shi LZ, Shah J, Berns MW, Bielinsky A-K. Chromosome tips damaged in anaphase inhibit cytokinesis. *PLoS One*. 2010;5:e12398. doi:10.1371/journal.pone.0012398.
6. Bakhoun SF, Kabeche L, Compton DA, Powell SN, Bastians H. Mitotic DNA damage response: at the crossroads of structural and numerical cancer chromosome instabilities. *Trends Cancer*. 2017;3:225–234. doi:10.1016/j.trecan.2017.02.001.
7. Ayra-Plasencia J, Machín F. DNA double-strand breaks lead to coalescence between segregated sister chromatid loci. *Nat Commun*. 2019;10(1):2862. doi:10.1038/s41467-019-10742-8.
8. Chung DKC, Chan JNY, Strecker J, Zhang W, Ebrahimi-Ardebili S, Lu T, Abraham KJ, Durocher D, Mekhail K. Perinuclear tethers license telomeric DSBs for a broad kinesin- and NPC-dependent DNA repair process. *Nat Commun*. 2015;6:7742. doi:10.1038/ncomms8742.
9. Dion V, Kalck V, Horigome C, Towbin BD, Gasser SM, Itami S, van de Wetering M, Poulosom R, Wright NA, Trotter MWB, et al. Increased mobility of double-strand breaks requires Mec1, Rad9 and the homologous recombination machinery. *Nat Cell Biol*. 2012;14:502–509. doi:10.1038/ncb2464.
10. Lawrimore J, Barry TM, Barry RM, York AC, Friedman B, Cook DM, Akialis K, Tyler J, Vasquez P, Yeh E, et al. Microtubule dynamics drive enhanced chromatin motion and mobilize telomeres in response to DNA damage. *Mol Biol Cell*. 2017;28:1701–1711. doi:10.1091/mbc.e16-12-0846.

Este documento incorpora firma electrónica, y es copia auténtica de un documento electrónico archivado por la ULL según la Ley 39/2015.  
Su autenticidad puede ser contrastada en la siguiente dirección <https://sede.ull.es/validacion/>

Identificador del documento: 3075810 Código de verificación: smutbmB+

Firmado por: JESSEL AYRA PLASENCIA  
UNIVERSIDAD DE LA LAGUNA

Fecha: 30/11/2020 12:24:14

María de las Maravillas Aguiar Aguiar  
UNIVERSIDAD DE LA LAGUNA

08/02/2021 13:50:06



INVESTIGATION

## Genome-Scale Genetic Interactions and Cell Imaging Confirm Cytokinesis as Deleterious to Transient Topoisomerase II Deficiency in *Saccharomyces cerevisiae*

Cristina Ramos-Pérez,<sup>\*,1,1</sup> Jessel Ayra-Plasencia,<sup>\*,†</sup> Emiliano Matos-Perdomo,<sup>\*,†</sup> Michael Lisby,<sup>‡</sup>

Grant W. Brown,<sup>§</sup> and Félix Machin<sup>\*,2</sup>

<sup>\*</sup>Unidad de Investigación, Hospital Universitario Nuestra Señora de Candelaria, 38010 Santa Cruz de Tenerife, Spain,

<sup>†</sup>Universidad de la Laguna, 38200 San Cristóbal de La Laguna, Santa Cruz de Tenerife, Spain, <sup>‡</sup>Department of Biology, University of Copenhagen, DK-2200, Denmark, and <sup>§</sup>Department of Biochemistry and Donnelly Centre, University of Toronto, Ontario M5S3E1, Canada

ORCID IDs: 0000-0003-1052-4214 (J.A.-P.); 0000-0001-9783-3591 (E.M.-P.); 0000-0002-4830-5247 (M.L.); 0000-0002-9002-5003 (G.W.B.); 0000-0003-4559-7798 (F.M.)

**ABSTRACT** Topoisomerase II (Top2) is an essential protein that resolves DNA catenations. When Top2 is inactivated, mitotic catastrophe results from massive entanglement of chromosomes. Top2 is also the target of many first-line anticancer drugs, the so-called Top2 poisons. Often, tumors become resistant to these drugs by acquiring hypomorphic mutations in the genes encoding Top2. Here, we have compared the cell cycle and nuclear segregation of two coisogenic *Saccharomyces cerevisiae* strains carrying *top2* thermosensitive alleles that differ in their resistance to Top2 poisons: the broadly-used poison-sensitive *top2-4* and the poison-resistant *top2-5*. Furthermore, we have performed genome-scale synthetic genetic array (SGA) analyses for both alleles under permissive conditions, chronic sublethal Top2 downregulation, and acute, yet transient, Top2 inactivation. We find that slowing down mitotic progression, especially at the time of execution of the mitotic exit network (MEN), protects against Top2 deficiency. In all conditions, genetic protection was stronger in *top2-5*; this correlated with cell biology experiments in this mutant, whereby we observed destabilization of both chromatin and ultrafine anaphase bridges by execution of MEN and cytokinesis. Interestingly, whereas transient inactivation of the critical MEN driver *Cdc15* partly suppressed *top2-5* lethality, this was not the case when earlier steps within anaphase were disrupted; *i.e.*, *top2-5 cdc14-1*. We discuss the basis of this difference and suggest that accelerated progression through mitosis may be a therapeutic strategy to hypersensitize cancer cells carrying hypomorphic mutations in *TOP2*.

### KEYWORDS

topoisomerase II  
*top2-4* and *top2-5*  
synthetic genetic  
array analysis  
mitotic exit  
network  
cytokinesis  
plasma membrane  
abscission  
anaphase bridges  
*Cdc14*

Upon chromosome replication, topological intertwinning arises between sister chromatids. These intertwinings often become interlocked

(*i.e.*, catenations) due to the confinement of the very long chromosomes in the reduced space of the nucleus. Catenations preclude sister chromatid segregation in anaphase, and the key enzyme in all life forms for removing them is topoisomerase II (Top2) (Nitiss 2009a; Vos *et al.* 2011). Top2 works by making transient double-strand breaks (DSBs) on one chromatid, allowing the passage of its sister through this break. Importantly, a human homolog of Top2, hTOPOII $\alpha$ , is the main target of first-line anticancer drugs including etoposide and doxorubicin (Deweese and Osheroff 2009; Nitiss 2009b). These drugs trap Top2-mediated DSBs and are called Top2 poisons. The resulting DSBs are more abundant and less efficiently repaired in cancer cells than in normal cells and this, in turn, leads to the selective killing of the tumor. Human TOPOII $\alpha$  is often mutated and/or downregulated during acquisition of secondary resistance to Top2 poisons, and this fact could be exploited for second-line

Copyright © 2017 Ramos-Pérez *et al.*

doi: <https://doi.org/10.1534/g3.117.300104>

Manuscript received February 23, 2017; accepted for publication August 11, 2017; published Early Online August 23, 2017.

This is an open-access article distributed under the terms of the Creative Commons Attribution 4.0 International License (<http://creativecommons.org/licenses/by/4.0/>), which permits unrestricted use, distribution, and reproduction in any medium, provided the original work is properly cited.

Supplemental material is available online at [www.g3journal.org/lookup/suppl/doi:10.1534/g3.117.300104/-DC1](http://www.g3journal.org/lookup/suppl/doi:10.1534/g3.117.300104/-DC1).

<sup>1</sup>Present address: Department of Biochemistry and Donnelly Centre, University of Toronto, Toronto ON M5S3E1, Canada.

<sup>2</sup>Corresponding author: Unidad de Investigación, Hospital Universitario Nuestra Señora de la Candelaria, Ctra del Rosario 145, 38010 Santa Cruz de Tenerife, Spain. E-mail: [fmachin@funcanis.es](mailto:fmachin@funcanis.es)

Este documento incorpora firma electrónica, y es copia auténtica de un documento electrónico archivado por la ULL según la Ley 39/2015.

Su autenticidad puede ser contrastada en la siguiente dirección <https://sede.ull.es/validacion/>

Identificador del documento: 3075810

Código de verificación: smutbmB+

Firmado por: JESSEL AYRA PLASENCIA  
UNIVERSIDAD DE LA LAGUNA

Fecha: 30/11/2020 12:24:14

María de las Maravillas Aguiar Aguilár  
UNIVERSIDAD DE LA LAGUNA

08/02/2021 13:50:06

## Apendix III

anticancer treatments (Larsen *et al.* 2003; Nitiss 2009b; Holohan *et al.* 2013).

*Top2* is essential for cellular viability. In unicellular eukaryotes and bacteria the study of *Top2* functions has been largely facilitated by the availability of conditional alleles. In the yeasts *Saccharomyces cerevisiae* and *Schizosaccharomyces pombe* early studies showed that inactivation of *Top2* by means of thermosensitive (*ts*) alleles leads to a mitotic catastrophe as determined by a sudden loss of viability once the cells reach anaphase (Holm *et al.* 1985; Uemura and Tanagida 1986). In agreement with a role in removing sister chromatid catenations, *Top2* inactivation yielded cells with DAPI-stained anaphase bridges and broken chromosomes once cells completed cytokinesis (DiNardo *et al.* 1984; Uemura and Yanagida 1984; Holm *et al.* 1985, 1989; Uemura and Tanagida 1986). In the case of *S. cerevisiae*, all these studies were carried out with two *ts* alleles isolated in independent screens, *top2-1* and *top2-4*. Both alleles yield *Top2-ts* proteins sensitive to poisons. In the same screen where *top2-4* was isolated, *top2-5* was also obtained (Holm *et al.* 1985). Later, *top2-5* was shown to be resistant to poisons and served as a key tool to understand the mechanism of action of this class of clinical drugs (Jannatipour *et al.* 1993; Perego *et al.* 2000). Nevertheless, the cell cycle of the *top2-5* strain was not characterized and has been assumed to be equivalent to that of the *top2-4* strain.

Here, we have revisited the cell cycle progression of cells expressing the broadly used *top2-4* allele and compared its behavior to a coisogenic *top2-5* strain. In addition, we have performed a genome-scale synthetic genetic array (SGA) analysis for these two *top2-ts* alleles. We show that *top2-5* goes faster through the cell cycle and gathers more genetic interactions related to mitotic progression than *top2-4*. In addition, we show that execution of the mitotic exit network (MEN) has specific deleterious effects on sublethal downregulation of *Top2-5*, and that this correlates with destabilization of anaphase bridges by cytokinesis.

## MATERIALS AND METHODS

### Yeast strain construction, cell cycle experiments, and fluorescence microscopy

All the strains used in this work are listed in Supplemental Material, Table S1 in File S1 together with their relevant genotypes. C-terminal tagging with GFP/RFP variants or an auxin-based degron system, gene deletions and *ts* allele transfers were carried out using standard PCR methods as described before (Tong *et al.* 2001; Janke *et al.* 2004; Nishimura *et al.* 2009).

Most strains were grown overnight in air orbital incubators at 25° in YPD media before every experiment. Cell cycle time course experiments and fluorescence microscopy were performed as described before (Quevedo *et al.* 2012; Silva *et al.* 2012; García-Luis and Machín 2014). Briefly, asynchronous cultures of *MATa* haploids were adjusted to OD<sub>600</sub> = 0.3 and then synchronized in G1 at 25° for 3 hr by adding 50 ng/ml (*bar1Δ* strains) or 5 μg/ml (*BARI* strains) of α-factor (T6901, Sigma-Aldrich). The G1 release was induced by washing the cells twice in YPD and resuspending them in fresh media containing 0.1 mg/ml of pronase E (81750, Sigma-Aldrich). Next, the culture was incubated at 37° for 4 hr and samples were taken every 30 min for direct visualization under a Leica DMI6000 fluorescence microscope. DNA was stained using DAPI (32670, Sigma-Aldrich) at 4 μg/ml final concentration after keeping the cell pellet 24 hr at -20°. In the experiments performed to visualize ultrafine anaphase bridges (UFBs), a synthetic complete medium containing 100 μg/ml adenine (SC+Ade) was used instead of YPD and images were taken with a Zeiss AxioImager Z1 fluorescence microscope.

Plasma membrane (PM) abscission and zymolyase digestion were employed to address progression of cytokinesis (Norden *et al.* 2006;

Mendoza *et al.* 2009; Quevedo *et al.* 2012). For membrane abscission, the PM reporter 2-PH-GFP (two GFP-fused pleckstrin homology domains of phospholipase C from *Rattus norvegicus*) was used. When this reporter was not available, PM was stained with 5 μg/ml Hoechst 33258 (94403, Sigma-Aldrich) for either 5 or 15 min at 37° before processing for fluorescence microscopy. Aside from the DNA, Hoechst dyes have great affinity for the lipid bilayer where they also become strongly fluorescent (Shapiro and Ling 1995). Zymolyase treatment was performed as described before (Quevedo *et al.* 2012). Briefly, samples were taken from the culture, fixed with 5% formaldehyde for 1 hr at 37°, and then washed twice with PBS and once with 1 M sorbitol in 50 mM KPO<sub>4</sub>, pH 7.5. Finally, the sample was split in two; one half was treated with 0.2 mg/ml zymolyase 20T (E1005, Zymo Research) in the above sorbitol buffer containing 4 mM β-mercaptoethanol for 20 min at 37°, whereas the other half was treated in the same conditions but without zymolyase (mock control).

For the time-lapse movies, an asynchronous culture was concentrated by centrifugation to three OD<sub>600</sub> equivalents and plated on YPDA (YPD, agar 2% w/v). Patches were made from this plate and mounted on a microscope slide. They were incubated at 37° in high humidity chambers to avoid drying of the agarose patch. Photos were taken every 30 or 60 min for 6 hr in order to minimize both photobleaching and cell damage by the excitation light.

For clonogenic assays, ~300 cells (as calculated from OD<sub>600</sub> measurements) from an asynchronous culture were seeded on two YPD plates. One plate was incubated at 25° for 3 d, whereas the other was first preincubated at 37° for 6 hr before being transferred to 25°. Proportion of survivors was calculated from the fraction of colonies that grew after the 37° preincubation normalized to the number of colonies on plates continuously grown at 25°. The same principle of temperature incubations was employed in the spot dilution assay. In this case, the asynchronous culture was first normalized to OD<sub>600</sub> = 1, then 1:10 serially diluted, and finally spotted on YPD plates (~5 μl per spot) with a 48-pin replica plater (R2383, Sigma-Aldrich).

Variation between independent experiments was evaluated by SEM. Comparisons between mean values for different strains or conditions were performed by the unpaired two-sided student's *t*-test. When percentages were calculated for selected cell phenotypes observed by microscopy, exact binomial 95% confidence intervals (CI95) were also included as error bars in order to inform about the accuracy of such observation. When percentages are mentioned in the main text, CI95 is indicated afterward in parentheses. Cells from at least two independent experiments were pooled for such calculations.

### Synthetic genetic array analyses

SGA was performed as described before (Tong *et al.* 2001; Baryshnikova *et al.* 2010; Li *et al.* 2011). In order to make the strain arrays (described in detail in Figure S1 in File S1), we first replaced the *TOP2* locus in the haploid *MATa* strain Y7092 with our query *top2-ts* alleles attached to the selection marker *natMX4* (resistance to nourseothricin). For consistency, we also attached the *natMX4* marker to our reference *TOP2* Y7092 strain. The new *natMX4* strains were then mated with the *MATa* mutant collections (4322 knockout strains for nonessential genes plus 1231 strains with thermosensitive alleles for essential genes). These panels of *MATa* strains bear the *kanMX4* marker (resistance to G418) at the mutated locus. Diploids were selected on YPD plates containing both nourseothricin and G418, and later sporulated and selected for *MATa* haploids containing both markers. Once the *TOP2*, *top2-4*, and *top2-5* arrays were constructed they were replicated on to plates with the same medium used in the *MATa* selection and exposed to the different temperature regimes described in the *Results* section.

The image analysis, processing, and fitness scoring of the arrays were done using SGAtools (<http://sgatools.ccb.utoronto.ca/about>) (Wagih *et al.* 2013). Gene Ontology (GO) enrichment analysis was performed using the Generic GO Term Finder (<http://go.princeton.edu/cgi-bin/GOTermFinder>) of Princeton University (Boyle *et al.* 2004). Networks were made with Cytoscape v3.3.0 (<http://www.cytoscape.org/cy3.html>) (Shannon *et al.* 2003).

#### Data availability

Strains are available upon request. File S1 contains additional material and methods, four supplemental figures, six supplemental tables, and legends for the SGA files included in File S2. File S2 is a zip compressed file which contains 12 Microsoft Excel files with raw and processed data for each SGA analysis.

## RESULTS

### Three nuclear segregation patterns can be revealed by live microscopy of *top2-4* and *top2-5* cells

We started this work by revisiting fluorescence microscopy time course experiments in the original *top2-4* and *top2-5* ts strains (Holm *et al.* 1985). As a control, we also included the *TOP2* reference wild-type allele in the same genetic background. We first engineered the strains in order to label the histone H2A (*HTA2* gene) with GFP. This strategy allowed us to complement the time course experiments with fluorescence videomicroscopy of the nuclear DNA without adding DNA intercalating dyes. We further labeled Rad52 with RedStar2 to assess DNA damage upon inactivation of Top2. Rad52 forms nuclear foci to repair DSBs through the homologous recombination repair pathway (Lisby *et al.* 2001).

All strains were arrested in G1 at the permissive temperature (25°) for 3 hr and then released at 37° to follow the progression through a synchronous cell cycle. As expected, the *TOP2* control cycled normally after the release, with segregation of the nuclear masses taking place very quickly at 90–120 min and no signs of DNA damage after that (Figure 1A, left panels). Separation between the segregated histone-labeled masses was clear and often laid close to the cell poles. Hereafter, we refer to this segregation phenotype as long-distance binucleated (LD-binucleated) and grouped cells within this phenotype provided that the distance between the split masses was >1 μm. From 150 min onwards, the *TOP2* strain split the daughter from the mother and asynchronously entered a second cell cycle. In contrast to *TOP2*, the *top2-4* mutant exhibited a phenotype of cells stuck in anaphase after 4 hr, in which ~75% of the cells were in a “dumbbell” state (*i.e.*, the bud as big as the mother) and ~35% (50% of dumbbells) had two very close nuclear masses as determined by histone labeling (Figure 1A, central panels; Figure 1, B and C). We refer to this abnormal form of nuclear segregation as short-distance binucleated (SD-binucleated, <1 μm of separation) (Figure 1D). Unexpectedly, the actual presence of chromatin anaphase bridges (CABs, *i.e.*, stretched histone-labeled DNA across the bud neck, Figure 1D) was low, with a SD-binucleated:CAB ratio of 5:1. The presence of SD-binucleated was constant from 150 min onwards. Coinciding with this change in the nuclear morphology, a steady increase of cells with Rad52 foci was also observed (up to 35% of cells by 240 min). In the case of *top2-5*, we observed a quicker G1-S entry and a different mix of cell morphologies by the end of the time course (Figure 1A, right panels; Figure 1B). Thus, we found a decrease of the dumbbell category from 150 min and the presence of “threesomes,” where the mother cell has rebudded, in up to 25% of the population, a percentage that was higher than that of *top2-4* (Figure 1B). Furthermore, there was only a transient peak of SD-binucleated at 120 min (Figure 1A, right

panels), with <10% of the cells having this morphology after 4 hr (Figure 1B). Likewise, Rad52 foci abruptly rose from 120 min, reaching 60% of all cells by 180 min, twice as many as in *top2-4* (Figure 1A, lower panels).

We next complemented the time course experiments with videomicroscopy aimed to follow up single cells throughout their first and second cell cycles (up to 6 hr). In order to do so, we filmed on agarose patches an asynchronous population of cells at the restrictive temperature and analyzed those cells that were in G1 (unbudded) at the time of the temperature shift. First, we filmed the *TOP2* strain as a control and found normal cell cycle progression for up to two generations for the mother and one generation for its first daughter (Figure 2A, upper chart). We also found little indication of cells undergoing arrest in G1 (categories 1, 5 and 9), in G2/M (categories 3, 7 and 11), or presenting CABs (categories 4, 8 and 12). By contrast, we found that *top2-ts* cells starting in G1 struggled to rebud in the second cell cycle (Figure 2A, mid and lower charts), with only a minority of cells that had done so by 6 hr (~20% of *top2-4* and *top2-5* mothers; *i.e.*, the sum of the orange bar values from morphological categories 6–13). As in the case of the time course with liquid cultures, the cell cycle on agarose patches was slightly quicker in *top2-5* than in *top2-4* (drop of category 1).

Videomicroscopy allowed us to gain insights about the time that cells spent with the SD-binucleated and CABs phenotypes (Figure 2B). Thus, around 5–10% of *top2-ts* cells had these phenotypes in two continuous frames (*i.e.*, aberrant segregation phenotypes lasted >1 hr). Although the low percentage and limited number of single cells analyzed precluded a definitive assessment, these long-lasting incomplete segregations occurred in *top2-4* cells more often. A close look at cells while transiting through anaphase (30 min frame intervals) confirmed the long-lasting nature of these “short distance” nuclear morphologies, as opposed to those cells that quickly ended up in the LD-binucleated morphology (Figure 2C). To confirm that the SD-binucleated phenotype was a proper split of nuclear masses rather than a mere relocalization of histones, we took samples and stained the DNA with DAPI. In all cases, the DAPI signal overlapped with the H2A-GFP (Figure 2D).

Finally, the use of live cell imaging also allowed us to visualize other striking aberrant anaphases. Although these phenotypes occurred in <1% of filmed cells, both G1 and early S phase (small bud) at the time of the temperature shift, they show remarkable instances of uncoupling between the nuclear division and the cell cycle in *top2-ts* (*e.g.*, rebudding before splitting the chromatin bridge) (Figure S2 in File S1).

### Cytokinesis progression correlates with the shape of the segregating nuclear mass in *top2-ts* mutants

Both the presence of dynamic SD-binucleated phenotypes and the low percentage of CABs were surprising for *top2-ts*, taking into account that depletion of Top2 is considered the prototypical model to elicit anaphase bridges. This led us to study *top2-ts* anaphases in more detail. First, we wondered about the completion of cytokinesis in these mutants. Previous reports have suggested that *top2-4* CABs delay cytokinesis (Mendoza *et al.* 2009). This delay would explain the observed accumulation of dumbbells and threesomes, but it would also predict an easy visualization of CABs due to the gross defects in sister chromatid resolution.

Cell wall digestion has often been used to check whether mother and daughter cells have finished cytokinesis yet not completed septum formation. We performed this digestion on *top2-ts* cells that were well into anaphase or beyond; *i.e.*, 4 hr after the G1 release at 37° (Figure 3A). Strikingly, dumbbells remained as such, although more than half of the threesomes were split in two (one budded and one unbudded cell,

Este documento incorpora firma electrónica, y es copia auténtica de un documento electrónico archivado por la ULL según la Ley 39/2015.

Su autenticidad puede ser contrastada en la siguiente dirección <https://sede.ull.es/validacion/>

Identificador del documento: 3075810

Código de verificación: smutbmB+

Firmado por: JESSEL AYRA PLASENCIA  
UNIVERSIDAD DE LA LAGUNA

Fecha: 30/11/2020 12:24:14

María de las Maravillas Aguiar Aguiar  
UNIVERSIDAD DE LA LAGUNA

08/02/2021 13:50:06

Appendix III

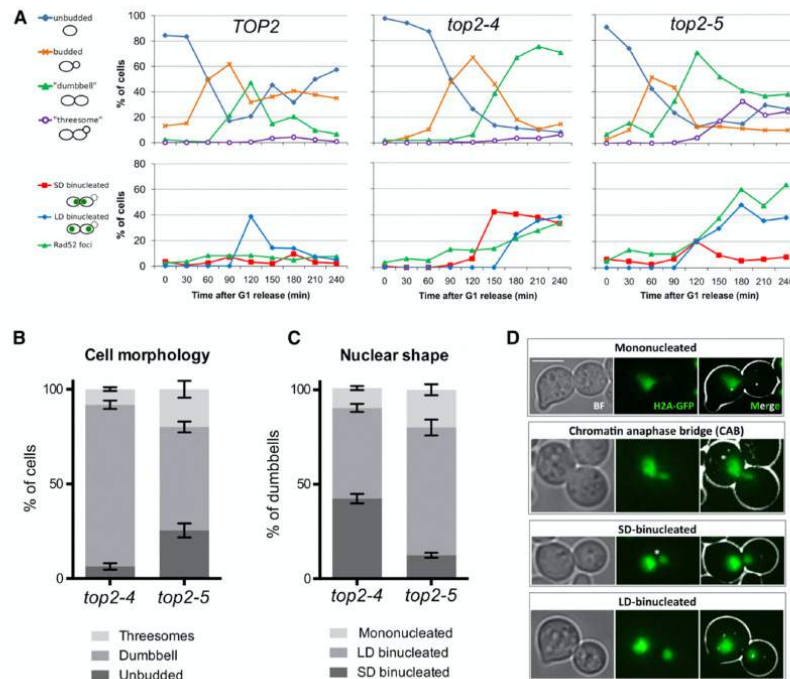


**Figure 1** Cell morphology and segregation of the nucleus upon inactivation of Top2 by the temperature-sensitive *top2-4* and *top2-5* alleles. (A) HTA2-GFP Rad52-RedStar2 yeast cells carrying different alleles of the *TOP2* gene (wild-type *TOP2* and thermosensitive alleles *top2-4* and *top2-5*) were synchronized in G1 at the permissive temperature (25°C) and then released into a synchronous cell cycle at 37°C for 4 hr. Samples were taken every 30 min and directly analyzed by fluorescence microscopy. More than 150 cells were counted for each time point. Upper charts depict the budding pattern of the population. Lower charts depict the percentage of cells with histone-labeled split nuclear masses that either remained at a short distance ( $\leq 1 \mu\text{m}$ ) from one another (“SD-binucleated”) or were separated by a longer distance (“LD-binucleated”). Percentage of cells with at least one Rad52 focus is also included. (B) Stacked bar chart of the observed end-point budding morphologies from three independent experiments (after 4 hr at 37°C, mean  $\pm$  SEM). (C) Stacked bar chart of the nuclear morphologies observed for the dumbbell subpopulation from (B). (D) Examples of different nuclear morphologies observed in cell dumbbells of *top2-ts* mutants. The asterisk highlights that SD-binucleated cells have an apparent segregation defect, yet a proper chromatin anaphase bridge (CAB) cannot be visualized. The bar corresponds to 5  $\mu\text{m}$ .

whose proportions thus became slightly higher upon digestion). This result was somewhat expected for *top2-4*, based on the higher prevalence of SD-binucleated dumbbells and previous reports (Mendoza *et al.* 2009); however, it was surprising for *top2-5* since dumbbells were mostly LD-binucleated and were steadily being split into two by 4 hr (Figure 1, A and B). Hence, we decided to complete the analysis of *top2-5* by directly checking abscission of the PM at the bud neck. In order to do so, we engineered the original *top2-5* strain to express the PM marker 2xPH-GFP. Interestingly, abscission (*i.e.*, PM resolved in two at the bud neck) had taken place in at least 50% of the dumbbells and all threesomes 4 hr after the G1 release (Figure 3, B and C). As for the other 50% of dumbbells that fell into a preabscission category, half of them had a full contracted furrow and the other half an open neck; *i.e.*, PM ingression at the cleavage furrow was absent or just partial. Interestingly, CABs were only visible in cells with an open cleavage furrow, although most of these cells were just mononucleated (~1:2 ratio). By

contrast, SD-binucleated cells always had either a contracted or a resolved PM (Figure 3B, photos).

**Chromatin anaphase bridges in *top2-ts* are stabilized by preventing mitotic exit**

Since there is PM ingression in *top2-ts* mutants, we next decided to check what the nuclear morphology looks like if ingression is fully abrogated. Cytokinesis is executed by the MEN, which also makes possible the telophase-to-G1 transition (Jaspersen *et al.* 1998; Meitinger *et al.* 2012; Weiss 2012). We chose two broadly-used *ts* alleles for essential genes involved in MEN to prevent cytokinesis, *cdc15-2* and *cdc14-1*. At 37°C, both mutants block cells in telophase with an open cleavage furrow (Bembenek *et al.* 2005); however, there are important differences between them. Cdc14 is the key MEN player, but it also has physiological roles unrelated to cytokinesis in early anaphase. Thus, Cdc14 gets activated twice in anaphase, first by the so-called FEAR

Este documento incorpora firma electrónica, y es copia auténtica de un documento electrónico archivado por la ULL según la Ley 39/2015.  
 Su autenticidad puede ser contrastada en la siguiente dirección <https://sede.ull.es/validacion/>

Identificador del documento: 3075810 Código de verificación: smutbmB+

Firmado por: JESSEL AYRA PLASENCIA  
 UNIVERSIDAD DE LA LAGUNA

Fecha: 30/11/2020 12:24:14

María de las Maravillas Aguiar Aguiar  
 UNIVERSIDAD DE LA LAGUNA

08/02/2021 13:50:06

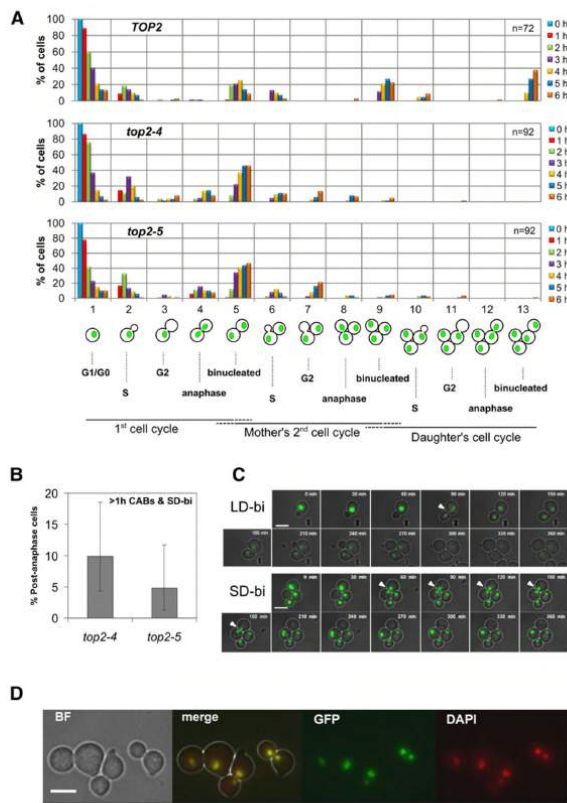


**Figure 2** Single-cell live microscopy of *top2-4* and *top2-5* alleles for the first two cell cycles at the restrictive temperature. (A) *HTA2-GFP* cells carrying different alleles of the *TOP2* gene (*TOP2*, *top2-4* and *top2-5*) were grown at 25°, concentrated to  $OD_{600} = 3$ , spread onto YPD agarose patches, and filmed under the microscope at 37° for 6 hr, taking images every 1 hr. Several films were independently recorded and the subpopulation of cells which were at G1 (unbudded) at the time of the temperature shift were followed (cell number is indicated on the upper right corner of each bar chart). Each hour, cells were either kept in their preceding category (starting at “1,” first cell cycle G1) or moved into one of the 13 categories shown on the X-axis. The bar charts represent the percentage of cells in each of these categories at any given time point. Horizontal dashed line ends under the categories indicate uncertainty about which cell cycle stage cells are in (e.g., category “5” grouped those cells which are in the first cell cycle’s telophase together with those mother and daughter cells in the second cycle’s G1). (B) Analysis of cells where anaphase lasted longer than 1 hr in the cells studied in (A); i.e., cells that remained in category “4” for at least two successive frames. Only cells that reached or passed the first anaphase were considered for the analysis. Error bars represent CI95 of the cell proportion. (C) The same *top2-ts HTA2-GFP* strains used for (A) were filmed again at 37° but taking images every 30 min. Representative cells where a CAB was seen are shown. The upper “LD-binucleated” example is from a *top2-5* cell and the lower “SD-binucleated” example is taken from a *top2-4* cell. White-filled triangles pointing to H2A-GFP CABs are included in the corresponding frames. (D) *HTA2-GFP top2-4* after 4 hr at 37° in liquid cultures showing a perfect colocalization of H2A-GFP and DAPI staining in cells with the SD-binucleated morphology. The bar corresponds to 5  $\mu$ m. BF, bright field.

network and then by MEN (Stegmeier and Amon 2004; Machin *et al.* 2016). *Cdc15* is only involved in the *Cdc14* activation by MEN. Importantly, whereas the single *cdc15-2* mutant allows full segregation of sister chromatids, single *cdc14-ts* mutants give rise to a thin CAB that comprises the ribosomal DNA (rDNA) chromosome arm (D’Amours *et al.* 2004; Machin *et al.* 2005).

First, we constructed *top2-5 cdc15-2* and *top2-5 cdc14-1* double mutants and checked whether they were better protected than the single *top2-5* mutant against transient *Top2* inactivation. Protection by *cdc15-2* has been reported before for *Top2* depletion through a degen allele (Baxter and Diffley 2008). We found that *top2-5 cdc15-2* survived slightly better than *top2-5* in the restrictive regime (Figure 4, A and B), whereas there was no difference for *top2-5 cdc14-1*. In order to address the nuclear morphology, we arrested these strains in telophase, together with the corresponding *TOP2 cdc15-2/cdc14-1* controls. We found that *top2-5 cdc15-2* could not resolve the CAB (Figure 4C). By contrast, full segregation of the histone signal was seen in all *TOP2 cdc15-2* cells. In the case of *top2-5 cdc14-1*, the nuclear segregation was worse; we observed that most of the nucleus was in the bud (Figure 4D). This synergistic nuclear segregation defect in *top2-5 cdc14-1* may

account for the lack of genetic suppression of *top2-5* despite *cdc14-1* also blocking cytokinesis (see *Discussion* chapter). Overall, these two double mutants demonstrate that the *top2-5* strain gives rise to actual CABs and that the contraction of the cytokinetic furrow quickly split this CAB apart (see below).

We also made a *top2-4 cdc15-aid* strain. We used *cdc15-aid* (*Cdc15* depletion by auxin addition rather than temperature shift) because it was difficult to phenotypically confirm *top2-4 cdc15-2* as *top2-4* alone got stuck as dumbbells (Figure 1). We also observed CABs when both *Top2-4* and *Cdc15-aid* were depleted [33% (24–43%)]. In this case, most CABs had a SD-binucleated appearance (Figure S3 in File S1).

#### Ultrafine anaphase bridges are also split apart in *top2-5*

A final cell imaging analysis we performed was to check UFBs in *top2-5* and address their fate after membrane abscission. These UFBs comprise mysterious forms of DNA that connect segregated nuclei and are refractory to classical DNA dyes and histone labeling (Chan *et al.* 2007). UFBs can, however, be detected with specific proteins that interact with them in anaphase; one such protein in yeast is *Dpb11* (Germann *et al.* 2014). Thus, we looked at a *top2-5* strain that had been triple-labeled

Este documento incorpora firma electrónica, y es copia auténtica de un documento electrónico archivado por la ULL según la Ley 39/2015.  
 Su autenticidad puede ser contrastada en la siguiente dirección <https://sede.ull.es/validacion/>

Identificador del documento: 3075810 Código de verificación: smutbmB+

Firmado por: JESSEL AYRA PLASENCIA  
 UNIVERSIDAD DE LA LAGUNA

Fecha: 30/11/2020 12:24:14

María de las Maravillas Aguiar Aguiar  
 UNIVERSIDAD DE LA LAGUNA

08/02/2021 13:50:06

Apendix III

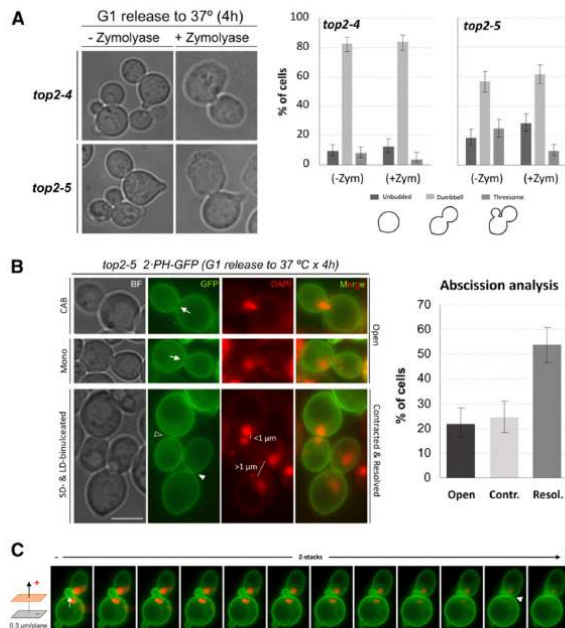


**Figure 3** Cytokinesis defects in *top2-ts* and correlation with the different abnormal nuclear segregation morphologies. (A) The same *top2-4* and *top2-5* strains used for Figure 2 were synchronized in G1 at the permissive temperature (25°) and then released into a synchronous cell cycle at 37° for 4 hr. A sample was then taken, fixed with formaldehyde, and split in two for addressing cytokinesis through the cell wall digestion assay; i.e., comparing cell morphologies after zymolyase or a mock treatment. On the left, representative pictures of cells for the mock control and zymolyase treatment. On the right, quantification of major cell morphologies. Error bars depict CI95 of the measured percentages. (B) A *top2-5* strain expressing the plasma membrane (PM) marker PH-GFP was released in a synchronous cell cycle as in (A). A sample taken after 4 hr was stained with DAPI and visualized under the microscope. On the left, representative cells showing different degrees of cytokinetic completion and their best corresponding nuclear shape across the neck. The arrow points to an “open” neck (no PM ingression) with either a CAB across (first cell) or mononucleated (second cell), the open arrowhead points to a “resolved” membrane at the neck (i.e., abscission with septum deposition in between) with a SD-binucleated nuclear morphology, and the filled arrowhead points to a “contracted” PM. (C) A complete Z-stack series of a representative threeome is shown. Note how the mother and the daughter have a resolved PM at the neck (filled arrowhead), whereas the mother and its second bud have an open neck (white arrow). The bar corresponds to 5 μm. BF, bright field.

with H2A-GFP, Dpb11-RFP, and the PM reporter Hoechst 33258, which becomes fluorescent in the CFP channel when bound to membranes (Shapiro and Ling 1995); we confirmed that Hoechst 33258 can also stain yeast PM *in vivo* and that a very short incubation (5 min) minimizes containing of the DNA (Figure S4 in File S1). In addition, we included a *top2-5 cdc15-2* strain to prevent cytokinesis, as well as the corresponding *TOP2 cdc15-2* control. First, we again observed PM abscission in *top2-5* at late time points of a synchronous cell cycle at 37°, whereas PM abscission was mostly absent in the *cdc15-2* strains (Figure 5A). Second, we again observed how CABs dropped as *top2-5* cells complete abscission, whereas CABs remained throughout the time course in the *top2-5 cdc15-2* strain (Figure 5B). Interestingly, few Dpb11-stained UFBs could be detected in either strain, whereas UFBs were relatively common in the *TOP2 cdc15-2* strain (30–40% of cells). Since there was no transient enrichment of UFBs relative to CABs during the drop of the latter in the *top2-5* strain, we conclude that UFBs are likely to be severed by PM abscission in this mutant. Moreover, we found a relocalization of Dpb11 to foci, which was specific for the *top2-5* strain (Figure 5C). This finding further indicates that DNA at the *top2-5* anaphase bridges is broken at the time of PM abscission (Germann *et al.* 2011).

**Synthetic genetic array analysis confirms mitotic exit and cytokinesis as deleterious enhancers of transient Top2 inactivation**

In order to weigh the overall negative contributions of mitotic exit and cytokinesis in each *top2-ts* allele, we carried out an SGA analysis with two collections of yeast mutants: the haploid gene deletion collection of nonessential genes (4322 knockout strains) and a collection of *ts* alleles

for essential genes (1231 *ts* strains) (Tong *et al.* 2001; Giaever *et al.* 2002; Li *et al.* 2011). SGA allows screening for genetic interactions in *S. cerevisiae* by comparing the fitness of the different mutant combinations (i.e., single mutants in the collections vs. double *top2-ts*/collection mutants). In addition, we decided to perform the SGA analysis in three different conditions that modify Top2 activity.

In our first analysis, we grew all the strains constantly at the permissive temperature (25°), and compared the collection of *top2-4* and *top2-5* double mutants with the corresponding *TOP2* counterparts as references. Thermosensitive alleles are expected to have a mild reduced fitness at the permissive temperature and, in our case, we indeed detected genetic interactions at 25°, 139 in *top2-4* and 167 in *top2-5* (Figure 6A, Table S2, and Table S3 in File S1). Eighty-four interactions were shared between *top2-4* and *top2-5*, and these interacted with both alleles in a similar way, either positively or negatively (Figure 6B and Table S4 in File S1). Among them was *top1Δ*, which is well known to have synthetic sickness with *top2-ts* alleles (Kim and Wang 1989). However, most of the observed genetic interactions were positive, which is typically a sign of suppressive pathways.

Next, we sought to study the changes that increasing the temperature would produce in the observed genetic interactions. We opted for two different incubations: one set of arrays was grown at semipermissive temperature (30°) for 2 d, and another set was incubated at 37° for 6 hr, and then shifted to 25° to allow growth of survivors. This transient restrictive regime gives enough time to complete one cell cycle without Top2 on solid media (Figure 2A), and indeed allowed us to observe the *cdc15-2* protection of *top2-5* (Figure 4A). In both cases we used the *top2-ts* arrays that were grown at 25° as controls to compare colony sizes. Thus, we obtained a large number of new interactions that, unlike

Este documento incorpora firma electrónica, y es copia auténtica de un documento electrónico archivado por la ULL según la Ley 39/2015.  
 Su autenticidad puede ser contrastada en la siguiente dirección <https://sede.ull.es/validacion/>

Identificador del documento: 3075810 Código de verificación: smutbmB+

Firmado por: JESSEL AYRA PLASENCIA  
 UNIVERSIDAD DE LA LAGUNA

Fecha: 30/11/2020 12:24:14

María de las Maravillas Aguiar Aguiar  
 UNIVERSIDAD DE LA LAGUNA

08/02/2021 13:50:06



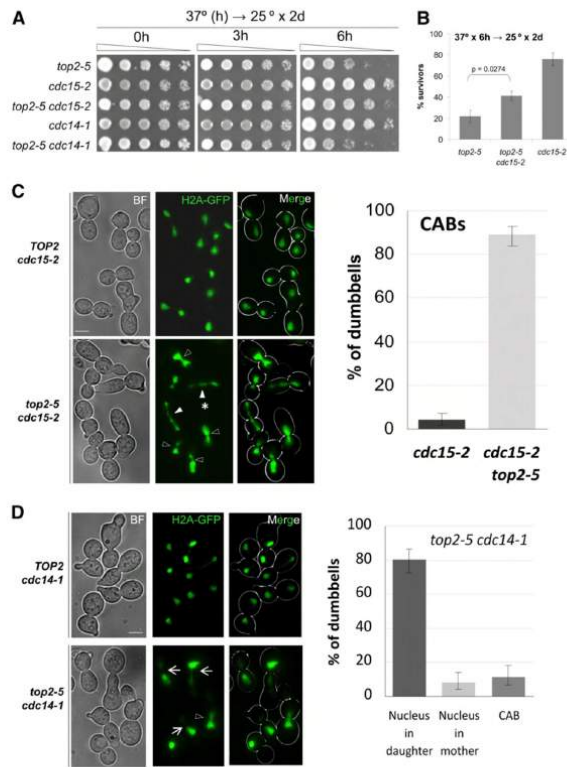


**Figure 4** The mitotic exit network (MEN) destabilizes top2-mediated chromatin anaphase bridges (CABs). (A) Spot dilution assay to compare survivability of different combinations of the top2-5, cdc14-1, and cdc15-2 alleles to a transient temperature shift to 37°. All strains are HTA2-GFP *bar1Δ* derivatives from the corresponding TOP2 and top2-5 coisogenic strains. (B) Clonogenic assay to compare survivability of the top2-5, cdc15-2, and top2-5 cdc15-2 strains to a transient 6 hr shift to 37° (mean ± SEM, n = 5). (C) The cdc15-2 HTA2-GFP and top2-5 cdc15-2 HTA2-GFP strains were synchronized in G1 at the permissive temperature (25°) and then released into a synchronous cell cycle at 37° for 4 hr. Samples were taken at the end of the experiment and analyzed by fluorescence microscopy. On the left, representative microscope fields for each strain. On the right, bar chart of cells with CABs (error bars are CI95). Open arrowheads point to examples of short CABs (~1/3 of observed CABs in top2-5 cdc15-2). Filled arrowheads point to examples of long CABs (~2/3 of observed CABs). The asterisk highlights the complex strung chromatin bridges seen in ~50% of the long CABs. (D) The cdc14-1 HTA2-GFP and top2-5 cdc14-1 HTA2-GFP strains were treated as in (C). On the left, representative microscope fields for each strain. On the right, bar chart of nuclear morphologies in dumbbells (error bars are CI95). Arrows point to cells where the bulk of the nucleus migrated to the bud, whereas open arrowheads point to CABs. Arrows and arrowheads point exactly at the bud neck. The bar corresponds to 5 μm. BF, bright field.

during constant growth at 25°, were mostly negative (Figure 6C, Table S5, and Table S6 in File S1). Ontological classification of significant interactions revealed common negative interactions at 37° × 6 hr with bioenergetics and autophagy (Table 1). This could be related to the heat shock treatment and putative roles of Top2 during chromosome reshaping and transcription reprogramming to cope with this stress (Pommier *et al.* 2016). Importantly, this classification also spotlighted a high number of positive interactions between top2-5 grown at 30° and/or 37° × 6 hr and thermosensitive alleles related to mitotic progression, especially anaphase/telophase progression (Figure 6D and Table 1). Many of the genes belong to the MEN, including CDC15, whereas others are related to the cytoskeleton or rDNA metabolism, which are known to undergo important modifications during anaphase (Machin *et al.* 2016). To a lesser extent, top2-4 was also enriched in mitotic division alleles when incubated at 37° × 6 hr, some of which overlap with those of top2-5 (e.g., STU1, CDC10 and MOB2) (Table S5 and Table S6 in File S1).

#### DISCUSSION

In this work we have presented single-cell biology studies and large-scale genetic interaction data that strongly support that the survival of a yeast cell transiently depleted from Top2 is negatively correlated with the

commitment to execute cytokinesis at the end of mitosis. To a great degree, our data confirm results by others who have previously explored such a possibility (Baxter and Difley 2008). Importantly, we have classified the different aberrant nuclear morphologies seen in top2-ts anaphases and correlated them with the degree of completion of cytokinesis.

In addition, we have found many positive genetic interactions between top2-ts and alleles or mutations that delay different stages of the cell cycle (Figure 6, Table 1, Table S2, Table S3, Table S4, Table S5, and Table S6 in File S1). We reason that such positive interactions, measured as improved fitness on a SGA, are better explained by: (i) fewer cells with CABs reaching the point-of-no-return (*i.e.*, cytokinesis) during the transient 37° × 6 hr shift; and (ii) the additional cell cycle delay allowing the reduced Top2 activity to end up resolving catenations, especially in the case of steady incubations at 25 and 30°. Again, these positive interactions support previous works that claimed that blocking the cell cycle in G1 or G2/M protects against transient Top2 depletion (Holm *et al.* 1985; Thomas *et al.* 1991).

Finally, our work also put forward some intriguing questions about why downregulation of Cdc14, the trigger of exit from mitosis, does not protect against Top2 deficiency. Last but not least, we uncovered surprising differences between the two top2-ts alleles used in this work, top2-4 and top2-5.

Appendix III

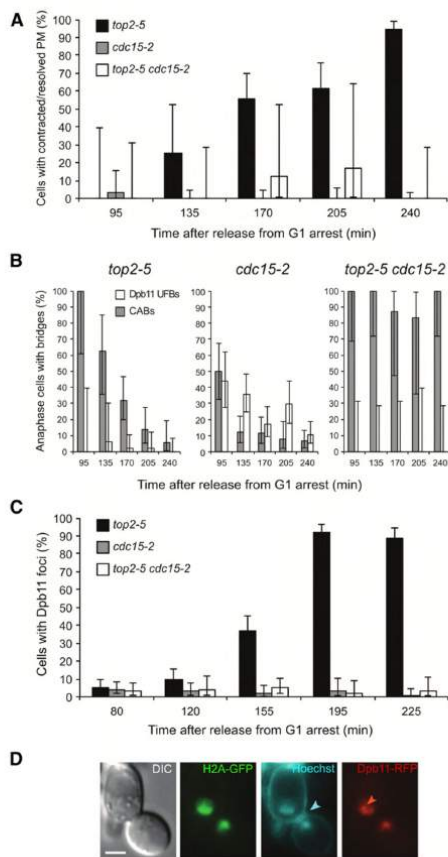


**Figure 5** Dpb11 Ultrafine bridges are also destabilized by cytokinesis in *top2-5*. Coisogenic *top2-5*, *cdc15-2*, and *top2-5 cdc15-2* strains bearing the *HTA2-GFP Dpb11-yEmRFP bar1Δ* genotype were released into a synchronous cell cycle at 37°. At the indicated time points, the plasma membrane (PM) was stained with 5 μg/ml Hoechst 33258 for 5 min at 37° before processing for fluorescence microscopy. (A) The time course of PM abscission (full contraction and resolution at the cytokinetic plane). Note how *top2-5* mutant cells progress to abscission. (B) The time course of both CABs and UFBs in anaphase cells. Note how *top2-5* mutant cells do not accumulate UFBs, not even transiently, while CABs are split apart. (C) The time course of Dpb11 foci formation. Note how *top2-5* mutant cells accumulate Dpb11 foci. Error bars depict CI95 ( $n = 50-200$ ). (D) The prototypical example of a late anaphase *top2-5* cell; i.e., PM has completed abscission, there is no longer a CAB connecting the mother and the daughter cell, nor are there any Dpb11-UFBs, and Dpb11 accumulates in foci within the split nuclear masses instead. The cyan arrowhead points to the resolved PM, whereas the red arrowhead points to a Dpb11 focus. The bar corresponds to 3 μm. DIC, differential interference contrast.

**On the nature and fate of the anaphase bridges that result from depleting Top2**

We started this work by revisiting earlier works from Botstein's and Sternglanz's laboratories on yeast cells cycling without Top2 activity (DiNardo *et al.* 1984; Holm *et al.* 1985). These studies reported that *S. cerevisiae* had no terminal phenotype at the *top2-ts* restrictive temperature. Rather, a mixture of unbudded and large-budded (dumbbell) cells was the final outcome of Top2 inactivation. In many dumbbell cells, failure in chromosome segregation was evident due to the presence of DAPI-stained anaphase bridges. They assumed that there were two classes of cells coming from a *top2-ts* G1-synchronized culture: those which get stuck as dumbbells with major defects in nuclear segregation, and those which complete cytokinesis and cell separation. In light of the unbudded progeny they observed, they concluded that the latter had gone through a devastating mitotic catastrophe. In general, our data fully support this conclusion (profiles of cell morphologies in Figure 1 and Figure 2). The most shocking difference is the relatively low percentage of visible anaphase bridges, which we here refer to as CABs since we used histone-labeled DNA (H2A-GFP). Of note, we also observed a small fraction of anaphase bridges when staining with either DAPI or Hoechst and, in addition, H2A-GFP and DAPI signals perfectly colocalized (Figure 2B). Instead of CABs, we often distinguished very close split nuclear masses just across the neck (SD-binucleated). The distance between the split signals was normally <1 μm. It is likely that this phenotype has been referred to as "anaphase bridge" in previous works. Notably, a similar phenotype was described before for a strain that depletes Top2 through a degron system and referred to as "cut" phenotype (Baxter and Diffley 2008). Besides, a similar terminal phenotype occurs in mouse *topo IIα*<sup>-/-</sup> embryos and in a significant fraction (~1/3) of epithelial cells treated with Top2 catalytic inhibitors (Wheatley *et al.* 1998; Akimitsu *et al.* 2003). Outstandingly, we have been able to correlate this SD-binucleated phenotype to ingression of the cleavage furrow at the cytokinetic plate. On the one hand, we observed that CABs were only visible when ingression was absent (Figure 3B). On the contrary, SD-binucleated required either full contraction or resolution of the PM at the neck (abscission). On the other hand, when we blocked MEN in *top2-ts* by depleting Cdc15, and hence we also blocked cleavage furrow ingression, the SD-binucleated morphology was absent and a CAB was seen instead (Figure 4C and Figure S4 in File S1). As mentioned already, the large-scale screen for genetic interactions also supports that commitment to execute cytokinesis is deleterious for *top2-ts* (Figure 6, Table 1, Table S2, Table S3, Table S4, Table S5, and Table S6 in File S1).

An intriguing question is what happens to the CAB during PM ingression and abscission. Two alternative hypotheses were possible: (i) the CAB is broken through cytokinesis, or (ii) the CAB becomes a histone- and DAPI-invisible UFB. Notably, a recent report has shown that thin channels of nuclear material are formed between the mother and the daughter cells when Top2 is depleted (Amaral *et al.* 2016). These channels go through cells that appear to have completed PM abscission, are fully surrounded by septum, and might be wide enough to accommodate UFBs. These channels might also explain why we observed PM abscission in many *top2-ts* dumbbells but were unable to split them upon zymolyase treatment (Figure 3, A and B). We have tried to address the fate of CABs during PM ingression by triple-labeling the PM, the CAB (H2A-GFP), and the UFB (Dpb11-RFP). Our data do support that most CABs (and UFBs) are broken apart at the time of PM abscission, (Figure 5). Thus, there was no change in the CAB/UFB ratio during the drop of anaphase bridges by PM abscission in *top2-5*. In addition, Dpb11 relocated to foci which, together with the formation

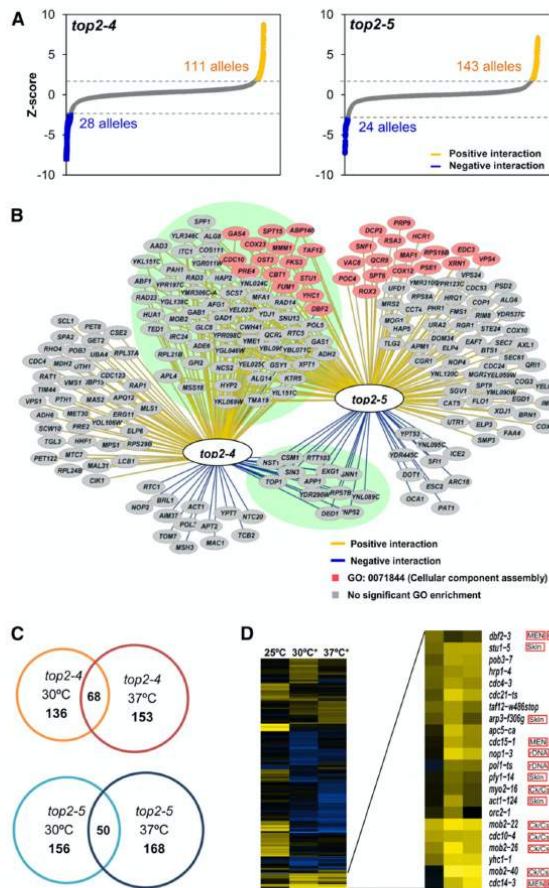


**Figure 6** SGA analyses identify the MEN as deleterious enhancers of Top2 downregulation. (A) The z-scores of the genetic interactions detected at permissive temperature (steady growth at 25°) are plotted. The *top2-ts* arrays of mutants were compared with the *TOP2* arrays as a control. 5553 alleles were screened in total. Positive and negative genetic interactions that meet the cutoffs (>2 or < -2) are indicated. (B) Network of the genes that interact with *top2-4* and *top2-5*. Green background encircles the 84 shared genes between the two *top2-ts*. Pink nodes indicate the positive interaction between *top2-5* and genes involved in the aggregation and bonding of cellular components (GO: 0071844). (C) The numbers of genetic interactions identified during steady growth at 30° and after 6 hr incubation at 37° are shown. Circle intersections depict number of genetic interactions shared between both treatments. (D) Heat map of *top2-5* SGA scores (those with  $P < 0.05$ ). Yellow, positive interactions; blue, negative interactions; black, no interaction. The 25° Column represents the z-score obtained comparing *top2-5* vs. *TOP2* at 25°, whereas the 30° and 37° × 6 hr columns compare *top2-5* at these temperature regimes vs. *top2-5* at 25°. MEN, mitotic exit network; Ck/Cs, cytokinesis/cell separation; Skln, cytoskeleton; rDNA, ribosomal DNA metabolism.

of Rad52 foci (Figure 1A), strongly points toward DSBs taking place in *top2-5* late anaphase. Since PM abscission, CAB/UFB disappearance, and Dpb11 foci accumulation could all be prevented in the *top2-5 cdc15-2* double mutant, we favor the hypothesis that all kinds of anaphase bridges are broken as a consequence of cytokinesis. Nevertheless, the alternative hypotheses of (i) Dpb11 relocating from UFBs to DNA repair foci upon CAB breakage or (ii) the UFB becoming too narrow for the current limits of fluorescence microscopy cannot be ruled out entirely and deserve further investigation in the future, especially in the light of the aforementioned channels.

Altogether, we propose a model where cells depleted from Top2 always form CABs at anaphase (Figure 7). These CABs can be massive and might often prevent the mitotic spindle from pulling the segregating sister chromatids away from each other, hence the short distances that separate the splitting masses across the bud neck. Alternative possibilities for such short distances are feasible but unlikely; e.g.,

Top2 is known to play no roles during mitotic spindle enlargement (Andrews *et al.* 2006). Importantly, these CABs do not prevent cleavage furrow ingression, which quickly changes them into SD-binnucleated (Figure 3B). Remarkably, cells depleted from the condensin subunit Brn1, which are thought to give rise to *top2*-equivalent anaphase bridges, do not delay execution of cytokinesis either (Cuylen *et al.* 2013), and only a short delay of 15 min was seen for karyokinesis in anaphase bridges restricted to the rDNA (Quevedo *et al.* 2012). What happens after full membrane ingression is less clear. However, DNA damage seems apparent (Figure 1 and Figure 5), suggesting that DNA is severed as reported previously (Holm *et al.* 1989; Baxter and Diffley 2008). Again condensin depletion leads to similar results (Cuylen *et al.* 2013). Strong support for this model was obtained when we blocked MEN and cytokinesis (*i.e.*, *cdc15-2*) in *top2-5* strains. Thus, CABs were stabilized in the *top2-5 cdc15-2* double mutant and no signs of DNA damage were detected (Figure 1 and Figure 5). Strikingly, though, even

Este documento incorpora firma electrónica, y es copia auténtica de un documento electrónico archivado por la ULL según la Ley 39/2015.  
 Su autenticidad puede ser contrastada en la siguiente dirección <https://sede.ull.es/validacion/>

Identificador del documento: 3075810 Código de verificación: smutbmB+

Firmado por: JESSEL AYRA PLASENCIA  
 UNIVERSIDAD DE LA LAGUNA

Fecha: 30/11/2020 12:24:14

María de las Maravillas Aguiar Aguiar  
 UNIVERSIDAD DE LA LAGUNA

08/02/2021 13:50:06

Appendix III

■ Table 1 Significant biological processes that genetically interact with top2-ts in different downregulating regimes

SGA group <sup>a</sup>	Gene Ontology <sup>b</sup>	P-value <sup>c</sup>
top2-4 – 30° (pos. int.)	Carbohydrate biosynthetic process (GO:0016051)	0.04323
top2-4 – 37° x 6h (pos. int.)	APC-dependent ubiquitin-dependent protein process (GO:0031145) Cell division (GO:0051301)	0.00681 0.00706
top2-4 – 37° x 6h (neg. int.)	Macroautophagy (GO:0034262)	0.03361
top2-5 – 30° (pos. int.)	Macromolecular complex subunit organization (GO:0043933) Organelle assembly (GO:0070925)	0.00115 0.04773
top2-5 – 37° x 6h (pos. int.)	Cell division (GO:0051301) Mitotic cell cycle process (GO:1903047) Mitotic cell cycle (GO:0000278) Mitotic nuclear division (GO:0007067) Mitotic cell cycle phase transition (GO:0044772) Cell cycle phase transition (GO:0044770) Cell separation after cytokinesis (GO:0000920) Nuclear division (GO:0000280) Regulation of cell division (GO:0051302)	1.49E-05 0.00017 0.00033 0.00035 0.0006 0.00068 0.02562 0.03884 0.04929
top2-5 – 37° x 6h (neg. int.)	Macroautophagy (GO:0034262) Cellular respiration (GO:0045333) Oxidative phosphorylation (GO:0006119) Generation of precursor metabolites and energy (GO:0006091) Phosphorylation (GO:0016310) Autophagy (GO:0006914) Homoserine metabolic process (GO:0009092) Sister chromatid biorientation (GO:0031134) Energy derivation by oxidation of organic compounds (GO:0015980)	0.00048 0.00067 0.00238 0.00301 0.01924 0.02062 0.02391 0.02391 0.04017

<sup>a</sup>The corresponding top2-ts double mutant arrays were grown at 25° x 2 d, 30° x 2 d, and 6 hr x 37° + 25° x 2 d. The genetic positive interactions (pos. int.) and negative interactions (neg. int.) refer to the comparison between the downregulating temperature regimes and steady growth at 25°.

<sup>b</sup>Gene Ontology (GO) enrichment analyses were done using the Generic GO Term Finder (<http://go.princeton.edu/cgi-bin/GOTermFinder>). GO terms that contained > 1500 genes were discarded, as they are usually too general. Similarly, redundant GO terms with < 10 genes were discarded.

<sup>c</sup>P-values were computed using a hypergeometric distribution, and adjusted with the Bonferroni correction.

complete block of MEN yielded only partial recovery when Top2-5 was reactivated (Figure 4A). In our study, this recovery was slightly smaller than the one previously reported (Baxter and Difley 2008), likely due to the fact that we incubated the cells at 37° for a longer period. It is probable that the partial recovery relates to cells restoring Top2 and Cdc15 functions at the same time after the 37–25° shift, although the possibility of CABs becoming irreversible upon a long absence of Top2 should not be ruled out completely. Indeed, we have shown before that rDNA bridges in *cdc14-1* eventually become challenging to resolve (Machin *et al.* 2006; Quevedo *et al.* 2012).

**On the putative synergistic role of Cdc14 in anaphase bridge resolution through the FEAR network**

Top2 is not the only universal player needed to avoid the occurrence of CABs during the mitotic cell division. The condensin complex also plays a key role in preventing CABs throughout all life kingdoms (Kalitsis *et al.* 2017). Previous works have placed condensin and Top2 within the same pathway to accurately remove sister chromatid catenations in *S. cerevisiae* (Baxter *et al.* 2011; Charbin *et al.* 2014). The master mitotic phosphatase Cdc14 controls resolution of sister chromatids by acting on overall transcription and thus favoring condensin

localization onto DNA, conditions that are especially critical for the highly transcribed rDNA array (Machin *et al.* 2016). This Cdc14 control over condensin takes place in early anaphase and is possible because Cdc14 is transiently activated there through the FEAR network. Cdc14 also plays an essential role for exit from mitosis at late anaphase through its second activation by MEN. The kinase Cdc15 is critical for Cdc14 activation by MEN but not by the FEAR network (Stegmeier and Amon 2004). In this work, we have seen two important differences when the top2-5 allele was combined with ts mutants for the *CDC14* and *CDC15* genes. First, top2-5 *cdc15-2* could partly rescue the reduced fitness of top2-5, whereas top2-5 *cdc14-1* did not (Figure 4, A and B). This was confirmed in the SGA analysis, where *cdc15-1* (*cdc15-2* was not present) also alleviated top2-5; whereas two out of the three included *cdc14-ts* alleles were neutral (*cdc14-1* and *cdc14-2*; just *cdc14-3* emerged as a suppressor). Second, top2-5 *cdc15-2* led to CABs that resembled the morphology of the SD- and LD-binucleated nuclear masses in top2-5; *i.e.*, addition of a bridge to these morphologies was the only difference (Figure 4C). Nevertheless, top2-5 *cdc14-1* gave a missegregation pattern that was clearly worse than either ts allele alone. In most cases the nuclear mass failed to split entirely, yet it localized within the daughter cell (Figure 4D). This phenotype is reminiscent of

Este documento incorpora firma electrónica, y es copia auténtica de un documento electrónico archivado por la ULL según la Ley 39/2015.  
 Su autenticidad puede ser contrastada en la siguiente dirección <https://sede.ull.es/validacion/>

Identificador del documento: 3075810 Código de verificación: smutbmB+

Firmado por: JESSEL AYRA PLASENCIA  
 UNIVERSIDAD DE LA LAGUNA

Fecha: 30/11/2020 12:24:14

María de las Maravillas Aguiar Aguilár  
 UNIVERSIDAD DE LA LAGUNA

08/02/2021 13:50:06

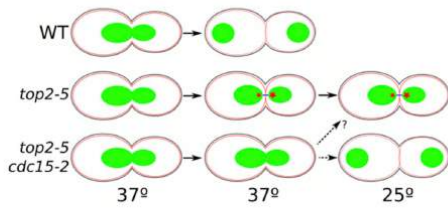


**Figure 7** Summary and model of anaphase progression in *top2-5* and *top2-5 cdc15-2* mutants. Cells with wild-type (WT, upper schematic) Top2 enter anaphase and quickly resolve catenations to yield LD-binucleated cells. Temperature-sensitive *top2-5* (middle schematic) also enters anaphase on schedule but fails to resolve catenations, yielding a chromatin anaphase bridge (CAB). CABs cover a short distance across the neck in many instances (SD-phenotype). Importantly, cytokinetic furrow ingression is not blocked and results in CABs being visibly severed into binucleated morphologies (Figure 1, Figure 2, Figure 3, Figure 4, and Figure 5). Two scenarios are possible: DNA is actually severed by cytokinesis, or the CAB is turned into a sort of Dpb11-free ultrafine bridge (blue line) (Figure 5). In any case, DNA damage arises and is sensed in the progeny (red stars). Damage might be worse in the daughter cells since ~20% of the mothers can rebud at least once (Figure 2). Blocking cytokinesis in *top2-5 cdc15-2* (lower schematic) stabilizes CABs. Resuming Top2 function after anaphase in *top2-5* (shift to 25°) yields an unviable progeny. Resuming Top2 and cytokinesis (Cdc15) at the same time gives a window of opportunity to recover and may yield at least one viable cell (dashed arrows). Green objects depict the nuclear masses (histone-labeled DNA); black lines on the cell surface depict cell wall; red thin lines depict the PM.

cells depleted of separase, the protease that breaks sister chromatid proteinaceous cohesion at the anaphase onset (McGrew *et al.* 1992). Taking into account that *cdc14-1* strains are also known to mistakenly segregate the nucleus to the daughter cell (Ross and Cohen-Fix 2004), the synergistic nuclear segregation defect in *top2-5 cdc14-1* may be due to the lack of a FEAR-dependent spindle pulling force back toward the mother. The alternative hypothesis is that Top2 and Cdc14 actually work in parallel pathways. This hypothesis would thus put forward that either condensin has Top2-independent roles or, alternatively, Cdc14 controls condensin-independent processes important for sister chromatid resolution. In support of the latter, Cdc14 depletion also results in an enrichment of regions with unfinished replication, particularly in the rDNA, as well as sister chromatids still connected through recombination intermediates (Dulev *et al.* 2009; García-Luis *et al.* 2014). However, similar problems have been described in *top2* mutants as well (Baxter and Diffley 2008; Fachinetti *et al.* 2010). Finally, it is worth mentioning that the highly asymmetric segregation of the nucleus we observed in *top2-5 cdc14-1* is the hallmark of mammalian epithelial cells treated with Top2 catalytic inhibitors (Gorbsky 1994; Wheatley *et al.* 1998).

#### On the similarities and differences between *top2-4* and *top2-5*

Temperature-sensitive alleles for TOP2 were originally thought to be equivalent. In the first screenings for such *top2-ts* alleles, just one was normally selected and deeply studied, assuming that the other *top2-ts* were identical. That was the case for *top2-4*, which has been widely used since and founded most of the knowledge we have about Top2 functions in yeast. Nevertheless, independent isolation of *top2-ts* from different labs showed later that *top2-ts* could carry intrinsic and variable

properties in terms of cell cycle progression, commitment to enter anaphase, etc. (Andrews *et al.* 2006). One of the first surprising findings was that there was a difference in terms of resistance to the clinically used Top2 poisons within the same *top2-ts* group where *top2-4* was isolated. Thus, *top2-5* proved to be resistant to poisons even at permissive temperature (Jannatipour *et al.* 1993). This fact led us to include coisogenic *top2-4* and *top2-5* strains in this work. Surprisingly, we found marked differences between them. In general, both *top2-ts* alleles shared many similarities: (i) they failed to arrest in G2/M; (ii) they formed short-lived CABs, which could be stabilized by depleting Cdc15; (iii) they had DNA damage coinciding with anaphase progression; (iv) they led to two classes of split nuclear masses in anaphase (SD- and LD-binucleated); and (v) the immediate progeny often failed to bud again, and when they did, budding was restricted to the mother. The differences were more related to the timing of the cell cycle events and relative proportions of several phenotypes (Figure 1). It is important to highlight that these differences were more obvious in time course experiments carried out in liquid cultures than when we filmed single cells on agarose patches (Figure 2). In the time course experiments, *top2-5* progressed through the cell cycle faster than *top2-4*. It also became stalled as dumbbells less frequently than *top2-4*. Likewise, SD-binucleated occurred less frequently in *top2-5*. Since *top2-5* had a quicker G1-S transition in cultures relative to cells filmed on agarose patches, the most trivial explanation for these differences lay in this G1-S transition, making later phenotypes appear earlier and evolve into others quicker. As for the reason behind this difference, we can hypothesize about two origins. On the one hand, the difference may relate to the genetic history of these strains through the numerous passes over the years. Taking into account that it has been shown that Top2-5 only keeps 33% of normal Top2 activity at 25° (Jannatipour *et al.* 1993), we believe that the *top2-ts* strains might be genetically unstable at 25°, which would in turn boost the probability of *top2-4* and *top2-5* being genetically different despite their coisogenic origins. On the other hand, there might be an intrinsic difference between the *top2-ts* alleles. In support of this second hypothesis we have the fact that the *top2-5* allele still gathered more genetic interactions than *top2-4* when transferred to the SGA background. It is difficult to speculate on the causes of such an intrinsic difference. There is only a missense mutation in the protein encoded by *top2-4*, a proline-to-glutamine change at position 820 (P820G), whereas Top2-5 has three in a cluster: R883P, R885I, and M887I (Thomas *et al.* 1991; Jannatipour *et al.* 1993). In both cases, mutations lay in the gyrase A motif near the catalytic center of the enzyme (Y782). Although it is plausible that the three mutations of *top2-5* render the enzyme less active than Top2-4, more work is needed to conclusively explain intrinsic differences upon the 37° shift. Lastly, an interesting possibility is that differences may correlate with the poison-resistant nature of Top2-5. This latter scenario would have important health-related implications and, therefore, it is worth testing in future works.

#### Conclusions and perspectives

In this work, we have characterized the consequences of depleting yeast cells from Top2 using two *top2-ts* alleles that differ in their resistance to chemotherapeutic Top2 poisons. As previously reported, the first cell cycle takes place with normal kinetics until anaphase, when *top2-ts* forms anaphase bridges. We have shown that these bridges are quickly split apart by PM abscission and can be maintained if mitotic exit is blocked. Finally we provide genetic evidence that stabilization of these bridges improve survivability upon transient Top2 inactivation. Since transient inactivation of targets is of the outmost importance to predict cell response to pharmacological drugs and also uncover adjuvant treatments, our results point toward upregulation of mitotic exit as a

Apendix III

putative target to synergistically promote cell death upon Top2 down-regulation/mutation in cancer cells.

**ACKNOWLEDGMENTS**

We thank other members of the labs for fruitful discussions and technical help. We also thank Manuel Mendoza for sending the plasmid to express the PM marker 2-PH-GFP. This work was supported by research grants PI12/00280 and BFU2015-63902-R to F.M. These grants were funded by the Spanish "Instituto de Salud Carlos III" and the Spanish Ministry of Economy and Competitiveness, respectively. Agencia Canaria de Investigación e Innovación y Sociedad de la Información supported C.R.-P. through a predoctoral fellowship (TESIS20120109). All these programs were cofinanced with the European Commission's European Regional Development Fund. The Danish Agency for Science, Technology and Innovation and the Villum Foundation supported the work performed by M.L. Funding to G.W.B. was provided by the Canadian Cancer Society Research Institute (Impact grant 702310) and the Canadian Institutes of Health Research (grant MOP-79368). The authors declare no conflicts of interest.

**LITERATURE CITED**

Akimitsu, N., N. Adachi, H. Hirai, M. S. Hossain, H. Hamamoto *et al.*, 2003 Enforced cytokinesis without complete nuclear division in embryonic cells depleting the activity of DNA topoisomerase IIa. *Genes Cells* 8: 393-402.

Amaral, N., A. Vendrell, C. Funaya, F.-Z. Idrissi, M. Maier *et al.*, 2016 The Aurora-B-dependent NoCut checkpoint prevents damage of anaphase bridges after DNA replication stress. *Nat. Cell Biol.* 18: 516-526.

Andrews, C. A., A. C. Vas, B. Meier, J. F. Giménez-Abián, L. A. Díaz-Martínez *et al.*, 2006 A mitotic topoisomerase II checkpoint in budding yeast is required for genome stability but acts independently of Pds1/securin. *Genes Dev.* 20: 1162-1174.

Baryshnikova, A., M. Costanzo, S. Dixon, F. J. Vizecoumar, C. L. Myers *et al.*, 2010 Synthetic genetic array (SGA) analysis in *Saccharomyces cerevisiae* and *Schizosaccharomyces pombe*. *Methods Enzymol.* 470: 145-179.

Baxter, J., and J. F. X. Diffley, 2008 Topoisomerase II inactivation prevents the completion of DNA replication in budding yeast. *Mol. Cell* 30: 790-802.

Baxter, J., N. Sen, V. L. Martínez, M. E. M. De Carandini, J. B. Schwartzman *et al.*, 2011 Positive supercoiling of mitotic DNA drives decatenation by topoisomerase II in eukaryotes. *Science* 331: 1328-1332.

Bembek, J., J. Kang, C. Kurischko, B. Li, J. R. Raab *et al.*, 2005 Crm1-mediated nuclear export of Cdc14 is required for the completion of cytokinesis in budding yeast. *Cell Cycle* 4: 961-971.

Boyle, E. I., S. Weng, J. Gollub, H. Jin, D. Botstein *et al.*, 2004 GO:Term-Finder—open source software for accessing Gene Ontology information and finding significantly enriched Gene Ontology terms associated with a list of genes. *Bioinformatics* 20: 3710-3715.

Chan, K.-L., P. S. North, and I. D. Hickson, 2007 BLM is required for faithful chromosome segregation and its localization defines a class of ultrafine anaphase bridges. *EMBO J.* 26: 3397-3409.

Charbin, A., C. Bouchoux, and F. Uhlmann, 2014 Condensin aids sister chromatid decatenation by topoisomerase II. *Nucleic Acids Res.* 42: 340-348.

Cuylen, S., J. Metz, A. Hruby, and C. H. Haering, 2013 Entrapment of chromosomes by condensin rings prevents their breakage during cytokinesis. *Dev. Cell* 27: 469-478.

D'Amours, D., F. Stegmeier, and A. Amon, 2004 Cdc14 and condensin control the dissolution of cohesin-independent chromosome linkages at repeated DNA. *Cell* 117: 455-469.

Deweese, J. E., and N. Osheroff, 2009 The DNA cleavage reaction of topoisomerase II: wolf in sheep's clothing. *Nucleic Acids Res.* 37: 738-748.

DiNardo, S., K. Voelkel, and R. Sternglanz, 1984 DNA topoisomerase II mutant of *Saccharomyces cerevisiae*: topoisomerase II is required for segregation of daughter molecules at the termination of DNA replication. *Proc. Natl. Acad. Sci. USA* 81: 2616-2620.

Dulev, S., C. de Renty, R. Mehta, I. Minkov, E. Schwob *et al.*, 2009 Essential global role of CDC14 in DNA synthesis revealed by chromosome underreplication unrecognized by checkpoints in *cdc14* mutants. *Proc. Natl. Acad. Sci. USA* 106: 14466-14471.

Fachinetti, D., R. Bermejo, A. Cocito, S. Minardi, Y. Katou *et al.*, 2010 Replication termination at eukaryotic chromosomes is mediated by Top2 and occurs at genomic loci containing pausing elements. *Mol. Cell* 39: 595-605.

García-Luis, J., and F. Machin, 2014 Mus81-Mms4 and Yen1 resolve a novel anaphase bridge formed by noncanonical Holliday junctions. *Nat. Commun.* 5: 5652.

García-Luis, J., A. Clemente-Blanco, L. Aragón, and F. Machin, 2014 Cdc14 targets the Holliday junction resolvase Yen1 to the nucleus in early anaphase. *Cell Cycle* 13: 1392-1399.

Germann, S. M., V. H. Oestergaard, C. Haas, P. Salis, A. Motegi *et al.*, 2011 Dpb11/TopBP1 plays distinct roles in DNA replication, checkpoint response and homologous recombination. *DNA Repair (Amst.)* 10: 210-224.

Germann, S. M., V. Schramke, R. T. Pedersen, I. Gallina, N. Eckert-Boulet *et al.*, 2014 TopBP1/Dpb11 binds DNA anaphase bridges to prevent genome instability. *J. Cell Biol.* 204: 45-59.

Giaever, G., A. M. Chu, L. Ni, C. Connelly, L. Riles *et al.*, 2002 Functional profiling of the *Saccharomyces cerevisiae* genome. *Nature* 418: 387-391.

Gorbisky, G. J., 1994 Cell cycle progression and chromosome segregation in mammalian cells cultured in the presence of the topoisomerase II inhibitors ICRF-187 [(+)-1,2-bis(3,5-dioxopiperazinyl-1-yl)propane; ADR-529] and ICRF-159 (Razoxane). *Cancer Res.* 54: 1042-1048.

Holm, C., T. Goto, J. C. Wang, and D. Botstein, 1985 DNA topoisomerase II is required at the time of mitosis in yeast. *Cell* 41: 553-563.

Holm, C., T. Stearns, and D. Botstein, 1989 DNA topoisomerase II must act at mitosis to prevent nondisjunction and chromosome breakage. *Mol. Cell Biol.* 9: 159-168.

Holohan, C., S. Van Schaeybroeck, D. B. Longley, and P. G. Johnston, 2013 Cancer drug resistance: an evolving paradigm. *Nat. Rev. Cancer* 13: 714-726.

Janke, C., M. M. Magiera, N. Rathfelder, C. Taxis, S. Reber *et al.*, 2004 A versatile toolbox for PCR-based tagging of yeast genes: new fluorescent proteins, more markers and promoter substitution cassettes. *Yeast* 21: 947-962.

Jannatipour, M., Y. X. Liu, and J. L. Nitiss, 1993 The top2-5 mutant of yeast topoisomerase II encodes an enzyme resistant to etoposide and amacrine. *J. Biol. Chem.* 268: 18586-18592.

Jaspersen, S. L., J. F. Charles, R. L. Tinker-Kulberg, and D. O. Morgan, 1998 A late mitotic regulatory network controlling cyclin destruction in *Saccharomyces cerevisiae*. *Mol. Biol. Cell* 9: 2803-2817.

Kalitsis, P., T. Zhang, K. M. Marshall, C. F. Nielsen, and D. F. Hudson, 2017 Condensin, master organizer of the genome. *Chromosome Res.* 25: 61-76.

Kim, R. A., and J. C. Wang, 1989 A subthreshold level of DNA topoisomerases leads to the excision of yeast rDNA as extrachromosomal rings. *Cell* 57: 975-985.

Larsen, A. K., A. E. Escargueil, and A. Skladanowski, 2003 Catalytic topoisomerase II inhibitors in cancer therapy. *Pharmacol. Ther.* 99: 167-181.

Li, Z., F. J. Vizecoumar, S. Bahr, J. Li, J. Warringer *et al.*, 2011 Systematic exploration of essential yeast gene function with temperature-sensitive mutants. *Nat. Biotechnol.* 29: 361-367.

Lisby, M., R. Rothstein, and U. H. Mortensen, 2001 Rad52 forms DNA repair and recombination centers during S phase. *Proc. Natl. Acad. Sci. USA* 98: 8276-8282.

Machin, F., J. Torres-Rosell, A. Jarmuz, and L. Aragón, 2005 Spindle-independent condensation-mediated segregation of yeast ribosomal DNA in late anaphase. *J. Cell Biol.* 168: 209-219.

3390 | C. Ramos-Pérez *et al.*



212

Este documento incorpora firma electrónica, y es copia auténtica de un documento electrónico archivado por la ULL según la Ley 39/2015.

Su autenticidad puede ser contrastada en la siguiente dirección <https://sede.ull.es/validacion/>

Identificador del documento: 3075810

Código de verificación: smutbmB+

Firmado por: JESSEL AYRA PLASENCIA  
 UNIVERSIDAD DE LA LAGUNA

Fecha: 30/11/2020 12:24:14

María de las Maravillas Aguiar Aguiar  
 UNIVERSIDAD DE LA LAGUNA

08/02/2021 13:50:06

- Machín, F., J. Torres-Rosell, G. De Piccoli, J. A. Carballo, R. S. Cha *et al.*, 2006 Transcription of ribosomal genes can cause nondisjunction. *J. Cell Biol.* 173: 893–903.
- Machín, F., O. Quevedo, C. Ramos-Pérez, and J. García-Luis, 2016 Cdc14 phosphatase: warning, no delay allowed for chromosome segregation! *Curr. Genet.* 62: 7–13.
- McGrew, J. T., L. Goetsch, B. Byers, and P. Baum, 1992 Requirement for ESP1 in the nuclear division of *Saccharomyces cerevisiae*. *Mol. Biol. Cell* 3: 1443–1454.
- Meitinger, F., S. Palani, and G. Pereira, 2012 The power of MEN in cytokinesis. *Cell Cycle* 11: 219–228.
- Mendoza, M., C. Norden, K. Durrer, H. Rauter, F. Uhlmann *et al.*, 2009 A mechanism for chromosome segregation sensing by the NoCut checkpoint. *Nat. Cell Biol.* 11: 477–483.
- Nishimura, K., T. Fukagawa, H. Takisawa, T. Kakimoto, and M. Kanemaki, 2009 An auxin-based degron system for the rapid depletion of proteins in nonplant cells. *Nat. Methods* 6: 917–922.
- Nitiss, J. L., 2009a DNA topoisomerase II and its growing repertoire of biological functions. *Nat. Rev. Cancer* 9: 327–337.
- Nitiss, J. L., 2009b Targeting DNA topoisomerase II in cancer chemotherapy. *Nat. Rev. Cancer* 9: 338–350.
- Norden, C., M. Mendoza, J. Dobbelaere, C. V. Kotwaliwale, S. Biggins *et al.*, 2006 The NoCut pathway links completion of cytokinesis to spindle midzone function to prevent chromosome breakage. *Cell* 125: 85–98.
- Perego, P., G. S. Jimenez, L. Gatti, S. B. Howell, and F. Zunino, 2000 Yeast mutants as a model system for identification of determinants of chemosensitivity. *Pharmacol. Rev.* 52: 477–492.
- Pommier, Y., Y. Sun, S. N. Huang, and J. L. Nitiss, 2016 Roles of eukaryotic topoisomerases in transcription, replication and genomic stability. *Nat. Rev. Mol. Cell Biol.* 17: 703–721.
- Quevedo, O., J. García-Luis, E. Matos-Perdomo, L. Aragón, and F. Machín, 2012 Nondisjunction of a single chromosome leads to breakage and activation of DNA damage checkpoint in G2. *PLoS Genet.* 8: e1002509.
- Ross, K. E., and O. Cohen-Fix, 2004 A role for the FEAR pathway in nuclear positioning during anaphase. *Dev. Cell* 6: 729–735.
- Shannon, P., A. Markiel, O. Ozier, N. S. Baliga, J. T. Wang *et al.*, 2003 Cytoscape: a software environment for integrated models of biomolecular interaction networks. *Genome Res.* 13: 2498–2504.
- Shapiro, A. B., and V. Ling, 1995 Reconstitution of drug transport by purified P-glycoprotein. *J. Biol. Chem.* 270: 16167–16175.
- Silva, S., I. Gallina, N. Eckert-Boulet, and M. Lisby, 2012 Live cell microscopy of DNA damage response in *Saccharomyces cerevisiae*. *Methods Mol. Biol.* 920: 433–443.
- Stegmeier, F., and A. Amon, 2004 Closing mitosis: the functions of the Cdc14 phosphatase and its regulation. *Annu. Rev. Genet.* 38: 203–232.
- Thomas, W., R. M. Spell, M. E. Ming, and C. Holm, 1991 Genetic analysis of the gyrase A-like domain of DNA topoisomerase II of *Saccharomyces cerevisiae*. *Genetics* 128: 703–716.
- Tong, A. H., M. Evangelista, A. B. Parsons, H. Xu, G. D. Bader *et al.*, 2001 Systematic genetic analysis with ordered arrays of yeast deletion mutants. *Science* 294: 2364–2368.
- Uemura, T., and M. Yanagida, 1984 Isolation of type I and II DNA topoisomerase mutants from fission yeast: single and double mutants show different phenotypes in cell growth and chromatin organization. *EMBO J.* 3: 1737–1744.
- Uemura, T., and M. Yanagida, 1986 Mitotic spindle pulls but fails to separate chromosomes in type II DNA topoisomerase mutants: uncoordinated mitosis. *EMBO J.* 5: 1003–1010.
- Vos, S. M., E. M. Tretter, B. H. Schmidt, and J. M. Berger, 2011 All tangled up: how cells direct, manage and exploit topoisomerase function. *Nat. Rev. Mol. Cell Biol.* 12: 827–841.
- Wagih, O., M. Usaj, A. Baryshnikova, B. VanderSluis, E. Kuzmin *et al.*, 2013 SGATools: one-stop analysis and visualization of array-based genetic interaction screens. *Nucleic Acids Res.* 41: W591–W596.
- Weiss, E. L., 2012 Mitotic exit and separation of mother and daughter cells. *Genetics* 192: 1165–1202.
- Wheatley, S. P., C. B. O'Connell, and Y. I. Wang, 1998 Inhibition of chromosomal separation provides insights into cleavage furrow stimulation in cultured epithelial cells. *Mol. Biol. Cell* 9: 2173–2184.

Communicating editor: S. Jaspersen

Este documento incorpora firma electrónica, y es copia auténtica de un documento electrónico archivado por la ULL según la Ley 39/2015.  
Su autenticidad puede ser contrastada en la siguiente dirección <https://sede.ull.es/validacion/>

Identificador del documento: 3075810 Código de verificación: smutbmB+

Firmado por: JESSEL AYRA PLASENCIA  
UNIVERSIDAD DE LA LAGUNA

Fecha: 30/11/2020 12:24:14

María de las Maravillas Aguiar Aguiar  
UNIVERSIDAD DE LA LAGUNA

08/02/2021 13:50:06

Appendix III

---

**Genome-scale genetic interactions and cell imaging confirm cytokinesis as deleterious to transient Topoisomerase II deficiency in *Saccharomyces cerevisiae*.**

Cristina Ramos-Pérez<sup>\*,†,1</sup>, Jessel Ayra-Plasencia<sup>\*,†</sup>, Emiliano Matos-Perdomo<sup>\*,†</sup>, Michael Lisby<sup>‡</sup>, Grant W Brown<sup>§</sup> and Félix Machín<sup>\*,2</sup>

\* Unidad de Investigación, Hospital Universitario Nuestra Señora de Candelaria, 38010, Santa Cruz de Tenerife, Spain.

† Universidad de la Laguna, 38200, San Cristóbal de La Laguna, Santa Cruz de Tenerife, Spain.

‡ Department of Biology, University of Copenhagen, DK-2200, Copenhagen, Denmark.

§ Department of Biochemistry and Donnelly Centre, University of Toronto, M5S3E1, Toronto, Ontario, Canada.

<sup>1</sup> Present address: Department of Biochemistry and Donnelly Centre, University of Toronto, M5S3E1, Toronto, Ontario, Canada.

<sup>2</sup> Corresponding author:

Félix Machín. Unidad de Investigación, Hospital Universitario Nuestra Señora de la Candelaria, Ctra del Rosario 145, 38010 Santa Cruz de Tenerife, Spain. Tel: +34922602951.  
E-mail: [fmachin@funcanis.es](mailto:fmachin@funcanis.es)

Este documento incorpora firma electrónica, y es copia auténtica de un documento electrónico archivado por la ULL según la Ley 39/2015.  
Su autenticidad puede ser contrastada en la siguiente dirección <https://sede.ull.es/validacion/>

Identificador del documento: 3075810 Código de verificación: smutbmB+

Firmado por: JESSEL AYRA PLASENCIA  
UNIVERSIDAD DE LA LAGUNA

Fecha: 30/11/2020 12:24:14

María de las Maravillas Aguiar Aguiar  
UNIVERSIDAD DE LA LAGUNA

08/02/2021 13:50:06



## SUPPLEMENTAL MATERIAL AND METHODS.

### Construction of yEmRFP-2xPH

First, a BamHI/SalI fragment of vector pML105 (Germann et al. 2014) containing PRC1p-CFP-2xPH was subcloned into the BamHI/SalI-digested *HIS3* vector pML104 (Germann et al. 2014) to generate pML106. Next, CFP was replaced with yEmRFP in vector pML106 by fusing a PRC1 promoter PCR fragment generated with BamHI-adapted primers PRC1-F and PRC1-yEmRFP-R from template pRS426GFP-2xPH(PLC $\delta$ ) (Stefan et al. 2002) to a yEmRFP PCR fragment generated with BspEI-adapted primers cherry.Fw and yEmRFPend-BspEI-R from template pNEB30 (Silva et al. 2012). The PCR fusion product was digested with BamHI and BspEI and cloned into BamHI/BspEI-linearized pML106 to produce plasmid pML111. The pML111 plasmid was partially digested with BsmI and transformed into strain ML8-9A for integration at the *his3-11,15* locus producing strain ML704.

Primers related to this construction were (5' to 3'):

PRC1-F	GTGGATCCTTCTGCACAAGAAG
PRC1-yEmRFP-R	CTTCTTCACCTTTTGAAACCATAGCGTATGTATACTTTAAG
cherry.Fw	ATGGTTTCAAAGGTGAAGAAG
yEmRFPend-BspEI-R	GAGTCCGGATTTATATAATTCATCCATACCACC

### References:

- Germann SM, Schramke V, Pedersen RT, Gallina I, Eckert-Boulet N, Oestergaard VH, Lisby M. 2014. TopBP1/Dpb11 binds DNA anaphase bridges to prevent genome instability. *J Cell Biol* **204**: 45-59.
- Silva S, Gallina I, Eckert-Boulet N, Lisby M. 2012. Live Cell Microscopy of DNA Damage Response in *Saccharomyces cerevisiae*. *Methods Mol Biol* **920**: 433-443.
- Stefan CJ, Audhya A, Emr SD. 2002. The yeast synaptojanin-like proteins control the cellular distribution of phosphatidylinositol (4,5)-bisphosphate. *Mol Biol Cell* **13**: 542-557.

Este documento incorpora firma electrónica, y es copia auténtica de un documento electrónico archivado por la ULL según la Ley 39/2015.  
Su autenticidad puede ser contrastada en la siguiente dirección <https://sede.ull.es/validacion/>

Identificador del documento: 3075810 Código de verificación: smutbmB+

Firmado por: JESSEL AYRA PLASENCIA  
UNIVERSIDAD DE LA LAGUNA

Fecha: 30/11/2020 12:24:14

María de las Maravillas Aguiar Aguiar  
UNIVERSIDAD DE LA LAGUNA

08/02/2021 13:50:06

SUPPLEMENTAL FIGURES.

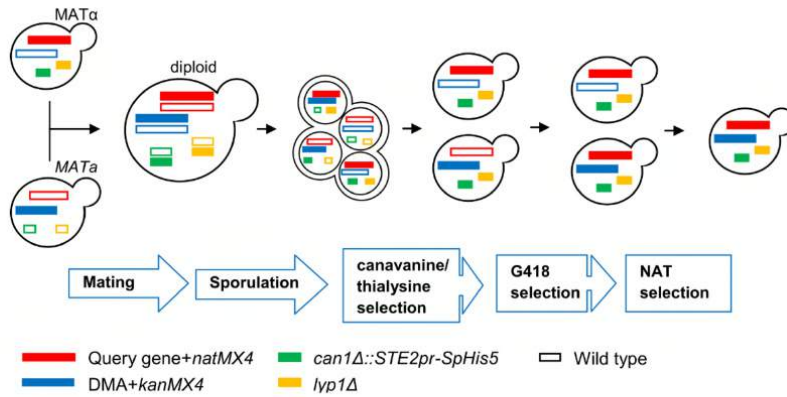


**Figure S1. Schematic of the generation of strain arrays for SGA analysis.** This technique is designed to detect genetic interactions by creating a subset of strains that have one query mutated gene in common and an array of other known mutations or deletions in their genome. We used the *ts* alleles *top2-4* and *top2-5* as our query genes, and scanned for genetic interactions with an array of mutants with deletions for 4322 non-essential genes and 1231 thermosensitive essential genes. We first replaced the *TOP2* locus in a haploid *MATa* strain (strain Y7092) with our query *top2-ts* alleles attached to the selection marker *natMX4* (resistance to nourseothricin -NAT-). For consistency, we also attached *natMX4* to the wild type *TOP2* locus, resulting in three Y7092 derivatives. The target Y7092 strain also carries other dominant selection markers such as *can1Δ* and *lyp1Δ*, which confer resistance to canavanine and thialysine, respectively. In addition, the deletion of *can1Δ* is linked to the construct *STE2pr-SpHis5*. *STE2pr* is a promoter that is only active in *MATa* haploid cells; allowing them to grow in media lacking histidine. The new *TOP2::natMX4*, *top2-4::natMX4* and *top2-5::natMX4* strains were then mated with the *MATa* deletion mutant array (DMA) and the *ts* mutant array (TSv6), which bear the *kanMX4* marker (resistance to geneticin -G418-) at the mutated loci. The result of this mating is a diploid with heterozygosity for all the markers. To select only the diploids and discard the cells that did not mate, the arrays were grown on plates containing both NAT and G418. After this, the diploids were plated onto sporulation media for 5 - 7 days. The plates were then replicated onto SD/MSG -his -arg -lys media with canavanine and thialysine in order to select for spores carrying the *MATa can1Δ lyp1Δ* genotype. The lack of histidine only allows the growth of *MATa* haploid (spores) cells carrying the *STE2pr-SpHis5* construct, whereas canavanine and thialysine kill all the cells carrying the WT alleles *CAN1* and *LYP1*, including all diploid. Next, we replicated the array onto the same media but adding G418, in order to select cells that carried the deletion mutation of the DMA or *ts* collection. Finally, we made a last selection onto the same media, this time adding also NAT, to select only the mutants that bear our query *TOP2::natMX4*, *top2-4::natMX4* and *top2-5::natMX4* alleles. Once the *TOP2*, *top2-4* and *top2-5* arrays were constructed they were replicated onto plates with the same medium used in the last selection step to maintain the selective pressure, and they were exposed to the different temperature regimes described in the Results section. The aforementioned genes are indicated with boxes with different sizes and colour lines. The presence of a modified allele is indicated by a filled box, whereas the WT allele is an empty box. Details on the different media compositions can be found at Tong, A. & Boone, C. *Yeast Gene Anal.* - Second Ed. 36, 369-707 (2007).

Este documento incorpora firma electrónica, y es copia auténtica de un documento electrónico archivado por la ULL según la Ley 39/2015.  
 Su autenticidad puede ser contrastada en la siguiente dirección <https://sede.ull.es/validacion/>

Identificador del documento: 3075810 Código de verificación: smutbmB+

Firmado por: JESSEL AYRA PLASENCIA  
 UNIVERSIDAD DE LA LAGUNA

Fecha: 30/11/2020 12:24:14

María de las Maravillas Aguiar Aguiar  
 UNIVERSIDAD DE LA LAGUNA

08/02/2021 13:50:06

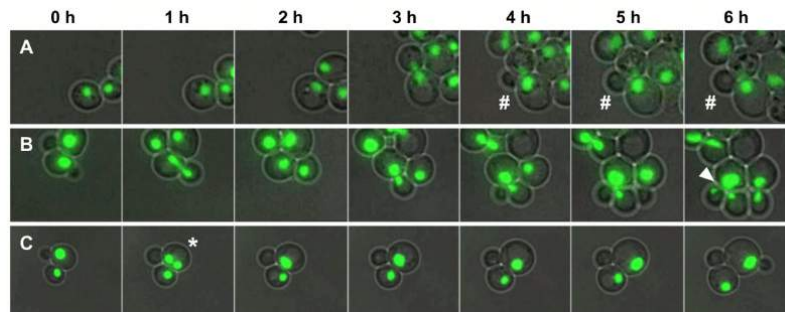


**Figure S2. Examples of uncoupling between nuclear division and cell cycle in *top2-ts* mutants.** *HTA2-GFP top2-ts* cells were filmed as in Figure 2A. **A.** A cell in which a new bud (#) comes out from the mother before it had finished segregating the DNA with the first bud (observed in two *top2-4* cells). **B.** An example of the formation of a double CAB (arrowhead) that connects the mother cells with its two daughters (observed in one *top2-5* cell). **C.** A nucleus trying to divide inside the mother cell, resulting in a temporarily binucleated single cell (\*) that then fuses the split nuclei back into one single nuclear mass (observed in one *top2-4* cell). The total number of cells filmed was 239 and include both *top2-ts* mutants as well as cells which were in either G1 or S phase (small bud) at the time of the temperature shift.

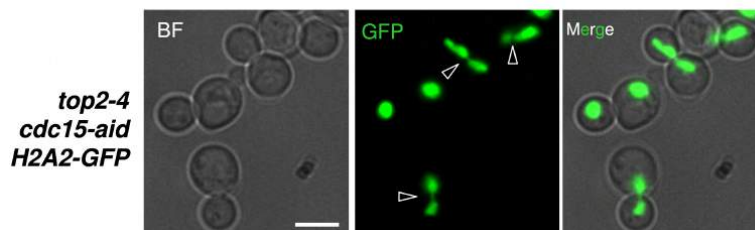


**Figure S3. Chromatin anaphase bridges are stabilized by blocking Mitotic exit in *top2-4*.** The *top2-4 cdc15-aid HTA2-GFP* strain was synchronized in G1 at 25° and then released at 37° in the presence of 1 mM of the auxin indolacetic acid (IAA) for 3 h. Scale bars correspond to 5 µm. BF, bright field. Hollow arrowheads point to examples of CABs. All arrowheads point exactly at the bud neck.

Este documento incorpora firma electrónica, y es copia auténtica de un documento electrónico archivado por la ULL según la Ley 39/2015.  
 Su autenticidad puede ser contrastada en la siguiente dirección <https://sede.ull.es/validacion/>

Identificador del documento: 3075810 Código de verificación: smutbmB+

Firmado por: JESSEL AYRA PLASENCIA  
 UNIVERSIDAD DE LA LAGUNA

Fecha: 30/11/2020 12:24:14

María de las Maravillas Aguiar Aguiar  
 UNIVERSIDAD DE LA LAGUNA

08/02/2021 13:50:06

Appendix III

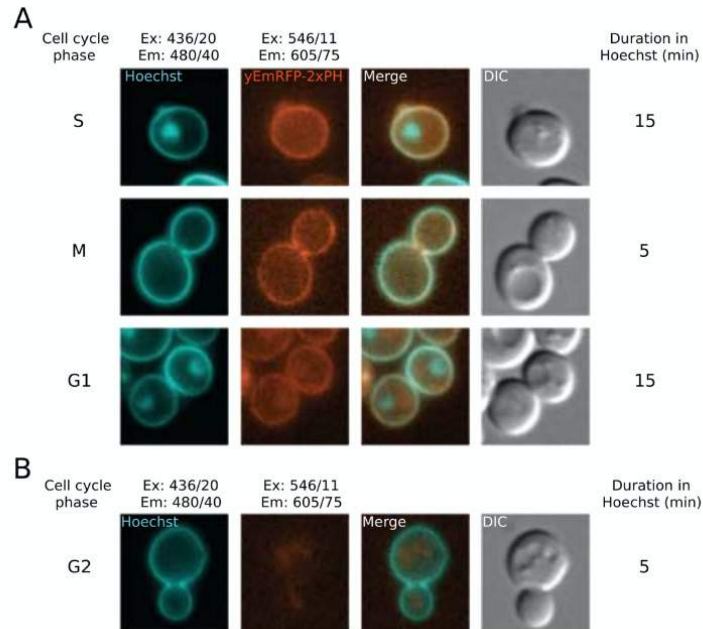


**Figure S4. Validation of Hoechst staining as a marker for the plasma membrane.** **A.** Hoechst colocalizes with the plasma membrane marker 2xPH. Cells expressing the plasma membrane marker yEmRFP-2xPH (ML704) were grown to exponential phase (OD = 0.2) in SC+Ade medium and stained with 5 µg/ml Hoechst 33258 for 5 min or 15 min as indicated before mounting on a microscope slide in fresh SC+Ade medium without Hoechst. Images show representative cells in S, M and G1 (post-abscission) phase of the cell cycle. **B.** Staining of control cells. Wild-type cells without the yEmRFP-2xPH marker (ML8-9A) were stained with 5 µg/ml Hoechst 33258 for 5 min before mounting on a microscope slide in fresh SC+Ade medium without Hoechst to confirm that Hoechst does not bleed-through into the RFP channel. DIC, differential interference contrast.

Este documento incorpora firma electrónica, y es copia auténtica de un documento electrónico archivado por la ULL según la Ley 39/2015.  
 Su autenticidad puede ser contrastada en la siguiente dirección <https://sede.ull.es/validacion/>

Identificador del documento: 3075810 Código de verificación: smutbmB+

Firmado por: JESSEL AYRA PLASENCIA  
 UNIVERSIDAD DE LA LAGUNA

Fecha: 30/11/2020 12:24:14

María de las Maravillas Aguiar Aguiar  
 UNIVERSIDAD DE LA LAGUNA

08/02/2021 13:50:06

**SUPPLEMENTAL TABLES.**

**Table S1. Strains used in this work.**

Strain name	Relevant genotype <sup>a</sup>	Origin
CH325	(S288C) <i>MATa ura3-52 his4-539am lys2-801am SUC2+ top2-4</i>	D. Botstein
CH326	(S288C) <i>MATa ura3-52 his4-539am lys2-801am SUC2+ top2-5</i>	D. Botstein
CH335	(S288C) <i>MATa ura3-52 his4-539am lys2-801am SUC2+ TOP2</i>	D. Botstein
FM1386	CH326; <i>H2A2(YBL003c):GFP:BleMX; Δbar1::URA3</i>	This work
FM1387	CH325; <i>H2A2(YBL003c):GFP:BleMX; Δbar1::URA3</i>	This work
FM1419	CH335; <i>H2A2(YBL003c):GFP:BleMX; Δbar1::URA3</i>	This work
FM1423	FM1387; <i>RAD52:RedStar2:NatMX</i>	This work
FM1437	FM1419; <i>RAD52:RedStar2:NatMX</i>	This work
FM1457	FM1386; <i>RAD52:RedStar2:NatMX</i>	This work
FM2021	FM1386; <i>cdc15-2:9myc:Hph</i>	This work
FM2086	FM1419; <i>cdc15-2:9myc:Hph</i>	This work
FM2105	CH326; [2-PH-GFP:URA3]	This work
FM2153	FM1386; <i>cdc14-1:9myc:Hph</i>	This work
FM2152	FM1419; <i>cdc14-1:9myc:Hph</i>	This work
FM2147	CH325; <i>H2A2(YBL003c):GFP:BleMX; ura3-52:ADH1:OsTIR1:9Myc:URA3; cdc15:AID*:Hph</i>	This work <sup>b</sup>
ML8-9A	(W303) <i>MATa ADE2 can1-100 ura3-1 his3-11,15 leu2-3,112 trp1-1 LYS2 RAD5</i>	M. Lisby
ML704	ML8-9A; <i>his3-11,15:yEmRFP-2xPH:HIS3</i>	This work
ML1009	FM1386; <i>tTA(tetR-VP16)-tetO2-DPB11-yEmRFP::KanMX</i>	This work <sup>c</sup>
ML1010	FM2021; <i>tTA(tetR-VP16)-tetO2-DPB11-yEmRFP::KanMX</i>	This work <sup>c</sup>
ML1022	FM2086; <i>tTA(tetR-VP16)-tetO2-DPB11-yEmRFP::KanMX</i>	This work <sup>c</sup>
Y7092	(S288C) <i>MATα can1Δ::STE2pr-Sphis5 lyp1Δ his3Δ1 leu2Δ0 ura3Δ0 met15Δ0</i>	C. Boone

Este documento incorpora firma electrónica, y es copia auténtica de un documento electrónico archivado por la ULL según la Ley 39/2015.  
 Su autenticidad puede ser contrastada en la siguiente dirección <https://sede.ull.es/validacion/>

Identificador del documento: 3075810 Código de verificación: smutbmB+

Firmado por: JESSEL AYRA PLASENCIA  
 UNIVERSIDAD DE LA LAGUNA

Fecha: 30/11/2020 12:24:14

María de las Maravillas Aguiar Aguilár  
 UNIVERSIDAD DE LA LAGUNA

08/02/2021 13:50:06

Appendix III

---

FM2181	Y7092; <i>TOP2:natMX</i>	This work <sup>d</sup>
FM2211	Y7092; <i>top2-4:natMX</i>	This work <sup>d</sup>
FM2241	Y7092; <i>top2-5:natMX</i>	This work <sup>d</sup>

<sup>a</sup> Semicolons separate independent transformation events during strain construction. Intermediate strains are omitted. Brackets indicate the relevant genotype is in a plasmid.

<sup>b</sup> This strain is *BAR1*. *AID\** stands for auxin-inducible degron system (asterisk denotes it carries the minimum effective sequence as reported in Morawska, M. & Ulrich, H. D. *Yeast* **30**, 341–51 (2013)). The *Cdc15* depletion was checked by absence of growth on a 1 mM auxin (indolacetic acid, IAA) YPD plate and full telophase arrest at 25°C after 3h with 1 mM IAA (data not shown).

<sup>c</sup> The *tTA(tetR-VP16)-tetO2-DPB11-yEmRFP::KanMX* cassette was PCR amplified an integrated at the *DPB11* locus.

<sup>d</sup> These strains are the basis for the corresponding *MATa* double mutants strain arrays (5,553 strains per *top2* allele; 16,659 in total), whose individual genotypes are omitted for the sake of space.

Este documento incorpora firma electrónica, y es copia auténtica de un documento electrónico archivado por la ULL según la Ley 39/2015.  
Su autenticidad puede ser contrastada en la siguiente dirección <https://sede.ull.es/validacion/>

Identificador del documento: 3075810 Código de verificación: smutbmB+

Firmado por: JESSEL AYRA PLASENCIA  
UNIVERSIDAD DE LA LAGUNA

Fecha: 30/11/2020 12:24:14

María de las Maravillas Aguiar Aguiar  
UNIVERSIDAD DE LA LAGUNA

08/02/2021 13:50:06

**Table S2. Genes that interact exclusively with *top2-4* at 25°C.**

<b>Positive interaction<sup>a</sup></b>	<p>ACA1, ADH6, AFR1, APQ12, AVT5, BLI1, BSP1, CCC2, CDC123, CDC19, CDC26, CDC37, CIK1, CSE2, CTH1, DBF4, DEP1, DON1, DUS3, ECM10, ECM23, EFT1, ELO1, ELP6, EMP46, ENT5, ERG11, ERG3, ESA1, FLD1, FMP41, FRE1, GCV1, GET2, GIR2, GRE2, HHF1, HKR1, INM2, IPT1, IST1, LCB1, LEA1, MAL31, MAS2, MBA1, MDH1, MDH2, MET30, MIC23, MLS1, MNS1, MPS1, MSB2, MSC7, MTC7, NAT5, NIT3, NPA3, NSE3, PBI2, PCF11, PCL9, PET122, PET8, PIN4, PPH3, PRE2, PTH1, PUT2, RAP1, RAT1, RAX2, RBD2, REX2, RHO4, RNH203, RPL24B, RPL37A, RPS29B, RPS6B, RSF1, SAS4, SCL1, SCW10, SCW11, SDH1, SGF73, SIF2, SIP3, SIP4, SKI2, SLI1, SLX4, SPA2, STU2, SWD3, SWT1, TIM44, TRK2, TVP23, UBA4, UBP15, UFD2, UTH1, VMS1, VPS1, YBL059W, YDR018C, YDR133C, YDR391C, YGL015C, YGL152C, YGL159W, YGR012W, YGR266W, YHR022C, YHR138C, YJL150W, YKL053W, YKL077W, YKR051W, YLR063W, YMR010W, YNL134C, YOL019W, YOL106W, YOR059C, YOR325W, YPL062W, YRB30</p>
<b>Negative interaction<sup>a</sup></b>	<p>AAD3, ABP140, ACT1, AIM18, AIM24, AIM26, AIM37, ALP1, AMD1, APS1, APS2, APT2, ARO80, ATG1, ATO2, ATP18, AVL9, BOP2, BRL1, CBR1, CDC21, CIC1, CKB1, COA1, COX23, CPR7, CWH41, CWH43, DEG1, EAR1, ECM19, ERC1, ERG5, EXG1, FMP25, FMP46, GAL83, GDE1, GRX6, HAP3, HDA1, HIM1, HMI1, IME2, KAR4, LCB1, LSM6, MAC1, MAM3, MCK1, MDM38, MET30, MGS1, MHT1, MIG1, MKC7, MKS1, MNL2, MRPL10, MSH3, MTC3, NHP10, NOP2, NSE4, NSE5, NTC20, OPI1, ORM2, OSW2, PAN2, PCL1, PDC1, PET122, PET20, PEX13, PHB2, PHD1, PIN2, PMD1, PML1, POB3, POL3, POL32, PRM2, PTM1, PUN1, RFX1, RHO4, RNH1, RPA14, RPA34, RPL14A, RPL34B, RPL40B, RPL8A, RPS11A, RPS25B, RPS29B, RPS4B, RRT12, RTC1, RTC4, RUD3, SAM2, SCY1, SDC1, SEC23, SEC26, SHH4, SHO1, SKG3, SLA1, SLM4, SNA2, SPA2, SSO2, STF1, STP3, STP4, SUA7, SVL3, SWA2, SWC7, SYC1, SYF1, TCB2, TFS1, THI7, THI73, TOM7, TOS6, TRM1, UBC12, UBP6, UBP8, UGA2, UPS2, URC2, UTH1, VAM7, VPS1, VPS51, VRP1, YAR1, YBR287W, YCF1, YCK3, YCT1, YDJ1, YDL119C, YDR161W, YEL059W, YGR250C, YGR272C, YHR140W, YJL021C, YKR104W, YLR108C, YLR152C, YLR236C, YLR241W, YLR269C, YLR391W, YLR444C, YML035C-A, YNL171C, YNL195C, YNR040W, YOL029C, YOL106W, YOR062C, YPL034W, YPL150W, YPR084W, YPR197C, YPT7</p>

<sup>a</sup> normalized growth of double *top2-ts/collection* mutants are compared to that of single collection mutants, both grown at 25°C.

Este documento incorpora firma electrónica, y es copia auténtica de un documento electrónico archivado por la ULL según la Ley 39/2015.  
 Su autenticidad puede ser contrastada en la siguiente dirección <https://sede.ull.es/validacion/>

Identificador del documento: 3075810 Código de verificación: smutbmB+

Firmado por: JESSEL AYRA PLASENCIA  
 UNIVERSIDAD DE LA LAGUNA

Fecha: 30/11/2020 12:24:14

María de las Maravillas Aguiar Aguilár  
 UNIVERSIDAD DE LA LAGUNA

08/02/2021 13:50:06

Appendix III

**Table S3. Genes that interact exclusively with *top2-5* at 25°C.**

<b>Positive interaction<sup>a</sup></b>	<p>ABZ2, ACE2, ACT1, AIM5, AIM7, ALD4, ALG6, ALT1, APJ1, APM1, ATG2, ATX1, AVT4, AXL1, BRN1, BTS1, CAT5, CCT4, CCW12, CDC14, CDC15, CDC24, CDC53, CGI121, CGR1, CLA4, CLB1, COG3, COP1, COX10, COX12, COX5B, CPR5, CSF1, CTS1, DAN1, DBF2, DCP2, DLD1, DOM34, EAF7, EAR1, EDC3, EGD1, ELM1, ELP3, ELP4, EOS1, FAA4, FLO1, FMS1, GAL83, HAP5, HCH1, HCR1, HDA1, HNT2, HOM3, HRP1, HRQ1, IME2, IRC6, IRC8, KNS1, LAT1, LCB2, LSC2, MAF1, MCH1, MCK1, MCX1, MDJ2, MEP1, MGR2, MOG1, MPH1, MRP8, MRS2, MYO2, NOP1, NOP4, OAF3, OAR1, OCA4, OCA6, ORC2, PAC11, PAM17, PCK1, PHO90, PHO91, PHR1, PLP1, PMP3, POC4, POL1, PRC1, PRP9, PSD2, PSE1, PUF3, PUT3, QCR9, QRI1, RAD16, RCY1, RGR1, RIM8, RNH201, ROG3, ROX3, RPL41B, RPS19B, RPS1B, RPS21A, RPS8A, RSA3, RTT109, SCJ1, SDS23, SEC28, SEC61, SGM1, SGN1, SMP3, SNC2, SNF1, SNO2, SNO4, SNZ2, SPI1, SPT6, SPT8, SSF1, STE24, SYT1, TLG2, UFD1, URA2, UTR1, VAC8, VHS1, VPS24, VPS4, XDJ1, XRN1, YAR044W, YBL083C, YBL086C, YBR259W, YCF1, YCL012W, YCL013W, YCS4, YDL023C, YDL094C, YDR134C, YDR179W-A, YDR537C, YEL057C, YEL059W, YER156C, YGR176W, YJL064W, YJR115W, YKR078W, YLL017W, YLR217W, YMD8, YML090W, YMR316C-A, YNL105W, YNL115C, YNL120C, YNR005C, YOR082C, YOX1, YPR011C, YPR038W, YPR123C, YPT52</p>
<b>Negative interaction<sup>a</sup></b>	<p>AAC3, AGA1, AKL1, ALG6, ARC18, ARF1, ASF1, ATG2, ATP10, BIM1, BRE2, BUB1, CAB5, CAF20, CAT5, CBP4, CCC1, CDC1, CDC10, CDC48, CGR1, CIN8, CKI1, CNB1, COX10, COX12, COX7, CSE2, CSG2, CTF4, CTM1, DFG16, DFG5, DMC1, DNM1, DOT1, DOT6, DPH5, DRS2, EMI5, ENT5, ERG6, ESC2, FMT1, FPR1, GID7, GIM4, GLO2, GRS1, GSM1, HAP2, HAP5, HCR1, HMS1, HPA3, HXK1, ICE2, IPL1, JHD2, KAP120, LAS17, LIP2, LPD1, LPX1, LSM1, MAF1, MAK10, MBA1, MBR1, MDH3, MMM1, MNE1, MNN10, MSB4, MSC6, MSN4, MTC6, MUB1, MUM2, NIP100, NOT3, NQM1, NSE3, NUP133, NUP188, OCA1, OST4, PAC10, PBA1, PBP4, PCF11, PEX12, PEX15, PMS1, PMT1, PPM2, PSO2, PUF4, QCR2, QCR9, RAD4, RGD1, RMD1, RMR1, RPL11B, RPL13A, RPL20B, RPL37A, RPL6B, RPS0A, RPS11B, RPS25A, RRM3, RTA1, RTC2, RTR1, RTS3, RVS167, SAC7, SAM1, SCT1, SDL1, SEC28, SEC39, SFI1, SIA1, SIC1, SIF2, SIT1, SLC1, SLP1, SNF1, SOK1, SOL4, SPO21, SPO71, SPT8, SWD1, TAD3, TEX1, TGS1, TPK2, TRI1, VAM6, VID30, VPS24, VPS4, VPS72, VPS9, XPT1, YBR099C, YCL075W, YDR445C, YEL010W, YER087C-A, YER181C, YGL260W, YGL262W, YGR021W, YHC1, YKR033C, YLR252W, YLR290C, YLR407W, YLR428C, YML090W, YNL095C, YNL109W, YNL296W, YNL320W, YOL035C, YOR019W, YOR041C, YPL102C, YPL113C, YPQ2, YPR123C, YPT11, YPT53, YSC83</p>

<sup>a</sup> normalized growth of double *top2-ts/collection* mutants are compared to that of single collection mutants, both grown at 25°C.

Este documento incorpora firma electrónica, y es copia auténtica de un documento electrónico archivado por la ULL según la Ley 39/2015.  
 Su autenticidad puede ser contrastada en la siguiente dirección <https://sede.ull.es/validacion/>

Identificador del documento: 3075810 Código de verificación: smutbmB+

Firmado por: JESSEL AYRA PLASENCIA  
 UNIVERSIDAD DE LA LAGUNA

Fecha: 30/11/2020 12:24:14

María de las Maravillas Aguiar Aguiar  
 UNIVERSIDAD DE LA LAGUNA

08/02/2021 13:50:06



**Table S4. Genes that interact with both *top2-4* and *top2-5* at 25°C.**

<b>Positive interaction<sup>a</sup></b>	AAD3, ABF1, ABP140, ADE6, ADH2, AFG1, ALG14, ALG8, APC5, APL4, ARP3, CBT1, CDC10, CDC20, CDC21, CDC4, COS111, COX23, CUP2, CWH41, DDI3, DOG2, ENO1, FKS3, FUM1, GAB1, GAD1, GAS1, GAS4, GLC8, GPI2, GSY1, HAP2, HUA1, HYP2, IRC24, ITC1, KTR5, LST4, MFA1, MMM1, MOB2, MSS18, NCS2, OST3, PAH1, PET10, PFY1, POB3, POL5, PRE4, QCR2, RAD14, RAD23, RAD3, RPL21B, RTC5, SCS7, SGV1, SNU13, SPF1, SPT15, STU1, SWM1, TAF12, TED1, TGL3, TMA19, UBP6, XPT1, YBL071C, YBL096C, YDJ1, YDL162C, YDR157W, YEL023C, YEL025C, YGL046W, YGL138C, YGL165C, YGR011W, YHC1, YIL151C, YKL069W, YKL151C, YLR346C, YME1, YMR306C-A, YMR310C, YNL024C, YPR098C, YPR197C
<b>Negative interaction<sup>a</sup></b>	ALG8, APL6, APP1, ATP23, BCK1, CDC8, CMC1, COA4, COQ10, COX5A, CSM1, CTP1, DAL81, DBF2, DDI1, DED1, EPS1, FLX1, FSH2, GSH1, HAP4, HAT2, HOM2, HOM6, HTZ1, HUR1, INP52, IZH1, MAS2, MDM35, MOT1, MPS1, MRP49, MRPL1, MSS18, NPR2, NST1, OMS1, PAT1, PMR1, PRP9, QRI1, RMD5, RPN11, RPO41, RPP1A, RPS27B, RPS7B, RTC6, RTS1, RTT103, RVS161, SAC3, SCS2, SEC21, SEC22, SIN3, SMI1, SNF4, SNN1, TAF5, THR1, TOP1, TPS2, TRM7, UME6, VIP1, YDR290W, YHL005C, YJR120W, YLR031W, YLR402W, YNL089C, YOR152C, YPR039W

<sup>a</sup> normalized growth of double *top2-ts/collection* mutants are compared to that of single collection mutants, both grown at 25°C.

Este documento incorpora firma electrónica, y es copia auténtica de un documento electrónico archivado por la ULL según la Ley 39/2015.  
 Su autenticidad puede ser contrastada en la siguiente dirección <https://sede.ull.es/validacion/>

Identificador del documento: 3075810 Código de verificación: smutbmB+

Firmado por: JESSEL AYRA PLASENCIA  
 UNIVERSIDAD DE LA LAGUNA

Fecha: 30/11/2020 12:24:14

María de las Maravillas Aguiar Aguiar  
 UNIVERSIDAD DE LA LAGUNA

08/02/2021 13:50:06

Appendix III

Table S5. Genes/alleles that interact with *top2-4* in any temperature regime.

Clusters <sup>a</sup>			
25°C <sup>b</sup>	30°C <sup>c</sup>	6h x 37°C <sup>d</sup>	
+	0	0	<i>ADH6, FUM1, YGL138C, YEL023C, AFG1, YEL025C, MAL31, MLS1, TED1, RAD23, MDH2, ITC1, RPL21B, YBL096C, YKL151C, YGR011W, MTC7, RPL37A, RTC5, GSY1, SCS7, UBA4, PAH1, SPF1, CBT1, CSE2, RPL24B, YME1, YNL024C, HAP2, RAD14, APL4, HHF1, YBL071C, YGL046W, YIL151C, PTH1, TMA19, GAD1, IRC24, XPT1, GAS4, COS111, pre2-v214a, mob2-26, mob2-14, hyp2-1159, mps1-417, gab1-2, rad3-ts14, pre4-ph, mob2-22, pre2-75, scl1-ph, mps1-3796, cdc4-1, OST3, pob3-7, hyp2-1, gpi2-774, lcb1-5, erg11-td, tim44-8, snu13-167w, YKL069W, cdc4-3, snu13-ph, PET8, ADE6, KTR5, MFA1, HUA1, NCS2, YPR098C, alg14-ph, pol5-2, yhc1-8, cdc123-4</i>
+	+	+	<i>YMR306C-A, FKS3, TGL3, ADH2, ELP6, GLC8, UBP15, taf12-w486stop, stu1-5, cdc10-4, abf1-101, SCW10</i>
0	+	+	<i>mob2-20, pfy1-14, apc5-ca, esa1-d414, sgv1-35, yhc1-1, cdc21-ts, arp3-f306g, AVT5, DEP1, RAX2, FLD1</i>
+	-	-	<i>UTH1, COX23, MSS18, ABP140, CWH41, AAD3, PET122, YPR197C, met30-6, RPS29B, YDJ1, SPA2, RHO4, ALG8, YOL106W, mas2-10</i>
0	+	0	<i>npa3-ph, YMR310C, YJL150W, BLI1, YLR063W, PUT2, REX2, YDR133C, SIP4, LST4, YBL059W, DUS3, MSC7, YGR266W, NIT3, ELO1, IPT1, SLX4, ACA1, PIN4, MBA1, PET10, SKI2, YNL134C, SGF73, ECM10, SIP3, YGL152C, YHR022C, PBI2, SLI1, MNS1, DOG2, MIC23, FRE1, RNH203, HKR1, ENO1, GRE2, MDH1, EMP46, INM2, ERG3, YDR157W, NAT5, PCL9, YKL053W, PPH3, TRK2, YKR051W, UFD2, UBP6</i>
0	0	+	<i>CTH1, GIR2, SIF2, YGL165C, CUP2, MSB2, IST1, YGR012W, YDR018C, FMP41, YGL015C, LEA1, RSF1, YRB30, EFT1, DD13, YHR138C, GCV1, ECM23, SDH1, BSP1, DON1, YOR325W, SCW11, RPS6B, YDL162C, YGL159W, SWD3, YPL062W, YOR059C, YOL019W, YFL052W, AFR1, TVP23, SWT1, YMR010W, SWM1, CCC2, nse3-ts4, dbf4-3, cdc20-2, cdc26-1, cdc19-1, pcf11-ts10, cdc37-1, stu2-12, RBD2, YDR391C, SAS4, YKL077W</i>
-	0	0	<i>INP52, APT2, TOM7, SNN1, YDR290W, EXG1, RPS7B, TOP1, lcb1-2, DBF2, brl1-3231</i>
0	-	-	<i>PET20, SHH4, VPS51, BOP2, YLR108C, YOL029C, YLR241W, STP3, YLR031W, CPR7, SMI1, MCK1, CBR1, APS2, SKG3, NPR2, URC2, VIP1, MHT1, RPA34, RUD3, GRX6, RPL40B, RPL34B, YHR140W, SCS2, RTC6, SDC1, MKS1, UPS2, PAT1, pob3-q308k, cdc21-1, mot1-1033, prp9-ts, SEC22, ALP1, TRM7, ALG8, YOL106W, mas2-10</i>
-	-	-	<i>MSH3, RTT103, RTC1, act1-2, CSM1, cdc2-7, YPT7, nop2-9</i>

Este documento incorpora firma electrónica, y es copia auténtica de un documento electrónico archivado por la ULL según la Ley 39/2015.  
 Su autenticidad puede ser contrastada en la siguiente dirección <https://sede.ull.es/validacion/>

Identificador del documento: 3075810 Código de verificación: smutbmB+

Firmado por: JESSEL AYRA PLASENCIA  
 UNIVERSIDAD DE LA LAGUNA

Fecha: 30/11/2020 12:24:14

María de las Maravillas Aguiar Aguiar  
 UNIVERSIDAD DE LA LAGUNA

08/02/2021 13:50:06

0	-	0	MDM38, YLR402W, HAT2, IME2, SAC3, YML035C-A, YPL034W, RFX1, OSW2, FMP46, RPP1A, SVL3, PHD1, YLR444C, SWC7, EAR1, SAM2, YPR084W, RPS27B, LSM6, YLR391W, MNL2, RNH1, SYC1, AIM26, YCK3, SWA2, YLR269C, PIN2, YNL171C, YDR161W, PUN1, RTC4, ERG5, RPS4B, RRT12, YLR152C, RPS25B, YEL059W, UBC12, TRM1, YCT1, THI7, EPS1, ORM2, ERC1, AIM24, RPL14A, FSH2, TFS1, YHL005C, SLA1, YGR272C, MRPL10, SNA2, SLM4, YLR236C, MGS1, RPO41, NHP10, HIM1, RMD5, YAR1, YPR039W, DEG1, KAR4, RPA14, ECM19, SSO2, YOR062C, MDM35, taf5-20, qri1-ph, RPS29B, YDJ1, SPA2, RHO4 ypr086w-ph, DDI1, ATO2, BRE1, AIM18, YOR152C, YGR250C, CTP1, TOS6, YCF1, COA1, PHB2, OPI1, PDC1, PTM1, YNL195C, FMP25, YKR104W, AMD1, ydr416w-ph, cdc8-1, nse4-ts3, rpn11-8, nse5-ts1, sec26-f856aw860a, sec23-1, cic1-2, sec21-1, HAP4, ATP18, MAM3, YNR040W, GSH1, PMD1, VAM7, MKC7, PCL1, PML1, RPS11A, UGA2, UME6, OMS1, FLX1, MRPL1, STP4, YJR120W, THR1, COA4, BCK1, SNF4, THI73, DAL81, HOM2, HMI1, MRP49, HAP3, CMC1, CKB1, HDA1, COQ10, MIG1, TPS2, UBP8, BST1, HOM6, YPL150W, PAN2, RVS161, PEX13, RTS1, YJL021C, GDE1, VRP1, YBR287W, PRM2, GAL83, YDL119C, SHO1, SCY1, MTC3, CWH43, POL32, PMR1, HUR1, COX5A, ATP23, UBP6, UTH1, COX23, MSS18, ABP140, CWH41, AAD3, PET122, YPR197C, met30-6
0	0	-	

<sup>a</sup> + : positive interaction, - : negative interaction, 0: no interaction

<sup>b</sup> normalized growth of double *top2-ts/collection* mutants are compared to that of single mutants in the collections, both grown at 25°C.

<sup>c</sup> normalized growth of double *top2-ts/collection* mutants grown at 30°C are compared to the same double mutants grown at 25°C. For instance, "+" at 25°C and "+" at 30°C indicates that there was a positive genetic interaction at 25°C that was enhanced at 30°C; "+" at 25°C and "0" at 30°C indicates that there was a positive genetic interaction at 25°C that was maintained to a same degree at 30°C; "+" at 25°C and "-" at 30°C indicates that there was a positive genetic interaction at 25°C that diminished at 30°C (either to neutral or negative interaction); "0" at 25°C and "+" at 30°C indicates that a positive genetic interaction at 30°C was seen that did not happen at 25°C; "0" at 25°C and "-" at 30°C indicates that a negative genetic interaction at 30°C was seen that did not happen at 25°C; etc.

<sup>d</sup> normalized growth of double *top2-ts/collection* mutants grown first during 6 h at 37°C and then at 25°C for 2 d are compared to the same double mutants grown always at 25°C. The interpretation of the genetic interactions is similar to the above paragraph.

Este documento incorpora firma electrónica, y es copia auténtica de un documento electrónico archivado por la ULL según la Ley 39/2015.  
 Su autenticidad puede ser contrastada en la siguiente dirección <https://sede.ull.es/validacion/>

Identificador del documento: 3075810 Código de verificación: smutbmB+

Firmado por: JESSEL AYRA PLASENCIA  
 UNIVERSIDAD DE LA LAGUNA

Fecha: 30/11/2020 12:24:14

María de las Maravillas Aguiar Aguilár  
 UNIVERSIDAD DE LA LAGUNA

08/02/2021 13:50:06

Appendix III

Table S6. Genes/alleles that interact with *top2-5* in any temperature regime.

Clusters <sup>a</sup>			
25°C <sup>b</sup>	30°C <sup>c</sup>	6h x 37°C <sup>d</sup>	
+	0	0	<i>COS111, GAS4, FUM1, TED1, YEL057C, YDR537C, YMR310C, GAS1, AFG1, YEL025C, RPL21B, YEL023C, YGL138C, EDC3, ITC1, IME2, RTC5, RAD23, FLO1, GSY1, HRQ1, UTR1, PHR1, YNL024C, YIL151C, YGR011W, IRC24, YBL071C, RAD14, GAD1, APL4, ABP140, AAD3, URA2, dbf2-3, ufd1-2, sec61-2, cdc24-1, smp3-1, spt6-14, prp9-1, cop1-1, pre4-ph, pse1-41, sgv1-80, alg14-ph, gab1-2, qri1-ts6, rgr1-100, OST3, snu13-ph, hyp2-1159, RIM8, nop4-3, gpi2-774, cct4-1, pol5-2, brn1-9, cog3-1, abf1-101, snu13-167w, YKL069W, rox3-182, dcp2-7, cdc53-1, spt15-i143n, rad3-ts14, YPR098C, POC4, APM1, MRS2, YPR197C, COX5B, PSD2, FAA4, ELP4, NCS2, EGD1, HUA1, ADE6, STE24, MFA1, KTR5, AXL1, CBT1, SCS7, FMS1, VAC8, ELP3, MOG1, PAH1, YBL096C, YEL059W, RPS19B, SPF1, YNL120C, MGR2, hyp2-2, TLG2, XRN1, YGL046W, YME1, RPS8A, DOM34</i>
+	+	+	<i>DAN1, cdc14-3, mob2-40, pol1-ts, nop1-3, cdc15-1, apc5-ca, cdc21-ts, cdc4-3, hrp1-4, pob3-7, RPL41B, YLR217W, AIM5, YCL013W, YDR179W-A</i>
0	+	+	<i>yhc1-1, mob2-26, cdc10-4, mob2-22, taf12-w486stop, stu1-5, YMR306C-A, ADH2, FKS3, YKL151C, TMA19</i>
+	-	-	<i>SPT8, SNF1, COX10, COX12, CAT5, QCR2, YML090W, VPS24, MMM1, YPR123C, HAP5, MSS18, HAP2, SEC28, MAF1, XPT1, CGR1, HCR1, VPS4, ALG8, QCR9</i>
0	+	0	<i>CGI121, MPH1, SGN1, YNL105W, YOR082C, UBP6, PAC11, YAR044W, MCH1, CSF1, YCF1, YOX1, RPS21A, YMR316C-A, DDI3, SGM1, SSF1, PET10, HDA1, OAF3, ATX1, ABZ2, DOG2, SYT1, PHO91, YDL094C, PHO90, PCK1, YJL064W, YBR259W, PLP1, RAD16, MCK1, ROG3, YDL162C, YDR157W, HNT2, HCH1, ENO1, GAL83, YKR078W, SNZ2, KNS1, LST4, MCX1, YER156C, PUT3, orc2-1, act1-124, myo2-16, pty1-14, arp3-f306g, PAM17, HOM3, EAR1, RPS1B, TGL3, SNO4, ELM1</i>
0	0	+	<i>ACE2, OAR1, MDJ2, ALT1, YNR005C, SCJ1, CUP2, SWM1, YJR115W, DLD1, YCL012W, YGR176W, YPR011C, SDS23, CTS1, CCW12, YNL115C, AVT4, APJ1, YGL165C, SPI1, VHS1, CPR5, YPT52, LAT1, YPR038W, MRP8, IRC8, SNO2, PRC1, YMD8, AIM7, OCA4, YLL017W, OCA6, YDR134C, PUF3, ALD4, IRC6, CLB1, YDL023C, LSC2, CLA4, YBL086C, YBL083C, MEP1, RCY1, lcb2-16, cdc20-2, ELM1, RTT109, RNH201, ATG2</i>
-	0	0	<i>RTT103, DBF2, YNL089C, YDR290W, CSM1, YDR445C, ESC2, DOT1, YNL095C, RPS7B</i>

Este documento incorpora firma electrónica, y es copia auténtica de un documento electrónico archivado por la ULL según la Ley 39/2015.  
 Su autenticidad puede ser contrastada en la siguiente dirección <https://sede.ull.es/validacion/>

Identificador del documento: 3075810 Código de verificación: smutbmB+

Firmado por: JESSEL AYRA PLASENCIA  
 UNIVERSIDAD DE LA LAGUNA

Fecha: 30/11/2020 12:24:14

María de las Maravillas Aguiar Aguiar  
 UNIVERSIDAD DE LA LAGUNA

08/02/2021 13:50:06

0	-	-	LIP2, RPS11B, MDH3, YPT11, HMS1, RMD5, NPR2, DFG16, cdc48-1, IZH1, ATP23, OMS1, SNF4, TEX1, EPS1, RRM3, HTZ1, ERG6, YCL075W, OST4, KAP120, YJR120W, UME6, SIA1, LPD1, HCR1, VPS4, ALG8, QCR9
0	-	0	PAC10, TPK2, PBP4, SIT1, HPA3, EMI5, VPS72, SAC3, YLR407W, YNL109W, YOL035C, DFG5, CTF4, PPM2, CCC1, DOT6, RPS27B, YER087C-A, YOR041C, JHD2, YGR021W, DPH5, APL6, RTS3, YKR033C, RAD4, DMC1, TRI1, YLR252W, SLC1, CNB1, SAM1, BIM1, MBR1, CTP1, YBR099C, YLR031W, SDL1, RTA1, RTC2, DRS2, YPR039W, ENT5, PUF4, YOR019W, CIN8, RPS0A, RPL11B, RPO41, RGD1, CAF20, SPO71, MSB4, GID7, VAM6, YHL005C, YER181C, PMS1, SCS2, LSM1, YPL102C, ASF1, SIF2, RPL13A, RTR1, GLO2, RPL37A, FSH2, NUP133, YLR402W, GIM4, RPP1A, HAT2, YEL010W, RPL6B, mas2-10, tad3-ph, prp9-ts, qri1-ph, sec39-ph, taf5-20, cab5-ph, nse3-ts3, pcf11-1, cdc1-4, mot1-1033, ATG2, XPT1, CGR1
0	0	-	SCT1, YGL262W, YPL113C, RVS161, COA4, YPQ2, MNN10, YOR152C, SMI1, PSO2, CSE2, SIC1, HUR1, PMR1, COX7, COQ10, HAP4, YNL296W, THR1, TPS2, BCK1, MBA1, MSC6, HOM6, AGA1, MRPL1, MSN4, COX5A, MNE1, TGS1, SWD1, CMC1, MAK10, SOK1, AAC3, BRE2, MUM2, MUB1, SAC7, MRP49, YGL260W, MTC6, SPO21, RTS1, RMR1, FLX1, VID30, CSG2, SLP1, RVS167, GSH1, YLR428C, PEX12, CBP4, FMT1, RPS25A, FPR1, NIP100, DNM1, las17-1, rpn11-8, sec21-1, ipl1-1, cdc8-1, PBA1, RPL20B, HOM2, NUP188, SEC22, ARF1, RTC6, YNL320W, ICE2, SOL4, HXK1, BUB1, YLR290C, YSC83, VIP1, CKI1, CTM1, LPX1, NQM1, PEX15, NOT3, MDM35, VPS9, TRM7, AKL1, DDI1, GRS1, GSM1, DAL81, RMD1, ATP10

<sup>a</sup> + : positive interaction, - : negative interaction, 0: no interaction

<sup>b</sup> normalized growth of double *top2-ts/collection* mutants are compared to that of single mutants in the collections, both grown at 25°C.

<sup>c</sup> normalized growth of double *top2-ts/collection* mutants grown at 30°C are compared to the same double mutants grown at 25°C. For instance, "+" at 25°C and "+" at 30°C indicates that there was a positive genetic interaction at 25°C that was enhanced at 30°C; "+" at 25°C and "0" at 30°C indicates that there was a positive genetic interaction at 25°C that was maintained to a same degree at 30°C; "+" at 25°C and "-" at 30°C indicates that there was a positive genetic interaction at 25°C that diminished at 30°C (either to neutral or negative interaction); "0" at 25°C and "+" at 30°C indicates that a positive genetic interaction at 30°C was seen that did not happen at 25°C; "0" at 25°C and "-" at 30°C indicates that a negative genetic interaction at 30°C was seen that did not happen at 25°C; etc.

<sup>d</sup> normalized growth of double *top2-ts/collection* mutants grown first during 6 h at 37°C and then at 25°C for 2 d are compared to the same double mutants grown always at 25°C. The interpretation of the genetic interactions is similar to the above paragraph.

Este documento incorpora firma electrónica, y es copia auténtica de un documento electrónico archivado por la ULL según la Ley 39/2015.  
 Su autenticidad puede ser contrastada en la siguiente dirección <https://sede.ull.es/validacion/>

Identificador del documento: 3075810 Código de verificación: smutbmB+

Firmado por: JESSEL AYRA PLASENCIA  
 UNIVERSIDAD DE LA LAGUNA

Fecha: 30/11/2020 12:24:14

María de las Maravillas Aguiar Aguiar  
 UNIVERSIDAD DE LA LAGUNA

08/02/2021 13:50:06

Apendix III

---

**LEGENDS TO EXCEL FILES INCLUDED IN FILE S2.zip**

**File: SGAtool data\_top2-4\_TSv6\_RT.xlsx**

Raw and processed SGA data of the permissive (25°) experiment where *top2-4* was the query allele used against the collection of thermosensitive alleles.

**File: SGAtool data\_top2-4\_TSv6\_30C.xlsx**

Raw and processed SGA data of Top2 constant downregulation (30°) experiment where *top2-4* was the query allele used against the collection of thermosensitive alleles.

**File: SGAtool data\_top2-4\_TSv6\_37Cx6h.xlsx**

Raw and processed SGA data of the transient Top2 inactivation (37° x 6h) experiment where *top2-4* was the query allele used against the collection of thermosensitive alleles.

**File: SGAtool data\_top2-4\_DMA\_RT.xlsx**

Raw and processed SGA data of the permissive (25°) experiment where *top2-4* was the query allele used against the collection of gene deletions.

**File: SGAtool data\_top2-4\_DMA\_30C.xlsx**

Raw and processed SGA data of Top2 constant downregulation (30°) experiment where *top2-4* was the query allele used against the collection of gene deletions.

**File: SGAtool data\_top2-4\_DMA\_37Cx6h.xlsx**

Raw and processed SGA data of the transient Top2 inactivation (37° x 6h) experiment where *top2-4* was the query allele used against the collection of gene deletions.

**File: SGAtool data\_top2-5\_TSv6\_RT.xlsx**

Raw and processed SGA data of the permissive (25°) experiment where *top2-5* was the query allele used against the collection of thermosensitive alleles.

**File: SGAtool data\_top2-5\_TSv6\_30C.xlsx**

Raw and processed SGA data of Top2 constant downregulation (30°) experiment where *top2-5* was the query allele used against the collection of thermosensitive alleles.

**File: SGAtool data\_top2-5\_TSv6\_37Cx6h.xlsx**

Raw and processed SGA data of the transient Top2 inactivation (37° x 6h) experiment where *top2-5* was the query allele used against the collection of thermosensitive alleles.

**File: SGAtool data\_top2-5\_DMA\_RT.xlsx**

Raw and processed SGA data of the permissive (25°) experiment where *top2-5* was the query allele used against the collection of gene deletions.

15

228

Este documento incorpora firma electrónica, y es copia auténtica de un documento electrónico archivado por la ULL según la Ley 39/2015.  
Su autenticidad puede ser contrastada en la siguiente dirección <https://sede.ull.es/validacion/>

Identificador del documento: 3075810 Código de verificación: smutbmB+

Firmado por: JESSEL AYRA PLASENCIA  
UNIVERSIDAD DE LA LAGUNA

Fecha: 30/11/2020 12:24:14

María de las Maravillas Aguiar Aguiar  
UNIVERSIDAD DE LA LAGUNA

08/02/2021 13:50:06

File: **SGAtool data\_top2-5\_DMA\_30C.xlsx**

Raw and processed SGA data of the Top2 constant downregulation (30<sup>o</sup>) experiment where *top2-5* was the query allele used against the collection of gene deletions.

File: **SGAtool data\_top2-5\_DMA\_37Cx6h.xlsx**

Raw and processed SGA data of the transient Top2 inactivation (37<sup>o</sup> x 6h) experiment where *top2-5* was the query allele used against the collection of gene deletions.

Este documento incorpora firma electrónica, y es copia auténtica de un documento electrónico archivado por la ULL según la Ley 39/2015.  
*Su autenticidad puede ser contrastada en la siguiente dirección <https://sede.ull.es/validacion/>*

Identificador del documento: 3075810 Código de verificación: smutbmB+

Firmado por: JESSEL AYRA PLASENCIA  
UNIVERSIDAD DE LA LAGUNA

Fecha: 30/11/2020 12:24:14

María de las Maravillas Aguiar Aguiar  
UNIVERSIDAD DE LA LAGUNA

08/02/2021 13:50:06



Este documento incorpora firma electrónica, y es copia auténtica de un documento electrónico archivado por la ULL según la Ley 39/2015.  
*Su autenticidad puede ser contrastada en la siguiente dirección <https://sede.ull.es/validacion/>*

Identificador del documento: 3075810      Código de verificación: smutbmB+

Firmado por: JESSEL AYRA PLASENCIA  
UNIVERSIDAD DE LA LAGUNA

Fecha: 30/11/2020 12:24:14

María de las Maravillas Aguiar Aguiar  
UNIVERSIDAD DE LA LAGUNA

08/02/2021 13:50:06



This is an open access article published under a Creative Commons Non-Commercial No Derivative Works (CC-BY-NC-ND) Attribution License, which permits copying and redistribution of the article, and creation of adaptations, all for non-commercial purposes.



Letters



Cite This: ACS Chem. Biol. 2018, 13, 1950–1957

## Lawson, Juglone, and $\beta$ -Lapachone Derivatives with Enhanced Mitochondrial-Based Toxicity

Laura Anaissi-Afonso,<sup>†,‡,∇</sup> Sandra Oramas-Royo,<sup>§,∇</sup> Jessel Ayra-Plasencia,<sup>†,‡</sup> Patricia Martín-Rodríguez,<sup>||</sup> Jonay García-Luis,<sup>†</sup> Isabel Lorenzo-Castrillejo,<sup>†</sup> Leandro Fernández-Pérez,<sup>||</sup> Ana Estévez-Braun,<sup>\*,§</sup> and Félix Machín<sup>\*,†</sup>

<sup>†</sup>Unidad de Investigación, Hospital Universitario Nuestra Señora de La Candelaria, 38010 Tenerife, Spain

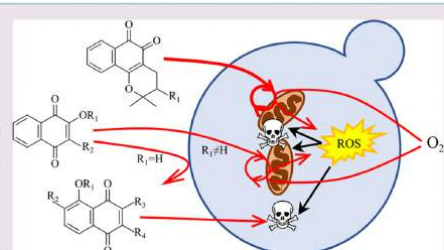
<sup>‡</sup>Universidad de La Laguna, 38206 Tenerife, Spain

<sup>§</sup>Instituto Universitario de Bio-Orgánica (CIBICAN), Departamento de Química Orgánica, Universidad de La Laguna, 38206 Tenerife, Spain

<sup>||</sup>Instituto Universitario de Investigaciones Biomédicas y Sanitarias (IUIBS), Departamento de Ciencias Clínicas, BIOPHARM, Universidad de Las Palmas de Gran Canaria, 35001 Las Palmas de Gran Canaria, Spain

### Supporting Information

**ABSTRACT:** Naphthoquinones are among the most active natural products obtained from plants and microorganisms. Naphthoquinones exert their biological activities through pleiotropic mechanisms that include reactivity against cell nucleophiles, generation of reactive oxygen species (ROS), and inhibition of proteins. Here, we report a mechanistic antiproliferative study performed in the yeast *Saccharomyces cerevisiae* for several derivatives of three important natural naphthoquinones: lawson, juglone, and  $\beta$ -lapachone. We have found that (i) the free hydroxyl group of lawson and juglone modulates toxicity; (ii) lawson and juglone derivatives differ in their mechanisms of action, with ROS generation being more important for the former; and (iii) a subset of derivatives possess the capability to disrupt mitochondrial function, with  $\beta$ -lapachones being the most potent compounds in this respect. In addition, we have cross-compared yeast results with antibacterial and antitumor activities. We discuss the relationship between the mechanistic findings, the antiproliferative activities, and the physicochemical properties of the naphthoquinones.



The quinone moiety is ubiquitously found in many natural products and is also a frequent byproduct in the metabolism of xenobiotics such as air pollutants (e.g., polycyclic aromatic hydrocarbons) and clinically used drugs (e.g., acetaminophen).<sup>1,2</sup> Quinones are often cytotoxic through two major mechanisms. First, quinones catalyze redox cycles fed by NAD(P)H and molecular oxygen (O<sub>2</sub>), the latter being transformed to harmful reactive oxygen species (ROS). Second, quinones are potent electrophiles; unsubstituted carbons in the quinone ring can react with nucleophilic biomolecules through a Michael-type addition mechanism. Sensitive nucleophiles include thiol groups in proteins, especially if they are in the thiolate form in physiological conditions (e.g., cysteine at the catalytic center of tyrosine phosphatases).<sup>3</sup> Other biologically important nucleophiles include heteroatoms of the four DNA bases and tubulin, which is the cytoskeleton protein that polymerizes to form the microtubules.<sup>4,5</sup>

Widespread quinones in nature include naphthoquinones (NQs) such as lawson, juglone, and lapachol, all of which have important human applications.<sup>4,5</sup> Lawson (2-hydroxy-1,4-naphthoquinone) is the principal dye of Henna (*Lawsonia inermis*) leaves,

which have been used for centuries in tattooing. Juglone (5-hydroxy-1,4-naphthoquinone) is found in plants that belong to the Juglandaceae family (e.g., *Juglans nigra*, also known as black walnut). Juglone has had several uses, from natural herbicide to natural dye for fabrics and food. Lapachol (2-hydroxy-3-prenyl-1,4-NQ) is thought to be the key active constituent of several plant preparations used in South American folk medicine (e.g., *Tabebuia avellanae* (Lapacho tree)). The conversion of lapachol to lapachones (a class of pyranonaphthoquinones) upon acidic exposure has also deserved special attention.<sup>6</sup> In recent years,  $\beta$ -lapachone (2,2-dimethyl-3,4-dihydro-2H-benzo[h]chromene-5,6-dione) has been extensively revisited, since it possesses unique antitumor activities.<sup>7,8</sup> Generally, the folk medicinal use of plant preparations enriched in NQs has been common for centuries and include ailments such as cancer and infections. When the NQs were purified and tested for

Received: April 2, 2018

Accepted: June 7, 2018

Published: June 7, 2018

ACS Publications © 2018 American Chemical Society

1950

DOI: 10.1021/acscchembio.8b00306  
ACS Chem. Biol. 2018, 13, 1950–1957

231

Este documento incorpora firma electrónica, y es copia auténtica de un documento electrónico archivado por la ULL según la Ley 39/2015.  
Su autenticidad puede ser contrastada en la siguiente dirección <https://sede.ull.es/validacion/>

Identificador del documento: 3075810

Código de verificación: smutbmB+

Firmado por: JESSEL AYRA PLASENCIA  
UNIVERSIDAD DE LA LAGUNA

Fecha: 30/11/2020 12:24:14

María de las Maravillas Aguiar Aguiar  
UNIVERSIDAD DE LA LAGUNA

08/02/2021 13:50:06

biological activities, they often showed cytotoxic properties against tumor cells, pathogenic bacteria, fungi, and protozoa.<sup>4–6</sup>

The outstanding knowledge on *Saccharomyces cerevisiae* biology and the availability of collections of genetically modified strains make this yeast a powerful tool in cell-based assays oriented toward the understanding of mechanism(s) of action of toxic drugs and xenobiotics. For instance, DNA-damaging and microtubule-depolymerizing agents are at the core of the classical chemotherapy against cancer. Eukaryotic cells respond to these agents through complex networks which, importantly, are conserved between yeast and human cells. Accordingly, both cell types counteract chemical damage to the DNA through the DNA damage response (DDR).<sup>9</sup> In yeast, Rad9 and Rad52 are essential for the DDR, and knockout mutants for their genes are hypersensitive to DNA damaging agents. Mad2, on the other hand, is a vital component of the spindle assembly checkpoint (SAC), which monitors the integrity of the microtubule-based apparatus for chromosome segregation;<sup>10</sup> the *mad2Δ* knockout mutant is hypersensitive to drugs that interfere with tubulin. Particularly important in quinoid compounds, yeast cells combat ROS and their toxicity through the oxidative stress response (OSR), in which Yap1 is a master regulator.<sup>11,12</sup> Consequently, a *yap1Δ* strain is hypersensitive to oxidative stress. In addition, *S. cerevisiae* is especially useful in dissecting the pleiotropic toxicity of quinones, because of its unique property of being a facultative aerobe.<sup>13,14</sup> This allows yeast cells to grow under hypoxic conditions as long as a fermentative carbon source (e.g., glucose) is available. This also implies that yeast cells can proliferate without a functional mitochondrial respiratory chain, which can be easily engineered in the laboratory by selection against the mitochondrial DNA (*rho0* genotype). Here, we obtained and biologically assayed several derivatives from the natural NQs lawsone, juglone, and  $\beta$ -lapachone. The transformations included (i) O-alkylations, (ii) C-alkylations, (iii) O-acylations, (iv) halogenations, and (v) aminations. Most chemical modifications add well-known functional groups that modify the electronic, lipophilic, and steric properties of the natural NQs (see Table S1 in the Supporting Information).

**Lawsone Ethers Produce Mitochondrial-Based Oxidative Stress in Yeast.** We studied 10 molecules that are closely related to lawsone (see Figure 1A): lawsone itself (1); five O-alkyl-lawsone derivatives with alkyl groups of different complexity [namely, methyl (2), ethyl (3), isopropyl (4), allyl (5), and propynyl (6)]; an acryloyl ester (7); the iodinated compound (8) and the derivative with an allyl group at C-3 (9). Since (9) is very similar to lapachol (10, 3-prenylated lawsone), another natural NQ, we chose to include the latter as well.

Dose–response growth inhibition curves of the reference *S. cerevisiae* strain BY4741 showed that lawsone was not toxic in the 1–128  $\mu$ M range (see Figure 1B). Strikingly, the O-alkylation reactions rendered active molecules with full growth inhibition at  $\sim$ 100  $\mu$ M. The inhibition profile was relatively similar for all O-alkyl derivatives. However, esterification, rather than etherification, rendered a nontoxic derivative (compare 7 with 5). The presence of additional functional groups at C-3 of the quinone ring (8, 9, and 10) scarcely improved toxicity.

As mentioned previously, quinones exert cytotoxicity through two major mechanisms: redox cycles and arylation of cell nucleophiles. Yeast mutants can be used to weigh the contribution of each mechanism and identify cell targets. Indeed, we found that the *yap1Δ* strain was more sensitive to the lawsone ethers than BY4741 (Figure 1B), pointing out that active derivatives cause toxicities through the generation of ROS. Regarding the

putative damage through electrophilic attack on either DNA or tubulin, we found that neither the double *rad9Δ rad52Δ* mutant nor the *mad2Δ* were as hypersensitive as *yap1Δ*. The minor increase in sensitivity of compounds 2, 4, 5, and 6 is likely via an indirect damage by ROS (further support below).

Halo inhibition assays confirmed this basic pattern, except for 7, in which an inhibition halo was observed (Figure 1C). Thus, 1, 4, 8, and 9 were inactive or at least as toxic as dimethyl sulfoxide (DMSO) alone (see Figure 1C, as well as Figures S1 and S2 in the Supporting Information). The halo assay has the advantage of forming a concentric gradient of concentrations that changes over time. This is useful to check cytostatic versus biocide toxicity and eventual adaptation to the drug. Accordingly, compounds 2, 5, and 6 had a clear inhibition halo surrounded by an area of partial inhibition after 24 h (Figure S2); both areas shrank after 48 h, pointing to a cytostatic effect followed by cell adaptation.

In the dose–response assay, *yap1Δ* was hypersensitive to compounds 2, 4, 5, and 6. In halo assays, *yap1Δ* also showed a greater inhibition zone with these compounds (see Figures 1C and 1D). Strikingly, growth under hypoxia dramatically narrowed the inhibition halo, both in BY4741 and *yap1Δ* (Figure 1D). Similarly, *rho0* derivatives of both strains had a reduced halo in normoxia. These results strongly point out that the mitochondrial respiratory chain is a target of these NQs and that O<sub>2</sub> itself is the source of toxicity. Altogether, this toxicity profile fits well with (i) ROS being generated by redox cycling at the mitochondria, and (ii) these ROS eventually overwhelm cell homeostasis. Overwhelming generation of ROS through redox cycles has been demonstrated previously for other NQs, such as menadione (vitamin K<sub>3</sub>).<sup>15,16</sup>

Finally, we also tested the effect that these NQs might have for the mitochondrial function. Although mitochondria are dispensable for growing in fermentable carbon sources such as glucose, they are strictly required in nonfermentable sources such as glycerol. We performed a normoxic halo assay in glycerol instead of glucose and found that compound 6 specifically potentiate the sensitivity of BY4741 (Figure 1E). This means that compound 6 not only produced ROS but also severely disrupted mitochondrial function.

**Juglone Derivatives Mostly Cause Toxicity through Oxidative Stress-Independent Mechanisms.** In the case of juglone (11), seven derivatives were analyzed: O-methyljuglone (12), two O-allyljuglones (13 and 14), O-acryloyljuglone (15), two amino juglone derivatives (16 and 17), and a brominated derivative (18). (See Figure 2A.)

Dose–response growth curves and halo assays showed that juglone was not cytotoxic, yet all other derivatives were (see Figures 2B and 2C, as well as Figure S3 in the Supporting Information). In contrast to lawsone derivatives, juglone derivatives that still carry the free hydroxyl group were active, though the most active compound was O-acryloyljuglone (15). Except for 16 and 17, there was neither hypersensitivity in *yap1Δ* mutants nor suppression of toxicity in hypoxia or in *rho0* variants (Figure 2D). These findings suggest that the toxicity of 12, 13, 14, 15, and 18 is not related to ROS. This could imply that toxicity is more related to their electrophilic potential instead; nevertheless, if so, the nucleophilic targets are neither DNA nor tubulin (Figure 2B and 2C). As mentioned, 16 and 17 were the only ones that might have moderate ROS-mediated toxicity; and 16 and 17 were also the only ones that disrupted mitochondrial function (Figure 2E). Interestingly, these two juglones carry an amino group at different carbon centers in the

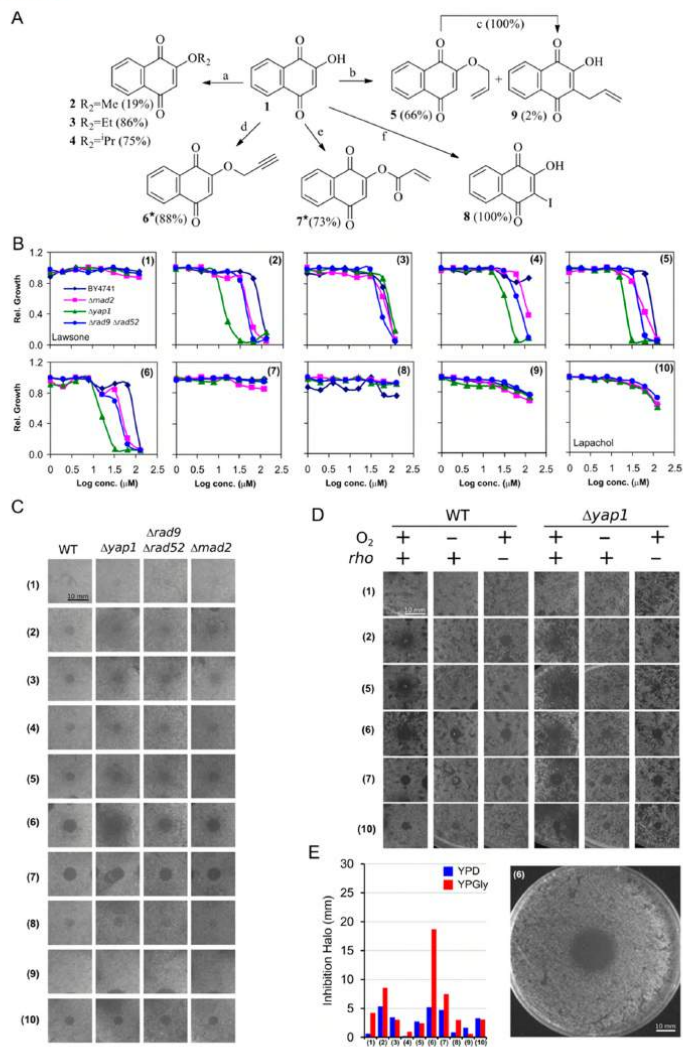


**Figure 1.** Yeast toxicity profiles of lawsone, lapachol, and derivatives thereof. (A) Scheme of preparation of lawsone derivatives. Reactives and conditions: (a) R<sub>2</sub>OH, HCl, reflux, 24 h; (b) allyl bromide, K<sub>2</sub>CO<sub>3</sub>, DMF, 15 h; (c) 1,4-dioxane, MW (180 °C), 15 min; (d) propargyl bromide, K<sub>2</sub>CO<sub>3</sub>, DMF, 72 h; (e) acryloyl chloride, K<sub>2</sub>CO<sub>3</sub>, DCM, 48 h; (f) NIS, DCM, reflux, 20 min. Asterisks denote novel derivatives. (B) Dose–response growth inhibition curves in the reference strain BY4741, OSR mutant *yap1Δ*, DDR double mutant *rad9Δ rad52Δ*, and SAC mutant *mad2Δ*. Growth was normalized to that of the vehicle (DMSO 1% (v/v)). (C) Halo of growth inhibition on solid media for the same strains (after 48 h). (D) Halo of growth inhibition for BY4741 and *yap1Δ* under normoxia and hypoxia (after 24 h and 72 h, respectively). In addition, normoxic inhibition halos for *rho0* strain derivatives are shown in the third and sixth columns (72 h). (E) Diameter of the inhibition halos for BY4741 growing on either YPD (fermentable glucose, 24 h) or YPGly (nonfermentable glycerol, 72 h). A photograph of the halo assay for compound 6 on YPGly is shown on the right in panel (E).

Este documento incorpora firma electrónica, y es copia auténtica de un documento electrónico archivado por la ULL según la Ley 39/2015.  
 Su autenticidad puede ser contrastada en la siguiente dirección <https://sede.ull.es/validacion/>

Identificador del documento: 3075810 Código de verificación: smutbmB+

Firmado por: JESSEL AYRA PLASENCIA  
 UNIVERSIDAD DE LA LAGUNA

Fecha: 30/11/2020 12:24:14

María de las Maravillas Aguiar Aguilár  
 UNIVERSIDAD DE LA LAGUNA

08/02/2021 13:50:06

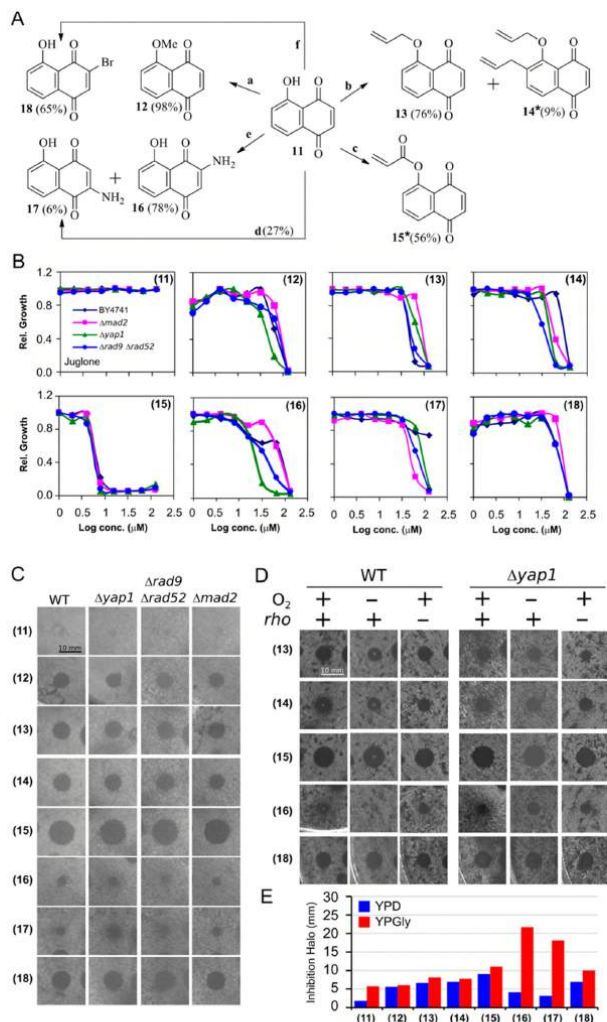


**Figure 2.** Yeast toxicity profiles of juglone and derivatives thereof. (A) Scheme of preparation of juglone derivatives. Reactives and conditions: (a) MeI, Ag<sub>2</sub>O, DCM, reflux, 72 h; (b) allyl bromide, Ag<sub>2</sub>O, DCM, reflux, 48 h; (c) acryloyl chloride, K<sub>2</sub>CO<sub>3</sub>, DCM, reflux, 96 h; (d) BzONH<sub>2</sub>·HCl, EtOH/Et<sub>3</sub>N, 4 h; (e) NaN<sub>3</sub>, H<sub>2</sub>O/HCl(10%)/MeOH, 29 h; (f) 1-Br<sub>2</sub>, HOAc, 15 min; 2-H<sub>2</sub>O/EtOH, reflux, 10 min. Asterisks denote novel derivatives. (B) Dose–response growth inhibition curves in BY4741, *yap1Δ*, *rad9Δ*, *rad52Δ*, and *mad2Δ*. (C) Halo of growth inhibition for the same strains (48 h). (D) Halo of growth inhibition for BY4741 and *yap1Δ* under normoxia and hypoxia (24 h and 72 h, respectively). In addition, normoxic inhibition halos for *rho0* strain derivatives are shown in the third and sixth columns (72 h). (E) Diameter of the inhibition halos for BY4741 growing on either YPD or YPGly.

quinone ring. It thus seems that this functional group might enhance toxicity against mitochondria.

**β-Lapachones Are Powerful Mitochondrial-Based Oxidative Stressors.** β-lapachone (19) is one of the most

clinically promising NQs. β-lapachone is a lapachol derivative obtained by intramolecular cyclization (Figure 3A).<sup>5</sup> We have previously shown that β-lapachone fulfills two of the findings that we show here for the subset of active lawsone derivatives;

Este documento incorpora firma electrónica, y es copia auténtica de un documento electrónico archivado por la ULL según la Ley 39/2015.  
 Su autenticidad puede ser contrastada en la siguiente dirección <https://sede.ull.es/validacion/>

Identificador del documento: 3075810 Código de verificación: smutbmB+

Firmado por: JESSEL AYRA PLASENCIA  
 UNIVERSIDAD DE LA LAGUNA

Fecha: 30/11/2020 12:24:14

María de las Maravillas Aguiar Aguiar  
 UNIVERSIDAD DE LA LAGUNA

08/02/2021 13:50:06

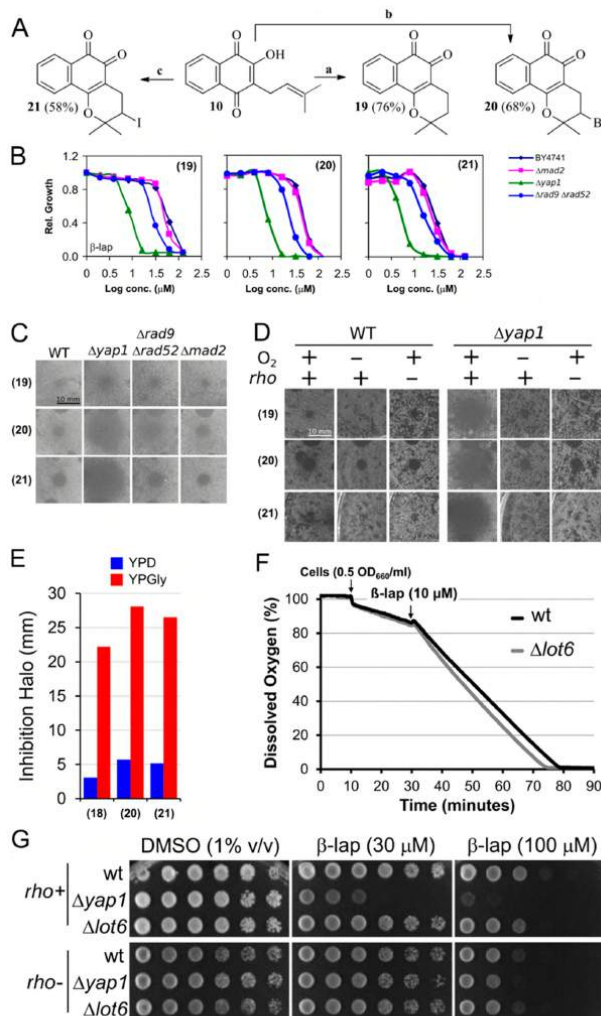


**Figure 3.** Yeast toxicity profiles of  $\beta$ -lapachone and derivatives thereof. (A) Scheme of preparation of  $\beta$ -lapachone derivatives from lapachol. Reactives and conditions: (a)  $H_2SO_4$ , 2 h; (b) 1-acetyl chloride, lutidine, 0 °C; 2-Br<sub>2</sub>, DCM, 15 min; (c) NIS, DCM, 24 h. (B) Dose–response growth inhibition curves in BY4741,  $yap1\Delta$ ,  $rad9\Delta$ ,  $rad52\Delta$ , and  $mad2\Delta$  strains. (C) Halo of growth inhibition for the same strains (48 h). (D) Halo of growth inhibition for BY4741 and  $yap1\Delta$  under normoxia and hypoxia (24 h and 72 h, respectively). In addition, normoxic inhibition halos for  $rho0$  strain derivatives are shown in the third and sixth columns (72 h). (E) Diameter of the inhibition halos for BY4741 growing on either YPD or YPGly. (F) Oxygen consumption in BY4741 and  $lot6\Delta$  before and after  $\beta$ -lapachone addition. First arrow denotes the addition of yeast cells; this triggers the first wave of  $O_2$  consumption through basal respiration. The second arrow denotes the addition of  $\beta$ -lapachone. (G) Spot assay for  $\beta$ -lapachone sensitivity in BY4741,  $yap1\Delta$  and  $lot6\Delta$  strains and their corresponding  $rho0$  derivatives.

i.e.,  $yap1\Delta$  hypersensitivity and suppression of toxicity in hypoxic conditions.<sup>17</sup> Therefore, we chose to study here  $\beta$ -lapachone and two halogenated derivatives (20 and 21). It seems that

halogenation of  $\beta$ -lapachone keeps its basic toxic profile while adding new toxicological features.<sup>17</sup> The three compounds showed strong  $yap1\Delta$  hypersensitive profiles (see Figures 3B and 3C, as

1954

DOI: 10.1021/acscchembio.8b00306  
 ACS Chem. Biol. 2018, 13, 1950–1957

235

Este documento incorpora firma electrónica, y es copia auténtica de un documento electrónico archivado por la ULL según la Ley 39/2015.  
 Su autenticidad puede ser contrastada en la siguiente dirección <https://sede.ull.es/validacion/>

Identificador del documento: 3075810 Código de verificación: smutbmB+

Firmado por: JESSEL AYRA PLASENCIA  
 UNIVERSIDAD DE LA LAGUNA

Fecha: 30/11/2020 12:24:14

María de las Maravillas Aguiar Aguiar  
 UNIVERSIDAD DE LA LAGUNA

08/02/2021 13:50:06

Table 1. Antiproliferative Activity of Natural NQs and Derivatives Thereof against Yeast, Bacteria, and Tumor Cell Lines

compound	<i>S. cerevisiae</i> <sup>a</sup>		<i>S. aureus</i> <sup>b</sup>		Tumor Cell Lines <sup>c,c</sup>		
	BY4741	MSSA	VISA	SkBr3	MCF-7	HEL	
	GI <sub>50</sub> (μM)	MIC (μM)	MIC (μM)	IC <sub>50</sub> (μM)	IC <sub>50</sub> (μM)	IC <sub>50</sub> (μM)	
<b>Lawsonia</b>							
1	>128	>128	>128	>10	>10	>10	
2	47.8 ± 9.8	64	32	6.1 ± 2.1	4.2 ± 1.1	6.7 ± 2.1	
3	56.1 ± 15.4	64	32	8.8 ± 2.1	3.5 ± 1.1	7.5 ± 2.1	
4	67.3 ± 35.2	128	64	>10	6.7 ± 2.1	8.5 ± 3.1	
5	54.3 ± 12.5	64	32	9.0 ± 1.8	4.3 ± 1.2	6.9 ± 1.7	
6	44.2 ± 11.9	64	32	8.5 ± 1.2	4.6 ± 1.7	3.2 ± 1.1	
7	>128	>128	>128	>10	>10	>10	
8	>128	>128	>128	>10	>10	>10	
9	>128	>128	>128	>10	>10	>10	
<b>Lapachol</b>							
10	>128	>128	>128	>10	>10	>10	
<b>Juglone</b>							
11	>128	>128	>128	3.6 ± 0.7	>10	1.7 ± 0.5	
12	64.6 ± 20.1	32	64	n.d. <sup>d</sup>	n.d. <sup>d</sup>	n.d. <sup>d</sup>	
13	71.3 ± 23.3	32	64	>10	>10	8.9 ± 1.8	
14	50.4 ± 42.5	32	32	n.d. <sup>d</sup>	n.d. <sup>d</sup>	n.d. <sup>d</sup>	
15	14.5 ± 2.3	32	64	4.8 ± 2.1	>10	5.4 ± 1.1	
16	31.4 ± 12.2	16	32	8.8 ± 1.7	4.3 ± 1.4	3.5 ± 1.2	
17	65.2 ± 21.8	64	32	9.6 ± 3.1	5.7 ± 2.1	5.3 ± 1.8	
18	44.8 ± 1.3	128	32	>10	>10	>10	
<b>β-lap</b>							
19	60.0 ± 18.0	32	8	1.6 ± 0.5	0.6 ± 0.5	0.7 ± 0.2	
20	43.3 ± 11.6	8	8	n.d. <sup>d</sup>	n.d. <sup>d</sup>	n.d. <sup>d</sup>	
21	44.6 ± 13.5	8	16	1.9 ± 1.1	1.5 ± 0.3	0.8 ± 0.3	

<sup>a</sup>Values represent mean ± SD (*n* = 3). <sup>b</sup>MSSA, methicillin sensitive strain ATCC25923; VISA, methicillin-resistant vancomycin-intermediate strain NRS402. MIC, minimum inhibitory concentration (>90% inhibition relative to DMSO 1% v/v). MIC (μM [μg/mL]) for reference antibiotics: Oxacillin (MSSA = 2.4 [1]; VISA > 300 [>128]); vancomycin (MSSA = 1.4 [2]; VISA = 11.2 [16]). <sup>c</sup>SkBr3, HER2-overexpressing human breast cancer cell line; MCF-7, human breast cancer cell line; HEL, human erythroleukemia cell line. IC<sub>50</sub> for adriamycin (reference cytotoxic compound): SkBr3 (0.1 ± 0.06); MCF-7 (0.6 ± 0.09); HEL (0.1 ± 0.03). <sup>d</sup>Not determined.

well as Figure S4 in the Supporting Information). The *yap1Δ* hypersensitivity was clearly superior to all other quinones tested here and was almost fully suppressed in hypoxia and in the *rho0* strains (Figure 3D). Mitochondrial function was severely impaired after treatment with β-lapachones (see Figure 3E).

Whereas both the *yap1Δ* hypersensitivity and the suppression of toxicity in hypoxia fit well with current cytotoxic models for β-lapachone; i.e., ROS generation and NAD(P)H exhaustion through redox cycling; the suppression in *rho0* strains and the strong mitochondrial dysfunction were unexpected. What makes β-lapachone different from most NQs is the capability to feed redox cycles through the otherwise detoxifying cytosolic enzyme NQO1 (also known as DT-diaphorase; EC 1.6.5.2), whose yeast counterpart is Lot6.<sup>18,19</sup> Thus, we quantified redox cycling after β-lapachone exposure in cells with NQO1 (WT) and without NQO1 (*lot6Δ*). To measure redox cycling, we monitored O<sub>2</sub> consumption *in vivo* (Figure 3F). The addition of just 10 μM β-lapachone led to a sudden acceleration of O<sub>2</sub> consumption (~3-fold); the new rate of consumption was steady until O<sub>2</sub> exhaustion, in agreement with a scenario whereby β-lapachone triggers redox cycles fed by O<sub>2</sub>. Noteworthy, we observed similar O<sub>2</sub> consumption profiles between WT and *lot6Δ* (Figure 3F). Not only that, the *lot6Δ* was as sensitive to β-lapachone as the reference strain, irrespective of whether these strains carry functional mitochondria (Figure 3G). Note that if β-lapachone was triggering redox cycles through Lot6, the *lot6Δ* mutant was expected to be resistant and consume

less O<sub>2</sub>. We also performed *lot6Δ* halo assays for all other NQs and observed neither hypersensitivity nor resistance, compared to the reference strain (see Figure S5 in the Supporting Information).

From this set of experiments, and our previous results,<sup>16,17</sup> we conclude that, in yeast, the following statements are valid: (i) β-lapachones are highly potent oxidative stressors that generate ROS through redox cycling; (ii) the origin of ROS is mitochondrial rather than cytosolic; and (iii) β-lapachone itself, any of its biotransformed metabolites,<sup>20</sup> and/or ROS largely disrupt mitochondrial function.

**Antiproliferative Activities against Pathogenic Bacteria and Tumor Cell Lines.** Finally, we determined the antiproliferative effect of these NQs against (i) two strains of the pathogenic gram-positive bacteria *Staphylococcus aureus* that differ in their resistance to clinically used antibiotics (MSSA and VISA), and (ii) three well-established human cancer cell lines. Generally, growth inhibition in yeast correlated well with the other antiproliferative activities. Accordingly, both lawsonia and lapachol showed poor activities whatsoever, but those derivatives with ROS-based toxicity in yeast were also toxic in bacteria and cell lines (Table 1). As for juglone and derivatives thereof, we observed a better selectivity. Juglone was only toxic in cancer cell lines, whereas its brominated derivative (18) was just the opposite (i.e., mildly toxic against bacteria and good against yeast, but without an antitumor profile). The novel compound (15) was the strongest against yeast. As for β-lapachone

1955

DOI: 10.1021/acscchembio.8b00306  
 ACS Chem. Biol. 2018, 13, 1950–1957

derivatives, they were the most selective antitumor compounds, in accordance with expectations from the literature. Interestingly, they were also the strongest against *S. aureus*.

**Remarks on Structure–Activity Relationships.** From our data, we conclude that the free hydroxyl group in lawsone and lapachol blocks antiproliferative activity. We believe that this polar hydroxyl group provides a barrier for the NQs to go through the plasma membrane, especially considering the  $pK_a$  predictions for these compounds (Table S1 in the Supporting Information). Thus, 2-hydroxy-naphthoquinones (lawsones) are mostly in a membrane-impenetrable ionized form at physiological pHs, whereas the ionized form is <10% in 5-hydroxy-naphthoquinones (juglones). This might well explain why juglone derivatives that maintained the free 5-hydroxyl group were active. Overall, the absence of an ionized form at physiological pHs is the best toxicity predictor (see Table S1). However, the nature/size of the newly added groups could indeed determine the main mechanism of toxicity, at least in yeast (e.g., ROS generation in 2/3-amino-juglones versus other juglones). It also seems that the position of the group drives which mechanism might be operative (e.g., a ROS-dependent toxicity for 2-O-alkyl-naphthoquinones and a ROS-independent mechanism for 5-O-alkyl-naphthoquinones).

In conclusion, we have studied the toxicity of several derivatives (four of them novel chemical entities) from the widespread natural NQs lawsone, juglone, lapachol, and  $\beta$ -lapachone. We have cross-compared antiproliferative activity between bacteria, yeast, and tumor cell lines, and we found that most NQs were unselectively toxic.  $\beta$ -lapachones were the NQs with the strongest antitumor activity. In yeast,  $\beta$ -lapachones were also the most potent oxidative stressors and the ones that most effectively disrupted mitochondrial function. It would be interesting to check if the observed mitochondrial-driven toxicity is important to understand the potent antitumor properties of  $\beta$ -lapachone. In addition, here, we show that both lawsone and juglone can be chemically modified to obtain new drugs with a similar mitochondrial-based toxicological profile, which make these natural NQs useful scaffolds for this class of antiproliferative drugs.

## MATERIALS AND METHODS

**Synthesis of Naphthoquinone Derivatives.** The naphthoquinone derivatives were prepared following the reactions shown in panels (A) in Figures 1–3. Details on each reaction and structural characterization of the obtained compounds are included in the Supporting Information. For biological assays, NQs were resuspended in DMSO (10 mM stocks).

**Yeast Strains and Elimination of Mitochondrial DNA.** The reference yeast strain was BY4741. All single mutants were commercial isogenic derivatives of BY4741 obtained from the Euroscarf collection (<http://www.euroscarf.de>). The double mutant strain  $\Delta rad9::kanMX4 \Delta rad52::matMX$  (FM1329) was constructed through standard PCR-based genetic engineering;<sup>21</sup> details are given in the Supporting Information. All yeast strains were grown in YP media (1% w/v yeast extract; 2% w/v peptone) supplemented with the corresponding carbon source (2% w/v glucose, YPD; or 3% w/v glycerol YPGly).

Mitochondrial DNA was eliminated through continuous growth (~20 generations) in YPD supplemented with 20  $\mu$ g/mL of the DNA intercalating agent ethidium bromide. The loss of mitochondrial DNA (*rho0* genotype) was checked by DAPI staining and inability to grow in YPGly (see Figure S6 in the Supporting Information).

All strains and their relevant genotypes are listed in Table S2 in the Supporting Information.

**Growth Inhibition Assays in Yeast.** We first followed a broth microdilution assay in 96-well plates, as previously described.<sup>16,17</sup> The NQ concentrations were 0, 1, 2, 4, 8, 16, 32, 64, and 128  $\mu$ M

(final concentration of DMSO was maintained at 1% (v/v)). The inoculum was set at an optical density at 620 nm ( $OD_{620}$ ) of 0.001 (~ $2.5 \times 10^4$  cells/mL). The growth was measured at  $OD_{620}$  after 48 h of incubation at 25 °C. The concentration that inhibited growth by 50% ( $GI_{50}$ ) was calculated by fitting a four-parametric curve to the experimental data (<http://www.changbioscience.com/stat/ec50.html>).

Because of caveats to use a liquid-based dose–response assay for the hypoxic condition, as well as the lower growth rates under several experimental conditions (hypoxia, glycerol, and *rho0* strains), we also assessed toxicity through a halo inhibition assay (see Figure S7 in the Supporting Information). The cell density on the plate surface was ~50 cells/mm<sup>2</sup>, and the amount spotted for each NQ was 10 nmol. More details are given in the Supporting Information.

Finally, growth inhibition on plates at defined drug concentrations was determined through spot assays as described previously.<sup>17</sup>

**Dissolved Oxygen (DO) Consumption Assay.** The assay was performed in a homemade hermetically closed container with entries for pH and O<sub>2</sub> electrodes (MU 6100 H S2 equipment, VWR, No. 665–0312). The culture volume within the container (100 mL) was constantly stirred at 180 rpm while recording DO every 30 sec. The temperature was kept at 30 °C. DO was initially brought to 100% by briefly bubbling pure O<sub>2</sub> through a third entry controlled with a stopcock. After 10 min, freshly grown cells were added through the stopcock to yield an 0.5  $OD_{620}$ ; after another 10 min, the quinone was added to yield a final concentration of 10  $\mu$ M.

**Determination of Antibacterial and Antitumor Activities.** For determination of bacterial minimum inhibitory concentrations (MICs), we followed a standard broth microdilution assay as previously described.<sup>22</sup> The NQ and DMSO concentrations were the same as that for yeast; the inoculum was ~ $10^5$  cells/mL. Growth was determined in cation-adjusted Mueller Hinton broth after 24 h at 37 °C.

To test cytotoxicity against tumor cell lines, we performed the MTT [3-(4,5-dimethylthiazol-2-yl)-2,5-diphenyl tetrazolium bromide] assay as previously described.<sup>23</sup>

## ASSOCIATED CONTENT

### Supporting Information

The Supporting Information is available free of charge on the ACS Publications website at DOI: 10.1021/acscchembio.8b00306.

Seven figures, two tables, and extended materials and methods (PDF)

## AUTHOR INFORMATION

### Corresponding Authors

\*Tel.: +34 922 318576. E-mail: aestebra@ull.es (A. Estévez-Braun).

\*Tel.: +34 922 602951. E-mail: fmachin@funcanis.es (F. Machin).

### ORCID

Félix Machín: 0000-0003-4559-7798

### Author Contributions

<sup>†</sup>These authors equally contributed to this work.

### Notes

The authors declare no competing financial interest.

## ACKNOWLEDGMENTS

This work has been funded by Spanish Ministerio de Economía y Competitividad (No. BFU2015-63902-R to F.M.; No. SAF 2015-65113-C2-1-R to A.E.B.; No. SAF 2015-65113-C2-2-R to L.F.P.). L.A.A. thanks Agencia Canaria de Investigación, Innovación y Sociedad de la Información (ACIISI) for a predoctoral fellowship (No. TESIS2017010039). P.M.R. is the recipient of a predoctoral fellowship from ULPGC-IUIBS. Grants and fellowships are cofunded by EU-ERDF.

DOI: 10.1021/acscchembio.8b00306  
ACS Chem. Biol. 2018, 13, 1950–1957

1956

237

Este documento incorpora firma electrónica, y es copia auténtica de un documento electrónico archivado por la ULL según la Ley 39/2015.

Su autenticidad puede ser contrastada en la siguiente dirección <https://sede.ull.es/validacion/>

Identificador del documento: 3075810

Código de verificación: smutbmB+

Firmado por: JESSEL AYRA PLASENCIA  
UNIVERSIDAD DE LA LAGUNA

Fecha: 30/11/2020 12:24:14

María de las Maravillas Aguiar Aguiar  
UNIVERSIDAD DE LA LAGUNA

08/02/2021 13:50:06

REFERENCES

- (1) O'Brien, P. (1991) Molecular mechanisms of quinone cytotoxicity. *Chem.-Biol. Interact.* 80, 1–41.
- (2) Kumagai, Y., Shinkai, Y., Miura, T., and Cho, A. K. (2012) The chemical biology of naphthoquinones and its environmental implications. *Annu. Rev. Pharmacol. Toxicol.* 52, 221–47.
- (3) Santa-María, I., Smith, M. A., Perry, G., Hernández, F., Avila, J., and Moreno, F. J. (2005) Effect of quinones on microtubule polymerization: A link between oxidative stress and cytoskeletal alterations in Alzheimer's disease. *Biochim. Biophys. Acta, Mol. Basis Dis.* 1740, 472–480.
- (4) Klotz, L. O., Hou, X., and Jacob, C. (2014) 1,4-naphthoquinones: From oxidative damage to cellular and inter-cellular signaling. *Molecules* 19, 14902–14918.
- (5) Qiu, H.-Y., Wang, P.-F., Lin, H.-Y., Tang, C.-Y., Zhu, H.-L., and Yang, Y.-H. (2018) Naphthoquinones: A continuing source for discovery of therapeutic antineoplastic agents. *Chem. Biol. Drug Des.* 91, 681.
- (6) Ravelo, Á. G., Estévez-Braun, A., and Pérez-Sacau, E. (2003) The chemistry and biology of lapachol and related natural products  $\alpha$  and  $\beta$ -lapachones. *Stud. Nat. Prod. Chem.* 29, 719–760.
- (7) Siegel, D., Yan, C., and Ross, D. (2012) NAD(P)H:quinone oxidoreductase 1 (NQO1) in the sensitivity and resistance to antitumor quinones. *Biochem. Pharmacol.* 83, 1033–40.
- (8) Oh, E. T., and Park, H. J. (2015) Implications of NQO1 in cancer therapy. *BMB Rep.* 48, 609–617.
- (9) Symington, L. S., Rothstein, R., and Lisby, M. (2014) Mechanisms and Regulation of Mitotic Recombination in *Saccharomyces cerevisiae*. *Genetics* 198, 795–835.
- (10) Lara-Gonzalez, P., Westhorpe, F. G., and Taylor, S. S. (2012) The spindle assembly checkpoint. *Curr. Biol.* 22, R966–R980.
- (11) Farrugia, G., and Balzan, R. (2012) Oxidative stress and programmed cell death in yeast. *Front. Oncol.* 2, 64.
- (12) Boronat, S., Domènech, A., Paulo, E., Calvo, I. A., García-Santamarina, S., García, P., Encinar Del Dedo, J., Barcons, A., Serrano, E., Carmona, M., and Hidalgo, E. (2014) Thiol-based H<sub>2</sub>O<sub>2</sub> signalling in microbial systems. *Redox Biol.* 2, 395–9.
- (13) Rodríguez, C. E., Shinyashiki, M., Froines, J., Yu, R. C., Fukuto, J. M., and Cho, A. K. (2004) An examination of quinone toxicity using the yeast *Saccharomyces cerevisiae* model system. *Toxicology* 201, 185–96.
- (14) Emadi, A., Ross, A. E., Cowan, K. M., Fortenberry, Y. M., and Vuica-Ross, M. (2010) A chemical genetic screen for modulators of asymmetrical 2,2'-dimeric naphthoquinones cytotoxicity in yeast. *PLoS One* 5, e10846.
- (15) Chaput, M., Brygier, J., Lion, Y., and Sels, A. (1983) Potentiation of oxygen toxicity by menadione in *Saccharomyces cerevisiae*. *Biochimie* 65, 501–512.
- (16) Quevedo, O., García-Luis, J., Lorenzo-Castrillejo, I., and Machín, F. (2011) No role of homologous recombination in dealing with  $\beta$ -lapachone cytotoxicity in yeast. *Chem. Res. Toxicol.* 24, 2106–8.
- (17) Ramos-Pérez, C., Lorenzo-Castrillejo, I., Quevedo, O., García-Luis, J., Matos-Perdomo, E., Medina-Coello, C., Estévez-Braun, A., and Machín, F. (2014) Yeast cytotoxic sensitivity to the antitumour agent  $\beta$ -lapachone depends mainly on oxidative stress and is largely independent of microtubule- or topoisomerase-mediated DNA damage. *Biochem. Pharmacol.* 92, 206–219.
- (18) Sollner, S., Nebauer, R., Ehammer, H., Prem, A., Deller, S., Palffy, B. a., Daum, G., and Macheroux, P. (2007) Lot6p from *Saccharomyces cerevisiae* is a FMN-dependent reductase with a potential role in quinone detoxification. *FEBS J.* 274, 1328–39.
- (19) Pink, J. J., Planchon, S. M., Tagliarino, C., Varnes, M. E., Siegel, D., and Boothman, D. A. (2000) NAD(P)H: Quinone oxidoreductase activity is the principal determinant of beta-lapachone cytotoxicity. *J. Biol. Chem.* 275, 5416–24.
- (20) Paludo, C. R., da Silva-Junior, E. A., de Oliveira Silva, E., Vessecchi, R., Pepporine Lopes, N., Tallarico Pupo, M., da Silva Emery, F., dos Santos Gonçalves, N., Alves dos Santos, R., and Jacometti Cardoso Furtado, N. A. (2017) Inactivation of  $\beta$ -Lapachone

Cytotoxicity by Filamentous Fungi that Mimic the Human Blood Metabolism. *Eur. J. Drug Metab. Pharmacokin.* 42, 213–220.

(21) Smith, J. S., and Burke, D. J. (2014) *Yeast Genetics: Methods and Protocols* (Smith, J. S., and Burke, D. J., Eds.). Springer, New York.

(22) Casero, C., Estévez-Braun, A., Ravelo, A. G., Demo, M., Méndez-Álvarez, S., and Machín, F. (2013) Achyrofurin is an antibacterial agent capable of killing methicillin-resistant vancomycin-intermediate *Staphylococcus aureus* in the nanomolar range. *Phytochemistry* 20, 133–8.

(23) Quintana-Espinoza, P., Martín-Acosta, P., Amesty, Á., Martín-Rodríguez, P., Lorenzo-Castrillejo, I., Fernández-Pérez, L., Machín, F., and Estévez-Braun, A. (2017) 5-Ethynylarylnaphthalimides as Antitumor Agents: Synthesis and Biological Evaluation. *Bioorg. Med. Chem.* 25, 1976–1983.

Este documento incorpora firma electrónica, y es copia auténtica de un documento electrónico archivado por la ULL según la Ley 39/2015.  
Su autenticidad puede ser contrastada en la siguiente dirección <https://sede.ull.es/validacion/>

Identificador del documento: 3075810 Código de verificación: smutbmB+

Firmado por: JESSEL AYRA PLASENCIA  
UNIVERSIDAD DE LA LAGUNA

Fecha: 30/11/2020 12:24:14

María de las Maravillas Aguiar Aguilár  
UNIVERSIDAD DE LA LAGUNA

08/02/2021 13:50:06



## Topoisomerase II deficiency leads to a postreplicative structural shift in all *Saccharomyces cerevisiae* chromosomes

Jessel Ayra-Plasencia, Cristina Ramos-Pérez, Silvia Santana-Sosa, Oliver Quevedo-Rodríguez, Sara Medina-Suárez, Emiliano Matos-Perdomo, Marcos Zamora-Dorta, Grant W Brown, Michael Lisby, Félix Machín

### Abstract

The key role of Topoisomerase II (Top2) is the removal of topological intertwinings between sister chromatids. In yeast, inactivation of Top2 brings about distinct cell cycle responses. In the case of the conditional *top2-5* allele, interphase and mitosis progress on schedule but cells suffer from a segregation catastrophe. We here show that *top2-5* chromosomes fail to enter a Pulsed-Field Gel Electrophoresis (PFGE) in the first cell cycle, a behavior traditionally linked to the presence of replication and recombination intermediates. We distinguished two classes of affected chromosomes: the rDNA-bearing chromosome XII, which fails to enter a PFGE at the beginning of S-phase, and all the other chromosomes, which fail at a postreplicative stage. In synchronously cycling cells, this late PFGE retention is observed in anaphase; however, we demonstrate that this behavior is independent of cytokinesis, stabilization of anaphase bridges, spindle pulling forces and even anaphase onset. Strikingly, once the PFGE retention has occurred it becomes refractory to Top2 re-activation. DNA combing, two-dimensional electrophoresis, genetic analyses and GFP-tagged DNA damage markers suggest that non-recombinational modifications of late replication intermediates may account for the shift in the PFGE behavior. The fact that this shift does not trigger G<sub>2</sub>/M checkpoints further supports this statement since checkpoints are active for other replicative stresses in the absence of Top2. We propose that the prolonged absence of Top2 activity leads to a general chromosome structural change. This change might interlock chromatids together with catenations and thus contribute to the formation of anaphase bridges in *top2* mutants.

- This scientific contribution has been published as a preprint in biorxiv. It is currently under peer review in Scientific Reports Magazine (Q1, Impact factor 2019: 3.998).



QR code for the manuscript

239

Este documento incorpora firma electrónica, y es copia auténtica de un documento electrónico archivado por la ULL según la Ley 39/2015.  
Su autenticidad puede ser contrastada en la siguiente dirección <https://sede.ull.es/validacion/>

Identificador del documento: 3075810 Código de verificación: smutbmB+

Firmado por: JESSEL AYRA PLASENCIA  
UNIVERSIDAD DE LA LAGUNA

Fecha: 30/11/2020 12:24:14

María de las Maravillas Aguiar Aguiar  
UNIVERSIDAD DE LA LAGUNA

08/02/2021 13:50:06



Este documento incorpora firma electrónica, y es copia auténtica de un documento electrónico archivado por la ULL según la Ley 39/2015.  
*Su autenticidad puede ser contrastada en la siguiente dirección <https://sede.ull.es/validacion/>*

Identificador del documento: 3075810      Código de verificación: smutbmB+

Firmado por: JESSEL AYRA PLASENCIA  
UNIVERSIDAD DE LA LAGUNA

Fecha: 30/11/2020 12:24:14

María de las Maravillas Aguiar Aguiar  
UNIVERSIDAD DE LA LAGUNA

08/02/2021 13:50:06



Este documento incorpora firma electrónica, y es copia auténtica de un documento electrónico archivado por la ULL según la Ley 39/2015.  
*Su autenticidad puede ser contrastada en la siguiente dirección <https://sede.ull.es/validacion/>*

Identificador del documento: 3075810      Código de verificación: smutbmB+

Firmado por: JESSEL AYRA PLASENCIA  
UNIVERSIDAD DE LA LAGUNA

Fecha: 30/11/2020 12:24:14

María de las Maravillas Aguiar Aguiar  
UNIVERSIDAD DE LA LAGUNA

08/02/2021 13:50:06



Este documento incorpora firma electrónica, y es copia auténtica de un documento electrónico archivado por la ULL según la Ley 39/2015.  
*Su autenticidad puede ser contrastada en la siguiente dirección <https://sede.ull.es/validacion/>*

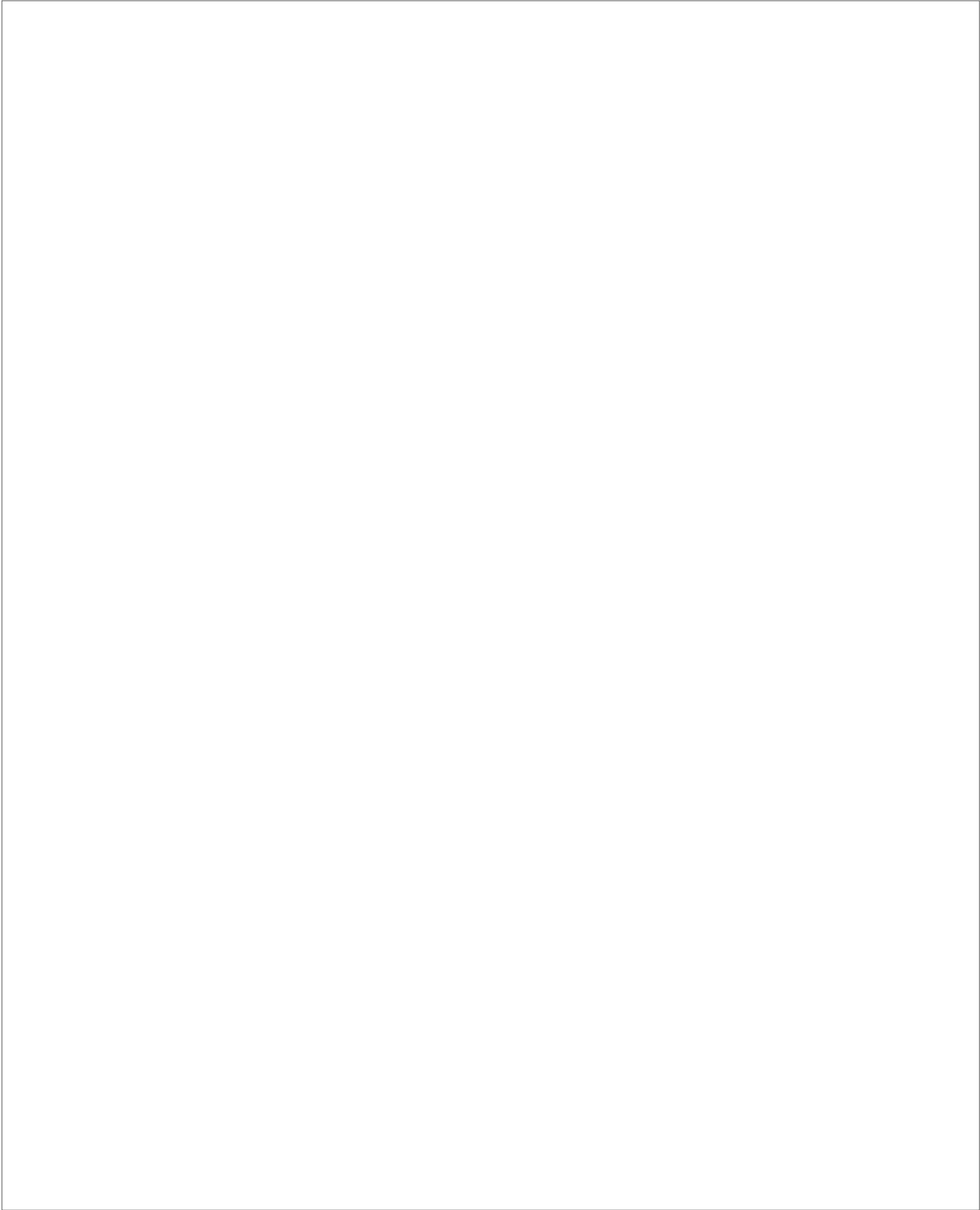
Identificador del documento: 3075810      Código de verificación: smutbmB+

Firmado por: JESSEL AYRA PLASENCIA  
UNIVERSIDAD DE LA LAGUNA

Fecha: 30/11/2020 12:24:14

María de las Maravillas Aguiar Aguiar  
UNIVERSIDAD DE LA LAGUNA

08/02/2021 13:50:06



Este documento incorpora firma electrónica, y es copia auténtica de un documento electrónico archivado por la ULL según la Ley 39/2015.  
*Su autenticidad puede ser contrastada en la siguiente dirección <https://sede.ull.es/validacion/>*

Identificador del documento: 3075810      Código de verificación: smutbmB+

Firmado por: JESSEL AYRA PLASENCIA  
UNIVERSIDAD DE LA LAGUNA

Fecha: 30/11/2020 12:24:14

María de las Maravillas Aguiar Aguiar  
UNIVERSIDAD DE LA LAGUNA

08/02/2021 13:50:06



Este documento incorpora firma electrónica, y es copia auténtica de un documento electrónico archivado por la ULL según la Ley 39/2015.  
Su autenticidad puede ser contrastada en la siguiente dirección <https://sede.ull.es/validacion/>

Identificador del documento: 3075810 Código de verificación: smutbmB+

Firmado por: JESSEL AYRA PLASENCIA  
UNIVERSIDAD DE LA LAGUNA

Fecha: 30/11/2020 12:24:14

María de las Maravillas Aguiar Aguilár  
UNIVERSIDAD DE LA LAGUNA

08/02/2021 13:50:06